José Luís Figueiredo
Mariette M. Pereira
Joaquim Faria

Editors

Catalysis from Theory to Application

An Integrated Course

(Página deixada propositadamente em branco)

I N V E S T I G A Ç Á O

José Luís Figueiredo
Mariette M. Pereira
Joaquim Faria
Editors

Catalysis from Theory to Application

An Integrated Course

(Página deixada propositadamente em branco)

To the memory of our colleague and friend
Eric Derouane (1944-2008)

(Página deixada propositadamente em branco)

PREFACE

The idea of this book started to take shape during the 1st Integrated Course on Catalysis which was organized in 2006 by the Portuguese Chemical Society (SPQ) through its Catalysis and Porous Materials Division (DCMP) and its Porto Delegation, in collaboration with six Universities and four Industrial companies.

The Course was organized according to the guidelines set up by the ERA-Net ACENET (Applied Catalysis European Network), with the objective of offering a broad and comprehensive survey of the field to PhD and MSc students in Catalysis. Indeed, most students graduating in chemistry or chemical engineering have only fragmented knowledge of catalysis. If they choose to work for a PhD degree or specialise in a selected topic in catalysis, they would probably never have an opportunity to learn the fundamentals of the topic in a systematic way. Therefore, ACENET strongly supports the implementation of such integrated courses across Europe.

The book follows approximately the structure of the Course and compiles most of the material presented therein. It starts with Heterogeneous Catalysis (Part A), followed by Homogeneous Catalysis (Part B), Photocatalysis (Part C) and Electrocatalysis (Part D). A final chapter on Experimental Design (Part E), and an additional chapter (7) in Part B were added for the sake of completeness. Several lectures have been combined in a single Chapter (as in Chapters 1 and 7, Part A, which include material from three different lectures, in each case), while others were not included in this edition. The coverage of the various topics is provided in sufficient

depth for an introductory text, and recommended references for further study are indicated where appropriate. Editing was kept at a minimum, therefore differences in style from chapter to chapter are unavoidable; additionally, the material presented in the different chapters is of the responsibility of their authors.

The Editors would like to take this opportunity to thank the Institutions and the people that made this project possible: Sociedade Portuguesa de Química, Fundação para a Ciência e a Tecnologia, the Universities of Coimbra, Porto, Aveiro, Évora, Technical University of Lisbon and New University of Lisbon, the supporting companies CIRES, Galp Energia, Hovione and Quimigal (now CUF-QI), all the authors, the lecturers not authoring any chapter (Michel Guisnet, Eric Derouane, Juan Carlos Bayón, Jacob Moulijn, Iluminada Gallardo, Sílvia Costa and Joaquim Vital), the colleagues responsible for the experimental sessions (João Rocha, Artur Silva and Carlos Sá) and also the students of the first Integrated Course on Catalysis, who made it all worthwhile.

We would also like to acknowledge various students of the Chemistry Department, University of Coimbra (Rui Nunes, Andreia Peixoto, Carlos Monteiro, Vanessa Simões, and Sara Pinto) for their assistance at various stages during the Course and also in the preparation of the manuscript. We are also grateful to Hovione for financially supporting the edition of this book. Finally, we hope that the book may be useful to students and researchers in the field of Applied Catalysis.

The Editors,
Mariette Pereira
Joaquim Luís Faria
José Luís Figueiredo

ÍNDICE

(Página deixada propositadamente em branco)

SECTION A

HETEROGENEOUS CATALYSIS

1. HETEROGENEOUS CATALYSIS: AN OVERVIEW

José Luís Figueiredo

Laboratório de Catálise e Materiais, Departamento de Engenharia Química, Faculdade de Engenharia, Universidade do Porto, R. Dr. Roberto Frias, 4200-465 Porto, Portugal.

1.1. INTRODUCTION

1.1.1. Applied catalysis: key to sustainability

It is appropriate to start this introductory chapter of the Integrated Course on Catalysis with a quote from the ACENET ERA-Net (European Network on Applied Catalysis) web page: *Applied catalysis is a strongly interdisciplinary field, encompassing chemistry, bioscience and materials and engineering science, among others. It also has a large potential to address many areas of socio-economic activity as well as key European challenges, such as sustainability and energy. The OECD estimates that 30% to 40% of the gross national products of developed economies, such as those of the EU Member States, depend on catalysts and catalytic technologies. As such, catalysis has a large impact on economic and social prosperity in Europe.*

Indeed, more than 80% of the chemical processes depend on catalytic technologies, with a worldwide value of products amounting to € 2×10^{12}/year. Moreover, catalytic technologies are essential in key areas for sustainable development, such as new energy vectors and renewable raw materials; clean, waste-free production of chemicals; pollution control and abatement. Catalysis is also a "green" technology, since the catalytic routes provide for higher atom efficiencies.

1.1.2. Historical perspective

It was Berzelius (J.J. Berzelius, 1779-1848) who coined the word *Catalysis* in 1835 (from the Greek, καταλειν, meaning to loose down, dissolve), by analogy to *Analysis*, in order to rationalize a number of isolated observations, such as the conversion of starch to sugar by acids, the decomposition of H_2O_2 by metals, the conversion of ethanol to acetic acid and the reaction between O_2 and H_2 in the presence of Pt. Although he had the merit to recognize a common feature in these processes, the nature of the phenomenon was not properly understood for the next 60 years. It was Ostwald (W. Ostwald, 1853-1932) who established the *kinetic* nature of catalysis, and the definition he proposed in 1895 has stood the test of time: "A catalyst is a substance that changes *the rate* of a chemical reaction without itself appearing in the products". Ostwald was awarded the Nobel Prize in Chemistry in 1909, and since then several other scientists were similarly recognized for their work on catalysis or related topics, as shown in Table 1.

TABLE 1 – Nobel Prizes in Catalysis or related topics

Year	Scientists	Research topic
1909	W. Ostwald	for his work on catalysis
1912	P. Sabatier	catalytic hydrogenation
1918	F. Haber	synthesis of ammonia
1931	C. Bosch, F. Bergius	high pressure methods
1932	I. Langmuir	surface chemistry
1963	K. Ziegler, G. Natta	stereospecific polymerization
2001	W.S. Knowles, R. Noyori, K.B. Sharpless	chiral catalysis
2005	Y. Chauvin, R.H. Grubbs, R.R. Schrock	olefin metathesis
2007	G. Ertl	catalytic reactions on surfaces

The development of the chemical industry in the 20th century closely parallels the evolution of catalysis. We can roughly consider three periods. Up to about

1940, the chemical industry was based on coal as a raw-material, and catalysts were mostly used for the production of base chemicals (ammonia, methanol, nitric and sulphuric acids), margarine (by catalytic hydrogenation), and liquid fuels by Fischer-Tropsch synthesis. Important concepts were introduced in this period by Sabatier (the reactants form *unstable intermediates* with the catalyst) and by Taylor (there are *active sites* on the catalyst surface, where chemical adsorption occurs). The Langmuir adsorption isotherm provided the basis to establish catalytic reaction mechanisms, while Brunauer, Emmett and Teller derived an isotherm for physical adsorption (the BET equation), which forms the basis of a method for determining the specific surface areas of catalysts.

The period from 1940 to 1970 was characterized by the availability of cheap oil, which led to the development of hydrocarbon refining and the petrochemical industry. Catalysts were used for the production of fuels (catalytic cracking, reforming), synthesis gas (by steam reforming) and polymers, as well as intermediates by selective oxidation processes. The synthesis of zeolites was a major advance in this period, which led to improved catalytic processes. Important concepts were introduced by Boudart (*structure sensitive* versus *structure insensitive* catalytic reactions) and by Weisz (*shape-selectivity* in catalysis by zeolites).

The so-called "oil-crisis" of 1972, and the subsequent discovery of abundant natural gas in the North Sea, provided the drive for the development of new hydrocarbon processes, capable of a more efficient use of energy and raw-materials. On the other hand, the introduction of legislation to curb pollution (especially from vehicles) led to the new area of *environmental catalysis*. The auto-exhaust catalytic converter was introduced in 1976 in the USA, and today this process is responsible for the largest consumption of catalysts. Significant progress was made in the preparation of catalysts and in understanding the mechanisms of catalyst deactivation. New micro and mesoporous materials (such as SAPOs, AlPOs, MeAPOs, TS1, MCM41) were synthesized and

applied in catalytic processes. New fields of application emerged, such as photocatalysis and electrocatalysis. In the 1990s, *sustainable development* became a major concern, leading to the concept of "Green Chemistry" and providing new opportunities for catalysis in the areas of fine chemicals and pharmaceuticals.

1.1.3. Basic concepts and definitions

We can define a catalyst as a substance which increases the rate of a chemical reaction without being consumed in the process. In doing so, the catalyst provides a new reaction mechanism, such as shown in Figure 1 for the reaction R → P, where **X** is the catalyst and RX an intermediate. The activation energy corresponding to the catalytic path is lower, therefore the reaction rate is much higher, since the rate constant $k = A \exp(-E/RT)$.

Thus, we have two steps in this mechanism:

$$R + \mathbf{X} \rightarrow RX$$

$$RX \rightarrow P + \mathbf{X}$$
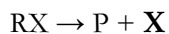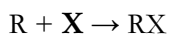
According to this definition, the catalytic reaction is a sequence of elementary steps which would repeat indefinitely, the catalytic cycle shown in Figure 2. However, in practice, and quoting J.J. Carberry, various deactivation mechanisms *conspire to deny catalysts immortality.*
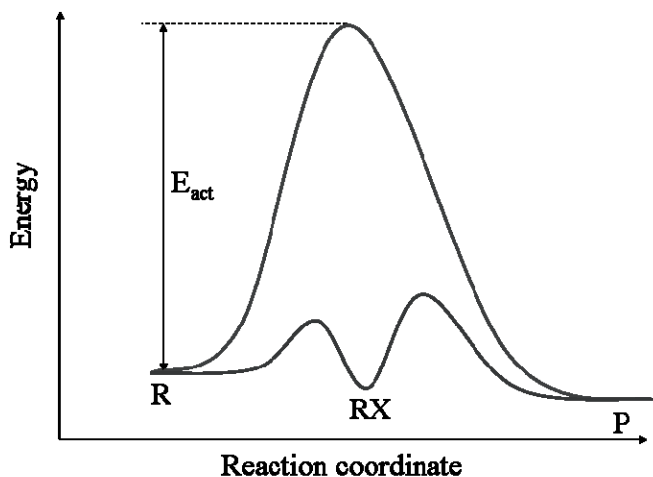
Figure 1 – Comparison of the catalytic and non-catalytic paths for the reaction.

Since the initial and final states are the same in the catalytic and non-catalytic reaction paths, the equilibrium constant $K = \exp(-\Delta G^o/RT)$ is not changed. The catalyst only affects the *kinetics* of the reaction, *i.e.* it increases the rate of approach to equilibrium. For an elementary step, the equilibrium constant is the ratio of the forward and reverse reaction rate constants; therefore, the catalyst increases the rate of both reactions to the same extent.
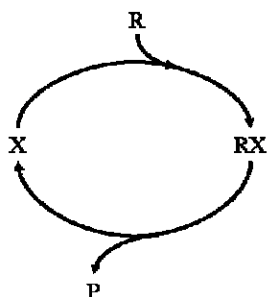
Figure 2 – Catalytic cycle for the reaction R → P.

One of the most important properties of a catalyst is its *selectivity*. Thus, different catalysts promote the formation of different products from the same

reactants. For instance, in the presence of a metal catalyst, such as Cu, ethanol is dehydrogenated to acetaldehyde, while metal oxides, such as alumina, catalyse the dehydration of ethanol to ethylene. Thus, each catalyst favours one among several reactions which are thermodynamically possible. This property is essential, for instance, when we want to obtain partially oxidized products, such as formaldehyde from methanol. If the catalyst is not selective, we will end up with the products of deep oxidation, CO_2 and H_2O. We can express the selectivity by the ratio between the rate of formation of the desired product, and the sum of the rates of formation of all other products. Alternatively, we can quote the *relative yield*, which is given by the ratio between the rate of formation of the desired product, and the rate of conversion of the reactant. Multiple reactions can be adequately described in terms of parallel (competitive) reactions, and series (consecutive) reactions.

The *activity* of a catalyst can be expressed by the number of revolutions of the catalytic cycle per unit time, or *turnover frequency*, TOF (s^{-1}). However, it is common practice to compare catalyst activities in terms of more accessible parameters, such as: the temperature needed to reach a given conversion, the conversion obtained under fixed conditions, the contact time needed to reach a given conversion (this depends on the reactor type), or the rate constants at fixed conditions.

The *stability* of the catalyst determines its useful life, which can be expressed by the number of turnovers of the catalytic cycle before the catalyst "dies".

Catalysis can be sub-divided into various disciplines:

- *Homogeneous* (or molecular) catalysis, when the reactants and the catalyst are in the same phase;

- *Heterogeneous* (or contact) catalysis, when the catalyst and the reactants are in different phases, and the reaction occurs at the *interface* between the phases. Several phase combinations are possible,

but most frequently the catalyst is a solid. The catalyst surface is not uniform, and reactions occur on specific locations, the *active sites*.

-   *Enzymatic catalysis* (or biocatalysis), when the catalyst is an enzyme. Enzymes are macromolecules, and although they are in the same phase as the reactants, we can find active sites on their structure. Therefore, enzymatic catalysis has a mixed character.

In the following sections, we will consider heterogeneous catalysis with solid catalysts.

1.2. HETEROGENEOUS CATALYSIS

1.2.1. Chemisorption

In heterogeneous catalysis, the reaction occurs at the interface between the phases. The interaction between the reactants and the catalyst surface is a phenomenon of chemical adsorption, or *chemisorption*, involving the formation of chemical bonds. Chemisorption occurs on *coordinatively unsaturated surface ions* which are the *active sites*. Typical concentrations of active sites are $10^{19}/m^2$ for metals, and $10^{15}/m^2$ for oxides. Sites may include more than one species, forming *multiplets* or *ensembles*. A chemisorbed species and the site to which it is bound constitutes the *adsorption complex.*

Saturated molecules, such as hydrogen or alkanes, can only be adsorbed after dissociation in two or more fragments which bind onto the surface (*dissociative* adsorption). On the other hand, molecules with π electrons or unpaired electrons can be adsorbed without dissociation (*associative* adsorption). Some examples of adsorption complexes are shown in Table 2.

TABLE 2 – Examples of adsorption complexes [Adapted from Ref. 1].

$$
\begin{array}{ccccc}
\underset{1}{\underset{Al_3^+}{\overset{\overset{H_3}{N}}{\cdot\cdot}}} &
\underset{2}{\underset{Pt}{\overset{\overset{O}{\underset{\|\|\|}{C}}}{}}} &
\underset{3}{\overset{O}{Pt\diagdown\underset{}{C}\diagup Pt}} &
\underset{4}{\overset{H\ \ H}{\underset{Pt\ \ Pt}{|\ \ \ |}}} &
\underset{5}{\overset{CH_3}{\underset{\underset{Pt\ \ \ Pt}{CH_2\ \ H}}{|}}}
\end{array}
$$
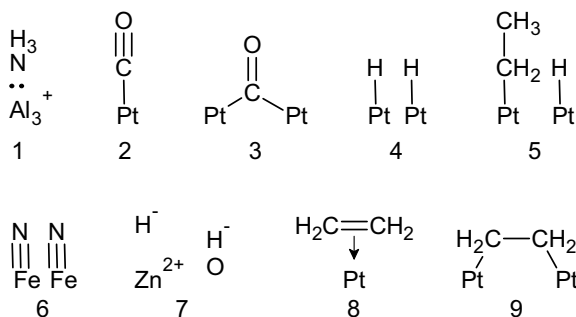
Case 1 represents the adsorption of NH$_3$ (a Lewis base) onto an Al^{3+} ion (a Lewis acid) coordinatively unsaturated on the surface of an aluminosilicate. Here, Al^{3+} is the active site for chemisorption of NH$_3$. Cases 2 and 3 are two modes of adsorption of CO on Pt. Cases 4 and 5 represent the dissociative adsorption of H$_2$ and C$_2$H$_6$, respectively, on Pt. A surface hydride is formed in 4, while a surface alkyl is formed in 5. Case 6 represents the dissociative adsorption of nitrogen on iron. In 7, H$_2$ was dissociatively adsorbed onto an active site formed by the ion pair Zn^{2+}O^{2-} on the surface of zinc oxide. Cases 8 and 9 represent different modes of ethylene adsorption onto Pt.

Chemisorption is the first step in the mechanism of the heterogeneous catalytic reaction, and it allows for the weakening of chemical bonds of the reactant molecules, thereby facilitating their conversion into products.

1.2.2. Industrial catalysts: Requirements and components

Heterogeneous catalysts must be prepared with an extensive and accessible surface, in order to present the required activity. The order of magnitude of the surface area required can be estimated knowing that, on average, each cm^3 of

catalyst must convert 10^{-6} mol/s of the reactant. Specific surface areas of several hundreds of m^2/g are common in heterogeneous catalysis.

Surface areas of this magnitude require the use of porous materials. In some cases, the catalyst is prepared as a porous material forming particles of adequate shape and size; this is mostly used with oxide catalysts. Alternatively, the catalyst may be dispersed in the form of small crystallites onto a porous support; this is especially used in the case of metals.

The most important parameters that determine the activity of a given catalyst formulation are its specific surface area and porosity. With porous catalysts, the reactants must diffuse into the pores, and this physical process occurs in parallel with the catalytic reaction. Diffusion limitations will be observed in many situations, especially in the case of large catalyst particles and small pore sizes. These aspects will be discussed in detail in Chapter A7.

Industrial catalysts can be classified in two groups:

- *Massive catalysts*, containing exclusively active species;

- *Supported catalysts*, when the active species are dispersed onto a refractory material, the *support* or *catalyst carrier*.

Active species include the catalytic agents themselves (most frequently, metals or oxides) and *promoters* (species which are not active by themselves, but which increase the activity and/or selectivity of the catalyst). In addition to the active species and support, catalyst particles may contain stabilisers and binders, in order to improve their mechanical resistance.

Examples of massive catalysts are the Pt-Rh gauze used in the oxidation of NH$_3$ for the production of nitric acid, the *skeletal catalysts* such as Raney-Ni, used in hydrogenations, and the amorphous silica-alumina formerly used as a cracking catalyst.

The most widely used support is alumina, especially in the form of γ-Al$_2$O$_3$, which is a high surface area phase. Silica (SiO$_2$) and activated carbons are also used in many applications. Examples of supported catalysts are Pt/Al$_2$O$_3$ for

the reforming of hydrocarbons, V_2O_5/SiO_2 used in the oxidation of SO_2 (production of sulfuric acid), and CoO-MoO_3/Al_2O_3 used as a hydrodesulfurization catalyst.

In general, the catalyst is prepared in the form of particles (spheres, granules, pellets and extrudates), their shape and size being determined by the type of reactor used and the physical state of the reactants.

Fixed-bed reactors are frequently used when the reactants are in the gas phase. The limiting factor here is the pressure drop through the bed. The catalyst particles are usually in the size range of 1.5 to 12 mm, because smaller particles would lead to very large pressure drops. When larger sizes are required (12-25 mm), as in the steam-reforming of hydrocarbons to produce synthesis gas, hollow particles are used, such as rings, in order to improve mass transfer rates. One important property of the catalyst is its crushing strength, since it must not fracture under the weight of the bed.

On the other hand, fluidized-bed and entrained-flow reactors require catalyst particles in the size range of 20-300 μm. In these reactors, as well as in moving-bed reactors, the spherical shape of the catalyst particles allows for higher attrition resistance.

Stirred tank reactors can be used with liquid reactants, and the catalyst must be in the form of small particles (75-200 μm) which can be suspended in the liquid.

Thus, the shape and mechanical resistance of the catalyst particles are the main factors which determine the correct fluid flow in the reactor.

For certain applications, structured catalysts are prepared, for instance, as *monoliths*. Such monoliths are currently used in the catalytic converters for automotive exhaust treatment, but their application to other processes is rapidly expanding. Monolith reactors have the advantage of presenting an open path for the fluid, with lower pressure drops in comparison to conventional fixed-bed reactors.

1.2.3. Activity and selectivity patterns

The general classification proposed by Bond[2] can be taken as a convenient starting point for a more detailed discussion of the activity and selectivity patterns of heterogeneous catalysts. Bond classified solid catalyst into three groups: metals, non-stoichiometric (semiconductor) oxides, and stoichiometric oxides.

As we can see in Table 3, each group exhibits catalytic activity for a certain set of reactions. This correlation between the chemical nature and the catalytic activity of a solid material can be interpreted in terms of its capacity to chemisorb the reactants, which is the first step in the mechanism of a heterogeneous catalytic reaction.

Thus, metals (in particular, transition metals) are good catalysts for reactions involving hydrogen and hydrocarbons, because they can easily adsorb these substances. However, only the noble metals can be used as oxidation catalysts; in the presence of oxygen, base metals would be oxidized.

Non-stoichiometric oxides can adsorb easily oxygen, which makes them good oxidation catalysts. However, only those oxides which are stable under hydrogen can be used as hydrogenation or dehydrogenation catalysts. In the presence of sulfur, the active phases are the corresponding sulfides, which are important hydrodesulfurization catalysts.

Stoichiometric oxides adsorb water easily, and therefore they can be used as dehydration catalysts. Some materials in this class present acid sites on their surfaces, which promote the formation of carbocations, and therefore they can be used as catalysts for alkylation, polymerization, cracking and isomerization.

TABLE 3 – Classification of solid catalysts [Adapted from Ref. 2]

Class	Functions	Examples
Metals	Hydrogenation Dehydrogenation Hydrogenolysis (Oxidation)	Fe, Ni, Pd, Pt, Ag, Cu
Non-stoichiometric oxides and sulphides	Oxidation Dehydrogenation Desulphurization (Hydrogenation)	NiO, ZnO, MnO_2, Cr_2O_3, Bi_2O_3-MoO_3, WS_2
Stoichiometric oxides	Dehydration	Al_2O_3, SiO_2, MgO
Acids	Polymerization Isomerization Cracking Alkylation	H_3PO_4, H_2SO_4, SiO_2-Al_2O_3 Zeolites

1.2.3.1. Metal catalysts

Metals are excellent catalysts for a wide variety of reactions. The active sites are exposed surface atoms, which can be characterized by the metal *dispersion*, defined as the ratio of the number of exposed metal atoms, to the total number of metal atoms. The smaller the crystallites, the higher will be the dispersion, and the exposed metal surface area.

The first key to interpret the activity of metals is their ability to chemisorb the reactants. Some metals (in particular, the transition metals) are able to adsorb dissociatively diatomic molecules such as H_2, O_2, N_2 and CO, and the atoms produced can then react easily on the surface with other adsorbed species. Polyatomic molecules can also be adsorbed with dissociation, by breaking bonds such as C-H, C-N, N-O, N-H, or P-H.

In most cases, reactions catalysed by metals occur between adsorbed species according to the Langmuir-Hinshelwood mechanism or, eventually, to the Rideal-Eley mechanism, as discussed in Chapter A3.

The *Principle of Sabatier* provides the second key to interpret the catalytic activity of metals. According to Sabatier, the catalyst forms an unstable intermediate compound with one of the reactants, which must have an optimal strength. It must be stable enough to be formed, but not too stable, otherwise it could not decompose to yield the product or products. The stability of the intermediate compound (which is the adsorption complex mentioned in section 1.2.1.) can be measured by the heat of adsorption, or any other parameter which is proportional to the heat of adsorption. This leads to the so-called *volcano curves*, an example of which is presented in Figure 3.

Thus, in order to select a catalyst for a given reaction we must find the metals which are able to chemisorb the reactants, from which we pick up those corresponding to an optimal strength of adsorption.

The following pattern of activity is observed in reactions involving hydrogen with or without hydrocarbons: Ru, Rh, Pd, Os, Ir, Pt>Fe, Co, Ni>Ta, W, Cr$\cong$Cu.

Noble metals are also excellent oxidation catalysts, and can be used for complete oxidations, such as:

$CO \rightarrow CO_2$, $RH \rightarrow CO_2 + H_2O$ (RH = hydrocarbons) and $NH_3 \rightarrow NOx + H_2O$.
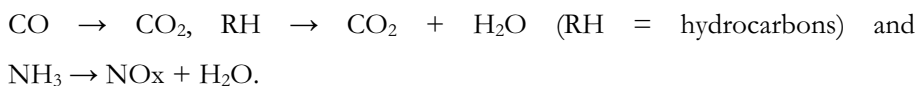
There are a few cases where the metal exhibits high selectivity; examples are the epoxidation of ethylene with Ag, and the conversion of ethylene into acetaldehyde with Pd. However, in general, the high activity of metals (which results from a high density of active sites, in the order of 10^{19} atoms per m^2) is accompanied by a poor selectivity, since various side reactions can be promoted by the catalyst. However, several methodologies are available to control the selectivity of a metal catalyst, which will be summarized below.
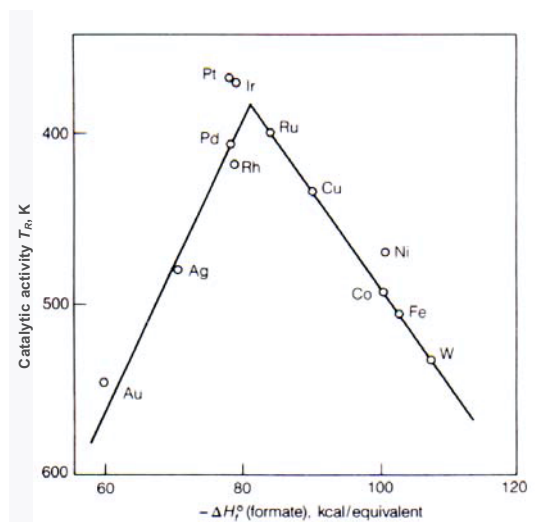
Figure 3 – Decomposition of formic acid catalysed by metals (Adapted from Ref. [3]).

In practice, metal crystallites are not perfect, and the crystallographic planes can exhibit defects and imperfections, such as steps and kinks. Atoms with lower coordination number, such as those in corners, edges, kinks and steps, are active sites of higher energy than those in the faces or terraces. Thus, we can change the properties of a catalyst by changing the crystallite size whenever the reaction occurs preferentially in one type of site.

M. Boudart[4] introduced a classification of the metal catalysed reactions in terms of structure sensitivity:

- *Structure-insensitive* (or *facile*) reactions, when the turnover frequency (TOF) is independent of the size, shape and other properties of the crystallites;

- *Structure-sensitive* (or *demanding*) reactions, when the TOF depends on the structural detail of the surface.

As a rule, reactions involving the breaking or formation of H-H, C-H or O-H bonds are insensitive to the structure, while those involving the breaking or formation of C-C or N-N bonds are structure-sensitive. Hydrogenation and dehydrogenation of hydrocarbons are of the first type, while the hydrogenolysis

of ethane and the synthesis of ammonia are structure sensitive. It has been shown that the active sites for structure insensitive reactions are simpler, in the limit they can be isolated atoms on the surface, while structure sensitive reactions require an *ensemble* of several adjacent metal atoms.

We can also modify the selectivity of the catalyst by using promoters (or modifiers), which can be classified into two groups: *structural* promoters, and *electronic* (or *bonding*) promoters. Examples of the first kind of effect are the sulphur passivation of metal catalysts, and the use of alloy or bimetallic catalysts. The objective is the same in both cases, namely to block the sites where unwanted reactions occur. Thus, structure sensitive reactions such as hydrogenolysis (which need a large ensemble of adjacent metal atoms) are prevented, while facile reactions, such as dehydrogenation, can still occur on isolated metal atoms. Figure 4 shows the classical work of Sinfelt[5] with Ni-Cu alloys. S-passivated metal catalysts are used, for instance, in the dehydrogenation of C_{10}-C_{14} paraffins, while bimetallic catalysts find application in the catalytic reforming of hydrocarbons to produce fuels with high octane number.

Another example of structural promotion is the incorporation of Al_2O_3 into the ammonia synthesis catalyst. During the reaction, Al_2O_3 promotes the restructuring of the iron crystals leading to the formation of [111] faces, which are 500 times more active than the [110] faces.

Electronic promoters can be electron-donor species (like potassium) or electron-acceptor species (like chlorine). For instance, in the ammonia synthesis catalyst, K (present as K_2O) supplies electrons to Fe, facilitating the dissociative adsorption of nitrogen. On the other hand, small amounts of chlorine are added during ethylene epoxidation with silver catalysts, in order to inhibit the complete oxidation into CO_2.

Other electronic effects include the role of oxide supports to stabilize different oxidation states of transition metal catalysts, and the *strong metal support*

interaction (SMSI) effect, most notorious with TiO_2 supported catalysts, where there is a partial charge transfer from the support to the metal.
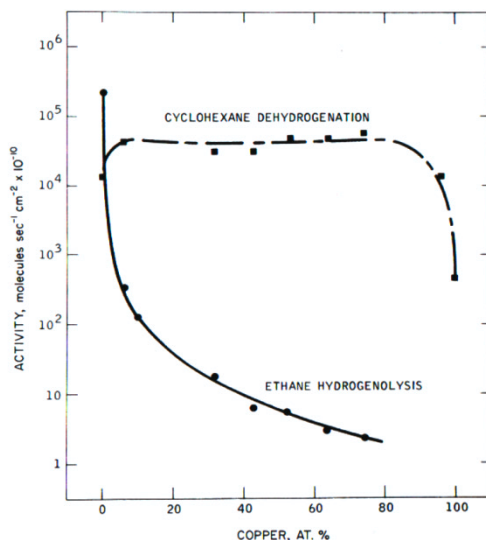
Figure 4 – Activities of Cu-Ni alloys for dehydrogenation and hydrogenolysis (Reproduced from Ref. [5]).

1.2.3.2. Non-stoichiometric oxide catalysts

Oxides and sulphides of transition metals may become *defect* or *extrinsic* semiconductors: when heated in air, they may gain or lose oxygen, becoming non-stoichiometric in terms of excess (p-type semiconductors) or deficiency (n-type semiconductors) of oxygen in the lattice, respectively. Examples of p-type semiconductors are NiO, CoO and MoS_2, while ZnO, Fe_2O_3 and V_2O_5 are n-type semiconductors. Figure 5 shows a schematic representation of the lattices of NiO (where   represents a cationic vacancy) and ZnO (with an interstitial Zn atom). The electrical conductivity is proportional to the concentration of *positive holes* in the first case, and to the excess of Zn in the second case.

Ni^{2+}	O^{2-}	Ni^{2+}	O^{2-}	Ni^{2+}	O^{2-}	Zn^{2+}	O^{2-}	Zn^{2+}	O^{2-}	Zn^{2+}	O^{2-}
O^{2-}	Ni^{2+}	O^{2-}	$\square$	O^{2-}	Ni^{2+}	O^{2-}	Zn^{2+}	O^{2-}	Zn^{2+}	O^{2-}	Zn^{2+}
Ni^{2+}	O^{2-}	$Ni^{2+\ominus}$	O^{2-}	$Ni^{2+\ominus}$	O^{2-}	Zn^{2+}	O^{2-}	Zn^{2+}	O^{2-}	Zn^{2+}	O^{2-}
O^{2-}	Ni^{2+}	O^{2-}	Ni^{2+}	O^{2-}	Ni^{2+}	O^{2-}	Zn^{2+}	O^{2-}	Zn^{2+}	O^{2-}	Zn^{2+}

(e Zn^+ appears above the third row in the ZnO lattice)
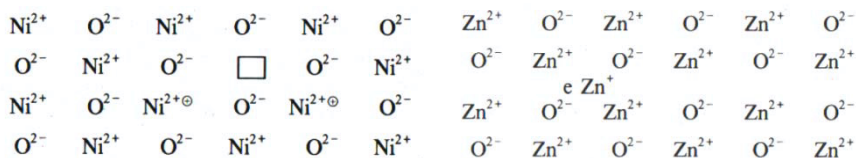
Figure 5 – Schematic representation of the lattices of NiO (p-type) and ZnO (n-type) semiconductors.

The catalytic behaviour of these two types of semiconductor oxides is different. With p-type oxides, the cation can access to a higher oxidation state. Therefore, the metal ions can supply electrons to oxygen, leading to the formation of adsorbed O^- species. On the other hand, on n-type oxides, oxygen adsorption can only occur on previously reduced surfaces. Conversely, the adsorption of reducing species is negligible on p-type oxides, and extensive on n-type oxides. As an example, let us consider the oxidation of CO. M_{is}^{n+} and O_{is}^{2-} are surface ions.

p-type:

$$M_{is}^{n+} + \tfrac{1}{2} O_2 \rightarrow M_{is}^{(n+1)+} O^-_{ads}$$

$$M_{is}^{(n+1)+} O^-_{ads} + CO \rightarrow M_{is}^{n+} + CO_2$$

n-type:

$$M_{is}^{n+} O_{is}^{2-} + CO \rightarrow M_{is}^{(n-2)+} + CO_2$$

$$M_{is}^{(n-2)+} + \tfrac{1}{2} O_2 \rightarrow M_{is}^{n+} O_{is}^{2-}$$
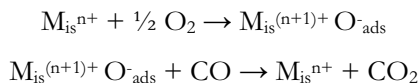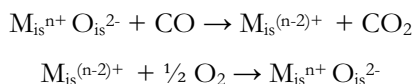
Thus, oxidation on p-type oxides involves adsorbed oxygen, while on n-type oxides it is the lattice oxygen which is involved. As a result, p-type oxides are more active.

The following pattern of activity is generally observed in oxidations, where the noble metals are included for comparison:

Pt, Pd $>$Ag$>$MnO, Co_3O_4, CuO$>$NiO$>$Fe$_2$O$_3$$>Cr_2O_3$$>V_2O_5$$>$ZnO

The excess of oxygen of p-type oxides cannot be maintained in reducing atmospheres (for instance, in dehydrogenations); therefore, only n-type oxides can be used. Cr, Mo and W oxides are the most active in hydrogenation, dehydrogenation and aromatization.

Neither p-type nor n-type oxides are useful catalysts for the partial oxidation of hydrocarbons. The first are too active, thus their selectivity is poor, leading to the products of complete oxidation; the latter are not active enough. Most of the selective industrial catalysts are mixed oxides, containing oxides of metals of groups 13-15 of the Periodic Table (In, Tl, Sn, Sb, Bi) together with n-type transition metal oxides (V, Mo, W). Examples of industrially important selective oxidations are the ammoxidation and the partial oxidation of propene, and the oxidative dehydrogenation of butenes:

$$C_3H_6 + NH_3 + 3/2\ O_2 \rightarrow CH_2{=}CHCN + 3\ H_2O$$
$$C_3H_6 + O_2 \rightarrow CH_2{=}CHCHO + H_2O$$
$$C_4H_8 + 1/2\ O_2 \rightarrow C_4H_6 + H_2O$$

These reactions are described by a special type of redox mechanism known as the Mars and van Krevelen[6] mechanism:

$$CAT\text{-}ox + R \rightarrow CAT\text{-}red + P$$
$$CAT\text{-}red + O_2 \rightarrow CAT\text{-}ox + H_2O$$

where CAT-ox and CAT-red represent the oxidised and reduced forms of the catalyst, respectively, R is the hydrocarbon reactant and P the desired selective oxidation product. Oxygen from the lattice is used to generate the desired product, while oxygen from the gas phase is used to regenerate the catalyst active sites.

1.2.3.3. Stoichiometric oxide catalysts

Stoichiometric oxides do not adsorb significant amounts of oxygen, hydrogen or carbon monoxide, since the cations cannot be oxidized or reduced. However, they may be used as catalysts for hydration/dehydration and similar reactions, because they can adsorb easily water and other polar substances.

Some of these oxides are solid acids, and in presence of hydrocarbons they can promote the formation of carbocations; therefore, they are good catalysts for reactions such as cracking, isomerization, polymerization and alkylation.

Among the solid acids, the aluminosilicates deserve special mention. Neither silica nor alumina are strong acids. However, aluminosilicates with 10-25% of Al_2O_3 are excellent cracking catalysts. The synthesis of these SiO_2-Al_2O_3 catalysts starts with the formation of a silica hydrogel, made up of a network of SiO_4 tetrahedra with silanol groups on the surface (Si-OH), followed by reaction with an aluminium salt, so that the hexacoordinated Al ions are incorporated into the surface as AlO_4 tetrahedra, as shown in Figure 6.

Figure 6 - Synthesis of SiO_2-Al_2O_3 catalysts (Reproduced from Ref. [7]).

Since each Al^{3+} is bound to four oxygens, each AlO_4 tetrahedron has a residual -1 charge, which requires the presence of a +1 charge to maintain electroneutrality. This compensation charge can be provided by H^+ ions, originating OH groups on the surface with high acid character. When the material is dehydrated by heating above 400 ºC, the Brønsted acid sites are

transformed into Lewis acid sites (the exposed Al^{3+} ion can accept an electron pair), as shown in Figure 7. Acid sites promote the formation of carbocations which are the intermediates in a chain reaction mechanism.

Figure 7 - Brønsted and Lewis acid sites on SiO_2-Al_2O_3 catalysts.

Amorphous SiO_2-Al_2O_3 were used as cracking catalysts prior to the introduction of zeolites. Zeolites are crystaline aluminosilicates with a porous structure consisting of channels or cavities of regular dimensions. These materials, which revolutionized the field of heterogeneous catalysis, will be discussed in detail in Chapters A5 and A8.

1.2.3.4. Bifunctional catalysts

Reactions such as dehydroisomerization and dehydrocyclization occur by a bifunctional mechanism, which requires the simultaneous presence of two types of active sites. The dehydrogenation/hydrogenation function is provided by the metallic phase, while an isomerisation function is provided by the acid sites. There is a cooperative effect of the two functions, as exemplified in Figure 8 for reactions of C_6 hydrocarbons. Bifunctional catalysts are used, for instance, in the reforming of hydrocarbons.

Figure 8 - Dehydroisomerization of methylcyclopentane on a bifunctional catalyst (Reproduced from Ref. [8]).

1.3. CATALYST DEACTIVATION

1.3.1. Deactivation mechanisms

In spite of what is implicit in its definition (*the catalyst increases the rate of a chemical reaction without itself being consumed in the process*), there are various phenomena which eliminate active sites available for reaction, contributing to a more or less rapid loss of catalyst activity. Deactivation mechanisms can be classified as follows:

<u>Poisoning</u> - strong chemisorption of an impurity onto the active sites, which will thereafter be unavailable for chemisorption of the reactants. It should be noted that just a small amount of poison (some μmol/g) can completely deactivate a catalyst. In terms of simple kinetic schemes, we can describe the process by an independent set of reactions:

$$A + X \rightarrow B + X$$

$$P + X \rightarrow PX$$

where A, B and P are the reactant, product and poison, respectively, X represents an active site and PX the strongly adsorbed poison.

<u>Fouling</u> - includes coking and carbon formation, which will cover the surface, physically blocking the access of the reactants to the active sites, as well as plugging of pores by particulates, coke or metals deposition. In comparison with poisoning there is quite a difference in scale, as the amount of coke that

deactivates a catalyst can be quite large (for instance, >10 % by weight). In addition, coking results from a series and/or parallel scheme with respect to the reactants/products:

$$A \rightarrow B \rightarrow Coke$$

Solid-state transformations: This category includes sintering (textural alterations), as well as solid state reactions between the catalyst components or between the catalyst components and the reactants/products, leading to changes in the nature of the solid phases. Sintering is the loss of surface area by textural changes; it is of physical nature, and depends mostly on the temperature. This mechanism is responsible for the agglomeration of metal crystallites in supported metal catalysts, and for the collapse of the porous structure in the case of oxide catalysts and supports.

In addition to these mechanisms, one can also consider the mechanical failure of the catalyst, for instance by particle attrition in moving and fluidized beds, by crushing or fracture of catalyst pellets in fixed beds, and the loss of washcoat in monolith catalysts. All these phenomena lead to reactor malfunctioning, and normally dictate the replacement of the catalyst.

In the following sections, we will briefly describe catalyst deactivation by poisoning, coking and solid state transformations.

1.3.2. Poisoning

This type of deactivation is reasonably well defined in chemical terms, since it involves a surface reaction between the poison and the active sites. Thus, the

nature of the active sites determines the type of compounds which can be toxic, as shown in Table 4.

Metals are poisoned by substances containing elements of groups 15 and 16 with unshared electron pairs or unoccupied orbitals, such as NH_3, H_2S and AsH_3, as well as metal ions with five or more d- electrons. In addition, molecules containing multiple bonds, such as CO, dienes, acetylene and aromatics may act as inhibitors.

Sulfur poisoning is the main cause of deactivation in a number of catalytic processes, such as hydrogenation, methanation, steam-reforming and Fischer-Tropsch synthesis. Indeed, sulfur is capable of irreversible adsorption at high coverages on most metal catalysts. For instance, it has been reported[9] that 15-100 ppb of H_2S can cause 3 to 4 orders of magnitude loss in activity of Ni, Co, Fe and Ru methanation catalysts. Such contamination levels are well below the sulfur concentrations found in many process feedstocks, even after desulfurization procedures.

TABLE 4 – Catalyst poisons

Catalyst	Active sites	Poisons
Metals	Exposed metal atoms	Molecules containing elements of groups 15 or 16 with unshared electron pairs; molecules with multiple bonds
Acids	Lewis or Brønsted acid centers	Basic molecules in the feed; basic impurities in the solid
Non-stoichiometric oxides	Coordinatively unsaturated surface ions	Any substance capable of changing the most favourable oxidation state of surface ions

Stoichiometric oxides, which are normally used as acid catalysts, are poisoned by bases. For instance, cracking catalysts can be poisoned by some nitrogen containing molecules found in petroleum feedstocks, such as pyridines, amines and quinolines.

Non-stoichiometric oxides possess active sites capable of accepting or donating electrons, favoring redox reactions. Therefore, any substance capable of changing the most favorable oxidation state of the surface ions will be a poison.

1.3.3. Solid state transformations

1.3.3.1. Sintering

Sintering refers to all temperature dependent phenomena which lead to growth of particles of the catalyst and to loss of surface area. Such textural changes can only occur when the atoms or ions of the solid are sufficiently mobile. For atoms or ions in the bulk, mobility can be observed at temperatures higher than $T_T = 0.5\ T_f$ (Tammann temperature), whereas those on the surface can show mobility at temperatures higher than $T_H = 0.3\ T_f$ (Hüttig temperature), where T_f (K) is the melting point of the substance. Therefore, it is generally accepted that sintering starts to become important somewhere between T_H and T_T. Thus, the melting point provides a very good measure of the thermal stability of a support or active phase.

Another factor which can affect the rate of sintering is the nature of the atmosphere in contact with the catalyst, in particular the presence of polar substances (such as H_2O, H_2S, HCl, NH_3). In the case of metal supported catalysts, two additional factors must be taken into consideration, namely the strength of the metal-support interaction and the presence of promoters or impurities, which can increase or decrease the mobility of the metal atoms on the surface.

The following general power law expression can be used to describe the sintering data, where D/Do is the normalized metal dispersion, and D_∞ is the limiting dispersion observed at sufficiently long times:

$$-d(D/D_o)/dt = k\ (D/D_o - D_\infty/D_o)^m$$

1.3.3.2. Solid state reactions

According to Delmon and Grange[10] , solid state reactions can be classified into the following groups:

- Without change in the global composition of the catalyst, including phase transitions, segregation of phases and reaction between solid phases;

- With change in the global composition of the catalyst, such as loss of components, reaction with the gas or liquid phase and formation of compounds with deposited impurities;

- Coupled processes, such as the simultaneous occurrence of two or more solid state reactions or the simultaneous occurrence of solid state reactions and textural changes.

In addition, the modifications that catalysts continuously undergo while they are acting under actual reaction conditions must also be considered.

1.3.4. Coke and carbon formation

The carbonaceous deposits commonly referred to as "coke" may be complex mixtures, containing a variety of materials of different structures and origins, ranging from hydrogen-deficient polyaromatic compounds to graphitic carbon. These "coke" components may contain pyrolytic carbons, tars, and catalytic carbons. Pyrolytic carbons and tars are formed at high temperatures by non-catalytic routes. Catalytic carbons are produced at much lower temperatures by heterogeneous surface reactions, the nature of the surface determining the type of carbon formed. Thus, metal oxide/sulfide catalysts produce coke mainly as a result of acid catalyzed polymerization reactions, and both high relative molecular mass polymers and carbon are found in the deposits. On the other hand, metallic catalysts promote the dissociative adsorption and dehydrogenation of hydrocarbons, producing highly crystalline carbon deposits at relatively low temperatures without the formation of any polycyclic aromatic

intermediates. Well ordered graphite, non-oriented carbons and carbon filaments (whiskers) have been identified in such deposits.

On acid catalysts, coke is produced by dehydrogenation of polycyclic aromatic compounds, which originate from alkene or aromatic intermediates. The following sequence of reactions may be envisaged:

a) Hydrocarbon cracking;

b) Oligomerization of the olefinic cracking products;

c) Cyclization of the oligomers;

d) Formation of monoaromatics by hydrogen transfer;

e) Alkylation of the monoaromatics, followed by cyclization and hydrogen transfer, producing polyaromatics.

All these reactions can be catalyzed by acid sites.

On zeolite catalysts, steric constraints limit the formation of coke molecules in the zeolite pores, since bimolecular reactions between bulky molecules are involved. Thus, the pore structure of the zeolite has a large influence on coke formation rates, and therefore, on deactivation. This subject will be discussed in more detail in Chapter A8.

Carbon formation from hydrocarbons on metal catalysts can be explained in terms of the following mechanism:

a) The hydrocarbon is adsorbed on the metal surface, leading to the production of chemisorbed carbon atoms by surface reactions such as hydrogenolysis and dehydrogenation;

b) These carbon atoms can dissolve in and diffuse through the metal, precipitating out at the grain boundaries or at the metal-support interfaces. As a result, metal crystallites will be lifted up from the surface of the catalyst and will be transported on top of the growing carbon filaments. This step is only possible with metals which can dissolve carbon, such as iron, cobalt and nickel.

c) Alternatively, the carbon species may react on the surface to originate an encapsulating film, leading to the deactivation of the catalyst. This can be prevented if the metal has the ability to hydrogenate the intermediates along the reaction path on the surface.

This mechanism is schematically described in Figure 9 for the case of nickel.

Figure 9 – Mechanism of carbon formation on nickel, and scheme showing the formation of carbon filaments (whiskers) by diffusion of carbon through the metal (Adapted from Ref. [11]).

Competition between carbon accumulation on the surface and carbon diffusion away from it determines whether the catalyst becomes deactivated or not. This depends on the nature of the reacting gas, temperature, hydrogen partial pressure and catalyst activity. At low temperatures, nucleation and growth of surface carbon is not very important, and the formation of carbon filaments prevails. In this case, the metal surface remains available for the main reaction, and there is no immediate deactivation by fouling. However, the growth of carbon filaments inside the pores of supported catalysts can lead to pellet fracture, leading to increased pressure drop in the reactor.

1.3.5. Deactivation of industrial catalysts

Table 5 presents examples of deactivation of industrial catalysts, where the different time scales of deactivation can be appreciated. But the general

conclusion is that all catalysts will loose their activity, sooner or later. The decision must then be taken, either to replace the catalyst or to regenerate it. Regeneration is possible, for instance, in the case of coked catalysts, as coke deposits are easily gasified by steam or air. Some poisons can also be removed by heating or by oxidation, but these treatments frequently lead to sintering and further deactivation. Sintering is generally an irreversible phenomenon; however, redispersion of the metal phase in Pt reforming catalysts can be achieved by an oxychlorination treatment. The disposal of spent catalysts is becoming a problem of great concern, as more strict environmental regulations are being enforced.

TABLE 5 – Examples of deactivation of industrial catalysts [Adapted from 12]

Process	Catalyst	Typical life (years)	Deactivation mechanism
Ammonia synthesis	Promoted Fe	5 - 10	Sintering
Methanation	Ni/Al_2O_3	5 - 10	Poisoning
Steam-reforming	Ni/Al_2O_3	2 - 4	Sintering, coking
Benzene oxidation	V+Mo oxides	1 - 2	Inactive phase
Ammonia oxidation	Pt-Rh gauze	0.1-0.5	Loss of Pt
Catalytic reforming	Pt/Al_2O_3 chlorinated	0.01-0.5	Coking
Catalytic cracking	zeolites	10^{-6}	Coking

Further reading

J.L. Figueiredo, F. Ramôa Ribeiro, *Catálise Heterogénea*, Fundação Calouste Gulbenkian, Lisboa, 2nd Edition, **2007**.

M. Guisnet, H.S. Cerqueira, J.L. Figueiredo, F. Ramôa Ribeiro, *Desactivação e Regeneração de Catalisadores*, Fundação Calouste Gulbenkian, Lisboa, **2008**.

References

1. R. Burwell, *Survey of Progress in Chemistry*, Academic Press, New York, **1977**, Vol. 8, pp.1.

2. G. C. Bond, *Heterogeneous Catalysis. Principles and Applications*. Oxford University Press, **1987**.

3. J.Fahrenfort, L. L. van Reyen, W. M. H. Sachtler in *The Mechanism of Heterogeneous Catalysis*, J.H. de Boer (editor), p. 23, Elsevier, Amsterdam, **1960**.

4. M. Boudart, *Adv. Catal.*, **1969**, *20*, 153.

5. J. H. Sinfelt, J. L. Carter, D. J. C. Yates, *J. Catal.*, **1972,** *24*, 283.

6. P. Mars, D.W. van Krevelen, *Chem.Eng.Sci.*, **1954,** *3*, 41.

7. B. Gates, J.R. Katzer, G.C.A. Schuit, *Chemistry of Catalytic Processes*, McGraw Hill, New York, **1979**.

8. J. M. Parera and N.S. Figoli, in *Catalytic Naphtha Reforming*, G.J. Antos, A.M. Aiteni, J.M. Parera (editors), Marcel Dekker, New York, **1995**.

9. P. K. Agrawal, W. D. Fitzharris, J. R. Katzer, *in Catalyst Deactivation*, B. Delmon and G. F. Froment (eds.), pp. 179, Elsevier, Amsterdam, **1980**.

10. B. Delmon and P. Grange*, in Progress in Catalyst Deactivation*, J. L. Figueiredo (editor), pp. 231, Martinus Nijhoff Publishers, The Hague, **1982**.

11. J. L. Figueiredo, *Erdöl und Kohle, Erdgas, Petrochemie*, **1989**, *42*, 294

12. P. J. Denny and M.V. Twigg, in *Catalyst Deactivation*, B. Delmon and G.F. Froment (eds.), pp.577, Elsevier, Amsterdam, **1980**.

2. BULK CATALYSTS

Isabel Maria de Figueiredo Ligeiro da Fonseca

REQUIMTE/CQFB, Departamento de Química, Universidade Nova de Lisboa, Faculdade de Ciências e Tecnologia, Quinta da Torre, 2825-516 Caparica, Portugal

2.1. INTRODUCTION

Catalytic materials exist in several forms and their preparation involves different protocols with a multitude of possible preparation schemes. The preparation of any catalyst involves a sequence of several complex processes many of them not completely understood. So changes in the preparative details may result in dramatic alteration in the properties of the final catalyst.

The goal is to produce and reproduce a catalyst that is stable, active and selective. The best procedure is sought which results in sufficiently high surface area, good porosity, and suitable mechanical strength. The catalytic properties are strongly affected by every step of the preparation together with the quality of the raw materials. The choice of a laboratory method to prepare a given catalyst depends on the physical and chemical characteristics desired in the final composition. For many years the preparation and development of heterogeneous catalysts were considered more alchemy than science with the predominance of trial and error experiments[1-6].

In 1970, the scientific bases for the preparation of the catalysts began to develop with significant integration and overlapping between the different sciences.

The wide number of variables can be reduced to a series of elementary steps or unit operations, which present quite strongly marked analogies from one catalyst to another and may therefore be described in a general way. Many excellent reviews have already been published[1-3].

Table 1 reports the main unit operations usually applied in catalyst preparation[2,4,6].

TABLE 1 - Unit operations in catalyst preparation[2,4,6]

Precipitation	Calcination
Gelation	Forming operation
Hydrothermal transformation	Impregnation
Decantation, filtration, centrifugation	Crushing and grinding
Washing	Mixing
Drying	Activation

The design of a catalyst covers all aspects from the choice of the active phases to the method of forming particles.

A heterogeneous catalyst is a composite material characterised by (1) relative amounts of different components (active species, physical and /or chemical promoters and supports) (2) shape (3) size (4) pore volume and pore size distribution (5) surface area[2,3].

Most catalyst formulations involve a combination of some or even all of these operations. However, even though the preparation procedures differ considerably from one catalyst to another three broad categories can be introduced to classify the catalysts with respect to the preparation procedure:

1. Bulk catalysts and supports
2. Impregnated catalysts
3. Mixed agglomerated catalysts

Bulk catalysts are mainly comprised of active substances such as silica-alumina for hydrocarbon cracking, Zn-Cr oxide catalyst for the conversion of $CO-H_2$ mixtures to methanol, iron molybdate for methanol oxidation. The supports are prepared by similar procedures (e.g. aluminas, silicas, silica-aluminas)[2,3].

2.2. BULK CATALYSTS PREPARATION

2.2.1. Precipitation

The first objective is to obtain a solid, which is generally achieved by precipitation. The aim of this step is to precipitate a solid from a liquid solution, either as a precipitate or as a gel.

Precipitation is the best known and most used procedure for the synthesis of both monometallic and multimetallic oxides. Precipitation results in a new solid phase (precipitate) that is formed discontinuously (i.e. with phase separation) from a homogeneous liquid solution[1-3].

Precipitation occurs in three steps:

- Supersaturation

- Nucleation

- Growth

Solubility curves are functions of temperature and pH. In the supersaturation region the system is unstable and precipitation occurs with any small perturbation, Figure 1.

Figure 1 - Supersaturation dependence on concentration, T and pH[2,3].

The supersaturation region can be approached either by increasing the concentration through solvent evaporation (A to C), lowering the temperature (A to B) or increasing the pH (which moves the solubility curve to D, and A into the supersaturation region). Supersaturation is reached by means of physical transformations (change in temperature or solvent evaporation) or chemical processes (addition of bases or acids, use of complex forming agents)[2,3].

In almost all cases, the formation of a new solid phase in a liquid medium results from two elementary processes which occur simultaneously or sequentially: (1) nucleation, i.e. formation of the smallest elementary particles of the new phase which are stable under the precipitation conditions and (2) growth or agglomeration of the particles.

In order to precipitate a solid from a homogeneous solution, a nucleus has to be formed first. The formation of a particle is governed by the free energy of agglomerates of the constituents of the solution. The total free energy change (ΔG) due to agglomeration, is determined by:

$$\Delta G = \Delta G_{bulk} + \Delta G_{interface} + \Delta G_{others}$$
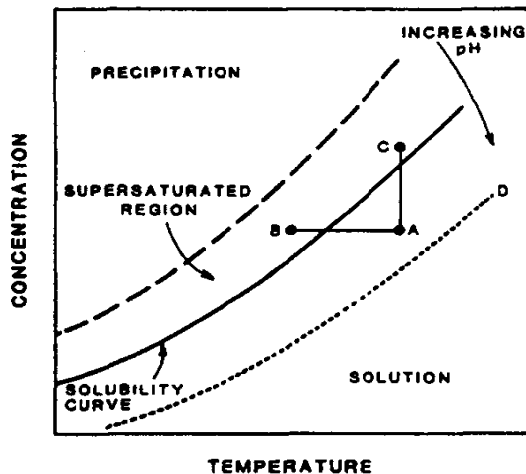
where ΔG_{bulk} is the difference of the free energy between solid species and solution species, $\Delta G_{interface}$ is the free energy change related to the formation of the interface, and ΔG_{others} summarizes all the other contributions as for instance trace impurities which can be neglected[5].

Agglomeration will be spontaneous if ΔG is negative. At supersaturation conditions ΔG_{bulk} is always negative, but energy is needed to create an interface; $\Delta G_{interface}$ is thus positive. For very small particles the total free energy change is positive[5].

If spherical particles are formed, ΔG_{bulk} increases with $4\pi r^3/3$, while the interfacial energy only increases with $4\pi r^2$. There is thus a critical size r of the agglomerate, from which on ΔG_{bulk} predominates in the total free energy change, the total free energy decreasing with the particle size. This critical size is the size of the nucleus[5].

The general process of formation of a solid from a solution can be described as indicated in Figure 2.
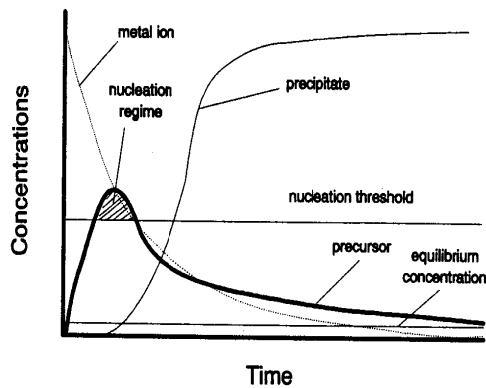
Figure 2 - Scheme for the formation of a solid product from solution[5].

The most important curve is the nucleation curve which describes the development of the precursor concentration with time. Such a precursor could be, for instance, the hydrolysis product of the metal ions in solution. Only if the precursor concentration exceeds a critical threshold concentration, will a nucleus form and the precipitation begins. The nucleus is defined "as the smallest solid phase aggregate of atoms, molecules or ions" which is formed during precipitation and which is capable of spontaneous growth. As long as the concentration of precursor stays above the nucleation threshold, new particles are formed. As soon as the concentration falls below the critical concentration, due to the consumption of precursors by nucleation or by the growth process, only particle growth of existing particles prevails. Particles with

a narrow particle size distribution will be obtained from a short nucleation burst, and a wide particle size distribution will result from nucleation over a longer period of time. The size of the particles finally resulting from a precipitation process will be dependent on the area of the shaded section between the nucleation curve and the nucleation threshold. The larger the area, more particles nucleate and smaller the particles will be. The nucleation process is strongly temperature dependent[5].

Nucleation may proceed spontaneously (homogeneous nucleation) or be initiated with seed materials (heterogeneous nucleation). These are solid impurities such as the dust or the rough edges of the vessel surface). The rate of nucleation can be accelerated by deliberate addition of seed nuclei[2].

Under conditions of high supersaturation, the rate of nucleation is much higher than the rate of crystal growth and leads to the formation of numerous but small particles. Under these conditions, amorphous precipitates can be obtained[1,3].

The growth process depends on the concentration, temperature, pH and ripening.

The sizes of the precipitate crystals diminish as their equilibrium solubility diminishes (i.e. as supersaturation increases), since Ostwald ripening is slowed down by the reduced transfer rate between the suspended particles[2].

Most precipitates are crystalline precipitates. Depending on the precipitation conditions, it is possible to obtain amorphous solids. If the supersaturation is very high, the aggregation rate can exceed the orientation rate and an amorphous solid is obtained. However, by ripening in the presence of the mother liquid, the amorphous solid can become crystalline[2].

Obtaining high supersaturation conditions is a difficult task in practice, as a result of the spontaneous evolution of the system towards a decrease of supersaturation by nucleation of the solid particles and consumption of reagents. High levels of supersaturation can only be obtained for short time and

within limited volumes of solution. The size and structure of the particles reduces to that of achieving a uniformly high level of supersaturation throughout the liquid before the nucleation starts, which may be quite difficult because of mass and heat transport limitations[1].

Usually precipitates with specific properties are desired. The properties include the nature of the phase formed, chemical composition, purity, particle size, surface area, pore size, etc as well as the requirements of downstream processes (drying, pelletizing or calcination).

Basically, all process parameters influence the quality of the final precipitates and fine tunning of the parameters is necessary in order to produce the required material. Figure 3 summarizes the parameters which can be adjusted in the precipitation processes and the properties which are mainly influenced by these parameters[3,5].

In general it is desirable to precipitate the desired material in such a form that the counterions of the precursor salts and the precipitating agent, which can be occluded in the precipitate during the precipitation, can easily be removed by a calcination step.

Favourable ions are nitrates, carbonates or ammonium which will decompose to volatile products during the calcinations. For catalytic applications usually hydroxides, oxohydrates, oxides are precipitated. In some cases, carbonates are subsequently converted to oxides or other species after calcination[5].

For economic reasons water is almost exclusively used as the solvent for the precipitation processes. Solubilities for most metal salts are much lower in organic solvents. However, there are some reports in the literature showing that organic solvents can be advantageous for the precipitation of certain materials.

Nucleation rates are extremely sensitive to temperature changes. Therefore precipitation temperature is a decisive factor to control the precipitate properties such as primary crystallite sizes, surface areas, and even the phases

formed. The optimum precipitation temperature is usually a parameter which has to be determined experimentally.
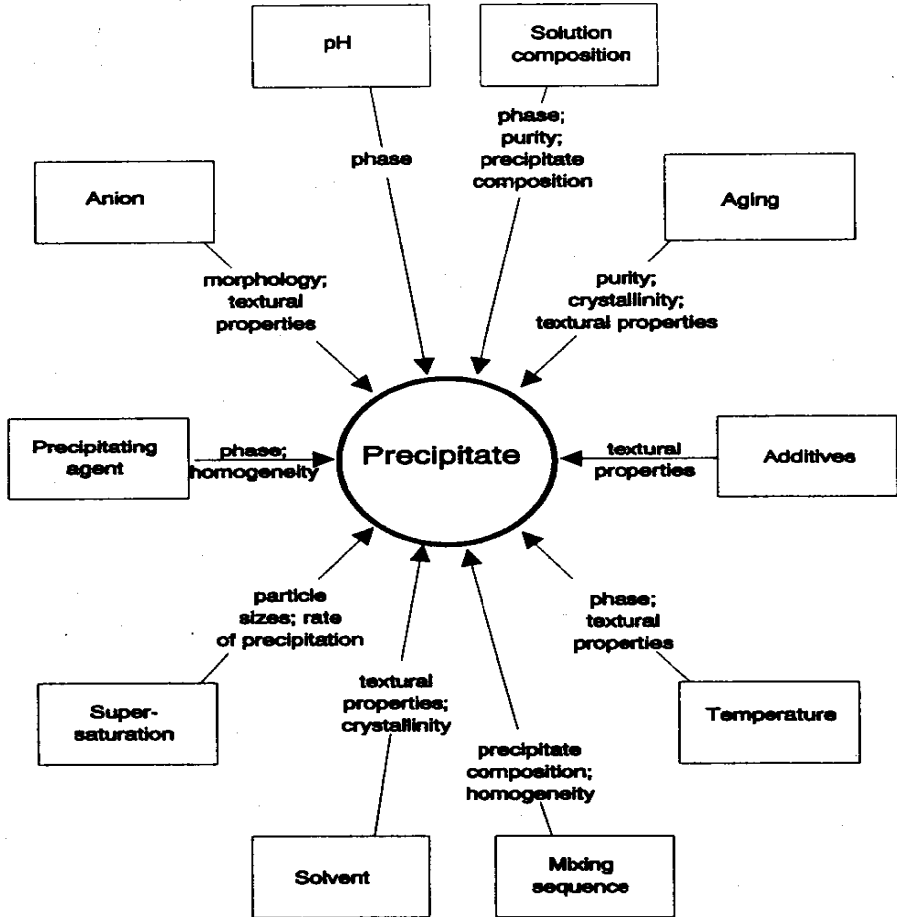
Figure 3 - Factors affecting the main properties of the precipitate[3,5].

Since the pH directly controls the degree of supersaturation, at least if hydroxides are precipitated, this should be one of the crucial factors in the precipitation processes. As for many other parameters, the influence of pH is not a simple one, and has to be investigated experimentally for a specific system. For instance, in the aluminium oxide system, the precipitation pH is

one of the variables which controls the nature of the phases (pH>8 bayerite, pH<8 boehmite)[5].

The properties of precipitates can be strongly influenced by additives. The most widely used additives are organic molecules which are added to the precipitate in order to control the pore structure. Such organic molecules can be removed during the calcination.

There are several ways to carry out the precipitation process, Figure 4.
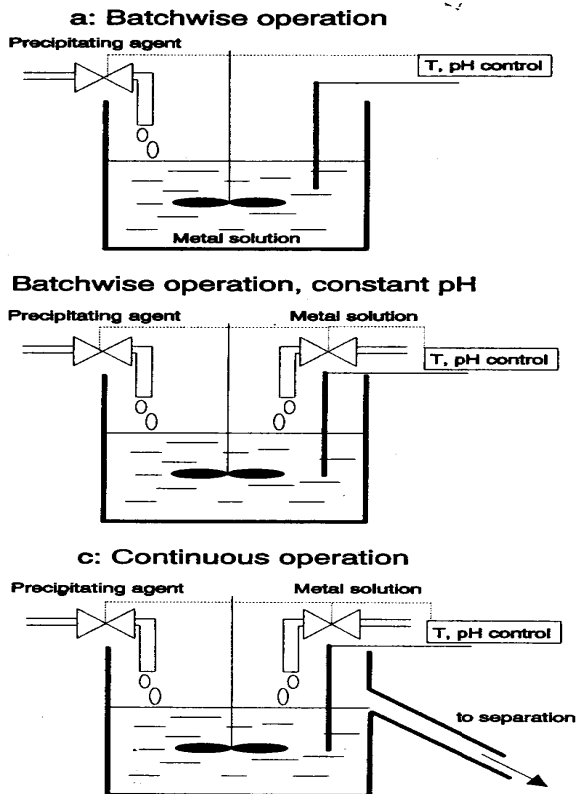
Figure 4 - Precipitation processes: a) batchwise process (pH and other parameters change continuously except T); b) pH is kept constant (residence time and composition change continuously); c) all parameters are kept constant[5].

The simplest one is the batch operation, where the solution from which the salt is to be precipitated is usually present in the precipitation vessel and the

41

precipitating agent is added. The advantage is that the operation is simple, but the change in the composition during the precipitation process is a severe disadvantage. The phase problems are avoided if a continuous process is employed for the precipitation. In a continuous process, all the parameters, such as temperature, concentration, pH and residence time of precipitate, can be kept constant. The continuous process usually allows precipitation at low supersaturation conditions since seeds are already present in the vessel[5].

During coprecipitation care must be taken in order to avoid independent or consecutive precipitations. Besides, the pH should be adjusted and kept constant during the operation: this can be done by mixing the starting solution continuously instead of adding one solution to another. Precipitation can be performed starting from either true solutions or colloidal solutions (sol). Figure 5 shows the characteristics of such solutions[2].

Figure 5 - Properties of colloidal particles[2].

Particles which show little or no attraction for water form hydrophobic colloids. These are easily flocculated and the resulting colloidal precipitates are easily filtered. Particles which show a strong affinity to water form hydrophilic colloids. These are very difficult to flocculate and the resulting jelly like mass is difficult to filter. Hydrophilic colloidal solutions can be prepared from many inorganic compounds such as silicic acid and the hydrous oxides of aluminium and tin. We will consider such gels in the gelation route[2].

2.2.2. Sol-gel (gelation) method

In contrast with the precipitation route, which is a discontinuous transformation, the gelation route, also known as the sol-gel method, is a homogeneous process which results in a continuous transformation of a solution into a hydrated solid precursor (**hydrogel**)[1].

The sol-gel process involves first the formation of a sol followed by that of a gel. A sol, which is a liquid suspension of solid particles ranging in size from 1nm to 1micron, can be obtained by the hydrolysis and partial condensation of a precursor such as an inorganic salt or metal alkoxide. The further condensation of sol particles into a three-dimensional network produces a gel which is a biphasic material with a solid encapsulating a solvent. Alternatively, a gel can be produced by destabilizing a solution of preformed sols. Sol-gel methods have several promising advantages over precipitation. In general, sol-gel syntheses have been recognised for their versatility which allows better control of the texture, composition, homogeneity and structural properties of the final solid[1,5].

The nanoscale chemistry involved in sol-gel methods is a more straightforward way to prepare highly divided materials.

Four main steps may be identified in the sol –gel preparation, Figure 6:

- formation of a gel
- aging of the gel
- removal of the solvent
- heat treatment
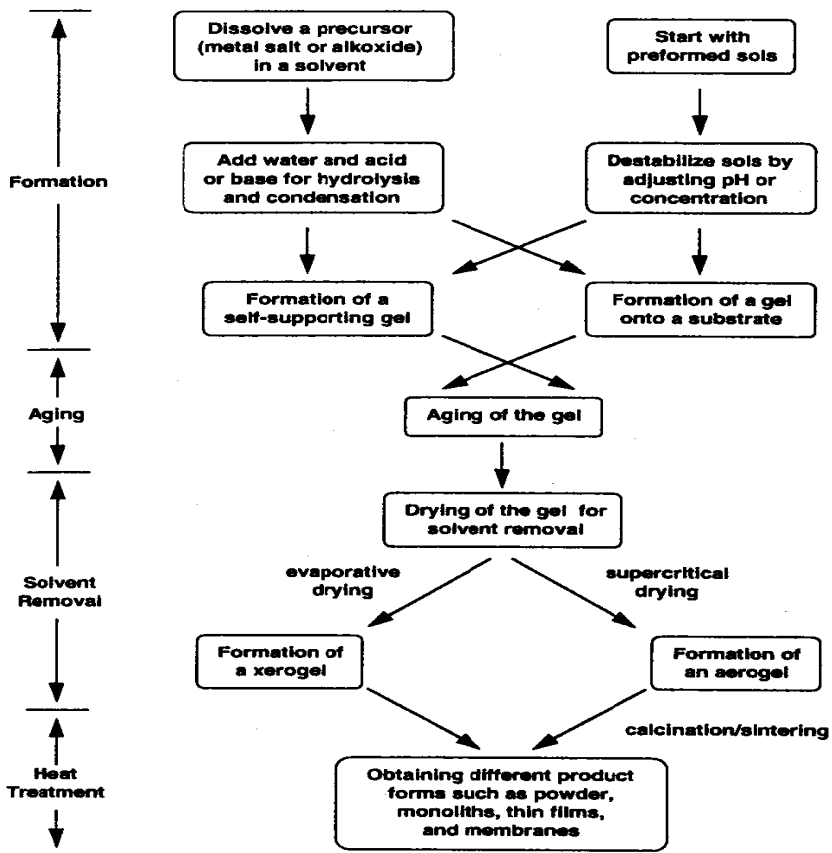
Figure 6 - Diagram showing the various steps of a sol-gel process[5].

The versatility of this preparation method lies in the number of parameters that can be manipulated in each step[3].

The precursor in a sol-gel preparation can be either a metal salt or alkoxide dissolved in an appropriate solvent, or a stable colloidal suspension of preformed sols. Metal alkoxides have been the most extensively used because they are commercially available in high purity and their solution chemistry has been well documented[5].

Hydrophilic colloidal solutions are formed of micelles that remain separated because of electrical charges on their surface in the surrounding solution. These charges create repelling forces which prohibit coagulation of the micelles. Such micelles are produced via chemical reactions of polymerization and polycondensation. The reticulation of these micelles gives rise to a hydrogel, a three-dimensional network. This framework is imbided by the solvent.

The point where hydrogel formation occurs, called *gelation*, depends on the micelle concentration, temperature, ionic strength of the solution and especially the pH. The mechanism of hydrogel formation is reported in Figure 7[2-4].

Path *H* leads from the sol to a hydrogel through the chemical reticulation of micelles surrounded by their double layers of electrostatic charges.
Path *F* leads from the sol to a flocculate of micelles through neutralization of their charges.
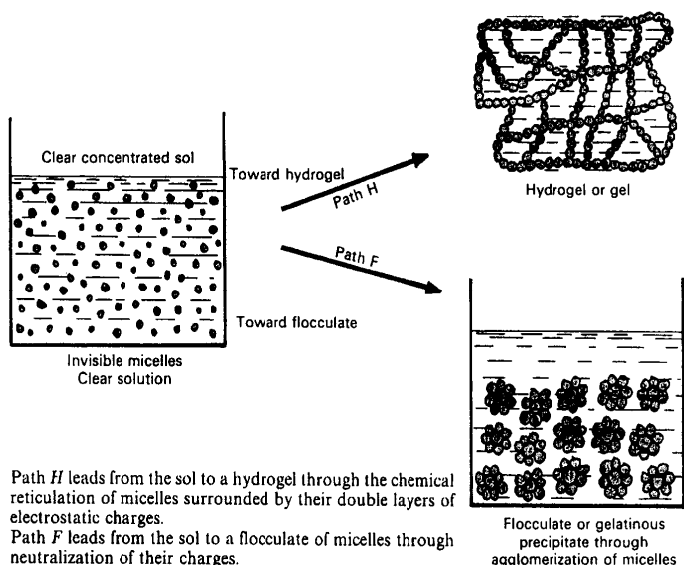
Figure 7 - Formation of gels and flocculates[2-4].

The chemistry of the processes can be represented by a sequence of acid or base catalysed nucleophilic additions or substitutions Hydrolysis (1) and Condensation (2)

(1) -M-OR + H_2O $\longrightarrow$ -M-OH + R-OH   **Hydrolysis**

(2) -M-OH +XO-M- $\longrightarrow$ -M-O-M- +X-OH   **Condensation**
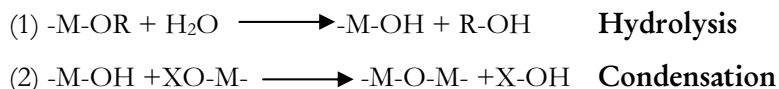
where X can be either H or R (an alkyl group).

Any parameter that affects either or both these reactions is thus likely to impact on the properties of the product. Key factors are the relative rate of hydrolysis and condensation, due their impact on the product properties.

The overall process produces a highly reticulated, metastable polymer with an open structure in which the primary units are held together either by chemical bonds, hydrogen bonds, dipole forces or van der Waals interactions. This framework is imbibed by the solvent, Figure 7, path H.

Figure 8 shows the rates of hydrolysis and condensation of tetraethylorthosilicate (TEOS), which is the most widely studied precursor, as function of pH[5].

Under acidic conditions hydrolysis occurs at faster rate than condensation and the resulting gel is weakly branched. Under basic conditions the reverse is true and the resulting gel is highly branched and contains colloidal aggregates. Subsequently dried and heat treated samples have different surface functionalities and pore structures. The gel characteristics also depend on the size of the alkoxide group attached to a particular metal atom, the amount of water used in the sol-gel preparation and the rate by which it is added, the temperature and the solvent. Among the classes of solvents, alcohols are largely used but other solvents (benzene) may also be used for some alkoxides. The catalysts introduced in the polycondensation stages are volatile acids (acetic acid) or bases (ammonia). The relative rates of competing reactions can be altered by changing the temperature.
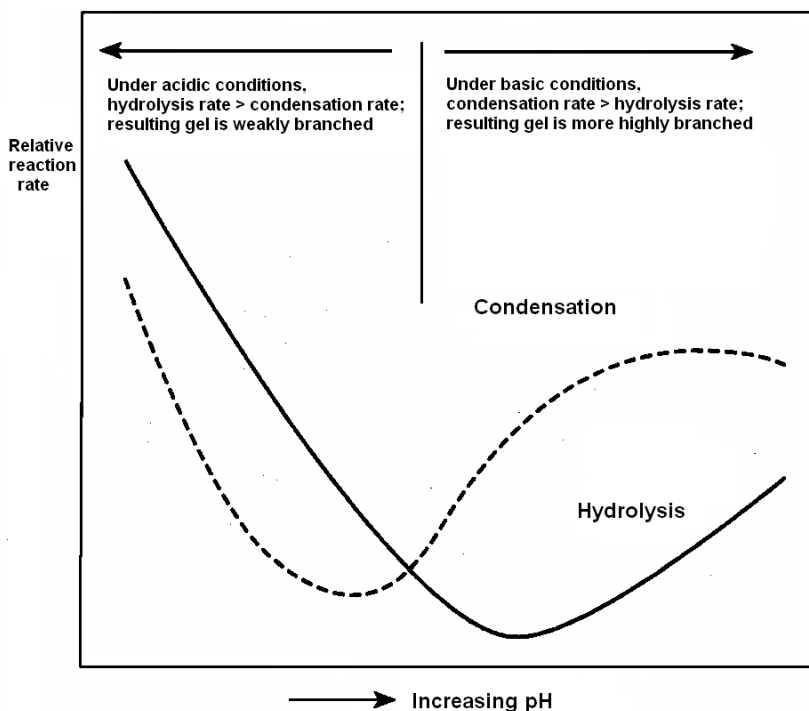
Figure 8 - Schematic diagram showing the variation of hydrolysis and condensation rates of TEOS with pH and the effect of relative rate on gel structure[5].

Using preformed sols instead of metal alkoxides as precursors is an attractive alternative to sol-gel preparation because recent advances in inorganic colloidal dispersions allow some control over the characteristics of the starting sols. The effects of the sol-gel parameters on the gel properties may be followed by an experimental observable known as *gel time.*

Gel time is defined as the time it takes for a solution to undergo a rapid rise in viscosity that corresponds to the transition from a viscous to an elastic fluid. At the *gel point* there is a continuous phase containing a structure that reflects the formation and branching of the particles under specific growth conditions. The *gelation times* range from a few minutes to 100h and the density of the

hydrogel increases with the increase of the original salts concentration in the solution and with the gelation rate[3,5].

Aging represents the time between the formation of a gel and the removal of a solvent. As long as the pore liquid remains in the matrix, a gel is not static and can undergo many transformations[5]. For alkoxide derived gels, condensation between surface functional groups continues to occur after the gel point. This process leads to a more cross linked network. However, extensive condensation causes the gel to shrink to the point that solvent is actually expelled in a phenomenon called *syneresis*.

Parameters that affect these aging processes include temperature, time, and pH of the liquid inside the pore. Common approaches in manipulating these parameters are immersing the gel in or washing it with another liquid, exposing the gel to a different humidity, heating the gel and using hydrothermal conditions[5].

The homogeneity of the hydrogel depends on the solubility of the reagents in the used solvent, the sequence of reactants addition, the temperature and the pH.

Flocculation of a sol can be obtained through the neutralization of the micelle charges and the flocculate precipitates more or less well. Hydrophilic sols give jelly–like flocculates that contain large amounts of water, Figure 7, path F. The flocculates are denser than hydrogels and the elementary solid particles have the dimensions of the original micelles. The surface area of the final solid depends on the original micelle size and also on the ripening and drying conditions[3].

The sol-gel method has been widely employed for the synthesis of micro and mesoporous materials, mixed oxides, composite powders, hydroxyapatite, layer double oxides, etc.[1-3,5].

2.3. HYDROTHERMAL TREATMENTS

Hydrothermal treatments refer to treatments of precipitates, flocculates or gels carried out at rather low temperature ($<300°C$) under ageing or ripening in the presence of the mother liquor[2,3].

They involve textural or structural modifications of the solid such as follows:

        small crystals ⟶ large crystals

        small amorphous particles ⟶ large amorphous particles

        amorphous solids ⟶ crystalline solid

        highly porous gel ⟶ low porosity gel (aging or syneresis of the gel)

        kinetically favoured phases ⟶ thermodynamically favoured phases

The variables in these types of operation for a given solid are the pH, temperature, pressure, time and concentration. The main difference between aging and hydrothermal treatments regards the reactions conditions (mainly T, P and time), aging being performed at room temperature and pressure for longer times. All textural or structural hydrothermal transformations obey to thermodynamic laws and thus proceed in a direction corresponding to a decrease in the free energy of the system. The hydrothermal synthesis of zeolites and mesoporous materials is a particular application of the hydrothermal treatment. Most hydrothermal treatments are performed in the presence of a liquid phase (mainly mother liquor). However they can also be performed in an atmosphere of steam, such as the steam stabilization procedure of zeolitesY [2,3].

2.4. SOLID PHASE RECOVERY

Decantation, filtration and centrifugation are the unit operations used to separate the solid from the mother liquor. The solid must be washed with water to eliminate impurities and the mother liquor.

The separation is easy for crystalline precipitates but difficult with flocculates and is useless with hydrogels. The separation method depends on the particle size of the solid, since small particles require centrifugation or filtration. Problems may arise when washing flocculates, since removal of counterions reverts flocculates to sol (*peptization*); thus care must be taken not to wash too much or allow settling times to become too long[2,3].

2.5. DRYING

Drying is the elimination of the solvent (usually water) from the pores of the solid. This is a routine procedure for crystalline solids but becomes critical for *flocculates* and even more for *hydrogels* that contain up to 90% of water[2,3].

In the case of hydrogels, as the pore liquid is evaporated from a gel network, the capillary pressure associated with the liquid-vapour interface within the pore can become very large for small pores, and removal of water can result in a collapse of the structure; therefore, drying has to be properly controlled when high porosity is desired[3,5].

Initially drying (in air) occurs through evaporation of the moisture from the outside surface of the hydrogel. The rate of water loss is constant and mass transfer is controlled by temperature, relative humidity and flow rate of air over the surface and size of the gel particles. This process continues until the moisture content is reduced to 50%, then the gel begins to shrink. The material so obtained is called *xerogel*. The subsequent moisture loss occurs with a declining rate in which evaporation is controlled by capillary forces. The saturation point decreases as pores become smaller and evaporation slows until water is forced into larger pores by concentration gradients. If evaporation occurs but removal of moisture is blocked by smaller pores, an internal pressure of steam develops and the structure collapses with loss of pore volume and surface area[2,3].

High temperature gradients should be avoided to reduce such effects. Vacuum drying at lower temperatures (-50 to -5ºC) or operating at temperatures higher than the critical temperature of water, avoids large capillary stresses. Most supercritical drying experiments have been done with alcohols or liquid CO_2 operating at temperatures higher than their critical temperatures. The solid structure maintains the textural properties of the wet gel and highly porous dry solids are obtained (*aerogels* or *carbogels*)[2,3].

One other approach is *freeze drying* in which the pore liquid is frozen into a solid that subsequently sublimes to give a product called a *cryogel*.

2.6. CALCINATION

After the removal of pore liquid further heat treatment is necessary to convert the solids into a catalytically useful form**.**

Calcination is carried out in air at temperatures higher than those used in the catalytic reactions or catalyst regeneration. Often heating is done in the presence of reactive gases (air, oxygen, hydrogen) in order to burn off any residual organics or to oxidize/reduce the solid.

When different atmospheres are employed (N_2, vacuum, etc) the term "heating" is used instead of "calcination". This operation can be carried out before or after the *forming operation*[2,3].

During calcination several processes occur such as loss of the chemically bonded water or CO_2, modification of the texture through sintering (formation of larger particles from small crystals or particles without the formation of a liquid phase, resulting in the loss of surface area and pore volume), modification of the structure, active phase generation and stabilization of the mechanical properties. Alumina calcination is an example of all these features[2].

Various types of sintering can result when calcining xerogels, with two extremes (1) sintering at constant pore radius, typical of xerogels with covalent bonds

(silica and silica alumina) in which the textural modification results in the reduction of the pore volume and (2) sintering at constant pore volume with an increase in the pore size, typical of xerogels with ionic bonds such as ferric hydroxide. Intermediate cases are observed between the two extremes, for instance calcining a xerogel with covalent bonds in the presence of steam, results in sintering at constant pore volume. The addition of a textural promoter inhibits sintering (addition of sodium to silica lowers the sintering temperature)[2,3].

The heating temperature and atmosphere must be properly chosen to obtain stable phases in the reaction and regeneration conditions avoiding sintering phenomena. Thus the physical characteristics of the product depend on parameters such as temperature, heating rate, time and gaseous environment[2,3].

It is common practice to subject the catalyst to a more severe heat treatment than it is likely to occur in the reactor to ensure at least the stability of its textural and structural properties during reaction.

Activation is a thermal treatment such as reduction, sulfidation, performed in special atmospheres in the reactor at the start up of the unit.

2.7. FORMING OPERATIONS AND SCALING-UP

The shaping of catalysts and supports is a key step in the catalyst preparation procedure. The shape and size of the catalyst particles should promote catalytic activity, strengthen the particle resistance to crushing and abrasion, minimise the bed pressure drop, lessen fabrication costs and distribute dust build-up uniformly[3]. The choice of the shape and size is mainly driven by the type of reactor, Table 2.

Moreover, for a given reactor the best shape and size of the catalyst particles depend on the hydrodynamics and heat and mass transfer limitations[3].

There are several techniques for shaping catalysts in microgranules (crushing and grinding), microspherical solids (spray drying), extrudates (extrusion), spheres (drop coagulation), pellets (dry tableting).

Ceramic monoliths can be manufactured by extrusion or by corrugation, the former being the technique mainly used and employing various materials, although cordierite and mullite are most often used especially as catalyst supports.

TABLE 2 - Different types of catalyst shapes[3]

Shape	Size	Type of reactor
Extrudate	$d = 1–50$ mm	Fixed bed reactor
	$l = 3–30$ mm	
Pellet	$d = 3–15$ mm	Fixed bed reactor
	$h = 3–15$ mm	
Granule, Bead	$d = 1–20$ mm	Fixed bed reactor
	$d = 1–5$ mm	
Sphere	$d = 1–10$ mm	Fixed bed reactor
		Moving bed reactor
Microspheroidal	$d = 20–100$ μm	Fluid bed reactor
		Slurry reactor

Metallic monoliths are produced exclusively by corrugation, followed by rolling up or folding into monoliths of the shape and size required[3].

When a catalyst is prepared with the goal of possible industrial application some attention should be devoted to its scaling-up in order to avoid useless reagents and/or preparation procedures. The first aspect is the role of the reagent purity, since analytical reagents are used in the laboratory while on a production scale technical grade reagents are employed. Also different preparation unit operations may offer unpleasant surprises. For example, some difficulties may arise in scaling–up precipitation, due to pH and temperature gradients, aging time, stirring geometry, etc. In the case of mixed co-precipitates, gradient concentrations may lead to lack of homogeneity due to

mixing. Other critical points may be the thermal treatments, especially calcinations, for which lack of homogeneity in the catalyst temperature and local gaseous atmosphere are very likely industrially, even in gas circulated ovens[3].

References

1.   J. Schwarz, C. Contescu, A. Contescu, *Chem.Review*, **1995**, *95*, 477-510.

2.   C. Perego, P. Villa, *Catalysis Today*, **1997**, *34*, 281-305.

3.   M. Campanati, G. Fornasari, A. Vaccari, *Catalysis Today*, **2003**, *77*, 299-314.

4.   J.F. Lepage, J. Cosyns, P. Courty, E. Freund; J.P. Franck, Y. Jacquin, B. Juguin, C. Marcilly, G. Martino, J. Miquel, R. Montarnal, A. Sugier, H. Van Landeghem; *Applied Heterogeneous Catalysis, Design, Manufacture, Use of Solid Catalysts*, Editions Technip, Paris, **1987**.

5.   G. Ertl, H. Knozinger, J.Weitkamp, *Handbook of Heterogeneous Catalysis*, Wiley-VCH, **1997**.

6.   J.L. Figueiredo, F. Ramôa Ribeiro, *Catálise Heterogénea*, editado pela Fundação Calouste Gulbenkian, **1987.**

3. MECHANISMS AND KINETICS IN HETEROGENEOUS CATALYSIS

José J. Melo Órfão

Laboratório de Catálise e Materiais, Departamento de Engenharia Química, Faculdade de Engenharia, Universidade do Porto, Rua Dr. Roberto Frias, 4200-465 Porto, Portugal

The main purpose of this chapter is to relate the steps of chemical nature in the mechanisms of heterogeneous catalytic reactions with the respective kinetic laws. For that objective, an essentially theoretical approach will be used, starting with simple concepts and gradually increasing the complexity. At the end, some generalizations will be made, which allow to answer the more practical problem of formulating mechanisms compatible with experimentally determined kinetic laws.

3.1. THE GENERAL MECHANISM OF HETEROGENEOUS CATALYTIC REACTIONS

In heterogeneous catalysis, the catalytic action involves the adsorption of reactant molecules on active sites on the surface of the solid catalysts; therefore, the transport of those molecules from the fluid phase to the surface, where the catalytic reaction effectively occurs, must be considered in the general mechanism. Similarly, the molecules of the reaction products are eventually desorbed and transferred in the opposite direction from inside the solid pores to the fluid phase.

Assuming a porous catalyst, the following sequence of processes must be generally considered:

1. Transport of reactants from the fluid phase to the catalyst particle surface;
2. Transport of reactants in the catalyst pores;

3. Adsorption of reactants on active sites;

4. Surface chemical reaction involving adsorbed species (molecules, atoms);

5. Desorption of products;

6. Transport of products in the catalyst pores to the particle surface;

7. Transport of products from the catalyst particle surface to the fluid phase.

These mechanistic steps are shown schematically in Figure 1 for the case of an isomerisation reaction A → P, taken as an example.
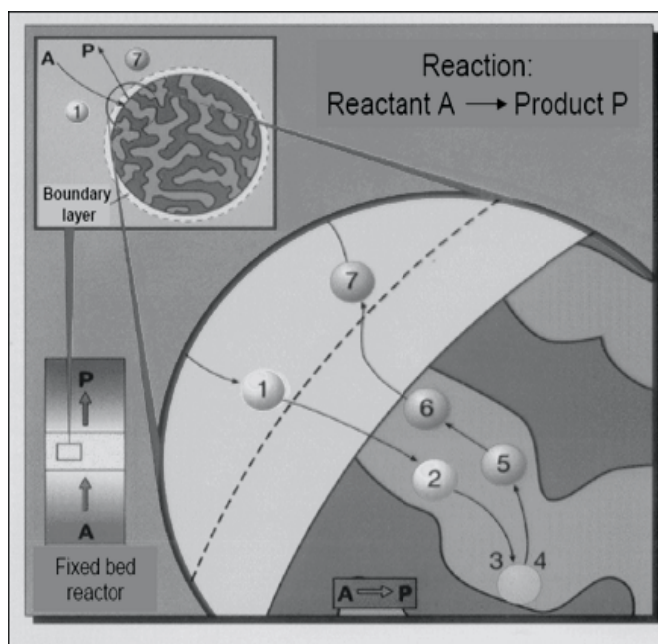
Figure 1 – General mechanism of the heterogeneous catalytic reaction A → P.

The presented sequence gives a general perspective about the mechanism of catalytic action in heterogeneous catalysis. However, this general picture may be simplified in some situations. For instance, in the presence of non porous catalysts, it is obviously not necessary to considerer the intraparticle transport

steps of both reactants and products. Additionally, in bimolecular reactions, both reactants may adsorb on the catalyst surface or, alternatively, only one of them adsorbs. The products of reaction may adsorb on the active sites, competing with the reactants, or not.

Steps 1, 2, 6 and 7 of the general mechanism described above are of physical nature. Their integration in modelling and in the design of catalytic reactors is described elsewhere in this book. Here, we will consider only the steps of chemical nature (adsorption/desorption – 3 and 5, surface reaction – 4), which constitute the basis of the catalytic reaction.

3.2. ADSORPTION/ DESORPTION EQUILIBRIUM

The adsorption of reactants (or at least one of them) on the active sites of the catalyst is the first step of chemical nature involved in the catalytic reaction. This weakens the chemical bonds in the molecules and promotes their transformation into products. Thus, in order to establish the kinetic laws of catalytic reactions, it is first necessary to consider the quantitative study of the adsorption processes, namely the description of the adsorption/desorption equilibrium. The associated experimental data for a given system adsorptive/adsorbent correspond to the equilibrium adsorption isotherm, which relates, at equilibrium, the concentration in the solid phase to the concentration in the fluid phase (or partial pressure in the case of gases) at constant temperature. A typical example is presented in Figure 2, where the dashed line represents the saturation of the active sites on the surface.
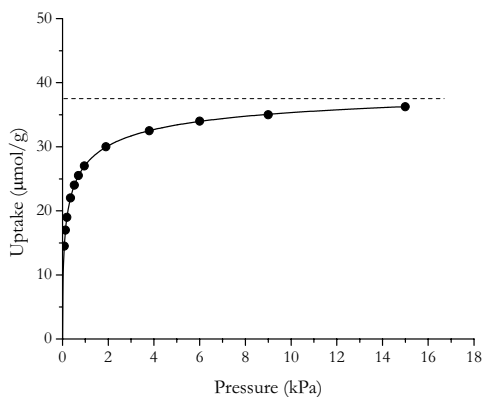
Figure 2 – Equilibrium adsorption isotherm of H_2 on a Pt/Al_2O_3 catalyst at room temperature.

3.2.1. Langmuir model

In 1916, Irving Langmuir developed a model for the adsorption/desorption equilibrium[1], which is based on some simplifying assumptions:

1) The adsorbed species (molecules, atoms, fragments of molecules) have no mobility over the surface;

2) Each active site may accommodate only one adsorbed entity, i.e. only a monomolecular layer (*monolayer*) is formed;

3) The adsorption process is energetically identical in all active sites, independently of the presence or absence of other species adsorbed on neighbouring sites, which means that the heat of adsorption does not depend on the amount adsorbed.

These assumptions are not satisfied for many real systems. However, the Langmuir model still provides a useful insight into the relationship between the extent of surface coverage and concentration (or partial pressure) at equilibrium conditions. Moreover, as we will see, the model is generally used as a basis for the formulation of rate equations in heterogeneous catalysis. Therefore, in the

scope of this chapter, only this equilibrium model will be considered, without further complications.

The Langmuir equation is derived on the basis of largely known simple kinetic concepts and the dynamical nature of equilibrium. Considering that each molecule A (for instance, in the gas phase) adsorbs on an active site *, the adsorption/desorption equilibrium may be represented by the elementary equation:

A + * = A*
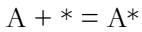
At equilibrium, the rates of adsorption and desorption are equal. Since these are elementary steps, we may write:

$$k_a \, P_A \, (1 - \theta_A) = k_d \, \theta_A$$

where $k_a = A_a \exp(-\dfrac{E_a}{R \, T})$ and $k_d = A_d \exp(-\dfrac{E_d}{R \, T})$ are, respectively, the rate constants of adsorption and desorption, E_a and E_d the corresponding activation energies, P_A the partial pressure and θ_A the fractional coverage or fraction of occupied sites, taken as a measure of the concentration of A adsorbed on the surface ($\theta_A = \dfrac{n^a}{n^a_m}$, where n^a is the adsorbed concentration at a given partial pressure and n^a_m is the maximum adsorbed concentration, which would correspond to the monolayer capacity). Of course, the above equation applies to gases; for adsorption of solutes in the liquid phase, the partial pressure is usually replaced by the molar concentration.

Considering that $K_A = \dfrac{k_a}{k_d} = \dfrac{A_a}{A_d} \exp(-\dfrac{E_a - E_d}{R \, T}) = B \exp(-\dfrac{\Delta H^{\circ}_{ads}}{R \, T})$ is the adsorption equilibrium constant and taking into account that ΔH°_{ads} is independent of the fractional coverage (one of the model assumptions), then we can obtain the Langmuir isotherm equation for a 1/1 stoichiometry:

$$\theta_A = \frac{n^a}{n_m^a} = \frac{K_A \, P_A}{1 + K_A \, P_A}$$

According to the van't Hoff equation $\left(\dfrac{d \ln K_A}{d\,T} = \dfrac{\Delta H_{ads}^{\circ}}{R\,T^2} \right)$, and knowing that

adsorption is an exothermal phenomenon, it is possible to conclude that the adsorption equilibrium constant decreases when the temperature increases. Several simulated Langmuir isotherms are shown in Figure 3.
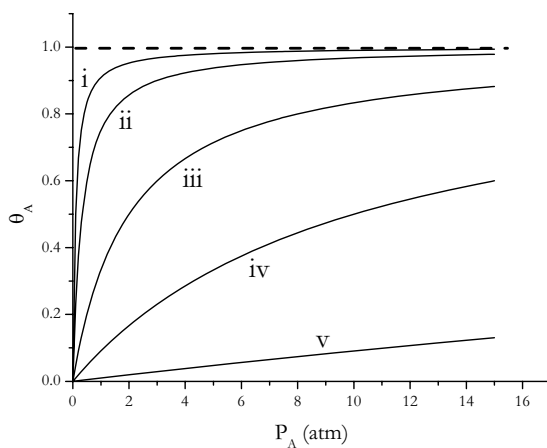
Figure 3 – Simulated Langmuir isotherms for different values of the equilibrium constant: (i) 10, (ii) 3, (iii) 0.5, (iv) 0.1, (v) 0.01 atm^{-1}.

The asymptotic forms of the model expression (also illustrated in Figure 3) correspond to:

a) For high temperatures and/or low pressures, $K_A \, P_A \ll 1$, and therefore $\theta_A \cong K_A \, P_A$, i.e. the isotherm approaches linearity;

b) For low temperatures and/or high pressures, $K_A \, P_A \gg 1$, and $\theta_A \cong 1$, i.e. the adsorbed amount approaches saturation (monolayer formation).

3.2.2. Extensions of the Langmuir model

In some cases, adsorption is dissociative, i.e. the molecules of the adsorptive dissociate during the process. A well studied example is the adsorption of hydrogen on metals (Ni, Co, Fe, Pt, Pd, etc). This corresponds to a 1 molecule/2 active sites stoichiometry, and the Langmuir equation presents a different form. Equilibrium may be represented by the equation:

$A_2 + 2 * = 2 A*$

Establishing the condition of dynamic equilibrium, similarly as before, it comes:

$$k_a \ P_{A_2} \ (1-\theta_A)^2 = k_d \ \theta_A^2$$

Rearranging and considering the definition of the adsorption equilibrium constant already presented, it is possible to arrive at the Langmuir equation applicable in this case:

$$\theta_A = \frac{\sqrt{K_{A_2} \ P_{A_2}}}{1+\sqrt{K_{A_2} \ P_{A_2}}}$$

This result can be generalized for a stoichiometry of 1 molecule of A/m active sites:

$$\theta_A = \frac{(K_A \ P_A)^{1/m}}{1+(K_A \ P_A)^{1/m}}$$

In the situations analyzed so far, it was considered that only one species adsorbs on the solid active sites (non-competitive adsorption). However, especially in the scope of catalytic reactions, various reactants and/or products may compete for the same type of active sites (competitive adsorption). For illustrative purposes, let us consider the simultaneous adsorption of two gases, A and B, both with a 1/1 stoichiometry:

$A + * = A*$

$B + * = B*$
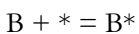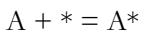
Noting that the concentration of vacant sites is now proportional to $(1 - \theta_A - \theta_B)$, we may write the following two equations:

$$k_{a_1}\ P_A\ (1 - \theta_A - \theta_B) = k_{d_1}\ \theta_A$$

$$k_{a_2}\ P_B\ (1 - \theta_A - \theta_B) = k_{d_2}\ \theta_B$$

Defining the adsorption equilibrium constants as $K_A = \dfrac{k_{a_1}}{k_{d_1}}$ and $K_B = \dfrac{k_{a_2}}{k_{d_2}}$,

and taking into account that $\dfrac{\theta_B}{\theta_A} = \dfrac{K_B\ P_B}{K_A\ P_A}$, it comes:

$$\theta_A = \frac{K_A\ P_A}{1 + K_A\ P_A + K_B\ P_B}$$

$$\theta_B = \frac{K_B\ P_B}{1 + K_A\ P_A + K_B\ P_B}$$

If several species compete for active sites of the same type, and all of them undergo adsorption according to a 1/1 stoichiometry, the Langmuir equation has the general form:

$$\theta_A = \frac{K_A\ P_A}{1 + \sum_i K_i\ P_i}$$

Similarly, when the adsorption of a certain species is dissociative, it is possible to show that the respective term $K_i\ P_i$ in the previous expression must be replaced by $\sqrt{K_i\ P_i}$. This is the case for the competitive adsorption of A_2 and B, where the former adsorbs dissociatively. By similar reasoning and algebraic calculations as before:

$$\theta_A = \frac{\sqrt{K_{A_2}\ P_{A_2}}}{1 + \sqrt{K_{A_2}\ P_{A_2}} + K_B\ P_B}$$

$$\theta_B = \frac{K_B\ P_B}{1 + \sqrt{K_{A_2}\ P_{A_2}} + K_B\ P_B}$$

Finally, it is important to mention that if two species A and B adsorb simultaneously on active sites of different chemical nature, of course there is no competition, and the Langmuir equations in the simpler form are the relevant ones (for instance, in the case of 1/1 stoichiometry, $\theta_A = \dfrac{K_A\ P_A}{1 + K_A\ P_A}$ and $\theta_B = \dfrac{K_B\ P_B}{1 + K_B\ P_B}$).

3.3. FORMULATION OF RATE LAWS BASED ON THE LANGMUIR MODEL

Kinetic laws can be easily derived from the appropriate expressions of the Langmuir model if the surface reaction is the rate controlling step of the catalytic reaction and all the other mechanistic steps correspond to adsorption of reactants and desorption of products. This arises from the approximation to equilibrium for all adsorption and desorption steps in those cases, a point that deserves a more detailed explanation, as well as the concept of rate controlling step.

As an example, let us consider a reversible catalytic reaction A = P, and assume that both the reactant and the product adsorb on the catalyst with a 1/1 stoichiometry. In addition, also assume that the surface reaction is rate controlling. Using the notation already presented, the reaction mechanism may be described by the sequence:

Step 1)   A + * = A*   (adsorption of A on active sites *)

Step 2)   A* = P*   (surface reaction; rate controlling step)

Step 3)   P* = P + *   (desorption of the product P)

It is important to mention that the rates of the three elementary steps (each one of them calculated as the difference between the respective forward and backward rates) are equal. Thus, it is not correct to define the controlling step as the slowest one. If this were true, the adsorbed reactant A would accumulate

on the catalyst surface. On the other hand, P cannot desorb from the surface at a rate higher than the rate of its formation in the previous step, in the same way as a powerful racing car is not able to overtake a bus in a narrow one-way street. For the reaction considered, the surface reaction controls the rate because both the corresponding forward and backward rates are very much lower than the forward and backward rates of the other steps of the mechanism, i.e. $r_{2f}, r_{2b} << r_{1f}, r_{1b}, r_{3f}, r_{3b}$. As the individual forward and backward rates of the non-controlling steps are comparatively very high, it is possible to assume that $\dfrac{r_{1f}}{r_{1b}} \cong 1$ and $\dfrac{r_{3f}}{r_{3b}} \cong 1$, which justifies the approximation to equilibrium for those steps (corresponds to the equality of rates in both directions).

It is now easy to understand how to formulate kinetic laws when the surface reaction is the rate controlling step and the other steps correspond to adsorption and desorption processes. As the later approach equilibrium, the concentrations of adsorbed species may be determined using the appropriate Langmuir model equations, presented in the previous sections of this chapter. Some illustrative examples will be considered in continuation.

3.3.1. Irreversible reaction A → P

The reaction mechanism is described by the elementary steps:

A + * = A*

A* → P*   (rate constant k)

P* = P + *
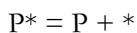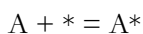
Note that, if the reaction is irreversible, at least one of the steps must be irreversible and that step is necessarily the rate controlling one, because the other steps approach equilibrium.

The rate law is expressed on the basis of the rate controlling step, i.e. $r = k\,\theta_A$. Considering the approximation to equilibrium, according to the Langmuir model, the fractional coverage of active sites by reactant A is

$\theta_A = \dfrac{K_A\,P_A}{1 + K_A\,P_A + K_P\,P_P}$, because A and P adsorb competitively on the active

sites. Therefore, $r = \dfrac{k\,K_A\,P_A}{1 + K_A\,P_A + K_P\,P_P}$. Since the temperature dependency of

the reaction rate (through kinetic and equilibrium constants) is not separable relatively to the concentrations (or partial pressures in this case) dependency, an

activation energy cannot be defined and the Arrhenius plot ($\ln r$ versus $\dfrac{1}{T}$) is

complex. However, if product P were strongly adsorbed on the catalyst, then

$K_P\,P_P \gg 1 + K_A\,P_A$, and the simplified rate equation $r = \dfrac{k\,K_A}{K_P}\dfrac{P_A}{P_P}$ would be

verified. This corresponds to an observed activation energy in all the temperature domain that is dependent on the activation energy of the surface reaction and on the heats of adsorption of A and P on the catalytic sites:

$E_{obs} = E + \Delta H_A^\circ - \Delta H_P^\circ$.

If product P were not adsorbed, $\theta_A = \dfrac{K_A\,P_A}{1 + K_A\,P_A}$ and $r = \dfrac{k\,K_A\,P_A}{1 + K_A\,P_A}$. This

expression presents two limiting cases. For low temperatures and/or high

pressures $K_A\,P_A \gg 1$ and $r = k = A\exp\left(-\dfrac{E}{R\,T}\right)$. In these conditions, the

reaction would be of zero order relatively to the reactant and its activation energy would correspond to the activation energy of the surface reaction step ($E_{obs} = E$). On the other hand, for high temperatures and/or low pressures it

is possible to say that $K_A\,P_A \ll 1$ and $r = k\,K_A\,P_A = A\,B\exp\left(-\dfrac{E + \Delta H_A^\circ}{R\,T}\right)P_A$,

which corresponds to a first-order reaction with $E_{obs} = E + \Delta H_A^\circ < E$, where

$\left(-\Delta H_A^\circ\right)$ is the heat of adsorption of reactant A. Outside these limits, the complete rate equation prevails and a single activation energy cannot be defined.

3.3.2. Irreversible bimolecular reaction A + B → P (both reactants adsorb on the same type of active sites) – Langmuir-Hinshelwood mechanism

The surface reaction occurs between the molecules of the two reactants adsorbed on neighbouring sites.

Assuming that P does not adsorb on the catalyst, it comes:

A + * = A*

B + * = B*

A* + B* → P + 2 *   (rate constant k)
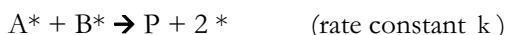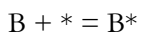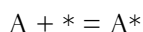
The rate of reaction is directly proportional to the concentrations of active sites occupied with A and B molecules, i.e. $r = k\,\theta_A\,\theta_B$. As the two reactants compete for the catalyst active sites, $\theta_A = \dfrac{K_A\,P_A}{1 + K_A\,P_A + K_B\,P_B}$ and

$\theta_B = \dfrac{K_B\,P_B}{1 + K_A\,P_A + K_B\,P_B}$. Therefore, $r = \dfrac{k\,K_A\,K_B\,P_A\,P_B}{\left(1 + K_A\,P_A + K_B\,P_B\right)^2}$.

3.3.3. Irreversible bimolecular reaction A + B → P (both reactants adsorb on active sites of different type)

Considering that P does not adsorb on the catalyst and representing by * and ● the two types of active sites present on the catalyst surface, we may write the reaction mechanism:

A + * = A*

B + ● = B●

A* + B● → P + * + ●   (rate constant k)
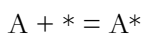
As in the previous case, $r = k \, \theta_A \, \theta_B$, but now the two reactants do not compete for adsorption on the same type of active sites. This means that $\theta_A = \dfrac{K_A \, P_A}{1 + K_A \, P_A}$ and $\theta_B = \dfrac{K_B \, P_B}{1 + K_B \, P_B}$, where K_A and K_B are the adsorption equilibrium constants of A and B, respectively on active sites * and ●. Therefore, the rate equation corresponding to this mechanism is

$$r = \frac{k \, K_A \, K_B \, P_A \, P_B}{\left(1 + K_A \, P_A\right)\left(1 + K_B \, P_B\right)} .$$

3.3.4. Irreversible bimolecular reaction A + B → P (only reactant A adsorbs on the active sites) – Rideal-Eley mechanism

The reaction mechanism has only two steps (adsorption of reactant A and surface reaction between A adsorbed on the catalyst and B in the gas phase):

A + * = A*

A* + B → P + *   (rate constant k)
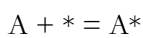
The reaction rate is expressed by the equation $r = k \, \theta_A \, P_B$. As only reactant A adsorbs on the catalyst, $\theta_A = \dfrac{K_A \, P_A}{1 + K_A \, P_A}$ and, consequently, $r = \dfrac{k \, K_A \, P_A \, P_B}{1 + K_A \, P_A}$.

3.3.5. Irreversible reaction 2A + B → P (both reactants adsorb on active sites of the same type and the product does not adsorb)

The equation representative of a reaction indicates which are the reactants and products and gives information about the stoichiometry (proportions relative to the combination of reactants and the formation of products). For instance, in the reaction under analysis, we can conclude that 2 mol of reactant A react with 1 mol of B to produce 1 mol of the product P. The equation presented in the section title could be written in a different form (e.g. A + ½ B → ½ P) without any loss of information. In the case of mechanistic equations, which intend to

describe the behaviour of individual entities (molecules, atoms, ions, free radicals, etc), the situation is not the same. Exemplifying for the adsorption of A, if we write A + * = A*, we mean that a reactant molecule "meets" a vacant site and adsorbs on it. On the other hand, if we assume that the adsorption step is represented by 2 A + 2 * = 2 A*, we mean that pairs of A molecules must be considered in order to make adsorption possible, which would be an absurd approach. Taking into account these preliminary comments and considering that the mechanism must obey the stoichiometry of the reaction, the most probable sequence of elementary processes involved are:

A + * = A*

B + * = B*

2 A* + B* $\rightarrow$ P + 3 *   (rate constant k)
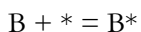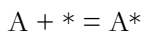
In the surface reaction (rate controlling step), the interaction of one adsorbed B molecule and 2 independently adsorbed A molecules in the vicinity originates a molecule of the product P and releases three active sites.

The rate of reaction is expressed by the equation $r = k \, \theta_A^2 \, \theta_B$. Considering the competition between A and B for the active sites, after substitution of the appropriate Langmuir model equations, it is possible to obtain

$$r = \frac{k \, K_A^2 \, K_B \, P_A^2 \, P_B}{\left(1 + K_A \, P_A + K_B \, P_B\right)^3} \, .$$

3.3.6. Irreversible reaction 1/2 A$_2$ + B $\rightarrow$ P (only reactant A$_2$ adsorbs dissociatively on the catalyst)

Taking into account the reaction stoichiometry and knowing that the adsorption of reactant A$_2$ is dissociative, the reaction mechanism is described by:

A$_2$ + 2 * = 2 A*

A* + B $\rightarrow$ P + *   (rate constant k)

The stoichiometry of the reaction is globally verified by the mechanism considered, since from a stoichiometric point of view each A_2 molecule combines with two B molecules to produce two P molecules. Of course, the same is true if one reads "mole" instead of "molecule". The rate equation is $r = k\,\theta_A\,P_B$. The adsorption of A_2 is dissociative and there is no competition.

Therefore, $\theta_A = \dfrac{\sqrt{K_{A_2}\,P_{A_2}}}{1 + \sqrt{K_{A_2}\,P_{A_2}}}$ and, making the substitution, it results that

$$r = \frac{k\,\sqrt{K_{A_2}}\,\sqrt{P_{A_2}}\,P_B}{1 + \sqrt{K_{A_2}}\,\sqrt{P_{A_2}}}.$$

3.3.7. Reversible reaction A = P (both compounds adsorb on the catalyst without dissociation)

This case was already considered at the beginning of section 3.3 while explaining the rate controlling step concept and the approximation to equilibrium for the remaining mechanistic steps. This example is solved here, at the end of the section, since the respective treatment is a little more complex than the previous situations. The corresponding mechanism involves the adsorption of reactant A, the desorption of product P and a reversible surface reaction as the rate controlling step:

A + * = A*   (equilibrium constant of A adsorption, K_A)

A* = P*   (rate constants k and k'; equilibrium constant K_{sr})

P* = P + *   (equilibrium constant of P desorption, $\dfrac{1}{K_P}$)
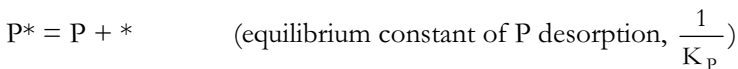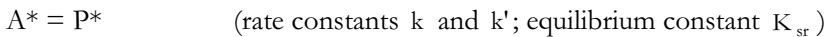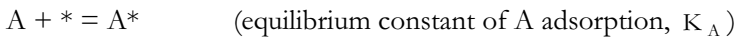
The rate law may be written as $r = k\,\theta_A - k'\,\theta_P$. Considering that there is a competition between A and P for adsorption, $\theta_A = \dfrac{K_A\,P_A}{1 + K_A\,P_A + K_P\,P_P}$ and

$$\theta_P = \frac{K_P \ P_P}{1 + K_A \ P_A + K_P \ P_P} \ . \quad \text{Therefore,} \quad r = \frac{k \ K_A \ P_A - k' \ K_P \ P_P}{1 + K_A \ P_A + K_P \ P_P} \ . \quad \text{Finally, taking}$$

into account that $K_{sr} = \dfrac{k}{k'}$, and that in this case the equilibrium constant of the

reaction, K, may be expressed in terms of the equilibrium constants of the

elementary steps according to $K = \dfrac{K_A \ K_{sr}}{K_P}$, the rate equation becomes

$$r = \frac{k \ K_A \left(P_A - \dfrac{P_P}{K} \right)}{1 + K_A \ P_A + K_P \ P_P} \ .$$

3.4. HOUGEN-WATSON METHODOLOGY

In the previous examples the surface reaction was always taken as the rate
controlling step of the various mechanisms considered; however, it is also
possible that either the adsorption or the desorption steps may control the
reaction rate. Moreover, in particular cases, more than one surface reaction may
be present in the mechanism. Finally, it is also possible that some reactions
have no rate controlling step. In all these situations, the method based on the
Langmuir equations for the adsorption/desorption equilibrium cannot be used
and a more general technique is necessary. This methodology was developed by
Hougen and Watson[2], and is very similar to the technique used for the same
purpose in the scope of homogeneous reactions. The Hougen-Watson method
has a wide range of application, although it is more complex than the technique
presented in the previous sections.

For illustrative purposes, we are going to consider only the example already
treated in the previous section. We will apply the new methodology not only to
the case of surface reaction controlling, proving that both methods are
equivalent, but also to the different situations of rate control by adsorption of
reactant or by desorption of product. The reaction is a reversible isomerisation

reaction A = P and it is assumed that both reactant A and product P may adsorb on the catalyst. Representing the active sites by Z, as usually done in the scope of this method, the reaction mechanism is:

A + Z = AZ   (rate constants k_A and k_{-A}; equilibrium constant $K_A = \dfrac{k_A}{k_{-A}}$)

AZ = PZ   (rate constants k_{sr} and k_{-sr}; equilibrium constant $K_{sr} = \dfrac{k_{sr}}{k_{-sr}}$)

PZ = P + Z   (rate constants k_P and k_{-P}; equilibrium constant $\dfrac{1}{K_P} = \dfrac{k_P}{k_{-P}}$)
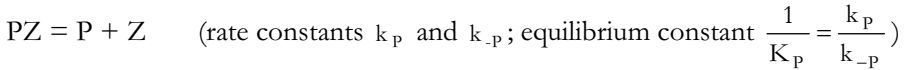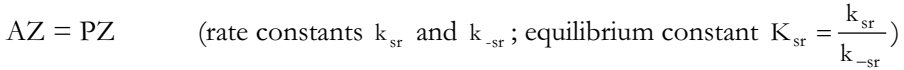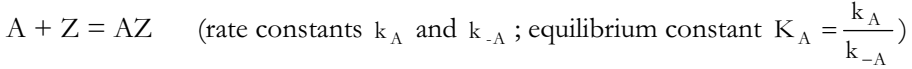
AZ and PZ represent the adsorption complexes on the surface of the catalyst and Z represents the vacant active sites. Additionally, as mentioned in the previous section, it is possible to prove that the reaction equilibrium constant is related to the equilibrium constants of the individual steps by the expression

$$K = \frac{K_A \, K_{sr}}{K_P} \, .$$

Case 1 – The surface reaction is the rate controlling step.

In the Hougen and Watson methodology, the concentrations of occupied sites are not expressed by the respective fractional coverages (dimensionless) as in the previous method. In this technique, those concentrations may be for instance mol/mass of catalyst or mol/area of catalyst and are represented by $[Z]$, $[AZ]$, $[PZ]$, etc. Therefore:

$$r = k_{sr} \, [AZ] - k_{-sr} \, [PZ] = k_{sr} \left([AZ] - \frac{[PZ]}{K_{sr}} \right)$$

Considering the approximation to equilibrium for the other two steps, we can write:

$$K_A = \frac{[AZ]}{P_A \, [Z]} \quad \Rightarrow \quad [AZ] = K_A \, P_A \, [Z]$$

$$\frac{1}{K_P} = \frac{P_P\ [Z]}{[PZ]} \quad \Rightarrow \quad [PZ] = K_P\ P_P\ [Z]$$

In order to express the concentrations of vacant and occupied sites as a function of the partial pressures of reactants and products, an additional equation is necessary. This equation is the balance of active sites:

$$[Z] + [AZ] + [PZ] = L$$

where L is the total concentration of active sites.

After substitution and rearrangement, we may conclude that:

$$[Z] = \frac{L}{1 + K_A\ P_A + K_P\ P_P}$$

To make obvious the compatibility between the present method and that based on the Langmuir equations for adsorption/desorption equilibrium, it is sufficient to notice that the fraction of vacant sites is

$$\frac{[Z]}{L} = \frac{1}{1 + K_A\ P_A + K_P\ P_P} = 1 - \theta_A - \theta_P$$

and to compare with the expressions of θ_A and θ_P shown in the previous section.

Returning to the rate law deduction, after substitution of the concentrations $[AZ]$ and $[PZ]$, we arrive at its final form:

$$r = \frac{L\ k_{sr}\left(K_A\ P_A - \dfrac{K_P\ P_P}{K_{sr}}\right)}{1 + K_A\ P_A + K_P\ P_P} = \frac{L\ k_{sr}\ K_A\left(P_A - \dfrac{P_P}{K}\right)}{1 + K_A\ P_A + K_P\ P_P}$$

Comparing this equation with that developed in the previous section, it is possible to conclude that they are similar. The only difference is related to the circumstance that the corresponding rate constants have not the same units, but if we put $k = L\ k_{sr}$ the similarity becomes perfect.

Case 2 – The adsorption of reactant A is the rate controlling step.

The mathematical procedure is similar to that used in the previous case. Then, without further explanations:

$$r = k_A \ P_A \ [Z] - k_{-A} \ [AZ] = k_A \left(P_A \ [Z] - \frac{[AZ]}{K_A} \right)$$

$$\frac{1}{K_P} = \frac{P_P \ [Z]}{[PZ]} \quad \Rightarrow \quad [PZ] = K_P \ P_P \ [Z]$$

$$K_{sr} = \frac{[PZ]}{[AZ]} \quad \Rightarrow \quad [AZ] = \frac{[PZ]}{K_{sr}} = \frac{K_P \ P_P \ [Z]}{K_{sr}}$$

$$[Z] + [AZ] + [PZ] = L \quad \Rightarrow \quad [Z] = \frac{L}{1 + \dfrac{K_P \ P_P}{K_{sr}} + K_P \ P_P} = \frac{L}{1 + \dfrac{K_A \ P_P}{K} + K_P \ P_P}$$

Finally, after substitution and rearrangement:

$$r = \frac{L \ k_A \left(P_A - \dfrac{K_P \ P_P}{K_A \ K_{sr}} \right)}{1 + \dfrac{K_P \ P_P}{K_{sr}} + K_P \ P_P} = \frac{L \ k_A \left(P_A - \dfrac{P_P}{K} \right)}{1 + \dfrac{K_A \ P_P}{K} + K_P \ P_P}$$

Contrarily to the first case and to all other situations analysed corresponding to rate control by surface reactions (see the previous section), in which the denominator of the rate equation is formed by a sum of 1 with various terms of the type $K_i \ P_i$ and/or $\sqrt{K_i \ P_i}$ (i are the species that adsorb competitively on the catalyst, i.e. A and P in the present example), in the rate law under analysis the term $K_P \ P_P$ remains in the denominator, but the other one is replaced for an expression that also contains the partial pressure of P. Therefore, P_A does not appear in the denominator of the rate equation.

Case 3 – The desorption of product P is the rate controlling step.

The rate law is initially written on the basis of the rate of the desorption step:

$$r = k_P \ [PZ] - k_{-P} \ P_P \ [Z] = k_P \left([PZ] - K_P \ P_P \ [Z] \right)$$

The approximation to equilibrium for the other two elementary steps leads to:

$$K_A = \frac{[AZ]}{P_A \ [Z]} \quad \Rightarrow \quad [AZ] = K_A \ P_A \ [Z]$$

$$K_{sr} = \frac{[PZ]}{[AZ]} \quad \Rightarrow \quad [PZ] = K_{sr} \ [AZ] = K_{sr} \ K_A \ P_A \ [Z]$$

The concentration of vacant sites can be deduced from the balance of active sites:

$$[Z] + [AZ] + [PZ] = L \quad \Rightarrow \quad [Z] = \frac{L}{1 + K_A \ P_A + K_{sr} \ K_A \ P_A} = \frac{L}{1 + K_A \ P_A + K_P \ K \ P_A}$$

After successive substitutions in the previous expressions, it comes:

$$r = \frac{L \ k_P \left(K_{sr} \ K_A \ P_A - K_P \ P_P \right)}{1 + K_A \ P_A + K_{sr} \ K_A \ P_A} = \frac{L \ k_P \ K_P \ K \left(P_A - \dfrac{P_P}{K} \right)}{1 + K_A \ P_A + K_P \ K \ P_A}$$

Taking as basis the rate expression deduced for the case of rate control by the surface reaction, the term $K_A \ P_A$ remains in the denominator and the other term (originally, $K_P \ P_P$) is replaced for one that contains the partial pressure of the reactant A.

3.5. GENERALIZATIONS ABOUT THE RATE LAWS OF HETEROGENEOUS CATALYTIC REACTIONS

Several authors analysed the rate equations corresponding to an extensive set of simple reaction stoichiometries and mechanisms involving a controlling step (adsorption of reactant, surface reaction, desorption of product) and one type of active sites. Perhaps the most relevant of those studies was carried out by Yang and Hougen[3]. Consequently, it was possible to establish various important generalizations, which may be summarized:

1) All the rate laws deduced by the two methods considered in this text present a general form of the type $r = \dfrac{(\text{Kinetic term})(\text{Driving force})}{(\text{Adsorption term})^{\text{Exponent}}}$.

2) When the surface reaction controls the rate, the adsorption term in the denominator has the form $1 + \sum_i K_i\, P_i$, the summation being extended to all adsorbed species, eventually including inert gases; if the adsorption of a certain species is dissociative, the corresponding term $K_i\, P_i$ in the sum is replaced by $\sqrt{K_i\, P_i}$.

3) If the adsorption of a reactant or the desorption of a product is rate controlling, the respective term $K_i\, P_i$ or $\sqrt{K_i\, P_i}$ in the denominator is replaced for a different one that contains the partial pressures of all the other species.

4) The exponent of the adsorption term is equal to the number of active sites involved in the rate controlling step.

5) The kinetic term in the numerator is equal to the product of the rate constant of the controlling step in the forward direction by the equilibrium constants of the previous steps and by the total concentration of active sites raised to an exponent equal to the number of active sites involved in the rate controlling step.

These main conclusions are important, since they allow writing directly the kinetic laws associated to known mechanisms. In addition, and probably more important from a practical point of view, they permit to formulate suitable mechanisms based on kinetic data, without extensive analyses.

EXAMPLE

For the heterogeneous catalytic reaction with equation $A_2 + B \rightarrow R + S$, write suitable mechanisms compatible with the following experimental rate laws:

$$1:\ r = \frac{\alpha\, P_{A_2}\, P_B}{\left(1 + \beta\, P_{A_2} + \gamma\, P_R + \delta\, P_S\right)^2}$$

$$2:\ r = \frac{\alpha\, P_{A_2}\, P_B}{\left(1 + \sqrt{\beta\, P_{A_2}} + \gamma\, P_R\right)^2}$$

$$3:\ r = \frac{\alpha\, P_{A_2}}{\left(1 + \sqrt{\beta\, \dfrac{P_R\, P_S}{P_B}} + \gamma\, P_B\right)^2}$$

$$4:\ r = \frac{\alpha\, \dfrac{P_{A_2}\, P_B}{P_S}}{1 + \sqrt{\beta\, P_{A_2}} + \gamma\, \dfrac{P_{A_2}\, P_B}{P_S}}$$

$$5:\ r = \frac{\alpha\, P_{A_2}\, P_B}{1 + \beta\, P_B + \gamma\, P_R}$$

$$6:\ r = \frac{\alpha\, P_{A_2}\, P_B}{\left(1 + \sqrt{\beta\, P_{A_2}} + \gamma\, P_B\right)^3}$$

The parameters α, β, γ and δ depend only on temperature.

1 – Surface reaction controlling; A_2, R and S adsorb on the catalyst surface with 1/1 stoichiometry; reactant B does not adsorb on the catalyst; the surface reaction involves two active sites, since both products adsorb on the catalyst.

$A_2 + Z = A_2Z$

$A_2Z + B + Z \rightarrow RZ + SZ$

$RZ = R + Z$

$SZ = S + Z$
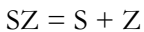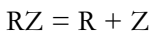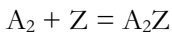
2 – Surface reaction controlling; only reactant A_2 and product R adsorb on the catalyst; A_2 adsorbs with dissociation; the surface reaction involves two active sites that correspond to those where the reactant A_2 adsorbs.

$A_2 + 2\,Z = 2\,AZ$

$2\,AZ + B \rightarrow RZ + S + Z$

$RZ = R + Z$
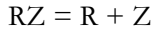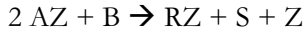
3 – Reactant A_2 adsorption controlling; dissociative adsorption of A_2 and simple (1/1) adsorption of B; R and S do not adsorb on the catalyst; two active sites involved in the rate controlling step.

$A_2 + 2\,Z \rightarrow 2\,AZ$

$B + Z = BZ$

$2\,AZ + BZ = R + S + 3\,Z$
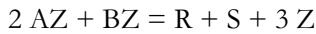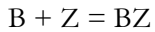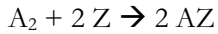
4 – Desorption of R controlling; one active site involved; dissociative adsorption of A_2; B and S do not adsorb on the catalyst.

$A_2 + 2\,Z = 2\,AZ$

$2\,AZ + B = RZ + S + Z$

$RZ \rightarrow R + Z$
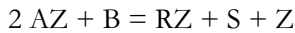
5 – Surface reaction controlling; only B and R adsorb on the active sites of the catalyst; one active site takes part in the rate controlling step.

$B + Z = BZ$

$A_2 + BZ \rightarrow RZ + S$

$RZ = R + Z$
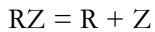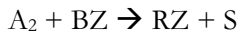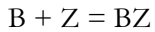
6 – Surface reaction controls the rate; A_2 adsorbs with dissociation; additionally, only the other reactant (B) adsorbs on catalyst; the rate controlling step involves three active sites.

$A_2 + 2\,Z = 2\,AZ$

$B + Z = BZ$

$2\,AZ + BZ \rightarrow R + S + 3\,Z$
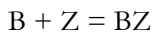
3.6. ABSENCE OF RATE CONTROLLING STEP

When there is no rate controlling step, no approximation to equilibrium can be considered. In these situations, the rate equation is deduced on the basis of the

steady state hypothesis for the intermediates (the complexes of adsorption), similarly to a well known technique used for homogeneous reactions.

In order to maintain the mathematical treatment as simple as possible, the technique for the determination of the kinetic equation from the mechanism is exemplified using a catalytic reversible isomerisation reaction A = P, and assuming that the product P does not adsorb on the catalyst. Therefore, the mechanism only involves the following two steps:

$$A + Z = AZ \quad \text{(rate constants } k_A \text{ and } k_{-A}; \text{ equilibrium constant } K_A = \frac{k_A}{k_{-A}})$$

$$AZ = P + Z \quad \text{(rate constants } k_{sr} \text{ and } k_{-sr}; \text{ equilibrium constant } K_{sr} = \frac{k_{sr}}{k_{-sr}})$$
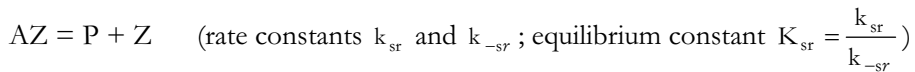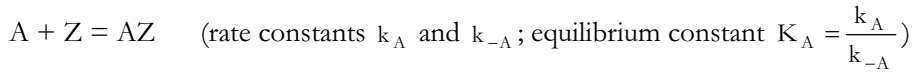
The rate equations associated to the two steps are, respectively:

$$r_1 = k_A \ P_A \ [Z] - k_{-A} \ [AZ] = k_A \left(P_A \ [Z] - \frac{[AZ]}{K_A} \right)$$

$$r_2 = k_{sr} \ [AZ] - k_{-sr} \ P_P \ [Z] = k_{sr} \left([AZ] - \frac{P_P \ [Z]}{K_{sr}} \right)$$

The concentrations of vacant and occupied active sites, respectively [Z] and [AZ], are determined by the balance of active sites and the steady state approximation for the intermediate AZ. As discussed before, the rates of all elementary steps of a mechanism are equal (in this case, $r = r_1 = r_2$). The mathematical formulation of the steady state condition for AZ is equivalent to the equality of the rates of the two steps. In this example:

$$r_{AZ} = k_A \ P_A \ [Z] - \frac{k_A}{K_A} [AZ] - k_{sr} \ [AZ] + \frac{k_{sr}}{K_{sr}} \ P_P \ [Z] \cong 0$$

$$[Z] + [AZ] = L$$

By solving this system of two equations, it is possible to obtain:

$$[AZ] = \frac{k_A \, P_A + \dfrac{k_{sr}}{K_{sr}} \, P_P}{\dfrac{k_A}{K_A} + k_{sr}} \, [Z]$$

and

$$[Z] = \frac{L}{1 + \dfrac{k_A \, P_A + \dfrac{k_{sr}}{K_{sr}} \, P_P}{\dfrac{k_A}{K_A} + k_{sr}}}$$

Making the substitutions in one of the rate expressions (r_1 or r_2) and taking into account that the equilibrium constant of the reaction is $K = K_A \, K_{sr}$, we may conclude that:

$$r = \frac{L \, k_A \, k_{sr} \left(P_A - \dfrac{P_P}{K} \right)}{\dfrac{k_A}{K_A} + k_{sr} + k_A \, P_A + \dfrac{k_{sr} \, K_A}{K} \, P_P}$$

As expected, this equation is more complex than the rate laws deduced previously. This complexity is associated to the level of generality it possesses. In particular, it is possible to extract the solutions corresponding to rate control by adsorption of A or by surface reaction. In the first case, considering the interpretation of the rate controlling step, $r_{1f}, r_{1b} \ll r_{2f}, r_{2b}$, or

$$k_A \, P_A \, [Z], \frac{k_A}{K_A} [AZ] \ll k_{sr} \, [AZ], \frac{k_{sr} \, K_A}{K} \, P_P \, [Z]. \quad \text{Thus,} \quad k_A \, P_A \ll \frac{k_{sr} \, K_A}{K} \, P_P$$

and $\dfrac{k_A}{K_A} \ll k_{sr}$. Making these simplifications in the general rate equation, it

comes $r = \dfrac{L \, k_A \left(P_A - \dfrac{P_P}{K} \right)}{1 + \dfrac{K_A}{K} \, P_P}$, which is in fact the rate law associated to the case

of rate control by adsorption of A. Reversing the direction of the inequalities,

i.e. assuming that r_{1f}, $r_{1b} \gg r_{2f}$, r_{2b}, and using the same procedure, it is possible

to obtain the expression $r = \dfrac{L\,k_{sr}\,K_A\left(P_A - \dfrac{P_P}{K}\right)}{1 + K_A\,P_A}$, which corresponds to rate

control by the surface reaction.

3.7. EMPIRICAL RATE LAWS

Along this chapter, we saw that the heterogeneous catalysis mechanisms lead to somewhat complex rate laws in which the temperature dependent parameters (rate and equilibrium constants) are not separated from the partial pressures (or molar concentrations) of reactants and products. Therefore, it may be concluded that heterogeneous catalytic reactions generally do not depend on temperature according to the well known Arrhenius law.

However, in many cases, it is possible and even desirable to use empirical rate equations of the type "power law", expressing the rate as

$$r = k^*\,P_A^a\,P_B^b\,... = k^* \prod_i P_i^{\alpha_i}$$

where the empirical rate constant k^* obeys the Arrhenius law:

$k^* = A^* \exp\left(-\dfrac{E^*}{R\,T}\right)$. Evidently, this type of expressions has no mechanistic

significance, but may be useful to compare the performance of a set of catalysts for a given reaction or the activities of various reactions in the presence of the same catalyst. However, we must notice that these largely used empirical rate laws are only valid inside the (usually narrow) range of experimental conditions used for its determination. Extrapolations, for instance in order to design catalytic reactors, are not allowed.

References

_____

1. I. Langmuir, *J. Am. Chem. Soc.*, **1916**, *38*, 2221-2295.

2. O.A. Hougen, K.M. Watson*, Ind. Eng. Chem.,* **1943***, 35,* 529-541.

3. K.Y. Yang, O.A. Hougen, *Chem. Eng. Progr.,* **1950**, *46*, 146-157.

(Página deixada propositadamente em branco)

4. Physisorption Of Gases By Solids: Fundamentals, Theories And Methods For The Textural Characterization Of Catalysts

M. Manuela L. Ribeiro Carrott

Centro de Química de Évora and Departamento de Química, Universidade de Évora, Colégio Luís António Verney, 7000-671 Évora, Portugal

4.1. Introduction

The knowledge of textural parameters, such as surface area, pore volume and pore width, usually contributes to the understanding of the behaviour of a catalyst in a process, since the extent of surface can be determinant for an efficient distribution of catalytically active sites, while the type of porosity can affect the accessibility and the diffusion process of reactant and product molecules through the porous structure.

Gas adsorption is a powerful means for textural characterization of powders and nanoporous solids[1,2,3]. This is not restricted to nitrogen adsorption at 77K, which is indeed an important case and used as routine, but it has been evident for a long time that the use of other adsorptives, namely organic vapours, and at higher temperatures is, in many situations, of fundamental importance for an adequate characterization.

Despite the fact that recent developments for the characterisation of porous solids have been dedicated to advanced computational methods for modelling adsorption in nanoporous materials, it is unquestionable that the classical methods of adsorption data analysis are those available for the majority of researchers needing to characterise their materials in everyday work and can still provide, in most cases, the necessary information. However, it is obvious that the methods have to be carefully selected and properly applied, for the particular system under study, otherwise the parameters may be significantly inaccurate or even meaningless.

Therefore, some classical methods to obtain surface area and pore volume will be addressed and their advantages and limitations will be critically evaluated on the basis of the type of mechanism of adsorption involved. A brief overview of some procedures for the determination of pore size and pore size distributions will also be considered.

4.2. PHYSISORPTION ON OPEN SURFACES AND INSIDE PORES

The selection of appropriate methods to analyse the adsorption data and to obtain valid textural parameters requires the understanding of the mechanism of physisorption involved. This will depend on several factors, the pore width being one of them and according to this IUPAC[1] has recommended that pores be classified as *micropore*, *mesopore* or *macropore* if the width is less than ~2nm, between 2 and 50 nm or superior to 50 nm, respectively. Therefore the physisorption mechanism will be addressed in this context, but it should be noted that it will depend also on the gas-solid interactions, the temperature and the dimension of adsorptive molecules, especially inside narrow pores.

Physisorption on macropores occurs as on a nonporous and energetically heterogeneous surface by a mechanism of *monolayer-multilayer* formation. It is well established that physisorption is not limited to a monolayer but that the second, third, etc., can start to form before the first layer is completed. Only when the surface is completely uniform, or nearly so, and in a few restricted gas-solid systems, adsorption can occur almost layer-by-layer. In all cases, when the pressure reaches the value of the saturation pressure p^o of the adsorptive at the operational temperature, the adsorbate condenses on the nonporous surface. In macropores this occurs at very high relative pressure (p/p^o), close to 1.

It should be noted that, in an energetically heterogeneous surface, the stronger the adsorbate-adsorbent interaction the more likely it is that the monolayer is

complete before significant adsorption on subsequent layers occur. If, on the other hand, the surface has very low affinity for the adsorptive, adsorption is very reduced at low pressures. It begins with the adsorption of some molecules on a few of the most favourable sites and then adsorbate-adsorbate interactions predominate leading to the multilayer, by the formation of clusters around those sites, with no defined monolayer.

Adsorption in mesopores starts with monolayer-multilayer coverage of the pore walls but, due to the existence of opposite walls, condensation occurs inside the mesopores at relative pressure inferior to 1. Therefore, two adsorption mechanisms are involved: monolayer-multilayer adsorption prior to *capillary condensation*. Capillary condensation in mesopores is often associated with hysteresis, that is: evaporation occurs at p/p^o lower than that of condensation. Hysteresis has been the subject of various interpretations, including the existence of ink-bottle shaped pores, differences in meniscus shape during condensation and evaporation in open-ended cylinders, or metastability of the adsorbate in adsorption or/and desorption branches, but it is not yet completely understood. However, it is now established that the appearance of hysteresis associated with capillary condensation depends on the particular adsorptive-solid pair and of temperature, and that, for a given adsorptive and pore geometry, hysteresis can eventually disappear as the temperature increases and/or the pore size decreases. For instance, adsorption measurements on MCM-41 materials have shown that reversible stepwise capillary condensation can occur in open-ended non-intersecting cylindrical pores under certain conditions.

With regard to micropores and most adsorptives (e.g. water can be a particular exception), two possible *micropore filling* mechanisms have been proposed by Gregg and Sing[4]. One occurs in very narrow micropores where close proximity of the walls, in relation to the size of the adsorbed molecules, leads to an enhancement of the adsorption energy in comparison with that occurring on an

open surface. Due to this the pores are filled at very low relative pressures without prior monolayer formation. This was called the *primary process of micropore filling* and occurs in micropores with dimensions close to the dimensions of the adsorbed molecules, usually designated *ultra*micropores. In slightly wider micropores, usually designated *super*micropores, or with smaller molecules, for instance for slit shaped pores with widths superior to two molecular diameters, it was proposed that firstly occurs monolayer coverage of the pore walls and pore filling subsequently occurs by a cooperative process. This *secondary process of micropore filling* is not accompanied by an enhancement in adsorption energy in comparison to an open surface and the micropores are completely filled at p/p° superior to those for the smaller micropores.

It should be pointed out again that the adsorption mechanism does not depend solely on absolute pore size but the other factors initially mentioned should be taken into account when considering the possible mechanisms of adsorption inside pores of a given size. For instance, adsorption regimes have recently been distinguished based on both pore size and temperature[5]. One should also be aware that it is possible for certain micropores to be filled by a secondary process with nitrogen and by a primary process with bulkier molecules, such as neopentane. It should be noted, in addition, that although an upper limit of 2nm for micropore width was considered by IUPAC, there is no rigid separation at 2 nm for micropore filling and reversible capillary condensation.

4.3. A Look At The Physisorption Isotherm As A First Diagnosis Of The Textural Characteristics

The starting point for textural characterisation of a material by physisorption of gases is the adsorption isotherm, usually presented in graphical form of the amount adsorbed per unit mass of solid (n_{ads}) as a function of the relative

pressure (p/p^o), at a constant temperature. The isotherm shape and its qualitative interpretation based on the possible mechanisms involved can provide valuable preliminary information, but of course not always conclusive, on the characteristics of the material.

The classification of IUPAC[1] includes six major types of physisorption isotherm, which can be complemented by the subdivision with a, b or c, proposed more recently[3] (not yet officially adopted by IUPAC), as illustrated in Figure 1.

Type I isotherms are straight away indicative of the presence of a microporous material with strong affinity for the adsorptive and with reduced surface area external to the micropores. Micropore filling is complete at very low relative pressures and, subsequently, the isotherm reaches a plateau as reduced external surface area is available for further significant adsorption. The subdivision in Ia or Ib, differing in the steepness of the approach to the limiting plateau, corresponds, respectively, to the occurrence of a primary or a secondary micropore filling process, as can easily be understood considering the mechanisms previously described. If both narrow and wider micropores are present, the isotherm will be type Ib, with the primary micropore filling being complete for the former at very low p/p^o. For instance, if with the same adsorptive one obtains a type Ia on a certain solid and a type Ib on another, it can be inferred that the latter material has wider micropores, solely or in addition to narrow micropores. On the other hand, a type Ib can be obtained with nitrogen at 77K, and a type Ia can be obtained for the same material with bulkier molecules.

Adsorption on a nonporous or a macroporous solid, or that possessing microporosity inaccessible to the adsorptive used, usually gives rise to a type IIa isotherm. The inexistence of a plateau is indicative of monolayer-multilayer adsorption, with condensation occurring only at $p/p^o \sim 1$. On an open and stable surface the isotherm is reversible. Certain materials, such as clays,

consisting of aggregates of plate-like particles leading to slit shaped pores, usually give rise to type IIb isotherms with a type H3 hysteresis loop[1].
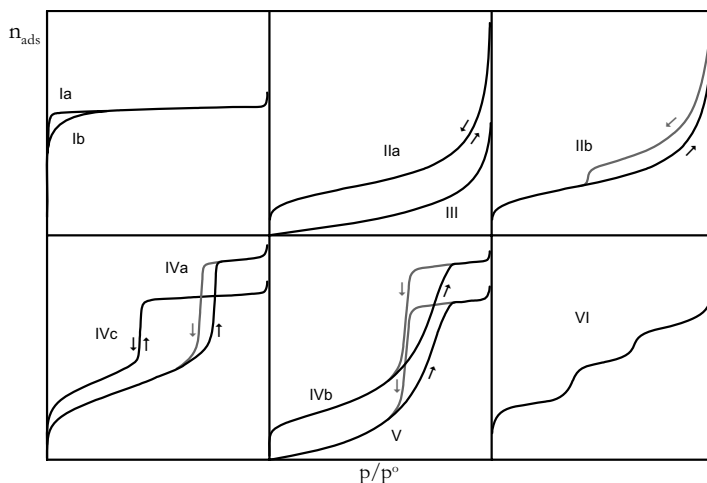
Figure 1 - The main types of gas-solid physisorption isotherms of the IUPAC classification1 complemented with the subdivision (a,b,c) proposed by Rouquérol *et al.*[3].

Type III and type VI isotherms are also obtained on nonporous materials, but restricted to a few systems. The convex nature of the type III from low p/p° indicates a very low affinity of the adsorptive for the material and cooperative multilayer adsorption, without monolayer coverage. On the other hand, the type VI isotherm reveals a stepwise layer-by-layer adsorption process on highly uniform open surfaces.

Type IV isotherms clearly indicate the presence of mesopores. At low relative pressures the isotherm is not very different from type II, but the rise of the isotherm starts before saturation pressure, indicative of the occurrence of capillary condensation inside the mesopores, and the isotherm tends to a plateau at high relative pressures. For a long time, type IV isotherms were generally associated with a hysteresis loop, such as type H1 or H2 loops[1], respectively, for IVa and IVb isotherms. However, one of the exciting features of MCM-41 materials for adsorption scientists was that they provided the first

reversible type IV isotherm, now called type IVc. The steepness of the condensation step and the shape of the hysteresis loop can give some indication about the pore structure. It is recognized that type IVa and IVc isotherms, are indicative of high uniformity of pore size. These could be obtained for instance on mesoporous materials with open-ended non-intersecting cylindrical pores of uniform diameter, with the same adsorptive and temperature, but in the IVc case the pores are sufficiently narrow for hysteresis not to occur at the operational temperature. Type IVb is less understood, but in many cases results from a complex network of interconnected pores of different size and shape.

Type V is similar to type III, resulting from weak adsorbate-adsorbent interaction, but the step, the plateau and hysteresis loop are indicative of a porous material. It should be noted that it can be either meso or micropores. For instance, highly microporous and hydrophobic carbon materials will give a type I isotherm with nitrogen or hydrocarbon vapours, while a type V will be obtained with water vapour.

The cases described are the simpler and extreme situations. If the material possesses several types of pores and also external surface, the resulting isotherm will be a composite. For instance, a microporous material with high external surface will give rise to a nitrogen isotherm with an overall shape similar to type II, but with type I character at low pressures. Also the hysteresis loops in Figure 1 are the most common, but other peculiar loops have been observed on, for instances, novel mesoporous materials.

4.4. SOME CLASSICAL THEORIES FOR THE QUANTITATIVE ANALYSIS OF ADSORPTION ISOTHERMS

4.4.1. The Brunauer-Emmett-Teller theory and the BET method

In spite of the criticisms that it has been subjected to and its limitations, it is undeniable that the equation based on the theory developed in 1938 by

Brunauer, Emmett and Teller (BET) is still the one most used for surface area determination and in many situations with great success. The model and assumptions underlying the BET equation can be resumed as: it considers a nonporous and energetically uniform surface, consisting of sites where the adsorption in the first layer occurs; the molecules in the first layer act as sites for adsorption of additional molecules leading to the multilayer formation that can start before the first layer is completed; "lateral" interactions adsorbate-adsorbate are considered negligible; at equilibrium pressures, the adsorbed amounts are constant in each layer, resulting from equal rates of adsorption and desorption for each layer; the second and subsequent layers are treated equally, but different from the first, namely the adsorption energy is considered to be the same as the molar energy of condensation of the adsorptive; the number of layers is assumed to be infinite at $p/p^o=1$.

On the basis of these assumptions of this kinetic theory of monolayer-multilayer adsorption, and also later on by a statistical mechanical treatment, the BET equation has been deduced, and is applied in a form such as:

$$\frac{p/p^o}{n_{ads}(1-p/p^o)} = \frac{1}{n_m\,C} + \frac{C-1}{n_m\,C}(p/p^o)$$

(1)

where n_m is the *monolayer capacity*, which is defined as the amount of adsorbate needed to cover the surface of unit mass of material in a complete single molecular layer, and C is a parameter related with the molar energy of adsorption in the first layer.

If the plot of $(p/p^o)/[n_{ads}\,(1-p/p^o)]$ versus p/p^o is linear, the n_m and C values can be obtained from the corresponding slope s and intercept b as:

$n_m = 1/(s+b)$ (2)

and

$C = s/b + 1$ (3)

The C value does not allow calculating the energy of adsorption of the first layer, but it merely gives a qualitative indication. The higher is the adsorption

energy of the first layer, the higher is the C value. Considering the definition of n_m it is easily understood that it can be converted into a specific surface area, A_s, using:

$$A_s = n_m \, a_m \, N_A \tag{4}$$

where a_m is the area occupied by one molecule in the monolayer (*molecular cross-sectional area)* and N_A is Avogadro's number. There are therefore two aspects on which the surface area relies: the proper way of obtaining n_m and to ascertain its physical meaning, and the validity of the a_m considered.

The linear region is always restricted to a low relative pressure range. Normally, it is neither inferior to a p/p^o of 0.01 nor superior to 0.3, but the exact range of linearity depends on the gas-solid system and in some cases is no higher than $p/p^o \sim 0.1$. Therefore the BET method should not be applied blindly but the plot has to be drawn. Some criteria have been proposed for choosing the adequate linear region of the BET plot[6,7], and one is certainly that the C value cannot be negative. Now, even if a nice linear plot is obtained, the n_m and A_s values may have doubtful physical meaning.

It is clear that one has to look for the situations where, at low pressures, surface coverage (on open surface or on pore walls) exclusively occurs and this will be the case for type II, IV and also Ib isotherms, and when primary micropore filling is absent. Usually, for type II isotherms the linear region extends to a reasonable range of relative pressure, but rarely higher than 0.3. For type IV and, in particular, for type Ib, special care has to be taken to consider only the range before capillary condensation or secondary micropore filling starts. The value of A_s will correspond to a total surface area, which in the case of type IV or type Ib isotherms will include the area of the pore walls and the external surface area. A better applicability of the BET method and validity of the n_m value (and also of A_s due to a_m) is found when the C value is in the range of ~50 to ~150. This is usually achieved with nitrogen at 77K on many solids, and

is one of the reasons for this adsorptive to be recommended for surface area determination.

When equation 1 is applied to type Ia isotherms, it may give a linear plot, although usually in a very limited range of low relative pressure. However, type Ia is obtained when primary micropore filling occurs, with no prior monolayer coverage of the pore walls. Therefore, the "n_m" certainly does not correspond to a *monolayer capacity*. This also applies if the resulting isotherm is type Ib or appears to be type II or IV but the material contains narrow micropores filled by a primary process. Recently, Rouquérol *et al.*[7] have presented a detailed examination of the applicability of the BET equation to microporous materials and suggested that in order not to lose its benefits, the quantity n_m could be called the "*BET strong retention capacity*".

Consequently, whenever primary micropore filling is present, the "A_s" will not be a surface area. Nevertheless, this figure can be presented for comparison purposes between several materials, but is usually referred to as an *apparent surface area*. Indication of the presence of primary micropore filling is, usually, provided by the very high C values obtained, namely of several hundreds or even thousands, in qualitative agreement with a considerable enhancement of adsorption energy in very narrow micropores.

For type III and V isotherms the "n_m" also does not correspond to a *monolayer capacity* as in these cases monolayer coverage does not occur at low pressures, being overtaken by multilayer adsorption starting in a few favourable sites. The corresponding C values are very low, reflecting very weak adsorbate-adsorbent interactions.

Now having ascertained when the n_m values can be reliable, we go to the other aspect: the conversion into surface area using equation 4. This requires the use of the right value for a_m. The usual way is to assume that the density of the adsorbed monolayer is the same as that of the bulk liquid adsorptive, and to calculate it from:

$$a_m = f \left(\frac{M}{\rho_L N_A} \right)^{2/3}$$

$$(5)$$

where M is the molar mass of the adsorptive, ρ_L is the density of the liquid adsorptive at the operational temperature and f is the packing factor, usually considered 1.091 for hexagonal close packing. However, for many systems it has been found that the values obtained in this way may not be adequate and, furthermore, that a_m for a certain adsorptive may not be the same on different adsorbents. In this context, the adsorptive that appeared to be the most suitable has been nitrogen at 77K and the corresponding a_m is $0.162nm^2$. Nevertheless, even in this case, there is some uncertainty in some systems. For instance, it has been suggested that on silica the a_m for nitrogen can vary with the degree of hydroxylation[3]. In fact, there has been some tendency for some adsorption scientists to favour argon for surface area determination. However, the "BET-nitrogen area", using a_m of $0.162nm^2$, is so universally used and associated with advantageous practical features, that it is unlikely that it will be replaced in the near future.

4.4.2. The Dubinin theory and the DR method

For the particular case of microporous materials, the theory of volume filling of micropores (TVFM), proposed in 1947 by Dubinin, lead to the well known Dubinin-Radushkevich (DR) equation which is still widely used.

The TVFM theory is based on the thermodynamic theory of potential of Polanyi that considers that the amount adsorbed is only dependent on the adsorption potential (A). Based on this theory there will be a characteristic curve (surface coverage versus A) invariant with temperature for each adsorptive.

In practical terms, the contribution of Dubinin was to propose for the characteristic curve the following mathematical expression in terms of fractional filling of the micropore volume:

$$V_{ads} / V_{mic} = \exp \{-[A/(E_o \beta)]^2\} \quad (6)$$

where A is the Polanyi adsorption potential given by:

$$A = RT \ln (p^o/p) \quad (7)$$

and V_{ads} is the volume adsorbed, V_{mic} is the micropore volume, E_o is constant for a given solid and designated *characteristic energy* and β is constant for a given adsorptive and designated the *affinity factor*. This later is a scale factor that allows superposition of the characteristic curves of different adsorptives obtained in the same material. Dubinin chose benzene as standard and, consequently, for other adsorptives y, $\beta=\beta(y)/ \beta(benzene)$.

By combining equations 6 and 7, the usual form of the DR equation is:

$$\log V_{ads} = \log V_{mic} - D \log^2 (p^o/p) \quad (8)$$

with

$$D = 2.303 [RT/(E_o \beta)]^2 \quad (9)$$

If a plot of $\log V_{ads}$ as a function of $\log^2 (p^o/p)$ is linear, the micropore volume and the E_o can be obtained from the intercept and slope, respectively. An aspect to take into consideration is that it is usually assumed that the density of the adsorbate is equal to that of the liquid, at the operational temperature, which may not be valid for all systems.

This equation should only be applied in the very low relative pressure range where primary micropore filling occurs. Therefore, the reliability of the parameters obtained greatly depends on the accuracy of pressure measurements and, in addition, care should also be taken in choosing the linear region. It has been found that equation 8 best applies to systems where only primary micropore filling occurs, and the linear region extends usually up to p/p^o of ~0.05. When secondary micropore filling also occurs, the linear region is shorter, and usually up to only p/p^o ~0.01 or 0.005. It should be noted that at

low pressures not only does primary micropore filling occur, but some adsorption on open surface and wider pores is not excluded. So, when these are also present to a significant extent, the "V_{mic}" obtained from applying equation 8, will be superior to the amount in ultramicropores, whatever care is taken in choosing the linear region.

Nevertheless, the comparison of values of "V_{mic}" (or without converting into liquid volume) obtained with different adsorptives is, usually, useful to elucidate the porosity.

Variants of the DR equation are the Dubinin-Astakov (DA) with an adjustable parameter N replacing the exponent 2 in equation 6, the more elaborate Dubinin-Stoeckli (DS)[8], that considers the sum of the contributions from several groups of pores, and, curiously, the Dubinin-Radushkevich-Kaganer (DRK), with analytical form similar to the DR equation, but that gives a good linear plot when applied to adsorption data on a nonporous surface[9]. This shows that if considerable external surface is present besides microporosity, an overestimation of the micropore volume can be obtained.

4.5. ANALYSIS OF ADSORPTION ISOTHERMS BY EMPIRICAL COMPARISON METHODS

4.5.1. Principle of the methods

The principle underlying any comparative method is that when isotherms of the same adsorptive on different materials are normalised, they become superimposed if the mechanism of adsorption is the same in the same pressure regions. In practice these comparison methods are usually applied by comparing an isotherm to be analysed with a reference isotherm, in a reduced form, of the same adsorptive obtained on a nonporous material with surface chemistry similar to that of the material under analysis. In early work, de Boer and co-workers proposed the existence of a *universal* curve for a given

adsorptive on different nonporous adsorbents, but subsequently they realized that the word universal should not have been used. It is now generally agreed that the reference material and the test adsorbent should have similar surface chemistry.

The reduced variable for the reference isotherm can be for instance n/n_m or n_{ads}/A_s, but the most well known are the $\underline{t}$ and α_s reduced variables proposed, respectively, by de Boer and by Sing.

The t is the *statistical thickness* of the adsorbed phase given by:

$$t = (n_{ads} / n_m) \; d' \tag{10}$$

where n_{ads} and n_m refer to the reference, with the latter being obtained by the BET method, and d' is the mean thickness of one adsorbed layer. Assuming again that its density is equal to that of bulk liquid adsorptive, d' can be calculated as:

$$d' = M/ (a_m \, N_A \, \rho_L) \tag{11}$$

where the terms are as previously defined. For instance, for nitrogen at 77K this assumes the value of 0.354nm.

The $\underline{\alpha}_s$ is simply:

$$\alpha_s = n_{ads}/ (n_{ads})_x \tag{12}$$

where $(n_{ads})_x$ is the adsorbed amount at a selected relative pressure of x, for the reference. For nitrogen at 77K this is usually done at p/p^o of 0.4, as at this pressure micropore filling is complete and in many systems capillary condensation in mesopores has not started yet.

The way to apply the t and the α_s methods and the type of information they provide are the same. The "t plot" or the "α_s plot" consists of representing the n_{ads} obtained on the material under analysis as a function of the t or α_s values taken from the reference adsorption isotherm (t or α_s against p/p^o) at the same p/p^o. Linearity is obtained in the p/p^o regions where the adsorption on the material under study occurs as on the reference material. Therefore, a value of

surface area for the material under analysis can be calculated by multiplying the slope $\underline{s}$ of a linear region by a calibration factor. It is easy to verify that for the t method, the expression takes the form:

$$A_s (t) = s (M/\rho_L)$$ (13)

where M and ρ_L refer to the adsorptive, while in the case of the α_s method it is:

$$A_s (\alpha_s) = s [A_s^{ref}/(n_{ads})_x]$$ (14)

where A_s^{ref} and $(n_{ads})_x$ are the values for the reference material.

So, by the comparison methods the surface area is obtained without the need to evaluate n_m for the material under analysis.

In both methods, if the linear regions have positive intercepts $\underline{b}$, these will correspond to adsorbed amounts in pores that are filled at pressures below the beginning of the linear regions and can be converted into pore volume, using:

$$V_p = \frac{n_p \, M}{\rho_a}$$ (15)

where n_p (equal to b) is the *pore capacity* that is the amount of adsorbate that completely fills the pores and ρ_a is the density of the adsorbate in the pores. Almost invariably, it is assumed that the adsorbate density is the same as in the bulk liquid, at the operational temperature. The uncertainty of this assumption may not be restricted to microporous materials. For instance, nitrogen at 77K often gives higher pore volumes than organic vapours at higher temperatures, not only in the case of microporous materials, but also for mesoporous materials, as verified on ordered mesoporous silicas[10]. Therefore the pore volume should always be indicated together with the adsorptive used.

In some situations, the area of walls of a group of pores can be obtained and the ratio of pore volume to surface area of its walls, known as the *hydraulic radius* (r_h), can be used to estimate the *pore size*. This is defined as the *pore width*, the distance between the opposite walls of the pore, and its relation with

r_h depends on the pore geometry. For instance, for an open-ended cylindrical pore, the width will correspond to pore diameter and for a set of these non-intersecting pores with the same width can be calculated as:

$$D_P = \frac{4\,V_P}{A_P}$$

(16)

while for a parallel-sided slit shaped pore, the width will be the distance between the opposite walls of the slit and for a group of these pores can be calculated as:

$$w_P = \frac{2\,V_P}{A_P}$$

(17)

In both cases, A_P is the area of walls of the group of pores, and may be obtained from the difference between the total surface area (A_s) and that external to the pores (A_{ext}).

4.5.2. Interpretation of the t or α_s plots

In Figure 2 are shown some ideal plots. To understand them it is now only necessary to bear in mind the principles and the mechanisms of adsorption earlier described.

If the material under analysis is completely nonporous as the reference, the plot will be like in Figure 2 (a), that is an extensive straight line that can be *extrapolated to the origin*. From the slope $\underline{s}$ and equations 13 or 14, the surface area can be obtained. In many cases, small deviations as illustrated in Figure 2 (a) can be detected before the linear region, at very low monolayer coverage, indicating differences in surface chemistry. In fact, it is very difficult to have a reference material with exactly the same surface chemistry as the material under analysis. Positive deviations indicate a higher interaction adsorbent-adsorbate in the material under analysis as compared to that on the reference, the opposite occurring for negative deviations. As the amount adsorbed increases the surface sites become screened and the plot is linear, allowing the determination of the

surface area. The presence of very narrow micropores, that are filled by a primary process, is detected by a positive intercept b of a linear region with slope s2, starting at very low t or α_s values, as illustrated in Figure 2 (b) for case A. The intercept b corresponds to n_p and can be converted into a *micropore volume* using equation 15. From the slope s2 and equation 13 or 14, the *external* surface area is obtained.

(a)   (b)   (c)
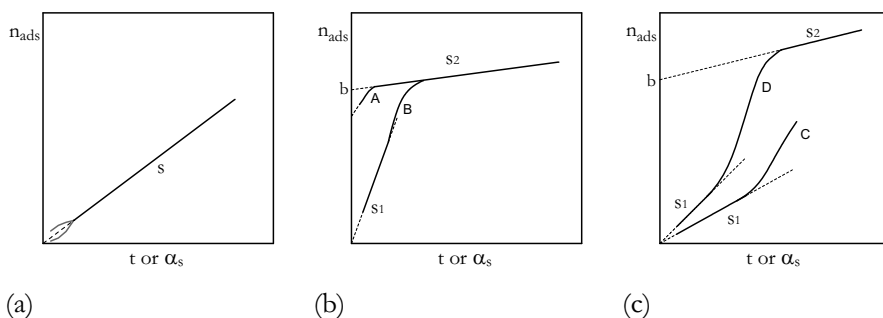
Figure 2 - Hypothetical t or α_s plots for (a) nonporous, (b) microporous or (c) mesoporous material.

If on the other hand, the t or α_s plot has a first linear region going through the origin, as in Figure 2 (b) case B, it indicates pore wall coverage without enhanced adsorption and therefore a secondary micropore filling process and the absence of primary micropore filling. The slope s1 of the first linear region will provide the *total* surface area, including external surface and that internal of the supermicropores. From the second linear region, after the pore filling is complete, it is possible to obtain the *external* surface from s2 and the *micropore volume* from b.

The presence of mesoporosity is detected by upward deviations after an initial linear plot, as shown in Figure 2 (c), indicating the onset of capillary condensation. So, from the slope s1 the *total* surface area, including mesopore area and external surface area, can then be obtained. If the situation is as

illustrated in Figure 2 (c) case C, nothing else can be obtained other than to note that there is mesoporosity. On the other hand, if the situation is as illustrated in Figure 2 (c) case D, then from the slope s2 and intercept b the *external* surface area and the *mesopore volume* can, respectively, be obtained.

In this situation, and also that described in the previous paragraph, the surface area of walls of the pores can be obtained ($A_p=A_s - A_{ext}$) and the mean pore width can be estimated from relations of the type of equations 16 or 17.

Now, if the plot is similar to those of case B in Figure 2 (b) and Figure 2 (c), but the first line cannot be extrapolated to the origin, that is with a positive intercept (not shown), it indicates that, in addition, primary micropore filling is also present. The intercept b will then include the amount adsorbed in all pores, allowing us to obtain the *total* pore volume, including that of the ultramicropores. The slope s2 will allow us to obtain the *external* surface area. If there is a good definition of the straight line s1, it may be possible to obtain from s1 the area of the external surface and of the rest of the pores (wider micropores or mesopores) as before, and the ultramicropore volume from the first intercept (not shown). However, in some cases this is not possible.

To overcome this limitation, an interesting method that can be useful is the method of n-nonane pre-adsorption, proposed in 1969 by Gregg and Langford and now used in combination with the t or α_s methods. Due to their narrow size, the n-nonane molecules are able to enter into narrow micropores, but due to the high physisorption energy, associated with the long chain, they remain there upon outgassing at room temperature or slightly higher, while being desorbed from wider pores and open surface. Therefore the method consists of determining the nitrogen adsorption isotherm on the material with and without n-nonane pre-adsorbed. If there is no blocking of wider pores by nonane retained in connected narrow pores, the analysis of the data will allow separation of the amount adsorbed in the narrow micropores from that on the

rest of the material and can provide a reliable estimation of the ultramicropore volume[11].

4.5.3. Some comments

Despite their empirical nature, these comparison methods are particularly useful, as they can provide in one single plot the analysis of the whole isotherm and important information, both qualitative and quantitative, about the porosity present in the sample.

For instance, sometimes the isotherm can appear type II or IV, but it is not certain if ultramicropores are absent. A high C from BET method can lead to suspicion, but definite confirmation is provided if the t or α_s linear plot cannot be extrapolated to the origin. Similarly for mesoporosity, the shape of the isotherm may be close to type II, if the pores are wide and there is a broad pore size distribution and high external area. An upward deviation in the comparison plot will confirm the presence of mesoporosity.

In many systems it is possible to separate different components contributing for the surface area, while from the BET method solely the total surface area is obtained. Furthermore, these comparison plots can make a direct correction for adsorption on the surface external to the group of pores and allow us to obtain solely the pore capacity. This is not the case when the micropore volume is obtained from the DR method and also when the total pore volume is estimated from the amount adsorbed at, for instance, p/pᵒ of ~0.95. First, it is quite evident that when the isotherm rises asymptotically at high relative pressure, the error will be enormous and the value obtained has no meaning. When there is a good plateau on a type IV isotherm, indicating low external area, the estimation at p/pᵒ of ~0.95 is satisfactory, but even so the amount adsorbed will include also adsorption on external surface and the corresponding liquid volume will be higher than the pore volume[10].

There are of course limitations in the comparison methods. One is that if the material has a very heterogeneous porosity, ranging from narrow micropores to wide mesopores, the plots are far from the ideal cases shown. It may be very difficult to ascertain the linear regions or they may be inexistent.

Another important aspect is that the information provided relies on the use of the correct reference isotherm. This can be a problem as there are not many reference data in the literature, regarding different nonporous materials and also adsorptives. Nevertheless, if there is no alternative, a reference isotherm of the same adsorptive but on a slightly different solid, can be used tentatively and, usually, the main problem is in the monolayer region. In some situations, the adequacy of a reference isotherm at low pressures can be checked by comparing the surface area obtained by the comparison method with the BET area. However, in many cases, one has to obtain one's own reference data. Sometimes it may not be necessary to use for reference a strictly nonporous material, which in fact is difficult to produce. For instance, if we submit a material to treatments that creates microporosity, but without changing the external surface and wide porosity, the data on the starting material may be used as reference for the modified samples. The comparison plots will be linear in the multilayer and condensation ranges and will allow us to probe the changes in the microporosity[12], as long as there are not very significant alterations in the surface chemistry.

4.6. PORE SIZE AND PORE SIZE DISTRIBUTIONS

The evaluation of real pore sizes is still a current problem, even when the pores have a simply defined geometry. As mentioned previously, an estimation of the mean pore width can be obtained in some situations from the t or α_s methods. However, limitations regarding the density of the adsorbate and the surface area[10], may lead to inaccurate pore sizes, although they can sometimes be used for comparative purposes in a series of samples. Furthermore, they only

provide an average value for a group of pores, which will be enough information if there is a very narrow range of pore sizes in the material. Another useful parameter is the pore size distribution (PSD), that is for instance a curve of dV_p/dD_p against D_p.

For mesopores this is commonly obtained from a single isotherm by using traditional methods, such as those of Barrett, Joyner and Halenda (BJH), Pierce, Cranston and Inkley (CI) and Dollimore and Heal (DH). These methods differ in details of computing procedure and assumptions, and examples are provided in the literature[3,4,13]. But all have in common the use of the Kelvin equation, which is based on classical thermodynamics and relates the radius of the meniscus with the p/p^o at which condensation or evaporation occurs. Afterwards, it is necessary to correct for the thickness of the pre-adsorbed film (using a reference curve) and assume a pore geometry in order to obtain the pore width.

Another common feature of these methods is that they underestimate the size of narrower mesopores, for which the macroscopic Kelvin equation no longer remains valid. A refined modification was proposed in the late 60s by Broekhoff and de Boer (BdB), by allowing for effects of curvature on the pore size analysis, which, although not used for many years, is now becoming more popular not only with nitrogen but also with other adsorptives[14]. In recent years, adsorption studies of nitrogen or argon on model adsorbents with cylindrical mesopores, and comparison with pore sizes calculated using density functional theory and molecular simulations, indicate that the Kelvin equation underestimates the size for pores of 20nm width or less, becoming progressively more inaccurate as the pore size decreases, and that the BdB modification extends the applicability to ~7-8nm[5]. Recently, improvements of the BdB method to smaller pores have been proposed for nitrogen adsorption[15].

However, if more adequate methods are not accessible, those like BJH, even when inaccurate in absolute terms of mesopore size, can be and, in fact, are still widely used to obtain qualitative information about the pore size uniformity from the PSD.

With regard to PSD for micropores the situation is still a complex issue. Certainly, methods based on the Kelvin equation cannot be applied, but others like the DS, Horvath-Kawazoe (HK), density functional theory and molecular simulations have been used. However, it appears that at present there is no established and reliable procedure to compute them from a single isotherm. For the characterisation of microporosity it is useful to employ several adsorptives of different molecular dimensions and to take into account the different stages of micropore filling and the eventual inaccessibility to the micropores.

4.7. CONCLUDING REMARKS

Gas-solid physisorption is one of the few non-destructive methods to characterise powders and nanoporous materials. In many cases values of surface area, pore volume and pore width can be obtained by proper analysis of gas adsorption isotherms. However, one should be aware that there are limitations that require care in the analysis of adsorption data and on the significance of the parameters obtained.

The first step is the qualitative interpretation of the adsorption isotherm. After this, a comparison method, such as t or α_s, is useful to obtain more detailed qualitative information about the type of porosity present. Then proceed to the quantitative analysis of the isotherm by the comparison methods and others which are appropriate for the system being studied.

Finally, it should be noted that the use of different carefully selected adsorptives is advisable as it can often provide important complementary information.

References

1. K.S.W. Sing., D.H. Everett, R.A.W. Haul, L. Moscou, R.A. Pierotti, J. Rouquérol, T. Siemieniewska, *Pure Appl. Chem.*, **1985**, *57*, 603.

2. J. Rouquérol, D. Avnir, C.W. Fairbridge, D.H. Everett, J.H. Haynes, N. Pernicone, J.D.F. Ramsay, K.S.W. Sing, K.K. Unger, *Pure Appl. Chem.*, **1994,** *66,* 1739.

3. F. Rouquérol, J. Rouquérol, K.S.W. Sing, *Adsorption by Powders and Porous Solids. Principles, Methodology and Applications*, Academic Press, London, **1999**.

4. S.J. Gregg, K.S.W. Sing, *Adsorption, Surface Area and Porosity*, 2nd Ed., Academic Press, New York, **1982**.

5. A.V. Neimark, P.I. Ravikovitch, A. Vishnyakov, *J. Phys.: Condens. Matter,* **2003**, *15*, 347.

6. J.B. Parra, J.C. Sousa, R.C. Bansal, J.J. Pis, J.A. Pajares, *Adsorption Sci. Tech.*, **1994**, *11*, 51.

7. J. Rouquérol, P.L. Llewellyn, F. Rouquérol in P.L Llewellyn., J. Rouquerol, F. Rodriguez-Reinoso, N. Seaton, (Eds.), *Characterization of Porous Solids VII*, *Studies in Surface Science and Catalysis*, Elsevier, Amsterdam, **2007**, vol. 160, pp. 49.

8. M.M. Dubinin, H.F. Stoeckli, *J.Colloid Interface Sci.*, **1980**, *75*, 34.

9. D. Hugi-Cleary, F. Stoeckli, *Carbon*, **2000**, *38*, 1309.

10. M.M.L. Ribeiro Carrott, A.J.E. Candeias, P.J.M. Carrott, P.I. Ravikovitch, A.V. Neimark, A.D. Sequeira, *Micropor. Mesopor. Mater.*, **2001**, *47*, 323.

11. P.J.M. Carrott, F.L. Conceição, M.M.L. Ribeiro Carrott, *Carbon*, **2007,** doi:10.1016/j.carbon.2007.01.008.

12. M. Ribeiro Carrott, P. Carrott, M.B. Carvalho, K.S.W. Sing, *J.Chem.Soc., Faraday Trans.*, **1991**, *87,* 185.

13. J.L. Figueiredo, F. Ramôa Ribeiro, *Catálise Heterogénea*, Fundação Calouste Gulbenkian, Lisboa, **1989**.

14. P.A. Russo, M.M.L. Ribeiro Carrott, A. Padre-Eterno, P.J.M. Carrott, P.I. Ravikovitch, A.V. Neimark, *Micropor. Mesopor. Mater.*, **2007**, doi:10.1016/j.micromeso.2007.01.032.

15. P. Kowalczyk, M. Jaroniec, A. P. Terzyk, K. Kaneko, D.D. Do, *Langmuir*, **2005**, *21*, 1827.

(Página deixada propositadamente em branco)

5. FUNDAMENTAL ASPECTS IN ZEOLITES SYNTHESIS AND POST-SYNTHESIS MODIFICATION

M. Filipa Ribeiro and Auguste Fernandes

IBB-Institute for Biotechnology and Bioengineering, Centro de Engenharia Biológica e Química, Departamento de Engenharia Química, Instituto Superior Técnico, Av. Rovisco Pais, 1049-001 Lisboa, Portugal.

5.1. HISTORICAL OVERVIEW

Zeolites (Greek, zein, "to boil"; lithos, "a stone") are minerals that have a micro-porous structure. The term was originally coined in the 18th century by a Swedish mineralogist named Axel Fredrik Crönstedt who observed, upon rapidly heating a natural mineral, that the stones began to dance about as the water evaporated. Using the Greek words which mean "stone that boils," he called this material zeolite. In 1784, Barthelemy Faujas de Saint-Fond, a French professor in geology, reported for the first time the peculiar properties of zeolites among minerals and formulated them in his book "Mineralogie des volcans ou description de toutes les substances produites ou rejetées par les feux souterrains" (published in 1784 in Paris). In his honor, a well-known zeolite was named Faujasite in 1842.

Natural zeolites are found in volcanogenic or metamorphic sedimentary rocks in contact with alkaline groundwater and are formed under particular geological conditions, e.g. low temperature (from 27 °C to 55 °C) and typical pH between 8 and 10; nature usually requires 50 to 50.000 years to complete zeolite formation. Until the early 1940s, attempts to synthesize zeolites were made by mineralogists. First efforts in reproducing natural zeolites in laboratory led, in 1940s, to Barrer[1] and Milton[2] works and the first preparation of synthetic zeolites, a mordenite analogous and the zeolite A (LTA structure), respectively.

The initial works in zeolites synthesis employed only inorganic reagents; in the early 1960s, organic compounds were also used as reagents source[3]. On the

threshold of Seventies, the use of quaternary ammonium salts allowed zeolites synthesis with a greater Si/Al ratio permitting the discovery of the zeolites Beta[4] and ZSM-5[5]. Since then, a large variety of new zeolite structures, including new zeotypes[6], among which aluminophosphates (AlPOs), silicoaluminophosphates (SAPOs)[7], gallo-phosphates (GAPOs)[7,8] and titanosilicates (such as ETS-10)[9] have been synthesized. These microporous materials present great variety of chemical compositions and frequently have structures with no zeolite analogue. More recently, mesoporous-structured materials, such as M41S and SBA families, have emerged. These mesoporous systems are synthesized using specific organic surfactants (long-chain organic molecules) and present pore sizes covering the 2-20 nm range[10].

As a result of the wide diversity observed in molecular sieve materials, concerning chemical composition, as well as structure or pores sizes, there are various synthesis methods, each one being optimized for a particular porous material, using specific experimental parameters. These different ways of preparation, the influence of the experimental parameters and also the molecular synthesis mechanisms, have been extensively described in many books[6,11-15], conference proceedings and review papers[16-18] . The International Zeolites Association (IZA) has also published a collection of procedures and methods related to the synthesis of many zeolites and similar materials known up to now[19].

5.2. INTRODUCTION TO ZEOLITES

5.2.1. Structure and pore system

Zeolites are a well defined class of natural or synthetic aluminosilicate materials. Their structure is formed by a three dimensional and regular network of SiO_4 and AlO_4 tetrahedra which are linked by their oxygen corners via a common oxygen atom (see scheme 1). Trivalent Al atoms in tetrahedral position (in the

zeolite framework), generate negative charges which are compensated by cations of different nature (Na^+, K^+, etc.).

$$(1)$$
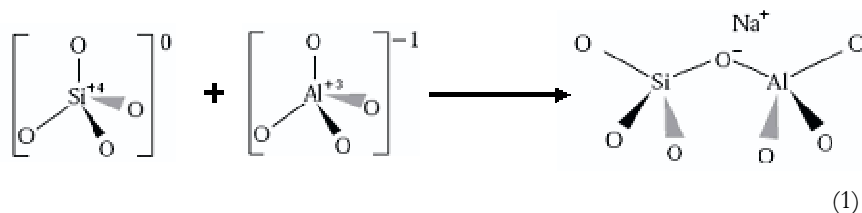
The framework of a zeolite contains channels, channel intersections and/or cages with dimensions ranging mostly from 0.2 to 1.5 nm. Inside these voids, water molecules and small cations which compensate the negative framework charge, are present. The chemical composition of a zeolite can hence be represented by a formula of the type:

$$(M^{m+})_{y/m} [(SiO_2)_x . (AlO_2^-)_y] . z H_2O \qquad (2)$$

where m is the valence of cation M, z is the number of water molecules per unit cell, $(x + y)$ is the number of tetrahedra SiO_4 and AlO_4^- per unit cell, and x/y is the so-called framework silicon/aluminum ratio (Si/Al). Lowenstein's rule prohibits that two contiguous tethrahedra contain tetracoordinated aluminum, i.e. Al-O-Al linkages are forbidden, or Si/Al $\geq$ 1. Silicon and aluminum in aluminosilicate zeolites are generally referred to as the T-atoms and are located at the vertices with the lines connecting them standing for T-O-T bonds.

In most zeolite structures the primary structural units, AlO_4 or SiO_4 tethrahedra, are assembled into secondary building units (SBUs) which may be simple polyhedra such as cubes, hexagonal prisms, or cubo-octahedra. The final framework structure consists of assemblages of the secondary units[13].

Actually more than 170 zeolite structures, covering the span of pore diameters from about 0.3 nm to 2nm, are approved. The database of the Structure

Commission of the International Zeolite Association (IZA) provides structural information on all zeolite structure types. This includes crystallographic data and drawings for all zeolite framework types, simulated XRD powder patterns for representative materials and relevant references (http://www.iza-structure.org/databases). A three letter code (eg. FAU for X and Y zeolite, MFI for zeolite ZSM-5, LTA for A zeolite, etc.) is assigned to each zeolite structure. Typical zeolite pore sizes using oxygen packing models are shown in Figure 1. Zeolites with eight-, ten- and twelve-membered ring pore openings for which, respectively, the terms small-pore, medium pore and large pore zeolites are used, strongly predominate, whereas the super-large-pore materials with pores formed by more than 12 TO4 tetrahedra and materials with pores formed by an unusual number of TO4 tetrahedra are still scarce. Zeolites with eight-membered ring pores are good catalysts for a limited number of reactions involving small reactant and product molecules (ex. conversion of methanol to olefins, MTO). For the majority of catalytic applications, medium and large pore zeolites will usually be preferred.
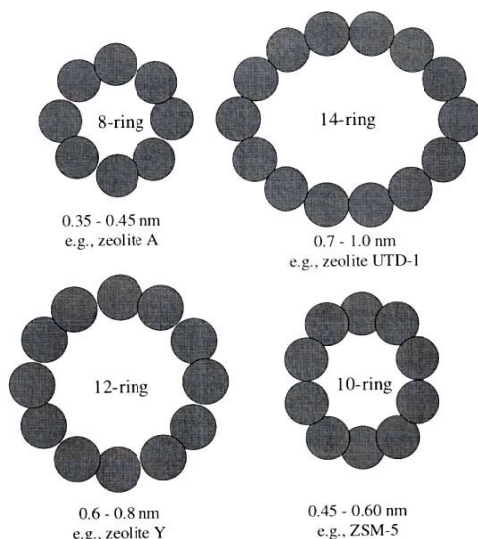
Figure 1 - Typical zeolite pore sizes illustrated with oxygen packing models.

Figure 2 shows examples of structures of four zeolites along with their respective void systems and pore dimensions. The faujasite (FAU) structure that corresponds to the synthetic zeolites X ($1 \leq Si/A\,l \leq 1.5$) and Y ($Si/Al < 1.5$) is formed using as secondary building unit the cube-octahedron, also referred to as a sodalite unit or β cage. The sodalite units are connected via their hexagonal faces, originating a three dimensional structure, with a twelve-membered-ring pore system. Its pore system is relatively spacious and consists of spherical cages, referred to as supercages, with a diameter of 1.3 nm, connected tetrahedrally with four neighboring cages through windows with a diameter of 0.74 nm formed by 12 TO_4 tetrahedra. ZSM-5 zeolite (Figure 2, line 2) is built using pentasil units. It has a three-dimensional pore structure with intersecting systems of ten-membered ring pores, one being straight and the other sinusoidal. Zeolite Theta-1 which is isostructural to zeolite ZSM-22 (Figure 2, line 3) possesses ten-membered ring pores and an unidimensional porous structure (TON structure).
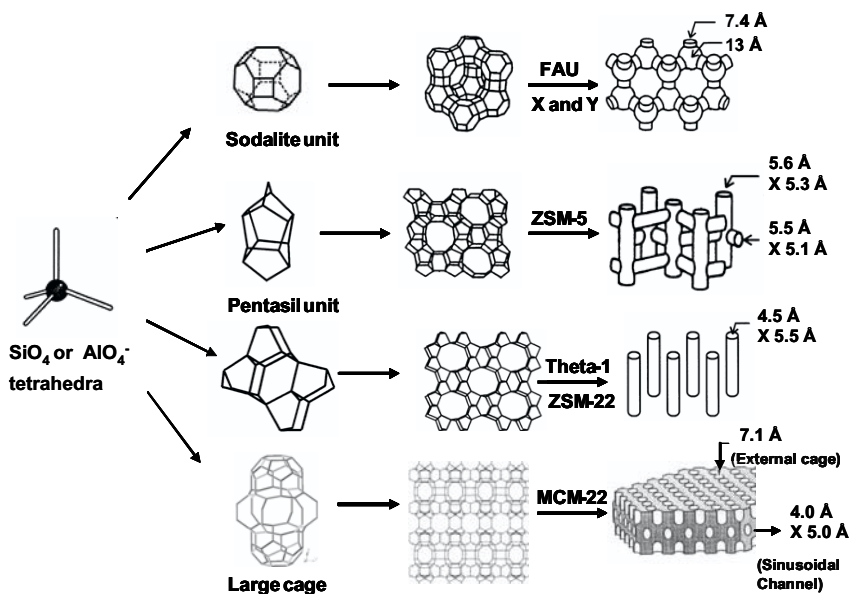
Figure 2 - Structures of four selected zeolites (Zeolites X and Y; ZSM-5; Theta-1 or ZSM-22 and MCM-22) and their micropore systems and dimensions.

The MWW zeolites family (line 4), including MCM-22, MCM-49, and ITQ-1, is an example of a bidimensional structure, differing only in Si/Al ratios. It contains two independent pore systems, both of them accessible through rings composed of ten tetrahedral T atoms. One of these pore systems is defined by two-dimensional, sinusoidal channels, while the other system consists of large supercages whose inner free diameter, 0.71 nm, is defined by 12 T-O species (12-rings) and whose inner height is 1.82 nm. These coexisting pore systems may provide opportunities for a wide variety of catalytic applications in the petrochemical and refining industries[14].

Zeolite Y is of extreme importance in heterogeneous catalysis because it is the active component in petroleum refining catalysts for fluid catalytic cracking (FCC process)[20]. ZSM-5 is another example of a zeolite which has gained enormous importance in heterogeneous catalysis. It is used industrially in the synthesis of ethylbenzene, isomerization of xylenes and in disproportionation of toluene, and it is often looked upon as the prototype of shape selective catalysts[21].

The shape and size of micropores may induce various kinds of shape selectivity, as reviewed by C. Marcilly[21]. Besides the highly favorable role in providing shape selectivity, the presence of micropores may in some cases also limit the catalytic performances of zeolites[22]. Bearing in mind that each zeolite structure can be modified by a plethora of post-synthesis techniques, an almost infinite variety of molecular sieve materials are nowadays at the researcher's and engineer's disposal. In many instances, one can tailor zeolite properties to a peculiar and desired application.

5.2.2. Chemical composition and properties of zeolites

Zeolites, in a narrow definition, are porous crystalline aluminosilicates having a uniform pore structure and exhibiting ion exchange behaviour. The ion exchange capacity of a zeolite depends on the chemical composition, i.e., a

higher ion exchange capacity being obtained in zeolites with lower SiO_2/Al_2O_3 ratio. The largest use (in volume) of zeolites is in detergent formulations, where they have replaced phosphates as water-softening agents, exchanging the sodium of the zeolite by the calcium and magnesium present in the water[14].

Today, a broad variety of zeolite-like microporous materials with T-atoms other than silicon and aluminum can be easily synthesized. These materials can be designated by the term zeotypes. The best known examples are microporous aluminophophates (AlPOs) or silicoaluminophosphates (SAPOs) and materials derived from them by incorporation of T-atoms other than Al and P [13]. The aluminophophate materials ($AlPO_4$-n) have a neutral framework and therefore have no ion exchange capacity. When some of the aluminum and/or phosphorus framework atoms are replaced by other atoms of different charge, as for example silicon, to form the so-called SAPO-materials, or with metals in addition or not to silicon, to form respectively the MeAPSO and MeAPO analogues, the framework becomes negatively charged with cation exchange properties and with weak to mild acidic catalytic properties. All these and related microporous materials, with still other T-atoms like Ti, V, Co, Fe, etc., are of considerable interest in catalysis. Titanium silicalite-1 (TS-1, MFI structure) is an example of a catalyst that is used on an industrial scale for the production of hydroquinone and catechol from phenol and hydrogen peroxide[23].

Many aluminosilicate zeolites can be synthesized over a wide range of aluminum contents, for example the zeolite ZSM-5 can be obtained with a Si/Al ratio from $\approx$ 10 to ∞. One of the technically most important members of the zeolite family, Faujasite, cannot be directly synthesized with Si/Al substantially higher than 2.5, at least not in economically reasonable crystallization times. It is, therefore, of great importance to find methods that can increase the Si/Al ratio. Various techniques for the post-synthesis modification of zeolite framework, i.e., by dealumination of the framework,

have been developed[24]. Conversely, the insertion of aluminum into the zeolite framework can be achieved as well[25].

Among the properties that are affected by the framework Al content, one can cite: the density of negative framework charge, the cation exchange capacity, the density of Brönsted acid sites, their strength, the thermal stability, the hydrophilic or hydrophobic surface properties and the unit cell dimensions. Brönsted acid sites in zeolites are characterized by bridging hydroxyl groups formed by the proton and a framework oxygen in an AlO_4 tetrahedron.

(3)

Upon severe heat treatment (> 500 °C) the Brönsted acid sites are removed (dehydroxylation) and water is split off with the concomitant formation of Lewis acid sites. The precise chemical nature of Lewis acid sites is less clear. They can be looked upon as tricoordinated aluminum and/or tricoordinated, positively charged Si in the framework[26].

(4)
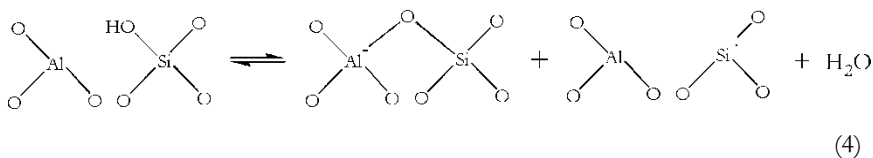
Zeolite catalysts are predominantly used in their acidic form (ex. FCC catalysts based on rare-earth exchanged FAU zeolites with small admixtures of ZSM-5, and catalytic dewaxing[27] using mordenite and ZSM-5), but they are also excellent supports for metals. These specific applications are not mutually exclusive; zeolite catalysts containing both acid sites and metal clusters (mono- or multimetallic) act as bifunctional catalysts. Zeolite supported metals are used for shape-selective hydrogenation, hydrodealkylation, isomerization,

hydroisomerization of naphtha fractions, hydrocracking of heavy petroleum distillates, CO hydrogenation, and other reactions. Details are given in some reviews[28]. More recently, the use of metal-containing zeolite catalysts (Cu, Co, Pd in ZSM-5 or other zeolites) for the selective catalytic reduction of nitrogen oxides with hydrocarbons, e.g. in exhaust gases from diesel engines, has become a topic of worldwide research[29].

The main emphasis of zeolite catalysts has been in reactions catalyzed by acids. However, if complete ion exchange with alkali metal ions such as K^+, Rb^+ or Cs^+ is carried out, it is possible to, not only, neutralize the Brönsted acid centers, but also prepare weakly basic zeolites[30]. This is particularly true if these neutral zeolites are then impregnated with alkali hydroxides[31].

5.2.3. Zeolite synthesis

Zeolites usually crystallize under hydrothermal conditions. The synthesis is, in general, carried out in a batch system where caustic aluminate and silicate solutions are mixed together and heated at a temperature held above the ambient at autogenous pressures for a defined period (hours, days or even weeks).

Figure 3 shows a simplified scheme of the different steps involved in the synthesis of a zeolite which can be summarized as follows:

1. The starting mixture is generally prepared using sources (mostly non crystalline) of the framework elements (Si and Al) and sources of the inorganic cations, in a basic medium (pH = 10-14). OH⁻ (or F⁻) mineralizing agents dissolve the starting mixture (depolymerization process) and a gel (mostly silicate and aluminate monomers/oligomers) is formed.

2. The gel (reaction mixture) is heated at temperatures above 100 °C in a sealed autoclave (see Figure 4), generating an autogenous pressure.

3. The reactants remain amorphous for some time, even after starting heating. This so-called "induction period" leads to the emergence of the first nuclei formed by the assembly of the secondary building units (SBUs), precursors of the zeolite crystals, as described by Barrer et al.[32].

4. After the induction time, the crystalline zeolite products grow up and can be detected (by XRD technique).

5. With time, amorphous gel is progressively replaced by crystalline zeolite product which is recovered by filtration, washing and drying.
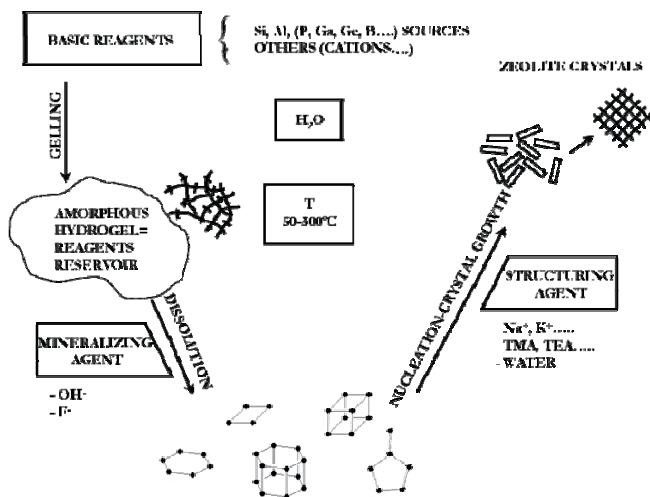
Figure 3 - Simplified mechanism of molecular sieve zeolite crystallization processes (Adapted from 15).
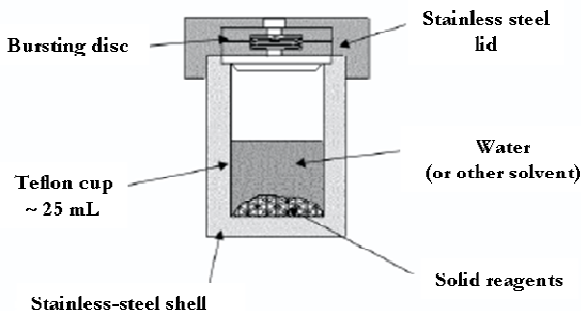
Figure 4 - A scheme of a Teflon™-lined, stainless steel autoclave typically used for hydrothermal synthesis.

Zeolites synthesis, like any other crystallization process, can be divided into three, distinct and fundamental steps, namely achievement of supersaturation, nucleation and crystal growth.

5.2.3.1. Solution supersaturation

Depending on concentration and temperature, a solution can be regarded as a stable, metastable or labile phase (see Figure 5).

The domains of stability and metastability are normally delimited by the solubility curve, corresponding to the equilibrium concentration of the solute C^* as a function of temperature. In contrast, the boundary between the metastable and labile region is not always well-defined. The degree of supersaturation (S) is defined as the ratio of the actual concentration C to the normal equilibrium concentration C^* ($S = C/ C^*$). Depending on the degree of solubility, crystallisation can occur or not: when the solution is in the stable region, no nucleation nor crystal growth can occur, while in the labile region spontaneous nucleation as well as crystal growth will occur. In the metastable domain, in principle only crystal growth can occur[15].
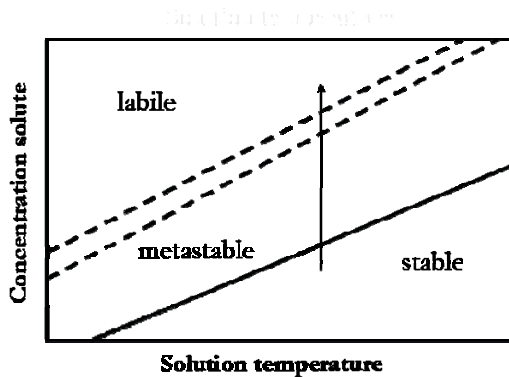
Figure 5 - The solubility-supersolubility diagram.

During the gel ageing (generally at a temperature slightly higher than that of the mixture), the concentration of soluble species, i.e. aluminosilicate precursors

increases with time (dissolution of the amorphous sources) and anionic aluminosilicate oligomer species appear. This increase of the solute concentration in solution, occurring usually at a constant temperature, will transform a stable solution into a metastable, and finally into a labile one.

5.2.3.2. Nucleation

Primary nucleation, from a supersaturated (labile) solution, can be homogeneous (from solution) or heterogeneous (provoked by foreign particles such as impurities). Secondary nucleation is induced by crystals and is a particular case of heterogeneous nucleation in which nucleating agents are crystals of the same phase. Obviously, heterogeneous nucleation can be avoided by filtration of the different solutes.

The nucleation is an activated process, and the nucleation rate J (number of nuclei formed per unit time) can be described using an Arrhenius-type equation:

$$J = A \exp (-\Delta G/RT) \qquad (5)$$

This equation predicts an exponential increase in the nucleation rate (J) as a function of temperature, and consequently, in the degree of supersaturation, since the concentration in solution increases exponentially with temperature. Experimentally, nucleation rate passes through a maximum, as the viscosity of the system increases, thus leading to nucleation inhibition.

5.2.3.3. Crystal growth

Zeolite crystal growth occurs at the crystal-solution interface by condensation of dissolved species, i.e. secondary building units, onto the surface of the crystals. The crystallization evolution observed with time shows a characteristic S-shaped curve representing the crystals yield as a function of the temperature, Figure 6. The crystallization profile can be described using the Kholmogorov

equation[33] $Z = 1-exp(kt^n)$, where Z is the ratio between the mass of the crystals at the instant t (M_t) and the mass of the crystals in the final product (M_f); k and n are constants that depend on the nucleation and growth conditions.
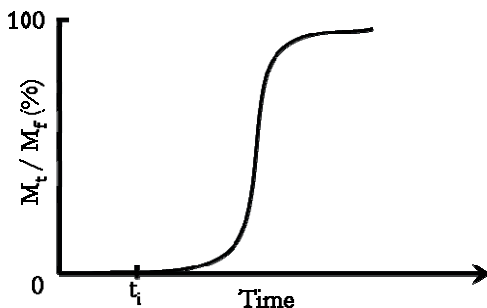
Figure 6 - Typical S-shaped crystallization curve showing crystals yield as a function of time: t_i corresponds to the end of the induction period.

The inflexion point of these sigmoidal curves corresponds to the passage of an auto-catalysed growth to a growth limited by the decrease, in solution, of the aluminosilicate precursors.

The size of zeolite crystals usually varies from a few tenths of a micrometer to a few tens of micrometers, but sometimes it can reach several hundred micrometers. The factors that normally determine the crystals size are: the initial supersaturation, the volume of the liquid fraction in the reaction mixture, the initial amount of nuclei, the overall nucleation rate during crystal growth and Ostwald ripening, i.e. the growth of the largest crystals at the expense of the smallest.

5.2.4. Synthesis parameters

Because many parameters can influence the zeolites formation, the synthesis of these molecular sieves is a difficult art that requires practice and precision,

above all when a particular material with specific structure and composition, and without any amorphous or crystalline impurities, is desired.

The procedure for zeolites synthesis involves many factors, physical and chemical, namely:

1. Nature of the reagents: the solvent, sources of framework atoms, sources of mineralizer, sources of inorganic cations and organic species.
2. Chemical composition of the reaction mixture.
3. Preparation of the starting mixture.
4. Reaction mixture ripening.
5. Seeding.
6. Crystallization temperature.
7. Heating time.
8. Agitation.
9. Pressure.
10. Reaction vessel.

All of these parameters are important but numerous. As a consequence, a large variety of microporous materials, with varying structure, chemical composition, crystal size and morphology can be prepared. Therefore, the overall description of a synthesis procedure should be as complete as possible. Hereafter, some of these parameters are discussed more in detail.

5.2.4.1. Source of framework atoms

The sources of the structural elements are various, each one presenting particular chemical properties (different reactivity) that will influence the synthesis, like the crystallization kinetics and also the catalytic properties of the final product.

In what concerns silicon, sources generally used are fumed silica, colloidal silica, silicon alkoxides, silicates and silicate hydrates. A special attention has to be

paid when deciding the type of source to use, each source having a particular reactivity, depending essentially on the size of the silica particles (when oxides are used), i.e. smaller the size of the particle, better the mineralization (hydrolysis) into crystallization precursor species. Some sources also contain impurities that can strongly influence the synthesis of a specific material, for example, when one wishes to obtain aluminum-free (silicalite) or high silica zeolites (high Si/Al ratios).

The aluminum sources are generally metal aluminates (especially sodium), aluminum hydroxide, aluminum oxide, pseudo-bohemite (AlOOH) and aluminum salts. As in the case of silicon, easily hydrolysable aluminum sources are generally preferred, and special attention is taken in what concerns the impurities present in the different sources.

5.2.4.2. Preparation and composition of the starting mixture

Every zeolite has a well-defined composition field, either large or reduced. The molar composition of the starting gel is usually expressed in terms of molar ratios of the oxides: Al_2O_3, $aSiO_2$, bM_xO, cR, dH_2O, where M is a metal (alkaline or alkaline earth) and R an organic species.

Generally, the specific crystallization field is illustrated using a ternary composition diagram for a given temperature and heating time. As an example, the ternary diagram presented in Figure 7 shows crystallization fields of zeolites A, X and Y.

The preparation conditions of the reaction mixture can also influence the final results, through the dissolution rate of the gels which mainly determine the nature and the concentration of the species present in the liquid phase, at a given time. This will depend essentially on: the reactivity of the reactants used, the method and order of their addition, the efficiency of the mixture homogenization, etc.. These parameters are of difficult control and may

originate problems and lack of reproducibility, for example in scaling-up procedures.
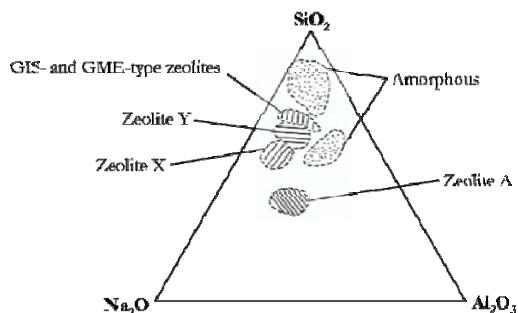
Figure 7 - Crystallization fields of zeolites A, X, Y and of type GIS and GME at 95 ºC, 24 h and $H_2O/Al_2O_3 = 140$. The fields shown correspond to compositions which were tested[34].

5.2.4.3. Effect of the mineralizer

Mineralizing agents are of crucial importance for nucleation and growth of zeolite crystals. Along with the OH^- anion largely employed to help in dissolution and crystallization processes, the F^- anion also plays a similar role and has been used in a few particular cases[35]. Both mineralizers are generally the counter-parts of the organic and inorganic cations used during the synthesis.

As a fact, reaction mixture pH generated by OH^- species helps zeolite formation by facilitating the dissolution of the precursors and the condensation of the aluminosilicate species. However, and because the nature of soluble species also depends on the pH (especially silicates species), the OH^- concentration will influence the crystals morphology and yield, together with the structure and composition of the final product. For example, alumina-rich zeolites crystallize preferably at a higher pH, a lower pH favouring silica-rich zeolites.

5.2.4.4. Effect of the organic template

Structure-directing agents (denoted as templates) contribute, in kinetic and thermodynamic aspects, to direct the framework formation of a specific zeolite. On one hand, aluminosilicate monomers and oligomers organize around the template by replacing water in the coordination sphere of the organic template, leading to zeolite precursors with a particular geometry that will govern the nucleation and growth of a singular zeolite. On the other hand, interactions between the organic molecule and the aluminosilicate species (coulombic, hydrogen and van der Waals bonds) tend to minimize the chemical potential of the framework, stabilizing the final zeolite. Figure 8 illustrates a schematic proposal of the mechanism for the synthesis of a zeolite (ZSM-5) that employs tetrapropylammonium as structure-directing agent.
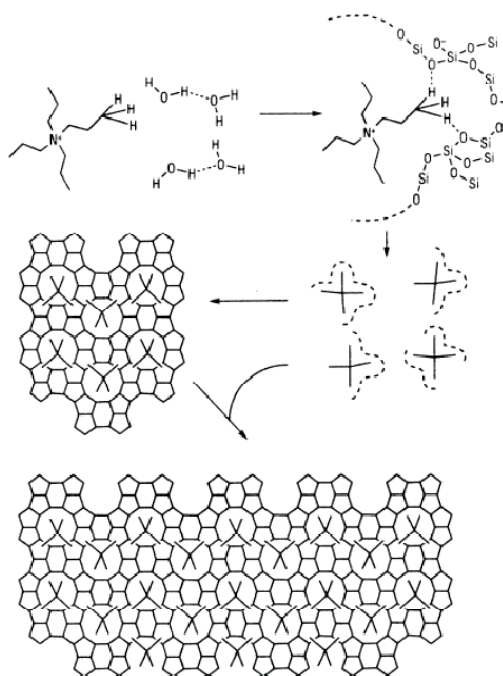
Figure 8 - Zeolite synthesis mechanism (adapted from 36).

Templates usually used are positively-charged species such as alkaline or organic cations. Neutral molecules (as for example water) that stabilize the framework by filling the pore voids can also play such a role. Other organic agents are also introduced as salts and basic molecules with OH⁻ as a counter-ion, the latter providing good pH regulation and control.

Thus, the selection of an organic template has to take into account some parameters like the charge density, the size and the shape, in order to provide the best stabilizing interactions. Template chemical properties, as solubility and basicity constant (pK_b), have also to be considered (reaction mixture pH regulation). Finally, templates can be simply used as pore filling or to control crystals morphology, purity degree and yield in product synthesis. As a general rule, a particular structure can be built using different template molecules and one template agent can be used to obtain several structures[37], even if sometimes only one structure-directing agent has to be used in order to synthesize a desired material, as in the case of SSZ-26 zeolite (see Figure 9).
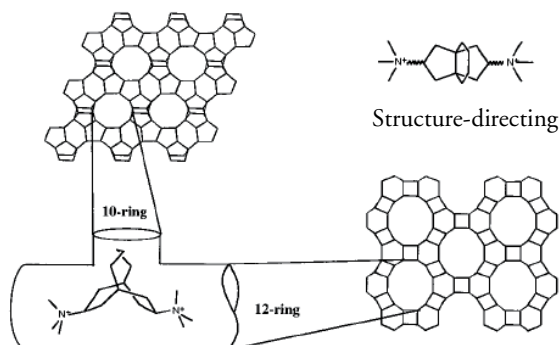
Figure 9 - Example of specific match between organic molecule used as template and asymmetric channels of SSZ-26 zeolite (adapted from 38).

5.2.4.5. Nature and sources of cations and organic templates

Inorganic cations are generally used for zeolite synthesis and especially alkali (Na^+, K^+, Li^+, Cs^+) and alkaline earth $(Ca^{2+}, Ba^{2+}, Sr^{2+})$ metals added as salts. In some cases, they can come from the sources of framework atoms (e.g. sodium aluminate or silicate). Organic molecules are rather preferred for the synthesis of silicon-rich zeolites and phosphor-containing microporous like AlPOs and SAPOs. Quaternary ammonium ions (tetramethyl TMA^+, tetraethyl TEA^+ and tetrapropyl TPA^+ ammoniums ions) are normally used (OH^- or halogen species X^- being the counter-ions) but it can also be mentioned the use of amines (dialkyl and trialkyl amines) that can be protonated or not, depending on the synthesis conditions. As an example, ZSM-5 zeolite (MFI structure) was first synthesized using Na^+ and organic templates, though TPA^+ has been shown to better direct MFI structure formation. The use of more complex organic molecules (crown ethers) along with Na^+ ions leads to the formation of zeolites with the FAU structure (with a higher Si/Al ratio), and the hexagonal FAU analog with the EMT structure. In the peculiar case of AlPOs, SAPOs and MeAPOs (metal-containing aluminophosphates), more than 100 organic molecules have been shown to play an effective template role. Table 1 presents some examples of templating agents typically used in the synthesis of these materials[13,39]. The structure code therein refers to zeolite type definition according to the International Zeolite Association. As observed in the table, some organic templates can favour only one, two or three particular structures (depending on the experimental conditions), while a peculiar template can be used for the formation of several different structures (as for example the tetraethylammonium TEA^+ ion).

TABLE 1 - Examples of organic molecules used as templates in the synthesis of AlPOs, SAPOs and MeAPOs materials. The designation (x) refers to AlPO-x, SAPO-x and MeAPO-x materials.

Designation (x)	Zeolite type (structure code)	template agent
5 (large pores)	AFI	cyclohexylamine
		Dipropylamine (DPA)
		N,N-dimethylbenzylamine (BDMA)
		Triethylamine (TEN)
		Tripropylamine
		Tetraethylammonium (TEA)
		Tetrapropylammonium (TPA)
11 (medium pores)	AEL	Dipropylamine (DPA)
		diisopropylamine
16 (very small pores)	AST	quinuclidine
18 (small pores)	AEI	Tetraethylammonium (TEA)
		N,N-diisopropylethylamine (DIPEA)
20 (very small pores)	SOD	Tetramethylammonium (TEA)
34 (small pores)	CHA	Tetraethylammonium (TEA)
		Isopropylamine (MIPA)
		Morpholine
36 (large pores)	ATS	Tripropylamine
37 (large pores)	FAU	Tetrapropylamine + Tetramethylamine
40 (large pores)	AFR	Tetrapropylamine
44 (small pores)	CHA	Cyclohexylamine
46 (large pores)	AFS	Dipropylamine (DPA)
VPI-5/MCM-9 (extra-large pores)	VFI	Dipropylamine (DPA) Tributylamine

5.2.4.6. Influence of physical parameters

5.2.4.6.1. Crystallization parameters

The crystallization temperature range generally used in zeolites synthesis is quite large, starting from ambient and going up to about 300 ºC. Some materials may crystallize over a wide temperature range, about 150 ºC, while others are only produced in a small interval of temperature of approximately 20 ºC. At low temperature (lower than 100 ºC), the most open structures such as zeolites A, X and Y (0.4 $cm^3.g^{-1}$) are generally obtained, while higher temperatures (120 ºC and above) favour less open materials like ZSM-5 (0.15-0.20 $cm^3.g^{-1}$), highly dense phases like quartz-type SiO_2, $AlPO_4$, or $GaPO_4$ (tridymite, cristobalite) being predominant at temperatures close to 200 ºC. On the other hand, Si/Al ratio also depends on the crystallization temperature, and as generally observed, the higher is the temperature, the higher is the Si/Al ratio, rich-aluminum zeolites being obtained at temperatures comprised between 25 and 100 ºC. The crystallization is normally faster at higher temperatures. The heating rate to reach the crystallization temperature is also of great importance, and it can be critical especially when a large autoclave or vessel is used. Agitation of the reaction mixture can be a very useful tool to avoid thermal gradients, since it permits to reach and maintain a good homogeneity of equilibrium temperature throughout the reaction mixture. However, agitation can also lead to a decrease of the supersaturation level, resulting in a diminution of the nucleation of the desired material and thus favouring the formation of other undesired phases. Along with traditional heating systems, microwave heating is also used[40], generally when high heating rate is desired. This heating method may favour temperature homogenisation and may lead to shorter induction period[17], but such a technique can be only used with small volumes.

5.2.4.6.2. Heating time

The complete crystallization of a specific zeolite can occur in a few hours or in several months, depending on the synthesis conditions. According to Ostwald's rule, for longer heating times, more stable phases can crystallize and contaminate the desired phase. So, the synthesis of a pure crystalline phase can be difficult due the appearance of a second or even a third phase before the complete formation of the former. This observation is illustrated in Figure 10, which shows that increasing heating time, ZSM-5 material transforms into mordenite which is converted into quartz. It can also be seen that the largest amount of ZSM-5 zeolites is obtained after heating for 24 h.
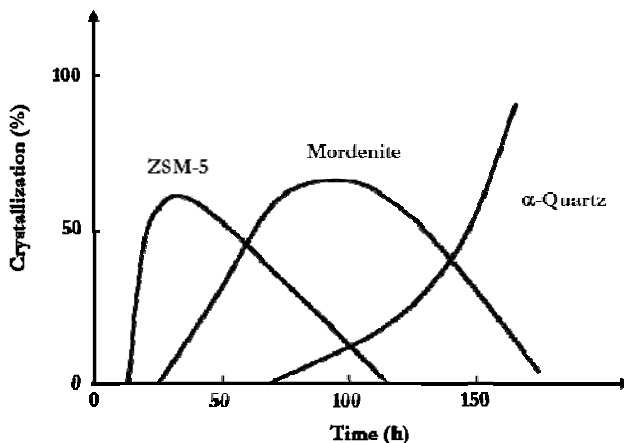
Figure 10 - Influence of the heating time during ZSM-5 zeolite organic-free synthesis performed at 190 ºC [41].

5.2.4.6.3. Template removal

To use a zeolite as molecular sieve, adsorbent or even heterogeneous catalyst, the organic/inorganic template present inside the material pores must be removed. When the structure directing species is an alkaline or alkaline earth metal, it is removed from the structure by ion exchange, using generally an ammonium salt (NH_4^+, NO_3^-) that will be decomposed at a moderate

temperature, leading to a proton H$^+$ compensating the negative charge of the framework.

When the template species is an organic molecule or ion, it is directly decomposed at temperatures sufficiently high to remove completely the template. However, such treatments sometimes result in species polymerization (appearance of coke residues) and/or structure damages (loss of crystallinity, pores collapse). The decomposition of the tetrapropylammonium cation into propylene (Hoffman mechanism) is a good example:

$$(C_3H_7)_4N^+X^- \quad \rightarrow \quad C_3H_6 \ + \ (C_3H_7)_3N \ + XH \tag{6}$$

where X can be an hydroxide anion or a framework oxygen.

To prevent coke formation or structure damages, a recent method has been purposed in the literature, consisting in the use of specific templates that decompose under mild conditions (aqueous solutions, temperature lower than 100 °C) with no calcination process needed[42,43]. One typical example related to ZSM-5 and ZSM-12 synthesis is shown in Figure 11: the organic template containing an acetal group is hydrolyzed and decomposed into two organic fragments that can be easily recovered and re-used. The main disadvantage of this technique is that such organic templates are generally used to specifically synthesize only a few zeolites.
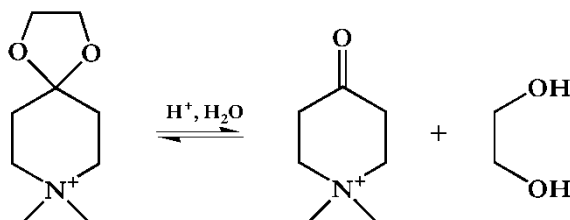
Figure 11 - Schematic decomposition of the directing-structure agent used in ZSM-5 synthesis (adapted from[42]).

5.3. ZEOLITE POST-SYNTHESIS MODIFICATIONS

For many purposes, zeolites and related materials are not utilized in the as-synthesized form. Rather, they are only employed after an appropriate post-synthesis modification.

Most of the "as-synthesized" zeolites do not possess any acidic properties (Na^+, K^+ as compensating cations). In addition, zeolites with low Si/Al ratios are not thermally stable (Si/Al lower than about 4) and the porosity of as-synthesized zeolites needs, under certain circumstances, to be improved. The preparation of zeolite catalysts containing highly dispersed noble or transition metals also requires several post-synthesis treatments, such as ion exchange or impregnation methods, followed in both cases by thermal decomposition of the metal precursor and reduction for the genesis of metal particles. Ion exchange is also the preferential method to transform a non acidic material into an acidic one. Thus, the dealumination process is the main modification treatment used to increase the thermal stability and to alter the acidity and porosity of a zeolite.

5.3.1. Ion exchange

The technique of ion exchange is frequently used to alter the properties of zeolites, e.g., to prepare acidic or basic catalysts, to tailor the pore size for specific adsorption processes and to introduce specific adsorption sites. The specific ion exchange capacity varies with the structure of the zeolite and the cations to exchange.

Ion exchange is generally a very simple technique in which the zeolite is suspended in an aqueous solution of a soluble salt containing the desired cation, preferentially under conditions which favour mass transfer, i.e, at elevated temperatures (80-90 °C) under stirring. When the zeolite crystals are immersed in an aqueous electrolyte, the zeolitic ions communicate with the

zeolite external solution, resulting in an exchange of ions between the solid phase and the solution.

$$A_z^+ + B_s^+ \leftrightarrows B_z^+ + A_s^+ \tag{7}$$

(subscripts s and z represent the solution and the solid respectively). An exchange is characterized by an isothermal exchange curve representing the variation of the B^+ concentration in the solid as a function of the B^+ concentration in the solution[11]. The rate of ion exchange depends on the concentration of ions of a size capable of penetrating the pores of the zeolite. At ambient temperature, the solution contains essentially fully hydrated cations with size larger than the pore opening of the zeolite, making the exchange very slow. The rate of exchange increases with rising temperature, as water is stripped from the ions and the hydration equilibrium shifts towards less hydrated ions.

Sometimes, the cation with its hydration shell is too bulky to enter the zeolite pores, or the salt with cation in the desired valence state is unstable or insoluble in water. In these and other instances, the desired form of the zeolite can often be made by solid-state ion exchange[44].

The most common application of ion exchange is the preparation of ammonium forms of zeolites to generate acidic catalysts. An acid form of a zeolite can be readily generated by aqueous ion exchange with ammonium ions, followed by a thermal treatment for decomposition of the ammonium ions inside the zeolite, leaving behind the acidic form of the zeolite where protons reside at the ion exchange sites.

$$NH_4^+ + (Na^+, Z^-) \rightarrow (NH_4^+, Z^-) + Na^+ \rightarrow (H^+, Z^-) + NH_3 \nearrow \tag{8}$$

A simple and standard example of an exchange is that used to replace sodium ions in zeolite NaY by ammonium ions. Zeolite NaY contains 9.9 % sodium (in weight). Available isothermal exchange curves show that, at room temperature, only about 73 % of the sodium ions can be exchanged, proving that a single exchange operation is not enough to eliminate all of the exchangeable sodium ions[45]. To reach higher exchange levels it will be necessary to perform several successive operations in fresh solutions.

Another example of ion exchange involves the preparation of zeolite supported metals by the exchange of K^+, Na^+, or NH_4^+ ions with Pt or Pd amine complex cations, e.g., $[Pt(NH_3)_4]^{2+}$. Direct reduction of this complex leads to the formation of large Pt agglomerates, therefore it is necessary to decompose the tetrammine complex prior to reduction with H_2. The ion exchanged zeolite is usually calcined prior to reduction of the metal ion. The temperature applied in the latter two steps determines the position and the dispersion of Pt^0 or Pd^0.

The reduction of zeolitic metal cations causes acid sites to be generated, so that a high loading with such cations may destabilize the zeolite upon reduction, particularly if the Si/Al is low.

$$([Pt(NH_3)_4]^{2+}, Z^{2-}) + H_2 \rightarrow Pt + 4\ NH_3 + (2\ H^+, Z^{2-}) \tag{9}$$
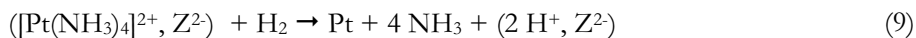
In many cases, careful attention must be paid to the pH of the exchange solution, which can affect the final metal dispersion. Thus, precipitation of metal hydroxides on the external surface of the zeolite, due to the local increase in pH when alkali ions are exchanged, should be avoided. In the case of first row transition metals, the use of very diluted solutions can be effective in reducing the formation of hydrolyzed species and precipitation can also be avoided by pH adjustment.

5.3.2. Dealumination techniques

The term dealumination, in the strict sense of the word, refers to the removal of aluminum from zeolite frameworks by chemical reactions generally resulting in lattice deficiencies. However, in its general use, it relates to a more complex process comprising the incorporation of other elements, especially silicon, into the transient framework vacancies temporarily left by the release of aluminum[24]. The processes that increase the Si/Al ratio of zeolite structures may be subdivided into two categories, according to the agent used: dealumination without any external Si addition and dealumination with external Si addition.

5.3.2.1. Dealumination without any external Si addition

This type of treatment involves three main routes: (1) removal of framework aluminum by chemical agents, generally by an acid, i.e., a direct acid leaching; (2) elimination of Al using high temperature calcinations in the presence of water steam (steaming method) and (3) high temperature calcinations in the presence of water steam followed by acid leaching.

5.3.2.1.1. Acid leaching

The direct acid leaching can be performed by refluxing the zeolite with inorganic acids such as nitric or hydrochloric acid, according to the following scheme:

$$(10)$$
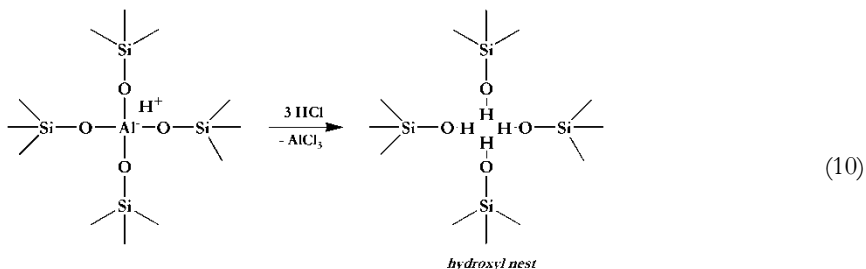
Depending on the acid concentration, up to 100 % of the framework aluminum can be removed. However, the thermostability of the products gradually decreases at dealumination degrees higher than 65 %. Moreover, the Si/Al ratio of the starting material must be higher than 4.5, otherwise destruction of the framework occurs during leaching.

This type of dealumination without silicon reinsertion in framework positions leads to the formation of defect sites generally denoted by the term "hydroxyl nest" as shown in the previous scheme, and originates the formation of secondary pore systems (meso and macropores). A scheme of a dealuminated structure containing atomic vacancies originated by Al extraction is shown in Figure 12.
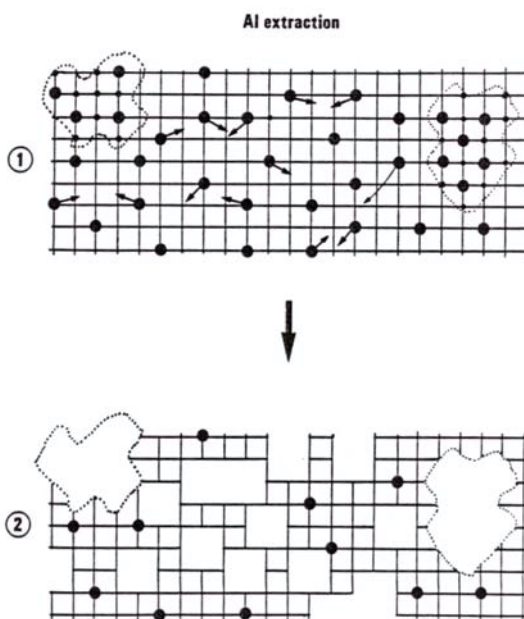
Figure 12 - Schematic representation of defect pores generated by acid leaching dealumination (adapted from 49).

The effectiveness of this technique depends on the zeolite used and attention must be paid to the concentration of acid solutions used for dealumination

treatments. It is obvious that dealumination of aluminum rich zeolite frameworks resulting in the formation of high lattice defect concentration can lead to a decrease of the stability of the crystal structure. For example, the structure of faujasite type zeolites completely collapses upon treatment with strong mineral acids, but using very low concentration of HCl, the structure of Y zeolite can be preserved. In the case of mordenite, direct acid leaching has been successfully used to generate mesopores[46].

5.3.2.1.2. Steaming

The hydrothermal dealumination of zeolite framework in the presence of water vapor, also called "steaming", has been reported as a method to increase the thermal stability of Y zeolite. This so-called "ultrastabilization" procedure became a matter of considerable interest because of the important industrial application of Y zeolite. However, when followed by a mild acid leaching, hydrothermal dealumination is also a useful method to create mesopores in the zeolite crystals and to obtain materials that combine zeolite micropores with mesopores that largely enhance the molecular accessibility inside the zeolite porosity [46].

Although thermal treatments without any water steam can also create defects in the zeolite structure[47,48], the use of water steam greatly enhances the mobility of aluminum and silicon species during the dealumination process.

Steaming is usually performed at temperatures above 500 °C with the zeolite in its ammonium or protonic form. When contacted with water steam, hydrolysis of Al-O-Si bonds takes place. The aluminum is finally expelled from the framework causing a vacancy (hydroxyl nest) or a partial framework amorphization. The amorphous material generated is a source of mobile silicon species, which can heal the vacancies in the framework left by expelled

aluminum atoms. Thus, part of the vacancies is filled while others grow to form mesopores, as depicted in Figure 13.
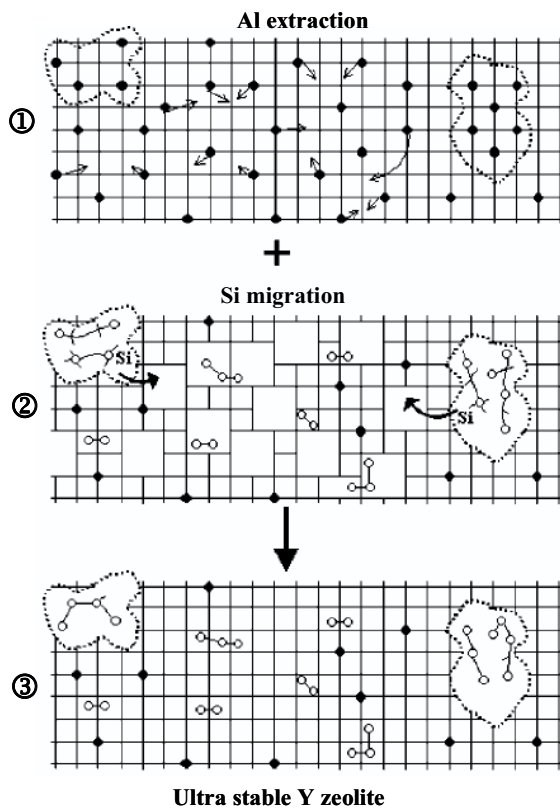
Figure 13 - Schematic picture of the formation of mesopores (adapted from 49). The grid denotes the zeolite framework, the black dots are framework Al atoms, the open circles are Al atoms extracted from the framework and the dotted lines indicate the mesopores.

$$(11)$$
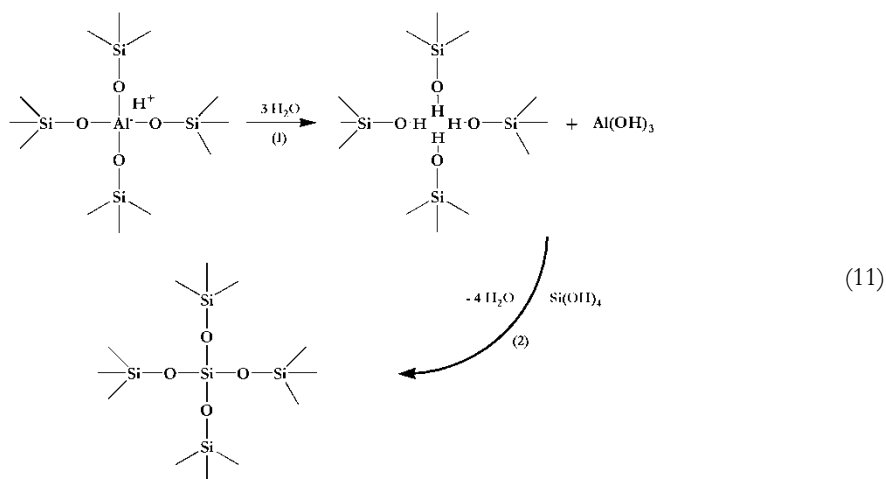
Scheme 11 illustrates that this mechanism of dealumination comprises an isomorphic substitution of framework aluminum for silicon species that come from the initial degradation of the zeolite structure, probably from a region rich in hydroxyl nests. In fact, steaming leads to a dealumination of the framework with silicon reinsertion in framework positions, the formation of extra-framework species and also to the formation of mesopores (d > 2 nm).

5.3.2.1.3. Post-steaming acid leaching

The purpose of acid leaching is to remove the extra-framework material created during the steaming process. Different extra-framework aluminum species, such as Al^{3+}, $Al(OH)_2^+$, $AlO(OH)$, AlO^+ and $Al(OH)_3$, have been suggested[26,50,51]. These extra-framework species (with a diverse nature) that are deposited in the micro and mesopores and on the external surface lead to a partial blockage of the porosity and the active sites, but they can be extracted by a mild acid leaching. If only steaming and no acid leaching is applied the bulk Si/Al ratio remains the same, but the framework Si/Al ratio increases. A mild acid leaching step, with either inorganic acids such as diluted nitric acid or organic (complexing) acids like oxalic acid, dissolves the extraframework

material. The acid leaching must only lead to unblocking of the microporosity, and in this case the mesopores are not actually formed during the process. Rather, the mesopores formed during the steaming process are emptied, resulting in a higher mesopore volume compared to zeolites that have only been steamed[52]. The strength of acid leaching has to be adapted to the framework Si/Al ratio of the steamed zeolites, otherwise a destruction of the solids could occur.

5.3.2.2. Dealumination with external Si addition

Rather than just being removed from the zeolite framework, aluminum can be also replaced directly by silicon. The two main routes that have been developed concern the treatment with hexafluorosilicates solution and silicon halides vapors, namely $SiCl_4$. Both treatments involve a mechanism of isomorphous substitution and do not lead to the formation of extra-framework species and secondary pore systems.

These dealumination methods are more efficient for zeolites with a very open structure (FAU, BEA)[24], but they can be also used to selectively remove aluminum from external surface of zeolite crystals with smaller pores[53,54].

5.3.2.2.1. Reaction with hexafluorosilicates

The principle of this dealumination method is to treat a zeolite slurried in water with an aqueous solution of an agent which extracts aluminum from the framework, providing ligands for the formation of a thermodynamically strongly favoured, soluble aluminum complex and serving as an extraneous source of silicon atoms filling up the framework vacancies formed upon extraction of aluminum. Breck and Skeels[55] realized that soluble hexafluorosilicate salts, especially the ammonium and lithium salts, meet the requirements of such a process that can be described by scheme 12.
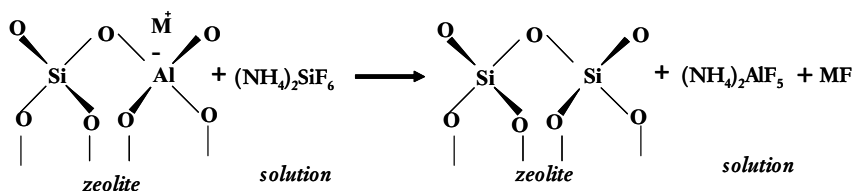
$$(12)$$

It is believed that the process proceeds in two steps, according to the following reaction scheme[26]:

1. removal of Al from the framework by HF formed from hydrolysis of ammonium hexafluorosilicate and originating hydroxyl nests

$$SiF_6^{2-} + H_3O^+ \leftrightarrows SiF_5OH^{2-} + HF \qquad (13)$$

$$SiF_5OH^{2-} + H_3O^+ \leftrightarrows SiF_4 + 2\,H_2O + HF \qquad (14)$$

$$SiF_4 + 2\,H_2O \leftrightarrows SiO_2 + 4HF \qquad (15)$$
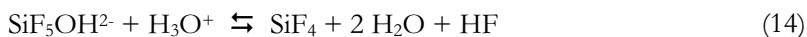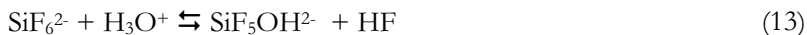
2. the insertion of Si atoms in the lattice vacancies left by Al release by reaction of SiF_4 species with hydroxyl nests.

In order to avoid too high concentration of defect sites leading to unstable products, the reaction rate of the first step should not exceed that of the second one. Thus, the pH of the slurry must be considered as a crucial parameter since it decisively controls the rate of aluminum extraction. This dealumination method requires the ammonium or hydrogen forms of zeolites and it is not applicable to sodium forms generally obtained as as-synthesized products.

5.3.2.2.2. Reaction with SiCl₄

The reaction of a zeolite with $SiCl_4$ is another dealumination method that involves gaseous silicon tetrachloride as dealumination agent and, at the same time, as extraneous silicon source. Under appropriate experimental conditions, framework silicon is directly and isomorphically substituted for aluminum in a strongly exothermic reaction without substantial lattice damage.

$$\text{(16)}$$
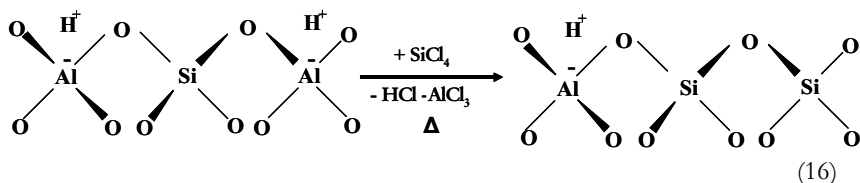
The applicability of this dealumination process is limited to zeolites with pore openings large enough to allow the penetration of the $SiCl_4$ molecule. The chemistry of this process may appear to be simple, but it is rather difficult and requires exact knowledge of this complex process[24] and great experience in its application to prepare completely, and especially partially dealuminated zeolites without significant damage to the lattice.

In practice, a stream of an inert gas saturated at ambient temperature with silicon tetrachloride is passed at high temperatures (about 450-500 °C) through a bed of the zeolite, preferentially pelleted without any binder. It is very important to avoid overheating due to released reaction heat, so it is recommended to contact the zeolite with $SiCl_4$ first at a lower temperature (about 200 °C), then to heat under the gas stream containing $SiCl_4$, at a moderate rate up to the reaction temperature and continue the treatment at this temperature during a certain time.

The degree of dealumination depends not only on the final reaction temperature but also on the reaction time. When applied to zeolites containing sodium, this dealumination process can lead to the intracrystalline deposition of $Na[AlCl_4]$, originated from reaction of $SiCl_4$ with Na^+ cations. The deposits of

this complex salt can difficult the dealumination, which may be strongly or completely inhibited, especially in the case of zeolites with one dimensional pore systems. Faujasites of extremely low Al content (Si/Al>200) and a minimum of framework vacancies and mesopores can be obtained by acid leaching and steaming of zeolite previously dealuminated with $SiCl_4$[24]. By treating NaZSM-5, a zeolite with smaller pores, with $SiCl_4$ vapour at temperatures between 450 and 650 ºC, only a slight increase in the bulk Si/Al ratio was observed, but the surface Si/Al determined by XPS revealed an higher value[56]. Thus, the external crystal shell was preferentially dealuminated upon contact with $SiCl_4$, obviously due to diffusion restrictions that explain that Al atoms on the external surface of ZSM-5 crystallites were removed more selectively than in the pores.

References

1. R.M. Barrer, *J. Chem. Soc.*, **1948**, 2158.

2. R.M. Milton, US Patent 2 882 243, **1959**.

3. R.M. Barrer, P.J. Denny, *J. Am. Chem. Soc.*, **1961**, *83*, 971.

4. R.L. Wadlinger, G.T. Kerr, E.J. Rosinski, US Patent 3 308 069, **1967**.

5. R.J. Argauer, G.R. Landolt, US Patent 3 702 886, **1972**.

6. R. Szostak, *Molecular Sieves - Principles of Synthesis and Identification*, Van Nostrand Reinhold, New York, 2nd Edition Blackie London, **1998**.

7. S.T. Wilson, B.M. Lock, C.A. Messina, T.R. Cannan and E. M Flanigen, *J. Am. Chem. Soc.*, **1982**, *104*, 1146.

8. E.M. Flanigen, R.L. Patton, S.T. Wilson, *Stud. Surf. Sci. Catal.*, **1989**, *37*, 13.

9. M.W. Anderson, O. Terasaki, T. Ohsuna, A. Philippou, S.P. MacKay, A. Ferreira, J. Rocha, S. Lidin, *Nature*, **1994**, *367*, 437.

10. A. Corma, *Chem. Rev.*, **1997**, *97*, 2373.

11. D.W Breck, *Zeolite Molecular Sieves*, John Wiley, New York, **1974**.

12. R.M. Barrer, *Hydrothermal Chemistry of Zeolites*, Academic Press, London, **1982**.

13. H. van Bekkum, E.M. Flanigen, P.A. Jacobs, J.C. Jansen, *Introduction to Zeolite Science and Practice*, Elsevier, Amsterdam, **2001**.

14. J. Čejka and H. van Bekkum, (Eds.), *Zeolites and Ordered Mesoporous Materials:Progress and Prospects,* Elsevier, Amsterdam, **2005**.

15. E.G. Derouane, F. Lemos, C. Nacache, F.R Ribeiro, *Zeolite Microporous Solids: Synthesis, Structure and Reactivity*", NATO ASI Series, Nº C352, Kluwer, **1992**.

16. E.J.P. Feijen, J.A. Martens and P.A. Jacobs, in G. Ertl, H. Knözinger and J. Weitkamp, Eds, *Handbook of Heterogeneous Catalysis,* Wiley-VCH, **1997**, 311.

17. C.S. Cundy, *Stud. Surf. Sci.Catal*, **2005,** *157*, 65 and references of table pp. 68.

18. C.S. Cundy, *Microporous and Mesoprous Materials*, **2005,** *82*, 1.

19. H. Robson, *Verified Synthesis of Zeolitic Materials*, 2nd rev., Elsevier, Amsterdam, **2001**.

20. M. Guisnet, F. Ramôa Ribeiro, *Zeólitos, Um Nanomundo ao Serviço da Catálise*, Fundação Calouste Gulbenkian, Lisboa, **2004**.

21. C. Marcilly, *Topics in Catalysis*, **2000**, *13*, 357.

22. J. Karger, D.M Ruthven, *Diffusion in Zeolites and Other Microporous Materials*, John Wiley and Sons N.Y., **1992**.

23. G. Belussi in G. Ertl, H. Knözinger and J. Weitkamp, Eds, *Handbook of Heterogeneous Catalysis*, Wiley-VCH, **1997**, 2329.

24. H.K. Beyer, in H.G. Karge and J. Weitkamp Eds., *Molecular Sieves Science and Technology*, *- Post-Synthesis Modification* I, Springer, **2002**, vol. 3, pp. 203.

25. A. Omegna, M. Vasic, Jeroen A. van Bokhoven, G. Pirngruber and R. Prins, *Phys. Chem . Chem . Phys .* **2004,** *6*, 447.

26. M. Guisnet, F.R. Ribeiro, *Les Zéolithes- Un Nanomonde au Service de la Catalyse*, EDP Sciences, **2006**.

27. Ian E. Maxwell, *J. of Inclusion Phenomena and Macrocyclic Chemistry*, **1986**, *4*, 1.

28. (a) W.M.H. Sachtler, Z.C. Zhang, *Advances in Catalysis*, **1993**, *39*, 129; (b) W.M.H. Sachtler in G. Ertl, H. Knözinger and J. Weitkamp, (Eds), *Handbook of Heterogeneous Catalysis*, Wiley-VCH, **1997**, pp. 365.

29. Y. Traa, B. Burger, J. Weitkamp, *Microporous and Mesoporous Materials*, **1999**, *30*, 3.

30. D.Barthomeuf, *Catal. Rev.-Eng. Sci.*, **1996**, *38*, 521.

31. R.J. Davis, *J. Catal.,* **2003**, *216*, 396.

32. R.M. Barrer, J.W. Baynham, F.W. Bultitude and W.M. Meier, *J. Chem. Soc.*, **1959**, 195.

33. S.P. Zhdanov, N.N. Feoktistova, L.M. Vtjurina, *Stud. Surf. Sci. Catal.*, **1991,** *65*, 287.

34. F. Delprato, *PhD. Thesis*, Université de Haute Alsace, Mulhouse, **1989**.

35. J.L. Guth, H. Kessler, R. Wey, in Y. Murakami et al., (Eds.), *Proc. 7th Int. Zeol.Conf.*, Elsevier, **1986**, 121.

36. M.E. Davis, A. Katz, W.R. Ahmad, *Chem. Mater.*, **1996**, *8*, 1820.

37. S.T. Wilson, *Stud. Surf. Sci. Catal.*, **1991**, *58*, 137.

38. M.E. Davis, *Chemtech*, **1994**, 22.

39. J.P. Lourenço, *PhD. Thesis*, Intituto Superior Técnico, Lisboa, **1996**.

40. J.C. Jansen, *Stud. Surf. Sci. Catal.*, **1991**, *58*, 77.

41. F.Y. Dai, M. Suzuki, H. Takahash, Y. Saito, in *Proc. 7th International Zeolite Conference*, Y. Murakami *et al.* (Eds.), Tokyo, **1986**, pp. 223.

42. H. Lee, S.I. Zones, M.E. Davis, *Nature*, **2003**, *425*, 385.

43. H. Lee, S.I. Zones, M.E. Davis, *J. Phys. Chem. B,* **2005**, *109*, 2187.

44. H.G. Karge, *Stud. Surf. Sci. Catal.*, **1997**, *105 C*, 1901.

45. M. Che, O. Clause, Ch. Marcilly, in *Preparation of Solid Catalysts*, G. Ertl, H. Knozinger, J. Weitkamp (Eds.), Wiley-VCH, Wienheim, **1999**, pp. 315.

46. S. van Donk, A.H. Jansen, J.H. Bitter, K.P. de Jong, *Catal. Review*, **2003**, *45*, 297.

47. K. Sato, Y. Nishimura, H. Shimada, *Catal. Lett.*, **1999**, *60*, 83.

48. J.P. Pariente, J. Sanz, V. Fornés and A. Corma, *J. Catal.*, **1990**, *124*, 217.

49. C.R. Marcilly, *Petrole et Techniques*, **1986**, *328*, 12.

50. J. Scherzer, in *Catalytic Materials: Relationship between Structure and Activity,* T.E. White, R.A. Della Betta, E.G. Derouane, R.T.K. Baker, (Eds.), ACS Symp. Ser., American Chemical Society, Washington D.C., **1984,** pp. 157.

51. G.H. Kuhl in *Catalysis and Zeolites- Fundamentals and Aplications*, J. Weitkamp, L. Puppe (Eds.), Springer, **1999**, pp. 81.

52. J. Lynch, F. Raatz, P. Dufresne, *Zeolites*, **1987**, *7*, 333.

53. J.M. Silva, M.F. Ribeiro, F. Ramôa Ribeiro, E. Benazzi, N.S. Gnep, M. Guisnet, *Zeolites,* **1996**, *16*, 275.

54. J.M. Silva, M.F. Ribeiro, F. Ramôa Ribeiro, N.S. Gnep, M. Guisnet, E.Benazzi, *React. Kinet. Catal. Lett.*, **1995**, *54*, 209.

55. D.W. Breck, G.W. Skeels in *Proceedings of the 6th International Zeolite Conference*, D. Olson, A. Bisio (Eds.), Butterworths, UK, **1984**, pp. 87.

56. S. Namba, A. Inaka, T. Yashima, *Zeolites*, **1986**, *6*, 107.

6. CHARACTERIZATION OF ACID CATALYSTS

A. Fernandes[1], J.M. Lopes[1], R. Ramos Pinto[1,2]

[1] IBB-Institute for Biotechnology and Bioengineering, Centro de Engenharia Biológica e Química, Departamento de Engenharia Química, Instituto Superior Técnico, Av. Rovisco Pais, 1049-001 Lisboa, Portugal.
[2] ISCSP - Instituto Superior de Ciências Sociais e Políticas, Pólo Universitário do Alto da Ajuda, Rua Almerindo Lessa, 1349-055 Lisboa, Portugal.

6.1. THE IMPORTANCE OF CHARACTERIZATION

The chemistry of a catalyst is closely related with its physical and chemical properties, only through its characterization it is possible to explain and predict the behavior of a catalyst in a catalytic process, namely its activity, selectivity and stability. This influence of physical and chemical properties makes its characterization essential to the understanding of the kinetics of any catalytic process.

In acid catalysis the acidic properties of the catalyst play a major role in its kinetics; as a consequence, it is mandatory to give particular attention to the characterization of any physical and chemical properties that influence acidity.

The acidity of a catalyst is essentially affected by the strength, amount, proximity and accessibility of its acid sites, aspects that are profoundly influenced by the structure of the catalyst and the nature of the acid sites.

In the following sub-chapters, two techniques will be described that are extensively used in catalytic research all over the world. IR spectroscopy, which is a very powerful tool for the characterization of the structural properties and the nature of the acid sites; Temperature Programmed Desorption, that enables to quantitatively describe the distribution of the acid sites. Finally, a description of an installation that enables to perform the laboratory evaluation of catalysts is presented. This kinetic evaluation is particularly important in the characterization of the active phase of the catalyst, in what concerns the

activity, selectivity for the formation of each product and stability of the main parameters.

6.2. INFRARED SPECTROSCOPY OF ZEOLITE CATALYSTS

6.2.1. Introduction

Infrared (IR) spectroscopy is a technique that deals with the monitoring of vibrations in molecules with a permanent dipolar moment. In the last 50 years, progress and development in IR, essentially the introduction of Fourier Transform Infrared (FTIR) spectrometers, has considerably improved this tool in terms of sensativity and quality of experimental spectra[1].

Zeolites are crystalline aluminosilicates that present a microporous system and are involved in many industrial applications (as adsorbents, molecular sieves and catalysts) mostly in petroleum refining and fine chemistry. The better understanding of the properties of these materials (degree of crystallinity, changes after post-treatments and surface acidity and/or redox properties when metal cations are presents) is thus the key for the improvement of their catalytic behaviour. Because FTIR spectroscopy allows to characterize not only the intrinsic properties of zeolites (framework) but also the interaction of the catalyst with molecular probes (in-situ experiments) and even reagents and products under catalytic reactions conditions (Operando spectroscopy), this technique has been widely used in catalysis research and represents certainly one of the most important tools for catalysts characterization, including zeolite-type materials.

6.2.2. Zeolite Framework Characterization

Zeolites can be described as materials with an infinitely extending three-dimensional assemblage of SiO_4 and AlO_4 tetrahedra units connected to each other by the sharing of oxygens ions. The presence of an AlO_4 tetrahedron in

the framework generates a negative charge compensated either by a proton (acidic properties), or by an extra-framework cation M^{n+} such as Na^+, K^+, NH_4^+, Ln^{3+} or MTI (metal transition ion) that present redox properties. Framework Si atoms can also be substituted with the aim of modifying catalyst properties: various examples in the literature have been reported and it can be mentioned here the isomorphous substitution of Si by B in the case of the ZSM-5 material (MFI structure)[2].

When zeolites are used as heterogeneous catalysts, some important parameters related to the degree of crystallinity, aluminium content and framework isomorphous substitution must be determined. FTIR spectroscopy in transmission mode of diluted samples in KBr pellets (typically 0.5 to 2 % in weight) is the easiest and more suitable technique to evaluate these parameters. Figure 1 shows a typical infrared spectrum of a zeolite material, the H-FER zeolite (KBr technique).
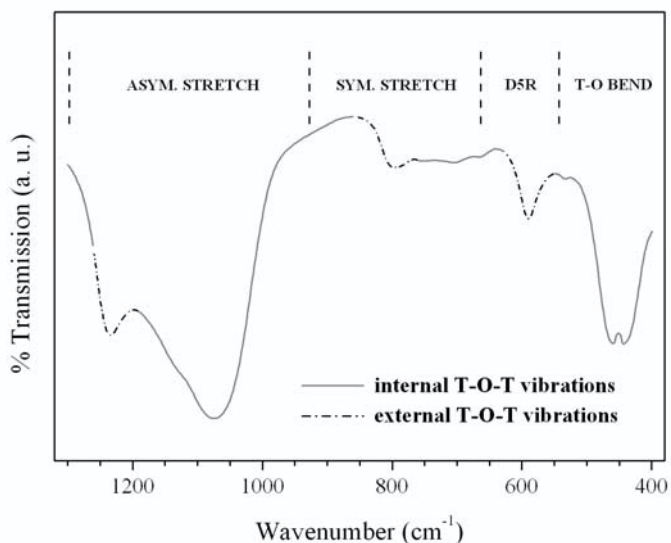
Figure 1 - Infrared spectrum of H-FER zeolite in the region of structural T-O-T bands.

Structural T-O-T bands of zeolites are generally divided in internal T-O-T vibrations and in external linkages between TO_4 tetrahedra (T = Si, Al): "internal" vibrations are only sensitive to the change of population of Si and Al in the framework, while "external" vibrations are also structure-sensitive[3] and may be used as a fingerprint of a particular zeolitic framework. For example, the band at 590 cm^{-1} observed in the IR spectrum of H-FER is characteristic of D5R (double 5-rings) subunits presents in pentasil zeolites.

Figure 2 shows the evolution of the D6R (double 6-membered rings or hexagonal prism) band frequency situated at 560-610 cm^{-1} as a function of Al framework and percentage of crystallinity in Y zeolites[4]. In the first case, a linear relationship between the band position and the Al content is observed and is attributed to electronegativity difference between Si and Al atoms. Therefore, this empirical correlation allows the prediction of the Si/Al ratio by a simple measurement of the band position. Examples of linear relationships are numerous and other structural bands (mainly asymmetric and symmetric T-O-T stretching bands at 1200-1000 and 850-750 cm^{-1}, respectively) can also be used. FAU zeolite certainly represents one of the examples most studied using these particular structural bands[5,6]. Consequently, zeolites dealumination processes can be monitored using this technique. In the second case (see below), using a reference considered 100% crystalline, it is possible to evaluate the samples crystallinity by comparing the band intensities. Moreover, isomorphous substitution of Si by heteroelements can be confirmed in the IR spectrum by the appearance of new structural bands, as in the case of silicon substitution by boron in MFI structure, the observation of the bands at 1380, 920, 700 and 620 cm^{-1} (ν(B-O) and ν(B-O-Si))[7].

A more detailed description of zeolite physical and chemical properties can be found in literature[8].
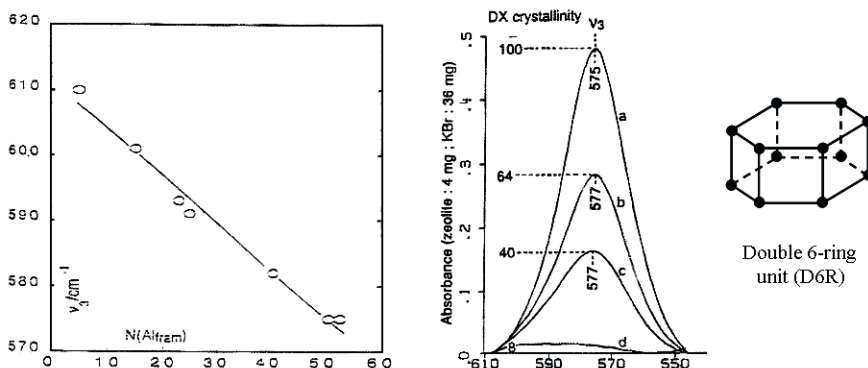
Figure 2 - Framework aluminium content and crystallinity of Y zeolites followed by IR structural bands.

6.2.3. Surface Acidity

Zeolites are generally used as heterogeneous catalysts, probably because of their interesting acidic properties. On the surface of the support, two different types of acid sites are present: the Brönsted acid sites (hydroxyl groups OH) providing labile protons H^+ and the Lewis acid sites, i.e. extraframework aluminium (electron acceptors). Brönsted acid sites are doubtless the main active sites in acid catalysis, the role of Lewis acid sites being essentially to enhance the strength of the latter. Because in hydrated zeolite, water molecules interact strongly with these hydroxyls groups, OH vibration bands are hidden and cannot be observed when measurements are performed with KBr diluted sample pellets. Since these KBr pellets cannot be heated (K^+ ions might diffuse into the zeolite pores and exchange with protons), one solution consists in preparing a self-supported thin wafer of the pure sample (10 to 20 mg) which is mounted on a special quartz sample holder and introduced into an IR vacuum cell that allows: 1) the sample to be outgassed at different temperatures and 2) the introduction (flow and/or adsorption) of gas (H_2, O_2, CO, NO, etc…) and volatile organic molecules, in a desired amount (see Figure 3).
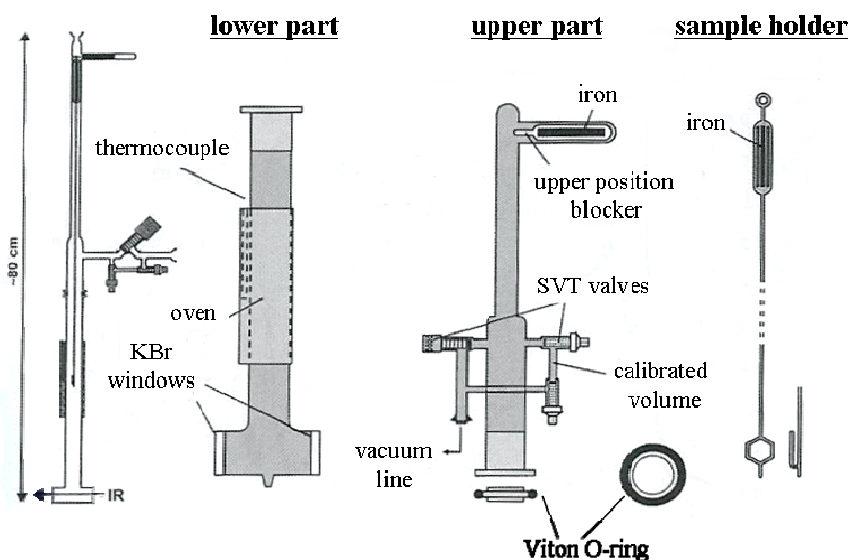
Figure 3 - Schematic representation of an in-situ IR cell (adapted from 9).

An example of IR spectrum obtained after pre-treatment (water removal) is shown in Figure 4 a) for the zeolite H-MCM22[10]. In the hydroxyls zone (4000-3000 cm^{-1}) two main bands are observed: the first one (sharp peak at 3745 cm^{-1}), corresponds to silanol groups (Si-OH) located at the external surface of zeolite crystallites and/or in structural defects; the second band situated at about 3620 cm^{-1} is associated to bridged Si(OH)Al groups, i.e. the Brönsted acid sites.
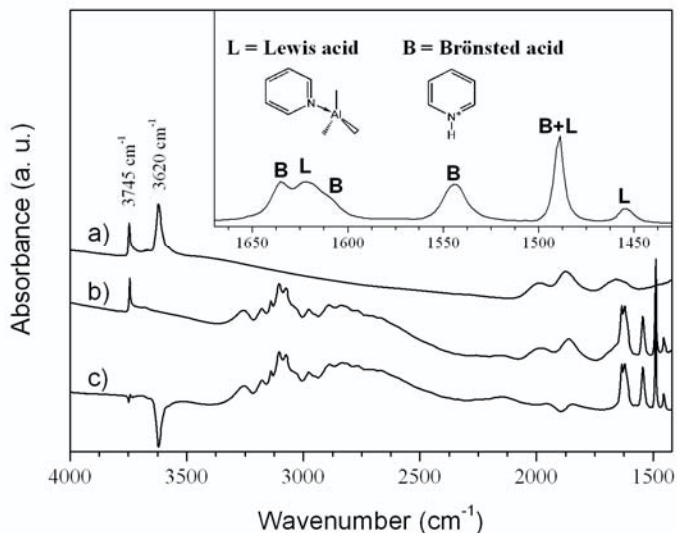
Figure 4 - Infrared spectra of: a) H-MCM22 after water evacuation, b) H-MCM22 after pyridine adsorption at 150 ºC and c) difference spectrum.

Nature, strength and accessibility of these acid groups are of crucial importance to understand catalytic activity of these supports. The use of molecular probes interacting with the surface of the catalyst is an attractive approach to identify and deeply characterize all these essential parameters. Different criteria for the selection of the molecular probes can be cited: 1) the probe molecule should be stable under the experimental conditions (to avoid dissociation or decomposition) and should adsorb easily on the support; 2) the probe molecule should present a dominating base character and rather weak acidic properties; 3) the IR spectrum of the sorbed probe molecule should permit to distinguish between sorption on protonic (Brönsted) and aprotic (Lewis) acid sites; 4) the probe molecule should allow to differentiate between acid sites of the same type, but of different strength; 5) the size of the probe molecule should be comparable to the size of the reactant to probe the concentration of acid sites relevant for a particular reaction. The most common molecular probe used is a base which will interact with both acid sites in different ways: nucleophilic

151

interaction with Lewis acid sites and H-bonding with hydroxyl groups leading, eventually, to a total deprotonation in the case of the Brönsted acid sites (strong hydrogen interaction). The spectrum b) in Figure 4 corresponds to pyridine (Py) adsorption and saturation at 150 ºC; the spectrum c) is obtained by difference between spectra a) and b). In the zone 1700-1400 cm^{-1} (Figure 5, insert), bands of Py interacting with the support become visible; the frequencies observed are different when comparing with liquid or gas phase Py and are characteristic of the molecule interacting with both Lewis and Brönsted acid sites. Using the values of the molar extinction coefficient ε for both Py species (PyH$^+$ and PyL), it is possible, from experimental results (after saturation and removal of physisorbed Py), to evaluate the concentration of both acid groups. The experimental determination of ε_B (PyH$^+$) and ε_L (PyL) is described in Figure 5. Successive introduction of a known (calibrated) volume of Py is accompanied by the increase of integrated area of both species, i.e. Py adsorbed on Lewis (band at 1455 cm^{-1}) and on Brönsted acid sites (band at 1540 cm^{-1}). The relation is linear and the value of ε can be obtained using equation (1). Final concentrations are calculated from equation (2). Typical values of ε_B and ε_L found in the literature (Emeis[11], Khabtou *et al.*[12], Guisnet *et al.*[13]) are summarized in the table below (see Figure 5).

Ammonia and aliphatic amines can also be used as probe molecules to quantify and to differentiate between Brönsted and Lewis acid sites and. However, these molecules are generally not stable upon sorption in temperature (dissociation, disproportion) and pyridine and derivates are often preferred.

The strength of Brönsted acid groups, which is an important parameter in catalysis, can be roughly evaluated using Py temperature-desorption experiments: the stronger the acid site the higher the Py desorption temperature. However, similar but more precise informations are also obtained using a weak base molecule[14] which will interact with the hydroxyl group only

via H-bonding, providing a red-shift of the OH frequency: the higher the frequency shift, the stronger the acid site.

$$\varepsilon = \frac{I \times S}{n} \ (1) \qquad c = \frac{n}{m} = \frac{I \times S}{\varepsilon \times m} (2)$$

	PyH$^{+(*)}$	PyL$^{(*)}$
Emeis	1.67	2.22
Khabtou et al.	1.5	1.8
Guisnet et al.	1.13	1.28

(*) cm/μmol
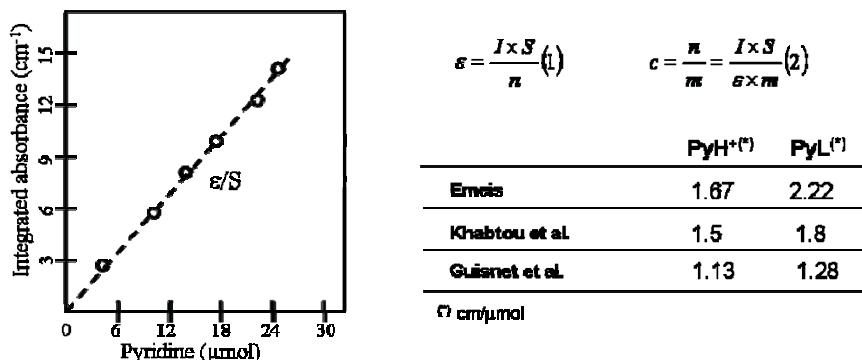
Figure 5 - Quantitative determination of acid sites concentration using Py adsorption. ε= molar extinction coefficient; I = integrated band area; n = number of Py vibrators, in moles; m = sample weight; S = wafer surface area.

The example of CO adsorption on H-ZSM5 zeolite is shown in Figure 6 (see below). As it can be shown, both frequencies (of OH and CO vibrator groups) are dramatically affected when CO molecule interacts with Brönsted acid sites. Thus, the evaluation of the chemical shifts of the ν(OH) frequency is a good measurement of the strength of the acid site, a typical shift of 250 to 400 cm^{-1} for zeolites supports being generally observed. Although CO presents almost all desired requirements (see above), the unique inconvenient of this probe is that the experiments must be done at very low temperatures (typically at the temperature of liquid nitrogen) because such a molecule is a weak base donor and presents a poor polarisability. Other weakly basic molecules, as for example nitriles, benzene and substituted benzenes, H_2 and N_2 are also often used.
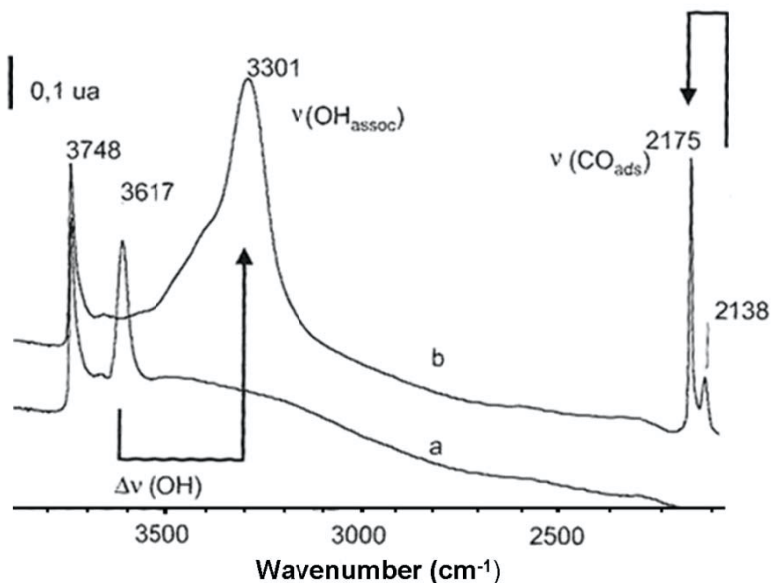
Figure 6 - IR spectra of H-ZSM5 zeolite before (a) and after CO adsorption at 100 K (b)[8].

The accessibility and location of the acid sites are also significant parameters to be considered, as they will influence the activity of the different acid sites. For this purpose, the main idea consists in using basic molecular probes of different size and shape: for example, using different substituted alkylamines and alkylpyridines allows to evaluate the accessibility of the different acid sites (such as the external sites from the internal ones). One important example refers to H-MFI zeolite where Py can interact with all the OH acid groups while external OH groups are only accessible to collidine molecule (trimethylpyridine). The same situation is observed in MCM22 zeolite where di-ter-butyl-pyridine was shown to be adequate probe to characterize acid OH groups located at the external surface of the zeolite[15] (external cups). On the other hand, the use of substituted pyridines also showed that it was possible to specify a molecular base interacting only with Brönsted acid sites (large, blocked up substituted pyridines will not interact with Lewis sites)[16].

6.2.4. Conclusion

It can be concluded that IR spectroscopy is a very powerful tool for catalyst investigations, in what concerns surface acidity and structural properties of zeolites. Moreover, zeolite containing metal ions (for bifunctional catalysis) can also be characterized using other specific molecular probes, i.e. electron donors, such as NO, CO, etc… gas molecules. However and because reactants generally interact with the catalyst surface in a different way, it is not straightforward to extrapolate these static mode results to predict the catalytic behaviour of the working material (during the reaction). Consequently:

1) IR spectroscopy of sorbed molecules, which are chemically similar to the reactants (similar shape and size, polarisability, base strength), is a better way to understand the physical and chemical properties of a particular catalyst. As example, Figure 7 shows the adsorption of n-pentane on H-ZSM5 zeolite: the total disappearance of the band at 3610 cm^{-1} after n-pentane adsorption demonstrates that similar reactants, during reaction, will be able to interact with all the Brönsted acid groups of the catalyst[15].

2) The study of the working catalyst using well-designed cell-reactor and rapid-scan/time-resolved infrared spectroscopy will provide better understanding of the reactions mechanisms, in particular in what concerns transition states and/or intermediate species detection[17].
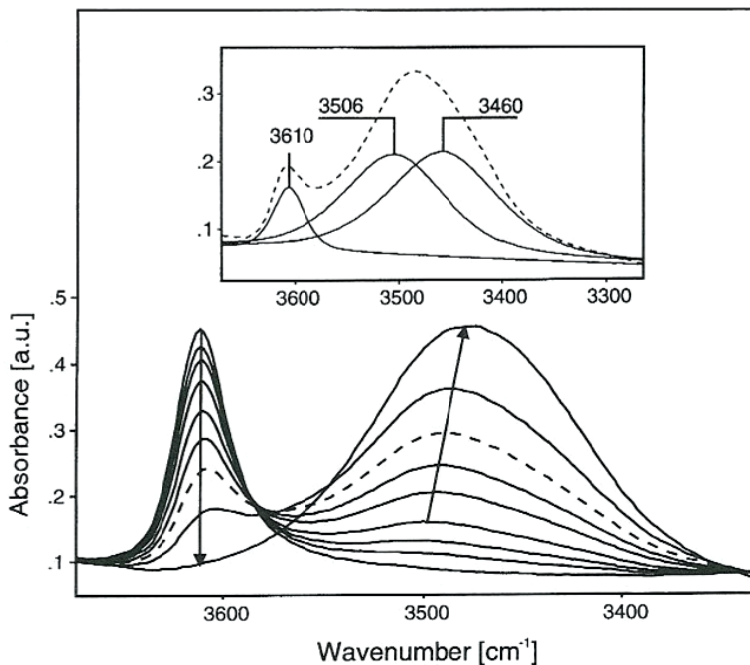
Figure 7 - Adsorption of n-pentane in H-ZSM5 zeolite.

6.3. TEMPERATURE PROGRAMMED DESORPTION

6.3.1. Description of the Technique

The Temperature Programmed Desorption (TPD) is a technique where, after the initial adsorption of the probe molecule, the temperature is increased in a controlled way and the amount of desorbed probe molecule as a function of time (and also temperature) is measured. This technique enables to quantitatively describe the distribution of the acid sites, which is essential to correlate the acidity and the activity of the catalysts.

The application of the TPD technique can be divided in two distinct stages:

Adsorption of the probe molecule in the acid sites

The catalyst sample is exposed to an excess of probe molecule, assuring that the entire catalyst surface is exposed to the probe and that at the end of the process each acid site has an adsorbed probe molecule. The adsorption must be performed under controlled temperature, between 120 and 150ºC, in order to avoid the presence of water molecules.

Desorption of the probe molecule from the acid sites

The temperature is raised in a programmed way (usually at a rate of 10ºC/min) until all the probe molecules have been desorbed and the acid sites regenerated to their initial protonic form. The temperature increase is usually performed in a single step, although it can also be performed in several steps.
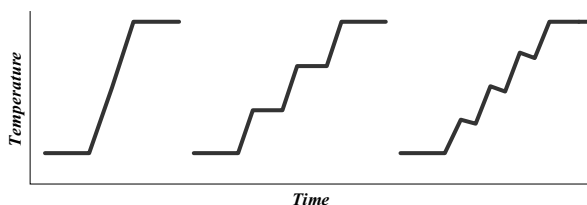
Figure 8 - The three most commonly used schemes, in TPD, for the programmed temperature increase.

6.3.2. The Probe Molecule

The most frequently used probe molecule is ammonia (NH_3), for two main reasons. Firstly, the fact that ammonia is a small molecule, enabling it to access to all the acid sites, even to the ones located in the smallest cavities. Secondly, the ammonia molecule is a strong base, which assures its adsorption even in the weaker acid sites, enabling the construction of a good acid scale, based in the chemisorption energy.

Several other molecules can be used as probes, like pyridine, carbon monoxide, carbon dioxide and even water, although ammonia is clearly the most common one.

Pyridine is also a strong base, even stronger than ammonia, although it's much larger molecular volume, frequently prevents it from accessing the acid sites in the smaller cavities, which strongly restricts its use as a probe molecule in TPD. The remaining of the referred molecules have similar or even smaller dimensions than ammonia: nevertheless, all of them are weaker bases than ammonia. The use of bigger probe molecules enables to withdraw information about the accessibility of the acid sites, when compared with results obtained using smaller probe molecules.

6.3.3. Analysis of the Results

During the desorption stage, the temperature, time and desorption rate of the probe molecule are registered. The rate of desorption can be determined, directly, through the detection of the probe molecules in the reactor effluent (usually with a Thermal Conductivity Detector), or indirectly, through the mass reduction of the catalyst sample, which can be obtained using a micro-balance.

The graphical representation of the desorption rate of the probe molecule as a function of temperature is commonly designated as "TPD curve".
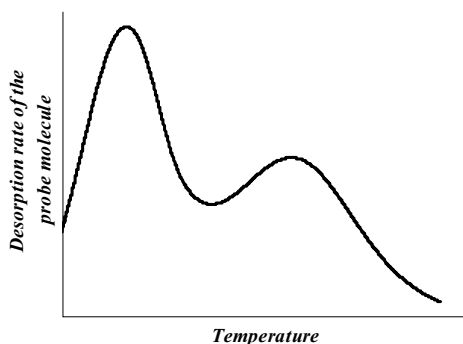
Figure 9 - Ammonia TPD curve for a ZSM-5 zeolite.

Assuming that each desorbed probe molecule corresponds to a protonic acid site, the TPD curve area is proportional to the number of sites, the total area corresponding to the total number of protonic acid sites. In a typical TPD curve the desorption of the probe molecules is dispersed through a wide range of temperature, which is, not only the result of the differences in the intensity of the bonds established between the probe molecule and the protonic acid sites, but also due to the dynamics of this experiment. The temperature increase induces an increase in the desorption rate constant of the probe molecule, although this desorption kinetics has a limit; as consequence, even if the catalyst had uniform sites, the desorption curve would demonstrate some degree of dispersion with temperature. Nevertheless, it is normally assumed that an increase in temperature of desorption of the probe molecule corresponds to a greater strength of the bond between the protonic site and the probe molecule. In order to quantify this distribution of the acidity of the sites, it is necessary to decompose the TPD curve in several sub curves, each one corresponding to a different acid strength. The area of each one of these sub-curves will be proportional to the number of protonic acid sites that have uniform acidity. Traditionally, this deconvolution of the TPD curve was obtained by performing several TPD experiments, where the only difference was the initial temperature of desorption, which was consecutively increased. The difference between the TPD curves of two consecutive experiments corresponds to the desorption of the probe molecule from sites with a very narrow range of acidity.
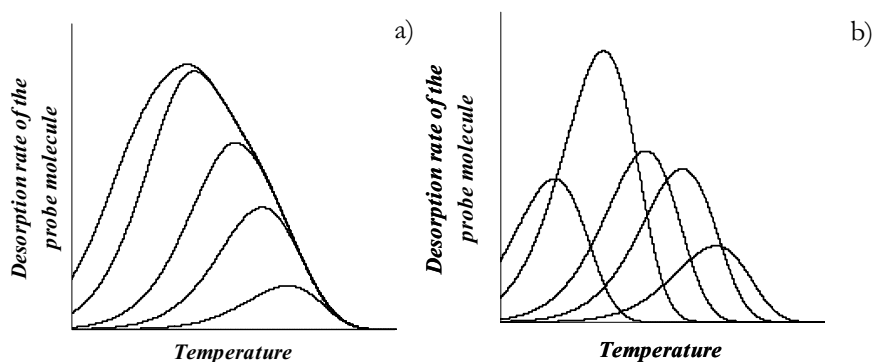
Figure 10 - Example of an experimental deconvolution of a TPD curve, where the TPD curves obtained experimentally and the result of their subtraction, are presented in figures a) and b), respectively.

The deconvolution of TPD curves using this technique is a very lengthy and difficult process to implement, as a consequence several alternative techniques based in a single experiment have been proposed. One of them is a numerical method, which enables to perform the deconvolution of the experimental TPD curve and, simultaneously, obtain for each sub curve indicative values of the amount and strength of the acid sites. Although the acidity distribution of a catalyst can be considered almost continuous, this technique assumes a discrete grid of desorption energy values, each one of these values corresponding to a different sub curve, and the TPD curve obtained experimentally is the result of adding all sub curves. Assuming that the desorption of the probe molecule, for a group of sites with equal energy, follows an irreversible first order kinetics, the desorption rate of the probe molecule is described by the following expression:

$$\frac{dq}{dt} = -\sum_{i=1}^{n}\left(k_i \cdot e^{-\frac{E_{a_i}}{R \cdot T}} \cdot q_i \right)$$

where dq/dt is the observed rate of desorption of ammonia at instant t, k_i is the pre-exponential factor, E_{ai} is the activation energy for the desorption of the

probe molecule from the acid sites i, R is the ideal gas constant and T is the absolute temperature.

Fitting this equation to the experimentally observed desorption rate curve, it is possible to determine the amount of acid sites (q_i) associated to each energy value (E_{ai}) in the chosen energy grid.
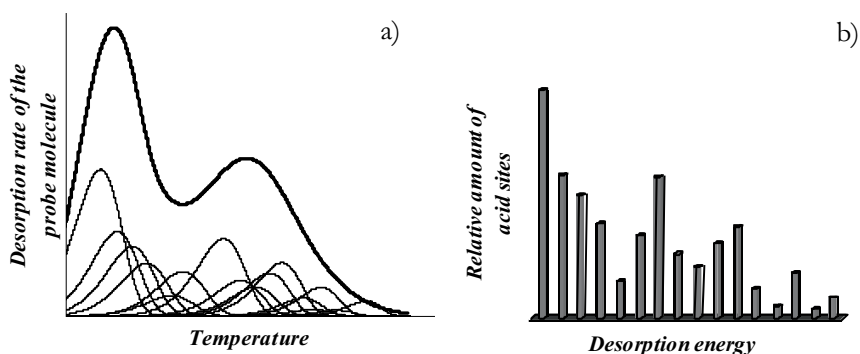
Figure 11 - a) TPD curve deconvoluted with the numerical technique described in the text; b) Acid site distribution as a function of desorption energy.

A more detailed description of this technique can be found in literature[18].

6.3.4. Importance of TPD

The activity of an acid catalyst is totally dependent on its acidity, in other words, it depends on the amount and strength of its acid sites, being impossible to consider these factors separately. As a consequence of this relation between acidity and activity, the characterization of the acidity of a catalyst is an essential step in order to understand its activity.

The TPD of probe molecules, in particular of ammonia, is a widespread technique and it is almost mandatory for anyone who wants to study the acidity of acid catalysts.

6.4. CATALYTIC TESTS

6.4.1. Catalytic Properties Evaluation

Industrial catalytic reactors may present a great variety of types, shapes and sizes, depending on the catalyst particles dimensions, reaction mixture phase (or multiphase), reaction thermicity, requested residence times, etc. Nevertheless, catalyst evaluation in the laboratory may be carried out in different reactors within a much narrower range of types.

In these laboratory tests, the catalyst may often be used as a powder, or in a fine granulometry, preventing in this manner the influence of possible mass transfer limitations on the observed reaction rates, allowing for an evaluation of the reaction kinetics. This kinetic evaluation is particularly important in the characterization of the active phase of the catalyst; its activity, selectivity for the formation of each product and stability being the main parameters to be known.

The aim of this section is to introduce the reader to heterogeneous catalytic tests at the laboratorial scale, so it will focus on the most frequently used laboratory reactors, and the simplest ones, which may be divided in two classes: fixed bed tubular reactors and slurry reactors. A more extensive approach to this subject can be found in literature[19].

6.4.2. Fixed Bed Tubular Reactors

This type of heterogeneous catalytic reactor is specially used for transformations in gaseous phase. The schematic experimental apparatus for its operation is presented in Figure12.

The data collected from the composition of the reactor effluent, allow the initial determination of the reactant conversion (x). The activity of the catalyst (Act), taken as the rate of the promoted reaction may be calculated from the conversion by considering a model for the reactor, usually the plug flow model:

$$F_{Ae}dx = Act.dw$$

where F_{Ae} is the reactant molar flow in the feed and dw the weight of catalyst. Performing different tests with different masses of catalyst, the initial activity will be obtained from the slope of the derivative of the curve defined in the representation of the conversion *vs* w/F_{Ae} , taken at the origin (zero conversion).
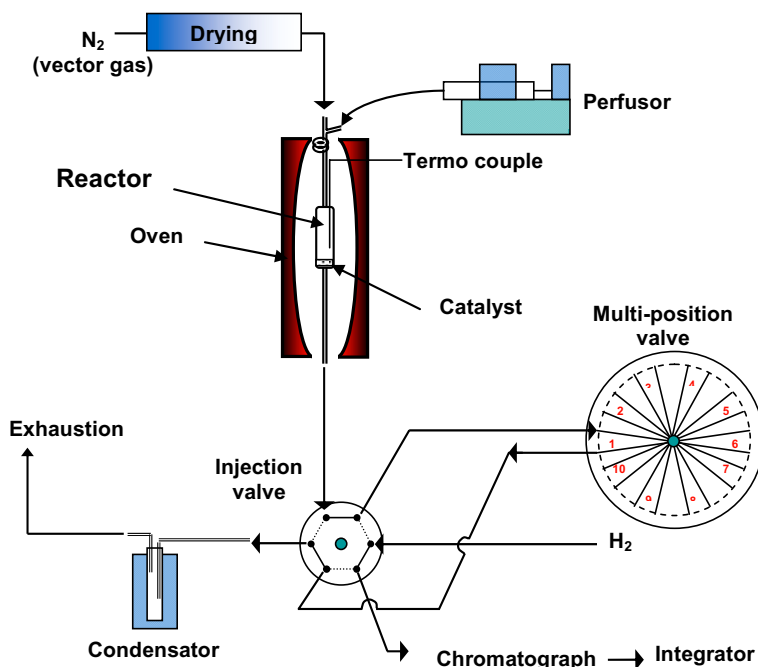
Figure 12 - Schematic representation of the experimental apparatus for operation with a continuous flow fixed bed tubular reactor in gaseous phase.

6.4.3. Slurry Reactors

In this case the transformation is carried out in a stirred vessel containing the catalyst. Most frequently it is operated in batch mode, processing liquid

163

reactants, and the experimental apparatus is considerably simpler than the one for the continuous gas phase transformations.

The composition analysis of samples taken from the reactor will allow the determination of the amount of the reactant in the reactor (n_A) as a function of time. The activity may then be calculated, assuming perfect mixing, and for a mass of catalyst w, by the expression:

$$Act. = \frac{1}{w}\frac{dn_A}{dt}$$

In the case of continuous operation, special care must be taken in order to maintain, as is usually desired, the catalyst inside the reactor. The analysis of the composition of the reactor effluent will allow the determination of the conversion, and the catalyst activity will be calculated, assuming also perfect mixing, by the expression:

$$Act. = \frac{F_{Ae}x}{w}$$

References

1. J. Ryczkowski, *Catal. Today*, **2001**, *68*, 263.

2. R. Aiello, J.B Nagy., J. Giordano, A. Katovic, F. Testa, *Comptes Rendus Chimie*, **2005**, *8*, 321.

3. A. Jentys, J.A. Lercher, *Techniques of Zeolite Characterization* in *Introduction to Zeolite Science and Practice*, H. Bekkum, E.M. Flanigen, P.A. Jacobs, J.C. Jansen (Eds.), Elsevier, Amsterdam, **2001**, pp. 345-386.

4. S. Khabtou, T. Chevreau, J.C. Lavalley, *Microporous Materials*, **1994**, *3*, 133.

5. J.R. Sohn, S.J. Decanio, J.H. Lunsford, *Zeolites*, **1986**, *6*, 225.

6. E.M. Flanigen, *Zeolite Chemistry and Catalysis*, ACS Monograph, **1976**, *171*, 80.

7. G. Coudurier, J.C. Védrine, *Pure & Appl. Chem.* **1986,** *58*, 1389.

8. M. Guisnet, F. Ramôa Ribeiro, *Zeólitos Um Nanomundo ao Serviço da Catálise*, Fund. Calouste Gulbenkian, Lisboa, **2004**.

9. F. Thibault-Starzyk, *Introduction à L'étude des Zéolithes par Spectroscopie Infrarouge* in *Les Matériaux Micro et Mésoporeux – Caractérisation,* Groupe Français des Zéolithes, F. Thibault-Starzyk (Eds.), EDP Sciences, **2004**, pp. 51-90.

10. A. Martins, J. Silva, M.C. Henriques, F.R. Ribeiro, M.F. Ribeiro, *Catal. Today*, **2005**, *107-108*, 663.

11. C.A. Emeis, *J. Catal.,* **1993**, *141*, 347.

12. S. Khabtou, T. Chevreau, J.C. Lavalley, *Microporous Materials,* **1994**, *3*, 133.

13. M. Guisnet, P. Ayrault, J. Datka, *Pol. J. Chem.,* **1997**, *71*, 1455.

14. H. Knözinger, S. Huber, *J. C. S. Faraday Trans.,* **1998**, *94*, 2047.

15. A. Corma, V. Fornés, L. Forni, F. Marquéz, J. Martinéz-Triguero, D. Moscotti, *J. Catal.* **1998**, *179*, 451.

16. J.A. Lercher, C. Gründling, G. Eder-Mirth, *Catal. Today* **1996**, *27*, 353.

17. H. Frei, Y.H. Yeom, *Time-resolved Step-scan and Rapid-scan Fourier-Transform Infrared Spectroscopy* in *In-situ Spectroscopy of Catalysts*, B.M. Weckhuysen (Eds.), ASP, USA, **2004**, pp. 32-46.

18. C. Costa, J.M. Lopes, F. Lemos, F. Ramôa Ribeiro, *J. Mol. Catal. A: Chem.,* **1999**, *144*, 221.

19. F. Lemos, J.M. Lopes, F. Ramôa Ribeiro, *Reactores Químicos*, IST Press, Lisboa, **2002**.

(Página deixada propositadamente em branco)

7. CHEMICAL REACTION ENGINEERING

Alírio E. Rodrigues

Laboratory of Separation and Reaction Engineering (LSRE), Associate Laboratory LSRE/LCM, Department of Chemical Engineering, Faculty of Engineering, University of Porto (FEUP)

In this chapter we briefly summarize the fundamentals of Chemical Reaction Engineering (CRE) needed to design and understand reactor operation. We start with the definition of chemical reactor and use chemical engineering principles to derive design equations for homogeneous ideal reactors (batch, plug flow and perfectly mixed reactors). Then heterogeneous catalytic reactors are introduced and the competition between diffusion and reaction in porous catalysts is addressed. Finally deviations to plug flow are introduced and a simple pseudo-homogeneous model of fixed bed reactor is discussed.

7.1. FUNDAMENTALS

7.1.1. Definition of chemical reactor

Let us start by recalling the definition of chemical reactor given by Levenspiel[1]:

A chemical reactor is a piece of equipment in which a fluid

    i.   can be heated or cooled;

    ii. can exchange mass/heat with a stagnant phase and

    iii. can be chemically transformed into different products.

This broad definition includes heat exchangers, fixed-bed operations as chromatography, adsorption, ion-exchange, etc and *last but not the least* the chemical reactor as commonly understood.

7.1.2. Chemical engineering principles

Le Goff[2] taught me in Nancy that the design of a chemical reactor involves, as any chemical engineering operation, the writing of the following equations:

   i.   conservation equations (mass, energy, momentum and electric charge balances);
   ii.   equilibrium laws at interfaces;
   iii. kinetic law of (bio)chemical reaction and mass/heat transfer;
   iv.   constitutive laws (e.g., ideal gas law, Hooke's law);
   v.   initial (IC) and boundary conditions (BC);
   vi.   optimization criterion.

The "supermarket" of chemical reactors is full of different reactor types: the "old" ideal reactors (batch, continuous reactors - plug flow and perfectly mixed reactors, semi-batch and "new" (microreactors, monoliths, reverse flow reactors, multifunctional reactors, etc). In any case there is a reaction going on inside the equipment; in the case of a single reaction involving species A_i with stoichiometric coefficients ν_i (>0 for products, <0 for reactants and zero for inerts)

$$\sum_i \nu_i A_i = 0 \tag{1}$$

7.1.3. Progress of a chemical reaction

The progress of a chemical reaction can be measured by the thermodynamic extent of reaction ξ introduced by De Donder. If we consider a batch system the change on the number of moles of species i (dn_i) in the time interval dt is a measure of the progress of the chemical reaction; therefore we can write:

$$dn_i = \nu_i d\xi \qquad (2)$$

or in the integrated form

$$n_i = n_{i0} + \nu_i \xi \qquad (3)$$

where n_{i0} is the number of moles of species i at time t=0.

Chemical engineers like dimensionless variables within bounds. That is the reason why they introduced the extent of reaction $X = \xi / n_0$ from the normalization of ξ by the total number of moles of active species $n_0 = \sum_i n_{i0}$ at t=0. The equation defining the extent of reaction X is then:

$$n_i = n_{i0} + \nu_i n_0 X \qquad (4)$$

More commonly we talk about conversion of a limiting reactant X_ℓ defined as:

$$n_\ell = n_{\ell 0}(1 - X_\ell) \qquad (5)$$

Obviously these quantities are related; the extent of reaction is equal to the conversion when the stoichiometric coefficient is (-1) and only one active species is present at time zero.

For continuous reactors in steady state similar relations hold if we substitute the number of moles n_i by the molar flow F_i.

7.1.4. Rate of reaction

For a single reaction $A \rightarrow products$ the reaction rate is just a function of the local composition, temperature and pressure, i.e.,

$$\Re = F(c_i, T, P) \tag{6}$$

The rate of formation of a species i, is simply $\Re_i = \nu_i \Re$ expressed in mole i/(m³ of mixture. s).

The above function can take different forms:

(i) $\Re = kc_A$ for first-order reactions;

(ii) $\Re = k; c_A > 0$ for zero order reactions (when there is no reactant the rate is zero);

(iii) $\Re = \dfrac{kc_A}{K_m + c_A}$ for Michaelis-Menten type kinetics;

(iv) $\Re = \dfrac{k_1 c_A}{(1 + k_2 c_A)^2}$ for linear reaction rate at low concentration and hyperbolic type kinetics at high concentrations. This rate equation applies to CO oxidation in car exhaust catalysts. Later we will see that even an isothermal perfectly mixed reactor with such kinetic law can have multiple steady states. These rate laws are illustrated in Figure 1.
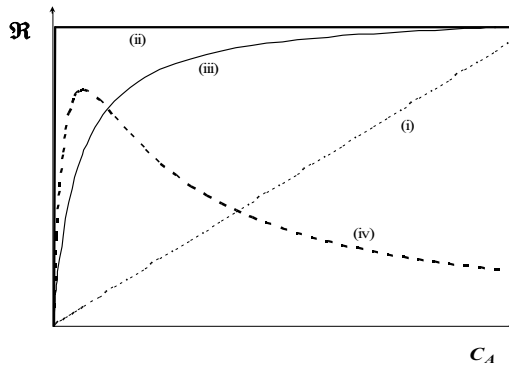
Figure 1 - Reaction rate laws.

7.2. DESIGN EQUATIONS OF ISOTHERMAL IDEAL REACTORS

7.2.1. Batch reactor

Model equations for isothermal batch, homogeneous, reactors[1,3], Figure 2 include mass conservation equation (material balance), reaction rate law, constitutive equation (ideal gas for example) and initial condition.
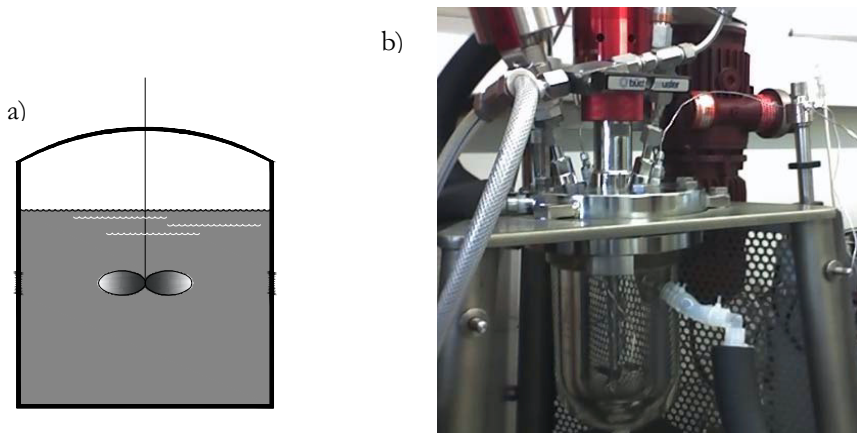
Figure 2 - Batch reactor: a) Schematic representation; b) Photo.

The mass balance equation for species i just states that the accumulation of species in the batch system is equal to the rate of formation of that species:

$$\frac{dn_i}{dt} = \Re_i V \tag{7}$$

In the above equation V is the volume of the mixture which can change as reaction progresses. For ideal gas systems:

$$V = \beta V_0 (1 + \alpha X) \tag{8}$$

where $\beta = \dfrac{P_o T}{P T_o}$ is a physical dilatation factor and $\alpha = \dfrac{\Delta \nu}{1 + \dfrac{n_I}{n_o}}$ is a chemical

dilatation factor with $\Delta \nu = \sum_i \nu_i$ and n_I is the number of moles of inert

species I.

Introducing the definition of extent of reaction X given by Equation (4) and the function V(X) given by Equation (8) in the mass balance, Equation (7) we get $\nu_i n_o \dfrac{dX}{dt} = \nu_i \Re_i V(X)$ and finally the design equation of a batch reactor:

$$t_{batch} = n_o \int_0^{X_b} \frac{dX}{\Re(X)V(X)} \tag{9}$$

where t_{batch} is the time needed to get the extent of reaction X_b.

You certainly realize that with consecutive reactions things are more complicated; if you "cook" too much you most probably will not get a good result. You must then stop the batch operation at the optimum point; an

example is the production of vanillin from lignin where there is an optimum time to get the higher vanillin concentration. After that time vanillin degrades…

7.2.2. Continuous perfectly mixed reactor (PMR)

For the isothermal PMR or continuous stirred tank reactor (CSTR) shown in Figure 3 the mass balance in steady state for species i states that: molar flow at the inlet (in)= molar flow at the outlet (s) + disappearance by reaction, i.e.,

$$F_{i,in} = F_{i,s} + (-\Re_i)V \tag{10}$$

Taking into account that: $F_{i,in} = F_{i,o} + \nu_i F_o X_{in}$ and $F_{i,s} = F_{i,o} + \nu_i F_o X_s$ we get the reactor volume of the perfectly mixed reactor needed to obtain the extent of reaction at the outlet X_s:

$$V_{PMR} = \frac{F_o(X_s - X_{in})}{\Re(X_s)} \tag{11}$$

where F_o is the total molar flow of active species in a reference state where the extent of reaction is zero and the rate of reaction is evaluated at the outlet conditions since in a PMR the composition at any point of the reactor is equal to that at the reactor outlet.
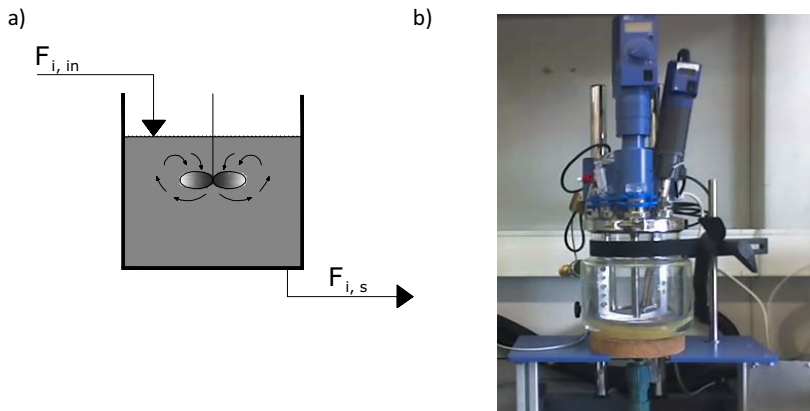
Figure 3 - Continuous perfectly mixed reactor: a) Schematic representation; b) Photo.

7.2.3. Plug flow reactor (PFR)

The plug flow reactor is sketched in Figure 4. In the plug flow all molecules take the same time to travel through the reactor until they exit the system. The velocity profile in a cross section of the tubular reactor is flat in plug flow; the space time is the reactor volume divided by the volumetric flow rate at the inlet conditions.
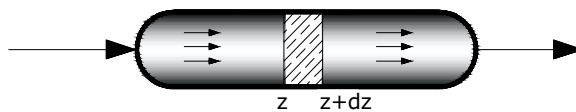
Figure 4 - The plug flow reactor (PFR).

Since in this type of reactor the composition is changing along the axial reactor coordinate we have to choose first the volume element where the mass balance for species i will be written. It is the volume between sections located at z and z+dz or $dV = A\,dz$. The mass balance over that volume element in steady state is again: molar flow entering the volume element at section z (or volume from the inlet V=Az) = molar flow at the outlet section of the volume element

located at z+dz (or volume from the inlet V+dV) + disappearance by reaction in the volume element dV, i.e.,

$$F_i\big|_V = F_i\big|_{V+dV} + (-\Re_i)dV \tag{12}$$

or

$$\frac{dF_i}{dV} + (-\Re_i) = 0 \tag{12}$$

The first term is the contribution of convection and the second term is the reaction contribution.

The integrated form taking into account the relation between molar flow F_i and reaction extent X is:

$$V_{PFR} = F_o \int_{X_{in}}^{X_s} \frac{dX}{\Re(X)} \tag{13}$$

7.2.4. Comparison between PMR and PFR

Now let us compare the volumes of PFR and PMR needed to treat a feed in order to reach a given extent of reaction X_s at the outlet. The single reaction $A \rightarrow products$ is assumed to be first order with respect to the concentration of reactant A. By plotting $\dfrac{F_o}{\Re(X)}$ as a function of X the area under the line in Figure 5 is the volume of the plug flow reactor; it is lower than the corresponding volume of the PMR which is the area of the rectangle with abcissa X_s and height $\dfrac{F_o}{\Re(X_s)}$.
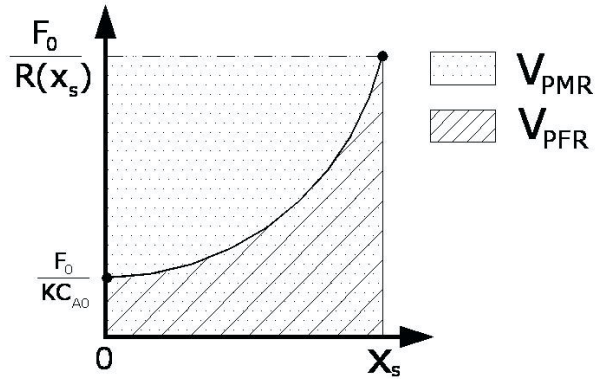
Figure 5 - Comparison of PFR and PMR for irreversible first order reaction.

7.2.5. Homogeneous versus heterogeneous reactors

In the above design equations the rate of reaction was expressed in terms of volume of reacting mixture. All design equations for ideal heterogeneous reactors are similar provided that the reaction rate is now $\Re^{'}$ expressed in mole/(kg catalyst.s) and the volume in homogeneous reactors is replaced by the mass of catalyst W_{cat}^{ideal}. If the feed mixture is not converted at all design equations for "ideal" continuous reactors are now:

Perfectly mixed reactor (heterogeneous):

$$W_{cat,PMR}^{ideal} = \frac{F_o X_s}{\Re^{'}(X_s)} \tag{14}$$

Plug flow reactor (heterogeneous):

$$W_{cat,PFR}^{ideal} = F_o \int_{0}^{X_s} \frac{dX}{\Re^{'}(X_s)} \tag{15}$$

176

The above equations imply that there are no mass transfer limitations, i.e., concentration of species inside catalyst particles is equal to the concentration in the bulk fluid phase around particles.

7.3. THE CATALYST PARTICLE. COMPETITION BETWEEN TRANSPORT PHENOMENA AND REACTION

7.3.1. Inventory of transport and reaction processes in porous catalysts

Consider a single reaction $A \to B$ occurring at the active sites of a catalyst particle surrounded by a bulk fluid phase where reactant A has concentration $c_{A,b}$.

The processes of transport and reaction shown in Figure 6 include:

1. diffusion of A through the fluid film around the particle (external or film diffusion);
2. diffusion of A in the catalyst pores (internal diffusion);
3. adsorption of A at the sites $A + S \Leftrightarrow AS$;
4. surface reaction at the sites $AS \to BS$;
5. desorption of B species $BS \Leftrightarrow B + S$;
6. diffusion of B through catalyst pores;
7. diffusion of B through the external film to the bulk fluid phase.

Mass transfer resistances can be present with concentration gradients for species both in the external fluid film and inside pores.
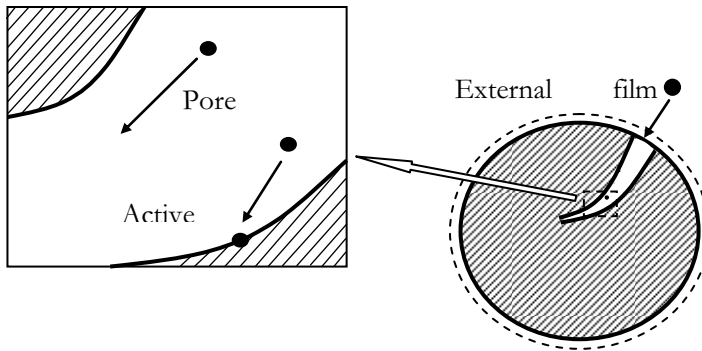
Figure 6 - Transport processes and reaction in porous catalysts.

7.3.2. Pore diffusion and reaction in porous catalysts: limiting situations of concentration profiles and effectiveness factor

Let us consider the competition of pore diffusion and reaction in an isothermal catalyst at steady state[4]. The concentration of species A at the surface is c_{As}. Three cases can be identified depending on the relative importance of pore diffusion rate and reaction rate:

a) pore diffusion rate >> reaction rate: the intraparticle concentration profile is almost flat; the catalyst operates in the chemical kinetics controlled regime;

b) reaction rate >> pore diffusion rate: the concentration profile inside the catalyst is in a thin region near the catalyst surface; the catalyst operates in the diffusion-controlled regime;

c) reaction rate and pore diffusion rate are of similar magnitude; the catalyst works in the intermediate regime.

The above situations are illustrated in Figure 7.
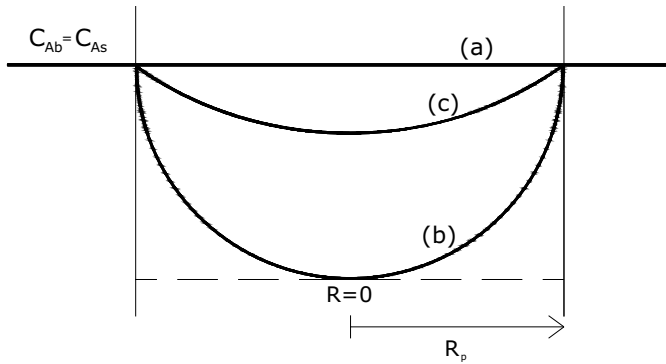
Figure 7 - Concentration profiles inside a catalyst particle with radius, R_p.

The parameter governing the competition of reaction and pore diffusion is the ratio of reaction rate and diffusion rate, i.e.,

$$\phi^2 = \frac{reaction\ rate}{diffusion\ rate} \tag{16}$$

where ϕ is the Thiele modulus.

In the chemical regime the observed reaction rate is $\Re'_{obs} = \Re'(c_{As})$; in the diffusion-controlled regime $\Re'_{obs} = \eta \Re'(c_{As})$ where η is the catalyst effectiveness factor. For a first order irreversible reaction in a catalyst $\Re' = kc_{As}$ and $\Re'_{obs} = k < c_{As} >$ based on the average concentration of A inside the catalyst.

The catalyst effectiveness factor is an important quantity since it will allow the calculation of real amount of catalyst needed to place inside the reactor to reach a given conversion in steady state; in fact $W_{cat} = \dfrac{W_{cat}^{ideal}}{\eta}$. The shape of a catalyst can be slab, infinite cylinder or sphere described by a shape factor s = 1

for slab, 2 for cylinder and 3 for spheres in such a way that the ratio of particle volume and external particle is $\dfrac{V_p}{A_p} = \dfrac{R_p}{s}$.

7.3.3. Concentration profiles inside a catalyst and catalyst effectiveness factor

Let us consider a slab isothermal catalyst with half-thickness ℓ shown in Figure 8.
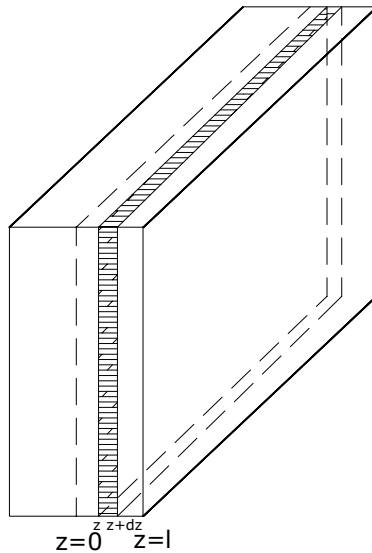
Figure 8 - Slab catalyst and volume element.

The mass balance in a particle volume element between sections at z and z+dz in steady state is:

Total flux of A "in"= total flux of A "out" + A consumed by reaction in the volume element

For first order reaction and diffusion flux governed by Fick's law we obtain:

$$D_{Ae} \frac{d^2 c_A}{dz^2} - kc_A = 0 \tag{17}$$

with boundary conditions: z=0 ; $dc_A/dz= 0$ (symmetry condition) and $z = \ell$; $c_A=c_{As}$.

Introducing dimensionless variables $\widetilde{c}_A = \dfrac{c_A}{c_{As}}$ and $x = \dfrac{z}{\ell}$ dimensionless model equation is:

$$\frac{d^2 \widetilde{c}_A}{dx^2} - \phi^2 \widetilde{c}_A = 0 \tag{18}$$

where $\phi^2 = \dfrac{\ell^2 k}{D_{Ae}}$.

Concentration profiles resulting from the solution of Equation (18) with the boundary conditions are given in Equation (19) and shown in Figure 9.

$$\widetilde{c}_A = \frac{\cosh(\phi x)}{\cosh \phi} \tag{19}$$
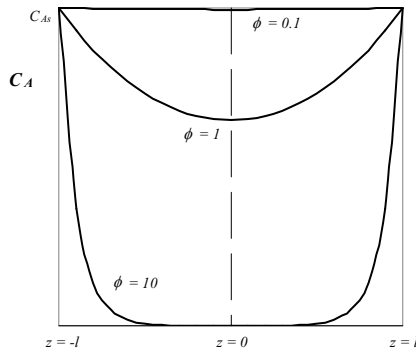
Figure 9 - Concentration profiles inside a slab catalyst.

The effectiveness factor is $\eta = \dfrac{\Re'_{obs}}{\Re'(c_{As})} = \dfrac{<\Re'>}{\Re'(c_{As})} = \dfrac{<c_A>}{c_{As}}$ which finally

leads to:

$$\eta = \frac{\tanh\phi}{\phi} \tag{20}$$

The plot of $\eta = f(\phi)$ is shown in Figure 10. For low Thiele modulus $\phi < 1/3$ the catalyst works in the chemical controlled regime and $\eta \approx 1$; for $\phi > 3$ the catalyst operates in the diffusion-controlled regime and the effectiveness factor is $\eta = \dfrac{1}{\phi}$.
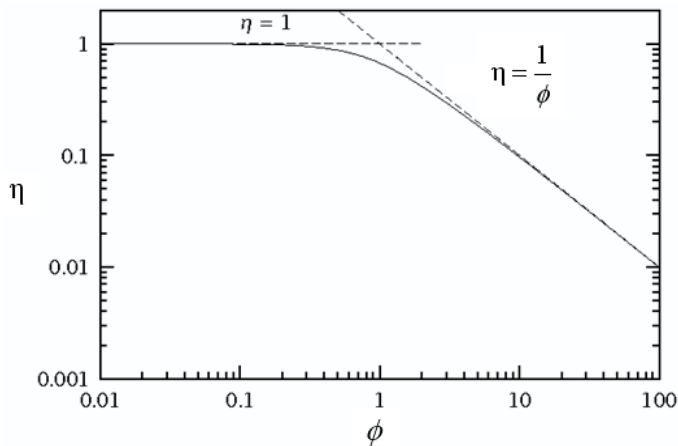
Figure 10 - Effectiveness factor η versus Thiele modulus ϕ: slab isothermal catalyst and first order irreversible reaction.

For spherical catalysts the effectiveness factor is:

$$\eta = \frac{3}{\phi}\left(\frac{1}{\tanh\phi} - \frac{1}{\phi}\right) \tag{21}$$

with the Thiele modulus based on the particle radius. In the diffusional – controlled regime the catalyst effectiveness factor is simply $\eta \approx \dfrac{s}{\phi}$ where s is the shape factor.

7.3.4. Criterion for absence of diffusion limitations

Let us consider again the slab catalyst and first order irreversible reactions. Weisz noted that $\eta\phi^2$ is expressed in terms of observable/measured quantities. In fact:

$$\eta\phi^2 = \frac{\mathfrak{R}'_{obs}}{\mathfrak{R}'(c_{As})}\frac{\ell^2 k}{D_{Ae}} = \frac{\mathfrak{R}'_{obs}}{kc_{As}}\frac{\ell^2 k}{D_{Ae}} = \frac{\mathfrak{R}'_{obs}\ell^2}{c_{As}D_{Ae}} \tag{22}$$

When $\phi < \dfrac{1}{3}$, $\eta \approx 1$ and $\eta\phi^2 \approx 0.1$; the criterion for absence of diffusion limitations is then:

$$\frac{\mathfrak{R}'_{obs}\ell^2}{c_{As}D_{Ae}} < 0.1. \tag{23}$$

7.3.5. Nonisothermal catalysts. Damkohler equation

Figure 11 is a sketch of a catalyst particle with concentration and temperature profiles when an exothermic reaction is taking place.
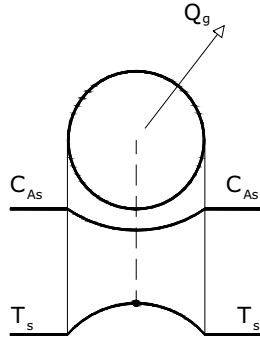
Figure 11 - Non isothermal catalyst particle with concentration and temperature profiles.

The heat generated by reaction in the section at radial position r is:

$$Q_g = \dot{N}(-\Delta H) \tag{24}$$

where $\dot{N}$ is the total molar flux crossing the section at position r (mol/s) by diffusion and $(-\Delta H)$ is the heat of reaction (J/mol). The heat generated has to be removed by conduction according to Fourier's law

$$Q_r = -A_r \lambda_e \frac{dT}{dr} \tag{25}$$

where A_r is the area of the sphere located at the radial position r, T is the temperature (K) and λ_e is the effective thermal conductivity of the catalyst.

At steady state the heat generated equals the heat removed, i.e., $\dot{N}(-\Delta H) = -A_r \lambda_e \frac{dT}{dr}$; taking into account that $\dot{N} = A_r D_{Ae} \frac{dc_A}{dr}$ we get

$A_r D_{Ae} \frac{dc_A}{dr}(-\Delta H) = -A_r \lambda_e \frac{dT}{dr}$ and finally, after integration between surface conditions and conditions at the radial position r:

$$T - T_s = \frac{D_{Ae}(-\Delta H)}{\lambda_e}(c_{As} - c_A) \tag{26}$$

Equation (26) was derived by Damkohler[5] a CRE pioneer. It relates concentration and temperature at any catalyst point. It allows a priori calculation of the maximum temperature T_m that the catalyst will reach for given operating conditions; in fact for c_A equal to zero we get:

$$T_m - T_s = \frac{D_{Ae}(-\Delta H)c_{As}}{\lambda_e} \tag{27}$$

or simply:

$$T_m = T_s(1 + \beta) \tag{28}$$

where $\beta_s = \dfrac{D_{Ae}(-\Delta H)c_{As}}{\lambda_e T_s}$ is the Prater thermicity factor.

7.4. THE FIXED-BED CATALYTIC REACTOR

7.4.1. Deviations from plug flow. Tracer experiments and Residence Time Distribution (RTD)

Here we will consider only a tubular, fixed bed catalytic reactor. In real reactors deviations from plug flow can occur and one should be able to calculate conversion in a tubular reactor for any kinetics provided that the macroscopic fluid flow is characterized. In fact the output of a reactor depends on the type of input, reaction kinetics, nature of fluid flow and state of micromixing.

The simplest way to get an idea on how the fluid travels through the reactor is by doing a tracer experiment[6]; at time zero a pulse of tracer is injected in the

feed stream and the tracer concentration at the outlet recorded as a function of time. This is illustrated in Figure 12.
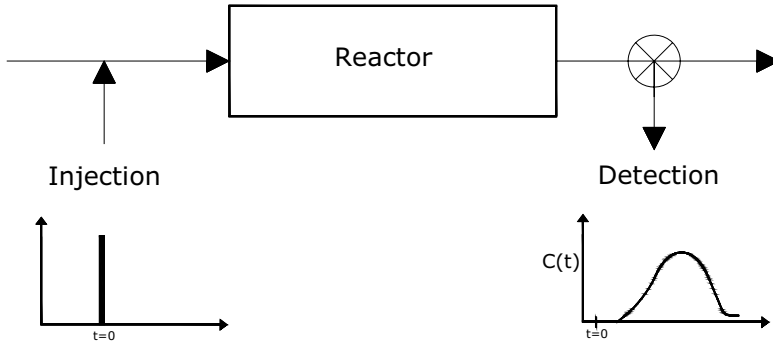
Figure 12 - A tracer experiment to evaluate the nature of macroscopic fluid flow.

A tracer is any substance which can be injected in the fluid flow we want to study with properties as close as possible to the fluid flowing through the system and easily detected at the outlet. Ideally tracer experiments should be done under nonreactive conditions.

From the tracer outlet concentration as a function of time the mean residence time can be calculated as the first moment of the response:

$$\bar{t}_r = \frac{\int_0^\infty t c_{out}(t)dt}{\int_0^\infty c_{out}(t)dt} \qquad (29)$$

and the variance of the tracer response as $\sigma^2 = \mu_2 - \mu_1^2$ measures the deviation to plug flow.

The theoretical Residence Time Distribution, E(t) is closely related to the normalized tracer response to an impulse of tracer $C(t) = \frac{c_{out}(t)}{c^o}$:

$$C(t) = \tau E(t) \tag{30}$$

where $\tau = \dfrac{\varepsilon V}{Q_o}$ is the space time and $c^o = \dfrac{n}{\varepsilon V}$ is a reference concentration of

tracer is the accessible volume to the fluid in the reactor. One should note that $E\,(t)$ dt is the fraction of tracer molecules leaving the reactor which spent a time between t and t+dt inside the system.

For total segregated flow it can be shown based on an association of plug flow reactors in parallel to cover all residence times, Figure 13, of the DTR that in steady state:

$$<c_{A,out}> = \int\limits_0^\infty c_{batch}(t)E(t)dt \tag{31}$$

where the information of both reaction kinetics (from batch experiments) and fluid flow (from tracer experiments, E(t)) are needed to calculate the reactant concentration at the reactor outlet.
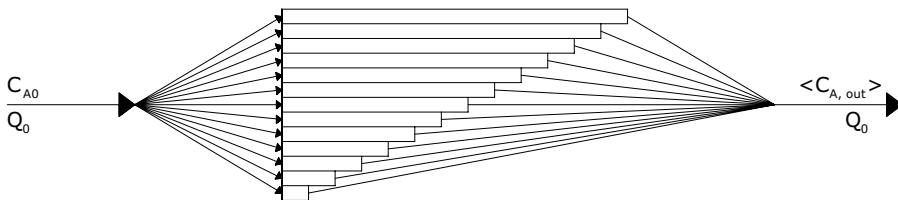
Figure 13 - A model of total segregated flow in a reactor: elements residing a time do not mix with fluid elements with different residence times.

In fact a mass balance at the outlet node, Figure 13, gives:

$$Q_o < c_{A,out} >= \sum_1 c_A(t_i)\Delta Q_i \tag{32}$$

or

$$< c_{A,out} >= \sum_1 c_A(t_i)\frac{\Delta Q_i}{Q_o} \tag{33}$$

Finally Equation (31) is obtained by remembering that $\dfrac{dQ}{Q_o} = E(t)dt$.

7.4.2. A pseudo-homogeneous model for a fixed-bed catalytic reactor

Models for catalytic reactors can be divided into pseudo-homogeneous and heterogeneous. In the first class no gradients of concentration and temperature are considered between the bulk fluid phase and catalyst particle; in the heterogeneous models at least one gradient of concentration/temperature is considered. Models can be also grouped in one-dimensional (1-D model, state variables depend only on the axial position) and bi-dimensional models (concentration and temperature depend also on the reactor radial position).

Here we look at the simplest 1-D pseudo-homogeneous model which assumes plug flow for the fluid phase and diluted feed; model equations include mass and energy balances:

$$u_o \frac{dc_{Ab}}{dz} + \Re(c_{Ab};T_b) = 0 \tag{34}$$

$$u_o \rho_f C_{pf} \frac{dT_{Ab}}{dz} - (-\Delta H)\Re(c_{Ab};T_b) + \frac{2U}{R_t}(T_b - T_e) = 0 \tag{35}$$

In the above equations u_o is the superficial fluid velocity, U is the overall heat transfer at the wall of the reactor with radius R_t and the fluid properties are density ρ_f and heat capacity C_{pf}. The first terms in both balances are the convective and reaction contributions; the third term in the energy balance represents heat losses at the wall.

A typical solution for the axial concentration and temperature profiles is shown in Figure 14 showing a hot spot in the temperature profile. The inlet feed conditions are T_o and c_{Ao}.

If the reactor operates adiabatically (U=0) the maximum temperature rise can be easily calculated (multiply the mass balance by the heat of reaction and add both Equations 34 and 35, etc.):

$$T_{max} - T_o = \frac{(-\Delta H)c_{Ao}}{\rho_f C_{pf}} \tag{36}$$
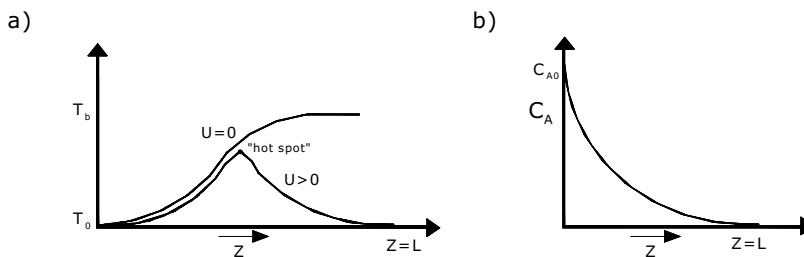
Figure 14 - Temperature a) and concentration b) profiles in a fixed-bed reactor.

This is an important calculation since one should know *a priori* the maximum temperature the catalyst may handle without damage and then find the appropriate operating conditions to meet the above constraint.

Last but not the least: this was a short introduction of CRE for non-chemical engineers. Those who want to learn more must be selective in reading – suggestions are given in the references.

Acknowledgement

I would like to acknowledge my PhD student Carla Pereira for providing me the notes taken during the lectures and for the art work.

References

_____

1. O. Levenspiel, *Chemical Reaction Engineering*, J. Wiley, New York, **1972**.

2. P. Le Goff, *Cours de Génie Chimique*, ENSIC, Nancy, **1970**.

3. J. Villermaux, *Génie de la Réaction Chimique*, Lavoisier, **1982**.

4. R. Aris, *The Mathematical Theory of Diffusion and Reaction in Permeable Catalysts*, Clarendon Press, Oxford, **1975**.

5. G. Damkohler, *Z. Elektrochem.*, **1936**, *42*, 846.

6. P.V. Danckwerts, *Chemical Engineering Science*, **1953**, *2*, 1.

8. SHAPE SELECTIVE CATALYSIS BY ZEOLITES

Luís Costa and Fernando Ramôa Ribeiro

Centro de Engenharia Biológica e Química, Departamento de Engenharia Química, Instituto Superior Técnico, Av. Rovisco Pais, 1049-001 Lisboa, Portugal.

Zeolites have a particular type of selectivity, called molecular shape selectivity[1,2] that is the result of the shapes and sizes of the molecules of reactants, products and intermediates being of the same magnitude as the shapes and sizes of the zeolite pores and cages where the active sites are located. This concept is the basis for many oil refining and petrochemical processes and the number of scientific publications on this subject in the past decade fully illustrates its importance: 600 papers in international scientific journals and 300 US patents[3]. There are essentially four major types of molecular shape selectivity[4,5,6]:

- for reactants: the pore mouths of some zeolites only allow some of the reactant molecules to diffuse through the channels and reach the active sites. This is reactant shape selectivity.
- for products: some of the products formed inside the pores are too bulky to diffuse towards the external medium. These products are converted into smaller molecules or deactivate the catalyst by blocking the pore exits. This is product shape selectivity.
- for transition states or intermediates: certain reactions are prevented because the intermediates or transition states are too bulky for the space available in the cages and pores of the zeolite structure. This is restricted transition state selectivity.
- the concentration effect[7,8]: it describes the concentration increase of hydrocarbons in zeolites, favoring bimolecular reactions over monomolecular ones. A special case of this effect, the so-called cage

effect, occurs in zeolites that present erionite cages (erionite, zeolite T). The mobility of molecules like *n*-heptane and *n*-octane is drastically reduced because these alkanes are perfectly adapted to the erionite cages. As a consequence, the diffusivity of *n*-paraffins with this number of carbon atoms is minimal, whereas their reactivity is maximized.

Another less common expression of molecular shape selectivity has been referred to: molecular traffic control[9] which may occur in zeolites such as ZSM-5 with more than one type of pores. Reactant molecules may preferentially penetrate through one type of pores while the products diffuse through pores of other dimensions, thus minimizing counter-diffusion phenomena.

Molecular diffusion plays an extremely important role in the case of zeolites. In porous solids, there are two diffusion regimes: molecular diffusion, where the mean free path of molecules is small compared to the pore diameter, the diffusion occurring by collisions between molecules; and Knudsen diffusion, by collisions with the walls, where the diffusivity is proportional to the reciprocal of the pore diameter.

In zeolites, there is a new type of diffusion that Weisz[10] named configurational, governed by the size and configuration of the molecules.

Recently, however, the role of the external acid sites of zeolites (and not just the ones located inside the pore structure) has attracted much attention due to the development of nanocrystalline zeolite synthesis, which led to the discovery of new types of shape selectivity: the nest effect, pore mouth catalysis and key-lock catalysis (Section 8.1.5).

8.1. Shape Selectivity And Applications In Industrial Catalytic Processes

Let us analyze the different types of shape selectivity and applications in past or present industrial catalytic processes, namely in the oil refining and petrochemical industries.

It is interesting to note that the first two types of shape selectivity discussed here, for reactants and for products, both occur either by size exclusion phenomena because of the pore apertures or by molecular diffusion differences. These are standard mechanisms recognizable in molecular sieves.

8.1.1. Shape selectivity for reactants

Weisz and Frilette[11] were not just pioneers of molecular shape selectivity catalysis, rather their experimental tests were at the origin of many industrial catalytic applications. The first results obtained by them in olefin hydrogenation[11] on zeolite A (pore aperture of 4 Å) are represented in Table 1.

TABLE 1 - Reactant shape selectivity in the hydrogenation of olefins over zeolite CaA with 0.3 % Pt (T = 25 ºC, 1 atm, $H_2/HC = 3$ and time-on-stream = 0.3 s).

Olefin	Conversion (%)
Propylene	52
1-butene	70
iso-butene	3

Analyzing the results, it can be concluded that though iso-butene is easier to hydrogenate than propylene and 1-butene, its conversion is almost zero. In fact, due to its kinetic diameter (5.3 Å) it cannot enter the pores of zeolite A, being transformed only over the external acid sites, and its conversion depends on the

crystallite size. The smaller they are, the greater their external area per mass of zeolite and, as such, the greater the number of external active sites per mass unit and, consequently, the conversion.

Many industrial applications of zeolites involve acid catalysis, for example cracking and isomerization. One important industrial process of the past (developed in the 1960's[12]) is selectoforming[13,14,15] over zeolite NiH-erionite with pore dimensions of 3.5×5.2 Å. As can be seen in Figure 1, the isoparaffins (5.3 Å), although easier to crack than n-paraffins (4.3 Å), cannot penetrate the pores, and therefore are not cracked unlike the n-paraffins. This leads to the increase of the gasoline octane index by increasing the percentage of isoparaffins, although with a higher production of light products. Cycloparaffins and aromatics are also not cracked which is advantageous since they are hydrocarbons with a high octane index.
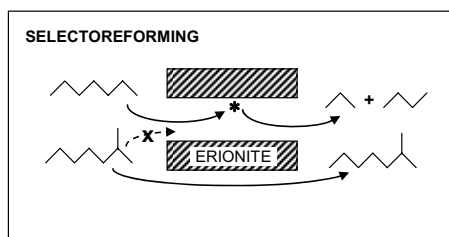
Figure 1 - Selectoforming (selective cracking) of n-paraffins over zeolite NiH-erionite.

Another very interesting application of shape selectivity for reactants was the M-forming process[16], given the strict regulations imposed by the European Union and other institutions at that time, banning the addition of alkyl-lead compounds to improve gasoline octane index values.

As shown in Figure 2, this process used zeolite ZSM-5 as one of the catalysts. There was a combination of an "intelligent" cracking reaction with aromatic alkylation. The n-paraffins and monobranched paraffins that had low octane index values entered the zeolite pores and were cracked. The resulting lighter

products alkylated the aromatic molecules, yielding alkyl-aromatic compounds with a high octane index. As a consequence, the industrial cracking catalyst formulations contained both H-ZSM-5 and REHY (zeolite HY exchanged with rare earths metals).
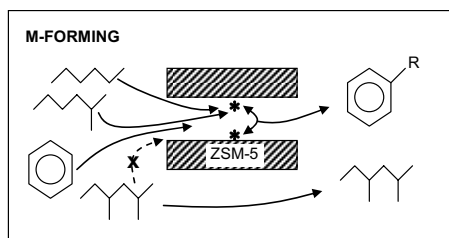
Figure 2 - M-forming (intelligent cracking and alkylation) over zeolite H-ZSM-5.

At the time of their development, these two processes played a key role in the implementation of environmental legislation to reduce the use of poisonous lead-containing compounds. However, decades later, new laws and directives were issued to regulate the amount of aromatics in fuels, in order to minimize their emissions by combustion engines. Since the fuels produced by selectoforming and M-forming presented high concentrations of aromatics, these processes were abandoned or reconverted.

8.1.2. Shape selectivity for products and restricted transition state selectivity

Its application with a greater impact on the petrochemical industry is the process of selective isomerization of xylenes. These aromatics are produced by reforming and, after distillation, their distribution corresponds to the thermodynamic equilibrium (25 % *o*-xylene; 50 % *m*-xylene; 25 % *p*-xylene). As *p*-xylene has the highest commercial value (basic raw material for the production of fibers and synthetic resins), it was imperative to obtain it in a

more selective way. One of the most typical processes uses ZSM-5 as catalyst[17], which present numerous advantages:

- high acidity and, thus, high activity in isomerization reactions;
- a porous structure with pore apertures ($5.4 \times 5.6 - 5.2 \times 5.8$ Å) that favor the diffusion of p-xylene (5.7 Å), Figure 3;
- the dimensions of the pores and their intersections (9 Å) prevent side reactions, such as disproportionation in toluene and trimethylbenzenes, Figure 4, or reactions leading to the formation of heavy carbonaceous compounds (often referred to as coke).
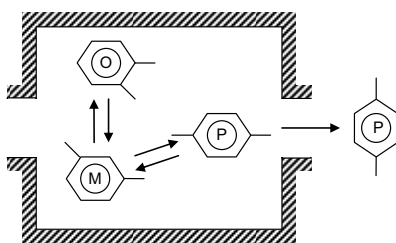
Figure 3 - Selective isomerization of p-xylene over ZSM-5.
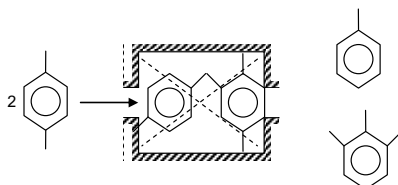
Figure 4 - Prevention of the disproportionation of xylenes over ZSM-5.

The influence of the zeolite structure in the selective isomerization of xylenes, preventing the disproportionation reaction by steric constraints during the formation of reaction intermediates, was evidenced by P. Weisz[18]. The relative values of the ratio between isomerization and disproportionation reaction rate constants are: 15 for zeolite Y, 70 for mordenite and 1000 for ZSM-5. Another important application of product shape selectivity in the petrochemical industry

is the process of toluene alkylation with methanol over zeolite ZSM-5[17,18,19]. The purpose is to selectively obtain *p*-xylene by increasing the diffusional limitations of the other two isomers by two different ways: a) geometrically, by increasing the crystal size of ZSM-5 and, consequently, lengthening the diffusional paths; b) chemically, for example by reducing the pore aperture *via* deposition of phosphorous salts[20] and partial deactivation of the superficial active sites. In the second case, it is possible to achieve selectivity values for *p*-xylene of 97 %, although with some loss of conversion.

8.1.3. Shape selectivity by concentration effect

Also called confinement effect, this shape selectivity type differs from the ones previously described because, instead of reducing the rate of an unwanted reaction, it accelerates a desired reaction[21]. The strong interactions between organic molecules and the pore walls of zeolites (zeolites can be considered as solid solvents[22]), lead to an increase of the reactant concentration inside the zeolite when compared to the bulk phase[24].

This has a significant impact in complex reaction systems, because it obviously favors bimolecular reactions over monomolecular ones. In catalytic cracking, for instance, REHY zeolites are 10 to 10^4 times more active than amorphous silica-alumina, partly also because of their high acid site strength and density. Moreover, the product distribution obtained with these two catalysts is very distinct: the zeolite yields a mixture richer in aromatics and alkanes and poorer in naphthenes and alkenes than silica-alumina. This is due to the zeolite favoring the rates of hydrogen transfer (bimolecular) reactions compared to cracking (monomolecular).

In fine chemical synthesis, generally in liquid phase, the solvent often competes with reactants and products for adsorption on the active sites or pore walls. In bimolecular reactions, the more polar reactant will adsorb preferentially in the

pores, sometimes blocking the access for the other reactant to be transformed. Also, the transformation of a low polarity reactant into a very polar product is autoinhibited, the polar product strongly adsorbing into the micropores and thus slowly diffusing to the bulk medium[23].

8.1.4. Other molecular shape selectivity aspects in micropores

A special type of shape selectivity, that has already been mentioned, is *molecular traffic control* [9], which may occur in zeolites with more than one type of channels, such as ZSM-5: linear pores with elliptic mouths and sinusoidal pores with almost circular pore mouths. According to Derouane and Gabelica[9], linear paraffins travel preferentially through the sinusoidal channels, while isoparaffins and aromatics diffuse through the linear channels, thus minimizing counter-diffusion phenomena.

One application in industrial catalysis is the production of gasoline from methanol over ZSM-5: the light reactants enter the sinusoidal channels and the reaction products (essentially isoparaffins and aromatics) diffuse through the linear channels. This process[25,26] was launched by Mobil, as a consequence of the 1973 oil crash, as an alternative to the production of gasoline from oil. Later, with the crude price falling, this process became less attractive due to its high cost and was abandoned in the late 1980's. The situation would be different today.

The *window effect*, proposed by Gorring[27], explains the periodical variation of the diffusion coefficients of n-paraffins with the number of carbon atoms. It has been observed in different zeolites, such as chabazite (CHA), erionite (ERI) and zeolite T (ERI-OFF).

Particularly in monodimensional molecular sieves, the *single file diffusion*[28] of reactants has an inhibitory effect on bimolecular reactions[29]. The behavior of mesoporous molecular sieves with non-intercrossing channels in the

isomerization of xylenes can be explained by *tunnel shape selectivity*[30]. In this case, xylene molecules that enter the pores undergo successive disproportionation and transalkylation reactions, favoring an exclusively bimolecular isomerization, selectively transforming *m*-xylene into *o*-xylene (*o*-/*p*- ratio is 4-5). This concept can also explain the high selectivity of ferrierites in the isomerization of *n*-butenes to isobutenes[31].

8.1.5. Catalysis and molecular shape selectivity on the external surface

The external acid sites of zeolites are generally considered as a source of problems in catalysis, since they are often responsible for undesirable side reactions and, as a consequence, several external surface passivation methods have been developed for zeolites. Recently, however, the external acid sites of intermediate pore zeolites have been found to selectively catalyze specific reactions[24].

Fraenkel *et al.*[32] first proposed that the alkylation of naphthalene with methanol over zeolite ZSM-5 essentially took place at the semi-intersections of channels, the pore mouths located on the external surface. Derouane *et al.*[33] later generalized and called this phenomenon the *nest effect*. However, shortly after, the explanation given by Fraenkel *et al.*[32] was refuted by Weitkamp *et al.*[34] for that particular example. Nevertheless, the nest effect was later revived to explain the unique selectivity of the bifunctional catalyst Pt/H-ZSM-22 (Pt/H-TON) in the transformation of long-chained *n*-alkanes that gave monobranched isomers in good yield[35]. The effects of *pore mouth catalysis* can be found in other systems, for example in the selective alkylation of benzene to ethylbenzene or cumene over one of the three independent pore systems of zeolite MCM-22[36].

A peculiar type of selectivity was observed in the isomerization of *n*-heptadecane over Pt/HTON: only 5 of the 219 bi-branched and 1171 tri-branched isomers could be detected. This catalysis mechanism resembles that of enzymes, a *key-lock* mechanism: the space between pores on the external surface of the zeolite crystal accurately determines the possible ramification positions on the hydrocarbon chain[37].

8.1.6. Characterization of zeolite pore structures

Zeolites can be grouped according to their pore dimensions in three categories, as represented in Table 2.

TABLE 2 - Classification of zeolites according to pore dimensions.

Zeolites	Adsorbed paraffins	Examples
Narrow pores (4.5 Å)	Linear paraffins	Erionite Zeolite A
Intermediate pores (5-6 Å)	Monobranched paraffins Monocyclic aromatics	ZSM-5 ZSM-48
Large pores (6.5-7.5 Å)	Multibranched aromatics	Offretite Mordenite Zeolite Y

Over one hundred zeolites have been synthesized and every month patent literature on new zeolites is published. Thus, it became necessary to characterize their porous structure (pore dimensions, cages, etc.) in order to select those with shape selectivity for a particular catalytic process.

One of the methods consists of determining the constraint index (CI)[38], defined as the ratio between the reaction rate constants of the cracking at 350 ºC of *n*-hexane and 3-methylpentane. Table 3 shows the constraint index for five zeolites of the three previously mentioned types.

The analysis of the constraint index values displayed in Table 3 reflects the differences in structure found for the various types of zeolites. As such, zeolite

Y and mordenite present CI values < 1, similar to those of amorphous silica-alumina, which corresponds to the intrinsic selectivity of the acid sites. Indeed, since n-hexane is more difficult to crack than 3-methylpentane and diffusional limitations are inexistent (both zeolites have large pores), it was expected that their ratios of cracking rate constants were less than 1.

TABLE 3 - Constraint index of several zeolites.

Zeolite (acid form)	Pore aperture (Å)	CI
Y	7.5	0.3
Mordenite	6.7 × 7.0	0.4
Offretite	6.4	6
ZSM-5	5.4 × 5.6 – 5.2 × 5.8	8
Erionite	3.6 × 5.2	40

Offretite and ZSM-5 show intermediate CI values. The differences in reactivity of the two alkanes are not due to diffusional limitations at the pore mouths (the molecules are smaller than the pore apertures), but rather to steric hindrance in the formation of reaction intermediates. According to Haag[39], the formation of intermediate carbocations occurs *via* a bimolecular mechanism, with a hydride transfer from the paraffin to a pre-adsorbed carbocation. The steric blockage is more significant for 3-methylpentane (larger kinetic diameter) than for n-hexane and consequently the CI value is higher than 1 for both zeolites.

Offretite, which possesses a pore structure with large cages as well as small channels formed by successive gmelinite cages, presents less steric hindrance than ZSM-5 which has no cages. As a consequence, offretite has a lower CI than ZSM-5.

Erionite, a zeolite with narrow pores, shows very high CI values because 3-methylpentane is too large to enter its pores, the reaction occurring only on

the external acid sites. By poisoning the external active sites with a bulky base molecule (unable to enter the pores), very high CI values are obtained for erionite.

This characterization method for the zeolite pore structure helps in grouping the zeolites according to Table 2. Zeolites with constraint indexes lower than 1 have large pores, between 1 and 12 they possess intermediate pores, and higher than 12 the zeolites have narrow pores.

Characterizing the pore structure based on the constraint index can, however, lead to incorrect assumptions due to the influence of several parameters, namely the acidity of the zeolite, the reaction temperature, the reaction time, etc… Therefore a strict procedure must be followed to evaluate the constraint index as described in the literature[38]. For instance, the constraint index of ZSM-5 determined at 500 ºC is 1.5, while at 350 ºC it has a value of 8. According to Haag[40], at higher temperatures there is a change in the cracking mechanism which becomes monomolecular and, therefore, there are no longer steric constraints in the reaction intermediate formation, especially for 3-methylpentane. Figure 5 illustrates how the CI of offretite increases with the reaction time[41]. That variation is explained by the quick coke deposition inside the large cages of offretite, preventing the access of 3-methylpentane to the narrow channels where only n-hexane travels.

These examples show that to characterize a zeolite pore structure, it is imperative to resort to other techniques, such as molecular adsorption or model reactions with well known kinetic diameters for the reactants, products and intermediates[42]. For bifunctional zeolitic catalysts, Jacobs *et al.*[43] use the hydroconversion of n-decane, a reaction that has been tested for zeolites with different and well-known pore structures and can then be applied to zeolites of unknown crystal structure.
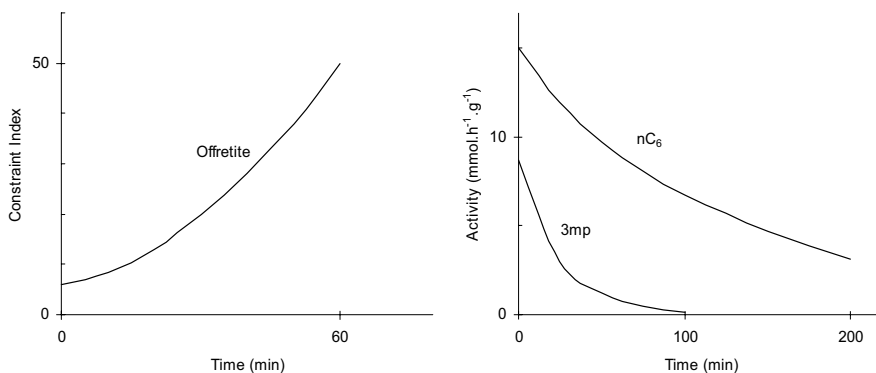
Figure 5 - Evolution of the constraint index of offretite and the activity towards *n*-hexane (nC$_6$) and 3-methylpentane (3mp) with the reaction time. Adapted from Bourdillon[41].

For acid zeolites, a frequently used reaction to characterize the pore apertures is the isomerization of *m*-xylene[42], since unlike the CI, it is independent of the site strength and of the free space around those centers. The disproportionation of xylenes[42] allows the characterization of the zeolite cage structure, although it presents the inconveniences of being affected by diffusional limitations and by the acid sites characteristics.

In summary, it can be said that the selectivity of reactions involving zeolites depends on several factors:

a) active site characteristics

b) diffusional limitations of reactants and products

c) steric hindrance during the formation of reaction intermediates

d) coke deposition, reactant impurities, etc.

The pore structure of zeolites may be characterized with model reactions, if the determinant factor is known. To characterize the pore apertures, factor b) (diffusional limitations) is key and one should use reactions such as the isomerization of *m*-xylene that involve monomolecular reaction intermediates, so as to prevent undesired steric hindrance effects that may mask the results.

203

In order to characterize the dimensions of the cages and channels of a zeolite structure, the ideal reaction is one where the reactant and product molecules are small to avoid diffusional limitations and the reaction intermediates are bimolecular and of known dimension, with their formation being independent of the characteristics of the acid sites.

8.1.7. Influence of shape selectivity on the rate of coke formation and deactivation of zeolitic catalysts

One final important aspect of shape selectivity and, thus, of zeolite pore structure is its influence on the rate of carbonaceous compounds formation and the consequent deactivation of zeolitic catalysts in reactions with hydrocarbons. The rate of coke formation depends on the operational conditions (temperature, presence of hydrogen or metals in the zeolite, etc.) and also on the zeolite pore structure, since it is a spatially demanding reaction[44].

Figure 6 represents the various reactions leading to coke formation, starting from paraffins. In narrow pore zeolites, only dehydrogenation and oligomerization reactions are possible, whereas in intermediate pore size zeolites (such as ZSM-5) cyclization reactions occur, leading to naphthenes and, by dehydrogenation, to aromatics. However, for these zeolites, the C/H ratio of carbonaceous compounds is usually less than 2. For large pore zeolites, alkylaromatics and polyaromatic rings are formed that, *via* dehydrogenation, yield coke, and compounds with C/H ratio of 0.5 are obtainable.
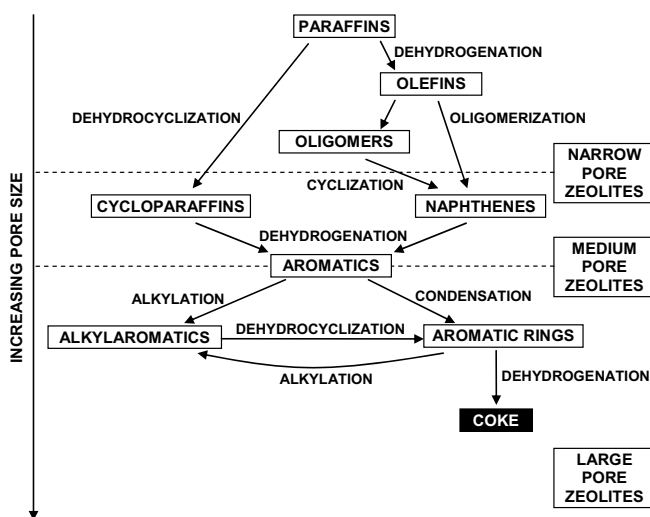
Figure 6 - Representation of coke formation in zeolites.

Rollmann[45] established a correlation between the coke percentage and the constraint index of zeolites: for the same operational conditions, the coke concentration can attain values of 1 % (by weight) for large pore zeolites (CI of 0.4), while for intermediate pore zeolites (CI of 8) the coke content is less than 0.05 % (by weight).

The deactivation of zeolitic catalysts by coke may occur by poisoning of the active sites or by blockage of reactant access to the active sites located on the inside of pores and cages. The deactivation is quicker in the second case and it depends essentially on the zeolite pore structure, as can be seen in Figure 7 that describes the variation of activity of four zeolites with different structures as a function of reaction time in the transformation of n-heptane[46].

The rate of coke formation is high when there is much space surrounding the active sites, since no steric hindrance exists. This is the case of zeolite Y and offretite that present large cages, and of mordenite that does not possess cages but has wide not interconnected linear channels. On the contrary, the rate of coke formation is low in ZSM-5, since it only has intermediate diameter channels.
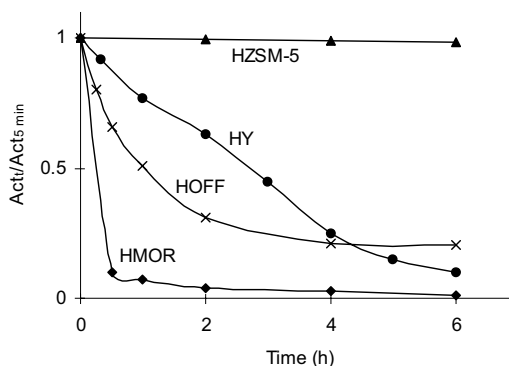
Figure 7 - Variation of A_R (activity for time t / activity after 5 min) as function of the reaction time, in the transformation of n-heptane (T = 450 ºC, p_{N2} = 0.7 bar, p_{nC7} = 0.3 bar) with four zeolites with different pore structures.

In what concerns the rate of deactivation, Figure 7, its value is high in mordenite because pore blockage quickly occurs as a result of monodimensional molecule circulation. The rate of deactivation is medium in zeolite Y and offretite, for although much coke formation is detected, the possibility of tridimensional circulation allows the molecules to maintain access to the active sites. Offretite, however, as seen in Figure 7, shows slow coke formation and deactivation rates after 2 h of reaction, because due to its pore structure molecular circulation takes place mostly through the small gmelinite cages as a result of blockage of the larger cages.

ZSM-5 displays a very slow deactivation rate as, besides having a low coke formation rate due to its pore size, the molecular circulation is tridimensional.

These considerations about the influence of the zeolite pore structure on coke formation and deactivation rates are better visualized in Figure 8, a schematic representation of the pore structures of mordenite, ZSM-5 and zeolite Y, the type of molecular circulation and the location of carbonaceous compounds formed during hydrocarbon reactions. Observing Figure 8, it can be said that mordenite has high coke formation and deactivation rates, that for ZSM-5 these rates are very low, and that for zeolite Y the coke formation rate is high

due to its large cages although a medium deactivation rate is observed because of its trimensional pore network.

(**a**) mordenite: non-communicating channels   (**b**) ZSM-5: communicating channels

(**c**) zeolite Y: communicating channels and cages
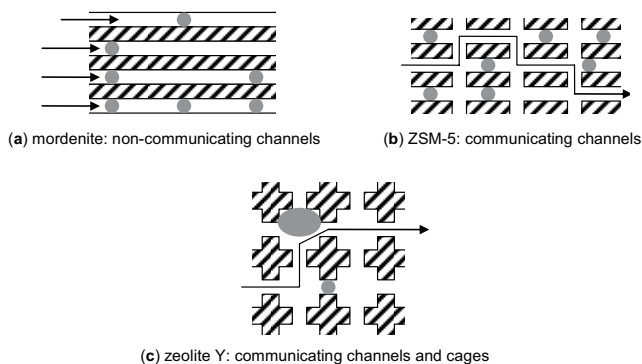
Figure 8 - Pore and cage blockage by coke formation in three types of zeolites: (a) mordenite, (b) ZSM-5 and (c) zeolite Y.

8.2. CONCLUSIONS

Zeolites can be considered microscopic catalytic reactors, with channels and cages whose dimensions differ according to their pore structure, on the inside of which the active sites are located.

Their very particular selectivity – molecular shape selectivity – is the basis for several zeolite applications in important catalytic processes in the oil refining and petrochemical industries. Several recent applications have appeared for fine chemical synthesis, some impacting on the synthesis of pharmaceutical compounds.

Since every month new zeolite patents are published, it is fundamental to assess their pore structure to select those with the required shape selectivity for a given catalytic process. The most common methods are determining the constraint index and studying model reactions, where the kinetic diameters of reactants, products and intermediates are well known.

Pore structure and shape selectivity also have a significant impact on the coke formation and deactivation rates of zeolitic catalysts in reactions with hydrocarbons. Coke formation is spatially demanding, its rate being lower in

zeolites with little space surrounding the active sites, which causes steric hindrance to the formation of these carbonaceous compounds. The deactivation rate is dependent on the extent of molecular circulation within the pore network of the zeolite, being higher when the structure is monodimensional, due to faster blockage of the access to the active sites located inside the pores.

Zeolites have yet to reveal further mysteries: recent advances in single file diffusion and tunnel shape selectivity in monodimensional zeolites, the nest effect on the external surface of zeolite catalysts or the extensive role of confinement effects. Molecular modeling coupled with tailored zeolite synthesis opens the way for new breakthroughs in the future.

Acknowledgments

References

_____

1. E. Derouane in B. Imelik *et al.* (Eds.), *Catalysis by Zeolites*, Elsevier Science Publishing Company, Amsterdam, **1980**, 5.

2. E. Derouane in F. Ramôa Ribeiro *et al.* (Eds.), *Zeolites: Science and Technology*, Martinus Nijhoff Publishers, The Hague, **1984**, 437.

3. T.L. Degnan Jr., *J. Catal.*, **2003**, *216*, 32.

4. N.Y. Chen, W.E. Garwood and F.G. Dwyer, *Shape Selective Catalysis in Industrial Applications*, Chemical Industries, Marcel Dekker, Inc. New York and Basel, *vol. 36*, **1989**, 2nd ed., *vol. 65*, **1996**.

5. N.Y. Chen, T.F. Degnan, C.M. Smith, Jr., *Molecular Transport and Reaction in Zeolites. Design and Application of Shape Selective Catalysts*, VCH Publishers, New York, **1994**.

6.   C. Song, J.M. Garcés, Y. Sugi (Eds.), *Shape Selective Catalysis, Chemical Synthesis and Hydrocarbon Processing*, ACS Symposium Series 738, American Chemical Society, Washington DC, **1999**.

7.   R.L. Gorring, *J. Catal.*, **1973**, *31*, 13.

8.   N.Y. Chen, S.J. Lucki and E.B. Mower, *J. Catal.*, **1978**, *52*, 453.

9.   E. Derouane and Z. Gabelica, *J. Catal.*, **1980**, *65*, 486.

10. P. Weisz, *Chem. Tech.*, **1973**, *3*, 498.

11. P. Weisz and J.V. Frilette, *J. Phys. Chem.*, **1960**, *64*, 382.

12. N.Y. Chen, J. Maziuk, A.B. Schwartz and P. Weisz, *Oil and Gas J.*, **1968**, *66*, 154.

13. N.Y. Chen and W.E. Garwood, *Ind. Eng. Process Res. Devel.*, **1978**, *17*, 513.

14. N.Y. Chen and W.E. Garwood, *J. Catal.*, **1978**, *53*, 284.

15. P.B. Weisz in C. Song, J.M. Garcés, Y. Sugi (Eds.), *Shape Selective Catalysis, Chemical Synthesis and Hydrocarbon Processing*, ACS Symposium Series 738, American Chemical Society, Washington DC, Chap. 2, **1999**.

16. N.Y. Chen and W.E. Garwood, communication to *Amer. Chem. Soc. Symp.*, Houston, **1980**.

17. N.Y. Chen, W.W. Kaeding and F.G. Dwyer, *J. Amer. Chem. Soc.*, **1979**, *101*, 6793.

18. S.L. Meisel, J.P. McCullough, C.H. Lechthaler and P. Weisz, *Leo Friend Symposium*, Amer. Chem. Soc., Chicago, **1977**.

19. S.A. Butter, US Patent 4007231, **1977**.

20. S.A. Butter and W.W. Kaeding, US Patent 3965208, **1976**.

21. M. Guisnet and J.P. Gilson in M. Guisnet and J.-P. Gilson (Eds.), *Zeolites for Cleaner Technologies*, Imperial College Press, Singapore, Chap. 1, **2002**.

22. E.G. Derouane, *J. Mol. Catal. A: Chemical*, **1998**, *134*, 29.

23. M. Guidotti, C. Canaff, J.M. Coustard, P. Magnoux and M. Guisnet, *J. Catal.*, **2005**, *230*, 375.

24. J.L. Figueiredo and F. Ramôa Ribeiro, *Catálise Heterogénea*, 2ª Edição, Fundação Calouste Gulbenkian, **2007**, 416.

25. C.D. Chang, J.C. Kuo, W.H. Lang, S.M. Jacob, J.J. Wise and A.J. Silvestai, *Ind. Eng. Chem. Proc. Res. Dev.*, **1978**, *17*, 255.

26. S.L. Meisel, J.P. McCullough, C.H. Lechthaler and P. Weisz, *Chemtech*, **1976**, *6*, 86.

27. R.L. Gorring, *J. Catal.*, **1973**, *31*, 13.

28. J. Kärger, M. Petzold, H. Pfeifer, S. Ernst and J. Weitkamp, *J. Catal.*, **1992**, *136*, 283.

29. V. Adeeva, T.W. de Haan, J. Jänchen, G.C. Lei, V. Schünemann, L.J.M. van de Ven, W.M.H. Sachtler and R.A. van Santen, *J. Catal.*, **1995**, *151*, 364.

30. M. Guisnet, S. Morin and N.S. Gnep in C. Song, J.M. Garcés and Y. Sugi (Eds.), *Shape Selective Catalysis, Chemical Synthesis and Hydrocarbon Processing*, ACS Symposium Series 738, American Chemical Society, Washington DC, Chap. 24, **1999**.

31. B. de Ménorval, P. Ayrault, N.S. Gnep and M. Guisnet, *J. Catal.*, **1998**, *174*, 185.

32. R. Fraenckel, M. Cherniavsky and M. Levy, *Proc. 8th Intern. Cong. Catal.*, Dechema: Frankfurt-am-Main, **1984**, *4*, 545.

33. E. Derouane, J.M. André and A.A. Lucas, *J. Catal.*, **1988**, *110*, 58.

34. M. Neuber and J. Weitkamp, *Stud. Surf. Sci. Catal.*, **1991**, *60*, 291.

35. J.A. Martens, R. Parton, L. Uytterhoeven, P.A. Jacobs and G.F. Froment, *Appl. Catal.*, **1991**, *76*, 95.

36. J.S. Beck, A.B. Dandekar and T.F. Degnan in M. Guisnet and J.P. Gilson (Eds.), *Zeolites for Cleaner Technologies*, Imperial College Press, Singapore, Chap. 11, **2002**.

37. J.A. Martens, W. Souverijns, W. Verrelst, R. Parton, G.F. Froment and P.A. Jacobs, *Angew. Chem.*, **1995**, *34*, 252.

38. J.V. Frilette, W.O. Haag and R.M. Lago, *J. Catal.*, **1981**, *67*, 223.

39. W.O. Haag, R.M. Lago and P. Weisz, *Faraday Discuss Chem. Soc.*, **1981**, *72*, 317.

40. W.O. Haag and R.M. Dessau, *Proc. 8th Intern. Congress Catal. III*, **1984**, 305.

41. G. Bourdillon, *Thesis*, Université de Poitiers, **1985**.

42. F. Ramôa Ribeiro, F. Lemos, G. Perot and M. Guisnet in R. Setton, Ed., *Chemical Reactions in Organic and Inorganic Constrained Systems*, Reidel Publishing Company, Dordrecht, **1986**, 141.

43. J. Martens, M. Tielen, P. Jacobs and J. Weitkamp, *Zeolites*, **1984**, *4*, 98.

44. L.D. Rollmann and D.E. Walsh in J.L. Figueiredo, Ed., *Progress in Catalyst Deactivation*, Martinus Nijhoff Publishers, The Hague, **1982**, 81.

45. L.D. Rollmann and D.E. Walsh, *J. Catal.*, **1979**, *56*, 139.

46. M. Guisnet, P. Magnoux and C. Canaff in R. Setton, Ed., *Chemical Reactions in Organic and Inorganic Constrained Systems*, Reidel Publishing Company, Dordrecht, **1986**, 131.

(Página deixada propositadamente em branco)

9. IMMOBILISATION OF METAL COMPLEXES ONTO SOLID SUPPORTS AND CATALYTIC APPLICATIONS

Cristina Freire and Clara Pereira

REQUIMTE/Departamento de Química, Faculdade de Ciências, Universidade do Porto, Rua do Campo Alegre, 4169-007 Porto, Portugal

9.1. INTRODUCTION

The immobilisation of transition metal complexes with catalytic properties onto supports is a theme of intense research, due to its importance towards the goals of Green Chemistry[1-8]. Complex immobilisation has been done in several supports such as organic polymers (insoluble and soluble polymers and dendrimers), carbon materials and porous inorganic materials (zeolites, mesoporous silicas and clay materials).

The main purpose of the immobilisation of homogeneous catalysts is to generate easily recyclable catalysts with improved catalytic properties when compared with their homogeneous counterparts. The activity and chemo- or enantioselectivities of the immobilised systems can be enhanced relatively to their free analogues due to two major key effects: the confinement effect[1-9] and the catalyst site isolation[3-8]. Furthermore, the immobilisation of the homogeneous catalysts also allows for the easy separation of the catalysts from the reaction media by simple separation procedures and consequently, the possibility for reuse in other catalytic cycles, which is typically one of the main advantages of the heterogeneous catalysts.

The improvement of the catalytic properties derived from the confinement effect results from the imprisonment of the substrate within the pores of the support, leading to enhanced interactions between the active catalyst and the substrate[9]. However, this is a two-edged sword, since several factors can also contribute to a decrease of the catalyst performance. In fact, a tight entrapment of the immobilised catalyst molecules can induce lower activity or chemo- and

enantioselectivity as a consequence of a compulsory conformation; in particular, the reduced enantioselectivity can be due to a constrained environment that prevents the chiral complex to adopt the special conformation which is required to induce chiral recognition[2,4,5]. Lower activities can also be a consequence of reduced or even blocked mass transport in the narrow pores, imposing limits to the effective range of substrates that can be used.

The improved catalytic activity can also occur upon the immobilisation of metal complexes onto solid supports due to complex site isolation since this effect prevents the reaction between the catalysts or its active forms, which is one of the main causes for homogeneous catalysts deactivation as it usually leads to the formation of catalytic inactive species[1,2,3-6].

This chapter will start with a general description of the different strategies for the immobilisation of transition metal complexes onto supports. In the following sections will be presented several examples of coordination compounds immobilised into several porous solid supports, such as carbon materials, zeolites, porous silicas and clay materials, in order to exemplify the different complex immobilisation procedures used for the diverse materials; references to the application of the immobilised systems in catalytic reactions will also be described.

9.2. GENERAL METHODS FOR METAL COMPLEX IMMOBILISATION

There are several approaches to immobilise transition metal complexes onto supports. One way to classify them is by the type of interaction between the support and the molecular species to be grafted. In this context, three different groups of support-molecule interactions can be considered:[1-8] i) *covalent bonding*, ii) *non-covalent interactions* (including physical adsorption and electrostatic interactions) and iii) *encapsulation*. Additionally, for covalent

bonding and non-covalent interactions, the interaction between the support and the molecular species can occur directly or through bifunctional molecules, previously attached to the support or bonded to the metal complex, which are usually named spacers or linkers. In Figure 1 are depicted schematically the different methods for the immobilisation of metal complexes onto supports, based on the type of interaction complex-support.
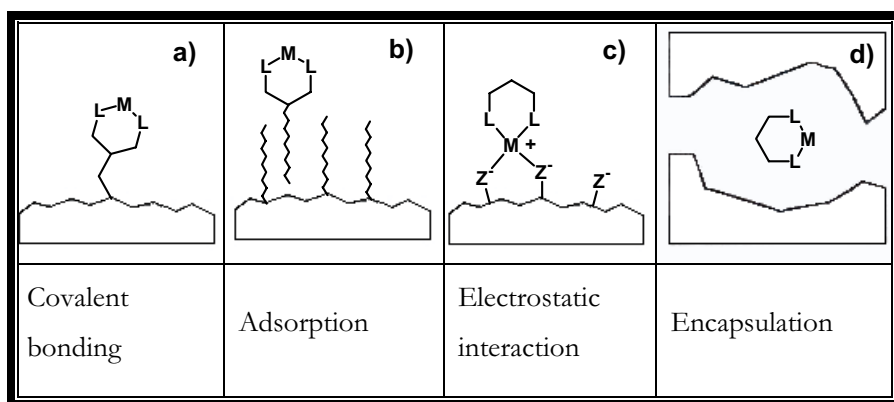
Figure 1 - Schematic representation of the different methods for the immobilisation of metal complexes onto supports, according to the type of interaction metal complex-support. Adapted from 2.

Covalent bonding of metal complexes onto supports is by far the most used strategy to immobilise transition metal complexes with catalytic properties[1-8]. It can be accomplished either directly by reaction of the metal complex with the support surface groups or mediated through a spacer previously grafted to the support or reacted with the complex. In the former case, the complex can react with the support surface groups through axial coordination to the metal centre or through the functional groups of the ligand coordinated to the metal, Figure 1a). On the other hand, the immobilisation of metal complexes *via* spacers involves the selection of a bifunctional molecule that must have groups capable of reacting with both the support surface functionalities and the complex (*via*

ligand functionalities or metal axial coordination). The selection of the spacer mainly depends on the type of support surface groups, but must also consider other characteristics namely its length, flexibility and the degree of surface coverage, which are very important to design heterogeneous catalysts with good catalytic performances. For example, in the case of asymmetric catalysis, the point of attachment of the tether to the ligand should be as far as possible from the stereogenic centre in order to minimise the disturbance of the chiral induction[2,5,7]. Among the different spacers available, the organo-siloxanes are the most used bifunctional molecules since they possess methoxyl groups which can easily react with surface hydroxyl groups (the majority of the surface groups present in the inorganic supports), as well as several other reactive functionalities, such as acid, halide, amine and mercapto, that can react with an enormous variety of groups in the metal complexes, through the ligand or by metal axial coordination; cyanuric chloride (CC), carbodiimide derivates and polyamines have also been used as linkers[1-8].

The most important advantage of this method is that the molecular species are linked to the support *via* chemical bonds and experience almost no leaching as far as all the bonds are stable in the reaction media. Nevertheless, an important drawback of this method is the large preparative effort, since it involves a multi-step procedure that usually includes, not only the functionalisation of the ligands coordinated to the metal, but also the grafting of spacers onto the support. Furthermore, the covalent bonding of metal complexes, directly or *via* spacers, can alter, to different extents, the electronic density within the metal which, in turn, can modify the performance of the catalysts in a way that may be difficult to foresee[3-8].

The group of *non-covalent interactions* between the support and the metal complex includes two methodologies for complex immobilisation: the *physical adsorption* and the *electrostatic interaction*[1-8]. The physical adsorption includes π-π and van der Waals interactions, hydrogen bonds and hydrophobic-

hydrophilic interactions between the support and the complex. The second approach consists of electrostatic interactions between the support and the complex and, therefore, charges of opposite signals are required between them. The non-covalent interactions can also occur directly between the support and the complex, Figure 1b),c) or through spacers; in the latter case, the interaction between the spacer and the complex can be of different nature, covalent or non-covalent.

The major advantage of non-covalent immobilisation methodology, when compared to the covalent bonding approach, is the easy preparation of these systems. However, their sensitivity to solvents is an important weakness, as it may cause extensive leaching of the active phase by simple manipulation of the experimental conditions used in the preparation of the immobilised complexes or during the catalytic reactions.

Encapsulation implies the physical entrapment of the metal complex within the pores of the support, Figure 1d), and as a starting-point, the assumption that no other interactions between the support and the metal complex exist besides the physical confinement[1-3,6,7,10]. Therefore, the encapsulation methodology is the one which can better mimic the catalytic behaviour of metal complexes in the homogeneous phase. This methodology depends on the respective sizes of the complex and the cavity where the complex should be entrapped. In order to prevent the leaching of the complex after encapsulation, the size of the complex has to be bigger than the dimensions of the cavity, which is the most important limitation of this method. Similarly to covalent bonding, this methodology also involves a multi-step approach which can, in some cases, be lengthy. In general, there are three approaches to encapsulate metal complexes: i) *in-situ synthesis* of the complex, ii) the *flexible ligand* approach and iii) *template synthesis*. In the first two cases, also termed '*ship-in-a-bottle*' approaches[3,6,7,10], the support is previously prepared and used as a nanoreactor, followed by the complex synthesis within the support cavities/pores. In the *in-*

situ synthesis, a molecular complex is used as a precursor which, after being adsorbed onto the support, is made to react with other reagents to give the desired complex, whereas in the *flexible ligand* approach, the metal salt is previously adsorbed in the support cavity and then complexed by the ligand added in liquid or gas phase to the support. Finally, in the *template synthesis*, the metal complex is used as a template in the synthesis of the support itself. Although this approach could be interesting from the view point of preparative synthesis, since the complex is prepared by the traditional methods outside the support, it has an important disadvantage, which is the impossibility of carrying out the step of support calcination at the usual temperature (500 ºC), since the complexes would decompose. These aspects have pernicious consequences on: i) the purity of the support, as the decomposition of the organic templates used in the synthesis is not complete and ii) the rigidity and stability of the support, since there is only a partial dehydration of the metal oxides.

The confirmation of the complex immobilisation is accomplished by the characterisation of the new hybrid materials. Due to their nature, their characterisation should involve techniques that give information on the immobilised molecular species and on the support. Although many techniques undoubtedly provide valuable results on the two components of these hybrid materials individually, the most useful information always emerges from the combination of several techniques; herein only the most common techniques will be referred.

The FTIR/Raman and UV-Vis spectroscopic techniques are important choices since they can provide information regarding the integrity of both the molecular complex and support and their changes upon complex immobilisation, simultaneously. Magnetic resonance methods (solid state nuclear magnetic resonance (NMR) and electron paramagnetic resonance (EPR)) are more significant techniques for the characterisation of the anchored species, metal complexes and spacers[11]. Elemental analysis (bulk contents by

chemical analysis and surface contents by X-ray photoelectron spectroscopy (XPS) or energy dispersive X-ray spectroscopy (EDS)) provide the metal complex loadings and indirect information about the homogeneous vs. surface distribution of the complex within the matrix; the analysis of XPS atomic spectra is also a key component in the characterisation of the hybrid systems[11]. Microscopy (scanning electron microscopy (SEM), transmission electron microscopy (TEM) and atomic force microscopy (AFM))[12] and X-ray diffraction (XRD)[11a] techniques allow for the evaluation of the morphology changes induced on the support by complex immobilisation and in the latter case, indirectly, of the complex distribution within the matrix. Thermal analysis techniques (thermogravimetry (TG) and differential scanning calorimetry (DSC)) provide information on the thermal and physical-chemical stabilities of both complex and support; temperature programmed desorption (TPD) can be of valuable importance in the case of carbon materials[11b]. Finally, N_2 adsorption/desorption isotherms permit directly the description of porous materials in terms of their surface areas and pores size distributions, and indirectly the distribution of the metal complexes within the supports[13].

9.3. IMMOBILISATION OF METAL COMPLEXES ONTO SOLID SUPPORTS AND APPLICATION IN CATALYSIS

9.3.1. Carbon materials

Research on the immobilisation of metal complexes onto carbon materials is scarce when compared with the inorganic supports such as zeolites, silicas and clay based materials. Nevertheless, carbon materials are unique supports as they can provide a variety of oxygen surface groups at the edges/defects of graphene sheets that can be tailored by adequate thermal/chemical treatments, besides the inherent physical/chemical reactivity associated with the graphene sheets, which are hydrophobic and present low polarity and a rich π-electron

density[14,15]. These properties can lead to a variety of strategies for the immobilisation of molecular species by all the methods referred above.

Although some examples of the modification of carbon materials surfaces by molecular species with catalytic properties dated from 1970[16,17], only recently, with the discovery of new allotropic forms of carbon, such as fullerenes[18] and carbon nanotubes (CNTs)[19], there was an astonishing growth of methods for carbon surface functionalisation with a plethora of chemical species for several applications[16,20-25].

The study of the direct immobilisation of functionalised [Cu(4-HOsalen)] complex onto activated carbon (AC) allowed the development and optimisation of a new direct anchoring methodology through ligand substituents[26]. The [Cu(4-HOsalen)] complex was directly anchored onto an air oxidised AC by stable chemical bonds formed in the reaction between hydroxyl ligand substituents and surface carbonyl and carboxylic anhydride groups. In the case of the surface carbonyl functionalities, a direct nucleophilic attack of the hydroxyl groups originated an ether bond to the complex, whereas for the surface carboxylic anhydrides the attack generated new carboxylic groups and an ester group, as depicted in Figure 2.
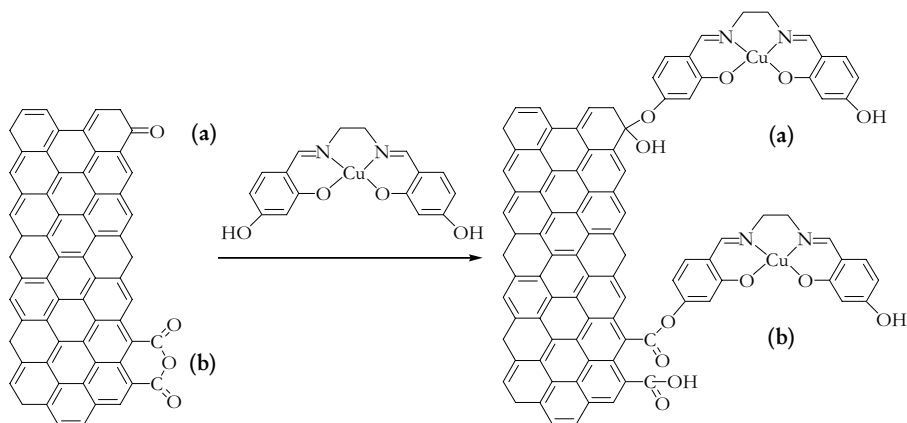
Figure 2 - Direct immobilisation of [Cu(4-HOsalen)] complex onto an air oxidised AC. Adapted from 26.

Two chiral Mn(III) *salen* catalysts (complexes (1) and (2)), bearing different chiral diamine bridges, Figure 3[27], were anchored by direct axial coordination of the metal centre to the phenolate groups created by sodium hydroxide treatment of an air oxidised commercial AC (CoxONa).
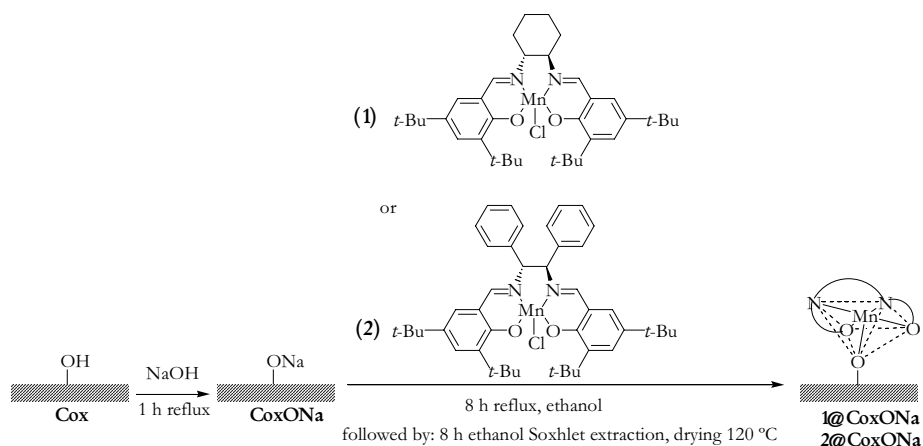
Figure 3 - Anchoring method for the immobilisation of two chiral [Mn(III)(*salen*)Cl] catalysts, (1) and (2), onto a modified air oxidised AC. Adapted from 27b.

The materials were active and enantioselective in the epoxidation of styrene and α-methylstyrene in dichloromethane at 0 °C using, respectively, *m*-chloroperbenzoic acid (*m*-CPBA) / 4-methylmorpholine N-oxide (NMO) and NaOCl as oxidants[27]. The immobilised complex (1) acted as a better heterogeneous catalyst than complex (2) in the asymmetric epoxidation of the alkenes, showing higher substrate conversions and enantiomeric excess percentage (ee%) values. Furthermore, the catalysts reuse led to no significant losses of catalytic activity and enantioselectivity for the epoxidation of α-methylstyrene using NaOCl, while a significant loss of enantioselectivity was observed for the epoxidation of styrene with the other oxidant. For both heterogeneous catalysts no significant metal leaching was observed after two

successive catalytic experiments, showing that the anchoring method was effective against active phase leaching.

A modified *Jacobsen*–type catalyst, possessing an hydroxyl group on the aldehyde fragment of the *salen* ligand, was anchored through cyanuric chloride (CC) spacer onto two modified ACs[28]: method A, an air oxidised AC functionalised with 3-aminopropyltriethoxysilane (APTES) and method B, a nitric acid AC treated with thionyl chloride and functionalised with 1,8-diaminooctane, Figure 4.
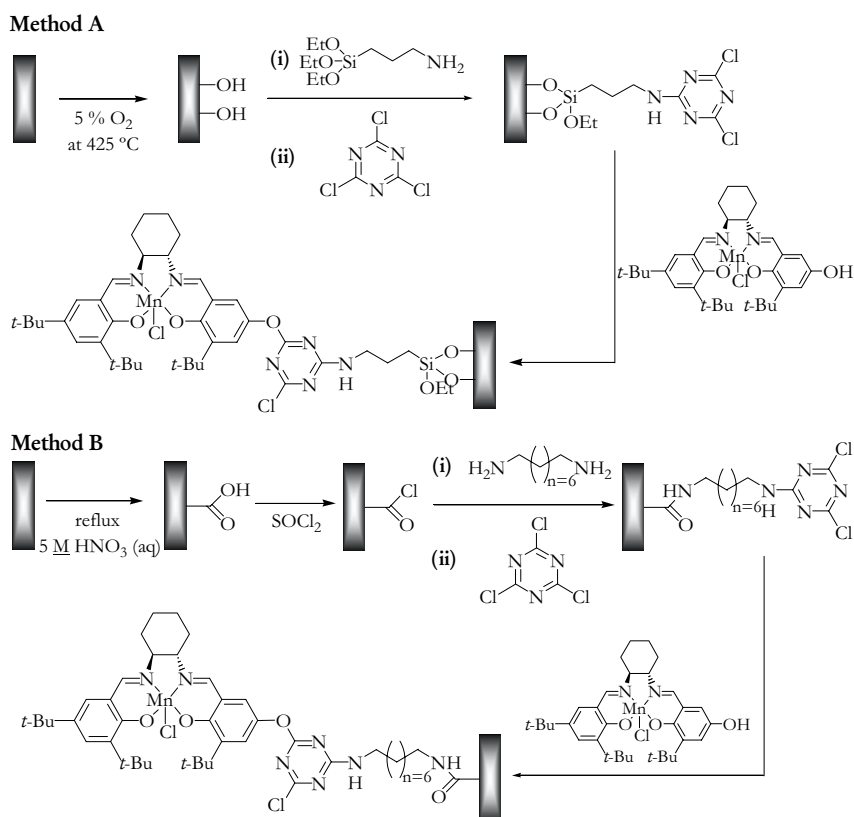
Figure 4 - Immobilisation of a modified *Jacobsen* catalyst onto AC through methods A and B. Adapted from 28.

The complex anchored more effectively in the former material (double anchoring efficiency). These supported materials acted as active and enantioselective heterogeneous catalysts in the epoxidation of α-methylstyrene, using NaOCl as oxidant[28]. Both catalysts showed higher substrate conversions (12 and 24%) than the homogeneous counterpart (10%). The increase in the distance of the [Mn(III)(*salen*)Cl] complex to the carbon surface did not have a significant effect in the ee% values (32 and 34%), which were lower than for the homogeneous catalyst (51%). Nevertheless, the catalyst bearing the shorter amine alkyl chain spacer showed higher catalytic activity.

Styryl functionalised vanadyl(IV) *salen* complexes (non-chiral and chiral versions) were covalently anchored onto mercapto-modified AC and single walled carbon nanotubes (SWCNTs), Figure 5[29]. The immobilisation procedure involved the acid oxidation of AC and SWCNTs, followed by the reaction of the carboxylic acid groups with thionyl chloride to give the acyl chloride groups, which were finally reacted with the spacer 2-mercaptoethylamine. The mercapto-functionalised AC and SWCNTs were then linked to the vanadyl complex through a radical chain addition of the mercapto groups to the terminal C=C functional group of the complex, initiated by 2,2'-azobisisobutyronitrile (AIBN); the modified SWCNTs were more efficient in the immobilisation of the [VO(*salen*)] complex.
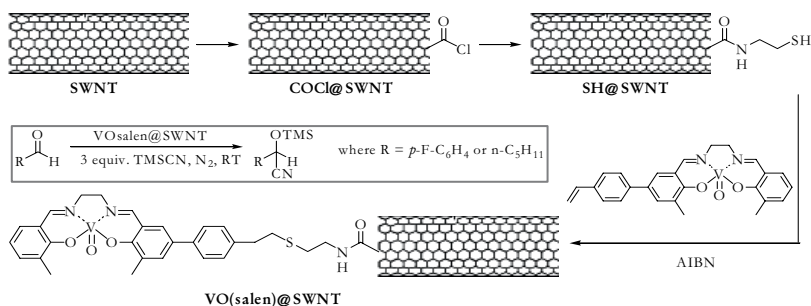
Figure 5 - Styryl functionalised-[VO(*salen*)] complex covalently anchored on mercapto-modified SWCNTs. Adapted from 29a.

These heterogeneous catalysts showed high activity in the cyanosilylation of benzaldehyde with substrate conversions of 83 and 93%, for mercapto-modified AC and SWCNT supports, respectively[29]. The SWCNT was shown to be a more suitable support for the VO complex relatively to the high-surface-area AC, since the latter support exhibited some adventitious activity. The asymmetric version of the reaction was also performed using the chiral vanadyl complex and, in this case, the SWCNT also behaved as a better support as the ee% was 66%, whereas for AC the ee% was 48% [29].

Several metal acetylacetonates, [M(acac)$_2$], have been anchored onto amine-functionalised ACs by using nitric acid oxidised ACs as starting supports[30,31]. The acid oxidised carbons, which possess carboxylic surface groups, were treated with thionyl chloride to give surface acyl chloride groups, which were then reacted with diamines. The subsequent attachment of [M(acac)$_2$] (M = Cu(II), VO(IV) and Co(II)) was achieved by Schiff condensation between the free amine groups of the grafted spacers and the C=O group of the acetylacetonate (acac) ligand, Figure 6. The [VO(acac)$_2$] complex was also anchored onto an air oxidised AC in which the phenol surface groups were previously made to react with APTES, followed by a Schiff condensation between the free amine groups and the acac ligand of the complex[30c].

The immobilised [Cu(acac)$_2$] was tested in the aziridination of styrene in acetonitrile using [N-(*p*-tolylsulfonyl)imino]phenyliodinane] (PhI=NTs) as nitrogen source[30b]. The styrene conversion and total turnover number (TON) of the heterogeneous reaction were similar (37 and 7%, respectively) to those of the reaction performed in the homogeneous phase (41 and 8%, respectively). The heterogeneous catalyst could be reused in further catalytic reactions for four times with successive increases in the styrene conversion and in the initial activity, with the total TON being higher than in the homogeneous reaction. No metal complex leaching was observed after the consecutive catalytic

reactions. The anchored [VO(acac)$_2$] complexes were tested in the epoxidation of 3-buten-2-ol using *tert*-butylhydroperoxide (TBHP) as oxygen source[30c]. The heterogeneous alkene conversions were similar to that observed in the homogeneous phase, although the oxidation rates were less than halved compared to the homogeneous system. The complex anchored through APTES exhibited higher catalytic efficiency than that anchored by the diamine. Upon reuse both materials presented no significant decrease in their catalytic properties.

(A)
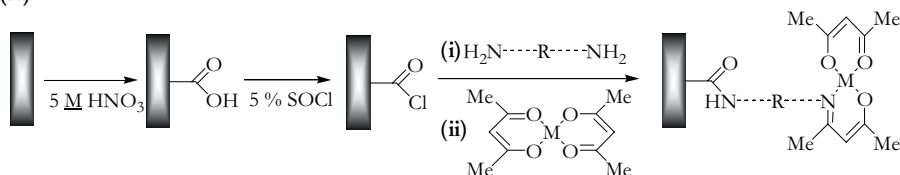
(B)
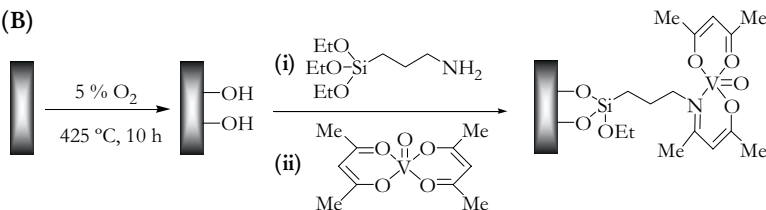
Figure 6 - (A) Immobilisation of [M(acac)$_2$] complexes onto an amine-functionalised acid oxidised AC; (B) Immobilisation of [VO(acac)$_2$] complex onto an amine-functionalised air oxidised AC. Adapted from 30c.

9.3.2. Zeolite materials

Microporous zeolites were one of the first inorganic materials to be used as supports for the immobilisation of transition metal complexes with catalytic properties. Due to the size and pore structure of these materials, complex immobilisation was usually performed using the encapsulation methods[10,32]. In literature, there are a lot of examples of the encapsulation of [M(*salen*)] type complexes prepared by the '*ship-in-a-bottle*' approaches (*in-situ synthesis* of the complex and *flexible ligand* approach)[33]; the *template synthesis* method is

usually used in the encapsulation of larger complexes, such as metalloporphyrins[34].

The $[Mn(bpy)_2]^{2+}$ complexes (bpy = 2,2'-bipyridine) were immobilised in the supercages of X and Y zeolites by the *in-situ synthesis* of the complex, Figure 7[35]. These new heterogeneous materials were effective catalysts in the cyclohexene epoxidation. Moreover, the zeolites supports affected the products distribution: with the NaX zeolite, the acidic sites were inexistent, leading to high 1,2-epoxycyclohexane selectivitity, whereas with NaY zeolite, the acidic sites promoted the epoxide opening to the *trans* diol and further oxidation to hydroxyketones, diketones or acids.
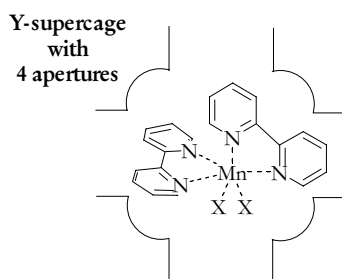
Figure 7 - Scheme of $[Mn(bpy)_2]^{2+}$ complexes encapsulated within the supercages of Y zeolite. Adapted from6.

Balkus *et al.* used the *in-situ synthesis* for the encapsulation of rhodium(III)-phthalocyanine within the supercages of NaX and NaY zeolites[36]. The encapsulation proceeded in two steps: i) rhodium exchange of X and Y zeolites and ii) ligand synthesis by diffusion of dicyanobenzene that condensed around the exchanged Rh ions forming the tetradentate macrocycle, which was too large to exit, Figure 8.
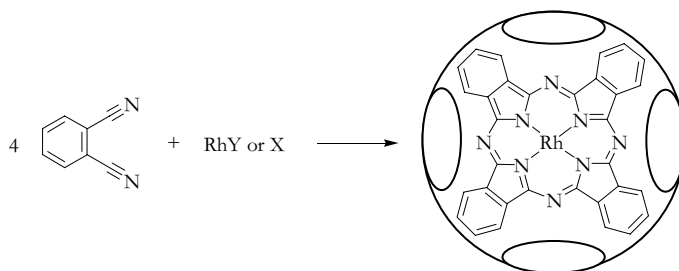
Figure 8 - Encapsulation of Rh-phthalocyanine onto X or Y zeolites. Adapted from 36.

9.3.3. Mesoporous silica materials

The ordered mesoporous silica materials, such as MCM-n, SBA-n and HMS-n, present several advantages as supports over zeolites since they have high specific surface areas and uniform and tunable pore sizes in the range of 2–50 nm, allowing the immobilisation of large metal complexes[37]. They possess silanol groups on their surfaces that can be easily functionalised with spacers (usually organo-siloxanes) allowing for the subsequent immobilisation of metal complexes by covalent bonding or non-covalent interactions, which is named *post-synthesis* grafting[38]. In another approach the mesoporous silicas can be prepared using silica precursors containing reactive groups for complex immobilisation, which is called the *direct synthesis* approach (co-condensation)[38a,39].

Two modified *Jacobsen*-type catalysts denoted as complexes (1) and (2) were grafted onto a hexagonal mesoporous silica (HMS) previously functionalised with APTES through the ligand, by using two different procedures: method A - direct anchoring of the complex (1); and method B - two-step procedure involving the covalent attachment of CC onto the APTES-functionalised HMS followed by the complex (2) immobilisation onto the CC functionalised HMS, as represented in Figure 9[40].
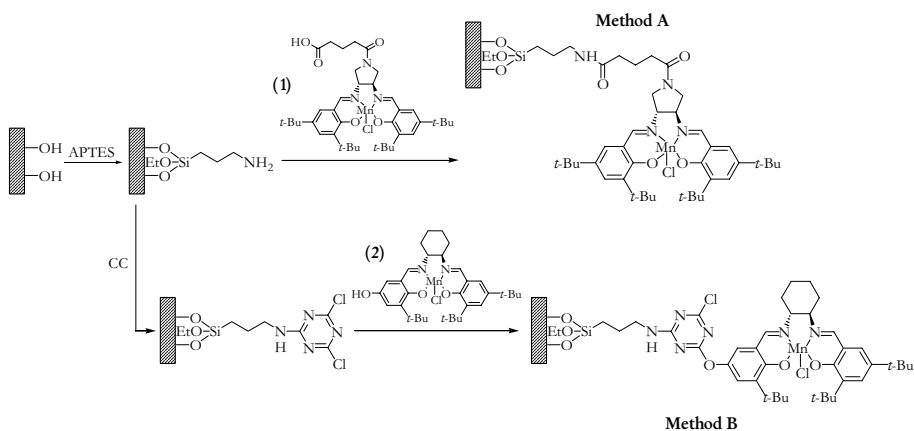
Figure 9 - Anchoring procedures used in the immobilisation of chiral complexes (1) and (2) onto APTES functionalised HMS, by methods A and B respectively. Adapted from 40.

The materials were tested in the asymmetric epoxidation of styrene and α-methylstyrene, at 0 °C, in dichloromethane using, respectively, *m*-CPBA/NMO and NaOCl as oxidant. They were active in the epoxidation reactions although leading to lower substrate conversions, TONs and turnover frequencies (TOFs) than those obtained in the homogeneous phase reactions. Furthermore, both catalysts were also enantioselective in the α-methylstyrene epoxidation, with the heterogeneous complex (1) catalyst showing higher ee% than the homogeneous counterpart. The heterogeneous catalysts were reused in the α-methylstyrene epoxidation, leading to similar catalytic activities and enantioselectivities. It was concluded that the direct covalent attachment of the complex through the diimine bridge was advantageous in the asymmetric induction (improved ee%), probably due to changes in the steric environment of the diimine bridge. On the other hand, the covalent attachment through one of the aldehyde fragments resulted in a negative effect in the ee%, which could be associated with the presence of CC as a mediator since it probably reduces the electron density of the Mn(III) centre.

In a novel approach, Zhang *et al.* prepared several Nb-doped silicas with different pore sizes[41]. In this way, different sites within the Nb-doped MCM-41 supports for the covalent attachment of an amine-functionalised Fe(III)-porphyrin, [Fe(III)(T$_{NH2}$PP)Br] (T$_{NH2}$PP is tetrakis-(4-aminophenyl)porphyrin) were provided. The Nb Lewis acids acted as anchors for amine substituents attached to the periphery of the porphyrin *via* N-Nb ligand interactions, Figure 10. This strategy allowed the heterogenisation of the metalloporphyrin without involving the metal centres, therefore leaving them accessible as active sites for catalytic oxidation reactions. The anchored metalloporphyrin acted as a fast and selective catalyst in the epoxidation of cyclohexene and cyclooctene in dichloromethane using PhIO. The authors found that the use of a Nb-doped MCM-41 support with larger pores led to better results since the large pore sizes, in association with the porphyrin peripheral attachment, facilitated the reagents and products diffusion as well as minimised the distortion of the porphyrin macrocycle geometry. Furthermore, in the case of the cyclooctene epoxidation, the support with larger pore sizes, led to even higher TON (196) than the homogeneous counterpart (170). The heterogeneous catalysts were stable upon reuse, without any metal complex leaching.
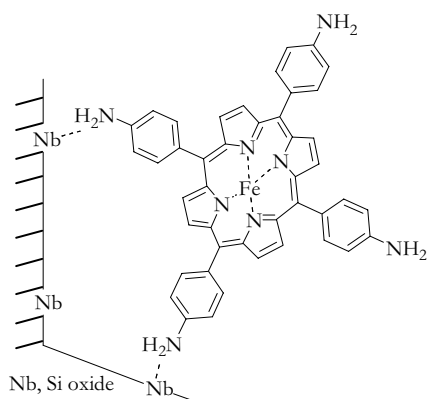
Figure 10 - Covalent attachment of [Fe(III)(T$_{NH2}$PP)Br] onto a Nb-doped MCM-41 support. Adapted from 6.

Cu(II) complexes bearing a bis(oxazoline) ligand, methylenebis[(4*S*)-4-phenyl-2-oxazoline], were anchored to the surfaces of MCM-41 and MCM-48 supports through the initial functionalisation of the bis(oxazoline) ligand with alkoxy-Si groups, as depicted in Figure 11[42]. When used in the enantioselective cyclopropanation of styrene with ethyl diazoacetate, the supported catalysts afforded higher yields and enantioselectivities than the corresponding homogeneous complexes. Upon reuse, the catalysts prepared with CuCl$_2$ deactivated faster than those with [Cu(OTf)$_2$] (OTf is trifluoromethanesulfonate), which presented very small deactivation, although showing a small decrease in the ee% values and *trans/cis* products ratio.
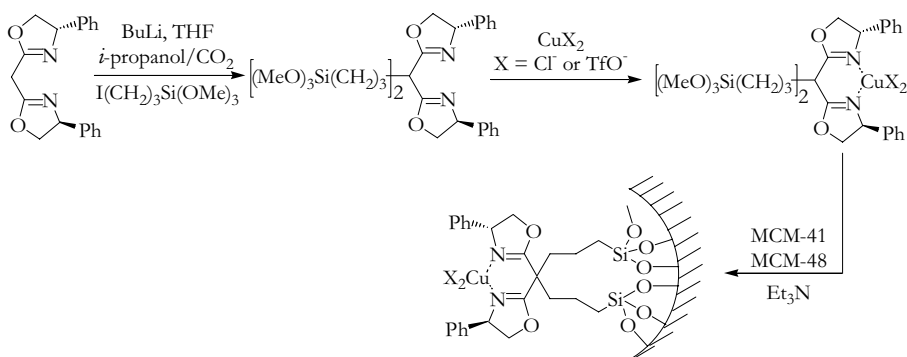
Figure 11 - Schematic representation of the immobilisation of Cu(II) bis(oxazoline) complexes onto MCM-41 and MCM-48 supports. Adapted from 42.

A chiral Pd(II) complex with a ligand derived from 1,1'-bis(diphenylphosphino)-ferrocene was anchored within the mesoporous MCM-41 support[43]. The synthesis strategy involved the following steps: i) reaction between (*S*)-1-[(*R*)-1,2'-bis(diphenylphosphino)ferrocenyl]-ethyl acetate and 3-(methylamino)propyltrimethoxysilane, resulting in a silane functionalised ferrocenyl ligand; ii) formation of the metallic ferrocenyl precursor by incorporation of palladium dichloride; and finally iii) reaction between the

ferrocenyl precursor and the mesoporous MCM-41, whose outer walls were previously deactivated by treatment with [Ph$_2$SiCl$_2$], Figure 12. The heterogeneous catalyst was tested in the enantioselective hydrogenation of ethyl nicotinate to ethyl nipecotinate, resulting in a 17 ee% whereas the homogeneous catalyst originated a racemic product. The heterogeneous catalyst also presented higher catalytic activity (TON = 291) than the homogeneous counterpart (TON = 98) and was remarkably stable.
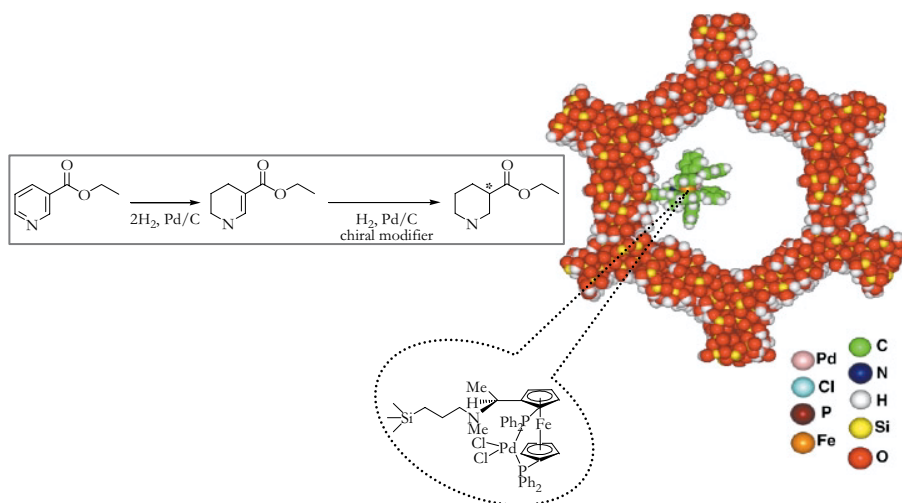
Figure 12 - Schematic representation of the Pd(II) complex encapsulated within MCM-41 and two-step catalytic hydrogenation of ethyl nicotinate to ethyl nipecotinate. Adapted from 43.

Zhou *et al.* reported the immobilisation of a [Cr(III)(*salen*)Cl] complex through metal axial coordination with NH$_2$ from APTES previously grafted into a MCM-41 support, Figure 13[44]. The material was an active catalyst in the asymmetric epoxidation of unfunctionalised alkenes in toluene using PhIO, giving significantly higher ee% than the value obtained with the free complex.
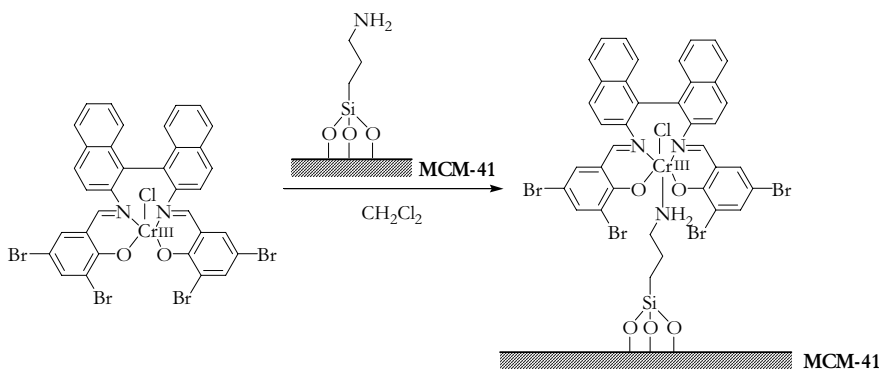
Figure 13 - Immobilisation of a [Cr(III)(*salen*)Cl] complex into a MCM-41 support functionalised with amine groups. Adapted from 44.

9.3.4. Clays and pillared clays materials

Clays and pillared clays (PILCs) are important low-cost materials that, besides the several applications in adsorption, catalysis and for environmental purposes, can also be used as catalyst supports[45].

9.3.4.1. Clays

The oldest and most used method for complex immobilisation in clays (cationic and anionic) has been the ionic interaction between the interlayer ions and metal complexes with groups of opposite charges[10,46]. Recently, complex immobilisation has also been performed by covalent bonding through spacers, namely organo-siloxanes, grafted at the edges of the clay sheets by using their surface hydroxyl groups[47].

A chiral [Mn(III)(*salen*)Cl] complex functionalised with sulphonate groups in the aldehyde moiety was successfully incorporated within a Zn(II)–Al(III) layered double hydroxide (LDH) host, by an anion exchange method, Figure 14[48]. The heterogeneous catalyst was effective in the stereoselective epoxidation of *R*-(+)-limonene and (-)-±-pinene, at room temperature, using molecular

232

oxygen as oxidant. It showed high conversion, selectivity and ee% values and could be recycled without efficiency loss. The authors suggested that the catalytic activity of the LDH-based complex was improved in comparison to the free complex as a result of several factors: ligand substituents, the presence of positive charge interactions in the LDH host and a sufficiently large gallery spacing which enhanced the substrate accessibility to the active centres.
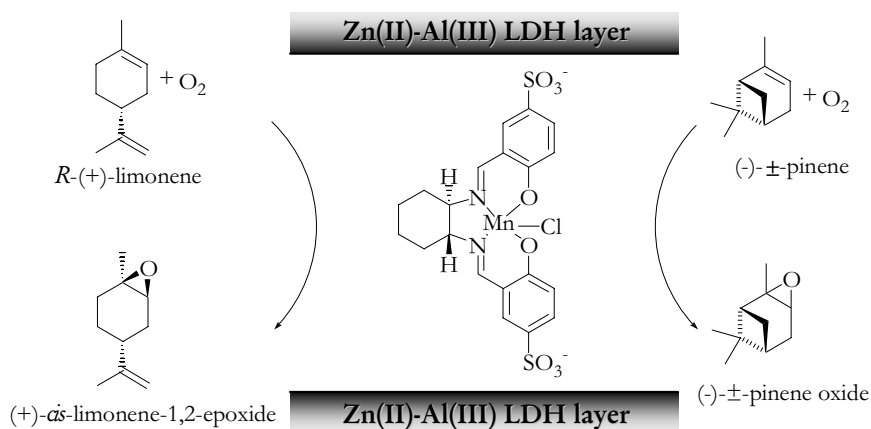
Figure 14 - Intercalation of a chiral anionic [Mn(III)(*salen*)Cl] complex within a Zn(II)-Al(III) LDH host and catalytic stereoselective epoxidation of *R*-(+)-limonene and (-)-±-pinene. Adapted from 48b.

The Cu(II) and VO(IV) acetylacetonates were immobilised onto two clays, Laponite (Lap) and K10-montmorillonite (K10), by two different immobilisation procedures: method A – direct complex anchoring ([M(acac)$_2$]@S, S = Lap or K10) and method B – complex anchoring through the APTES spacer previously attached onto the clays surface ([M(acac)$_2$]APTES@S)[49]. In the case of Cu(II) based materials, method A resulted in global complex anchoring efficiencies of 97 and 51 % for Lap and K10 based materials respectively; for method B, the opposite tendency was observed with 71 % and approximately 100 % for APTES-functionalised Lap and K10 supports. For [VO(acac)$_2$] based materials, method A led to complex

anchoring efficiencies of 87 and 35 % for Lap and K10, whereas method B resulted in 82 and 88 % for the APTES-based Lap and K10. It was concluded that the direct complex immobilisation mainly occurred through covalent bonding between the metal centre and the clay surface hydroxyl groups. In the case of the APTES-functionalised clays, it mostly proceeded by Schiff condensation between the free amine groups from grafted APTES and the carbonyl group of the acac ligand as depicted in Figure 15[49].
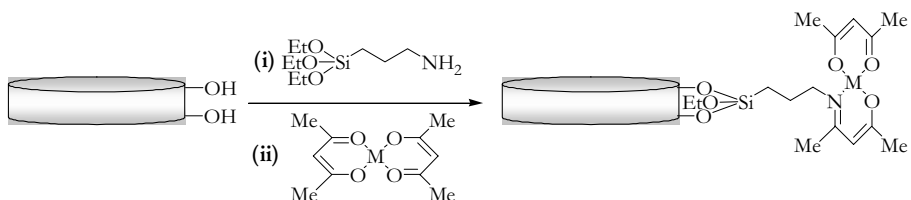
Figure 15 - Immobilisation of [M(acac)$_2$] complexes (M = Cu(II),VO(IV)) onto Lap and K10 clays previously functionalised with APTES. Adapted from 49.

The [VO(acac)$_2$] based materials were tested in the geraniol epoxidation in dichloromethane using TBHP as the oxidant and the catalysts were reused in other 4 cycles[49b]. The [VO(acac)$_2$]APTES@K10 material was the most efficient and stable catalyst upon reuse, resulting in a geraniol conversion and 2,3-epoxygeraniol regioselectivity comparable to the homogeneous phase reaction. In the case of Lap based materials, the [VO(acac)$_2$]@Lap was more catalytically efficient than [VO(acac)$_2$]APTES@Lap. After 5 catalytic cycles, a quite high leaching was detected for [VO(acac)$_2$]@K10, demonstrating that the APTES functionalisation prevented, to a large extent, the complex leaching. On the contrary, both Lap based materials presented similar leaching percentages.

9.3.4.2. Pillared Clays

The PILCs are a relatively recent class of porous materials prepared by direct intercalation of ionic oligomers between the clay interlayers that, after calcination, form pillars, creating an interlayer space of molecular dimensions

and a well-defined porous network[45b,c]. These solids can present pores that have intermediate dimensions between those typical of microporous zeolites and those of mesoporous silicas, allowing for the immobilisation of metal complexes by a great variety of methods.

One example of the encapsulation of metal complexes by different procedures is the study of the encapsulation of the non-chiral [Mn(saldPh)Cl] complex into an aluminium pillared clay, named Al-WYO, prepared using the parent clay Wyoming which is a montmorillonite clay from USA (Wyoming) and aluminium polyoxications[50]. The complex immobilisation was performed by: method A – *in-situ* Mn(III) complex synthesis within the PILC by a two-step procedure consisting of i) adsorption of Mn(II) chloride within the PILC, followed by ii) diffusion of the ligand and subsequent reaction with the metal centre; method B– simultaneous pillaring/encapsulation, with addition of the Mn(III) complex after the oligomer species formation; method C– simultaneous pillaring/encapsulation, with addition of the complex to the initial clay dispersion. The schematic representation of the different immobilisation methods is summarised in Figure 16.

In all cases, the Mn(III) complex was mainly physically encapsulated within the matrix, with nearly 20 % of complex immobilisation efficiency, although with some distortions due to physical restrictions imposed by the support and/or to host-guest interactions. All the materials were catalytic active in the styrene epoxidation in acetonitrile using PhIO, showing high styrene epoxide selectivities, although being lower than that observed for the homogeneous reaction. When compared with the homogeneous counterpart, the catalysts prepared by methods B and C presented similar styrene conversions and styrene epoxide yields, whereas the one prepared by method A led to lower values. After reuse for four cycles, although some decrease in their catalytic activities was observed, the catalysts prepared by methods B and C were more

stable. The recovered catalysts showed some metal complex leaching and deactivation, which was responsible for the decrease in the catalytic activities.
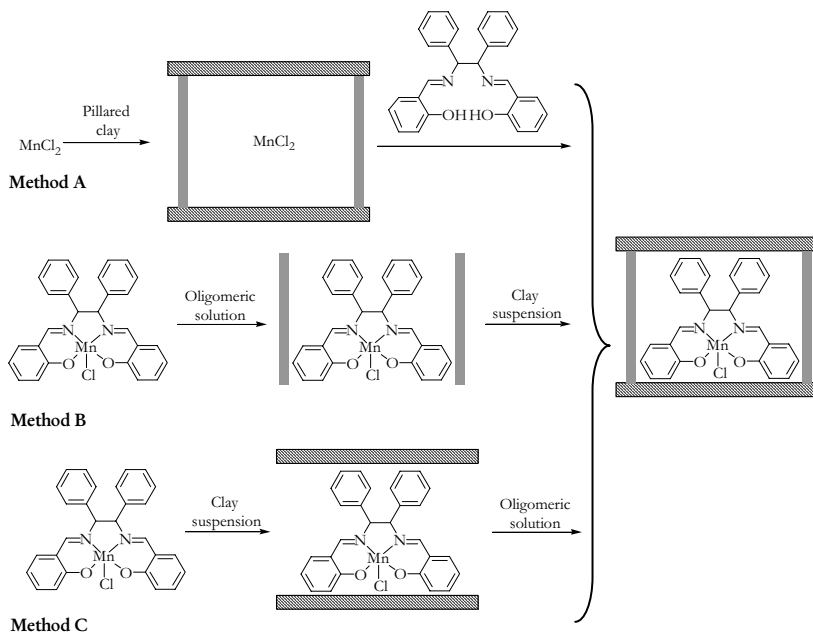
Figure 16 - Immobilisation of [Mn(III)(saldPh)Cl] complex within Al-WYO following three different methods, A, B and C. Adapted from 50.

9.4. CONCLUDING REMARKS

The quest for novel solid supports for the immobilisation of transition metal complexes as well as new strategies for the complexes immobilisation have been themes of increasing importance towards the goals of Green Chemistry. In the field of catalysis the main purpose of the metal complexes immobilisation is the preparation of heterogeneous materials with improved catalytic properties, when compared to their homogeneous congeners, and that can be recycled.

In this chapter, the general methods for the immobilisation of transition metal complexes with catalytic properties onto supports were presented according to the type of interaction between the support and metal complex. The examples

presented to demonstrate the immobilisation methodologies were restricted to solid supports, such as carbon materials, zeolites, mesoporous silicas and clay based materials. Among these supports, carbon materials and PILCs are probably those to which a greater variety of complex immobilisation methods can be applied.

References

1. J. Bird in *Catalyst Supports and Supported Catalysts*, A.B. Stiles (Eds.), Butterworths, Boston, **1987**.

2. *Chiral Catalyst Immobilisation and Recycling*, D.E. de Vos, I.F.J. Vankelecom, P.A. Jacobs (Eds.), Wiley-VCH Verlag, Weinheim, **2000**, pp. 19.

3. I.W.C.E. Arends, R.A. Sheldon, *Appl. Catal. A*, **2001**, *212*, 175.

4. Q.-H. Fan, Y.-M. Li, A.S.C. Chan, *Chem. Rev.*, **2002**, *102*, 3385.

5. C.E. Song, S. Lee, *Chem. Rev.*, **2002**, *102*, 3495.

6. D.E. de Vos, M. Dams, B.F. Sels, P.A. Jacobs, *Chem. Rev.* **2002**, *102*, 3615.

7. Q.-H. Xia, H.-Q. Ge, C.-P. Ye, Z.-M. Liu, K.-X. Su, *Chem. Rev.* **2005**, *105*, 1603.

8. J.M. Notestein, A. Katz, *Chem. Eur. J.* **2006**, *12*, 3954.

9. F. Goettmann, C. Sanchez, *J. Mater. Chem.*, **2007**, *17*, 24.

10. F. Bedioui, *Coord. Chem. Rev.,* **1995**, *144*, 39.

11. (a) J. W. Niemantsverdriet, *Spectroscopy in Catalysis. An Introduction*, VCH, Weinheim, **1995**. (b) J.P. Sibilia, *A Guide to Materials Characterization and Chemical Analysis*, 2nd Ed., Wiley, London, **1996**.

12. *Handbook of surface imaging*, A.T. Hubbard (Eds.), CRC Press, Boca Raton, **1995**.

13. G. Leofanti, M. Padovan, G. Tozzola, B. Venturelli, *Catal. Today*, **1998**, *41*, 207.

14. H. Marsh, F. Rodríguez-Reinoso, *Activated Carbon*, Elsevier, Oxford, **2006**.

15. *Chemistry and Physics of Carbon*, , L.R. Radovic (Eds.), vol. 28, Marcel Dekker, New York, **2003**.

16. C.M. Elliott, R.W. Murray, *Anal. Chem.,* **1976**, *48*, 1247.

17. K. Kinoshita, *Carbon Electrochemical and Physicochemical Properties*, Wiley, New York, **1988**.

18. (a) A. Hirsch, M. Brettreich, *Fullerenes: Chemistry and Reactions*, Wiley-VCH, Weinheim, **2004**. (b) K.M. Kadish, R.S. Ruoff, *Fullerenes: Chemistry, Physics, and Technology*, Wiley-VCH, Weinheim, **2000**.

19. (a) S. Iijima, *Nature*, **1991**, *354*, 56. (b) S. Reich, C. Thomsen, J. Maultzsch, *Carbon Nanotubes: Basic Concepts and Physical Properties*, Wiley-VCH, Weinheim, Germany, **2004**.

20. J.L. Figueiredo, M.F.R. Pereira, M.M.A. Freitas, J.J.M. Órfão, *Carbon*, **1999**, *37*, 1379.

21. (a) A. Vinu, K.Z. Hossian, P. Srinivasu, M. Miyahara, S. Anandan, N. Gokulakrishnan, T. Mori, K. Ariga, V.V. Balasubramanianc, *J. Mater. Chem.,* **2007**, *17*, 1819. (b) M.J. Lázaro, L. Calvillo, E.G. Bordejé, R. Moliner, R. Juan, C. R. Ruiz, *Microporous Mesoporous Mater.*, **2007**, *103*, 158.

22. (a) A. Hirsch, *Angew. Chem. Int. Ed.*, **2002**, *41*, 1853. (b) S. Banerjee, M.G.C. Kahn, S.S. Wong, *Chem. Eur. J.,* **2003**, *91*, 899. (c) S. Banerjee, T. Hemraj-Benny, S.S. Wong, *Adv. Mater.,* **2005**, *17*, 17.

23. (a) D. Tasis, N. Tagmatarchis, V. Georgakilas, M. Prato, *Chem. Eur. J.*, **2003**, *9*, 4001. (b) D. Tasis, N. Tagmatarchis, A. Bianco, M. Prato, *Chem. Rev.,* **2006**, *106*, 1105.

24. J.L. Bahr, J.M. Tour, *J. Mater. Chem.,* **2002**, *12*, 1952.

25. (a) R.F. Parton, P.E. Neys, P.A. Jacobs, R.C. Sosa, P.G. Rouxhety, *J. Catal.,* **1996**, *164*, 341. (b) R.C. Sosa, R.F. Parton, P.E. Neys, O. Lardinois, P.A. Jacobs, P.G. Rouxhet, *J. Mol. Catal. A: Chem.*, **1996**, *110*, 141.

26. A.R. Silva, M.M.A. Freitas, C. Freire, B. de Castro, J.L. Figueiredo, *Langmuir*, **2002**, *18*, 8017.

27. (a) A.R. Silva, C. Freire, B. de Castro, *Carbon*, **2004**, *42*, 3003. (b) A.R. Silva, V. Budarin, J.H. Clark, B. de Castro, C. Freire, *Carbon*, **2005**, *43*, 2096.

28. A.R. Silva, V. Budarin, J.H. Clark, C. Freire, B. de Castro, *Carbon,* **2007**, *45*, 1951.

29. (a) C. Baleizão, B. Gigante, H. Garcia, A. Corma, *J. Catal.,* **2004**, *221*, 77. (b) C. Baleizão, B. Gigante, H. Garcia, A. Corma, *Tetrahedron*, **2004**, *60*, 10461.

30. (a) A.R. Silva, M. Martins, M.M.A. Freitas, J.L. Figueiredo, C. Freire, B. de Castro, *Eur. J. Inorg. Chem.,* **2004**, 2027. (b) A.R. Silva, J.L. Figueiredo, C. Freire, B. de Castro, *Catal. Today,* **2005**, *102-103*, 154. (c) B. Jarrais, A.R. Silva, C. Freire, *Eur. J. Inorg. Chem.,* **2005**, 4582.

31. (a) A. Valente, A.M. Botelho do Rego, M.J. Reis, I.F. Silva, A.M. Ramos, J. Vital, *Appl. Catal. A,* **2001**, *207*, 221. (b) P. Oliveira, A.M. Ramos, I. Fonseca, A. Botelho do Rego, J. Vital, *Catal. Today,* **2005**, *102–103*, 67.

32. (a) K.J. Balkus Jr., A.G. Gabrielov, *J. Inclusion Phenom. Mol. Recognit. Chem.*, **1995**, *21*, 159. (b) D.E. de Vos, P.P. Knops-Gerrits, R.F. Parton, B.M. Weckhuysen, P.A. Jacobs, R.A. Schoonheydt, *J. Inclusion Phenom. Mol. Recog. Chem.*, **1995**, *21*, 185.

33. (a) P. Chen, B. Fan, M. Song, C. Jin, J. Ma, R. Li, *Catal. Commun.,* **2006**, *7*, 969. (b) C. Jin, W. Fan, Y. Jia, B. Fan, J. Ma, R. Li, *J. Mol. Catal. A: Chem.,* **2006**, *249*, 23. (c) M. Salavati-Niasari, *J. Mol. Catal. A: Chem.*, **2006**, *245*, 192. (d) J. Połtowicz, K. Pamin, E. Tabor, J. Haber, A. Adamski, Z. Sojka, *Appl. Catal. A: General*, **2006**, *299*, 235.

34. J. Haber, K. Pamin, J. Połtowicz, *J. Mol. Catal. A: Chem.*, **2004**, *224*, 153.

35. P.P. Knops-Gerrits, D.E. de Vos, F. Thibault-Starzyk, P.A. Jacobs, *Nature*, **1994**, *369*, 543.

36. K.J. Balkus Jr., A.A. Welch, B.E. Gnade, *J. Inclusion Phenom. Mol. Recognit. Chem.*, **1991**, *10*, 141.

37. (a) C.T. Kresge, M.E. Leonowicz, W.J. Roth, J.C. Vartuli, J.S. Beck, *Nature*, **1992**, *359*, 710. (b) J.S. Beck, J.C. Vartuli, W.J. Roth, M.E. Leonowicz, C.T. Kresge, K.D. Schmitt, C.T.-W. Chu, D.H. Olson, E.W. Sheppard, S.B. McCullen, J.B. Higgins, J.L. Schlenker, *J. Am. Chem. Soc.* **1992**, *114*, 10834. (c) P.T. Tanev, T.J. Pinnavaia, *Science*, **1995**, *267*, 865.

38. (a) F. Hoffmann, M. Cornelius, J. Morell, M. Fröba, *Angew. Chem. Int. Ed.*, **2006**, *45*, 3216. (b) A. Corma, H. Garcia, *Adv. Synth. Catal.*, **2006**, *348*, 1391.

39. A. Vinu, K.Z. Hossain, K. Ariga, *J. Nanosci. Nanotech.*, **2005**, *5*, 347.

40. A.R. Silva, K. Wilson, J.H. Clark, C. Freire, *Microporous Mesoporous Mater.*, **2006**, *91*, 128.

41. L. Zhang, T. Sun, J.Y. Ying, *Chem. Commun.*, **1999**, 1103.

42. R.J. Clarke, I.J. Shannon, *Chem. Commun.*, **2001**, 1936.

43. S.A. Raynor, J.M. Thomas, R. Raja, B.F.G. Johnson, R.G. Bell, M.D. Mantle, *Chem. Commun.*, **2000**, 1925.

44. X.-G. Zhou, X.-Q. Yu, J.-S. Huang, S.-G. Li, L.-S. Li, C.-M. Che, *Chem. Commun.*, **1999**, 1789.

45. (a) H.H. Murray, *Appl. Clay Sci.*, **2000**, *17*, 207. (b) Z. Ding, J.T. Kloprogge, R.L. Frost, G.Q. Lu, H.Y. Zhu, *J. Porous Mater.*, **2001**, *8*, 273. (c) A. Gil, L.M. Gandía, M.A. Vicente, *Catal. Rev. - Sci. Eng.*, **2000**, *42*, 145.

46. (a) J.M. Fraile, I. Pérez, J.A. Mayoral, O. Reiser, *Adv. Synth. Catal.*, **2006**, *348*, 1680. (b) J.M. Fraile, J.I. García, M.A. Harmer, C.I. Herrerías, J.A. Mayoral, *J. Mol. Catal. A: Chem.*, **2001**, *165*, 211.

47. (a) N.N. Herrera, J.-M. Letoffe, J.-P. Reymond, E. Bourgeat-Lami, *J. Mater. Chem.*, **2005**, *15*, 863. (b) A.M. Shanmugharaj, K.Y. Rhee, S.H. Ryu, *J. Colloid Interface Sci.*, **2006**, *298*, 854.

48. (a) S. Bhattacharjee, J.A. Anderson, *Chem. Commun.*, **2004**, 554. (b) S. Bhattacharjee, J.A. Anderson, *Catal. Lett.*, **2004**, *95*, 119.

49. (a) C. Pereira, S. Patrício, A.R. Silva, A.L. Magalhães, A.P. Carvalho, J. Pires, C. Freire, *J. Colloid Interface Sci.*, **2007**, *316*, 570. (b) C. Pereira, A.R. Silva, A.P. Carvalho, J. Pires, C. Freire, *J. Mol. Catal. A: Chem.*, **2007**, doi:10.1016/j.molcata.2007.11.034

50. B. Cardoso, J. Pires, A.P. Carvalho, I. Kuźniarska-Biernacka, A.R. Silva, B. de Castro, C. Freire, *Microporous Mesoporous Mater.*, **2005**, *86*, 295.

10. Transportation Fuels: New And Future Trends (From Petroleum To Biomass)

Jean-François Joly and Jean-Luc Duplan

Institut Francais Du Petrole – IFP-Lyon, BP n° 3, 69390 Vernaison - France

10.1. Introduction

Over the next thirty years, the most rapid increase in energy demand is expected to come from the transport sector (+2.1%/yr versus 1.7%/yr for total demand). At present, this sector relies almost exclusively on petroleum products, which raises two key issues: oil dependence and the reduction of greenhouse gases. In this context, after over 20 years of industrial development, the outlook for biofuels looks bright. The advantages of biofuels are well known. They provide an alternative to petroleum fuels in the transport sector and offer better environmental performance. With respect to the later, the main reason for using biofuels is that they reduce greenhouse gas (GHG) emissions.

Petroleum-based motor fuels account for more than 95% of the energy used in road transport worldwide. These fuels have already undergone substantial improvement. In addition to the specifications already scheduled for implementation, new ones may be enforced between now and 2020 to account for EU air quality targets and/or new modes of combustion in spark ignition and diesel engines. Beyond this time horizon, alternative fuels offer a solution to reduce greenhouse tailpipe emissions while retaining the internal combustion engine.

Today trends in transportation fuels have to take into account first generation biofuel (ethanol from sugar and biodiesel from oleaginous crops) as well as natural and liquefied pretroleum gases used in gasoline engines. In the future, new second generation fuels will be based on abundant carbon resources: coal, natural gas and the renewable lignocellulose biomass from wood, crops haulm

or waste. Sugar part of the later could be converted by biological processes and all those carbon sources could feed a flexible gasification for synthetic Fischer Tropsch fuel process chain.

In 2003, the transport sector consumed 1,500 Million Tonnes of Oil Equivalent (Mtoe) worldwide. Alternative motor fuels, i.e. natural gas for vehicles (NGV), liquefied petroleum gas (LPG) and biofuels, only represented about 40 Mtoe, less than 3% of the total.

If we consider the predicted growth of transport fuel on a world scale, Figure 1 and Table 1, we come to the following conclusions:

- all fuels are expected to grow ;
- the fastest growth will be observed for kerosene ;
- gasoline, the dominant fuel in 2005, will be superseded by middle distillates (kerosene and Diesel).
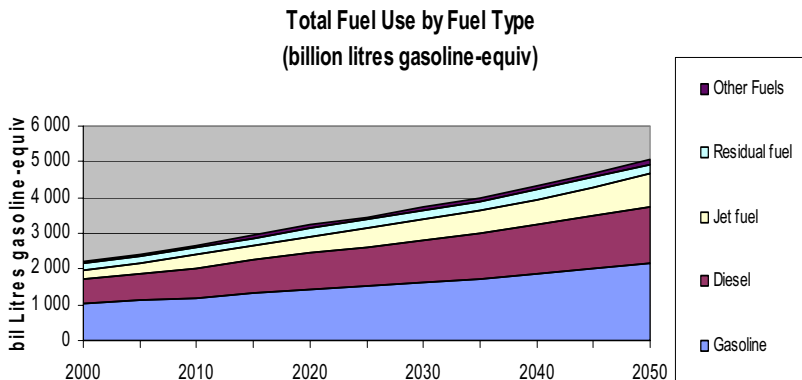
Figure 1 - An extrapolation of motor fuel use – (source IFP).

The fast growth of kerosene has important consequences. Kerosene is very difficult to substitute, because of the very stringent specifications of this fuel (necessary for aircraft safety). Also, the current aircrafts have a very long life (at

least 30 years). Thus, there will be a competition between Diesel and kerosene, leading to constraints on Diesel (this is not necessarily the case for gasoline).

TABLE 1 - World fuel use by fuel type (%) (source IFP)

	2005	2010	2020	2030
Gasoline	46.2	44.8	44.3	43.6
Diesel	31.2	31.6	31.8	31.7
Jet Fuel	12.3	13.1	14.3	15.7
Residual	8.0	7.6	6.9	6.5
Other	2.3	2.8	2.6	2.5

The introduction of a significant percentage of biomass derived Diesel components will not only help to control to some extent fossil carbon dioxide emissions, but also to fill the gap. The development of biodiesel is observed not only in Europe – where private car dieselization is increasing – but also in countries like Brazil and the US, where mainly gasoline is used for private cars. Different processes are under study; for some of them, pilot units have already been developed. In the short and medium term, it may be possible to exploit synfuels (GTL, CTL and BTL) produced from natural gas, coal and biomass. In the longer term, hydrogen may provide a breakthrough.

10.2. Alternative Motor Fuels Today: Natural Gas For Vehicles (NGV), Liquefied Petroleum Gas (LPG), And "First Generation" Biofuels.

10.2.1. Natural gas for vehicles (NGV)

The use of NGV for transport represents a very low percentage of total consumption of natural gas (mainly used for electricity production and heating) and of the world automobile fleet. The need for high-pressure storage and relatively heavy infrastructure limits large-scale development. Its greatest potential is concentrated in captive fleets of vehicles (e.g. buses and trucks) that make many short runs in downtown areas. In terms of environmental impact, this technology outperforms liquid hydrocarbon fuels provided that the engine is optimized for its use: no odors, no black fumes, no particulates, soot or evaporative emissions; CO emissions are reduced by 90% and NO_x by 60%; if the engine is optimized to run on natural gas, CO_2 emissions can be cut by 5 to 10% compared to the diesel engine.

10.2.2. Liquefied petroleum gas (LPG)

LPG (a blend of butane and propane) can be obtained directly in operations to remove hydrocarbon liquids at the field, in which case it is obtained directly or from crude oil refining. LPG motor fuel presents certain environmental advantages: high octane number, ensuring good resistance to engine knock; zero sulfur, lead and benzene emissions; low evaporative emissions.

It also has disadvantages: the need to develop a distribution network, the high additional cost of vehicle purchase and product availability. The global LPG fleet has grown 25% in 3 years, up from 7.5 million in 2000 to 9.5 million in 2003, which corresponds to consumption of 16.5 Mt.

10.2.3. "First generation" biofuels

Compared with the use of NGV and LPG, one major advantage of biofuels is that, blended with conventional motor fuels, they are compatible with the existing distribution system and that major vehicle modifications are not required.

Interest in biofuels is constantly increasing, driven by two concerns: protection of the environment and an imperative need for alternative energies.

Biofuels, synthesized from renewable plant resources, may represent an alternative, offering a partial response to the problem of CO_2 emissions in the transport sector and bring the beginnings of a solution to our dependence on energy.

For these reasons the European Commission promulgated a directive in 2003 aimed at establishing a 5.75% biofuel content in gasoline and gas oil in 2010, and substituting 20% of fossil fuels for alternative fuels (biofuels, natural gas, hydrogen, etc.) in the transport sector by 2020.

In this context, IFP has been leading research and development initiatives, some of these for twenty years, for industrial purposes, the principal aim of which is to reduce biofuel production costs. However, the area of cultivable land required combined with the competing needs associated with food crop uses mean that the production potential of biofuels is limited. As a result, research is now focusing on second-generation technologies using plant waste along with non-food resources, such as straw or wood. Second-generation technologies will be discussed later in this paper.

Today there are two principal biofuels currently in use: ethanol and biodiesel, Figure 2.
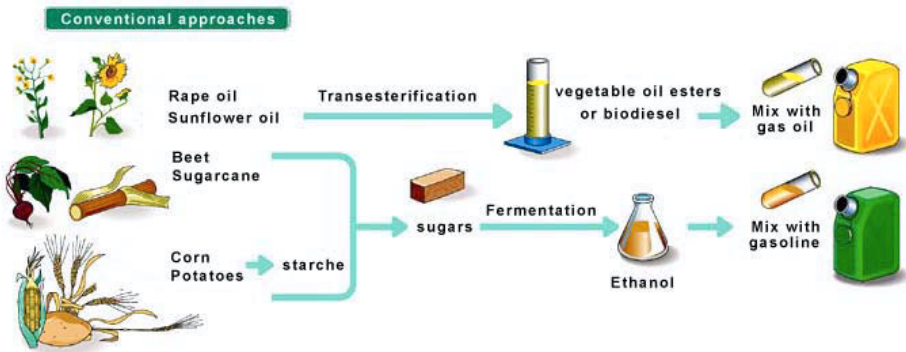
Figure 2 - Main routes for "first generation" biofuels production pathways.

10.2.3.1. Ethanol for gasoline engines

The most widely used biofuel in the world today is ethanol, blended with gasoline.

Ethanol can be used pure, in a blend or in its ether form (ETBE), obtained in reaction with refinery isobutene. If it used pure or in a very high concentration (e.g. 85% or E85), then vehicle modifications are necessary (injection systems, engine adjustment systems, compatibility of plastics and gaskets, special cold-start strategies for pure ethanol).

Ethanol is made from two types of crop: sugar-producing crops (sugar cane, sugar beets) and amylaceous plants (wheat, corn). All of these production processes require a fermentation stage to convert the sugar to ethanol, as well as a more or less advanced distillation stage to separate the alcohol from water. In EU, ethanol can be incorporated in blends in relatively low contents (5 to 10%) but ethanol can be first converted into ETBE by addition of isobutene, via a catalytic etherification.

10.2.3.2. Biodiesel (VOME, e.g. Vegetable Oil Methyl Ester) for diesel engines

VOME are produced from vegetable oils made from rapeseed, sunflower, soybean or palm. Unsuitable for direct use in modern diesel engines, vegetable oils need to be transformed by means of transesterification with an alcohol (currently methanol), via a catalyst, to obtain vegetable oil methyl esters and glycerin. VOME are mostly incorporated in blends in concentration ranging from 1 to 5%, and, in certain cases, to 30%.

The use of the methyl ester of vegetable oils has been proposed as early as 1983 by Guibet et al[1] and one of the first industrial units has been started in France near Compiègne on a design by IFP. VOME is produced from the trans-esterification of vegetable oils, especially from rapeseed in France, a chemical process which uses methanol of petrochemical origin. VOME is in widespread use in Europe, mainly mixed with gas oil to a concentration of 5%. In France, blended with gas oil in proportions varying between 2 and 5%, it is currently available at the pump with no specific identifying name, thus consumers are already using this biofuel, often without realizing it.

The transesterification of triglycerides to fatty acid methyl esters (FAME) with methanol is a balanced and catalyzed reaction, as illustrated in Figure 3. An excess of methanol is required to obtain a high degree of conversion.

$$
\begin{array}{cccccc}
R_1{-}COO{-}CH_2 & & & R_1{-}COOCH_3 & & HO{-}CH_2 \\
R_2{-}COO{-}CH & + & 3\ CH_3OH \xrightleftharpoons{catalyst} & R_2{-}COOCH_3 & + & HO{-}CH \\
R_3{-}COO{-}CH_2 & & & R_3{-}COOCH_3 & & HO{-}CH_2 \\
\text{triglyceride} & & \text{methanol} & \text{methyl esters} & & \text{glycerol}
\end{array}
$$
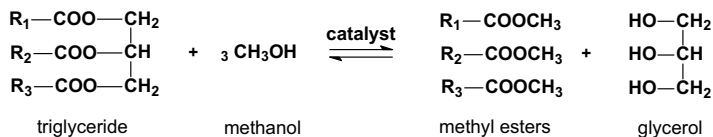
with R1, R2, R3 = hydrocarbon chain from 15 to 21 carbon atoms

Figure 3 - Overall reaction for transesterification of vegetable oil (triglycerides) to produce biodiesel (methyl esters).

The conventional industrial biodiesel processes are based on homogeneous catalysis. Sodium hydroxide or sodium methylate are the most often used catalysts in industrial processes. The removal of homogeneous catalyst from the reactor effluent requires further downstream operations. Typical process scheme is illustrated in Figure 4.
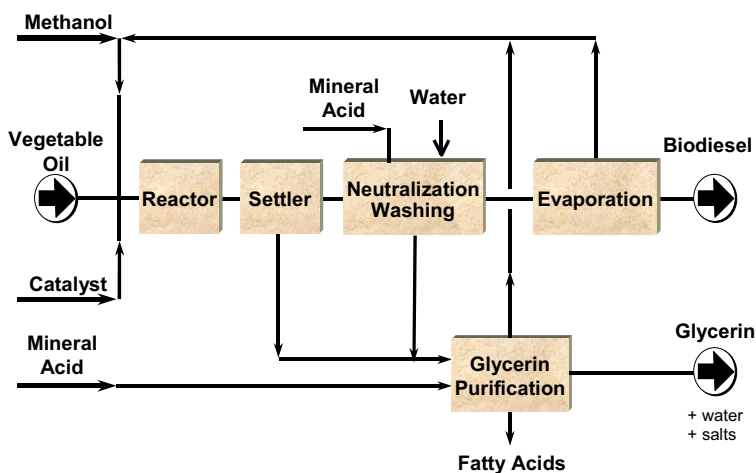
Figure 4 - Global scheme for a typical continuous homogeneous catalyzed process.

A new vegetable oil ester production process, developed by IFP and known as Esterfip-H™, has recently been marketed by Axens, Figure 5. This new process uses a solid catalyst developed at IFP[2], of the same type as those commonly used in traditional refineries, but not, as yet, adapted to biodiesel production. It was analysis of the disadvantages of homogeneous catalysis processes that led IFP and Axens teams to focus research on a solid catalyst[3].
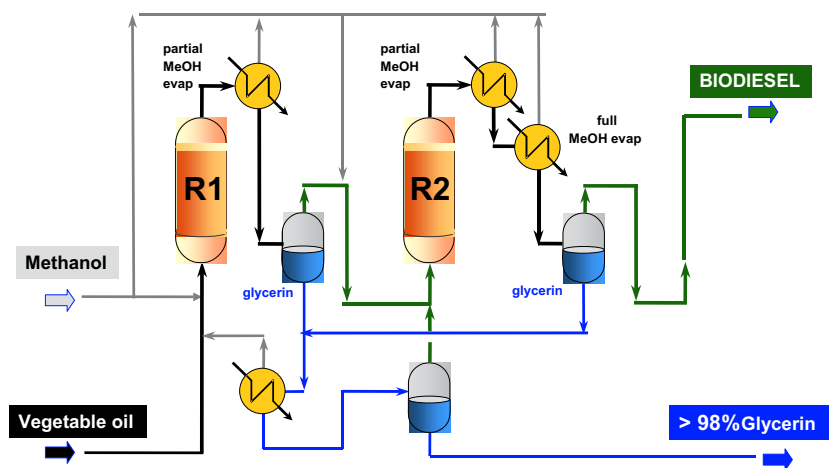
Figure 5 - Simplified flow sheet of the new heterogeneous process, Esterfip-H™.

This new heterogeneous catalyst process offers the main following advantages : high biodiesel yield can be obtained, since there is no ester loss due to soap formation;

- the crude glycerol obtained is salt free and has a very high glycerol purity, thus allowing new direct ways of valorisation ;
- there is neither chemical products consumption, nor waste streams.

To be acceptable, the ester must respect specifications (for the case of Europe: EN14214). The critical specifications are related to the cold properties and stability. These specifications limit the choice for the starting vegetable oils, as discussed below. In Europe, rape seed and oleic sunflower oils are used, in Brazil soybean oil.

Replacement of fossil derived methanol by ethanol is an interesting objective:

- the ethyl ester would be 100% derived from biomass;
- this is a way to incorporate some ethanol in the Diesel pool. This would help to fit the motor fuels consumption in Europe, where the gasoline / Diesel usage ratio is low and still decreasing, which makes ethanol a not optimal biofuel in this context.

However, this proves not easy for several reasons. First, the reaction is slower: higher amount of catalyst and/or higher temperatures are needed for ethyl esters production in order to balance the lower ethanol reactivity. Second, ethanol is a better solvent for oil and ethyl esters.

Research is in progress in order to find the way to produce ethyl esters in the most economical way[4]. Heterogeneous catalysis should be a better way to produce ethyl esters than homogeneous catalysis, since methanol substitution by ethanol involves less technical difficulties.

10.3. ALTERNATIVE MOTOR FUELS TODAY... SUMMARY

The alternative motor fuels most in use in the world today are biofuels (ethanol and FAME), LPG (liquefied petroleum gas) and NGV (natural gas for vehicles).

LPG (liquefied petroleum gas) and NGV (natural gas for vehicles): large-scale development is limited by specific distribution networks.

ETBE and VOME: Compatible with the existing distribution systems. However, production costs and restricted land volume, because of competition with food crops, led R&D work to find solutions to produce new biofuels. Those solutions will focus on an abundant and available renewable resource, lignocellulose biomass (wood, straw and other waste). Two alternatives could be considered: a biological conversion to ethanol or higher alcohols or thermochemical pathway as gasification to produce a syngas (H_2 and CO) coupled with a fuel synthesis Fischer-Tropsch unit. Gasification offers flexibility regarding both feedstock and final product, but it requires additional developments and improvements to reach economic profitability. Gasification process is well known for the conversion of coal, petroleum coke or heavy petroleum residues to syngas. From biomass feed, the main obstacles are the cleaning system of the syngas and the variability of the feedstock with time. As

for the FT synthesis, the industrial operability has been proved for a long time by Sasol on Coal or Shell on natural gas.

10.4. ALTERNATIVE MOTOR FUELS TOMORROW: SYNFUELS - GTL (GAS TO LIQUID), CTL (COAL TO LIQUID) AND "SECOND GENERATION" BIOFUELS.

Synthetic fuels can be produced from any raw material ("feed") at all containing carbon and hydrogen, be it coal, biomass (agricultural, household or industrial waste, etc.) or natural gas.

The fuels obtained will have comparable characteristics. However, primarily for economic reasons, it is natural gas that is mostly used today. Indeed, due in particular to the nature of the feeds, the R&D investment required is financially greater for the other types (CTL - Coal to Liquid, BTL - Biomass to Liquid).

10.4.1. Gas to Liquids (GTL) synfuels

Natural gas seems to have potential as an energy source for the transport industry, especially when it is transformed into a "so-called synthetic fuel", which can then be used directly in conventional combustion engines.

Several industry players have decided to invest in this area recently. For example, Shell was the first company to launch itself into synthetic fuel production from natural gas at its Bintulu site in Malaysia. This small production unit (12,500 barrels/day) has been operational since 1993 and remains the only factory in the world producing what is known as GTL fuel (Gas to Liquid). Although the cost of these units still represents a significant brake on their development, several sites capable of producing tens of thousands of barrels per day are being planned.

The synthetic fuel production chain consists of three stages, Figure 6:

First, syngas is produced from natural gas using vapor and/or oxygen. The syngas obtained should have a ratio of H_2 to CO of about 2. In addition to these 2 elements, a small amount of CO_2 is generated (about 5% of the total gas). In general, two basic processes are used to make syngas from natural gas: steam reforming and partial oxidation.

Steam reforming:

$CH_4 + H_2O + Heat \rightleftarrows 3H_2 + CO$

Partial oxidation:

$CH_4 + 1/2\ O_2 \rightleftarrows 2H_2 + CO + Heat$
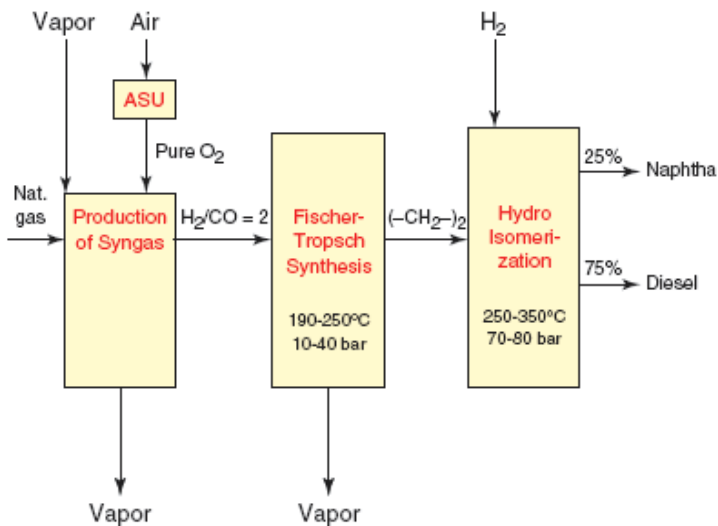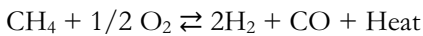
Figure 6 - Basic diagram for a gas-to-liquids unit (source IFP).

Next comes the most important step in the GTL production chain: Fischer-Tropsch synthesis, used to convert syngas into long paraffinic chains of hydrocarbons.

These long chains must be broken and reshaped. This is done by hydroisomerization (a gentle hydrocracking method at about 50-80 bar), then

products undergo conventional fractioning to obtain a naphtha cut (about one-quarter) and a diesel cut (about three-quarters).

Gas oil obtained using this process is of excellent quality: it contains no sulfur or aromatic substances (benzene, toluene, etc.), and its combustion in cars results in very low particle emissions. Its cetane number, which reflects combustion quality, is very high.

The GTL industry is still in its early days. Gradually, technological and design advances will no doubt help reduce the unit cost of investment. It seems evident that FT diesel has a bright future and that it fits into a general trend in favor of developing new motor fuel production pathways, such as CTL (Coal-to-Liquids), BTL (Biomass-to-Liquids) and, in the longer range, hydrogen.

10.4.2. Coal to Liquids (CTL)

Although it costs more, CTL technology is a possible solution. Direct or indirect liquefaction technologies have been developed.

This alternative is attractive for countries possessing coal in abundance. World coal reserves, which can ensure production for more than 200 years at the present rate, are concentrated in countries like China and India, which should see sharp growth in their energy consumption in the years to come. By way of an example, let us consider China. Since little research was done in this area over the last 20 years, significant advances can be expected in the future.

10.4.3. "Second generation" biofuels

The so-called second-generation biofuels can be defined as those using lignocellulosic biomass as the raw material. The principal advantage is that they can be used to extract value from the most abundant carbon source on our planet.

Lignocellulosic biomass is composed mainly of three polymers from the cell wall of plants: cellulose, hemicellulose and lignin, present in varying proportions, depending on the plant, Table 2 and Figure 7.

TABLE 2 - Composition of lignocellulosic biomass, it also contains other elements (inorganic, silica, etc.) in proportions ranging from 0,5 to 10%.

Biomass	Lignin (%)	Cellulose (%)	Hemicellulose (%)
Softwood	27-30	35-42	20-30
Hardwood	20-25	40-50	20-25
Wheat straw	15-20	30-43	20-27
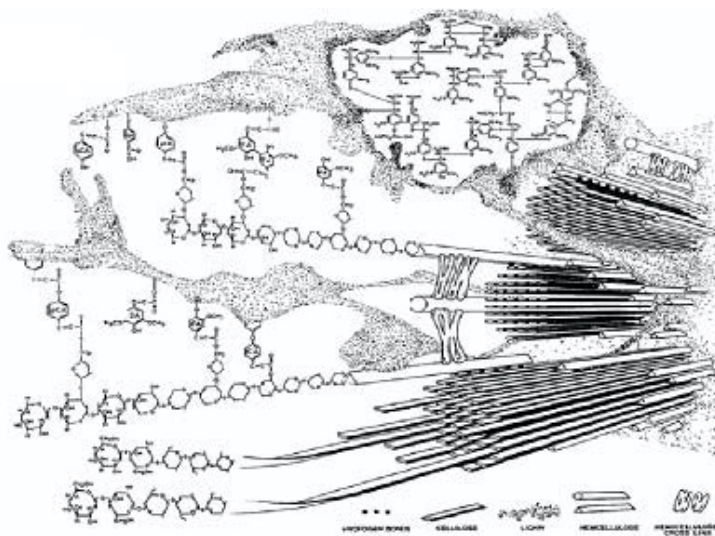
Figure 7 - Simplified representation of lignocellulose.

10.5. ETHANOL FOR GASOLINE ENGINES

Since the beginning of the 1980s, IFP has been researching and developing a production process for acetone butanol and/or ethanol from lignocellulosic biomass such as cereal straw, corn stalks, wood residues and even organic waste such as water treatment plant sludge. The addition of these oxygenated

compounds to unleaded gasoline leads to an increase in the octane number and a reduction in pollutant emissions in exhaust gas.

In this process, of the three main polymers making up the lignocellulosic biomass, cellulose and hemicelluloses are converted into ethanol by biological methods whilst lignin is used as an energy source. This biological conversion method has been researched on a representative pre-industrial scale. IFP is currently trying to improve the process by removing the last technological barriers, firstly the only moderate efficiency of enzymatic hydrolysis of lignocellulosic matter and, secondly, the poor performance of ethanolic fermentation of pentoses produced by the hemicellulose fraction, Scheme 1.
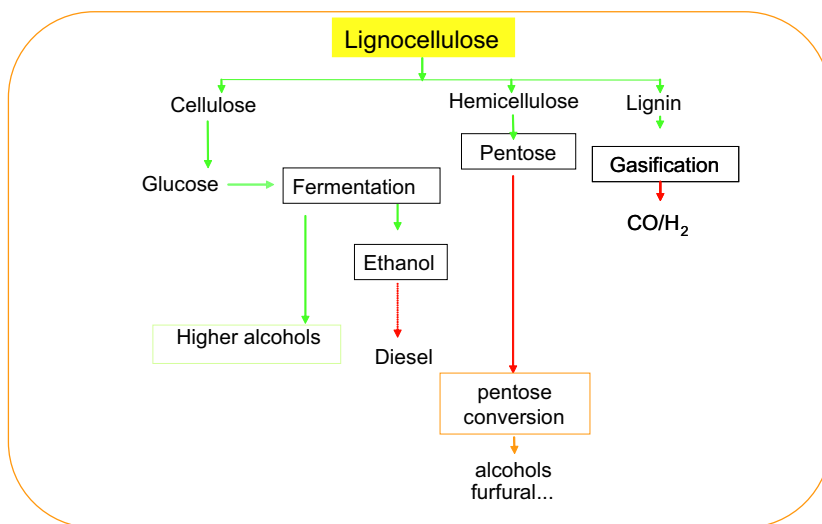
Scheme 1

10.6. ETHANOL FOR DIESEL ENGINES

Ethanol will become a commodity, as a very important component of the gasoline pool, and may be used as a starting material for light olefin production. However, as has been discussed in the introduction of this paper, it would be of high interest to convert ethanol to diesel.

The required chemistry:

$$\text{ethanol} \xrightarrow{\text{dehydration}} \text{ethylene} + \text{water}$$

$$\text{ethylene} \xrightarrow{\text{oligomerization}} \text{linear oligomers } C_4 - C_{20}$$
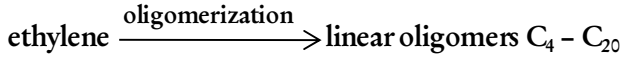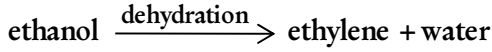
is well known, but the available processes are not adapted to the production of motor fuels, such a production requiring low cost processes and catalysts, with still a fair selectivity.

10.7. GASOIL FROM LIGNOCELLULOSE

Lignocellulose is a natural composite material whose main compounds are known as cellulose, hemicellose, and lignin. Cellulose and hemicelluloses are polysaccharides whereas lignin is considered as an amorphous polymer built with propyl-methoxy-phenols type constitutional units. Various inorganic compounds as sulphur, chlorine, iron, alkali metals and alkaline-earth metals are part of this natural material.

Lignocellulose can be used as a source of carbon and hydrogen in order to produce liquid fuels. Similarly to the use of coal, two routes have been identified and are summarized on Figure 8 hereunder.
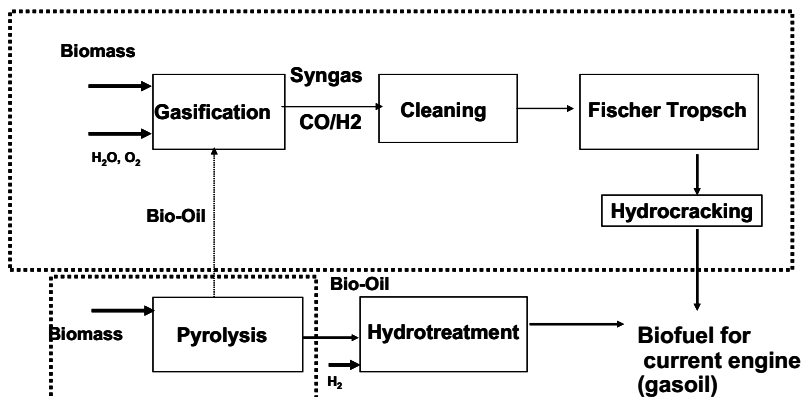
Figure 8 - Main routes for conversion of lignocellulose to liquid fuels.

Contrarily to the previously discussed processes, e.g. Biodiesel (VOME, e.g. Vegetable Oil Methyl Ester) that require highly specific plants, and can transform only part of those plants, (the "oily part"), second generation processes will transform the whole plant, i.e. lignocellulosic material (a complex mixture of oses: cellulose, hemicellulose and lignin) obtained from forestry and agriculture sources (wood, straw, dedicated crops, plant waste). This appears to be the most promising approach to significantly increase the production of biodiesel and bio middle distillates.

Four main steps are involved in the thermochemical route (middle distillates from lignocellulosic material):

- **step 1**: biomass pretreatment, generally required before biomass can be admitted to step 2. This usually involves thermal and mechanical transformations. Two methods can be used: pyrolysis[5] and torrefaction[6]. Pyrolysis uses heat to break biomass down into three phases: solid (coal), liquid (bio-oil) and gas (mostly carbon dioxide, carbon monoxide, hydrogen and methane). Although these bio-oils look very much like petroleum, see Figure 8, they are actually quite different. They contain several hundred chemical compounds (e.g. phenols, sugars, alcohols, organic acids and aromatic compounds) in proportions that vary greatly, and present the particularity of not being miscible with any petroleum product. These oils are then introduced directly into the gasifier. Current research is seeking to convert these oils directly to motor fuels via hydrogen treatments. Although attractive, this direct pathway seems hard to implement, given the quantities of hydrogen needed and the fact that the chemical nature of the bio-oils produced is very different from that of conventional automotive fuels. Torrefaction makes it easier to grind wood and thus obtain a finely divided solid suitable for certain gasification technologies. Torrefaction is like a final drying operation (temperature: 240 to

300°C, residence time: up to one hour). Carried out at temperatures much lower than in pyrolysis, this process is much less energy intensive;

- **step 2**: gasification[7] at high temperature with oxygen to obtain synthesis gas ($CO+xH_2$). Purification of the raw synthesis gas is a critical step. Gasification is a thermal operation that takes place in the presence of a gaseous reactive (water vapor, oxygen) and produces what is called a syngas that mostly contains hydrogen and carbon monoxide. In a BTL process, which aims to produce a liquid motor fuel, the constraints imposed on syngas are severe: maximize production of carbon monoxide (CO) and hydrogen (H_2) while achieving a H_2/CO ratio (about 2) compatible with motor fuel synthesis. It is also vital to eliminate impurities that would otherwise "poison" the catalyst used in Fischer-Tropsch synthesis. No specific biomass gasification technology has reached the industrial stage. Most of the solutions that have been put forward are derived from technologies for natural gas, coal or petroleum already in industrial use. Cleaning of the synthetic gas produced by gasification consists of filtration and elimination of certain compounds (H_2S, COS, HCl, HCN, NH_3, tars, alkali metals, etc.). This is a critical step for the feasibility and industrial profitability of the technology[8];

- **step 3**: Fischer-Tropsch synthesis to yield high molecular weight n-paraffins;

- **step 4**: hydrocracking of these paraffins to yield the final products (some gasoline, appropriate as a steam cracking feedstock, kerosene and Diesel, lubricating oil).

Figure 8 - Bio oil produced by lignocellulose pyrolysis, Bio-Oils composition: Water: 20-30 % C: 44-47 %; H: 6-7 %; O: 46-48 % N: 0,2 % max; S < 0,01 % density 1,2 Conradson Carbon : 10 - 20 %.

The thermochemical route is clearly not as technologically mature as GTL or CTL, and is still in the R&D stage. Projects have been implemented to demonstrate the technology, notably within the framework of European programs.

A number of research projects now underway, especially in the United States and Europe, are focusing on second-generation technologies. IFP is a major player[9] on the research scene both in France, where it is involved in the national bioenergy research plan, and in Europe, where it is leading the NILE3 Project bearing on the production of ethanol from lignocellulosic materials.

10.8. CONCLUSION

The alternative motor fuels most in use in the world today are biofuels (ethanol and FAME), LPG (liquefied petroleum gas) and NGV (natural gas for vehicles). In the medium term, the synfuels produced from natural gas (GTL), coal (CTL) and biomass (BTL) for which industrial or pilot projects exist

should come into greater use. In a more distant future, hydrogen may position itself as a replacement fuel provided that certain obstacles are overcome, particularly that of cost.

References

1. R. Stern, J.C. Guibet, J. Graille, *Revue Institut Français du Pétrole*, **1983,** *38*, 121-136.

2. L. Bournay, D. Casanave, B. Delfort, G. Hillion, J.A. Chodorge, *Catalysis Today*, **2005**, *106*, 190-192.

3. R. Stern, G.Hillion, J.J. Rouxel, US Patent 5908946, **1999**.

4. Hoang LeChien, FR 2,78 ,116, **1998**.

5. T. Bridgwater, *Fast Pyrolysis of Biomass*, *A Handbook,* vol. 2, CPL Press, UK, **2002**.

6. A. van der Drift, ECN, *Initial Biomass Treatment for Large Scale Fischer-Tropsch Production from Imported Biomass*, BTLtec,Munich, **2006.**

7. H. Knoef, *Handbook Biomass Gasification*, BTG Biomass Technology Group, Netherland, **2005**.

8. H.L. Iversen, B. Gobel in *Handbook Biomass Gasification*, H. Knoef (Ed.), BTG Biomass Technology Group, Netherland, **2005**, pp. 189.

9. D. Ballérini, *Les Biocarburants: États des Lieux, Perspectives et Enjeux du Développement*, Ed. Technip, Paris, **2006**, pp. 226.

SECTION B

HOMOGENEOUS CATALYSIS

(Página deixada propositadamente em branco)

1. HOMOGENEOUS CATALYSIS

Mariette M. Pereira and Andreia F. Peixoto

Departamento de Química, Faculdade de Ciências e Tecnologia, Universidade de Coimbra, Rua Larga, 3004-535, Coimbra, Portugal.

1.1. INTRODUCTION

In homogeneous catalysis the catalyst and the reactants are in the same phase.

Despite the large number of known homogeneous catalytic reactions (e.g. acid-base catalysis, Diels-Alder reactions), large-scale homogeneous catalysis was only dramatically improved with the development of organometallic chemistry between 1950 and 1960. Development of the synthesis of new ligands, especially phosphorous type ligands, provided the starting point for finely tuned tailored catalysts.

Nowadays, there are several examples of industrial homogeneous catalysts using transition metal complexes where activity and selectivity improved significantly: i) Ziegler and Natta olefin polymerization (1954/1955) ii) the Monsanto acetic acid process (1970) iii) nickel catalysed hydrogenation (Dupont), iv) the cobalt catalysed carbonylation of methanol (BASF) and the cobalt catalysed hydroformylation (Ruhrchemie-Shell), v) the molybdenum catalysed epoxidation of propene (Halcon)[1].

The first industrial homogeneous processes were developed for bulk chemistry, but the recognition that chiral ligands could give optical induction with pro-chiral substrates extended their application to fine chemistry. Stereoselective synthesis using organometallic catalysis is now one of the most valuable subjects of these research areas and some of the homogeneous catalysts available almost reach enzymatic selectivity. So, many raw materials and fine chemicals can be produced by means of homogeneous catalytic processes involving specific stereochemical synthetic requirements for pharmaceutical and agrochemical intermediates. In order to enhance, the activity and selectivity, of

the homogeneous catalysts it is also very important to optimize ligand design using modern computational methodologies.

The following chapters contain a concise description of the mechanism, catalyst structure and industrial applications in hydroformylation, hydrogenation, oxidation, palladium C-C coupling, methathesis, aldehyde alkylation and carbonylation reactions, Scheme 1, and also their potential industrial applications.
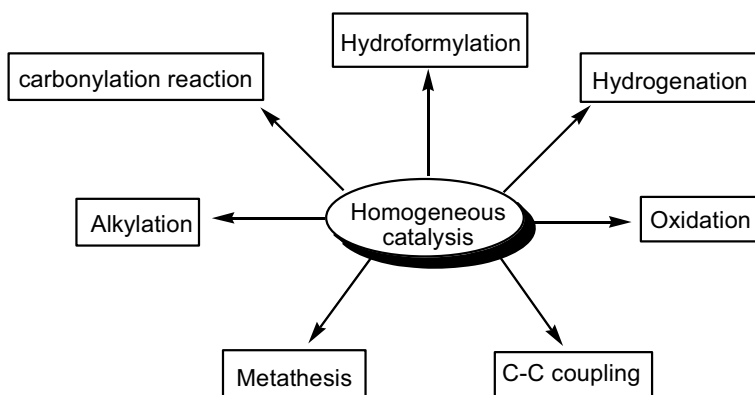
Scheme 1

1.2. GENERAL PROPERTIES OF ORGANOMETALLIC COMPLEXES

1.2.1. The 18-electron rule

The 18-electron rule is a simple way to decide if a given d-block transition organometallic complex is likely to be stable. A low-valent transition metal has one s orbital, three p orbitals and five d orbitals. To fill all the orbitals it is necessary to have 18 e-.

18-electron rule: a stable complex (with the electron configuration of the next highest noble gas) is obtained when the sum of electrons donated from ligands, metal-d-electrons and of the overall charge of the complex equals 18[2,3,4].

There are two conventions for counting electrons: the ionic and the covalent models. Both methods lead to the same result but they differ in the way the electrons are considered, i.e., whether they come from the metal or from the ligands. Let us consider $MoH_4(PR_3)_4$ as selected example. If we adopt the covalent model the H atom is considered as $1e^-$ ligand and $:PR_3$ $2e^-$ ligand. With this model the Mo is zero valent contributing with six electrons, plus four electrons from H•, plus eight electrons from four $:PR_3$, so $(6e^- + 4e^- + 8e^-) = 18e^-$. Using the ionic model, however, we have just two electrons from Mo^{4+}, eight from H: and eight from $:PR_3$ so, $(2e^- + 8e^- + 8e^-) = 18e^-$.

In the covalent convention the metal is always considered as zero valent and the ligands as neutral species, while the ionic convention considers the metal as a cation and the ligand as an anion. Table 1 presents the number of electrons donated to the metal following the electron-neutral convention and the ionic convention of a set of organometallic complexes.

Most organometallic complexes obey the 18-electron rule, except transition metals with d^8 configuration, such as Rh(I), Ir(I), Ni(II), Pd(II) and Pt(II), which have a strong preference to form square planar 16-electron complexes, Scheme 2. In these complexes the d_{z^2} orbital does not participate in ligand bonding.

TABLE 1 – Number of electrons that ligands formally donate to metal centre, using the covalent and the ionic model

	Heptacity η	Neutral/ Covalent	Oxid. State/ Ionic
-H, -Cl, -Br, -I, -OR $-NC\overset{O}{\underset{R}{\diagdown}}$	1	1	2
:C≡O :SR$_2$:PR$_3$ C=C C=Ö	2	2	2
$H_2C{=}\overset{H}{C}{-}CH_2 \leftrightarrow H_2C{-}\overset{H}{C}{=}CH_2$ (cyclopropenyl)	3	3	4
(cyclobutadiene) (butadiene)	4	4	4
(cyclopentadienyl) (indenyl⁻)	5	5	6
(benzene)	6	6	6

Rh (I)   – 8 e⁻
Cyclooctadiene   – 4 e⁻
Acetylacetonate   – 4 e⁻
                  ‾‾‾‾‾
                  16e⁻

Scheme 2

1.2.2. Metal - alkene bond

Olefins bind to transition metals via π orbitals by donating electrons into empty metal d-orbitals. This bond is stabilized by back-donation of electron density from an occupied d-orbital with appropriate symmetry, into the π^* orbital. So, the metal acts as a Lewis acid (electron acceptor) and as a Lewis base (electron donor), relative to the olefin, Scheme 3.
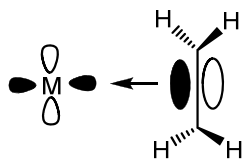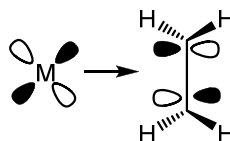
π − donation

d(π)-π* back-donation

Example:
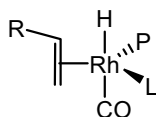
Scheme 3

1.2.3. Metal - Hydride

*Hydrid*e is the name given to a hydrogen atom with one more electron (H:⁻).

Actually, the term *Hydride* was enlarged to describe compounds of hydrogen with metals. They can be classified according to the nature of their chemical bonding: ionic, covalent and metal hydride transition metal complexes.

In ionic hydrides the hydrogen receives an electron from a more electropositive metal to form a negative ion (H:⁻) and a positive ion (M⁺). These hydrides are formed with alkali or alkali earth metals (ex. NaH, LiH; MgH_2) and are used as basic reagents in organic synthesis.

In neutral covalent hydrides the hydrogen is covalently bonded to a more electropositive element such as a *p*-block (boron, aluminium or beryllium). Hydrides that are soluble in organic solvents are widely used as reducing agents in organic synthesis, namely sodium borohydride ($NaBH_4$), lithium aluminium hydride ($LiAlH_4$) and diisobutylaluminium hydride (DIBAL)[5].

Transition metal hydride complexes play an important role in organometallic chemistry because they can easily undergo insertion reactions to give stable reaction intermediates with new M-C bonds, as described in the hydroformylation and hydrogenation sections. The complex *cis*-$FeH_2(CO)_2$ is the first example of transition metal hydride complex described by Walter Hieber´s Laboratory in Munich in 1931.

The metal hydride complexes can vary from acidic to hydric, depending on the nature of the metal center. This property depends on the charge, type of ligands and electronegativity of the metal. For example[6], $[VH(CO)_6]$ and $[CoH(CO)_4]$ are strong acids but $[HCo(CO)_3PPh_3]$ presents a pKa of 6.96. Metal hydride complexes can be terminal M-H, Scheme 4a, bridging two metal centers, Scheme 4b and more recently Kubas described the dihydrogen ligand (non-classical hydrides), Scheme 4c[7].

In non-classical ligands the H_2 can act as σ donor into an empty d_σ orbital on the metal and concomitantly the σ* orbital of H_2 accepts d_π electrons from d-orbitals of the metal, Scheme 4d.
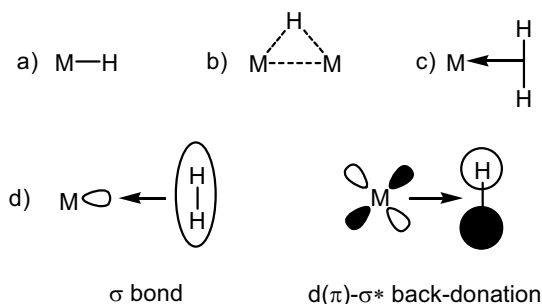
Scheme 4

1.2.4. Metal – CO bond

Carbon monoxide, CO, is a soft unsaturated ligand that is able to donate electrons via σ-bonding and is also able to accept d_π electrons by back-bonding from the filled d-orbitals of metal to the π* orbital of the CO, Scheme 5.

After metal binding, the CO molecule is polarized, with the carbon being more sensitive to nucleophilic attack and the oxygen more sensitive to electrophilic attack. The CO bond polarizibility and the bond strength are both clearly dependent on the other ligands of the organometallic complex. This aspect is discussed in more detail in Section 1.2.5.

σ bond   d(π)-π∗ back-donation
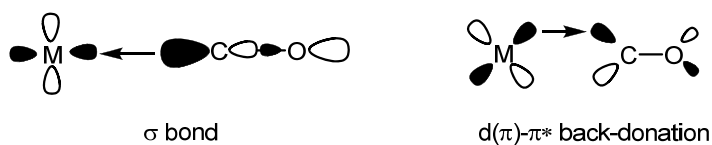
Scheme 5

1.2.5. Phosphine and phosphite ligand

Phosphines (PR₃) are a very important class of ligands since their electronic and steric properties can be modulated. The design and synthesis of the appropriate phosphine ligand allows the preparation of catalysts with high activity and selectivity for a large number of homogeneous catalysed reactions. Phosphines can act as Lewis bases because they have a lone pair on the phosphorous atom and also as π-acids, due to back-bonding of electrons from the d-orbitals of the metal to empty σ* orbital of a P-R bond, Scheme 6.

empty   fill   fill   empty

σ bond   d(π)-d(π) back-donation   d(π)-σ∗ back-donation
                (classical theory)   (modern theory)
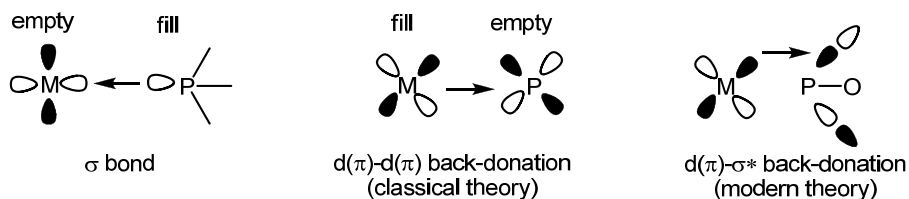
Scheme 6

The π-acidity is strongly dependent on R groups of the PR₃ ligand. The order of increasing π-acidity is:

$$P(alkyl)_3 < P(aryl)_3 < P(O\text{-}aryl)_3 < PCl_3 < CO < PF_3$$
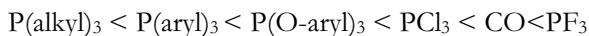
The σ-basicity and π-acidity of the phosphorous ligands was firstly obtained experimentally by Tolman[8] by measuring the stretching frequencies of the coordinated carbon monoxide ligands in complexes like $NiL(CO)_3$. Table 2 shows the values of the electronic parameter χ obtained from the differences of CO IR symmetric stretching frequencies for different PR_3 ligands. L= $P(^tBu)_3$ is used as reference with χ=0. The presence of strong σ-donors ligands, like $P(alkyl)_3$, increase the electron density on Ni with a concomitant increase of metal-CO back donation and a fall in υ (CO) infra-red frequency. Meanwhile, strong π-acceptor ligands like PF_3 or phosphites compete with CO for metal back-donation and so, the CO stretching frequencies and χ parameter increase. Tolman also quantified the steric effect of phosphorous ligands using the cone angle parameter. It is obtained using a space-filling model of the $M(PR_3)$ group. The metal is located at a distance of 2,28 Å from the phosphorous atom, and a cone that just contains all the atoms of the substituents on the phosphorous atom is constructed, Scheme 7. The cone angles θ obtained for selected phosphorous ligands using the Tolman approach are presented in Table 2.

TABLE 2 – Typical values of the Tolman electronic parameter χ and cone angle for different phosphorous ligands (PR_3).(Adapted from ref [7])

R	χ	θ
t-Bu	0	182
n-Bu	4	132
Phenyl	13	145
O-Phenyl	29	128
F	55	104
O-Bu^{t}C$_6$H$_4$O	29	194

It should be emphasized that these are empirical models and that the cone angle value is generally greater than the angles obtained directly by

crystallography. As is described in the next chapters, for catalytic purposes it is almost impossible to obtain an ideal separation of steric and electronic parameters to rationalize the effects of the structure of the ligand.

Tolman´s Cone Angle
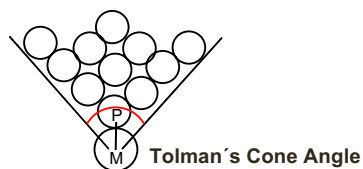
Scheme 7

1.3. FUNDAMENTAL REACTIONS OF TRANSITION METALS INVOLVED IN A CATALYTIC CYCLE

1.3.1. Substitution reactions

As described earlier, stable transition metal complexes have 16 or 18 valence-electrons, which mean that all their d-orbitals are filled. So, the first step of all homogeneous catalytic processes is the formation of a vacant site. To start the catalytic cycle it is necessary to substitute one ligand with a solvent molecule (weak bond) to make the coordination of the substrate possible. There are two possible mechanisms: dissociative, Scheme 8a, and associative, Scheme 8b, as in organic S_N1 and S_N2 substitution reactions, respectively.
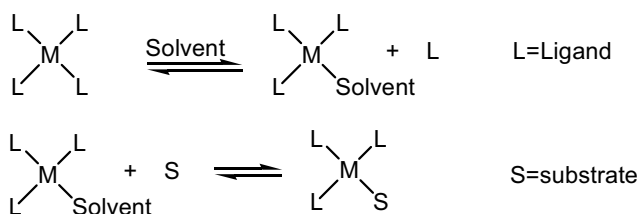
a) Dissociative mechanism, 1st step: leaving group departs; 2nd step: incoming group takes its place.
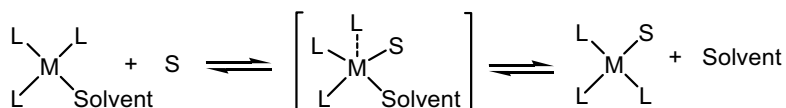
b) Associative mechanism, 1st step: incoming group attaches; 2nd step: leaving group departs.

Scheme 8

1.3.2. Oxidative addition and reductive elimination

In the oxidative addition of a substrate A-B into a metal complex the metal inserts between A and B with the cleavage of the A-B bond and the formation of two new bonds M-A and M-B, Scheme 9.
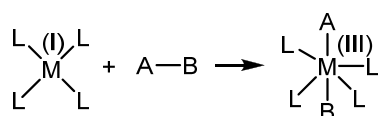
Scheme 9

In the oxidative addition reactions the A and B are reduced and the metal is oxidized by two units. The coordination oxidation number and the electron count are increased by two units.
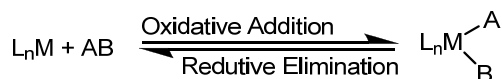
Example:
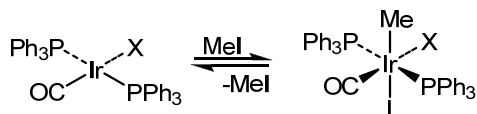
Scheme 10

The reverse reaction, reductive elimination, leads to the extrusion of an A-B molecule from the **A-L$_n$M-B** complex, Scheme 10. These two reactions often occur as elementary steps in homogeneous catalytic reactions.

1.3.3. Insertion and elimination reactions

Oxidative addition and reductive elimination reactions bring about changes in the metal oxidation state, while with insertion reactions only the ligands in the metal coordination sphere are transformed.

There are two main types of insertion reactions, 1,1-insertion and 1,2-insertion. In 1,1-insertion the **X** ligand and the metal are bound to the same atom, Scheme 11a), and in a 1,2-insertion reaction the **X** ligand and the metal are bound to adjacent atoms, Scheme 11b).
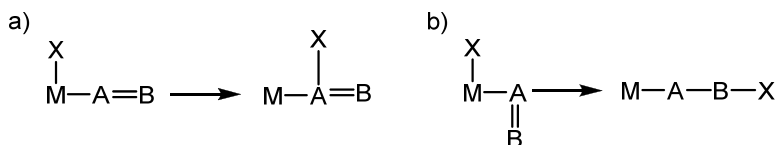
Scheme 11

The type of insertion strongly depends on ligand structure. A CO ligand only gives a 1,1-insertion, where the M and the X group are both attached to the carbon atom. This reaction involves the migration of the methyl group to a *cis* CO (migratory insertion reaction). But alkenes coordinated to metals can undergo M-H 1,2-insertion reactions, Scheme 12. These processes are very

important since they occur in several homogeneous catalytic systems, as shown in the next chapters.
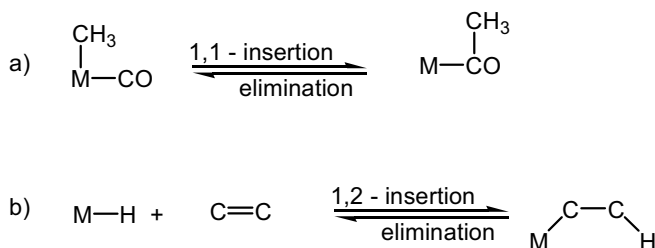
Scheme 12

The reverse reaction is called β-elimination. It involves the decomposition of transition metal σ-alkyl complexes by initial hydrogen transfer from ligand to metal with the concomitant creation of a metal vacant site, Scheme 13.
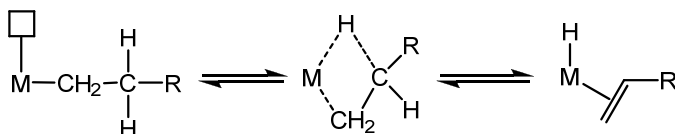
Scheme 13

β-elimination is prevented in complexes where the alkyl ligand has no β-hydrogens, e.g., -CH$_3$ and -CH$_2$CMe$_3$.

The catalytic hydroformylation reaction has been chosen to illustrate the above-mentioned selectivity and reactivity aspects of organometallic complexes in homogeneous catalysis. The industrial applications of hydroformylation reactions are discussed in more detail in Chapter B10.

1.4. SELECTIVITY IN HYDROFORMYLATION WITH RHODIUM MODIFIED CATALYSTS

The hydroformylation reaction was first discovered in Germany by Otto Roellen in 1935. It allows the direct synthesis of aldehydes, by *cis* addition of hydrogen and carbon monoxide to olefins, catalysed by transition metal complexes. It is one of the homogeneous catalytic processes that is quite widely used in industry, see Chapter B10, and it occurs with 100% atom economy, Scheme 14.
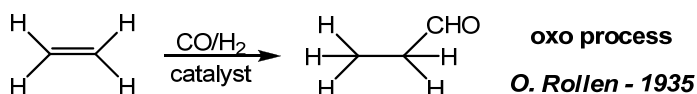
Scheme 14

Since aldehydes are very important raw materials, due to their easy transformation into other functional groups, hydroformylation becomes an important tool for synthetic proposes, Scheme 15.
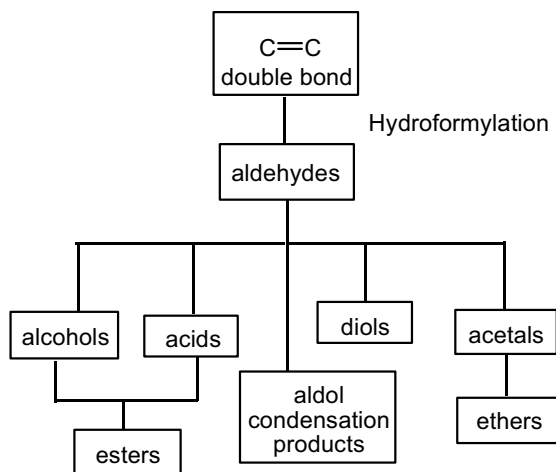
Scheme 15

1.4.1. Monodentate phosphorous ligands and selectivity

Despite its former industrial application, the use of the metal-catalyzed hydroformylation reaction has grown in organic synthesis only recently. This is mainly due to major difficulties in controlling the various aspects related to the activity and selectivity of this reaction. There are four aspects that may require optimization before hydroformylation can be used as a powerful tool for aldehyde synthesis: chemo-, regio-, enantio- and diastereoselectivity.

In the last decades considerable research work has been done to improve the activity and selectivity of this catalytic process with systematic studies of the metal and ligand effect[9].

It is generally accepted that rhodium aryl phosphorous complexes are the most active and chemoselective catalysts for hydroformylation reactions, Scheme 16.

$$[M]\text{- Catalyst precursor } + \text{ }[L]\text{- Modifying ligand}$$

$$CO \mid H_2$$

$$HM(CO)_xL_y$$
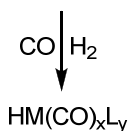
M = Rh >> Co > Ir, Ru > Os > Pt > Pd > Fe > Ni
L = PPh$_3$, P(OR)$_3$ > P(n-C$_4$H$_9$)$_3$ >> NPh$_3$ > AsPh$_3$, SbPh$_3$ > BiPh$_3$

Scheme 16[10]

The chemoselectivity of the catalytic process is the ratio of the total amount of aldehydes formed to the overall side products. The typical side reactions of the hydroformylation catalytic process are hydrogenation of the C=C double bond and/or the C=O double bond, and/or isomerisation reaction, Scheme 17b).
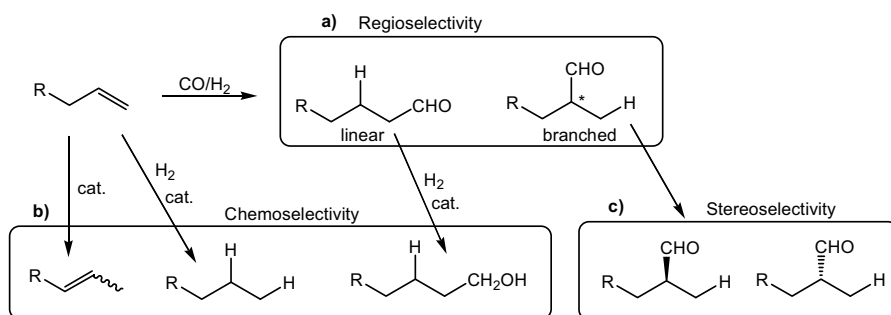
Scheme 17

The substitution of cobalt catalysts by rhodium-phosphorous modified catalysts almost solves the problem of chemoselectivity for unsubstituted olefins. A detailed discussion of these aspects and the influence of the substrate structure on the chemoselectivity can be read in recent reviews[10,11,12,13]. Control of the regioselectivity (ratio of one aldehyde to total amount of aldehydes) of the hydroformylation reaction catalysed by rhodium-phosphorous ligands, to form linear or branched aldehydes, is still one of the major problems remaining for academic and industrial researchers, Scheme 17a). Regioselectivity depends first and foremost on substrate structure, due to the different stability and reactivity of hydrometalation products, but it also depends on reaction parameters (pressure and temperature) and, strongly, on the electronic and steric parameters of the phosphorous ligand coordinated to the rhodium. Further discussion of all these aspects and reaction mechanism can be read in Chapter B3 and B10 and also in excellent reviews on the subject[10,11,13].

The stereoselectivity encompasses two aspects: diastereoselectivity and enantioselectivity. The diastereoselectivity is the preference for the formation of one diastereomer over the others, starting from a chiral substrate and using a non-chiral catalyst.

The diastereoselective hydroformylation of natural chiral produts like steroids[14] or terpenes[15] containing disubstituted or endocyclic double bonds was possible

277

after the synthesis of the bulky phosphite *tris(o-t-*butylphenyl)phosphite,[16] $P(O\text{-}o\text{-}^tBuC_6H_4)_3$. The large cone angle of this phosphite, combined with the weak σ-basicity and a strong π-acidity, prevents the coordination of a second ligand to the metal centre, favouring the CO dissociation and the coordination of the internal hindered double bonds with consequent increase of the reaction rate[17].

For example, in the hydroformylation of (*1R*)-(-)-myrtenyl acetate catalysed by $Rh/P(O\text{-}o\text{-}^tBuC_6H_4)_3$, a preferential coordination of the metal through the less hindered face of the substrate was observed, with 100% of diastereoselectivity[18] for the aldehyde *trans* to the isopropylidene bridge, Scheme 18.
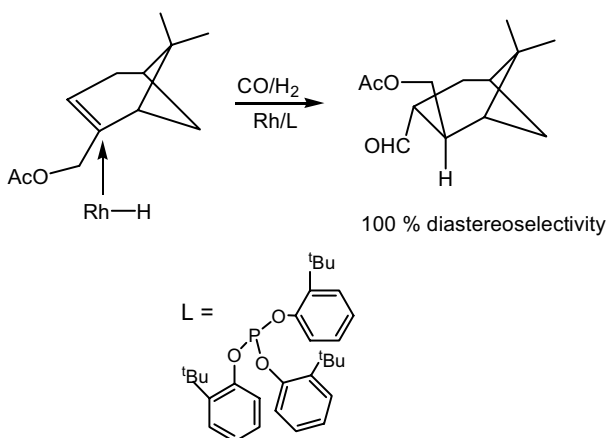
Scheme 18

1.4.2. Bidentate phosphorous ligands and selectivity

The introduction of diphosphines and diphosphites as ligands has been very important since they helped to significantly improve several aspects of reaction selectivities, especially regio- and stereoselectivity. It is now well established that the bite angle of the diphosphorous ligand is an important parameter to promote the design of the ligand so as to optimize the desired properties. The

general concept of natural bite angle (β_n) was first introduce by Casey[19], and is defined as the chelation angle (P-M-P bond angle) determined after optimization, using molecular mechanic calculations, of the diphosphine ligand backbone. There is accumulating evidence in the literature that ligands with bite angles around 90º (dppe) preferentially form axial-equatorial catalytic species, Scheme 19A and ligands with bite angles around 120º (xantphos) preferentially form *bis*-equatorial complexes, Scheme 19B[20].
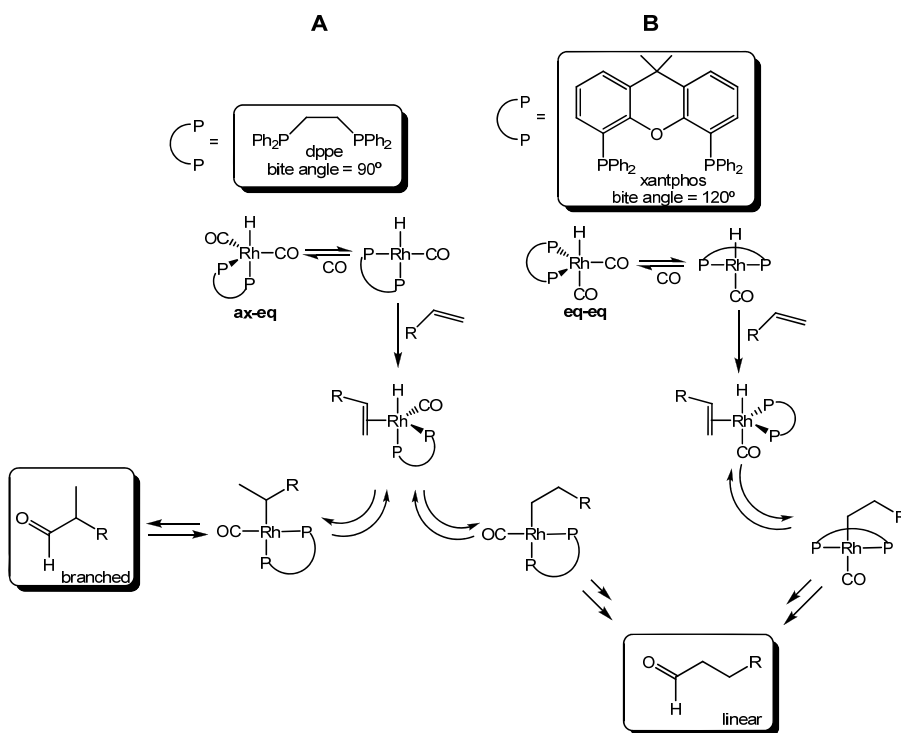
Scheme 19

The axial-equatorial active species is less hindered while the equatorial-equatorial complexes exhibit more steric hindrance around the metal. Therefore, the first catalytic system allows coordination by the primary or secondary olefin carbon atoms with concomitant formation of linear or

branched aldehyde (low regioselectivity) and the *bis*-equatorial species allow the preferential formation of the terminal σ-alkyl complex favouring the formation of the linear aldehyde (higher regioselectivity).

The introduction of bidentate phosphorous rhodium ligands not only helped to greatly improve the regioselectivity of the hydroformylation catalytic reaction, but was also responsible for the remarkable progress in the development of asymmetric catalysts. The breakthrough was the discovery of the phosphite/phosphine ligand, BINAPHOS, by Takaya and Nozaki,[21] which gave 98% regioselectivity for branched aldehyde and up to 94% ee, in the rhodium catalytic hydroformylation of styrene, Scheme 20.
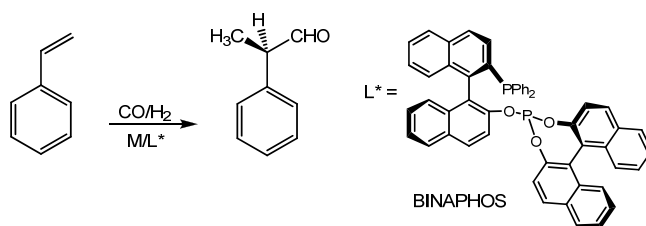
Scheme 20

It has been shown by *in situ* NMR that [RhH(CO)$_2$(*R,S*)-BINAPHOS] exists as a single species in which the phosphine moiety occupies an equatorial position and the phosphite an apical position that is *trans* to the hydride, Scheme 19.

A large number of chiral sugar diphosphite ligands have been synthesized, by Claver and Castillon[22], also representing landmark work, with ee of up to 90% in the hydroformylation of styrene, Scheme 21a). It is well documented that these ligands coordinate preferentially equatorial-equatorial and form an 8 member chelate.

M. R. Cobley[23] described the easy synthesis of rhodium bidentate diphospholanes, Scheme 21b), which form only 5 member chelate rings and

coordinate in equatorial-apical form, also give excellent enantioselectivities on styrene hydroformylation (up to 94%).
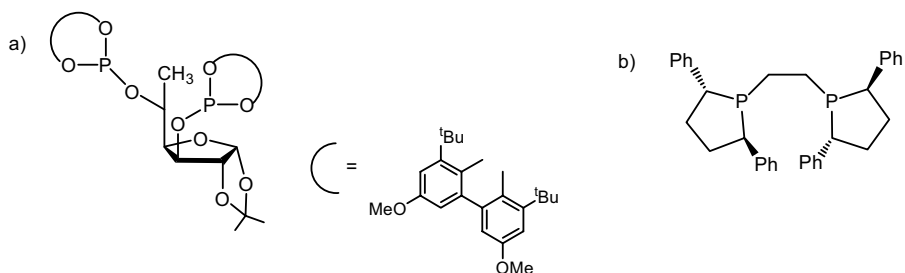
Scheme 21

From these studies it is possible to conclude that the crucial point for designing a ligand for asymmetric hydroformylation seems to be the exclusive formation of a single catalytic active species and neither the size of the chelate ring size, nor the chelating position

Even though hydroformylation has never been used in asymmetric industrial hydroformylation reactions, the easy synthesis of these new ligands and their stability will open new prospects for future applications in asymmetric chemical synthesis.

Acknowledgments

References

1. P.W.N.M. van Leeuwen, *Homogeneous Catalysis*, Kluwer Acad. Pub., **2004**.

2. R. H. Crabtree, *The Organometallic Chemistry of the Transition Metals*, 4th ed. Wiley, New York, **2005**.

3. M. Bochmann, *Organometallics 1. Complexes With Transition Metal-Carbon σ-Bonds*, Oxford, **1994**.

4. A. F. Hill, *Organotransition Metal Chemistry*, Royal Society of Chemistry, Bristol, **2002**.

5. K. Yvon, B. Bertheville, *J. Alloys and Compounds*, **2006**, *425*, 101.

6. D. Astruc, *Organometallic Chemistry and Catalysis*, Springer-Verlag Berlin, **2007**.

7. G. J. Kubas et al., *J. Am. Chem. Soc.*, **1984**, *106*, 451.

8. A. Tolman, *Chem Rev.*, **1977**, *77*, 313.

9. P.W.N.M. van Leeuwen, C. Claver, *Rhodium Catalyzed Hydroformylation*, Kluwer Acad. Pub., **2000**.

10. B. Breit, W. Seiche, *Synthesis*, **2001,** *1*, 1.

11. B. Cornils, W.A. Herrmann, *J. Catal.*, **2003**, *216*, 23.

12. B. Breit, *Topics in Current Chemistry*, **2007**, *279*, 139.

13. F. Ungváry, *Coord. Chem. Rev.*, **2007**, *251*, 2087.

14. R. Skoda-Földes, L. Kollár, *Chem. Rev.*, **2003**, *103*, 4095.

15. J. G. da Silva, H. J. V. Barros, A. Balante, A. Bolaños, M. L. Novoa, M. Reyes, R. Contreras, J. C. Bayón, E. V. Gusevskaya, E. N. dos Santos, *Appl. Catal. A*, **2007**, *326*, 219.

16. P. W. N. M. van Leeuwen, C. F. Roobeek, *J. Organomet. Chem.*, **1983**, *258*, 342.

17. P. C. J. Kamer, A. van Rooy, G. C. Schoemaker, P. W. N. M. van Leeuwen, *Coord. Chem. Rev.*, **2004**, *248*, 2409.

18. A. F. Peixoto, M. M. Pereira, A. M. S. Silva, C. M. Foca, J. C. Bayón, M J. S. M. Moreno, A. M. Beja, J. A. Paixão, M. R.. Silva, *J. Mol. Cat A: Chem.*, **2007**, *275*, 121.

19. C. P. Casey, G. T. Whiteker, M. G. Melville, L. M. Petrovich, J. A. Gavney, D. R. Powell, J. Am. Chem. Soc., **1992**, *114 (2)*, 5535.

20. a) P. C. J. Kamer, P. W. N. M. van Leeuwen, J. N. H. Reek, *Acc. Chem. Res.*, **2001**, 34, 895; Z. Freixa, P. W. N. M. van Leeuwen, *Dalton Trans.*, **2003**, 1890.

21. N. Sakai, S. Mano, K. Nozaki, H. Takaya, *J. Am. Chem. Soc.*, **1993**, *115*, 7033.

22. M. R. Axet, J. Benet-Buchholz, C. Claver, S. Castillón, *Adv. Synth. Catal.*, **2007**, *349*, 1983.

23. A. T. Axtell, C. J. Cobley, J. Klosin, G. T. Whiteker, A. Zanotti-Gerosa, K. A. Abboud, *Angew. Chem. Int. Ed.*, **2005**, *44*, 5834.

2. HOMOGENEOUS HYDROGENATION IN THE SYNTHESIS OF PHARMACEUTICALS

Maria José S. M. Moreno[a] and Rui M.D. Nunes[b]

[a] Centro de Estudos Farmacêuticos (CEF), Faculdade de Farmácia, Universidade de Coimbra, Rua do Norte, 3000-295 Coimbra, Portugal.
[b] Departamento de Química, Faculdade de Ciências e Tecnologia, Universidade de Coimbra, Rua Larga, 3004-535, Coimbra, Portugal.

2.1. INTRODUCTION

Nowadays, it is estimated that 90% of chemicals have come into contact with a catalyst at some stage in their manufacturing process. However, the number of fine and pharmaceutical processes currently using catalysts is still relatively small compared to major bulk chemical and refining processes as a whole.

In the manufacture of pharmaceuticals the ratio of finished product to raw material input is lower than for a commodity chemical, the synthetic processes are more elaborate due to their structural complexity, which means that more residual waste, including by-products and co-products, spent solvents and reactants as well as equipment cleaning residues are produced[1].

The present challenge for this sector is how to continue to meet healthcare needs by providing safe and efficacious products in an economically viable manner but without the adverse environmental side effects. These new and unmet requirements claim for strategies, concepts and issues related to sustainable development and environmentally friendly chemistry (green chemistry) are yet to be accomplished[2,3].

The use of catalysts, renewable feedstocks, alternative solvents / solventless reactions, process intensification, sustainable use of energy as well as innovative engineering is therefore essential. This pool of environmentally acceptable technology should be explored and incorporated into research and development (R&D) in order to attain prevention/reduction of environmental, health and safety impacts.

Catalysts not only can improve the selectivity of a reaction but they may also cut a multi-step synthetic sequence to a single step conversion, thereby reducing the energy requirement of the process and decreasing the waste produced. In industrial processes, heterogeneous catalysis is usually preferred as it facilitates recovery of the catalyst after reaction and allows a continuous operation mode. On the other hand, homogeneous catalytic systems generally allow faster reaction rates and higher chemo-, regio- and enantioselectivities[4]. As these are crucial goals in the synthesis of chiral pharmaceuticals and vitamins, the potential of homogeneous catalysis has also been used in their manufacture because it is compatible with the batch-type processes commonly used in the pharmaceutical industry.

As described in Chapter B1, homogeneous metal complexes containing chiral ligands are synthetically versatile catalysts that achieve very high enantioselectivity for a variety of catalytic reactions. The homogeneous hydrogenation of certain functionalized olefins is the best studied enantioselective catalytic reaction and it is also used in industrial production. In fact, the set of results reported so far in the literature makes homogeneous catalysis an attractive method for performing the chemo-, regio- and enantioselective hydrogenation of unsaturated groups when occurring in multifunctional molecules.

This chapter deals with homogeneous hydrogenation catalysts and mechanisms, the importance of the enantioselective homogeneous hydrogenation in the synthesis of bioactive compounds, and some applications of this reaction to the synthesis of intermediates and end-products, useful for the pharmaceutical industry. It is by no means a comprehensive text on the impressive evolution of the homogeneous catalytic hydrogenation of organic unsaturated compounds and so references to monographs[5], reviews[6], book chapters[7,8,9,10] and books[11,12,13] are given to help the reader to gain further familiarity with the subject.

2.2. HOMOGENEOUS HYDROGENATION CATALYSTS

Homogeneous hydrogenation is usually performed using a wide variety of soluble metal complexes as catalysts. These may be made from transition metals (rhodium, ruthenium, iridium, molybdenum) and appropriate ligands which are able to activate molecular hydrogen to add the two H atoms to an organic unsaturated substrate. It should be emphasised that in the absence of an adequate catalyst the hydrogenation, which is an exothermic reaction, is constrained by its high activation energy.

Wilkinson's catalyst, $Rh(PPh_3)_3Cl$, named after the Nobel Laureate who discovered the extreme importance of this compound in homogeneous catalysis[14], has been intensively studied since the 1960s. This catalyst is a square planar 16-electron complex that can be prepared from the reaction of rhodium trichloride with triphenylphosphine in ethanol, Scheme 1. It was the first catalyst to be routinely used to perform hydrogenations at room temperature and atmospheric pressure and is still the most widely used catalytic complex in synthetic chemistry.

$$RhCl_3(H_2O)_3 + CH_3CH_2OH + 3PPh_3 \longrightarrow RhCl(PPh_3)_3 + CH_3CHO + 2HCl + 3H_2O$$
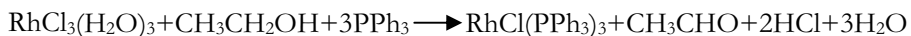
Scheme 1

The activity of homogeneous catalysts is strongly affected by the number of substituents at the C=C bond. Wilkinson´s catalyst allows the preferential hydrogenation of unsubstituted and terminal alkenes in the presence of internal alkenes[8]. The geometrical isomer *cis* reacts faster than the *trans* analog. Conjugated alkenes and dienes require higher pressures, and it is possible to hydrogenate the less substituted double bond of unsymmetrical allenes. Other easily reduced groups such as ciano, nitro, azo, and carbonyl remain unchanged. Catalyst performance is established as a function of the following criteria: enantioselectivity, chemoselectivity, productivity expressed as turnover number

or as substrate/catalyst ratio, and activity given as average turnover frequency, as previously described in Chapters A1 and B1. To be acceptable in the synthesis of pharmaceuticals a catalyst should at least exhibit an ee > 90%. For high value products, enantioselective hydrogenation TONs have to be >1000 or >50,000 for less expensive products, while TOFs should be >500 h^{-1} for small and >10,000 h^{-1} for large scale products[15,16].

The adequate design of a catalyst can provide significant improvement of its performance for a specific transformation. Experience has shown that varying the ligand structure may enable the tuning of the electronic and steric properties of catalytically active complexes to improve the outcome of catalytic reactions, especially in terms of their rates and selectivities. Exploitation of the ligand effects on the properties of metal complexes has, therefore, led to the successful development of a plethora of homogeneous catalysts that have useful catalytic activity in the production of a broad range of compounds[10].

For a chiral compound the biological activity of the two enantiomers can differ considerably, and so remarkable efforts have been made by the pharmaceutical industry to produce synthetic chiral pharmaceuticals and vitamins as enantiopure (ee >99%) or enantio-enriched compounds. For this purpose, the homogeneous complexes of Ru and Rh, with chiral phosphorous ligands (three-coordinated phosphorus ligands with P-C, P-O or P-N bonds), have proven to be among the most active and versatile catalysts providing good to excellent enantioselectivity in a range of different transformations[17,18]. In principle, both enantiomers of a product are accessible since both enantiomers of a chiral catalytic complex can be prepared. Actually, this is a remarkable difference from enzymatic catalysis, which can produce only one of the enantiomers.

binap Ar=Ph
tolbinap Ar=p-Tol

biphep

dipamp (R=o-anisyl)

Glup

josiphos

diop

bpm1 R=POPh$_2$
Ar=m-tolyl

bppfoh

duphos
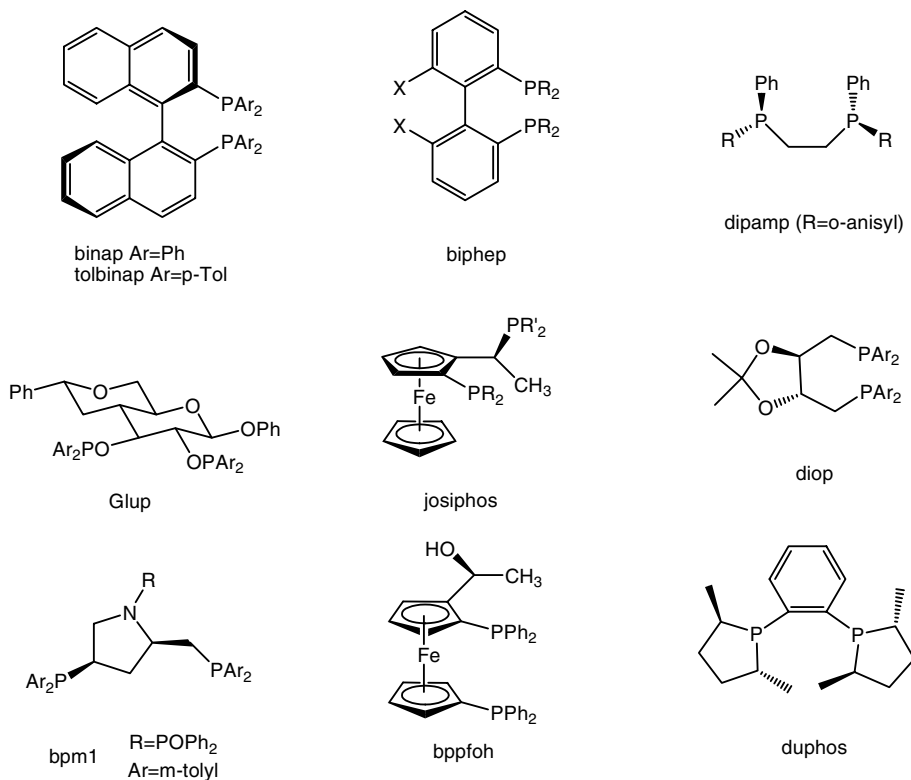
Scheme 2

A wide variety of chiral diphosphines which are able to induce enantiocontrol in catalytic reactions have been synthesised and are commercially available. Several bidentate ligands[18] are of particular interest, Scheme 2, in the enantioselective hydrogenation of unsaturated prochiral substrates for the synthesis of commercially relevant target molecules. These include dipamp, in which two chiral P atoms bear two sterically different substituents, 2,2´-bis(diphenylphosphino)-1,1´-binaphtyl (binap) and its axially chiral analogues containing two PAr$_2$ moieties attached to a chiral backbone, bis(phospholanyl)benzenes (duphos) with two chiral phosphacycloalkanes connected to an achiral scaffold, ferrocenyl-based diphosphines with planar

chirality (josiphos, bppfoh) and the sugar based diphosphonite (glup). The presence of an extra functional group, that can be varied and tuned to control the orientation of the reactant, confers inherent advantages to biphep and josiphos ligands[6,19].

Rh complexes containing the binap ligand exhibit high enantioselectivity in the catalytic hydrogenation of prochiral substrates containing C=C bonds; also vital for a successful result is the presence of polar substituents, e.g. acetamido group, which promotes an auxiliary complexation function, see section 2.3. Other electron-rich diphosphines, such as duphos, allow efficient enantioselective hydrogenations. Monophosphorous ligands have also been reconsidered since it was found that they may provide comparable or even higher optical yields than those produced by diphosphine chelates[20].

Homogeneous catalytic hydrogenation of carbonyl compounds is not so widespread. For this purpose Ru (II) complexes are more active than Rh (I) analogs. Excellent enantioselectivities, as well as good to very good activities, have been achieved using binap–Ru(II) catalysts and analogues for carrying out the industrial hydrogenation of aldehydes and ketones containing other polar groups, such as amino, hydroxyl, ester, amide and sulfate, which allow an additional interaction with the metal complex, ensuring high enantiomeric excesses[21].

The hydrogenation of multifunctional compounds has been and continues to be the subject of both academic and applied research, aiming at the design of highly active and selective catalysts. This is often mentioned as a decisive factor for the commercial success of a catalytic process. However, reaction parameters such as the substrate/catalyst ratio, additives/promoters, solvent, pH of the reaction mixture, temperature, and pressure as well as catalyst separation are also critical issues. Thus, in each case, these parameters have to be carefully optimised to reach the desired catalytic effect. For instance, the systematic variation of P-ligands on Rh catalysts prepared *in situ*, together with the

modulation of reaction parameters, e.g. solvent, substrate/catalyst ratio, temperature, and pressure, allows the hydrogenation of Δ^4-3-oxosteroids (cholestane, androstane and pregnane series) to the corresponding saturated ketones (5α-isomer), with the desirable chemo and stereoselectivity[22,23], Scheme 3.
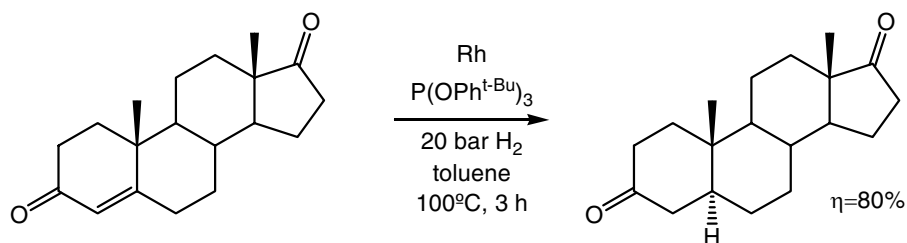
Scheme 3

It must be mentioned that, for this type of substrate, the thermodynamically more stable 5α-isomer is preferentially produced by the homogeneous catalytic systems, while the 5β-isomer is the main product under heterogeneous catalytic conditions. This reversal of stereoselectivity has deserved particular attention because it can be useful in the synthesis of steroid molecules such as hormones and vitamins.

2.3. MECHANISTIC CONSIDERATIONS

The detailed catalytic cycle for the hydrogenation of alkenes using Wilkinson´s complex, was first proposed by Halpern based on kinetic and ^{31}P NMR spectroscopic studies[24]. The author proposed two possible routes for the reaction mechanism: associative (oxidative addition of H_2 molecule to the 16 electron species [RhCl(PPh$_3$)$_3$]) and dissociative (oxidative addition of H_2 molecule to the 14 electron species [RhCl(PPh$_3$)$_2$]). However, the RhCl(PPh$_3$)$_2$ reacts with H_2 at least 10000-fold faster than the RhCl(PPh$_3$)$_3$, and is therefore

the active intermediate. In this dissociative pathway the initial dissociation of one triphenylphosphine ligand from the catalyst occurs, being replaced by a solvent molecule, giving a 14-electron complex, Scheme 4. Subsequent oxidative addition of H_2 to the metal takes place. In this step, the H-H bond undergoes either homolytic cleavage, forming a metal dihydride, or a heterolytic cleavage, producing one M-H bond and a proton, Scheme 5a.
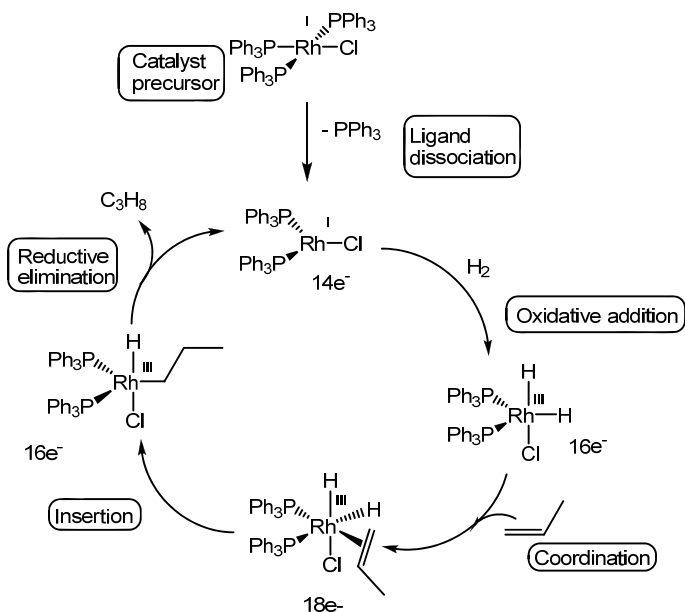
Scheme 4

A second function of the metal is the formation of complexes with the unsaturation C=X, most probably via a π-bond, thereby activating the second reactant, Scheme 5b, and placing it close to the M-H fragments. For the olefins, this coordination affords the 18-electron octahedral dihydride alkene complex. The intramolecular transfer of hydride to produce the [Rh(alkyl)Cl(PPh$_3$)$_2$] intermediate is the rate determining step for the whole process. Reductive elimination of the alkane product from this alkyl hydride intermediate occurs rapidly, completing the cycle, Scheme 4. Studies with deuterium have shown

that the *cis*-addition to the double bond is preferred and very little isomerization or hydrogen exchange occurs. Besides the changes mentioned in the electronic environment (14-, 16-, and 18-electron species), the proposed cycle involves changes in the oxidation state (I and III) and coordination numbers (from 3 to 6).

Activation of hydrogen   Activation of unsaturated bond
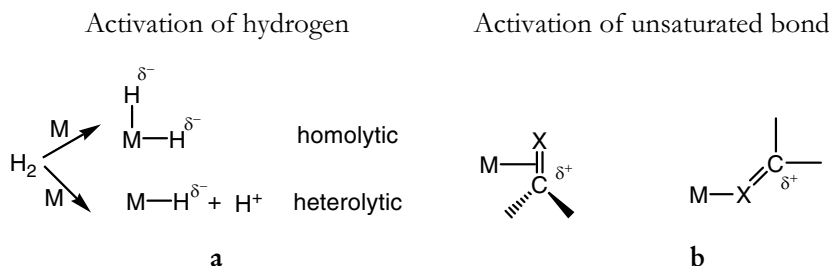
Scheme 5

The mechanism of rhodium-catalyzed asymmetric hydrogenation focused on prochiral enamides, as hydrogenation substrates, and rhodium chiral diphophines complexes as catalyst precursors, has been thoroughly studied. Halpern and Brown[24,25] showed that under catalytic conditions the molecule of the prochiral alkene coordinates to the rhodium atom originating two diastereomeric catalyst-substrate complexes, Scheme 6. Thus, in this case, hydrogen reacts with the preformed Rh-substrate complex and not via the dihydride route, as with the Wilkinson complex. There may be a preferential pathway in this oxidative addition of H_2. Indeed, the less stable complex can react faster with hydrogen than the major adduct, i.e., it is the relative reactivity of the diastereomers that regulates the stereochemistry of the hydrogenation, leading to the opposite result from that expected from the relative concentrations of the two Rh-substrate complexes.
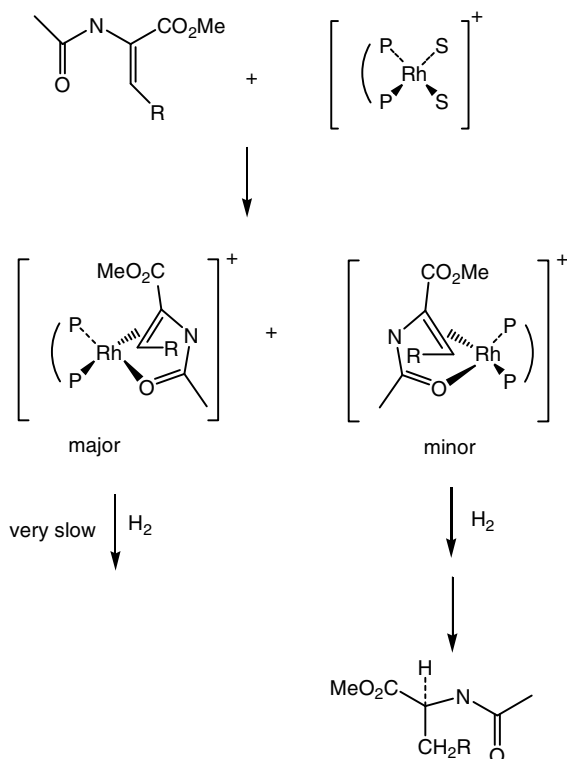
Scheme 6

2.4.   ENANTIOSELECTIVE   CATALYTIC   HYDROGENATION: INDUSTRIAL APPLICATIONS FOR PHARMACEUTICALS

Molecular chirality is of the utmost importance since it affects the biological activity and function of compounds. In fact the two enantiomers of a given bioactive compound such as a pharmaceutical or an agrochemical can cause different biological effects. Therefore, such isomers, named as eutomer (highest activity) and distomer (lower, no or undesirable activity), are regarded as distinct species. As regulation has evolved, over the last two decades, to the stage where it now demands the evaluation of both enantiomers before approval, this has driven the pharmaceutical industry to systematically produce synthetic chiral pharmaceuticals and vitamins as enantiomerically pure

compounds[1]. A major approach involves enantioselective catalysis, where prochiral starting materials are transformed into enantiopure molecules by using chiral catalysts[15-19]. This methodology can play an important role in the development of pharmaceuticals because it offers one of the most efficient, low-waste methods for producing enantiomerically pure compounds, thus promoting green sustainable chemistry.

TABLE 1 - Production Processes for C=C and C=O Catalytic Hydrogenation[18]

Substrate	Reaction Conditions	Product	ee (%)	TON	TOF h[-1]
MeO, COOH, AcO, NHAc	Rh/dipamp, 25°C, 10 bar	MeO, COOH, AcO, NHAc — Monsanto: intermediate in the synthesis of L-dopa (Parkinson)	95	2×10^4	1000
OH	Ru(OOCCF$_3$)$_2$ / binap 20°C, 100 bar	OH — Takasago: citronellol and intermediate for vitamin E	97	5×10^4	500
O, OH	Ru$_2$Cl$_4$Et$_3$N/ tolbinap 50°C, 25 bar	OH, OH — Takasago: intermediate for (S)-oxfloxazin (bactericide)	94	2×10^3	300
O, NHCOPh, COOMe	RuI$_2$cymee/ tolbinap	OH, NHCOPh, COOMe — Takasago: intermediate for carbapenem (antibiotic)	97	1×10^3	200
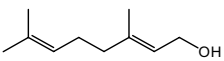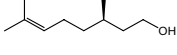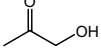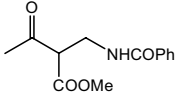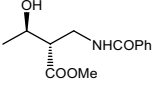
The first industrially interesting application was the asymmetric hydrogenation of cinnamic acid derivatives (prochiral enamides) with a cationic rhodium complex, having the chiral diphosphine, DIPAMP as ligand, Scheme 2, thus producing L-Dopa, a chiral drug used for the symptomatic treatment of

Parkinson´s disease, Table 1. Since then, most academic and industrial research has been focused on catalytic hydrogenation.

TABLE 2 - Pilot Processes for C=C and C=O Catalytic Hydrogenation[18]

Substrate	Reaction Conditions	Product	ee (%)	TON	TOF h⁻¹
	Ru(OAc)₂/ biphep1 60⁰C, 7 bar	Roche: intermediate for cilazapril (HIV protease inhibitor)	>99	2×10^4	830
	Ru(OAc)₂/ biphep2 30⁰C, 270 bar	Roche: intermediate for mibefradil (calcium antagonist)	94	1×10^3	400
	Ru/ biphep2 50⁰C, 9 bar	Chirotech (for Pfizer): intermediate for candoxatril (anti-hypertensive)	99	1×10^3	300
	Rh(OOCF₃)/ bpm 1 40⁰C, 40 bar	Roche: intermediate for pantothenic acid (vitamin)	91	2×10^5	1.5×10^4
	RhCl/ bppfoh 50⁰C, 80 bar	Ciba-Geigy (Solvias): levoprotiline (anti-depressant)	97	2×10^3	125
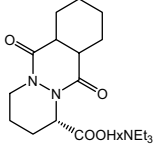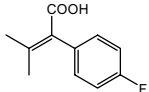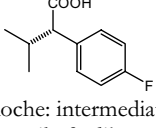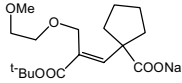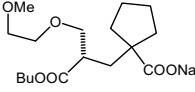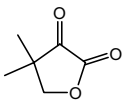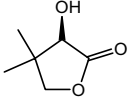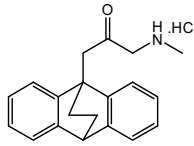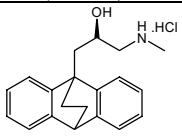
The technological potential, broad scope and scientific excellence of this methodology received recognition in the 2001 Nobel Prize, awarded to W. S. Knowles and R. Noyori for their work in this field.

Though enantioselective catalysis has made great strides, and its importance has been widely recognized, still relatively few enantioselective catalytic reactions are actually in use on an industrial scale. Some representative processes for the production of intermediates for the synthesis of pharmaceuticals through the enantioselective catalytic hydrogenation of C=C and C=O bonds are included in Table 1[18].

The information available in the literature for these unsaturated substrates contains some other efficient and competitive homogeneous hydrogenations, which are at a pilot stage. They operate in multi-10kg scales, Table 2, showing high feasibility for further commercial production[18].

In the industrial applications reported here, the ruthenium and rhodium metal complex catalysts have found a widespread application and the predominant ligands are chiral bidentate phosphines. In every case the unsaturated bonds to be hydrogenated (C=C or C=O) carry additional O or N functions which are also able to coordinate to the catalyst, improving the reaction enantiocontrol.

Other processes still on the bench stage of industrial development have also been shown to be suitable for the manufacture of pharmaceuticals[15,18].

2.5. CONCLUDING REMARKS

Homogeneous catalysis is an efficient, low-waste method to perform the chemo, regio and enantioselective hydrogenation of C=C or C=O groups present in multifunctional molecules. The results reported make this process especially valuable in the production of pharmaceuticals.

Awareness of the potential of enantioselective catalysis has been increasing significantly, along with growing know-how and experience in catalytic process development. Therefore, it can be expected that applications of existing and

new catalysts are likely to expand the industrial impact of this transformation in the near future.

Pharmaceutical industries need selective, recoverable and reusable catalysts. These challenges are leading much current research into how to combine the best characteristics of homogeneous and heterogeneous catalysts to achieve more sustainable catalytic hydrogenations. In this context, the utilization of unconventional media such as water (biphasic), ionic or supercritical liquids can play an important part in improving environmental performance.

Acknowledgments

References

1.   J. Messelbeck, l. Shuterland, *Environmental Health Perspectives*, **2000**, *108*, pp. 997.

2 . M. Lancaster, *Green Chemistry - An Introductory Text*, Royal Society of Chemistry, Cambridge, **2002**.

3.   P.T. Anastas, M.M. Kirchhoff, T.C. Williamson, *App. Catal. A*, **2001**, *221*, pp. 3.

4.   R..A. Sheldon, I. Arends, U. Hanefeld, *Green Chemistry and Catalysis*, Wiley-VCH Verlag GmbH & Co. KgaA Ed., Weinheim, **2007**.

5.   P.W.N.M. van Leeuwen, G. van Koten, *Catalysis: An Integrated Approach,* 2nd. Ed., Elsevier Science Pub, Amsterdam, **1999**, *123*, 289.

6.   R. Sánchez-Delgado, M. Rosales, *Coord. Chem. Rev.,* **2000**, *196*, 249.

7.   L.A. Oro in I.V. Horváth, E. Iglesia, M.T. Klein, J.A. Lercher, A.J. Russel, E.I. Stiefel (Eds), *Encyclopedia of Catalysis*, John Wiley & Sons, **2003**, Vol. 4, pp. 55.

8.   J.C. Bayon in L.A. Oro, E. Sola (Eds), *Fundamentos y Aplicaciones de la Catálisis Homogénea*, Zaragoza, **2000**, Chapter 8, pp. 113.

9.   P.W.N.M. van Leeuwen, in *Encyclopedia of Physical Science and Technology*, 3rd Ed, Academic Press, **2002**, Vol. 2, pp.457-489.

10.   P.W.N.M. van Leeuwen, in *Hydrogenation - The Success Story of Asymmetric Catalysis in Homogeneous Catalysis-Understanding the Art*, Kluwer Academic Publishers Eds., Dordrecht, **2004**, Chapter 4, pp.75-100.

11.   J.G. de Vries, C.J. Elsevier (Eds.), *The Handbook of Homogeneous Hydrogenation*, Wiley-VCH Verlag GmbH & Co. KgaA Ed., Weinheim, **2007**.

12.   P.A Chaloner., M.A. Esteruelas, F. Joó, L.A. Oro, *Homogeneous Hydrogenation*, Kluwer Academic, Dordrecht, **1994**.

13.   R.S. Dickson, *Homogeneous Catalysis with Compounds of Rhodium and Iridium*, D. Reidel Publishing Company, **1985**.

14.   J.A. Osborn, F.H. Jardine, J.F. Young, G. Wilkinson, *J. Chem. Soc. A*, **1966**, 1711.

15.   H.-U. Blaser, B. Pugin, F. Spindler, *J. Mol. Cat. A: Chem.*, **2005**, *231*, 1.

16.   H.-U Blaser, *Chem Comm.*, **2003**, 293.

17.   H.-U Blaser, C. Malan, B. Pugin, F. Spindler, H. Steiner, M. Studer, *Adv. Synth. Catal.*, **2003**, *345*, 103.

18.   H.-U. Blaser, F. Spindler, M. Studer, *Appl. Catal. A*, **2001**, *221*, 119.

19.   W. Tang, X. Zhang, *Chem. Rev.*, **2003**, *103*, 3029.

20.   A. M. Kluwer, C. J. Elsevier, in ref 11, Chapter 14, pp.375.

21.   M. L. Clarke, G. J. Roff, in ref 11, Chapter 15, pp.413.

22.   R.M.D. Nunes, A.F. Peixoto, A.R. Axet, M.M. Pereira, M.J. Moreno, L. Kollar, C. Claver, S. Castillon, *J. Mol. Cat. A: Chem.*, **2006**, *247*, 275.

23.   L. Kollár, S. Tôrös, B. Heil, Z. Tuba, *J. Mol. Cat.*, **1988**, *47*, 33.

24.   J. Halpern, *Pure Appl.Chem.*, **2001**, *73*, 209 and references cited.

25.   J.M. Brown, P.A. Chaloner, *J. Am. Chem. Soc.,* **1980**, *102*, 3040.

3. KINETICS OF HOMOGENEOUS CATALYTIC PROCESSES

Luis G. Arnaut

Departamento de Química, Faculdade de Ciências e Tecnologia, Universidade de Coimbra, Rua Larga, 3004-535, Coimbra, Portugal.

3.1. INTRODUCTION – APPLIED CATALYSIS: KEY TO SUSTAINABILITY

The rate of conversion for the general form of a chemical reaction,

$$\alpha\ A + \beta\ B + ... \rightarrow \chi\ X + \psi\ Y + ... \tag{I}$$

where α, β, χ, ψ are the stoichiometric coefficients of the species involved, can be defined with respect to any reactant or product provided that the stoichiometry of the reaction is taken into consideration. In solution, the reaction rate takes the form

$$v = -\frac{1}{\alpha V}\left(\frac{dn_A}{dt}\right) = -\frac{1}{\beta V}\left(\frac{dn_B}{dt}\right) = \frac{1}{\chi V}\left(\frac{dn_X}{dt}\right) = \frac{1}{\psi V}\left(\frac{dn_Y}{dt}\right)$$

$$= -\frac{1}{\alpha}\left(\frac{d[A]}{dt}\right) = -\frac{1}{\beta}\left(\frac{d[B]}{dt}\right) = \frac{1}{\chi}\left(\frac{d[X]}{dt}\right) = \frac{1}{\psi}\left(\frac{d[Y]}{dt}\right) \tag{1}$$

The velocities of elementary chemical reactions depend on a great number of factors, in particular the nature of the reactants, concentrations or pressures, temperature, light, catalysts and the solvent used. However, it is the nature of the reactants and the presence, or not, of a catalyst, that play the most fascinating role in generating the great diversity of reaction rates experimentally observed.

Almost all reaction rates depend on the concentration of reagents, while for reversible reactions they also are affected by those of products. The mathematical expression which relates the reaction velocity and the concentration of species present is called the law of reaction velocity, the

kinetic law, or most simply the rate law. Assuming that the reaction being considered involves an elementary process,

a A + b B $\rightarrow$ x X + y Y   (II)

 the corresponding rate law can be written

$$v = k[A]^a[B]^b$$ (2)

where the powers a and b are known as the partial orders of reaction for components A and B, and the proportionality constant k is called the specific rate constant for the reaction, or simply the rate constant. This constant is independent of the concentrations of the reagents, but depends on the temperature, pressure and reaction medium. The partial orders can only be identified with the stoichiometric coefficients when we are dealing with an elementary reaction.

Equation I represents a general chemical reaction with a global stoichiometry, whereas reaction II refer to an elementary reaction where a molecules of A collide with b molecules of B. The probability of such a collision is negligible when a+b>2. However, a rate law may have a sum of partial orders (molecularity) larger than 2, or even be a non-integer or a negative number. When such cases occur, we are necessarily in the presence of a sequence of elementary reactions, and the global reaction is the sum of that sequence. The sequence of elementary reactions is named reaction mechanism. The rate law depends on the reaction mechanism and is usually obtained by experimental methods. The reaction mechanism must agree with the global (stoichiometric) reaction and with the rate law. Occasionally, a mechanism may invoke the participation of intermediates that have not been observed, but that are required by indirect evidence to justify, for example, the selectivity experimentally observed. The molecularity each elementary step included in the reaction mechanism is usually 1 or 2. These rules do not unequivocally lead to one single mechanism. A given mechanism may be conform to all the experimental evidence available at a certain time, and later be shown to be

inconsistent with the presence of an intermediate detected by new analytical methods, or be modified by the observation of a parallel reaction[1].

A rate law may involve a species that is neither a reactant nor a product. When the partial order of that species is positive, it accelerates the reaction, but when it is negative, it acts as an inhibitor, because its presence reduces the reaction rate. Catalysts are substances which, although they are not included in the overall stoichiometric equation of a process, appear in the rate law with a partial order greater than zero. Occasionally, a reaction can undergo autocatalysis when, under the conditions described, a product of the reaction participates in the rate law of this process. Although caution needs to be used with such a definition, from the above a catalyst may increase the rate of a reaction without being consumed during it. The note of caution comes from the fact that in some processes, e.g. Friedel-Crafts alkylations and acylations of aromatic compounds using Lewis acid catalysts, the catalysts are used up in other steps of the process. Normally a good catalyst can lead to enormous enhancements in reactions rates even when only present in very small quantities. In any case, the catalyst always has a partial order in the rate law that largely exceed its stoichiometric coefficient in the overall stoichiometric equation.

Catalysts do not alter the position of equilibrium in a reaction. Their effect, instead, arises from the fact that in their presence a pathway with a lower activation energy becomes available to the reactants, as can be seen in Figure 1. The uncatalysed route still exists, but this new mechanism becomes kinetically more favourable. As a consequence, in the presence of a catalyst, the form of the rate equation will be changed with the addition of a new term, which becomes more important than the uncatalysed reaction. Returning to the general reaction mechanism 1 and rate law 2, the new rate law including the effect of catalysts will take the general form

$$v = k \, [A]^a \, [B]^b + \, k_{cat} \, [A]^{a'} \, [B]^{b'} [C]^{c'} \tag{3}$$

where C represents the catalyst. When the catalyst is a solid, such as the case of heterogeneous catalysis, its concentration is constant and does not appear as an independent term in this equation. Its effect will be included in the value of k_{cat}. As a general rule, to see the effects of catalysis, if the reaction order is unchanged it is necessary that $k_{cat}[C]^c > 0.1 \, k$.
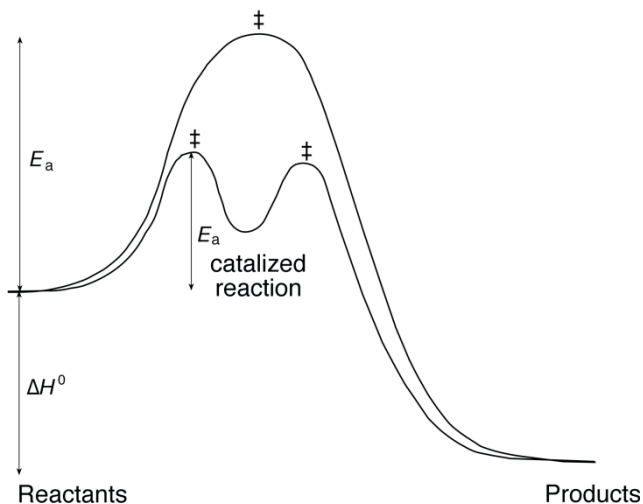
Figure 1 - Potential energy profiles of catalysed and uncatalysed reaction paths. The transition states are represented by ‡.

It is useful to distinguish between homogeneous catalysis, where reactants, products and catalyst are all in the same phase, and heterogeneous catalyst, where the catalyst is present in a different phase from the reactants and products. As an example we can consider the hydrogenation of carbon-carbon double bonds to transform them into single bonds. This can be carried out homogeneously using the Wilkinson catalyst, which is a complex of the transition metal rhodium, or heterogeneously, using particularly metallic platinum. This hydrogenation is very important in both the pharmaceutical and food industries, as it leads to the efficient production of saturated products

from unsaturated compounds. Partly for his work in developing such homogeneous catalysts through the study of transition metal complexes, Wilkinson received the Nobel prize in chemistry. The most obvious advantage of homogeneous catalysis is that it offers a good contact between the catalyst and the reactants, which means that the effective concentration of the catalyst is higher than in heterogeneous catalysis. This gain should be translated into more selective and mild reaction conditions. On the other hand, the disadvantage of homogenous catalysis is that the final product and the catalysts are usually in the same phase and they must be separated at the end of the reaction. In the separation processes, the catalyst may be lost.

Homogeneous catalysis is a success story of organometallic chemistry. Ever since hydroformylation was found in 1938 that catalytic processes opened the way for organometallic chemistry in the chemical industry. Today, homogeneous catalysis plays a relevant role in various industrial processes, namely, in the hydroformylation of propene and other olefins in butanol and biodegradable detergents, and in the hydrogenation of unsaturated vegetal fats into margarine. In this chapter we discuss in detail the kinetics of hydroformylation and hydrogenation reactions.

3.2. KINETICS OF HYDROFORMYLATION

In 1938, Otto Roelen found that reacting ethylene with CO and H_2 at high pressures and temperatures in the presence of metal oxides, leads to the formation of propionic aldehyde

$$HCR=CH_2 + CO + H_2 \xrightarrow[\text{oxide}]{\text{metal}} \begin{array}{l} RCH_2CH_2CHO \\[2ex] RCHCH_2 \\ \quad| \\ \;CHO \end{array} \qquad \text{(III)}$$
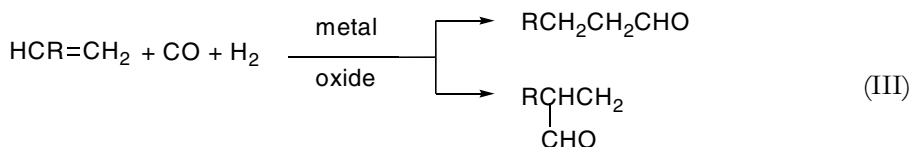
Heck and Breslow[2,3] carried out a detailed mechanistic study of this reaction. These authors obtained spectroscopic evidence that the reaction involved, in a

first step, the addition of the cobalt hydrotetracarbonyl to olefins. Later they demonstrated the reversibility of this step by synthesizing ethylcobalt tetracarbonyl by another method and verifying that at high temperatures they could obtain ethylene. Furthermore, they observed that when the reaction was made under a one atmosphere pressure of CO, it was inhibited with respect to the same reaction under a nitrogen atmosphere, and presumed that ethylcobalt tetracarbonyl probably lost a carbon monoxide molecule to give a tricarbonyl, which forms a π-complex with the olefin. Thus, they deduced that the addition to olefins should involve cobalt hydrotricarbonyl rather than cobalt tetracarbonyl. Next, they assumed that the π-complex should rearrange to an alkylcobalt tricarbonyl, which should react with CO and give an alkylcobalt tetracarbonyl. The alkylcobalt tetracarbonyl and the acylcobalt tricarbonyl are in equilibrium and the reduction of the latter gives the final product. The formation of the π-complex intermediate is also in agreement with the isomerization of olefins by cobalt hydrotetracarbonyl. Based on these observations, Heck and Breslow proposed the mechanism illustrated in Figure 2. This illustration emphasises the fact that the global transformation of ethylene, CO and H_2 in propionaldehyde occurs without consumption or formation of cobalt complexes. Alternatively, the most important steps of this mechanism can be written in terms of a series of chemical equilibria that close with and irreversible step.

$$HCo(CO)_4 \underset{k_{-1}}{\overset{k_1}{\rightleftarrows}} HCo(CO)_3 + CO$$

$$RCH = CH_2 + HCo(CO)_3 \underset{k_{-2}}{\overset{k_2}{\rightleftarrows}} RCH_2CH_2Co(CO)_3$$

$$RCH_2CH_2Co(CO)_3 + CO \underset{k_{-3}}{\overset{k_3}{\rightleftarrows}} RCH_2CH_2COCo(CO)_3 \qquad \text{(IV)}$$

$$RCH_2CH_2COCo(CO)_3 + H_2 \overset{k_4}{\longrightarrow} RCH_2CH_2CHO + HCo(CO)_3$$

$$HCo(CO)_3 + CO \underset{k_1}{\overset{k_{-1}}{\rightleftarrows}} HCo(CO)_4$$
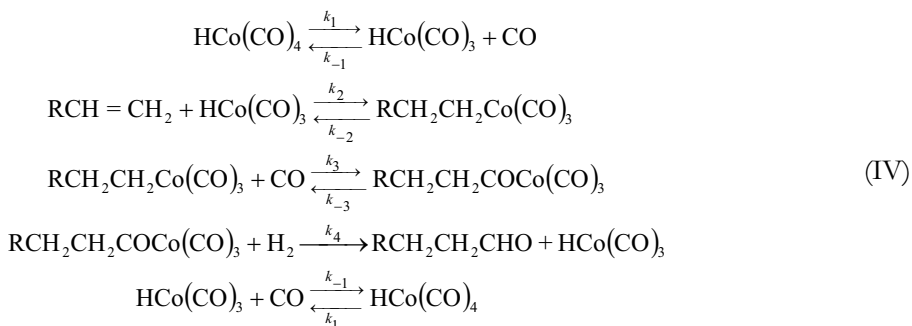
This formulation makes obvious the fact that the overall reaction, which is the sum of all the elementary steps, is identical to reaction III. It should be noted that this mechanism was proposed without information on the rate law. The rate law for hydroformylation can be written in terms of the rate of formation of the aldehyde

$$v = \frac{d[RCH_2CH_2CHO]}{dt} = k_4[H_2][RCH_2CH_2COCo(CO)_3] \tag{4}$$

but this expression is not satisfactory because it involves the concentration of an intermediate species, which is not known. The rate laws must always be expressed exclusively in terms of reactants, products or other species with easy to determine concentrations. The previous rate law only becomes useful when the intermediate concentration is expressed in terms of reactants, products and, if necessary, catalysts. In the case of a mechanism where a series of reversible equilibria are established before the irreversible step, such as mechanism IV, the mechanism can be simplified assuming that the irreversible step is the slowest step, which becomes the *rate-determining step* of the reaction. This view assumes that the previous equilibria are attained rapidly compared with the rate of the irreversible step. According to the *pre-equilibrium approximation*, the concentrations of the intermediates can be obtained from the equilibria where they are involved

$$K_1 = \frac{[HCo(CO)_3][CO]}{[HCo(CO)_4]}$$
$$K_2 = \frac{[RCH_2CH_2Co(CO)_3]}{[RCH=CH_2][HCo(CO)_3]} \tag{5}$$
$$K_3 = \frac{[RCH_2CH_2COCo(CO)_3]}{[CO][RCH_2CH_2Co(CO)_3]}$$
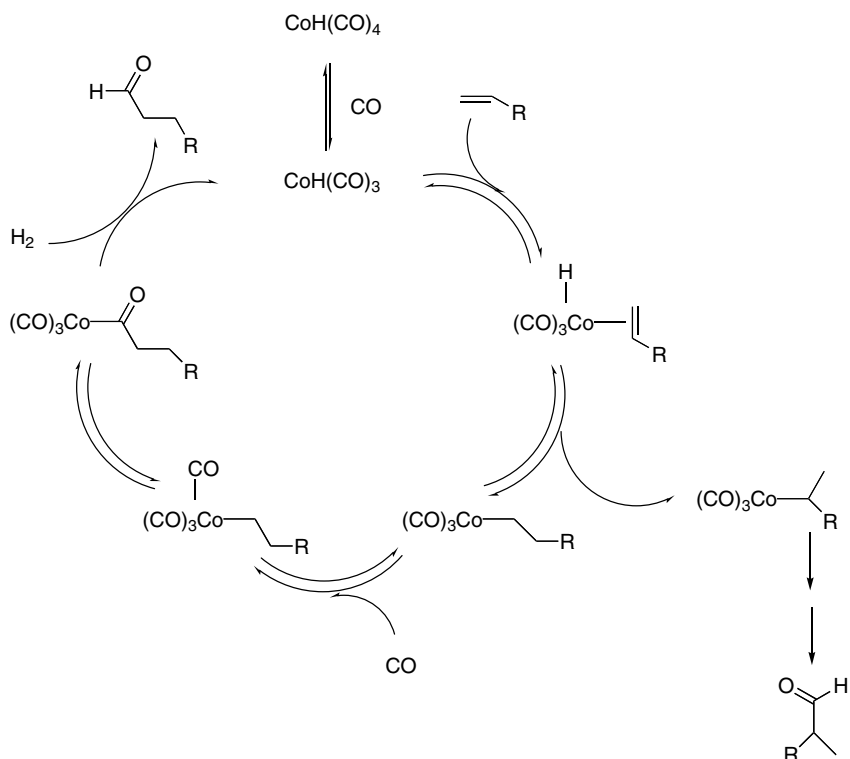
Figure 2 - Hydroformylation catalyzed by cobalt, according to the Heck-Breslow mechanism.

and the equation for the rate law becomes

$$v = K_1 K_2 K_3 k_4 [H_2][RCH = CH_2][CO]^2 [HCo(CO)_4] \tag{6}$$

The expression above implies that an increase in the concentration of CO leads to an increase in the rate of the reaction. This is in conflict with the observation mentioned before that, in the experimental conditions most currently employed, CO is an inhibitor of this reaction, that is, the rate constant decreases when the pressure of CO increases. This observation can only be accommodated changing the assumptions made before on the establishment of fast pre-equilibria. Instead, it is possible to use the *steady-state approximation*.

According to the steady-state approximation, if the concentration of an intermediate does not change significantly with the time, such as the concentration of the π-complex, it is possible to write

$$v = \frac{d[RCH_2CH_2Co(CO)_3]}{dt} = k_2 \big[RCH=CH_2\big][HCo(CO)_3] + k_{-3}\big[RCH_2CH_2COCo(CO)_3\big] - (k_{-2}+k_3[CO])\big[RCH_2CH_2Co(CO)_3\big] \approx 0 \tag{7}$$

that is

$$\big[RCH_2CH_2Co(CO)_3\big] = \frac{k_2[RCH=CH_2][HCo(CO)_3]+k_{-3}[RCH_2CH_2COCo(CO)_3]}{k_{-2}+k_3[CO]} \tag{8}$$

Using the expression above for the concentration of the π-complex together with the pre-equilibrium approximation for the concentration of the alkylcobalt tricarbonyl

$$\big[RCH_2CH_2COCo(CO)_3\big] = K_3[CO][RCH_2CH_2Co(CO)_3] \tag{9}$$

we obtain

$$v = k_4[H_2]K_3[CO]\frac{k_2[RCH=CH_2][HCo(CO)_3]+k_{-3}[RCH_2CH_2COCo(CO)_3]}{k_{-2}+k_3[CO]} \tag{10}$$

This expression can be simplified considering that the most current experimental conditions employ high pressures (100-300 atmospheres of 1:1 CO-H_2) and high concentrations of olefin, hence $k_3[CO]>>k_{-2}$ and $k_2[RCH=CH_2][HCo(CO)_3]>>k_{-3}[RCH_2CH_2COCo(CO)_3]$. If such cases, the expression above reduces to

$$v = k_4[H_2]K_3\frac{k_2[RCH=CH_2][HCo(CO)_3]}{k_3} \tag{11}$$

and from the first equilibrium we obtain the final expression

$$v = \frac{K_1 k_2 K_3 k_4}{k_3}\frac{[RCH=CH_2][H_2][HCo(CO)_4]}{[CO]} \tag{12}$$

which is in agreement with the inhibitor effect of CO in the most current experimental conditions.

The slow steps of the mechanism naturally attract more interest from the kinetic point of view because they will determine the rate of the reaction. In the mechanism of hydroformylation there are two intramolecular reactions involving hydrogen atoms that may have appreciable barriers: the transfer of the hydrogen from the metal to the π-complex, and the migration to the carbonyl. These reactions were studied by SCF calculations[4] that gave the geometries of reactants and products in each step presented in Figures 3 and 4. These calculations tend to overestimate the bond lengths of these bonds, but give important insights into the most important transformations that occur along the reaction coordinate for each reaction. In both cases there is the breaking of a Co-H bond and the formation of a H-C bond. However, whereas in the case of hydrogen transfer to the π-complex the reaction is exothermic by -25 kcal/mol, in the case of the migration to the carbonyl the reaction is endothermic by 20 kcal/mol. This energetic effect is decisive and places the barrier height of the first hydrogen transfer at 15 kcal/mol, and that of the second at 50 kcal/mol lower, according to the SCF calculations.

Industrial applications of hydroformylation reactions increasingly use rhodium carbonyl complexes with phosphines and, in particular, the $RhH(CO)(PPh_3)_3$ catalyst. The mechanism of the rhodium-catalysed hydroformylation is more complex than that of the catalysis by cobalt, and is illustrated in Figure 5. The intermediates involved in this catalytic cycle are too unstable to be isolated, but it was possible to identify some of them by NMR and infrared spectroscopies[5,6].
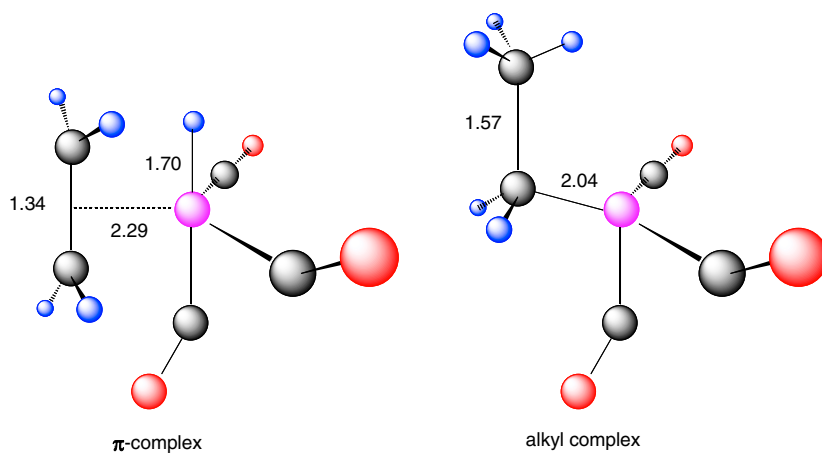
Figure 3 - Reactant and product in the transfer of an H-atom from the metal to the π-complex.
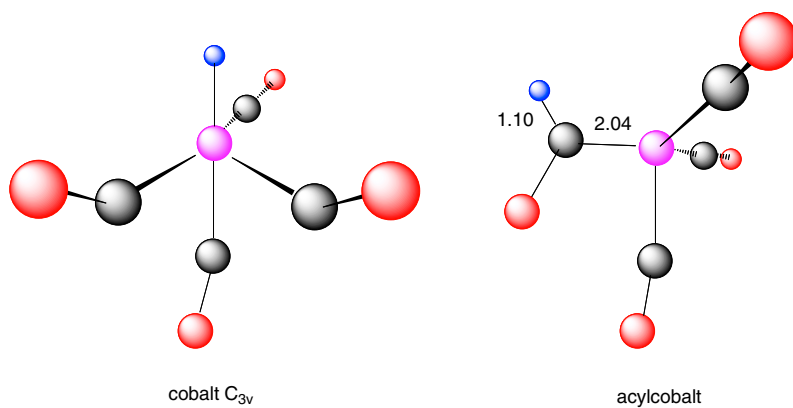
Figure 4 - Reactant and product in the migration of an H-atom from the metal to the carbonyl.
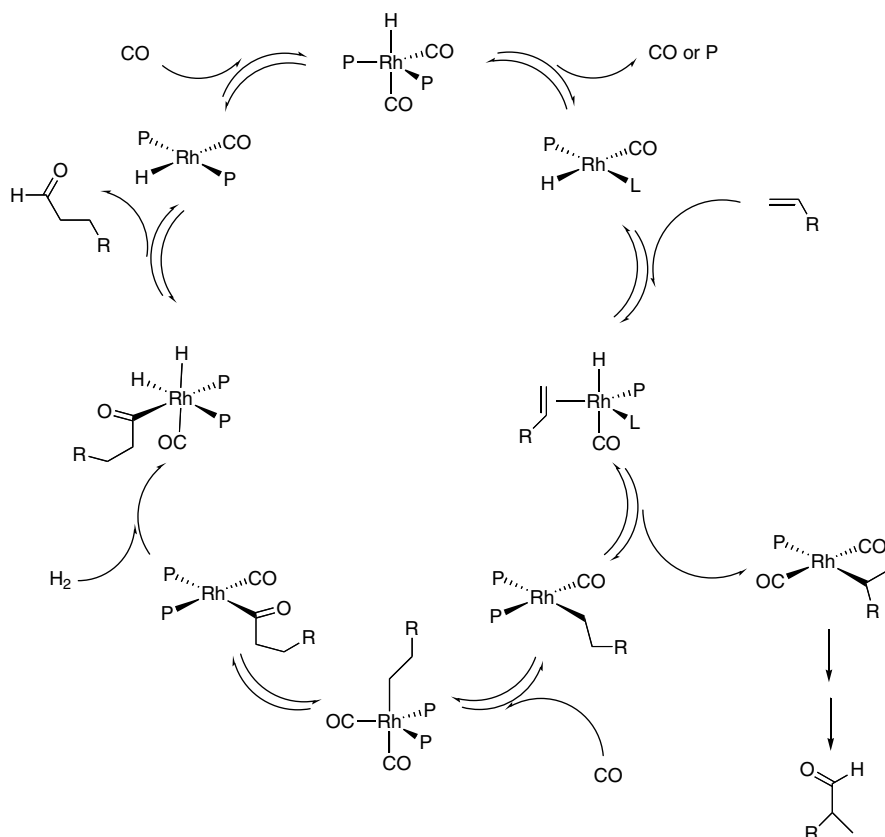
Figure 5 - Hydroformylation catalysed by rhodium, where L=CO or P, and P=PPh₃.

The first step is the attack of the olefin to the species RhH(CO)(PPh₃)₂ with 16 electrons which leads, through the π-complex, to the alkyl complex. This complex recovers the 18 electrons with the addition of a CO molecule, followed by the insertion to form the acyl derivative. This derivative undergoes the addition of a hydrogen molecule to form the dihydroacyl complex. In the last step, the addition of another hydrogen atom to the carbon atom of the acyl group followed by the release of the aldehyde, the oxidation state of the metal is changed and this probably is the rate-determining step of the reaction rate. The following steps reflect the equilibria between rhodium complexes coordinated with one or two CO molecules. It should be noted that in this case

the reaction rate also decreases when the concentration of carbon monoxide increases. In order to obtain a high selectivity towards the formation of a linear aldehyde, it is necessary to maintain a high concentration of triphenylphosphine. This assures the presence of the bisphosphine complex in the cycle, necessary to catalyse the formation of the linear aldehyde. The preference of this complex for linear aldehydes is due to steric restrictions dictated by the volume of triphenylphosphine in the alkyl complex.

With the rhodium catalyst, activation energies of 18 kcal/mol were obtained for the hydroformylation of several substrates[7], which suggests that the SCF calculations previously described tend to overestimate the reaction barriers of these reactions. Alternatively, the reaction barriers can be calculated with semi-empirical methods, as discussed in the following section.

3.3. KINETICS OF HYDROGENATION

The Wilkinson catalyst, RhCl(PPh$_3$)$_3$ [8], was the first homogeneous catalyst to be employed for a large number of hydrogenations under atmospheric pressure and room temperature. The complexity of the mechanism is at the origin of many unsatisfactory mechanistic proposals. However, the kinetic studies of some elementary steps allowed Halpern to obtain the mechanism illustrated in Figure 6[9].

The rate law of this mechanism is given by

$$v = \frac{K_1 k_4 K_5 k_6 [\text{olefin}][\text{H}_2]}{K_1 k_4 K_5 [\text{olefin}][\text{H}_2] + K_1 k_4 [\text{H}_2][\text{P}] + K_5 k_6 [\text{olefin}][\text{P}]} [\text{Rh}]_{total} \tag{13}$$

that can also be written as

$$k_{cat}^{-1} = \frac{[\text{Rh}]_{total}}{v} = \frac{1}{k_6} + \left(\frac{1}{K_5 k_6 [\text{olefin}]} + \frac{1}{K_1 k_4 [\text{H}_2]} \right)[\text{P}] \tag{14}$$

to illustrate that the reciprocal of the rate constant of the catalysis increases (that is, the reaction is inhibited) with an increase in the triphenylphosphine

concentration, but that this reciprocal decreases (the rate is accelerated) with an increase in the concentration of the olefin or of hydrogen.

The rate constants of some of these steps were measured from the hydrogenation of cyclohexane in benzene at 25 ^{0}C, and the following values were obtained: k_1= 0.68 s^{-1}, k_2= 4.8 M^{-1} s^{-1}, k_{-2}= 2.8x10^{-4} s^{-1}, K_5=3.0x10^{-4}, k_{-1}/k_4=1,0, k_6=0.22 s^{-1}. It is interesting to see that the rate constant of the rate-determining step of the catalytic cycle is of the same magnitude as that of the dissociation step of the complex RhCl(PPh$_3$)$_3$ that originates the catalytically active species.
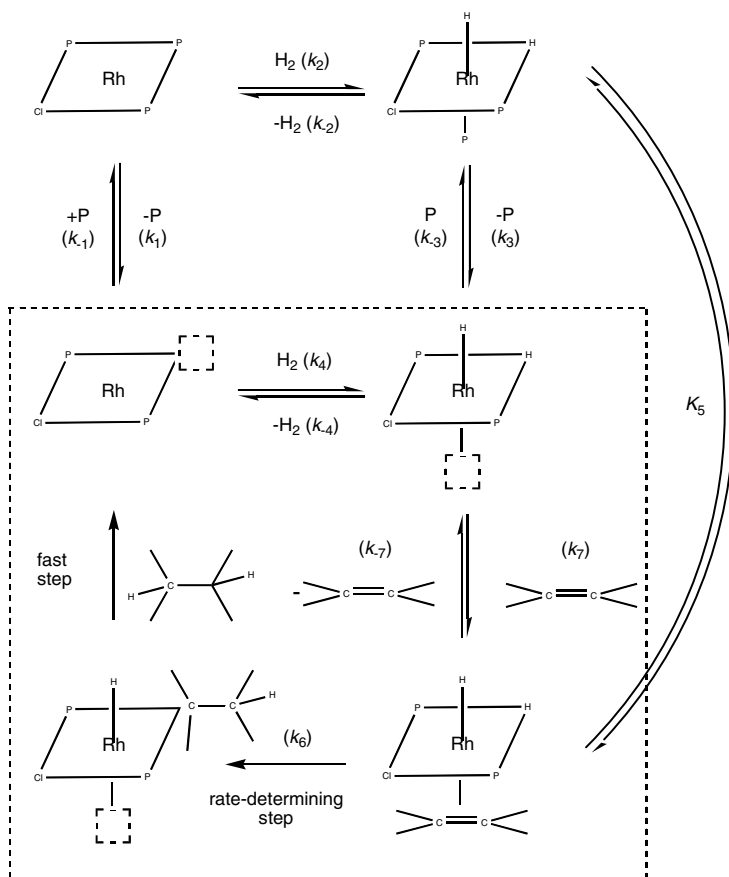
Figure 6 - Most important steps in the mechanism of hydrogenation of olefins, according to Halpern. The catalytic cycle is encompassed by the dashed rectangle. P=PPh$_3$.

These reactions were also studied by SCF calculations and the energies obtained are shown in Figure 7, relative to the energy of the reactants[10]. It should be noted that the energy difference between the first and the last species is the reaction energy $H_2+CH_2=CH_2 \rightarrow CH_3$—$CH_3$. Experimentally the reaction energy is 33 kcal/mol, 25% less than the calculated value, which recommends caution in analysing the values of Figure 7. According to these calculations, the slowest step is the insertion of the olefin, because it has the highest activation energy, although it is more exothermic than the subsequent step of reductive elimination. Experimentally, when the olefin is cyclohexene, the enthalpy of activation of the rate-determining step is 22 kcal/mol [8].

The difference between the transition state energies of olefin insertion and alkane reductive elimination can be understood on the basis of their structures and SCF calculations, Figure 8. The transition state for insertion corresponds to an intramolecular H-atom transfer, similar to that illustrated in Figure 3. On the other hand, the elimination is similar to the migration represented in Figure 4. H-atom transfer reactions have high barriers when they involve saturated hydrocarbons. If we represent the breaking of the H-Co bond of $HCo(CO)_4$ by its Morse curve using the bond dissociation energy $D_0^{298}=66.4$ kcal/mol [11], frequency $\omega_e=1934$ cm^{-1} [12] and equilibrium bond length $l_{eq}=1,556$ Å [13], and the making of the CH bond in the alkyl group by the parameters of ethane[15], we can employ the Intersecting/Interacting State Model to calculate the energy barrier[16]. Running the calculations over the Internet in the site designed for this purpose[17], we obtain a barrier of 6.5 kcal/mol for the reaction energy of -36 kcal/mol. More details on these calculations, including the format of input and output files, are given in the Appendix. This calculation can be refined considering the difference between the energies of interaction in Co-π and Co-C(alkyl). The excessive reaction energy employed above is probably due to the neglect of this difference. We can compensate for the difference in energies of

interaction increasing the energy of the H-Co bond by 11 kcal/mol, which leads to the correct reaction energy, -25 kcal/mol. With this reaction energy, the energy barrier increases to 9 kcal/mol. This barrier is compatible with the activation energy of 18 kcal/mol observed for the hydroformylation catalyzed by RhH(CO)(PPh$_3$)$_3$, because the insertion is not the rate-determining step of this catalytic cycle. Decreasing the exothermicity of the reaction to -10 kcal/mol, increases the barrier to 14 kcal/mol. Give the dependence of the barrier height on the exothermicity, it is not surprising that the rate-determining step may change from the H-atom transfer to the H-atom migration.

H-atom migrations may have smaller barriers than H-atom transfers for the same exothermicity because the formation of a three-centred species may be more efficient in stabilizing the transition state of a bond-breaking–bond-forming reaction. This stability may come from the higher electronic density of a three-centred transition state.
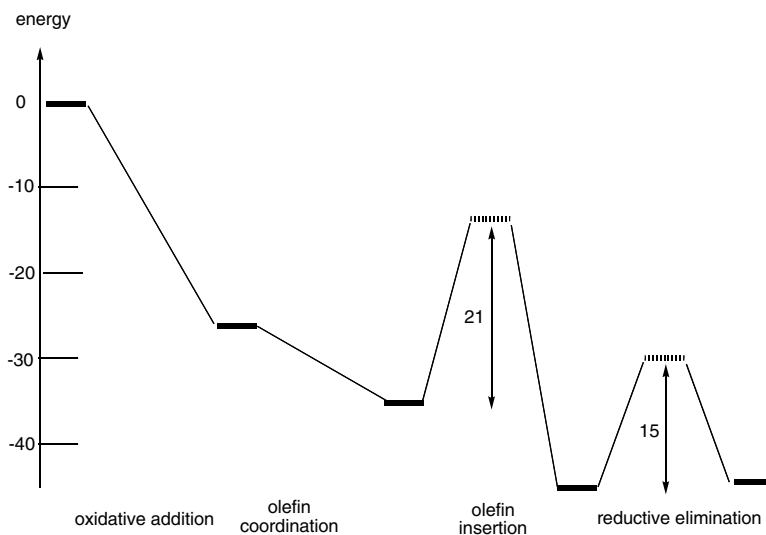
Figure 7 - Potential energy profile for the catalytic cycle of the hydrogenation of olefins, in kcal/mol. The thick lines indicate intermediates, with the zero energy at RhCl(PPh$_3$)$_2$+H$_2$+C$_2$H$_4$, and the final products RhCl(PPh$_3$)$_2$+C$_2$H$_6$. The dashed lines indicate transition states and the numerical values are the activation energies relative to the corresponding precursors. The activation energies of the first two steps are approximately zero.

transition state for insertion   transition state for elimination
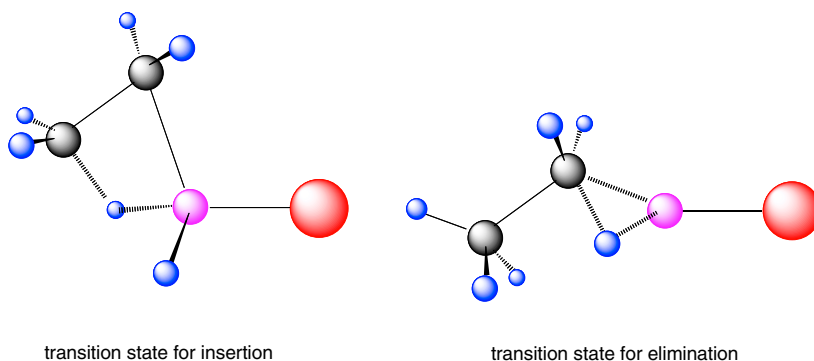
Figure 8 - Transition sates for the insertion of the olefin and for the reductive elimination of the alkane.

3.4. FINAL REMARKS

Homogenous catalysis has been a fertile ground for the proposal of sophisticated reaction mechanisms. The confidence in such mechanisms depends on their ability to explain and predict the rates of the catalysed reactions. This emphasises the need to make kinetic measurements to evaluate the possible reaction paths and decide whether a given species is, or not, a true reaction intermediate of the catalytic cycle. In the words of Halpern, "That such kinetic measurements are essential for the elucidation of catalytic mechanisms is hardly surprising in view of the fact that catalysis is, by definition, purely a kinetic phenomenon"[9].

Today, it is appropriate to complement these words of Halpern with the argument that the viability of a given elementary step of a reaction mechanism must be evaluated with an appropriate theoretical model. Semi-empirical methods are well suited for such evaluation because they combine fast calculations with clear relations between molecular structure and reactivity.

Acknowledgement

Appendix

This appendix presents the input and output files employed in the calculation of the rates of bond-breaking–bond-making processes using the Intersecting/Interacting State Model, ISM. The formats employed are consistent with those of the Internet application that runs ISM calculations[17].

Sequence of input data

The first line is the
'label'

The second line starts with the number "1" to signal a proton transfer calculation. Then, in order, pK_{aHA}, p_A, q_A, pK_{aHB}, p_B, q_B, K_c. The last value is used to calculate the reaction energy, when this is not calculated from the difference in pK_a, and is only used in the calculation if the parameter has a value less than 100.

The third line is
m_B, m_H, m_A, $D_{HA,298}{}^0$, ω_{eAH}, $l_{AH,eq}$, $D_{HB,298}{}^0$, ω_{eBH}, $l_{BH,eq}$, D_{0BA}, D_{0AB}, I_P, E_A, I_P, E_A, σ, j, T_{av}, angle.
The masses (m_B, m_H, m_A) are in amu, the bond dissociation energies ($D_{HA,298}{}^0$, $D_{HB,298}{}^0$) and the hydrogen-bond binding energies (D_{0BA}, D_{0AB}) are in kcal/mol, the observed infrared stretching frequencies (ω_{eAH}, ω_{eBH}) in cm^{-1}, the equilibrium bond lengths ($l_{AH,eq}$, $l_{BH,eq}$,) in Å, the ionization potentials and electron affinities (I_P, E_A) in eV, the statistical factor (σ) is adimensional, j=0 for "intramolecular" reactions using $\kappa(T)K_c k_B T/h$ as pre-exponential factor and j=3 otherwise, T_{av} is the temperature in K for the calculation of the reaction free-energy from pK_a, and *angle*=180^0.

The following lines are, in sequence,
"labels"
T, k_{exp}
Representing temperature (in K, for the rate calculation) and the experimental rate (when available, but not zero).

Key to output data

The first line is the 'label'
The second line informs on the success in finding all the solutions for the equations, the smoothness of the adiabatic reaction path at the transition state and whether the transition state was located at the maximum of the classical or vibrationally-adiabatic reaction paths.

The third line informs on the location of the several maxima, in terms of bond orders.

The fourth line informs on the location of the several minima, in terms of bond orders.

The fifth line gives the calculated electrophilicity index (m), the sum of bond extensions from reactants and products to the transition state (d), and the calculated activation energy (E_{calc}) without tunnelling corrections.

The sixth line gives the spectroscopic Morse constant and electronic dissociation energies.

The seventh line gives the bond order of precursor and successor H-bonded complexes.

The eighth line gives the H-bond stretching frequencies ($\overline{}_{AB}$ and $\overline{}_{BA}$), electronic dissociation energies and equilibrium bond lengths

The ninth line gives the symmetric stretching frequency, and the curvatures of the classical reaction path and of the vibrationally-adiabatic reaction path at the classical transition state.

The tenth line gives the energy of the several maxima relative to the classical energy of the reactants.

The eleventh line gives the energy of the several minima relative to the classical energy of the reactants.

The twelfth line gives the adiabatic reaction energy and the zero-point energies of reactants and products.

Thirteenth line gives the vibrationally-adiabatic and classical barriers.

The following lines give the several components of the reaction rates.

HCo(CO)$_4$ **CH$_3$CH$_3$**

Input file

'CH3CH2+HCo(CO)4 -> CH3CH3+Co(CO)4'
0 0 1 1 0 1 1 1 -25
12 1 59 66.4 1934 1.556 101.1 2954 1.094 0 0 17.423 0 13.598 0 1 0
280   120
'298'
298 1.1e10

Output file

'CH3CH2+HCo(CO)4 -> CH3CH3+Co(CO)4'

did all the roots converge? Y   discontinuity = -1 localization of s=0:classical
b.o.cl = 0.270   b.o.ad = 0.238   b.o.ts2 = 0.545   b.o.ts3 = 0.000
b.o.min1 = 0.518   b.o.min2 = 1.000
mTST = 1.000   dTST = 0.785   angle = 120.0   Ecalc = 7.730
betaBC = 1.573   DBC = 68.394   betaAB = 1.883   DAB = 104.614
b.o. nHC = 1.000   b.o. nAH = 0.000
freqAC = 0.000   DAC = 0.000   lAC = 0.000   freqCA = 0.000   DCA = 0.000
            lCA = 0.000
freqsym = 356.589 freqtunnelMEP = 1150.346   freqtunnelVAP = 0.000
Vmax = 9.163   Vadmax = 11.435 Vadmax2 = 5.126 Vadmax3 = 0.000
Vadmin1 = 4.918   Vadmin2 = 0.000 VadminAC = 2.870   VadminCA = -20.617
Ad r ene = -23.487 ZPEBC = 2.870   ZPEAB = 4.383
Ad barrier = 8.565 kcal/mol   Cl barrier = 9.163 kcal/mol

T	ATST	k thermal	tunnel corr.	k semicl
298.0	6.2098E12	3.2488E6	4.2216E0	1.3715E7

References

1. S.J. Formosinho, L. G. Arnaut, *Cinética Química*, Universidade de Coimbra, **2003**.

2. R.F. Heck, D.S. Breslow, *J. Am. Chem. Soc.*, **1960**, *82*, 4438.

3. R.F. Heck, D.S. Breslow, *J. Am. Chem. Soc.*, **1962**, *84*, 2499.

4. D. Antolovic, E.R. Davidson, *J. Am. Chem. Soc.*, 1987, *109*, 5828.

5. D. Evans, J.A. Osborn, G. Wilkinson, *J. Chem. Soc. A*, **1968**, 3133.

6. C. K. Brown, G. Wilkinson, *J. Chem. Soc. A*, **1970**, 2753.

7. R. Chansarkar, K. Mukhopadhyay, A.A. Kelkar, R.V. Chaudhari, *Catal. Today*, **2003**, *79/80*, 51.

8. J.A. Osborn, F.H. Jardine, J.F. Young, G. Wilkinson, *J. Chem. Soc. A*, **1966**, 1711.

9. J. Halpern, *Inorg. Chim. Acta*, **1981**, *50*, 11.

10. N. Koga, C. Daniel, J. Han, X.Y. Fu, K. Morokuma, *J. Am. Chem. Soc.*, **1987**, *109* 3455.

11. V. D. Parker, K. L. Handoo, F. Roness, M. Tilset, *J. Am. Chem. Soc.*, **1987**, *113* 7493.

12. W.F. Edgell, R. Summitt, *J. Am. Chem. Soc.*, **1961**, *83*, 1772.

13. E.A. McNeil, F.R. Scholer, *J. Am. Chem. Soc.*, **1977**, *99*, 6243.

14. L. G. Arnaut, A. A. C. C. Pais, S. J. Formosinho, M. Barroso, *J. Am. Chem. Soc.*, **2003**, *125*, 5236.

16. L.G. Arnaut, S.J. Formosinho, H.D. Burrows *Chemical Kinetics*, Elsevier, **2007**.

17. http://www.ism.qui.uc.pt:8180/ism/, L.G. Arnaut, M. Barroso and D. Oliveira, **2006**, Coimbra.

(Página deixada propositadamente em branco)

4. Homogeneous Catalysis: Oxidations

Beatriz Royo

Instituto de Tecnologia Química e Biológica, Universidade Nova de Lisboa, Av. da Republica, Apartado 127, 2781-901 Oeiras, Portugal

4.1. Introduction

Oxidation reactions catalyzed by transition metals are among the most important reactions in nature. They are responsible for the activation of molecular oxygen (O_2) in living species and fundamental for the chemical industry. In industry, oxidations catalyzed by transition metals cover a variety of reactions and are used for the production of bulk chemicals, which are building blocks for the production of many other products. Oxidation reactions are also basic for the synthesis of complex organic molecules, such as pharmaceutical products where the stereochemistry is of upmost importance[1].

State of the art oxidation technologies should be characterized by high atom economy and selectivity, broad substrate scope, use of environmentally benign oxidation reagents, and sufficient catalysts stability and productivity. Moreover, for industrial applications, systems which are simple and easy to work up are important. Among the readily available oxidants, molecular oxygen seems to be the perfect reagent for an oxidation reaction. However, only one oxygen atom of an oxygen molecule is used productively for oxidation. The second oxygen atom reacts with a reducing agent present to form by-products, which are thus formed in stoichiometric amounts. Apart from molecular oxygen, hydrogen peroxide (H_2O_2) has been shown to be environmentally benign by a similar atom-economy with its side product being water. In addition, it is readily available and can be used safely without much precaution.

In this chapter some important examples of oxidation reactions, which represent industrial processes of great importance, will be discussed.

4.2. WACKER PROCESS FOR THE OXIDATION OF OLEFINS TO CARBONYL COMPOUNDS

It has been known since 1894 that ethylene is oxidized to acetaldehyde by palladium chloride as a stoichiometric reagent (Equation 1)[2]. However, it was not until 1950s that it was discovered that the reaction could be made catalytic (in Pd) by linking it to a Cu-based redox system. This process was developed by the German enterprise Wacker Chemie[3]. The Wacker synthesis of acetaldehyde combines Equation 2 and 3 to yield a catalytic acetaldehyde synthesis. The overall reaction is equivalent to direct oxidation of ethylene by O_2 (Equation 4).

$$C_2H_4 + PdCl_2 + H_2O \rightarrow CH_3CHO + Pd + 2\ HCl \tag{1}$$

$$Pd + 2\ CuCl_2 \rightarrow PdCl_2 + 2\ CuCl \tag{2}$$

$$2\ CuCl + 2\ HCl + \tfrac{1}{2}\ O_2 \rightarrow 2\ CuCl_2 + H_2O \tag{3}$$

Total: $\quad C_2H_4 + \tfrac{1}{2}\ O_2 \rightarrow CH_3CHO \tag{4}$
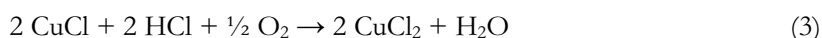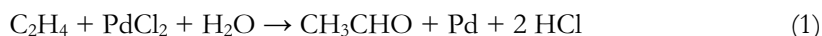
The Wacker process was one of the first successes of homogeneous catalysis although its use has declined over the last twenty years for two main reasons. First, manufacturing plants are expensive to build and maintain, because they must be constructed to withstand a corrosive environment. Second, another procedure, which yields acetic acid directly from synthesis gas, has been developed and now supplants the Wacker process. The mechanisms and kinetics of these reactions have been studied in detail. The major features of the mechanism seem to be well established, Scheme 1. The initial step is coordination of ethylene to Pd(II) which activates the double bond towards nucleophilic attack from water. The so-formed Pd-CH$_2$-CH$_2$-OH moiety undergoes β-H elimination to give a coordinated vinyl alcohol, Pd(η^2-CH$_2$-CH(OH)). Further rearrangement of this ligand at the coordination sphere of Pd leads Pd(0) from Pd(II) by reductive elimination of HCl and liberation of

acetaldehyde, CH_3CHO. The last step regenerates Pd(II) at the expense of Cu(II). The Cu(I) species that results is reoxidized to Cu(II) by O_2. The process requires large amounts of copper salts, chlorides and acid to maintain the catalytic cycle.

Scheme 1 - Major Features of the Wacker Synthesis of Aldehyde.

Recently, Sheldon reported a modification for the Wacker process using a water-soluble palladium complex with a bidentate diamine ligand, Figure 1[4]. This catalyst provided a system for performing Wacker-type reactions in water under neutral, copper-and chloride-free conditions.

Figure 1 - Water-soluble PhenS*Pd(OAc)$_2$ catalyst.

This modification allows the direct reoxidation of Pd(0) to Pd(II) by O$_2$. In a first step a palladium dimer with two bridging hydroxy ligands is dissociated via coordination of the olefin, this is followed by intra-molecular attack of the hydroxide on the coordinated olefin. The resulting β-hydroxyalkyl palladium complex decomposes into the 2-alkanone and a zerovalent species. The latter is reoxidized with dioxygen, giving a palladium peroxide. Coupling of this peroxide with one equivalent of zerovalent palladium-PhenS* regenerates the starting Pd-dimer, Scheme 2.
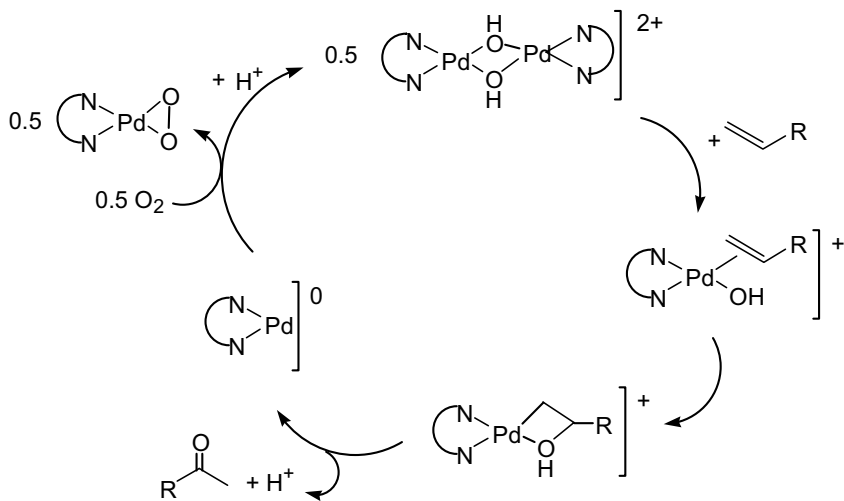
Scheme 2 - The catalytic cycle proposed for olefin oxidation with aqueous soluble Pd(II) catalysts.

4.3. EPOXIDATION OF OLEFINS

Epoxidation, oxygenation of olefins to form cyclic epoxide groups, Scheme 3, is an important reaction in organic synthesis because the formed epoxides are intermediates that can be converted to a variety of products. This reaction is also very attractive in asymmetric cases since it can lead to two chiral carbons in one step.
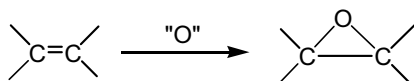
Scheme 3 - Epoxidation reaction.

Propylene oxide is a major industrial commodity, around 4.5 million tons are produced each year. Although a number of epoxidation processes that use various catalysts and oxidants have been developed, a chlorine-using noncatalytic process and catalytic processes based on expensive oxidants (organic peroxides and peracids) are still used extensively[5].The most important technical epoxidation processes, based on high valent transition metal catalysts in combination with alkyl hydroperoxides as the oxygen source, are the SHELL (heterogeneous processes that uses *tert*-butylhydroperoxide in the presence of a titanium/silica catalyst) and the ARCO/HALCON (which employs soluble molybdenum(VI) as catalysts) processes for propylene oxide.

Metal catalyzed epoxidations with alkyl hydroperoxides show the following characteristic features: (i) metals with low oxidation potentials and high Lewis acidity in their highest oxidation state are superior catalysts and show the following order of reactivity: Mo>W>V>Ti; (ii) the active catalysts contains the metal in its highest oxidation state (an induction period is observed during which catalysts precursors such as $Mo(CO)_6$ is oxidized to its highest oxidation state); (iii) strongly coordinating solvents, particularly alcohol and water, severely retard the reaction competing for coordinating sites on the catalyst (hydrocarbons and chlorinated hydrocarbons are the preferred solvents); (iv)

reactions are usually performed in the temperature range 80-120 ˚C; (v) the rate increases with increasing substitution of the double bond by electron-donating alkyl groups, consistent with an electrophilic epoxidizing agent; (vi) the epoxidation is sterospecific, *cis*-olefins give only *cis*-epoxides.

The high selectivities observed with a wide range of olefins and the stereospecificity of the epoxidation are consistent only with a heterolytic mechanism. This is a general agreement that involves rate-controlling oxygen transfer from an electrophilic alkylperoxo metal complex of the olefinic double bond. However, despite extensive studies, the detailed mechanism of the oxygen transfer step remains controversial. A mechanism was proposed by Sheldon, which involves coordination of the alkyl hydroperoxide through the oxygen atom to the molybdenum metal center and then the oxygen is transferred to the olefin, Scheme 4.
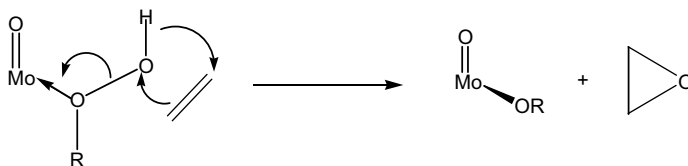
Scheme 4 - Oxygen transfer mechanism proposed by Sheldon.

Subsequently, Sharpless reasoned, on the basis of steric arguments, that the mechanism involving coordination of the alkyl hydroperoxide ligand through the distal rather than the proximal oxygen, was more likely, Scheme 5.
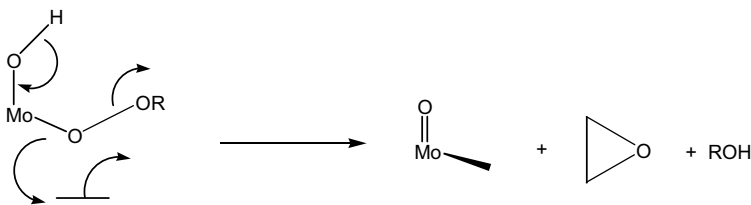
Scheme 5 - Oxygen transfer mechanism proposed by Sharpless.

An alternative mechanism for oxygen transfer was proposed by Mimoun. In this mechanism, initial coordination of the olefin to the metal is followed by its rate-limiting insertion into the metal-oxygen bond giving a pseudocyclic dioxometallocyclopentane. The latter decomposes to the epoxide and the metal alkoxide, Scheme 6.
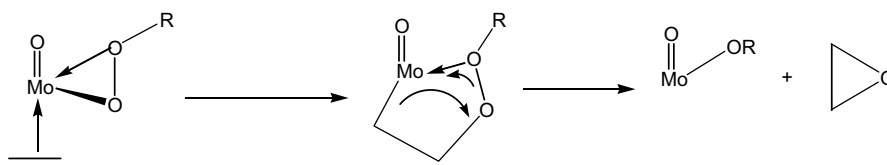
Scheme 6 - Oxygen transfer mechanism proposed by Mimoun.

Several organometallic derivatives of transition metal oxides are powerful epoxidation catalysts. Methyltrioxorhenium (MTO) catalyzes the epoxidation of olefins in the presence of H_2O_2. MTO reacts with H_2O_2 under formation of an isolable bisperoxo complex. If only a moderate excess of H_2O_2 is applied, a monoperoxo complex is formed, and this monoperoxo complex is also an epoxidation catalysts, Scheme 7. The most important drawback of the MTO catalyzed process is the concomitant formation of diols instead of the desired epoxides, especially in the case of more sensitive substrates. Sharpless found that the biphasic system (waterphase/organic phase) and addition of a significant excess of pyridine as Lewis base not only hamper the formation of diols but also increase the reaction velocity in comparison to MTO catalyst precursor. Several organomolybdenum oxides, particularly those of formula η^5-$(C_5H_5)MoO_2Cl$ and η^5-$(C_5H_5)MoO_2R$ are also powerful epoxidation catalysts if applied together with *tert*-butylhydroperoxide[6].
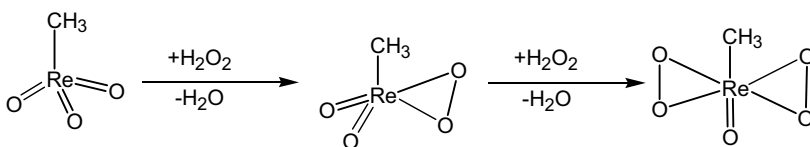
Scheme 7 - Reaction of MTO with H_2O_2.

4.4. ASYMMETRIC EPOXIDATION OF OLEFINS

The discovery by Sharpless that titanium complexes containing asymmetric ligands can catalyze the enantioselective oxidation of allylic alcohols to the corresponding epoxyalcohols has been of considerable impact[7]. The Sharpless oxidation employs a catalyst prepared by treating a titanium alkoxide, titanium tetraisopropoxide, $Ti(OPr^i)_4$, with a tartrate ester such as the natural (+) isomer of diethyltartrate, Scheme 8. The high enantioselectivity of this reaction is attributed to precoordination of the alcohol function to the titanium center, which serves to orient the face of the incoming double bond. Although they are rather sluggish catalysts (they are used almost in reagent quantities in some transformations) and require handling of organic peroxides on large scale. Also they are limited to allylic alcohols as substrates; the oxidation of simple olefins shows little enantioselectivities. Probably, the best known of the applications of Sharpless chemistry is the synthesis of a chiral epoxide as an intermediate to (+)-disparlure, the pheromone for the gipsy moth, commercialized by J.T Baker in 1981. The basis for a truly economical use of enantioselective epoxidation on a large scale came with the recognition in 1984 that the addition of molecular sieves to the reaction mixture allows the use of 5 mol % Ti/tartrate complex in a truly catalytic and reproducible manner. Upjohn and ARCO have both utilized this development as the basis of commercial routes for the production of C8-epoxyalcohols in 98% and (*S*)- and (*R*)-glycidol in more that 88 % *ee* (enantiomeric excess).
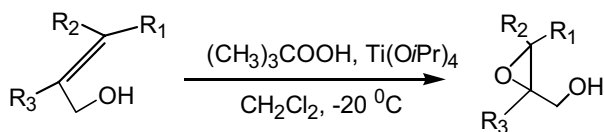
Scheme 8 - Asymmetric epoxidation of allylic alcohols.

A more recent alternative approach, developed by Jacobsen and Katsuki, provides an efficient method for unfuctionalized olefins using NaOCl as oxidant in the presence of Mn complexes of chiral Schiff-bases as catalysts[8], Figure 2. The proposed mechanism of the Jacobsen-Katsuki epoxidation is based on investigations by Kochi *et al.* with achiral salen ligands, where Mn^V-oxo complexes are postulated to be the catalytically active species, Scheme 9.
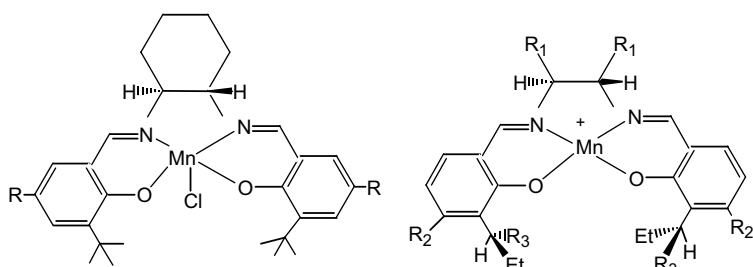
Figure 2 - Jacobsen-Katsuki catalysts for asymmetric epoxidation.
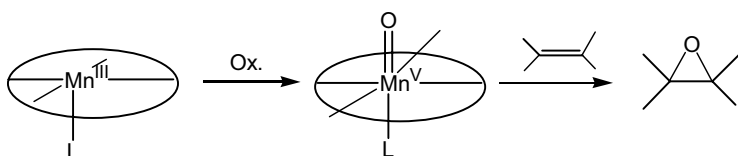
Scheme 9 - Formation of Mn^V-oxo complexes in Jacobsen-Katsuki catalysts.

Although the factors controlling the reactivity and enantioselectivity are now well understood, a controversy has erupted over the mechanism of oxygen transfer to the double bond. The concerted path A and pathways proceeding

via radical intermediates (path B) and manganaoxetanes (path C) seem operate depending on the nature of the olefin substituents, Scheme 10.
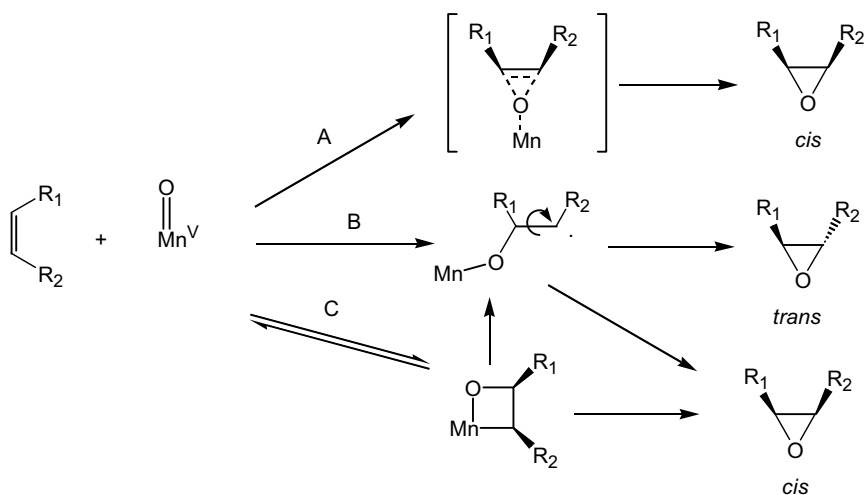
Scheme 10 - Three mechanisms for oxygen transfer: A concerted, B via radicals, C via manganaoxetane intermediates.

 In addition significant progress using organic catalysts based on chiral ketones has been reported[9]. The sugar-derived system developed by Shi is able to epoxidize trisubstituted *trans* alkenes and certain *cis* alkenes with good to excellent stereocontrol, although is not selective for terminal olefins[10].

However, the recent reports of Katsuki and Beller in which Ti- and Ru-based complexes are used for asymmetric epoxidation with H_2O_2, have doubtless changed the state of the art in the area of metal-catalyzed asymmetric epoxidation. Katsuki has recently developed a titanium-salen catalyst, Figure 3, for asymmetric epoxidation of unfuctionalized olefins using aqueous hydrogen peroxide. High yields and high enantioselectivity (up to 98 % ee) has been achieved for several olefins[11].

The Beller´s method uses H_2O_2 in the presence of ruthenium-pyboxazines complexes for the epoxidation of substituted aromatic olefins obtaining high yields and with *ee* values up to 84 % of the corresponding epoxides[12]. The

strategy was the use of a combination of two meridional ligands which provided the ability to tune both the activity and the asymmetric induction by using the ruthenium(pybox)(pyridinedicarboxylate), Figure 3. The original catalyst [Ru(pybox)(pydic)] was reported by Nishima *et al.* to catalyze the epoxidation of *trans*-stilbene in the presence of PhI(OAc)$_2$ as the stoichiometric oxidant[13].
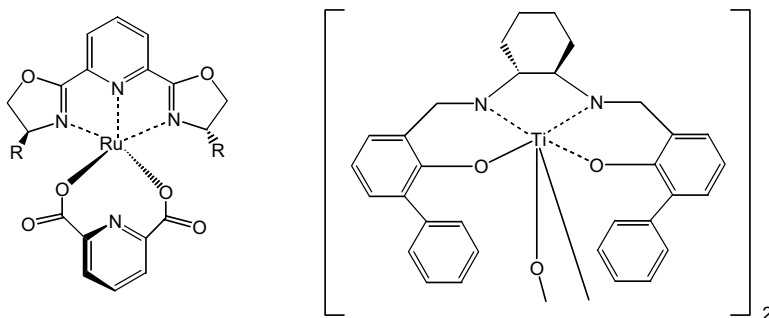
Figure 3 - Ruthenium(pybox)(pyridinedicarboxylate) and Ti-salen catalysts for asymmetric epoxidation.

The use of molybdenum-peroxo complexes for the industrial scale epoxidation of alkenes has been extensively explored over the last 40 years, beginning with homogeneous Mo(VI) catalysts in the Halcon and Arco processes[14]. Early reports of asymmetric epoxidation with a chiral molybdenum complex include the use of a stoichiometric molybdenum-(*S*)-lactic acid piperidineamide system by Schurig, Kagan and co-workers. However, weak coordination of ligands with the molybdenum has resulted in very little success having been achieved. This stage has changed by the recent report on the successful Mo-BHA (BHA = bishydroxamic acid, Figure 4, catalyzed asymmetric oxidation of mono-, di-, and trisubstituted olefins under mild condition to give epoxides in high yields and excellent selectivity[15].
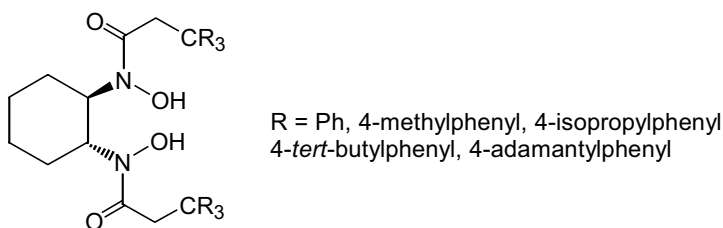
Figure 4 - Bishydroxamic acid (BHA).

4.5. ASYMMETRIC DIHYDROXYLATION

Osmium tetroxide is one of the most selective oxidants known; it dihydroxylates all olefins and it reacts only with olefins[16]. Thus, being an ideal substrate-selective catalyst but at the same time toxic and expensive, it is highly desirable to develop good reoxidation systems for osmium, rendering the dihydroxylation catalytic on osmium. Several reoxidation systems have been developed, of which the two most commonly used today are based on *N*-methylmorpholine *N*-oxide (NMO)[17] and $K_3[Fe(CN)_6]$[18], the latter being mainly used in asymmetric dihydroxylation. The Upjohn dihydroxylation allows the syn-selective preparation of 1,2-diols from alkenes by the use of OsO_4 as catalyst and a stoichiometric amount of an oxidant such as NMO.

The toxic and volatile OsO_4 can be prepared in situ by the oxidation of $K_2OsO_2(OH)_4$ with NMO. NMO is also the cooxidant that enables the use of a catalytic amount of OsO_4, because this reagent is able to reoxidize an Os(VI) species to an Os(VIII) species, Scheme 11. After the dihydroxylated product is released from the complex through hydrolysis, reoxidation of the metal takes place by NMO regenerating the catalyst. If the olefin concentration is too high, a second equivalent of the substrate might bind to the catalytic center in the absence of the chiral ligand, and undergo a dihydroxylation. This side reaction will decrease the enantioselectivity. This mechanistic insight leads to Sharpless to develop an optimized version by slow addition of the olefin. The slow

addition ensures a low concentration of the olefin in the reaction mixture, favouring the hydrolysis over the reaction with a second olefin molecule.
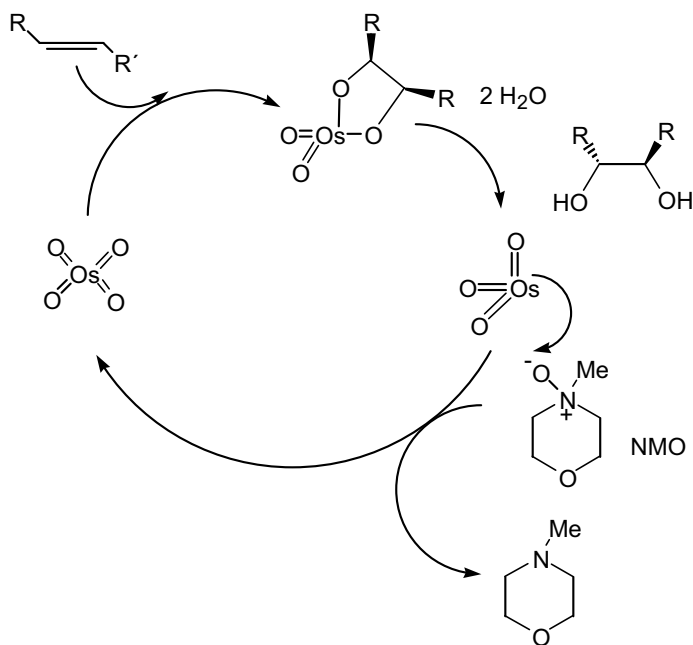
Scheme 11 - Upjohn procedure for the osmium-catalyzed dihydroxylations.

The key step is the cycloaddition of OsO$_4$ to the olefin. There has been some speculation regarding the actual addition step, for which experimental data suggest the possible involvement of two separate steps. Thus, the question arises during these discussions of whether the key step takes place via an initial (3+2)-addition or by a (2+2)-addition followed by expansion of the metallacycle, Scheme 12. Quantum chemical calculations have shown an initial (3+2)-addition of OsO$_4$ to be energetically more favorable.
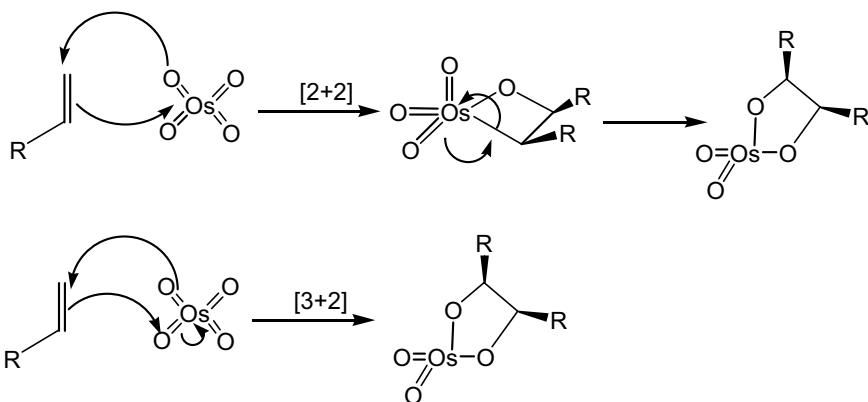
Scheme 12 - [2+2]- and [3+2]-addition of the olefin to OsO$_4$ in the OsO$_4$-catalyzed dihydroxylation.

Another protocol for asymmetric dihydroxylation is based on the use of K$_3$[Fe(CN)$_6$]. On the basis of the substantial improvement of enantioselectivities in asymmetric dihydroxylation by using K$_3$[Fe(CN)$_6$] as the oxidant, industrial research led to the development of an *In situ* electrochemical reoxidation of K[Fe(CN)6][19].

Very few procedures for reoxidation of osmium(VI) by H$_2$O$_2$ or O$_2$ are known. Milas reported that H$_2$O$_2$ could be employed as a direct reoxidant for Os(VI), but in many cases leads to nonselective reactions with low yields due to over-oxidations[20]. In addition, former publications[21] and patents[22] demonstrate that in the presence of OsO$_4$ and oxygen mainly nonselective oxidation reactions take place. However, Krief *et al*. recently designed successfully a reaction system consisting of oxygen, catalytic amounts of OsO$_4$ and selenides for the dihydroxylation of α-methylstyrene under irradiation with visible light[23]. Beller has also demonstrated that Os-catalyzed dihydroxylations of various olefins can be performed efficiently in the presence of dioxygen or air. Using α-methylstyrene as a model substrate it is shown that in the presence of very small catalyst-to-substrate ratios (up to 1:4000) high yield of the corresponding 1,2-diol are possible at slightly elevated oxygen pressures. In the presence of

chiral dihydroquinidine or dihydroquinine derivatives (Sharpless ligands), asymmetric dihydroxylations take place, albeit lower enantioselectivities compared to those obtained under the Sharpless conditions[24]. An alternative method based on the biomimetic osmium-catalyzed dihydroxylation by H_2O_2 has showed good results. In this process, the Os(VI) is recycled to Os(VIII) by a coupled catalytic ETM system based on NMO/flavin, leading to a mild and selective electron transfer[25].

References

1. *Transition Metals for Organic Synthesis*, M. Beller, C. Bolm (Eds.), VCH-Wiley, New York, **1998**, Vol. 2, pp. 155.

2. F.C. Philips, *J. Am. Chem. Soc.*, **1894**, *16*, 255.

3. J. Smidt, W. Hafner, R. Jira, J. Sedlmeier, R. Sieber, R. Rütlinger, H. Kojer, *Angew. Chem.*, **1959**, *71*, 176.

4. G.-J. Ten Brink, I.W.C.E Arends, G. Papadogianakis, R.A. Sheldon, *J. Chem. Soc. Chem. Commun.*, **1998**, 2359.

5. K.A. Jørgensen, *Chem. Rev.*, **1989**, *89*, 431.

6. F. E. Kühn, A. M. Santos, W. A. Herrmann, *Dalton Trans.*, **2005**, 2483.

7. T. Katsuki, B.K. Sharpless, *J. Am. Chem. Soc.*, **1980**, *102*, 5974.

8. T. Katsuki, *Adv. Synth. Catal.*, **2002**, *344*, 131.

9. W. Adam, C.R. Saha-Möller, P. A. Ganesphure, *Chem. Rev.*, **2001**, *101*, 3499.

10. Y. Shi, *Acc. Chem. Res.*, **2004**, *37*, 488.

11. Y. Sawada, K. Matsumoto, S. Kondo, H. Watanabe, T. Ozawa, K. Suzuki, B. Saito, T. Katsuki, *Angew. Chem. Int. Ed.,* **2006**, *45*, 3478.

12. M.K. Tse, C. Döbler, S. Bhor, M. Klawonn, W. Mägerlein, H. Hugl, M. Beller, *Angew. Chem. Int. Ed.*, **2004**, *43*, 5255.

13. H. Nishiyama, H. Shimada, H. Itoh, H. Sugiyama, Y. Motoyama, *Chem. Commun.*, **1997**, 1863.

14. M.N. Sheng, G.J. Zajaczek (ARCO), GB 1.136.923, **1968**; J. Kolar (Halcon), US 3.350.422, US 3.351.635, **1967**.

15. A.U. Barlan, A. Basak, H. Yamamoto, *Angew. Chem. Int. Ed.*, **2006**, *45*, 5849.

16. H.C. Kolb, M.S. VanNieuwenhze, K.B. Sharpless, *Chem. Rev.*, **1994**, *94*, 2483.

17. V. VanRheenen, R.C. Kelly, D.F. Cha, *Tetrahedron Lett.*, **1976**, 1973.

18. M. Minato, K. Yamamoto, J. Tsuji, *J. Org. Chem.*, **1990**, *55*, 766.

19. Y. Gao, C.M. Zepp, *Chem. Abstr.,* **1994**, 120, 119437j.

20. N.A. Milas, J.H.Trepagnier, J.T. Nolan, M.I. Iliopulos, *J. Am. Chem. Soc.*, **1959**, *81*, 4730.

21. J.F. Cairns, H.L. Roberts, *J. Chem. Soc. C,* **1968**, 640.

22. R.S. Myers, R.C. Michaelson, R.G. Austin. (Exxon Corp.) US-4496779, **1984**.

23. A. Krief, C. Colaux-Castillo, *Tetrahedron Lett.*, **1999**, *40*, 4189.

24. C. Döbler, G.M. Mehltretter, U. Sundermeier, M. Beller, *J. Am. Chem. Soc.,* **2000**, *122*, 10289.

25. S. Y. Jonsson, K. Färnegardh, J.-E. Bäckvall, *J. Am. Chem. Soc.*, **2001**, *123*, 1365.

5. POLYOXOMETALATES IN OXIDATIVE CATALYSIS OF ORGANIC COMPOUNDS

Ana M. V. Cavaleiro

Departamento de Química da Universidade de Aveiro, CICECO, Campus de Santiago, 3810-193 Aveiro, Portugal, anacavaleiro@ua.pt

5.1. INTRODUCTION

Polyoxometalates (POM) are a large class of oxoanions formed by group 5 and 6 metals, with general formula $[M_mO_y]^{n-}$ or $[X_xM_mO_y]^{p-}$, x < m, M = molybdenum, tungsten, vanadium, niobium and, less frequently, tantalum. These anions are also referred as iso- and heteropolyoxoanions, respectively. Isopolyoxoanions (IPA) dominate the chemistry of high oxidation states of the elements M in aqueous solution, since mononuclear oxoanions, like MoO_4^{2-}, WO_4^{2-} or VO_4^{3-}, are only found at comparatively high pH. Heteropolyoxoanions (HPA) have other elements (X) in their chemical composition, collectively called heteroatoms, besides oxygen and the predominant metal M, referred as the addenda. More than 70 elements of all parts of the periodic table are known as heteroatoms and different heteroatoms may be found in the same anion[1,2].

Structurally, polyoxometalates are aggregates of MO_x polyhedra (predominantly octahedra) sharing corners, edges or faces[1,2]. Common structural types are frequently referred by the name of the discoverer of the structure, Table 1.

The number of known polyoxometalates is very large and new species are being prepared even now[2,3]. The use of polyoxometalates (particularly polyoxomolybdates and polyoxotungstates) in catalysis is very diverse, including acid and redox catalysis, in homogeneous or heterogeneous conditions. This fact is directly related to the large variety of composition, structure and chemical behaviour of these anions, whose compounds are soluble in different solvents, depending on the chosen counter-cations.

TABLE 1 - Examples of polyoxometalates.

Type	Formula	Structure type
Isopolyoxoanion (IPA)	$[Mo_7O_{24}]^{6-}$, $[V_{10}O_{28}]^{6-}$	
	$[Nb_6O_{19}]^{8-}$	Lindqvist
Heteropolyoxoanion (HPA)	$[PW_{12}O_{40}]^{3-}$, $[CoW_{12}O_{40}]^{5-}$	Keggin
	$[Co(OH)_6Mo_6O_{18}]^{3-}$, $[TeMo_6O_{24}]^{6-}$	Anderson
	$[CeW_{10}O_{36}]^{8-}$, $[UW_{10}O_{36}]^{8-}$	Weakley
Mixed IPA	$[V_2W_4O_{19}]^{4-}$	Lindqvist
	$[Nb_3W_3O_{19}]^{5-}$	Lindqvist
Mixed HPA	$[PV_2Mo_{10}O_{40}]^{5-}$	Keggin
	$[SiMo_3W_9O_{40}]^{4-}$	Keggin

This chapter aims at giving a brief overview of some catalytic systems with polyoxometalates, developed in the last decades, for the oxidation of organic compounds in homogeneous conditions (excluding photocatalysis), and give the reader an insight on their potentialities.

Some types of polyoxometalates with importance in oxidative catalysis are represented in Figure 1 and Figure 2. Here are shown the parent Keggin and Wells-Dawson HPA, as well as the mixed anions (that is, anions with more than one type of addenda atoms) and related HPA that have metallic centres, like iron, manganese or other first-row transition metal. These have strong influence on the catalytic behaviour.
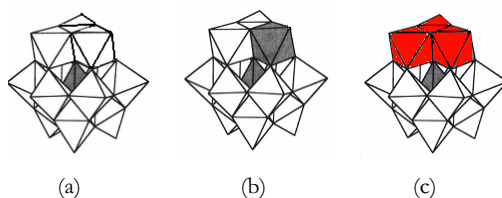
Figure 1 - Structure of some Keggin type polyoxometalates with importance in oxidative catalysis: (a) the α-isomer of the parent Keggin anion, like α-$[PW_{12}O_{40}]^{3-}$; (b) mono-substituted Keggin anion, like α-$[PW_{11}O_{39}Fe(H_2O)]^{4-}$, or mixed Keggin anion, like α-$[PMo_{11}VO_{40}]^{4-}$; (c) tri-substituted Keggin anion, like α-$[SiW_9O_{37}Fe_3(H_2O)_3]^{7-}$, or mixed Keggin anion, like α-$[PW_9V_3O_{40}]^{6-}$. The coloured octahedra correspond to the FeO_6 or VO_6 units. The central tetrahedron corresponds to PO_4 or SiO_4 groups. If the coloured octahedra are absent, structures (b) and (c) correspond to the mono- and tri-lacunary anions, like α-$[SiW_{11}O_{39}]^{8-}$ and α-A,B-$[PW_9O_{34}]^{9-}$, respectively.
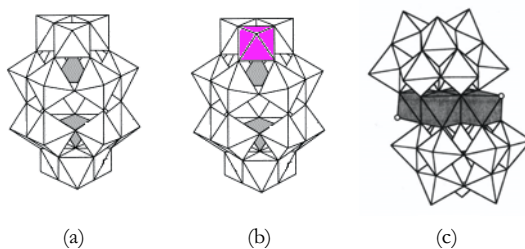
Figure 2 - Structure of some polyoxometalates related to the Keggin structure with importance in oxidative catalysis: (a) the parent Wells-Dawson anion, like α-$[P_2W_{18}O_{62}]^{6-}$; (b) mono-substituted Wells-Dawson anion, like α-$[P_2W_{17}O_{61}Fe(H_2O)]^{7-}$; (c) sandwich-type Baker-Figgis anion, like $[Fe_4(H_2O)_2(\alpha$-B-$PW_9O_{34})_2]^{6-}$. The coloured octahedra correspond to FeO_6 and the included tetrahedra to PO_4 groups. If the coloured octahedron is absent, structure (b) corresponds to the monolacunary anions, like α-$[P_2W_{17}O_{61}]^{10-}$.

5.2. PROPERTIES OF POLYOXOMETALATES RELEVANT TO CATALYSIS

By far, Keggin-type HPA constitute the most studied class of polyoxometalates for homogeneous or heterogeneous catalysis. This group, Figure 1, include the

α-isomers[i] of the parent Keggin anions, $[XM_{12}O_{40}]^{n-}$, the mono-lacunary, $[XM_{11}O_{39}]^{n-}$, and the mono-substituted anions $[XM_{11}O_{39}M'L]^{n-}$, among others (M = Mo, W; X = P, Si, B, etc.; M' = 1st row transition metal, Ru, etc., L = H_2O, OH^-, O^{2-}). The importance of Keggin-type HPA in catalysis is a consequence of a unique set of properties, which may be varied in a systematically controlled way by change of the composition, through choice of the heteroatom X or of the number and type of lacunae (in the case of lacunary anions, Figure 1) or substituting metals. The most relevant properties that are shared by many Keggin-type polyoxometalates are the following: high Bronsted acidity, thermal robustness, stability against oxidants, reversible redox reactions, solubility in different media, lability of lattice oxygen and photochemical reactivity. Secondary structure, that is, the three dimensional arrangement of polyoxoanions and cations in the solid, has also an important role in heterogeneous catalysis[4-7]. This structure is rather variable, depending upon the counter-cations, hydration degree and preparative conditions.

Keggin heteropolyacids, $H_n[XM_{12}O_{40}]\cdot aq$, are strong acids in aqueous solution and in the solid state, with the acidity varying in the series[5] $H_3PW_{12}O_{40}$ > $H_4PW_{11}VO_{40}$ > $H_4SiW_{12}O_{40}$ and $H_3PMo_{12}O_{40}$ > $H_5PMo_{10}V_2O_{40}$ > $H_4SiMo_{12}O_{40}$. In fact, the acid-base and redox properties of Keggin-type POM can be varied over a wide range by altering the chemical composition. The thermal stability of these anions also varies with the composition and occasionally with the counter-cations. The anions may be stable up to temperatures as high as 550ºC, depending on X and, slightly, on substituting metals. For example, tungstophosphates $[PW_{11}O_{39}]^{7-}$ and $[PW_{11}MO_{39}]^{5-}$, M = Mn, Co, Ni, Cu, as K^+ salts, are stable up to 450-500ºC, whereas $[PW_{11}FeO_{39}]^{4-}$ does not decompose until 550ºC. The same anions in tetrabutylammonium

---

[i] The prefix α- and others used for isomer identification will be omitted in this text from herein, except when relevant. For information on the isomerism of Keggin-type and related HPA, see ref [1].

salts decompose around 300ºC[8], originating the parent $[PW_{12}O_{40}]^{3-}$. The relative stabilities usually follow the order[9] tungstosilicates > tungstophosphates > tungstoborates. Heteropolyoxotungstates are thermally more stable than similar heteropolyoxomolybdates.

The solubility of the anions in different media is controlled by the counter-cations. Heteropolyacids and salts of Li^+, Na^+ and K^+ are water soluble, whereas Cs^+ and NR_4^+ salts do not dissolve in water, the latter being soluble in different organic solvents. Heteropolyacids are also soluble in many organic solvents.

Keggin-type anions are able to accept reversibly up to six electrons on the vanadium, tungsten or molybdenum atoms, and thus are potential oxidants[1,10]. Besides, in substituted HPA, oxidation or reduction of other metallic centres may occur. Electrochemical techniques have proved to be quite useful for the identification and characterisation of this type of anions and the knowledge of their electrochemical activity in different solvents may help to understand their behaviour as oxidative catalysts. Figure 3 shows typical cyclic voltammograms for the anion $[PW_{11}O_{39}Fe(H_2O)]^{4-}$ in two different solvents[11,12]. The number of redox processes identified and the values of the peak potentials are clearly dependent upon the solution media.

The electron-accepting properties of Keggin anion are important for oxidative catalysis when electron transfer mechanisms are predominant. In other cases, it is the lability of some oxygen atoms of the clusters and/or the possibility of being involved in complexation reactions that make them good catalysts for oxidation of organic compounds. The photochemical properties of Keggin anions have been explored in photocatalysis, but this is out of the scope of this chapter.

The set of characteristics just described for Keggin-type anions is extensive to many related anions, including Wells-Dawson[13] and sandwich species, Figure 2.

Obviously, not all of them are found for all polyoxometalates, but what has been described may be considered as a general trend.
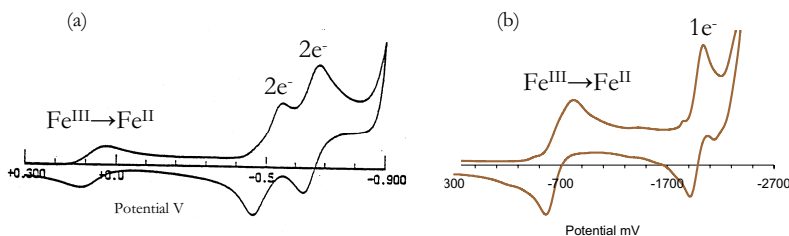
Figure 3 - Cyclic voltammograms at a glassy carbon working electrode of $[PW_{11}O_{39}Fe(H_2O)]^{4-}$ in different media[11,12]: (a) potassium salt in aqueous solution, pH 2.2 (1 mM solution, $HClO_4/NaClO_4$ supporting electrolyte and saturated Ag/AgCl as reference electrode); (b) tetrabutylammonium (TBA) salt in acetonitrile (10 mM solution, $TBAClO_4$ as supporting electrolyte and Ag/Ag^+ as reference electrode). The different waves correspond to processes occurring at the W atoms, except when indicated.

5.3. THE SYNTHESIS OF KEGGIN-TYPE AND RELATED POLYOXOMETALATES

Keggin type and related POM important for oxidative catalysis are generally prepared in aqueous solutions through simple reactions between species with the constituent atoms, at controlled stoichiometric proportion, reaction temperature and pH[1,9,13]. An example is shown in Figure 4. The possibility of being synthesised in large amounts from reagents commonly available is another advantage of this type of polyoxometalates. Different processes are used for isolation of solid compounds with these anions, depending on the chosen counter-cation. K^+ or Cs^+ salts usually precipitate from concentrated aqueous solutions. Alkylammonium salts may be precipitated by addition of a correspondent salt (like tetrabutylammonium bromide or chloride) to the aqueous solution of the anion or isolated from an organic phase using the alkylammonium salts as phase transfer agents. The specialized literature must

be consulted for each particular case. A few heteropolyacids and simple salts may be acquired from reagent suppliers.
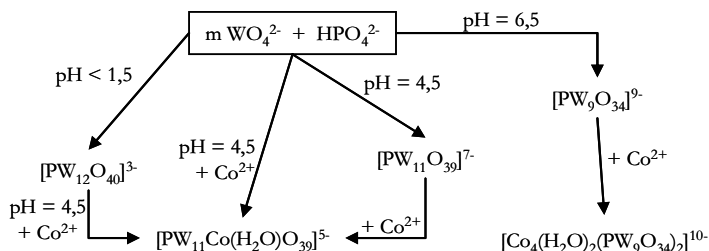
Figure 4 - Schematic representation of the synthesis of several related polyoxotungstates in aqueous solutions.

5.4. CATALYTIC APPLICATIONS OF POLYOXOMETALATES

Catalysis with polyoxometalates is a very important field of research that has been the subject of much work[14]. Keggin heteropolyacids and their simple salts have been used during the last thirty years in many types of homogeneous and heterogeneous catalytic systems, whereas new systems have been developed, more recently, with Wells-Dawson, sandwich, and poly-substituted Keggin anions. The roles of POM in catalysis have been reviewed extensively[4-7,14-25]. Several industrial processes based on catalysis with HPA have been developed and commercialized, namely the hydration of propene (1972), isobutene (1984) and *n*-butene (1985), the oxydation of methacrolein (1982), and the polymerization of tetrahydrofuran (1987)[26]. Finke[23] has compiled the 8 newer classes of polyoxoanion-based catalysts developed in the last 20 years or so, as presented in Table 2.

From herein, this chapter will be centred on oxidative homogeneous catalysis. A few systems will be referred, with no attempt to present a comprehensive review on the subject. The efforts to prepare supported catalysts derived from the homogeneous systems will be left aside. The readers will find information in the many reviews available[14-21,24,25].

TABLE 2 - Newer classes of polyoxoanion-based catalysts (adapted from reference[23]).

Catalyst type (catalytic reaction)	System composition
–Pseudo-liquid phase acid catalyst	$Cs_{2.5}H_{0.5}[PW_{12}O_{40}]$
–Wacker-type catalyst	$Pd^{2+/0}$, $[PMo_{12-n}V_nO_{40}]^{(3+n)-}$
–Mono-substituted polyoxoanion "Inorganic porphyrin analogs" (oxidations)	$[PW_{11}Mn^{III}O_{39}]^{4-}$, $[P_2W_{17}Mn^{III}O_{61}]^{7-}$ and others
–Multiple metal-substituted polyoxoanions (oxidation chemistry)	$[Co_4(H_2O)_2(PW_9O_{34})_2]^{10-}$ $[WZnRu_2(H_2O)_2(ZnW_9O_{34})_2]^{10-}$ $[PW_9Fe_{3-x}Ni_x(OAc)_3O_{37}]^{(9+x)-}$
–The Ishii-Venturello/H_2O_2 system (epoxidations)	$[(PO_4)(WO_5)_4]^{3-}$, other peroxocomplexes
–Solid state organometallic cation/non-basic polyoxoanion (hydroformylations)	$[L_3Rh(CO)(CH_3CN)_n]^{4+}$ $[SiW_{12}O_{40}]^{4-}$
–Basic-polyoxoanion-supported organo-metallics (oxidations)	$[(1,5-COD)Ir \cdot P_2W_{15}Nb_3O_{62}]^{8-}$ $[(CH_3CN)_nM^{II}/P_2W_{15}Nb_3O_{62}]^{7-}$ M^{II} = Fe, Co, Ni
–Polyoxoanion-stabilized $M(0)_n$ nanocluster "soluble heterogeneous catalysts"	$[Ir(0)_{\sim 300} \cdot (P_2W_{15}Nb_3O_{62})^{9-}]_{\sim 66}$

5.5. APPLICATIONS OF POLYOXOMETALATES IN OXIDATIVE HOMOGENEOUS CATALYSIS

5.5.1. Reaction types

The number of oxidative reactions catalysed by POM is fairly large and, due to the chemical and structural versatility of this class of anions, their role is not always understood. Reaction conditions seem to have a large influence on the outcome, and several oxidants and solvents have been used. Important reactions that have been studied include oxidation of alkanes (hydroxylation, dehydrogenation, etc.), epoxidation of alkenes and allylic alcohols, oxidation of

alcohols and other oxygenated organic compounds[15,17-19,24]. The three main general types of functions that POM may have in oxidative catalysis are listed in Table 3.

TABLE 3 - Types of reactive systems involving POM

A	Reaction of POM with the substrate	$Substrate + POM_{ox} \rightarrow Product + POM_{red}$ $POM_{red} + O_2 \rightarrow POM_{ox} + H_2O$
B	Reaction of POM with the oxidant	$Oxidant + POM \rightarrow [POM\text{-}Oxidant]_{activated}$ $[POM\text{-}Oxidant]_{activated} + Substrate \rightarrow$ $POM + Product$
C	Reaction at the POM substituting metal	$LM + Oxidant \rightarrow LM=O$ $LM=O + Substrate \rightarrow LM + Product$ L represents the lacunary POM

In systems type A (Table 3), the POM acts as an oxidizing agent, which is re-oxidized by O_2 or other oxidant to complete the catalytic cycle. Vanadium and molybdenum containing POM are usually used in this type of reactions. Systems type B rely on the activation of the oxidizing agent through any type of interaction with the POM. A variation of system type B occurs when the activation of the oxidant initiates a radical reaction. In systems type C, the activation of the oxidant takes place at the substituting metal of Keggin or Wells-Dawson type-anions or at the multi-metal "belt" of sandwich HPA. It should be noted that the mechanism of catalysis with POM is frequently unknown, notwithstanding the intense recent efforts. In addition, more than one type of reaction may take place in the same catalytic process. For example, if one substituted polyoxotungstate is used, the activation of the oxidising agent may take place at the substituting metal or at the W atoms. The oxidants most

used are, among others, O_2, H_2O_2, *tert*-butylhydroperoxide (TBHP) and iodosylbenzene.

5.5.2. Catalysis with vanadomolybdophosphates

Vanadomolybdophosphates $[PMo_{12-n}V_nO_{40}]^{(3+n)-}$, with n = 2-6 have been used since the work published around 1975 by Russian researchers. The HPA are mainly used as O_2-regenerable oxidants, in a process type A, Table 3. These are the catalysts used in the gas phase oxidation of methacrolein to methacrylic acid (heterogeneous catalysis) and have shown some success in the delignifying of wood pulp[18,19]. Many examples are found in the literature concerning homogeneous reactions catalysed by vanadomolybdophosphates, such as the oxidation of propane to isopropyl alcohol and acetone, dehydrogenation of α-terpinene to p-cymene, oxidation of 2-methylnaphthalene to a quinone, oxidative cleavage of 2-methylcyclohexanone yielding a ketoacid, oxidation of aldehydes to carboxylic acids, and oxidation of alkylphenols[18,19,27].

A system based on $[PMo_{12-n}V_nO_{40}]^{(3+n)-}$ and Pd^{2+}, Figure 5, developed for ethylene oxidation to acetaldehyde and propylene to acetone, functions analogously to the known Wacker system, with vanadium(V) having the same role as Cu^{2+} [18,19,28].
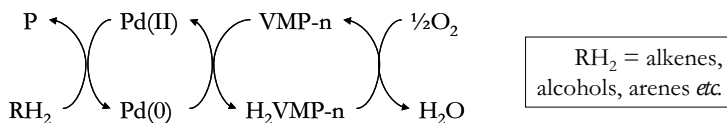
Figure 5 - Schematic representation of the Wacker type $Pd^{2+/0}$, $[PMo_{12-n}V_nO_{40}]^{(3+n)-}$ (VMP-n) oxidation system, known as the Catalytica system[18,28].

5.5.3. Catalysis with transition metal substituted polyoxotungstates

The interest on the use of Keggin and Wells-Dawson-type transition metal mono-substituted polyoxotungstates (TMSP) in oxidative catalysis started with the suggestion that they could be considered as metalloporphyrins (MP) analogues[29-31]. Both $[XW_{11}M(L)O_{39}]^{n-}$ and $[X_2W_{17}M(L)O_{61}]^{n-}$ may be described as metal complexes of a transition metal M with the mono-lacunary anions ($[XW_{11}O_{39}]^{n-}$ and $[X_2W_{17}O_{61}]^{n-}$) and L (usually water) as ligands. So, MP and TMSP have in common the fact that they are metal complexes that may have the metal in different oxidation states and that they may be dissolved in polar and non-polar media. As already referred, the polyoxotungstates are not prone to oxidative degradation and are easily prepared in large amounts and in good yield. This seemed to be advantageous in comparison to metalloporphyrins. Later, it was found that Keggin type polyoxometalates could be susceptible to degradation by reaction with H_2O_2, particularly in aqueous solutions, leading to the formation of tungsten peroxocomplexes.

The first studies were reported in the 1986-1989 period, with the anions $[PW_{11}M(H_2O)O_{39}]^{n-}$, M = Co, Mn, Fe, and others, and concerned the epoxidation of alkenes with iodosylbenzene, alkane oxidation with *t*-butylhydroperoxide and phenol oxidation with O_2 [29-31]. Early work was reviewed in 1995[17]. By and large, the studies of the catalytic oxidations with TMSP showed that the results depended on substrate, oxidant, solvent, catalyst and reaction conditions. An example, concerning the oxidation of cyclohexene[32], is shown in Figure 6. TMSP catalysed epoxidations have been continuously studied since then[17,19,25,33].

The oxidation of allylic alcohols, like geraniol, with H_2O_2 provided an interesting example of regioselectivity. Geraniol has two double bonds where epoxidation may occur, Figure 7, as well as the possibility of being involved in

allylic oxidation. In several conditions, reactions catalysed by mono- or multi-TMSP afforded the 2,3-epoxygeraniol as the main product[34,35].
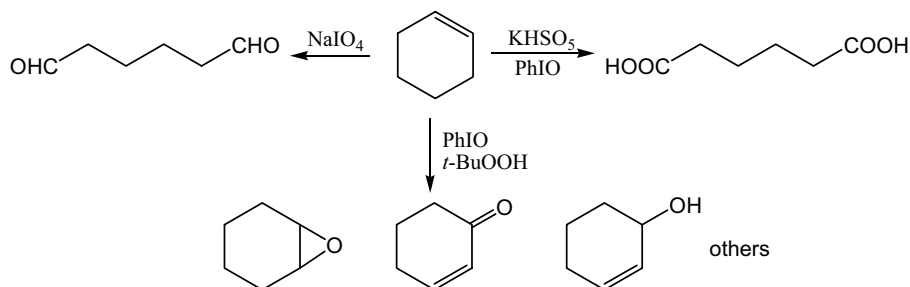
Figure 6 - Oxidation of cyclohexene with different oxidants in the presence of tetrahexylammonium salt of $[SiW_{11}Ru(H_2O)O_{39}]^{5-}$ in 1,2-dichloroethane (or 1,2-dichloroethane/water)[32].

Several studies on the oxidation of cyclohexane in the presence of mono-substituted Keggin-type anions are resumed in Table 4. The reaction products were cyclohexanol and cyclohexanone for all studies except those with H_2O_2 (last two lines of Table 4). In these cases, large amounts of cyclohexyl hydroperoxide were formed, in addition to cyclohexanol and cyclohexanone, when excess of oxidant was used. Similar results were obtained in the oxidation of cyclooctane[36,37].
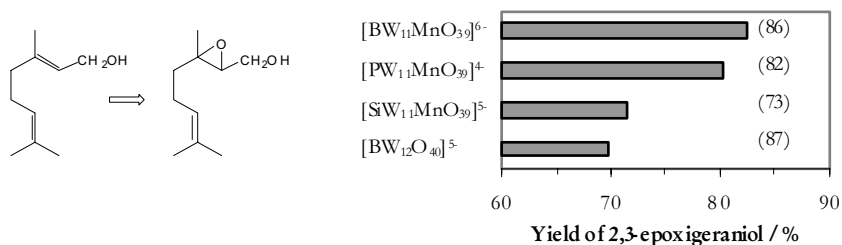
Figure 7 - Oxidation of geraniol by H_2O_2 in acetonitrile, after 3 h, at room temperature. Numbers in brackets indicate selectivity/% [34].

Not many systems have been developed for alkane oxidations using multi-substituted POM. The most studied are based on sandwich anions like $[WZnMn_2(ZnW_9O_{34})_2]^{12-}$ and others, which have been used in a large array of experiments with interesting results[19]. For instance, with this catalyst, cyclohexane was transformed into cyclohexanone with high selectivity, using O_3 as oxidant[45]. This and other examples[41,45-48] are presented in Figure 8.

TABLE 4 - Oxidation of cyclohexane with different oxidants in the presence of Keggin-type TMSP. For products, see text. (TON = turnover number).

Oxidant Solvent	Temp. ºC	Higher result	TMSP	Ref.
TBHP CH$_3$CN	65	TON= 30	$[PW_{11}MO_{39}]^{5-}$, M =Co, Mn, Cu, Fe	31
TBHP 1,2-dichloroethane	60	Conversion 23%	$[SiW_{11}RuO_{39}]^{5-}$	38
PhIO CH$_3$CN/CH$_2$Cl$_2$	20	Conversion 46%	$[PW_{11}MnO_{39}]^{5-}$	39
TBHP CH$_2$Cl$_2$/H$_2$O	22	Conversion 9%	$[PW_{11}RuO_{39}]^{5-}$	40
TBHP 1,2-dichloroethane	75	TON= 79	$[PW_{11}MnO_{39}]^{5-}$	41
TBHP Benzene	60	TON= 72	$[SiW_{11}MO_{39}]^{n-}$, M =Fe^{III}, Co^{II}, Ru^{III}, Rh^{III}	42
MCPBA CH$_3$CN	RT	Conversion 3 %	$[PW_{11}CoO_{39}]^{5-}$	43
H$_2$O$_2$ CH$_3$CN	80	TON= 352	$[PW_{11}MO_{39}]^{n-}$, M =Co^{II}, Mn^{II}, Fe^{III}	44
H$_2$O$_2$ CH$_3$CN	80	TON= 1307	$[BW_{11}MO_{39}]^{6-}$, M = Fe	36

Other studies on the functionalization of hydrocarbons and oxidation of other organic compounds catalysed by TMSP have been published and reviewed[13,17,19,24]. Different modes of reaction may take place, depending on reaction conditions and on the specific polyoxometalate used. Reactions of the POM with the oxidant, including those with the substituting metals, may give rise to radical formation, as noted before. TMSP are known to be involved in radical and in non-radical reactions. This may depend on the particular substituting metal, but also on the oxidant used. Globally, TMSP are potentially multifunctional catalysts.
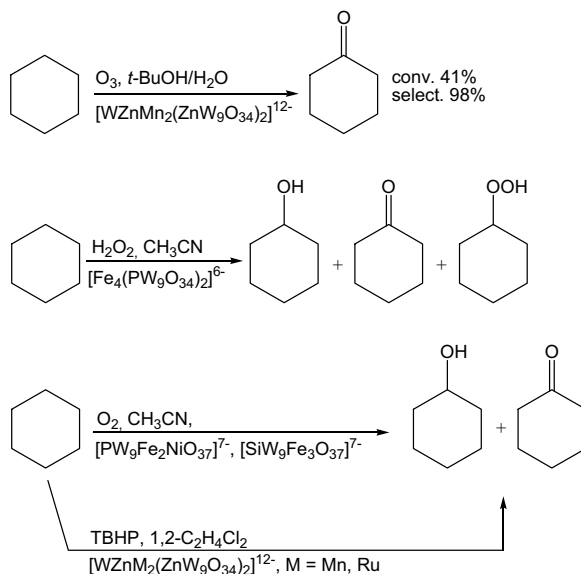
Figure 8 - Oxidation of cyclohexane in the presence of multi-TMSP[41,45-48].

5.5.4. Reactions with hydrogen peroxide and the Ishii-Venturello system

Hydrogen peroxide is a mild oxidant (E^o = 1,76 V in acid media), with high active oxygen content, that has many applications in the oxidation of organic compounds[49,50]. Hydrogen peroxide is considered to be very attractive, since

diluted aqueous H_2O_2 is comparatively cheap, environmentally clean (water is the only reaction product) and easy to handle. Nevertheless, it has a complex (and not always controllable) oxidation chemistry and low intrinsic reactivity, the same as with O_2. Frequently it requires some type of activation, Figure 9, and thus the need for a catalytic system. A drawback is the possibility of occurrence of dismutation, leading to its unproductive transformation into water and O_2 [50].

The use of H_2O_2 for oxidations catalysed by polyoxometalates started near thirty years ago[16,17]. One of the first systems studied was developed by Japanese researchers and was used in an array of oxidation reactions. Ishii and co-workers performed an enormous amount of research in a biphasic system, combining $H_3PW_{12}O_{40}$ with cetylpyridinium chloride as a phase transfer agent[18]. Later it was shown that the polyoxotungstate was only the catalyst precursor and that the active catalysts were one or more peroxotungstate complexes that formed in the reaction of $[PW_{12}O_{40}]^{3-}$ with H_2O_2. Among these, the so-called Venturello complex, Figure 10, was identified. The catalytic system is now called Ishii-Venturello, and is used in many reactions like epoxidations, alcohol oxidations, arene hydroxylations, etc.[18,25].
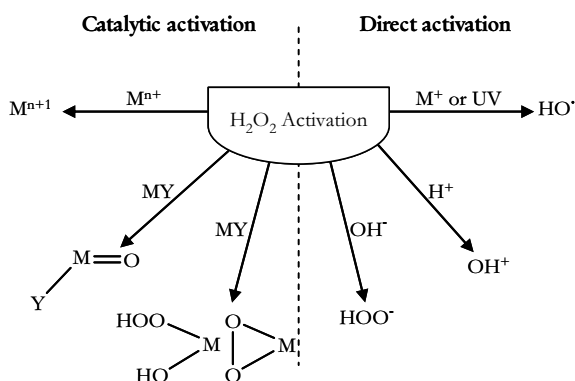
Figure 9 - Different types of activation of hydrogen peroxide[50].

In aqueous solution, TMSP like $[PW_{11}MO_{39}]^{5-}$, M =Co, Mn, Cu, are also prone to react with hydrogen peroxide to yield peroxotungstates, but this reaction usually does not occur in nonaqueous media. Care has thus to be taken in studies performed with this type of catalyst, with the need to control the amount of water in the reaction media and verify the stability of the polyoxometalates on an individual basis. This is particularly important when dealing with anions with P, which may be the real catalysts or just the catalyst precursors.

Reactions with hydrogen peroxide and Keggin-type polyoxotungstates are far from being understood, but provide interesting examples of the versatility of these anions. Iron(III)-substituted Keggin or sandwich anions have been used in the oxidation of cycloalkanes (through a radical process) with extensive hydroperoxidation occurring in reactions with excess of hydrogen peroxide[37,46]. Manganese(III) substituted POM are better catalysts for epoxidation reactions. Lacunary anions, nevertheless, were also found to be catalytically active in both type of oxidations, and the importance of the lacunae is now being recognised.

(a)

$$[PW_{12}O_{40}]^{3-} + H_2O_2 \xrightarrow[\text{water}]{pH = 2\text{-}4} [PO_4\{WO(O_2)_2\}_4]^{3-} \xrightarrow{\text{Phase transfer}} \text{Reaction media}$$

(b)
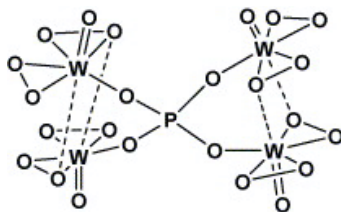
Figure 10 - Ishii-Venturello system: (a) Ishii reaction scheme; (b) structure of Venturello peroxocomplex.

350

5.6. A Few General Rules For The Use Of Polyoxometalates In Catalysis

So far, many papers have been published on catalytic studies with polyoxometalates, Figure 11, and several research lines have emerged from these studies. The possible combinations of POM/oxidant/reaction conditions are numerous and probably the work in this research area is going to continue, as the focus is changing for the need of more environmentally friendly systems, including reactions performed in aqueous solutions[14,24]. A few general rules for the use of polyoxometalates in catalysis may be indicated[20]. For acid catalysis, it is recommended to use a tungsten heteropolyacid and, if necessary, modify the acidity by alkali or alkaline-earth metal replacement of protons. For oxidative catalysis in liquid phase there are several choices. If the POM is to operate as an oxidant, a polyoxomolybdate, preferentially substituted by vanadium or other metal, should be used. The reduction potential variation is as follows V/Mo < Mo < W. For oxidations with peroxides and other oxygenation reactions, lacunary or metal substituted polyoxotungstate should be used. Finally, for heterogeneous oxidation catalysis in gas phase, it is necessary to consider the thermal stability of the anions.
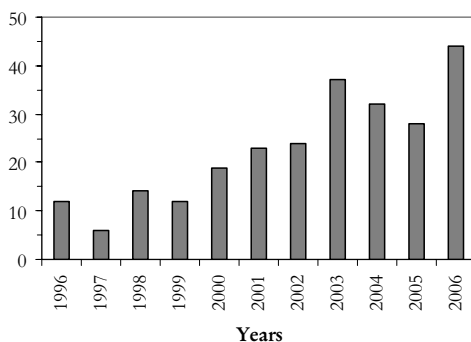
Figure 11 - Number of papers published each year between 1996 and 2006 (total 251). Data retrieved from ISI Web of Knowledge, with the keywords "polyoxometalate and catalysis".

Acknowledgements

References

_____

1. M.T. Pope, *Heteropoly and Isopoly Oxometalates*, Springer-Verlag, Berlin, **1983**.

2. M.T. Pope in *Comprehensive Coordination Chemistry II*, J.A. McCleverty, T.J. Meyer (Eds.), Elsevier, **2004**, pp. 635.

3. *Polyoxometalate Chemistry: From Topology via Self-assembly to Applications*, M.T. Pope, A. Muller (Eds.), Kluwer, Dordrecht, **2001**.

4. M. Misono, *Catal. Rev. Sci. Eng.*, **1987**, *29*, 269.

5. N. Mizuno, M. Misono, *J. Mol. Catal.*, **1994**, *86*, 319.

6. T. Okuhara, N. Mizuno, M. Misono, *Adv. Catal.*, **1996**, *41*, 113.

7. N. Mizuno, M. Misono, *Chem. Rev.,* **1998**, *98*, 199.

8. J.A. Gamelas, F.A.S. Couto, M.C.N. Trovão, A.M.V. Cavaleiro, J.A.S. Cavaleiro, J.D.P. Jesus, *Thermochim. Acta*, **1999**, *326,* 165.

9. A.M.V. Cavaleiro, J.D. Pedrosa de Jesus, H.I.S. Nogueira, in *Metal Clusters in Chemistry,* P. Braunstein, L.A. Oro, P.R. Raithbay (Eds.), Wiley-VCH, Weinheim, **1999**, vol. 1, pp. 444.

10. M. Sadakane, E. Stechhan, *Chem. Rev.*, **1998**, *98*, 219.

11. F.A.R.S. Couto, A.M.V. Cavaleiro, J.D.P. Jesus, J.E.J. Simão, *Inorg. Chim. Acta*, **1998**, *281*, 225.

12. M.S. Balula, J.A. Gamelas, H.M. Carapuça, A.M.V. Cavaleiro, W. Schlindwein, *Eur. J. Inorg. Chem.*, **2004**, 619.

13. L.E. Briand, G.T. Baronetti, H.J. Thomas, *Appl. Catal. A*, **2003**, *256*, 37.

14. C.L. Hill, *J. Mol. Catal. A*, **2007**, *262*, 2.

15. W.P. Griffith, *Trans. Met. Chem.*, **1991**, *16*, 548.

16. C.L. Hill, in *Catalytic Oxydations with Hydrogen Peroxide as Oxidant*, G. Strukul (Ed.), Kluwer, **1992**, pp. 253.

17. C.L. Hill, C.M. Prosser-McCartha, *Coord. Chem. Rev.*, **1995**, *143,* 407.

18. I.V. Kozhevnikov, *Chem. Rev.*, **1998**, *98,* 171.

19. R. Neumann, *Prog. Inorg. Chem.*, **1998**, *47*, 317.

20. F. Cavani, *Catal. Today*, **1998**, *41*, 73.

21. L.I. Kuznetsova, G.M. Maksimov, V.A. Likholobov, *Kinet. Catal.,* **1999**, *40,* 622.

22. T. Okuhara, N. Mizuno, M. Misono, *Appl. Catal. A*, **2001**, *222*, 63.

23. R.G. Finke, in *Polyoxometalate Chemistry: From Topology via Self-assembly to Applications*, M.T. Pope, A. Muller (Eds), Kluwer, Dordrecht, **2001**, pp. 363.

24. R. Neumann, *Modern Oxidative Methods*, in J. E. Bäckvall (Ed.) Wiley-VCH, Weinheim, **2004**, Chap. 8.

25. N. Mizuno, K. Yamaguchi, K. Kamata, *Coord. Chem. Rev.*, **2005**, *249*, 1944.

26. M. Misono, in *Polyoxometalates: From Platonic Solids to Anti-Retroviral Activity*, M. T. Pope, A. Muller (Eds), Kluwer, Dordrecht, **1994**, pp. 255.

27. A.M. Khenkin, R. Ben-Daniel, A. Rosenberger, I. Vigdergauz, R. Neumann, in *Polyoxometalate Chemistry: From Topology via Self-assembly to Applications*, M.T. Pope, A. Muller (Eds.), Kluwer, Dordrecht, **2001**, pp. 347.

28. J.H. Grate, D.R. Hamm, S. Mahajan, in *Polyoxometalates: From Platonic Solids to Anti-Retroviral Activity*, M.T. Pope, A. Muller (Eds.), Kluwer, Dordrecht, **1994**, pp. 281.

29. (a) D.E. Katsoulis, M.T. Pope, *J. Am. Chem Soc.*, **1984**, *106*, 2737; (b) D.E. Katsoulis, M.T. Pope, *J. Chem Soc., Chem. Commun.*, **1986**, 1186.

30. C.L. Hill, R.B. Brown, *J. Am. Chem. Soc.*, **1986**, *108*, 536.

31. M. Faraj, C.L. Hill, *J. Chem Soc., Chem. Commun.*, **1987**, 1487.

32. R. Neumann, C. Abu-Gnim, *J. Am. Chem. Soc.*, **1990**, *112*, 6025.

33. O.A. Kholdeeva, T.A. Trubitsina, M.N. Timofeeva, G.M. Maksimov, R.I. Maksimovskaya, V.A. Rogov, *J. Mol. Catal. A*, **2005**, *232*, 173.

34. (a) I.C.M.S. Santos, M.M.Q. Simões, M.M.M.S. Pereira, R.R.L. Martins, M.G.P.M.S. Neves, J.A.S. Cavaleiro, A.M.V. Cavaleiro, *J. Mol. Catal. A*, **2003**, *195*, 253; (b) M.S.S. Balula, Ph.D. thesis, University of Aveiro, **2003**.

35. W. Adam, P.L. Alsters, R. Neumann, C.R. Saha-Moller, D. Sloboda-Rozner, R. Zhang, *J. Org. Chem.*, **2003**, *68*, 1721.

36. I.M.S. Santos, M.S.S. Balula, M.M.Q. Simões, M.G.P.M.S. Neves, J.A.S. Cavaleiro, A.M.V. Cavaleiro, *Synlett*, **2003**, 1643.

37. M.S.S. Balula, I.C.M.S. Santos, M.M.Q. Simões, M.G.P.M.S. Neves, J.A.S. Cavaleiro, A.M.V. Cavaleiro, *J. Mol. Catal. A*, **2004**, *222*, 159.

38. R. Neumann, C. Abugnim, *J. Chem. Soc., Chem. Commun.*, **1989**, 1324.

39. D. Mansuy, J.F. Bartoli, P. Battioni, D.K. Lyon, R.G. Finke, *J. Am. Chem. Soc.*, **1991**, *113*, 7222.

40. M. Bressan, A. Morvillo, G. Romanello, *J. Mol. Catal.,* **1992***, 77*, 283.

41. R. Neumann, A.M. Khenkin, *Inorg. Chem.* **1995**, *34*, 5753.

42. Y. Matsumoto, M. Asami, M. Hashimoto, M. Misono, *J. Mol. Catal. A*, **1996**, *114*, 161.

43. W. Nam, S.J. Yang, H. Kim, *Bull. Korean Chem. Soc.*, **1996**, *17,* 625.

44. M.M.Q. Simões, P.M.D.N. Domingues, A.M.V. Cavaleiro, J.A.S. Cavaleiro, A.J. Ferrer-Correia, R.A.W. Johnstone, *J. Mol. Catal. A*, **1999**, *144*, 461.

45. R. Neumann, A.M. Khenkin, *Chem. Commun.,* **1998**, 1967.

46. I.C.M.S. Santos, J.A.F. Gamelas, M.S.S. Balula, M.M.Q. Simões, M.G.P.M.S. Neves, J.A.S. Cavaleiro, A.M.V. Cavaleiro, *J. Mol. Catal. A*, **2007**, *262*, 41.

47. N. Mizuno, C. Nozaki, T. Hirose, M. Tateishi, M. Iwamoto, *J. Mol. Catal. A,* **1997**, *117*, 159.

48. N. Mizuno, *Catal. Surv. Jpn.*, **2000**, *4,* 149.

49. *Catalytic Oxidations with Hydrogen Peroxide as Oxidant*, G. Strukul (Ed.), Kluwer, Dordrecht, **1992**.

50. C.W. Jones, *Applications of Hydrogen Peroxide and Derivatives*, Royal Society of Chemistry, RSC Clean Technology Monographs, Cambridge, **1999**.

6. Carbon-Carbon Bond Formation Mediated By Palladium(0)

Maria da Graça P. M. S. Neves, Mário M. Q. Simões and J. A. S. Cavaleiro

Chemistry Department, University of Aveiro, 3810-193, Aveiro.

6.1. Introduction

Nowadays it is difficult to find any organic chemistry journal that does not refer synthetic methodologies involving the use of catalysts or reagents based on transition metal compounds. Many reactions, known to be impossible to achieve by traditional synthetic methodologies, have been developed using such complexes. It is widely recognized that palladium is one of the most versatile transition metals for promoting or catalyzing some organic reactions and can be used either in the Pd(0) or Pd(II) oxidation state. While Pd(II) compounds are utilized as stoichiometric reagents or catalysts, Pd(0) is always used as catalyst[1-3].

In this chapter, a brief view of the principal cross-coupling reactions mediated by palladium(0) involving carbon-carbon bond formation will be presented and discussed.[1-3] The application of those reactions on the synthesis of natural compounds with pharmacological interest and on fine chemical synthesis will highlight the actuality, potentiality and the versatility of palladium(0).

Palladium, recognized as an important metal of the 21st century, was isolated from platinum and identified as a separate elemental metal in 1803 by William Hyde Wollaston[4]. This brilliant researcher made important contributions to several fields of science such as astronomy (the dark lines in the solar spectrum, a crucial tool in stellar astronomy today), biochemistry (he discovered cystine, the first amino acid), physiology (he was the first to postulate that human hearing is limited to certain frequencies) and physics (in atomic theory and

crystallography). He even had an island in the Arctic named after him, in recognition of a navigational instrument he invented.

However, the attitude of Wollaston concerning the isolation of palladium suffered a great criticism by the scientific community - thinking on its commercial value he decided not to announce how to do it. On that time, this kind of attitude was considered not to be very correct and even called in question the existence of the new metal. During years he made and sold the metal and only revealed how to do it just before his death in 1826. Nonetheless, the importance of this achievement was recognized, with the Royal Medal from the Geological Royal Society awarded to Wollaston.

6.2. CATALYTIC CYCLE MEDIATED BY Pd (0)

The fundamental reactions of transition metal complexes[2] to be considered here are summarized in Scheme 1. All the catalytic processes start with Pd(0) species, which then reacts with organic halides (or pseudohalides) R-X by an oxidative addition process affording R-Pd(II)-X intermediates. These intermediates, depending on the reaction conditions, can react with organometallics (*via* transmetallation, sequence **A**) or with unsaturated compounds (*via* insertion, sequence **B**) affording easy accesses to new compounds. The regeneration of Pd(0) occurs in both cases after a reductive elimination step. These palladium catalyzed reactions are generally tolerant to a wide range of functionalities and therefore can be used on the synthesis of complex organic molecules.

Pd(0)

reductive elimination
R-R´´(H)

H-X
reductive elimination

R-X
oxidative addition

H-Pd-X

$C=C$
R

β-elimination

(A)
transmetallation

R-Pd-R´´(H)

R-Pd-X

$C=C$
H

insertion
(B)

$R-C-C-Pd-X$
H

M'-X

M'-R''
M'-H

Scheme 1
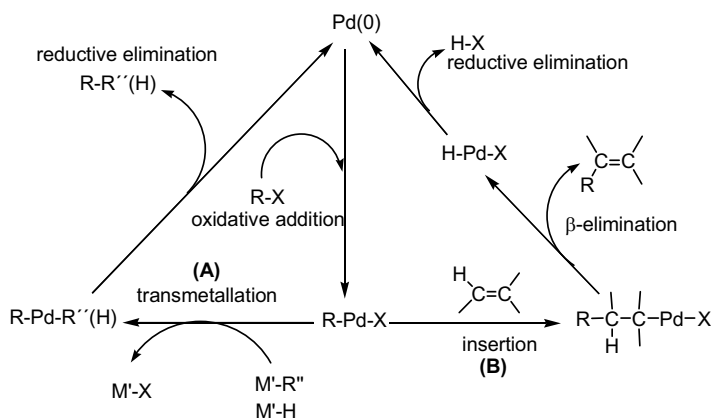
6.2.1. The catalyst

6.2.1.1. Palladium(0) Sources

The most common sources of palladium(0) complexes are the commercially available tetrakis(triphenylphosphine)palladium(0), $Pd(PPh_3)_4$ and DBA (dibenzylidene-acetone) complexes of palladium(0), like $Pd_2(dba)_3(dba)$ and $Pd_2(dba)_3(CHCl_3)$; in the latter ones each Pd is coordinated with three olefinic double bonds, Figure 1, and the other molecule of DBA or $CHCl_3$ is not directly connected to the metal. The complexes with DBA can be used to prepare other palladium-phosphine complexes by a ligand exchange reaction. The structures of other phosphines commonly used as ligands in those complexes are also shown in Figure 1.
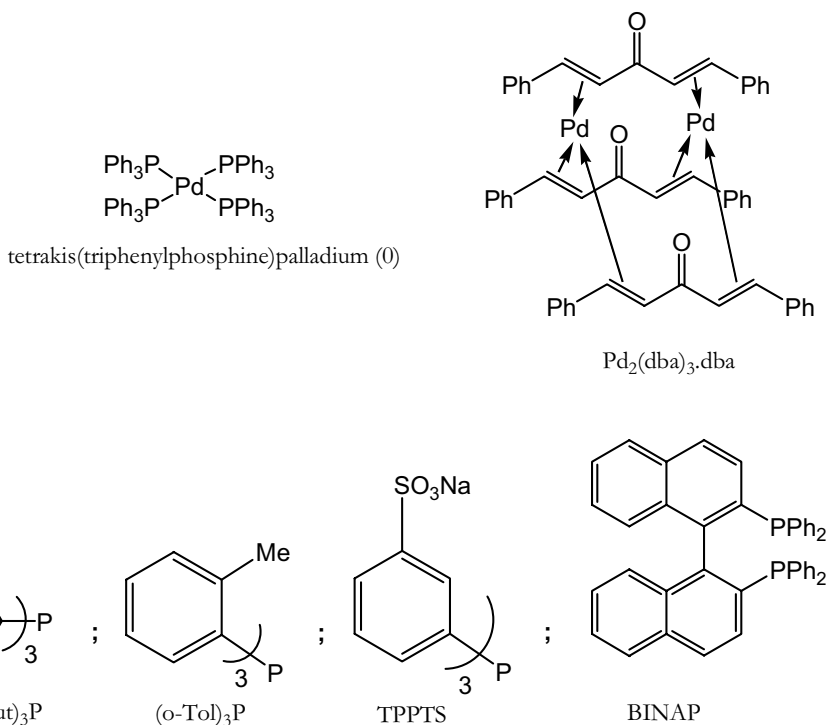
Figure 1 - Structures of commercially available Pd(0)-phosphine complexes and of other phosphines that are also used as ligands in those complexes.

6.2.1.2. *In situ* formation of Pd(0) by reduction of Pd(II)

Frequently, in reactions requiring Pd(0), the formation of the active complex may be achieved more conveniently by reduction of a soluble Pd(II) complex like $(PhCN)_2PdCl_2$, $(MeCN)_2PdCl_2$ or $Pd(OAc)_2$, without the need to synthesize and isolate the corresponding Pd(0) complex. The reduction of Pd(II) to Pd(0) can be achieved with amines, phosphines, alkenes and organometallics. Scheme 2 illustrates how this reduction process occurs in the presence of an amine or an alkene[5].

$$\overset{II}{Pd}L_2X_2 + Et_3N \xrightarrow{\text{ligand exchange}}$$

Scheme (top):

$\overset{II}{Pd}L_2X_2 + Et_3N \xrightarrow{\text{ligand exchange}}$ [iminium intermediate with H, $\overset{II}{Pd}L_2X$, N with Et, Et, and $X^{\ominus}$]

$\downarrow$ -hydride elimination

$HX + \overset{0}{Pd}L_2 \xleftarrow{\text{reductive elimination}} H\overset{II}{Pd}L_2X$

Scheme 2:

$\overset{II}{Pd}L_2X_2 \xrightarrow[{=\!=}]{\text{ligand exchange}} \overset{II}{Pd}LX_2 \xrightarrow[{=\!=}\ \ L]{\text{migratory insertion and association}}$ [Pd complex with X, X, H, L, L]

-hydride elimination

$HX + \overset{0}{Pd}L_2 \xleftarrow{\text{reductive elimination}} H\overset{II}{Pd}L_2X$ and vinyl–X

Scheme 2

More recently, catalysts known as palladacycles[6] (Figure 2) were developed and are recognized as very efficient in the activation of poor reactive halides.
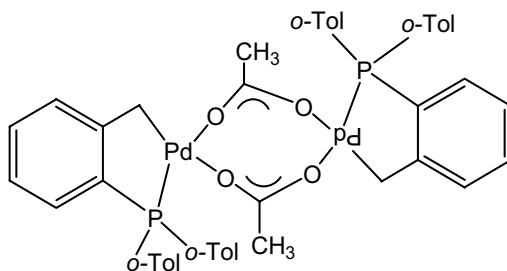
Figure 2 - Structure of a palladacycle catalyst.

359

6.2.2. Some Reactions Catalysed by Pd(0)

6.2.2.1 Mizoroki-Heck or Heck reaction: Cross coupling with alkenes

The cross-coupling of organic halides with alkenes in the presence of catalytic amounts of Pd(0) and a base to afford new alkenes, Scheme 3, was reported independently by Mizoroki and Heck, but this reaction is usually known as the "Heck reaction"[1-3,5].

X=I, Br, (Cl), OSO$_2$CF$_3$ (triflate), N$_2^{\oplus}$, COCl, SO$_2$Cl

[Pd]=Pd(0) - phosphine complexes
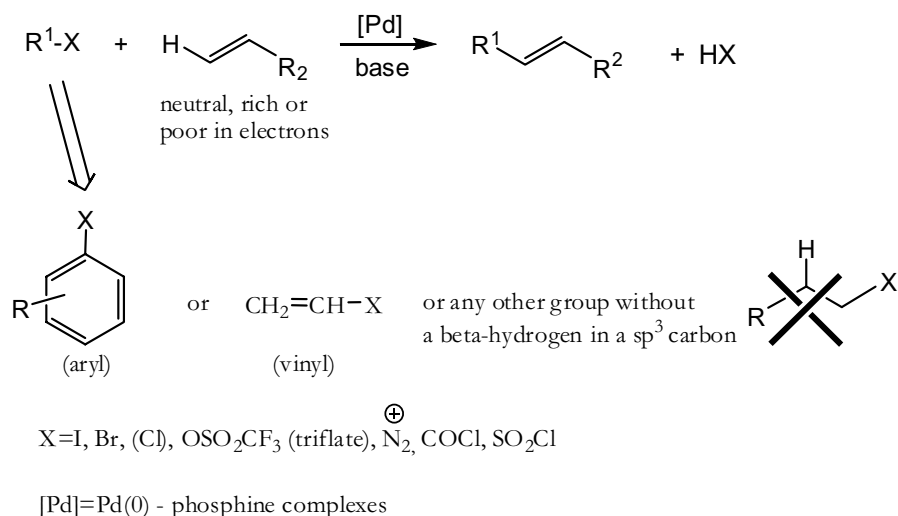
Scheme 3

In these reactions the alkene can be neutral, rich or poor in electrons, but the best selectivities are obtained with electron-poor alkenes. The R^1 group generally adds to the least hindered end and the formation of the *E*-alkene is thermodynamically favoured. With electron-rich alkenes the R^1 group adds to both ends, but a good control on the selectivity can be achieved with cyclic enolethers/enamines where the addition of R^1 group occurs next to the heteroatom. The organic halides are usually of the aryl, heteroaryl or alkenyl

types, but other groups can be used if a beta-hydrogen is not present in a sp^3 carbon.

As it was referred above, all these reactions start with an oxidative addition of the halide to Pd(0), which is favoured by the increase of the electron density on palladium. The usually observed rate of oxidative addition with C_{aryl}-halogen bonds increases according to the following order: C-F < < < C-Cl < < C-Br < C-I (with fluorides being almost inert). In the Heck reaction, pseudohalides like diazonium salts, triflates, aroyl halides and aroyl anhydrides (after decarbonylation under certain conditions) and sulfonyl halides (with evolution of SO_2) can also be used as the R^1-X component. These pseudohalides usually undergo facile oxidative addition to Pd(0) complexes.

The Heck reactions are usually performed in aprotic solvents like dimethylformamide, dimethylacetamide or dimethyl sulfoxide and the conditions used (such as the time and temperature) are related with the reactivity of the halide. The bases used to neutralize the hydrogen halide formed during the C-C coupling can be triethylamine, sodium acetate or aqueous sodium carbonate. The catalyst (1-5 mol%) can be one of the Pd(0) phosphine complexes referred above or can be obtained *in situ* by reduction of a salt of Pd(II) in combination with a phosphine.

The two examples shown in scheme 4 reflect some of the comments just mentioned about the Heck reaction, namely the use of Pd(AcO)$_2$ for the *in situ* formation of Pd(0), the addition of the R^1 group to the least hindered end of the double bond and the formation of the *E*-alkene.
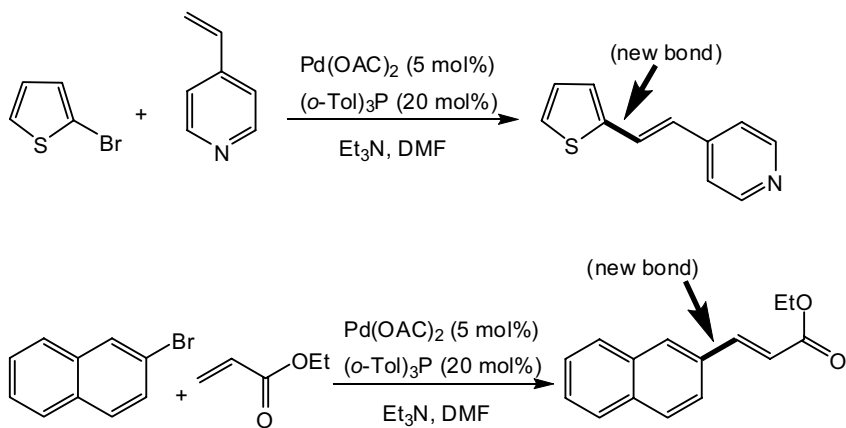
Scheme 4
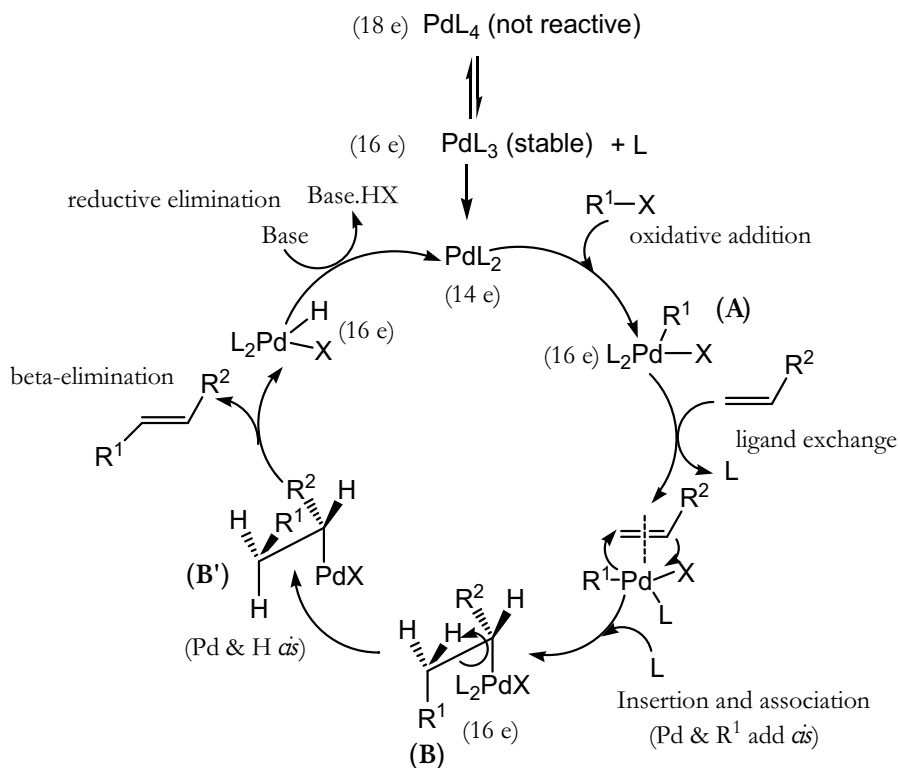
Scheme 5

The mechanism of the Heck reaction is usually explained through the general path **B** shown in Scheme 1. A more detailed analysis of the catalytic cycle, Scheme 5, can easily justify why the formation of the *E*-alkene is preferential. After the oxidative addition of the organic halide R^1-X to Pd(0), the insertion of the alkene into the intermediate R^1-X-Pd occurs in a *syn* fashion (intermediate B). For the beta-elimination to occur from this intermediate, in order to provide the new alkene, the beta-hydrogen must be *syn* and coplanar to the Pd atom, and an eclipse conformation with the bulky groups in a transoid situation must be adopted (conformation B').

The potentiality of the Heck reaction in the production of fine chemicals was explored by Hoechst AG and Hoechst Celanese in the synthesis of Naproxen using palladacycles as catalysts, Scheme 6. Albermarle has been also exploring this reaction on the synthesis of the same drug but using other catalyst[7,8]. This important non-steroidal anti-inflammatory drug acts by reducing the levels of the prostaglandin cyclooxygenase, one of the chemicals responsible for pain, fever and inflammation.

Scheme 6

363
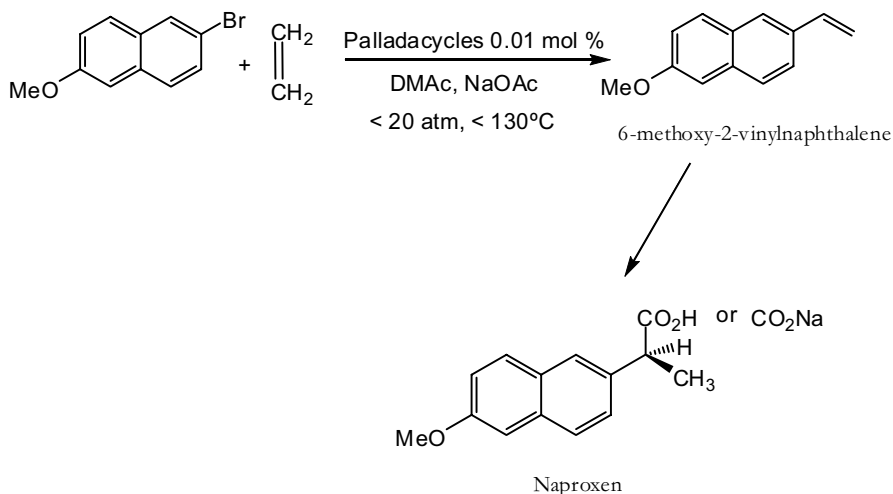
Other chemicals, like the sun-screen agent octyl *p*-methoxycinnamate, the anti-asthma agent Singulair, the anti-migraine drug Elitripan and LTD$_4$ receptor antagonists are also being produced by the industry using the Heck approach[7,8].
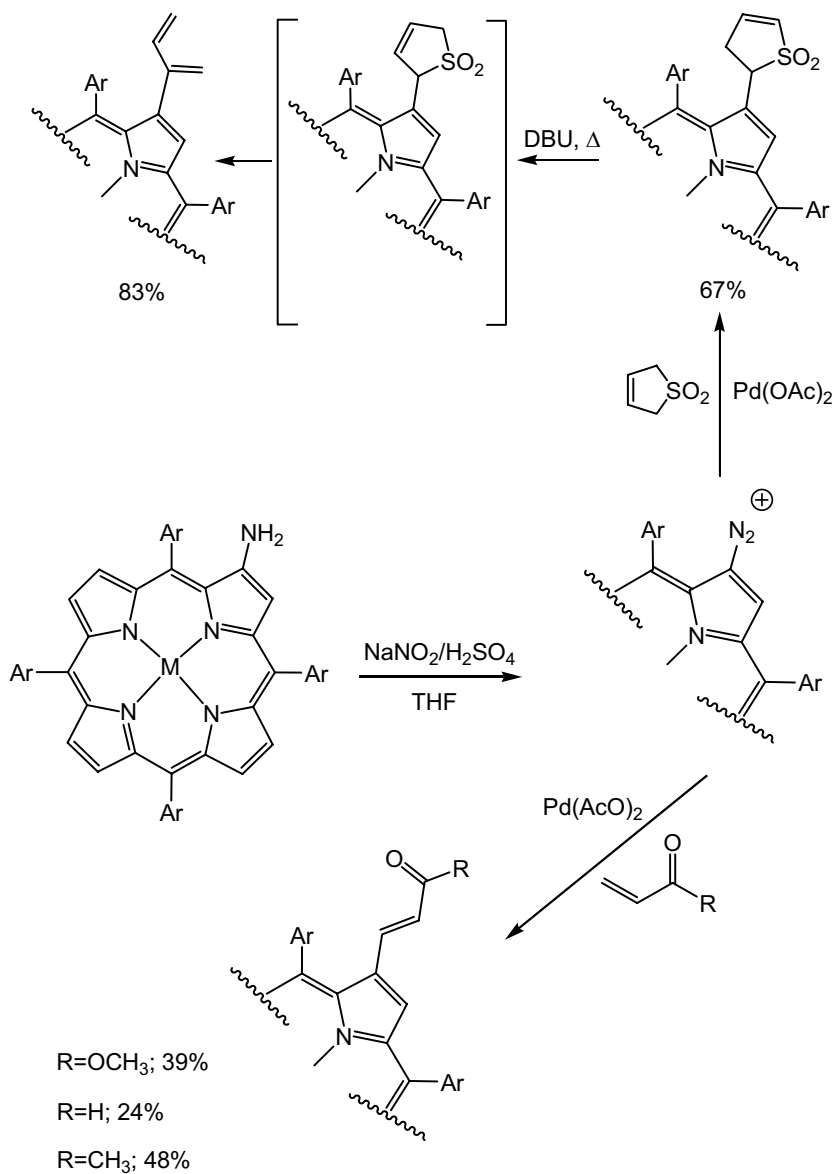
Scheme 7

However, it is recognized that the number of commercial applications is still very small. This weakness can be justified by: (i) the high price of palladium; (ii) the decomposition of conventional catalysts at high temperatures (palladacycle catalysts can be a solution for this problem, since they are much more stable than Pd-phosphine complexes and can be used at higher temperatures); (iii) the most reactive reagents like iodides and triflates are expensive; (iv) the activation of the more accessible chloroaromatics requires special Pd catalysts (more reactive); (v) recycling the catalyst and the salt waste are problems that still require solution.

The possibility of using pseudohalides, like diazonium salts, in Heck reactions, was explored for the first time in the field of porphyrins by the Aveiro group, Scheme 7. With this approach a beta position of *meso*-tetraphenylporphyrin was functionalised with unsaturated substituents and the porphyrin containing the diene system was used as precursor in the preparation of novel porphyrin-phthalocyanine dyads[9,10].

6.2.2.2. Cross-coupling with organometallic compounds

Palladium(0) also catalyses the coupling of halides or pseudohalides with organometallic compounds of the main group metals such as Mg, Zn, B, Al, Sn, Si or Hg, Scheme 8[1-3,5].

The features of R^1 - X are analogous to those described for the Heck reaction, an aryl or alkenyl halide or pseudohalide, but other groups can be used if a beta-hydrogen in a sp^3 carbon is absent. The R^2 component in the organometallic compounds can be any group, even with a beta-hydrogen. These reactions, depending on the organometallic used, are usually identified by the name of the principal authors responsible for their development: the Tamao-Kumada-Coriu reaction, when M=MgX (nickel is used more often than

Pd), the Negishi reaction, when M=ZnX, the Migita-Kosugi-Stille reaction or just Stille reaction, when M=SnR$_3$ or the Suzuki-Miyaura coupling when M=B(OR)$_2$. The catalyst can be one of the phosphine complexes of Pd(0) referred above or can be obtained *in situ* by the reduction of a Pd(II) salt in combination with a phosphine.

$R^2 =$ any group, even with a beta-hydrogen

M $=$ MgX, ZnX, SnR$_3$, B(OR)$_2$, SiR$_3$, Cu, ZrCp$_2$Cl, AlMe$_2$, etc.

$$R^1\text{-}X \quad + \quad R^2\text{-}M \quad \xrightarrow{\text{Pd(0)}} \quad R^1\text{-}R^2 \quad + \quad M\text{-}X$$

or any other group without a beta-hydrogen in a sp^3 carbon

X $=$ I, Br, (Cl), OTf, OPO(OR)$_2$, others
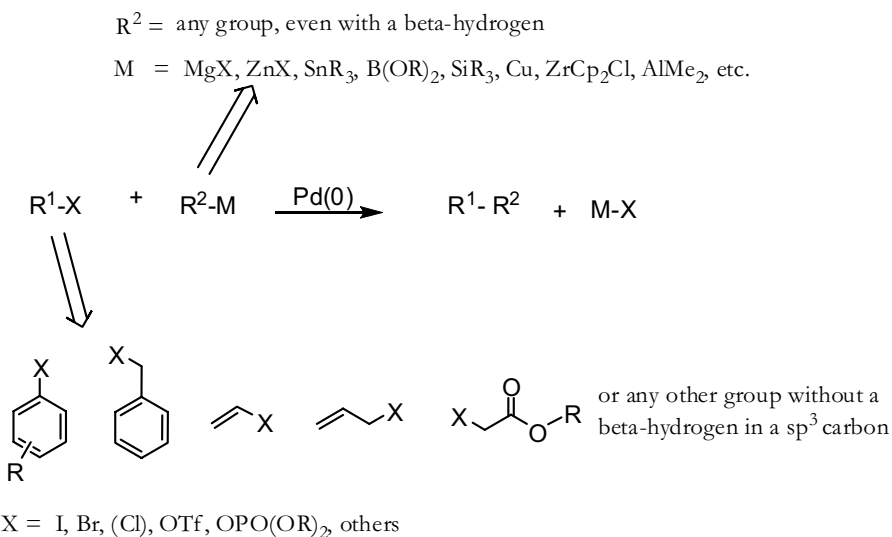
Scheme 8

The mechanism of all these processes (Scheme 1, *via* **A**) starts with an oxidative addition, followed by transmetallation and then a reductive elimination, Scheme 9.
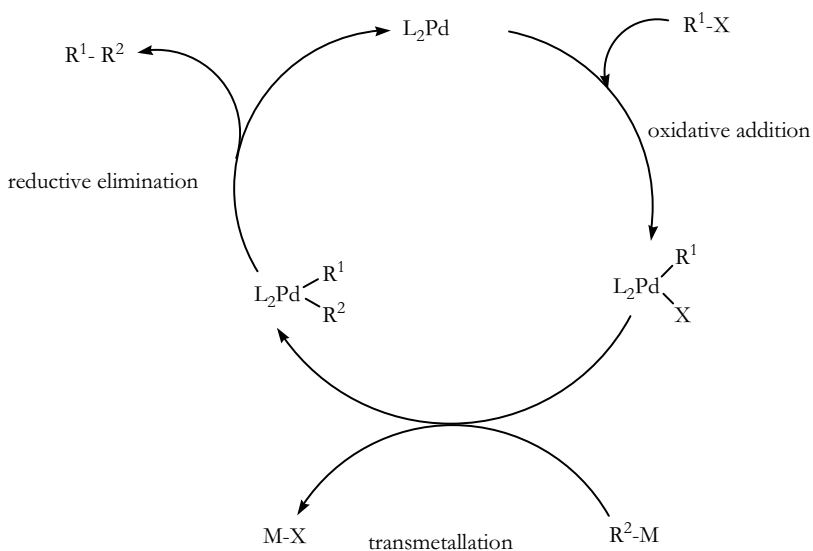
Scheme 9

Some simple examples of compounds that can be prepared by this type of crossing coupling reactions[2] are shown in Scheme 10. The new C-C bonds formed are highlighted.
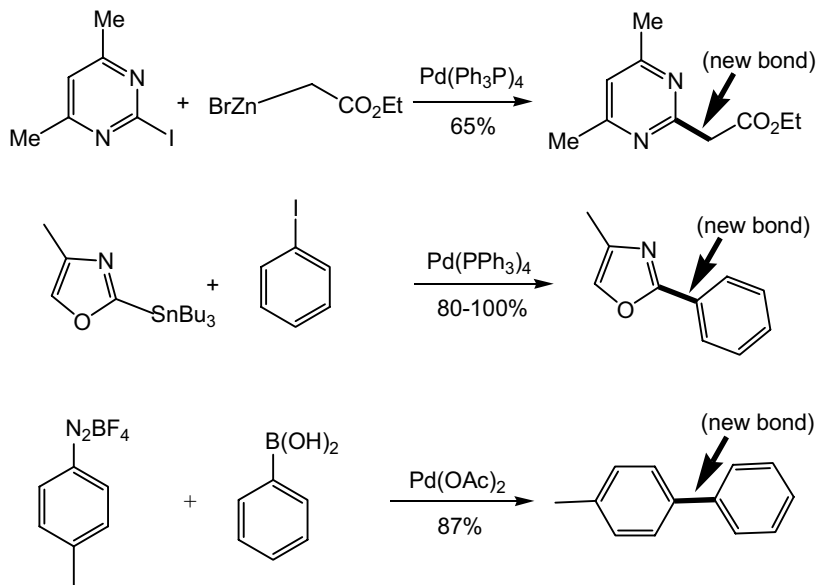
Scheme 10

In the case of the Stille reaction (Scheme 10, second reaction) a pertinent question that arises is: why is the heteroaryl group transferred and not the butyl group? This is related with the rate of transfer of those groups from Sn to Pd, usually easier in the following order:

$$RC\equiv C > RCH=CH > Ar > CH_2=CHCH_2 > ArCH_2 > \text{alkyl groups}$$
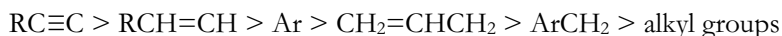
So, alkyl groups are only transferred if other groups are not present.

The tolerance of the organo-zinc, -tin and -boron compounds to a wide range of functional groups and the efficiency of these reactions offer unique conditions that have been largely explored by many research groups working on the complex chemistry of natural compounds.

For example, in the total synthesis of Macrolactin A, a macrolactone isolated in 1989 from a deep-sea coring bacterium with interesting pharmacological properties,[i] the Stille reaction was used in inter and intramolecular steps as it is exemplified in Scheme 11[11,12].

---

[i] Preliminary studies showed high inhibition of HIV replication in T-lymphoblast cells, high activity against a variety of multi-resistant gram-positive and gram-negative pathogens and strong growth inhibiting effect on vancomycin-resistant enterococci and methicillin-resistant *Staphylococcus aureus*.

OH

TBSO

TBSO

+ Bu₃Sn

OPiv

PdCl₂(MeCN)₂

DMF, 82%

OH

TBSO

TBSO

OPiv

(new bond)

OMOM

SnBu₃

O

I

O

MeO

MeO

Pd₂(dba)₃, AsPh₃

DMF, 60 ºC, 58%

(new bond)

OMOM

MeO

MeO

O

O

OH

HO

HO

(-)-Macrolactin A

O

O

Scheme 11

369
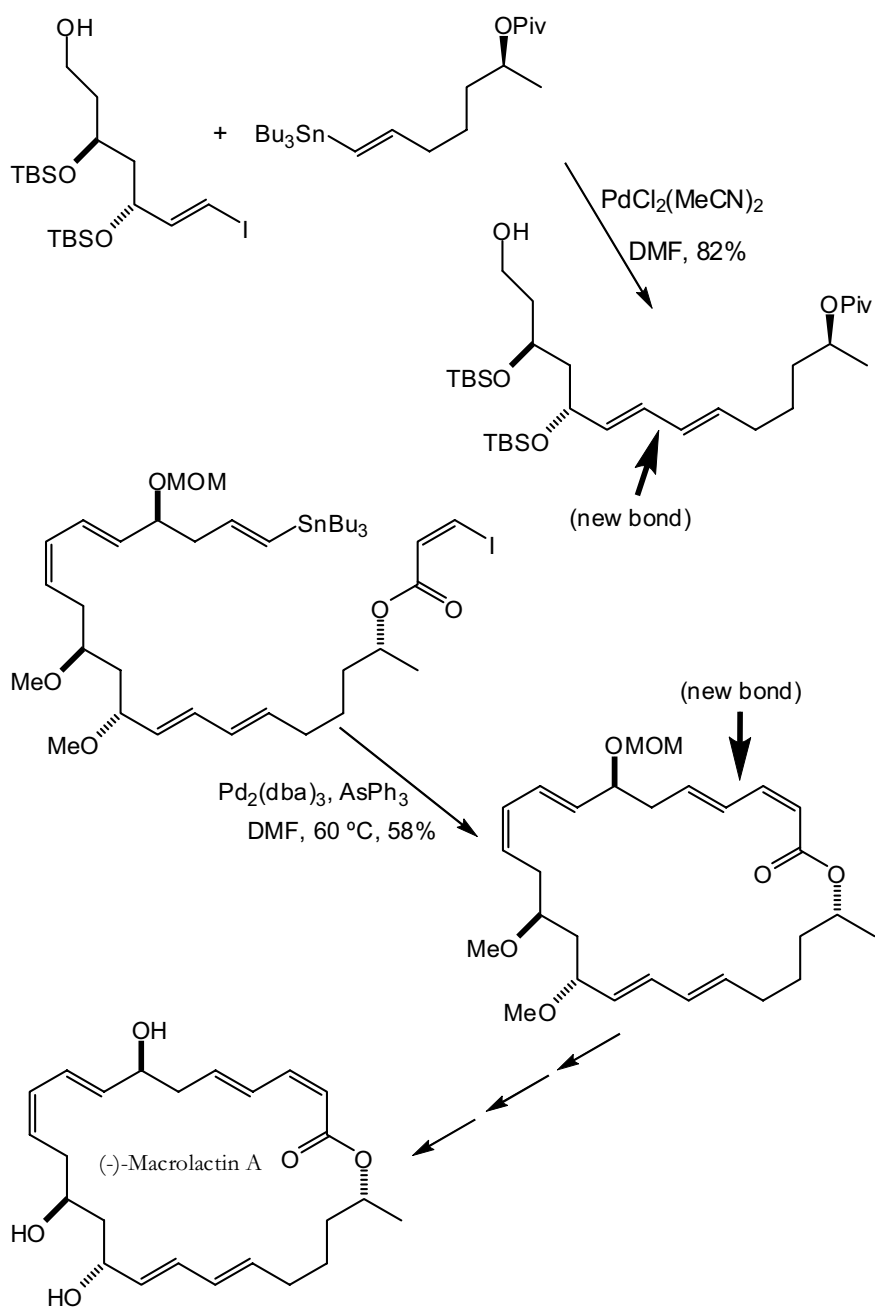
It is recognized that the Suzuki coupling, despite the multistep synthetic approaches usually required for the synthesis of the boronic acids, has some advantages when compared with the other approaches using organometallic reagents: i) lower toxicity of the complexes and of the by-products; ii) tolerance of a broader range of functional groups. Therefore, this coupling is being explored not only by academic researchers but also by industry, namely in the production of advanced materials by Dow, Sigma-Aldrich and Merck. Novartis and BASF are using this approach on the synthesis of Valsartan, an antihypertensive drug, and of Boscalid, a fungicide, respectively, Scheme 12[8,13].

Valsartan (Novartis)   Boscalid (BASF)
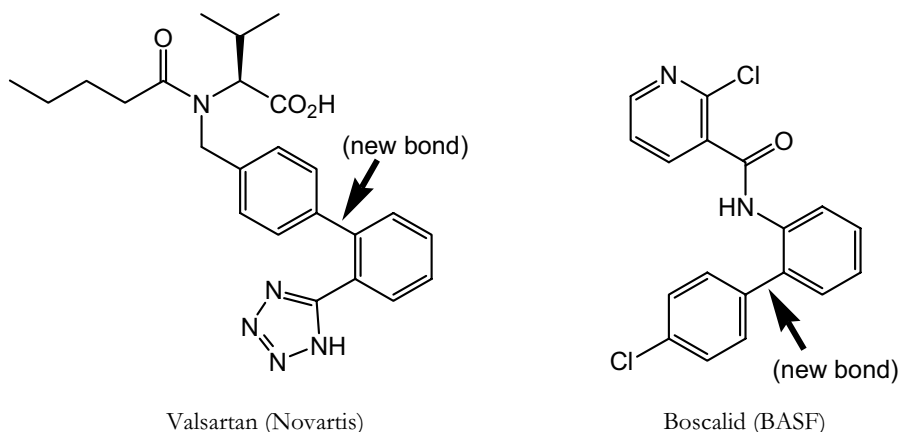
Scheme 12

6.2.2.3. The cross-coupling with terminal alkynes

Palladium(0) is also very efficient in the coupling of organic halides with terminal alkynes and this transformation is known as the Sonogashira reaction. These reactions are usually performed in the presence of a copper(I) salt and a base, Scheme 13. Organic halides are usually of the aryl or alkenyl type, affording respectively arylalkynes or conjugated enynes. Interestingly, in these reactions alkenyl chlorides react smoothly without any special conditions[1-3,5].

R^1-X + ≡—R^2 $\xrightarrow[\text{base, CuI}]{\text{[Pd]}}$ R^1—≡—R^2

X=I, Br, (Cl), OSO$_2$CF$_3$ (triflate)

[Pd]=Pd(0) - phosphine complexes

R—⬡—X   or   CH$_2$=CH-X

(aryl)   (vinyl)
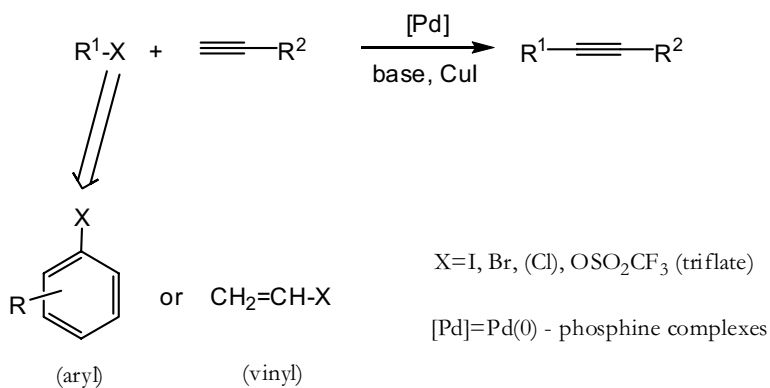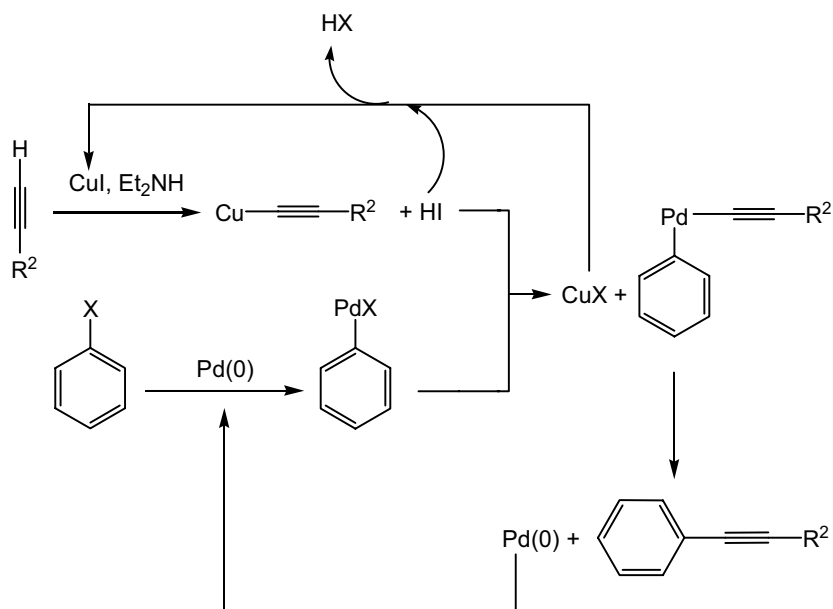
Scheme 13

Scheme 14

The mechanism of the reaction, Scheme 14, is similar to the mechanism of the cross-coupling with organometallic compounds after the generation of the alkynyl copper (terminal alkynes are acidic) obtained in the presence of the co-catalyst and the base.

The conditions used in the Sonogashira coupling reaction are very mild and thermally sensitive substrates can be used. When alkenyl halides are used, the configuration of the double bond is maintained and the coupling can be carried out in a stepwise methodology,[5] Scheme 15. This approach is being explored in the synthesis of intermediates of enediyne antibiotics, well known as potential anticancer compounds,[2] Scheme 16.
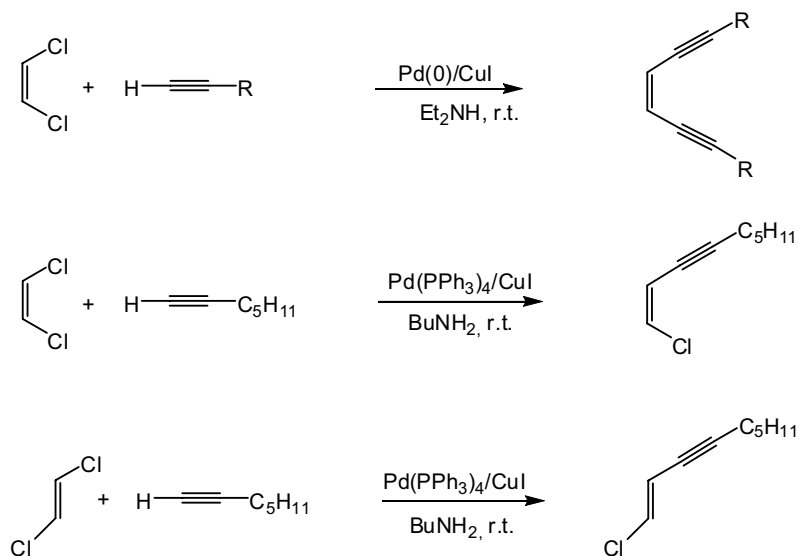
Scheme 15

Sandoz is using the Sonogashira reaction on an industrial scale for the synthesis of Terbinafin, Scheme 17, the active substance of the antimycotic Lamisil[8]. Palladium(0) is generated *in situ* and the reaction occurs with high stereoselectivity (the configuration of the double bond is maintained).

Scheme 16

Terbinafin
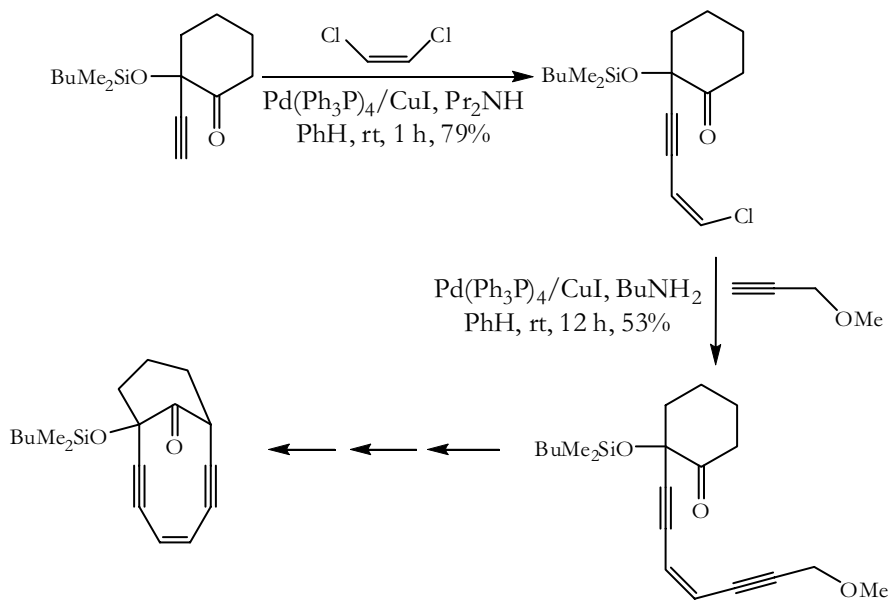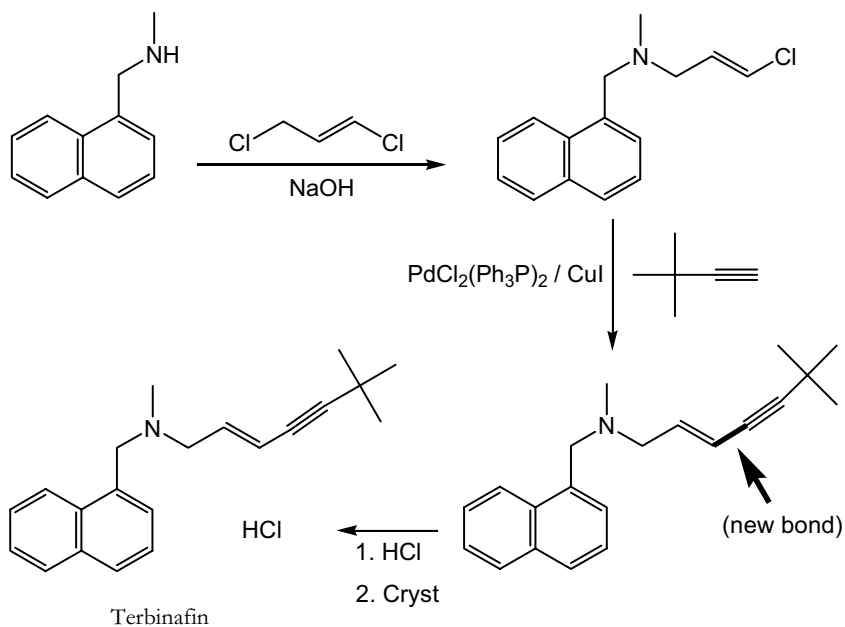
Scheme 17

6.2.2.4. Extension of the cross-coupling reactions catalysed by Pd(0) to internal alkynes, 1,3-dienes and under carbonylation conditions

The cross-coupling reactions just discussed can be extended to internal alkynes, Scheme 18, and to 1,3-dienes,[1,2] Scheme 19. With internal alkynes and after the oxidative addition step, an insertion of the triple bond in the reactive intermediate R^1-X (exemplified for R^1=Ph) occurs in a process similar to the Heck reaction. However, contrary to what happens in Heck reaction, where this step is followed by a facile beta-elimination, the intermediate obtained, an alkenylpalladium species, is stable. This "living species" can then suffer further transformations, like Heck reactions and all type of transmetallation processes just discussed, Scheme 18.
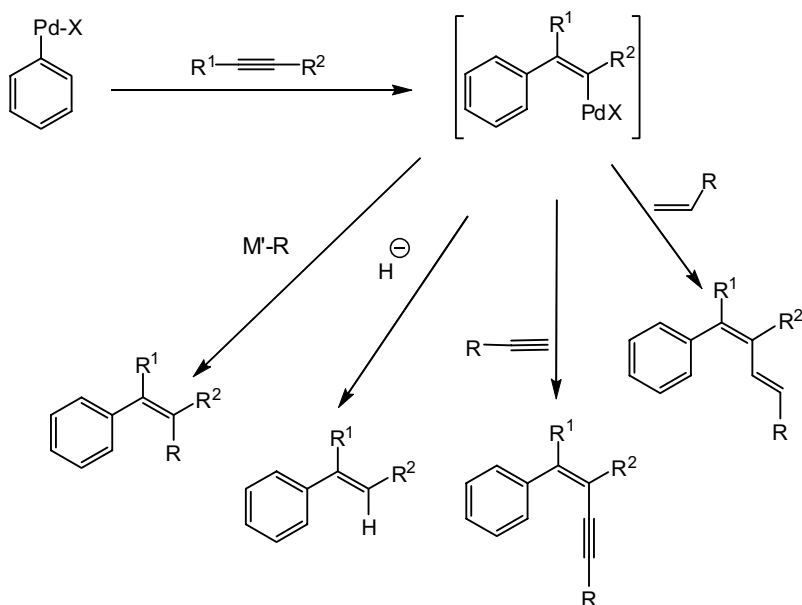
Scheme 18

With the 1,3-diene systems pi-allyl intermediates are obtained. These intermediates can suffer the expected beta-elimination but also cross-coupling through transmetallation and nucleophilic attack, Scheme 19.
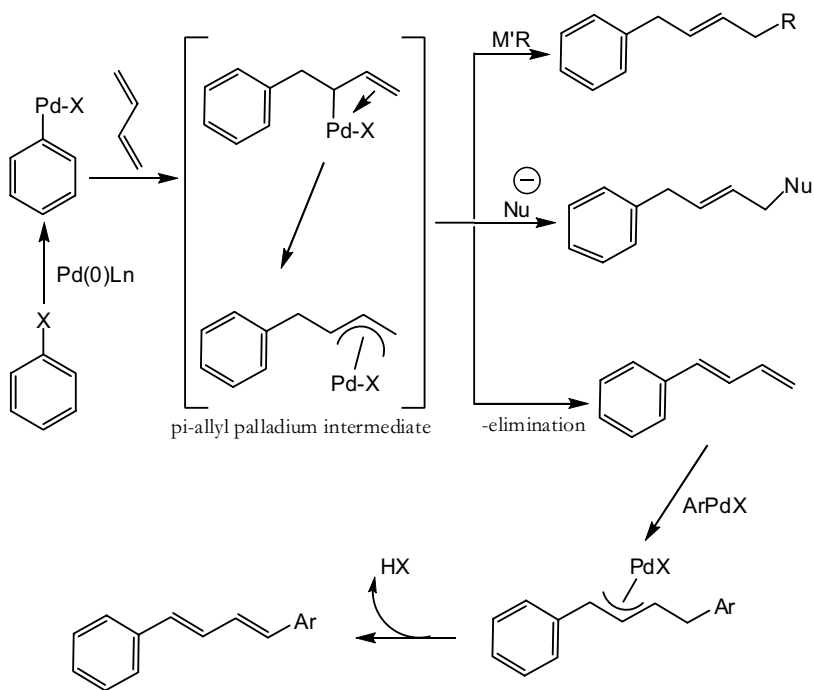
Scheme 19

The potentiality of this type of living processes, well documented in the literature[1,2], is exemplified in Scheme 20 for the construction of the steroid skeleton.

Useful compounds like ketones and aldehydes can also be obtained from aryl halides and alkenyl halides through Pd-catalysed carbonylation reactions. After the oxidative addition an insertion of CO affords acylpalladium halides that can suffer transmetallation with hydrides, Scheme 21, or with alkylmetal compounds affording, after a reductive elimination process, aldehydes and

ketones, respectively. If the reaction is terminated with nucleophiles, like water, alcohols and amines, acid, ester and amides are obtained instead.

Scheme 22 shows how an aldehyde and a ketone can be prepared through the trapping of the acylpalladium complexes by a hydride donor and an alkylmetal reagent.
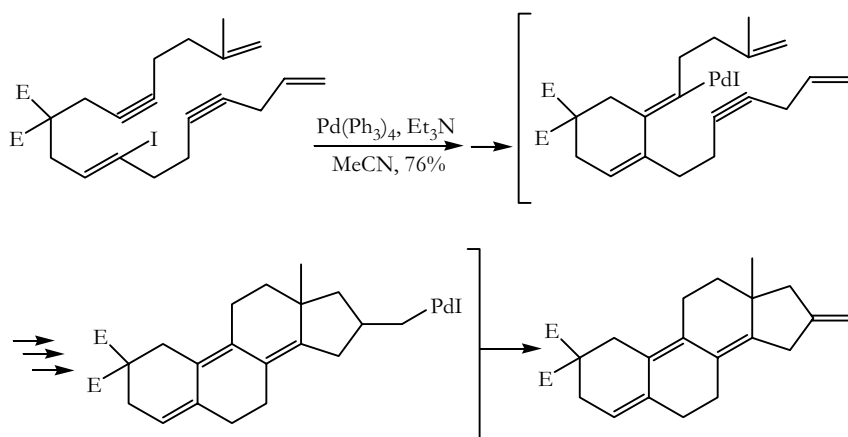
Scheme 20
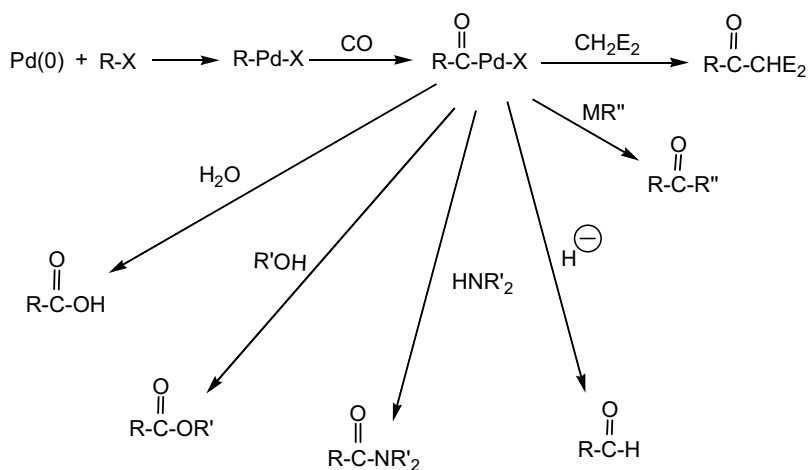
Scheme 21
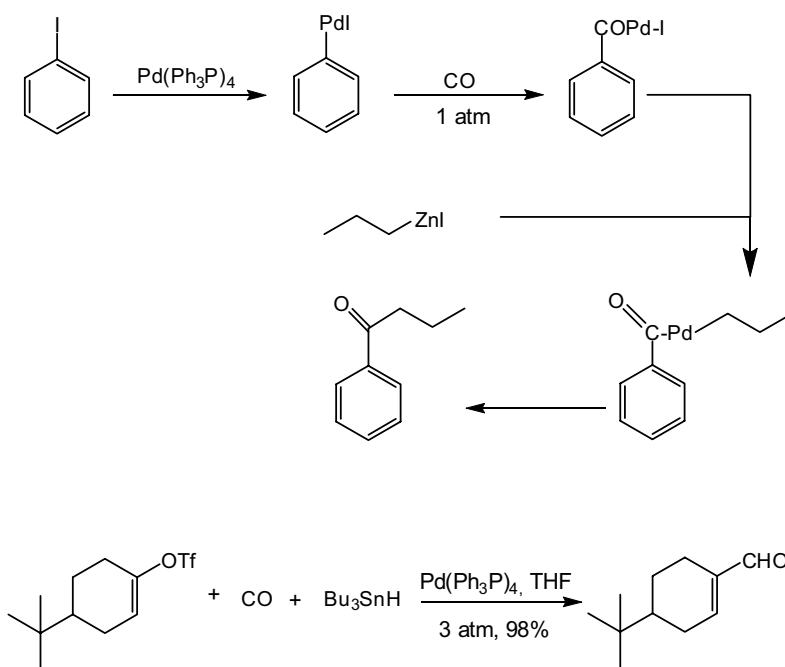
Scheme 22

6.3. FINAL REMARKS

Palladium catalysis offers a rich and versatile chemistry and actually it is recognised as a "must" for all synthetic organic chemists[2]. In this document, a simple introduction to basic palladium(0)-catalysed transformations involving carbon-carbon bond formation was covered and exemplified, when possible, with reactions of interest for a practical application. The authors would like to emphasise that they did not have the pretension of being exhaustive on the subject that is well documented in excellent textbooks and in scientific journals.

References

1. J. Tsuji, *Palladium Reagents and Catalysts, Innovations in Organic Synthesis*, Wiley: New York, **1995**.

2. J. Tsuji, *Transition Metal Reagents and Catalysts, Innovations in Organic Synthesis*, Wiley: New York, **2000**.

3. M. Beller, C. Bolm, *Transition Metals for Organic Synthesis, Building Blocks and Fine Chemicals*, Wiley-VCH: Weinheim, **1998**.

4. http://www.stillwaterpalladium.com/history4.html

5. J. Clayden, N. Greeves, S. Warren, P. Wothers, *Organic Chemistry*, Oxford University Press: Oxford, **2001**.

6. A. Zapf, M. Beller, *Chem. Commun.*, **2005**, 431.

7. A. Zapf, M. Beller, *Top. Catal.*, **2002**, *19*, 101.

8. H.U. Blaser, A. Indolese, A. Schnyder, *Current Science*, **2000**, *78*, 1336.

9. K. Ludtke, C.M.A. Alonso, M.G.P.M.S. Neves, A.M.S. Silva, J.A.S. Cavaleiro, Hombrecher H.K., *Heterocycl. Commun.* **1997**, *3*, 503.

10. C.M.A. Alonso, M.G.P.M.S. Neves, A.C. Tomé, A.M.S. Silva, J.A.S. Cavaleiro, *Tetrahedron Lett.*, **2000**, *41*, 5679.

11. M.A.J. Duncton, G. Pattenden, *J. Chem. Soc., Perkin Trans. 1*, **1999**, 1235.

12. A.B. Smith, G.R. Ott, *J. Am. Chem. Soc.*, **1998**, *120*, 3935.

13. A.M. Rouhi, *Chemical Engineering News*, **2004**, *82(36)*, 49.

7. ALKENE METATHESIS

Eduardo Nicolau dos Santos and Renata Cristina Nunes

Departamento de Química –ICEx, Universidade Federal de Minas Gerais, 31270-901 Belo Horizonte-MG, Brasil.

7.1. INTRODUCTION

Alkene metathesis is formally the bond breaking of alkene double bonds to form alkylidene fragments, which are recombined to generate new alkenes. The reaction is illustrated in Scheme 1, where ethene and 2-butene are converted in propene through a metathesis catalyst.
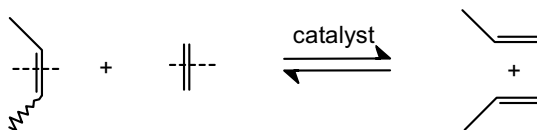
Scheme 1

The importance of alkene metathesis has been acknowledged in the 2005 Nobel Prize in Chemistry, awarded to Ives Chauvin from Institute Francais du Petrole (IFP), Richard Schrock from Massachusetts Institute of Technology (MIT), and Robert Grubbs from California Institute of Technology (CALTECH), who have given significant contribution to the field.[1]

Alkene metathesis is catalyzed by (supported) metal oxides of molybdenum, tungsten, and rhenium (heterogeneous catalysts), as well as Ziegler-type combinations, especially the ones containing (oxo)chlorides of tungsten, molybdenum, and rhenium in the presence of aluminum or tin organometallics (homogeneous catalysts). More recently, well defined metal-alkylidene complexes have been developed and employed with unprecedented success.

Alkene metathesis has been discovered in industry and, since the early times, it has been employed in many large scale industrial processes.[2] Nowadays, it has assumed enormous importance in organic synthesis of fine chemicals as it allows direct routes to chemical structures, which would be otherwise difficult to access.[3] Although heterogeneous catalysts have found a wide application in industry, the focus of this chapter will be on homogeneous catalysts.

7.2. MECHANISM

In the first proposition for the metathesis mechanism, it was postulated that two olefins coordinate concomitantly to the catalytic site (metal centre) to form a "quasicyclobutane" intermediate and the alkylidene fragments would be exchanged in a pair-wise fashion, Scheme 2.
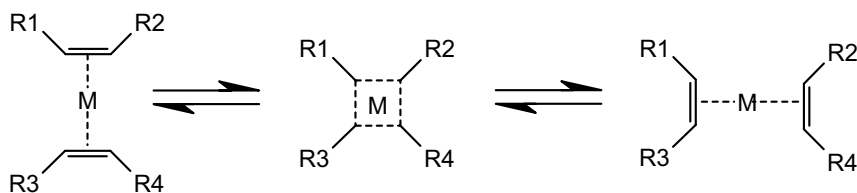
Scheme 2

Chauvin and Hérisson[4] observed that the reaction of a mixture of cyclopentene and 2-pentene led to C-9, C-10, and C-11 dienes in a 1: 2: 1 ratio, even at the beginning of the reaction. This result was inconsistent with the pair-wise mechanism, which would predict only C-10 dienes at the beginning. They proposed an alternative mechanism in which a metal-carbene or metal-alkylidene ($M=CHR_1$) is the key intermediate, Scheme 3. Once formed, the metal-carbene is coordinated by an alkene, which reacts to form a metalacyclobutane. This species either decomposes to the original alkene and metal-carbene (back reaction) or form a new metal-carbene ($M=CHR_2$) and a

new alkene (R_1CHCHR$_3$). The new metal-carbene will further react to promote alkylidene exchange among the alkenes present in the medium through the same mechanism and, if the catalyst lives long enough, *a thermodynamic equilibrium among the alkenes* will eventually be achieved. For a rather long period, both mechanisms have coexisted in literature. After experiments of ring closing metathesis (see item 7.4.2.) with a special diolefin (phenanthrene) as well as with deuterium-labeled alkenes, it was demonstrated that the product distribution was consistent with the carbene mechanism, but not with the pairwise one, after which the carbene mechanism has become widely accepted[5].
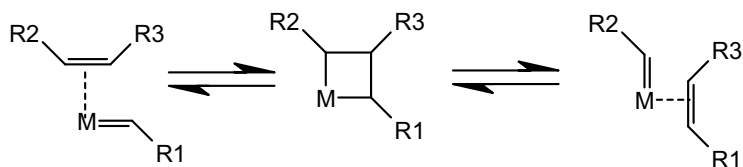
Scheme 3

7.3. CATALYSTS

7.3.1. Heterogeneous

Heterogeneous catalysts are preferred for large scale processes employing unfunctionalized alkenes. Nevertheless, they are very sensitive to feedstock impurities and are not useful for the metathesis of substrates containing functional groups. In this chapter we will limit this topic to some examples of catalysts that have found industrial applications, as shown in Table 1.[2] The likely pathway to the formation of active species on metallic oxides is the reaction of the olefin with the oxometal species on the catalyst surface, Scheme 4.
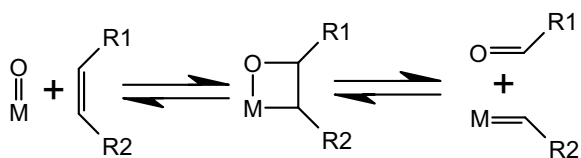
Scheme 4

TABLE 1 - Industrial heterogeneous catalysts for olefin metathesis

Catalyst	Example of Industrial Process
WO_3/SiO_2	Conversion of 2-butene and ethene to propene (OCT process) shown in Scheme 1
$WO_3/SiO_2 + MgO$	Dimers of isobutene to neohexene (intermediate for a fragrance and an anti-fungal agent)
Re_2O_7/Al_2O_3	Cycloalkenes and ethene to α,ω-diolefins (Shell FEAST process)
MoO_3/Al_2O_3-cobalt-promoted (CoMox)	Metathesis between low molecular weight ($<C_{10}$) and high molecular weight ($> C_{18}$) alkenes of the SHOP process to produce alkenes in the range C_{11}-C_{14}

7.3.2. Homogeneous (Ill-Defined)

A large variety of transition metal complexes in combination with an alkylating agent produces a catalytic system capable of promoting alkene metathesis. The most active ones are (oxo)chlorides of tungsten, molybdenum, and rhenium in the presence of an organometallic compound of aluminum or tin bearing alkyl or aryl groups. Some active combinations are shown in Table 2[6].

The system WCl_6/EtAlCl$_2$/EtOH (Calderon's catalyst) is very active in the metathesis of alkenes without functional groups even at room temperature, and so are many of the systems shown in Table 1. Nevertheless, few systems such as WCl_6/Me$_4$Sn; $WOCl_4$/Me$_4$Sn; $WCl_4(OC_6H_3$-2,6-Br$_2)$/Bu$_4$Pb are active to

promote the metathesis of *acyclic functionalyzed* olefins, and their activity is much lower.

TABLE 2 - Catalytic systems active in the metathesis of alkenes

Tungsten	Molybdenum	Rhenium
$WCl_6/BuLi$	$MoCl_5/Ph_4Sn$	$ReCl_5/Bu_4Sn$
WCl_6/Ph_4Sn	$MoCl_3(NO)/EtAlCl_2$	$ReCl(CO)_5/EtAlCl_2$
$WOCl_4/EtAlCl_2$	$Mo(NO)_2(OAc)_2/EtAlCl_2$	$ReOCl_3(PPh_3)/EtAlCl_2$
$W(CO)_5(PPh_3)/EtAlCl_2/O_2$	$[Mo(NO)_5](BF_4)_5/EtAlCl_2$	

The catalytic combination generates the carbene species through the alkyl chain transfer from the alkylating agent to the transition metal, followed by an α-hydrogen elimination, as exemplified in Scheme 5(a). Oxo ligands or additives such as alcohols or some oxygenated impurities may facilitate the formation of carbenes by assisting the α-elimination as exemplified in Scheme 5(b)[6].
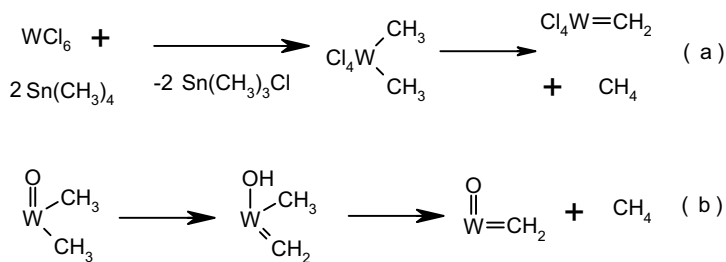
Scheme 5

Combinations involving a ruthenium source, a strained cycloalkene or substituted acetylenes generate *in situ* a metathesis catalyst. Such type of systems is used both in industry and laboratory, as exemplified below. A combination of $RuCl_3$ and HCl in butanol gives a very efficient catalyst for the ring opening metathesis polymerization (see item 7.4.4) of norbornene, a strained olefin[2]. A system generated by $RuCl_3$, PCy_3 and 1,4-butynediol

diacetate is effective for the self-metathesis of 1-octene[7]. Combinations of organometallics of Ru, an N-heterocyclic carbene precursor, and a Brönsted basis have been used for ring opening metathesis polymerization (see item 7.4.4.) and enyne metathesis (see item 7.4.8.)[8].

In conclusion, the catalysts generated *in situ* for metathesis are easier to prepare as compared to the well defined metal-alkylidene complexes (see item 7.3.3.) and have found considerable application in industry, mainly in metathesis polymerization. Nevertheless, their scope of application is limited by a series of factors, such as low tolerance to impurities or functional groups, fast deactivation by intermolecular mechanisms, the formation of different kinds of catalytic sites and large initiation periods.

7.3.3. Homogeneous (Well-Defined)

7.3.3.1. Schrock Catalysts

The development by Schrock's group of the well-defined metal-alkylidene complexes active in olefin metathesis is an example of catalyst design, strongly supported by the study of the related organometallic chemistry[9]. The basic structure of the catalysts has W or Mo in a high oxidation states as the central atom, a bulky imido ligand, two electron-withdrawing alkoxides, and an alkylidene. The complexes **1** and **2** are examples of highly active catalysts.

1   **2**
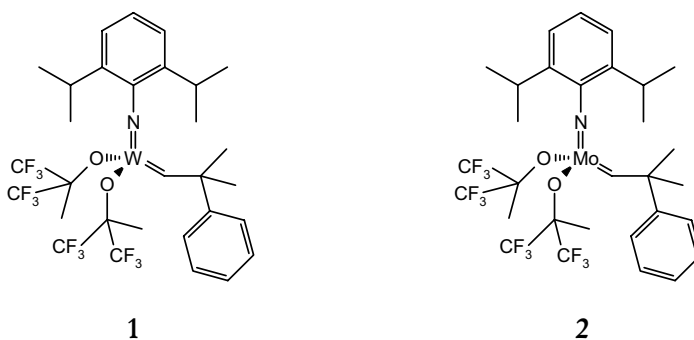
The need for a high oxidation state complex from groups 6 or 7 of the periodic table could be anticipated from the heterogeneous or homogeneous systems previously described. The bulkiness of all ligands helps to prevent the bimolecular deactivation pathways (see item 7.3.4.). The imido ligand is formally a four-electron donor and keeps the coordination number of the complex at four in a pseudo-tetrahedral geometry. The electron withdrawing effect of the alkoxides facilitates the olefin coordination by enhancing the Lewis acidity at the metal center. The electron counting of the complexes ($14e^-$) and their geometry allow the direct olefin coordination without the need of a ligand loss.

These complexes have the advantage of being highly active for metathesis, but are quite sensitive to impurities and need to be manipulated under high quality inert atmosphere. Tungsten complexes are more active, but their higher sensitivity to impurities and lower tolerance to functional groups at the substrate makes the molybdenum catalysts more useful for most of the applications.

7.3.3.2. Grubbs Catalysts

Although less active than W or Mo alkylidenes, the development of robust ruthenium catalysts for alkene metathesis allowed to broaden the application of this reaction in organic synthesis, as these catalysts are more tolerant to functional groups and less sensitive to impurities[5]. The first active catalysts contained, besides the alkylidene moiety, a bulky electron donating phosphine, which is necessary to stabilize the catalyst and favor the metalacyclobutane formation. Complex **3**, also known as 1st generation Grubbs' catalyst, is an example of an active catalyst. Mechanistic studies have shown that the catalyst activation begins with the loss of a neutral ligand from the pentacoordinated 16-electron species (*e.g.* **3**) to form a 14-electron species, which is coordinated by the alkene and react to form a metalacyclobutane intermediate, as shown in

Scheme 3. Cyclohexylphosphine (PCy₃) was found to be the optimal phosphine ligand, as phosphines with larger cone angles are too labile to stabilize the catalyst, whereas phosphines with smaller cone angles binds too tightly and disfavor the catalyst activation.

A breakthrough in the development of ruthenium catalysts was the employment of Arduengo's type N-heterocyclic carbenes instead of phosphines to stabilize the catalysts. The use of the bulky 1,3-bis(2,4,6-trimethylphenyl)-4,5-dihydroimidazolium allowed the substitution of only one phosphine in **3** to produce **4**. Catalyst **4**, also known as 2ⁿᵈ generation Grubbs' catalyst, is more efficient than **3** for the metathesis of dissubstituted alkenes and has enhanced activity for alkenes bearing electron withdrawing groups. The activation of **4** (loss of PCy₃) is slower than the activation of **3**, which makes difficult some applications, such as polymerization to obtain polymers with narrow polydispersity (narrow molecular weight distribution). The complex **5**, also known as 3ʳᵈ generation Grubbs catalyst, contains the more labile 3-bromopyridine instead of PCy₃ and is an extremely active, although less stable, metathesis catalyst.

3   4   5
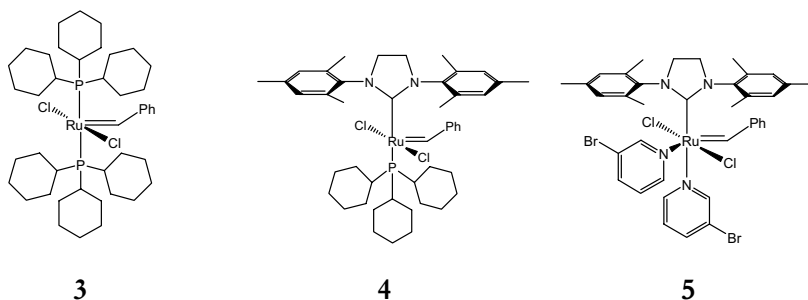
7.3.3.3. Chiral Catalysts

A great challenge in the olefin metathesis field is to develop catalysts able to perform *enantioselective metathesis*. In order to do this, the catalyst must have

a chiral element, but there is no catalyst capable of performing enantioselective metathesis for every substrate in high enantiomeric excess, since a fine tuning between the substrates and the catalyst is necessary. Schrock and Hoveyda have developed a family of catalysts whose general structure resembles complex **6**. Through the variation in the chiral biphenolate (or binaphtolate) ligands as well as the imido ligands, a series of catalysts with different activities and selectivities, has been produced and, for a particular transformation, the best catalyst of the series can be chosen[9].
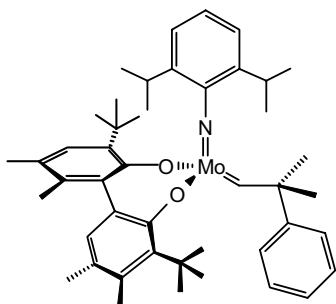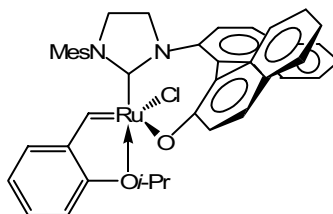
| 6 | 7 |

In some cases the Ru complex **7** and analogous, although less active than the molibdenum ones, are more convenient because they give a better chemoselectivity to the desired product[10].

7.3.4. Catalyst Deactivation

The mechanisms for catalysts deactivation discussed below are quite general, but are particularly relevant to the systems generated *in situ*. Although traces of oxigenated impurities can promote the activity of the system, many molecules containing heteroatoms (impurities or subtracts themselves) may lead to catalyst deactivation through a Wittig-type reaction, as shown in Scheme 6.
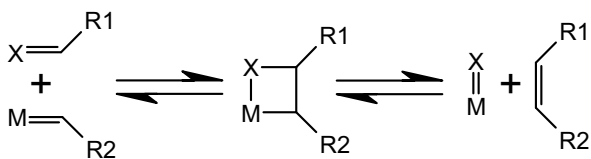
Scheme 6

Another general pathway of catalyst deactivation is by means of a bimolecular mechanism, in which two species containing alkylidenes approach to form an alkene and a metal complex not bearing an alkylidene (M) that is inactive for metathesis, Scheme 7.
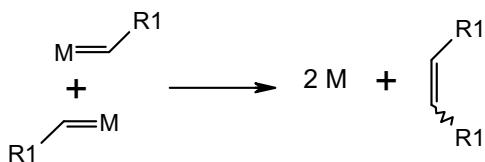
Scheme 7

7.4. Types Of Alkene Metathesis And Related Reactions

A general representation of the types of alkene metathesis is shown in Scheme 8, and explained in items 7.4.1.-7.4.5. Tandem processes involving alkene metathesis are commented in item 7.4.6. Alkyne and enyne metathesis are rapidly introduced in items 7.4.7. and 7.4.8., respectively.
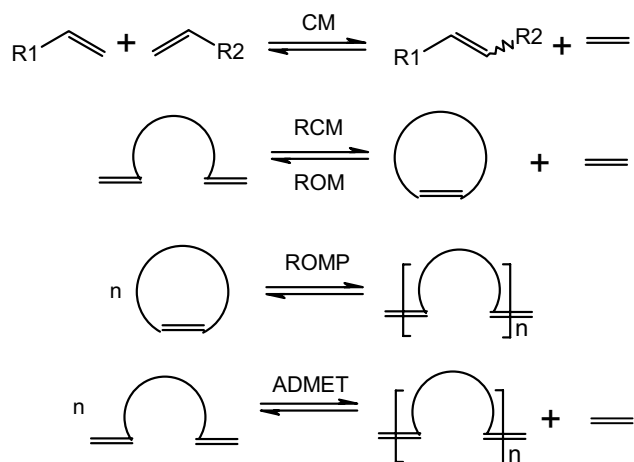
Scheme 8

7.4.1. Cross-Metathesis (CM)

The cross metathesis (CM) is the reaction in which two different acyclic alkenes couple together to yield new acyclic alkenes. The reaction tends to reach thermodynamic equilibrium among the various olefins present in the medium and the selectivity for the coupling tends to be low. When ethene or another volatile compound is one of the products, the reaction can be driven to completion by the withdrawal of the volatile product. Self metathesis (the coupling of two molecules of the same kind, *e.g.* $2R_1CHCH_2$ to form R_1CHCHR_1 and ethene) tends to reduce the selectivity of the crossed product, but it can be minimized with the appropriate choice of alkene counterparts and catalyst[11]. Besides the large scale applications shown in Table 1, CM has gained importance in organic synthesis[3]. For example, Garsubellin A, a substance extracted from a type of wood that has been studied for the treatment of Alzheimer's disease, can be synthesized through the CM of the precursor shown in Scheme 9 with methylbut-2-ene employing **4** as catalyst[12].
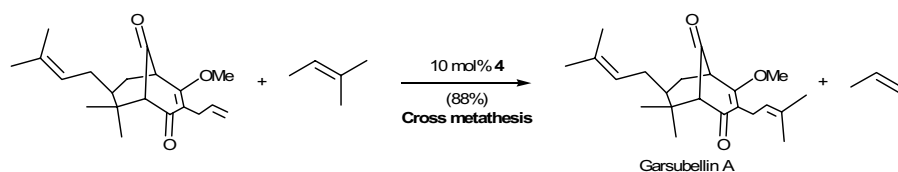
Scheme 9

7.4.2. Ring Closing Metathesis (RCM)

Ring Closing Metathesis (RCM) is a useful reaction in which an acyclic diene generates a cyclic alkene with liberation of ethene (if both double-bonds are terminal). The reaction may be driven to completion by ethene removal, but oligomerization and polymerization (see item 7.4.4.) are often side reactions that reduce the selectivity. In spite of this, RCM has become a very useful tool to synthesize cyclic compounds. For example, a key intermediate for (+)-Mevinolin, an inhibitor of an enzyme involved in cholesterol biosynthesis, can be produced by RCM of the acrylic ester, shown in Scheme 10, employing **3** as catalyst[13].
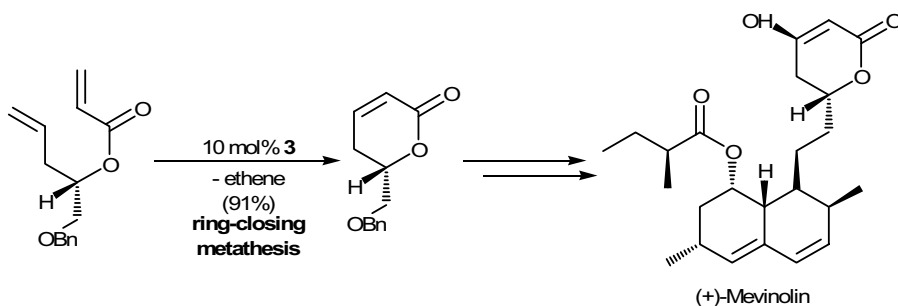
Scheme 10

7.4.3. Ring Opening Metathesis (ROM)

The reverse of RCM is called Ring Opening Metathesis (ROM) and is also useful to generate α,ω-dienes from easily available cycloolefins, such as cyclooctene, as in the Shell FEAST process exemplified in Scheme 11. The

390

reaction can be driven to the desired decadi-1,9-ene in the presence of an excess of ethene.
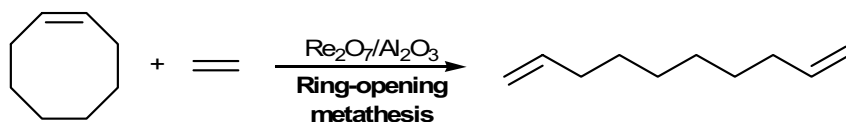
Scheme 11

A more elaborate example of ROM is shown in Scheme 12, in which chiral diolefin can be synthesized from a norbornadiene derivative and an excess of an α-olefin, in the presence of the chiral Ru complex **7**. It is worth mentioning that molybdenum catalysts, such as **6**, lead mainly to the oligomerization of the starting cycloolefin[10].
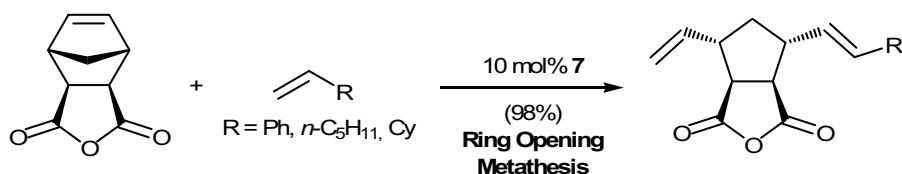
Scheme 12

7.4.4. Ring Opening Metathesis Polymerization (ROMP)

Ring Opening Metathesis Polymerization (ROMP) is nowadays a very useful tool to synthesize polymers from (functionalized) cyclic alkenes. A large variety of monomers can be employed in the process, which allows for a wide variety of structures for the polymers, and, in consequence, a large variation of their physical-chemical properties. Applications go from polymers for ballistic protection to biocompatible ones. In addition, very narrow molecular weight distributions may be obtained if the catalyst initiation is fast (*e.g.* with Schrock or 3rd generation Grubbs catalysts). The catalyst often remains linked to the end

of the polymer chain after the monomer is totally consumed. The addition of more monomer leads to a further growth in the polymer chain, in a process called "living polymerization". If a different kind of monomer is added, a block copolymer is obtained, which opens up possibilities for further variations in the properties of the polymers. As an example, the ROMP of norbornene is shown in Scheme 13.
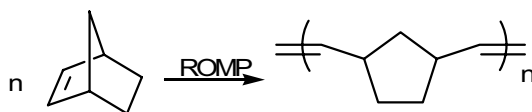
Scheme 13

7.4.5. Acyclic Diene Metathesis Polymerization (ADMET)

Acyclic Diene Metathesis Polymerization (ADMET) is the polymerization of an α,ω-diene with the release of ethene, as exemplified in Scheme 14, in which 1,4-pentadiene is polymerized to linear poly-1,4-pentadiene, a widely used synthetic rubber. ADMET opens the scope of metathesis polymerizations even more as acyclic dienes may be polymerized to form polymers distinct from those obtained with ROMP or other preparation methods. Unique well-defined polymer architectures can be obtained by simple monomer design. For example, the polymerization of various dienes branched with protected amino acids or peptides yield polymers with physical properties desired in bio-olefins. Such type of polymers may be applied in membranes, proteomics, chiral separation media, drug delivery systems, and surfaces for artificial implants[14].

poly-1,4-pentadiene
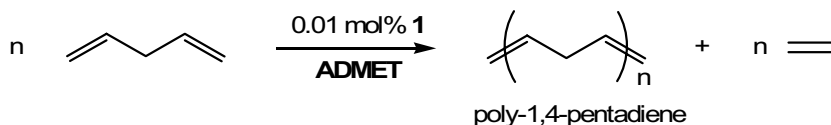
Scheme 14

7.4.6. Tandem Metathesis

The fact that ruthenium complexes can promote metathesis, hydrogenation, hydrogen transfer, and isomerization opens the possibility for the employment of ruthenium metathesis catalysts in tandem sequences[15]. The ruthenium center can be transformed into a suitable catalyst for each step of the sequence, either naturally or by the addition of modifiers such as ligands or reagents. An outstanding example of such a sequence is the synthesis of R-(-)-Muskone, a valuable component of fragrances, by a one-pot (Ru-catalyzed) three step process, shown in Scheme 15. Following RCM of the readily available diene (step a), the addition of 3-pentanone and NaOH initiates the transfer dehydrogenation of the resulting alcohol and affords a macrocyclic ketone (step b). Finally, the double-bond hydrogenation (step c) is achieved simply by the addition of H_2 resulting in (R)-(-)-Muscone in 56% overall yield[16].
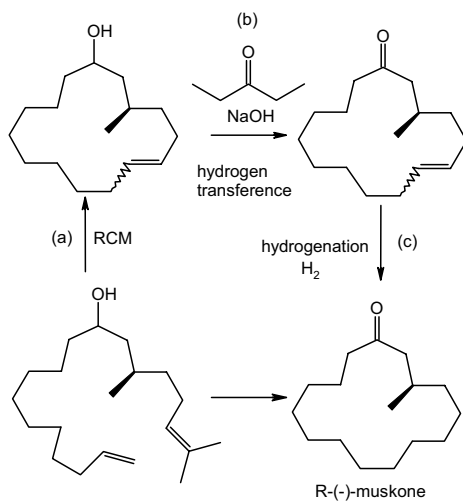
Scheme 15

7.4.7. Alkyne Metathesis

Alkyne metathesis is a direct analogue of the alkene metathesis reaction and involves the mutual exchange of alkylidyne units between two acetylene moieties through a mechanism similar to that shown in Scheme 3. The general representation of this reaction is shown in Scheme 16 for both the intramolecular (ring closing alkyne metathesis) and intermolecular (alkyne cross metathesis) versions. Terminal alkynes tend to polymerize in the presence of metathesis catalysts and for organic synthesis, the precursors are normally disubstituted alkynes. Cyclotrimerization to form substituted benzenes is also an important side reaction. A useful catalyst for this reaction is the well-defined alkylidyne complex (t-Bu-O)$_3$W($\equiv$C-t-Bu) **8**[17].
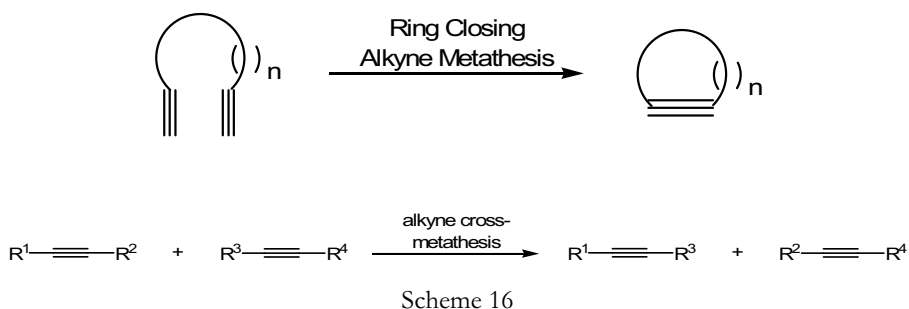
Scheme 16

For example, the key step in the total synthesis of (+)-citreofuran, a bioactive molecule, is the ring-closing alkyne metathesis shown in Scheme 17[17].
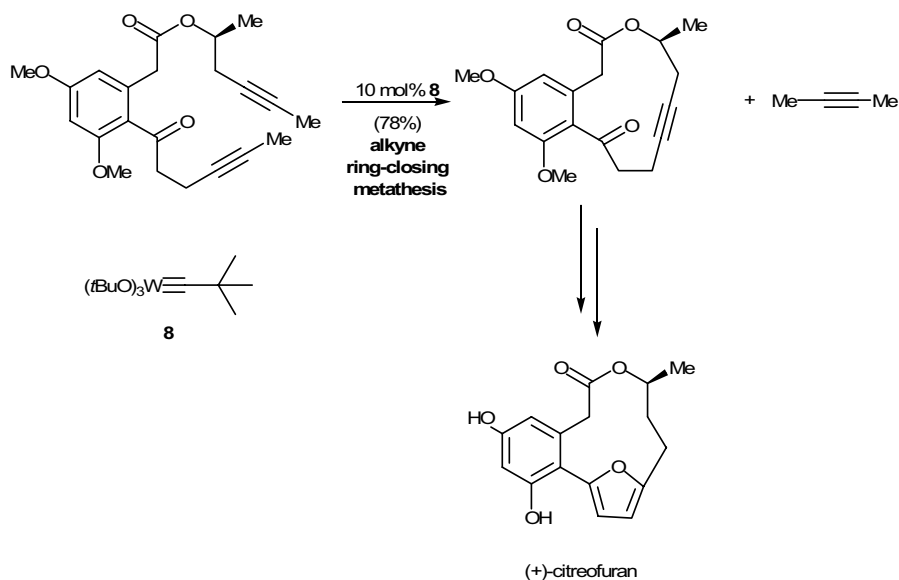
Scheme 17

7.4.8. Enyne Metathesis

Enyne metathesis involves the union of an alkene with an alkyne to form a 1,3-diene system. The generic representation of its intramolecular version (ring closing enine metathesis) is depicted in Scheme 18. It is a useful method for the construction of 1,3-diene systems from simple precursors under mild conditions. Besides the fact that dienes are interesting in themselves, this transformation may be followed by others, such as cycloadditions, which allows the building of complex molecules in few steps.
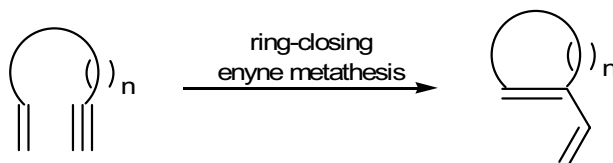
Scheme 18

For example, the total synthesis of the tricyclic alkaloid (-)-stermoamide has been achieved employing the first generation Grubbs catalyst **3** to perform the ring closing metathesis of the enyne, shown in Scheme 19. In a few steps from the diene, the target molecule has been obtained[18].
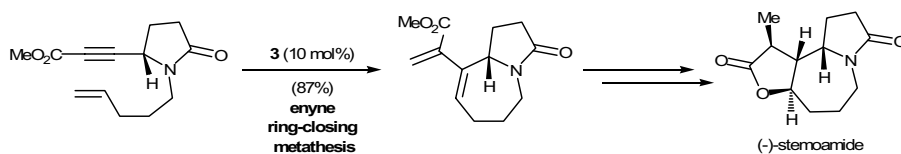
Scheme 19

The intermolecular version of the reaction is also known, but its utility is limited due to the usually low selectivity obtained.

7.5. CONCLUSIONS

Since its serendipitous discovery, alkene metathesis has experienced enormous advances. Heterogeneous catalysts and ill-defined homogeneous catalysts, although very useful in large scale processes, have severe limitations in the transformation of alkenes bearing functional groups. Well-defined metal-alkylidene complexes with optimized structures of W or Mo (Schrock's catalysts) or Ru (Grubbs' catalysts) have broadened the scope of this reaction, either by the enhancement of functional group tolerance or by the increase in the selectivity of the catalysts. Nowadays, alkene metathesis, as well as the related alkyne metathesis and enyne metathesis, has become a useful tool in organic synthesis.

References

1. www.nobelprize.org

2. J.C. Mol, *J. Mol. Cat. A: Chem.*, **2004**, *213*, 39.

3. K.C. Nicolaou, P.G. Bulger, D. Sarlah, *Angew. Chem. Int. Ed. Engl.*, **2005**, *44*, 4490.

4. J.-L. Herisson, Y. Chauvin, *Makromol. Chem.*, **1971**, *141*, 161.

5. R.H. Grubbs, *Tetrahedron,* **2004**, *60*, 7117.

6. J.C. Mol in *Applied Homogeneous Catalysis with Organometallic Compounds*; W.A. Herrmann, B. Cornils (Eds.); VHC, Weinheim, **1996**; 1, 318.

7. P.O. Nubel, C.L. Hunt, *J. Mol. Catal. A: Chem.*, **1999**, *145*, 323.

8. D. Sémeril, C. Bruneau, P.H. Dixneuf, *Adv. Synth. Catal.*, **2002**, *344*, 585.

9. R.R. Schrock, *J. Mol. Cat. A: Chem.*, **2004**, *213*, 21.

10. J.J. van Veldhuizen, D.G. Gillingham, S. B. Garber, O. Kataoka, A.H. Hoveyda, *J. Am. Chem. Soc.*, **2003**, *125*, 12502.

11. A.K. Chatterjee, T.-L. Choi, D.P. Sanders, R.H. Grubbs, *J. Am. Chem. Soc.*, **2003**, *125*, 11360.

12. S.J. Spessard, B.M. Stoltz, *Org. Lett.*, **2002,** *4*, 1943.

13. A.K. Ghosh, H. Lei, *J. Org. Chem.*, **2000**, *65*, 4779.

14. T.E. Hopkins, K.B. Wagener, *J. Mol. Cat. A: Chem.*, **2004**, *213*, 93.

15. D.E. Fogg, E.N. dos Santos, *Coord. Chem. Rev.*, **2004**, *248*, 2365.

16. J. Louie, C.W. Bielawski, R.H. Grubbs, *J. Am. Chem. Soc.*, **2001**, *123*, 11312.

17. R.S. Schrock, *Angew. Chem. Int. Ed.*, **2006**, *45*, 3748.

18. A. Kinoshita, M. Mori, *J. Org. Chem.*, **1996**, *61*, 8356.

(Página deixada propositadamente em branco)

8. ENANTIOSELECTIVE ALKYLATION OF ALDEHYDES WITH ORGANOZINC REAGENTS

M. Elisa Serra

Departamento de Química, Faculdade de Ciências e Tecnologia, Universidade de Coimbra, Rua Larga, 3004-535, Coimbra, Portugal.

8.1. BASIC CONCEPTS

A commonly accepted definition of enantioselective synthesis is "a process that allows the transformation of an achiral substrate into a chiral product, in a chiral environment". This chiral environment can be provided by the solvent, another reagent or a catalyst. The enantioselective alkylation of aldehydes with organozinc reagents, a method of obtaining chiral alcohols, is one of the many types of enantioselective synthesis. Before the discussion of this specific topic, it is useful and convenient to review some basic concepts related to enantioselective synthesis.

Why is it important to have methods for obtaining chiral products? In synthetic procedures it is frequently normal to obtain more than one of the many possible stereoisomers of a product. However, these stereoisomers are actually different compounds, possessing distinct properties, namely with respect to taste, aroma and biological activity, among others. When the product is being synthesized with a specific objective in mind, the existence of methods for exclusively obtaining the stereoisomer with the exact properties required is of the utmost importance.

8.1.1. Approaches to enantioselective synthesis

There are three basic approaches to enantioselective synthesis[1], Figure 1:

1 - Reaction of a chiral substrate or of a chiral auxiliary-modified substrate with another reagent to give a chiral product. In this case, the chiral substrate (or

chiral auxiliary-modified substrate) is responsible for inducing chirality in the reaction product. In cases where a chiral auxiliary is used, the procedure involves, first of all, reaction of the chiral auxiliary with the substrate in a reversible fashion. In this modified form, reaction occurs with a second reagent to give the chiral product. Finally, through a simple procedure the chiral auxiliary is removed, making it possible to re-use it in another reaction. There are some inconveniences in this approach. One of them is that stoichiometric quantities of auxiliary, with respect to the substrate, are required. Although the auxiliary may be partially or even totally recovered, this still means additional costs of reagents. Moreover, the transformation of the substrate may not be straightforward, leading to additional synthetic difficulties and time expenditure.

1st approach:

$$S^* \xrightarrow{R} P^*$$

$$S + A^* \longrightarrow S\text{-}A^* \xrightarrow{R} P^* + A^*$$

2nd approach:

$$S \xrightarrow{R^*} P^*$$

3rd approach:

$$S \xrightarrow{Cat^*} P^*$$
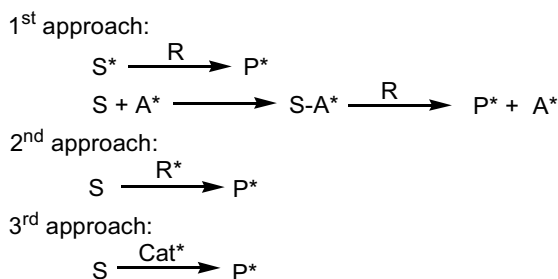
Figure 1 - Basic approaches to enantioselective synthesis.

2 - Reaction of a chiral reagent with an achiral substrate. In this approach the reagent, not the substrate, is responsible for the chiral induction in the reaction product. This approach is somewhat similar to the first, with the difference that the inducer of chirality is always incorporated in the product. Thus, the process never requires an additional step for removing the chiral auxiliary.

3- The reaction is carried out in the presence of a chiral catalyst, which is responsible for the induction of chirality in the product. The catalyst may be a metal complex or a ligand which interacts with the reagents, in this way inducing chirality in the product. In this approach, the enantioselective catalysis approach, only small quantities of chiral material are required to originate large

quantities of chiral product. Accordingly, enantioselective catalysis is undoubtedly the most convenient and possibly inexpensive approach to optically pure products.

Due to its very attractive characteristics, there are presently numerous applications of enantioselective catalysis in fine chemistry. Some of these are indicated in Table 1[2].

TABLE 1 - Applications of enantioselective catalysis in fine chemistry

Reaction	Chiral Catalyst	Product	Application
Hydrogenation	Ru/*(S)*-BINAP	*(S)*-Naproxen	pharmaceutical
Enamide Hydrogenation	Rh/DIPAMP	L-DOPA *(L)*-Phenylalanine	pharmaceutical food additive
Allylic Amine Isomerization	Rh/*(S)*-BINAP	*(L)*-Menthol	chemical aroma
Allylic Acohol Epoxidation	Ti(O^{i}Pr)$_4$/*t*-BuOOH/ diisopropyl tartarate	Dispalure glycidol	pheromone intermediate
Ciclopropanation	Cu/chiral schiff base	Cilastatin	pharmaceutical

8.1.2. Importance and applications of chiral secondary alcohols

Synthetic procedures for efficiently obtaining chiral secondary alcohols are of great interest because of the vast application of these compounds in fine chemistry. Optically active secondary alcohols incorporate many structures with biological activity. They are structural units in pharmaceuticals, perfumes, herbicides and pesticides. Chiral alcohols are also used as pheromones, while others are important components of liquid crystals. Besides these uses for optically active secondary alcohols, there is the purely synthetic facet, since the hydroxyl group is an excellent precursor for many other functionalities, being very useful in organic synthesis for obtaining a wide variety of chiral compounds. Figures 2 and 3 indicate several examples of useful chiral alcohols,

all of which are terpene derivatives[3]. The two enantiomers of citronelol are precursors in the synthesis of various antibiotics, while (-)-menthol is a common component of cold and flu remedies. Some terpenes are responsible for aromas and scents: (R)-lavandulol is a perfume component and the enantiomers of diendiol I and linalool contribute to the characteristic aroma of *Muscat* wines[4].

| citronelol | (-)-menthol | *(R)*-lavandulol | diendiol I | linalool |
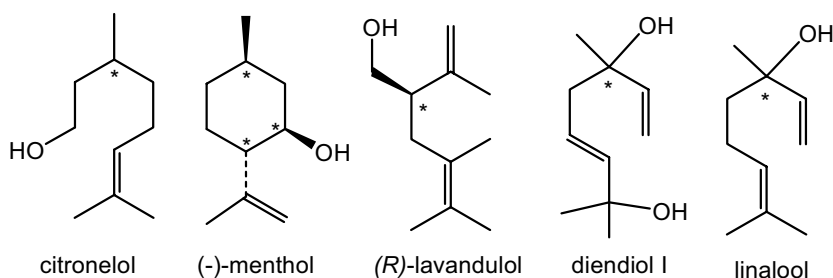
Figure 2 - Some useful optically active terpinols.

The structures of some pheromones are found in Figure 3. All of these are chiral secondary alcohols.
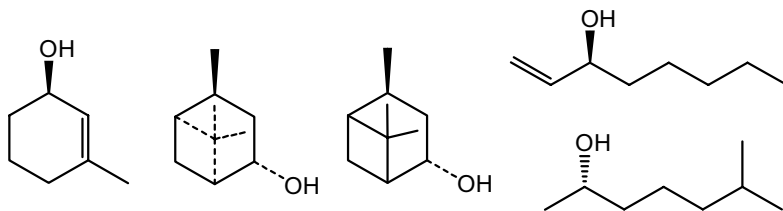
Figure 3 - Pheromones which are optically active secondary alcohols.

8.2. CHIRAL ALCOHOLS FROM THE ENANTIOSELECTIVE REDUCTION OF KETONES

Because of their importance, numerous methods have been explored for the synthesis of optically active secondary alcohols. Many of these synthetic procedures involve the transformation of prochiral ketones, namely, through

enantioselective reduction. These reductions can be carried out with molecular hydrogen or, alternatively, with hydrogen donors in the presence of a chiral metal complex catalyst. The reduction of ketones can also be accomplished with metal hydrides in the presence of a chiral ligand and with borane derivatives.

Organoaluminates, which are common hydride donors have been frequently used for obtaining chiral alcohols, the induction of chirality occurring through the coordination of a chiral ligand to the aluminum. One reagent of this type is the organoaluminate modified with binol, which gives alcohols with optical purities greater than 95%[5], Figure 4.

R₁	R₂	ee (%)
Ph	Et	98
Ph	Me	95
Ph	Pr	100
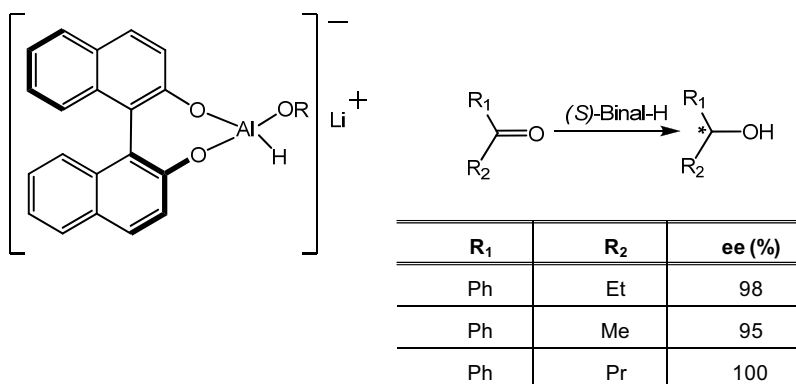
Figure 4 - Use of a binol modified hydride donor for enantioselective reductions of ketones.

Chiral organoboranes are also very efficient in the enantioselective reduction of prochiral ketones. Itsuno[6] and Corey[7] prepared chiral boranes by reacting BH_3 with chiral aminoalcohols 2-amino-3-methyl-1,1-diphenylbutanol and diphenylprolinol, giving the organoboranes known as the Itsuno and Corey organoboranes, respectively, Figure 5.
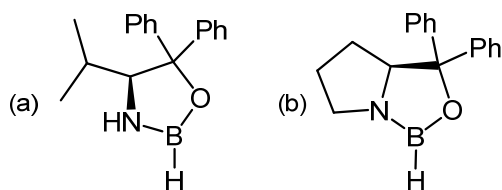
Figure 5 - The Itsuno (a) and Corey (b) organoboranes.

These reducing agents give chiral secondary alcohols from phenylalkyl ketones, Ph(R)CO, with ee greater than 90%, Table 2.

TABLE 2 - Enantioselective reductions of phenylalkyl ketones using the Itsuno and Corey organoboranes.

R	Itsuno reagent (ee%)	Corey reagent (ee%)
Me	94	97
Et	94	90
n-Bu	100	--

8.3. CHIRAL ALCOHOLS FROM THE ENANTIOSELECTIVE ALKYLATION OF ALDEHYDES

Aldehydes constitute another source of chiral secondary alcohols. In this case, the transformation results from the addition of different organometallic reagents such as lithium, magnesium, copper, aluminium, titanium and zinc derivatives to aldehydes in the presence of a chiral ligand.

The first example of the use of organometallic reagents in enantioselective alkylation was reported by Mukaiyama[8], in 1978. He tried to enantioselectively alkylate benzaldehyde with butyllithium and diethylmagnesium in the presence of a chiral amino alcohol derived from proline, Figure 6. The products were obtained with ee of 95% and 92%, respectively. In spite of the high selectivity, the method presents a problem. Since these organometallic reagents themselves

react with the aldehyde without requiring the intervention of the ligand, there is always a competing non-catalytic pathway which gives a racemic product. In order to favor the enantioselective process without competition from the non-selective one, stochiometric or greater quantities of chiral ligand are required.
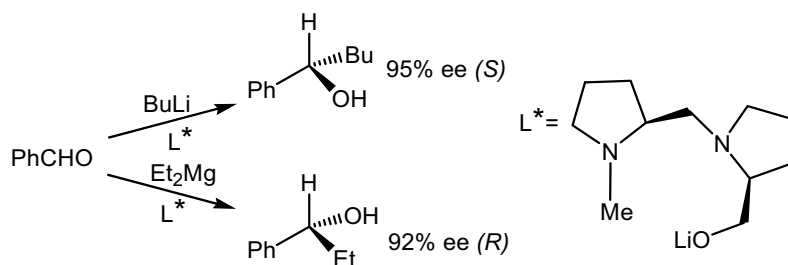
Figure 6 - Alkylation in the presence of the proline derived Mukaiyama ligand, L*.

8.3.1. Alkylations with organozinc reagents

Organometallic zinc reagents do not react directly with aldehydes. However, in the presence of an excess of a chiral ligand, Mukaiyama was able to alkylate benzaldehyde with diethylzinc to give racemic 1-phenyl-1-propanol, concluding that in this case the ligand efficiently activated the organozinc reagent, allowing, for the first time, the addition of this type of reagent to the carbonyl group of an aldehyde.

Why does the organozinc reagent only add to the carbonyl in the presence of the ligand? Dialkylzincs are linear molecules, only slightly polar and reactive, Figure 7(a). In the presence of the chiral ligand, both molecules coordinate giving rise to significant changes in the structure of the former. The molecule acquires an approximately tetrahedral geometry with a 145° R-Zn-R angle and the Zn-R bond becomes longer with a more nucleophilic R, Figure 7(b). As a consequence of these structural changes, the dialkylzinc becomes much more reactive[9].
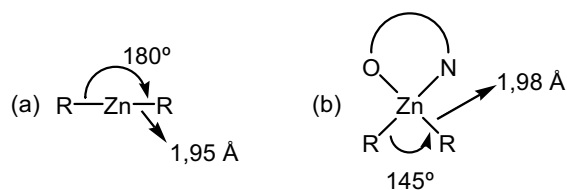
Figure 7 - Structural characteristics of (a) a dialkylzinc molecule and (b) a coordinated dialkylzinc molecule.

Since dialkylzincs only react with aldehydes in the presence of a ligand, the problem of competition with the direct addition to give a racemate does not exist in the enantioselective process. Therefore, having found the appropriate ligand, this system has the ideal characteristics for a catalytic enantioselective process.

The first efficient enantioselective ligand found for alkylations was (S)-leucinol, Figure 8. With 2 mol% of this ligand, benzaldehyde reacted with diethyl zinc to give 1-phenyl-1-propanol with 49% ee[10]. Although not exceptionally selective, this result encouraged further search for more efficient ligands.

Noyori was able to greatly improve the selectivity of enantioselective alkylations using (-)-DAIB[11], Figure 8. The alkylation of benzaldehyde with diethylzinc gave a product with 99% ee. Other aromatic aldehydes also gave high enantiomeric excesses with this ligand, Table 3. With these results, the addition of diethylzinc to aldehydes in the presence of chiral ligands was established as a valid procedure for the enantioselective synthesis of secondary alcohols.
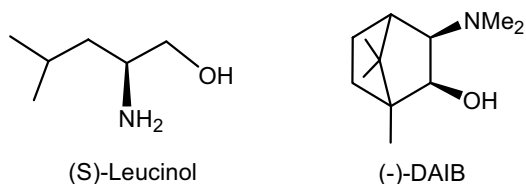
Figure 8 - First enantioselective chiral ligands for alkylations with dialkylzinc.

TABLE 3 - Enantioselective alkylation of aldehydes with (-)-DAIB.

aldehyde	ee (%)
p-chlorobenzaldehyde	93
p-methoxybenzaldehyde	93
ferrocenylaldehyde	81

Both (*S*)-leucinol and (-)-DAIB are β-amino alcohols but this is not the only type of chiral ligands that efficiently and selectively catalyse enantioselective alkylations. Besides β-amino alcohols, other amino alcohols, diamines, disulfonamides, aminosulfonamides, diols, disulfides and aminosulfides, among others, are also used as catalysts in these reactions. The role of these ligands is to activate the organometallic reagent and to induce chirality in the reaction product. Of all types of ligands tested, so far the majority of the most selective were found to be β-amino alcohols.

8.3.2. Mechanism of the enantioselective alkylation with organozinc reagents

The mechanism of the enantioselective alkylation of aromatic aldehydes with dialkylzinc reagents catalysed by chiral ligands is presented in Figure 9[12], for the addition of a dialkylzinc to benzaldehyde in the presence of a chiral β-amino alcohol. After coordination of the ligand (i) with one molecule of ZnR_2, a zinc alcoxide (ii) is formed. In this intermediate, the zinc atom behaves as a Lewis acid and the oxygen of the amino alcohol as a Lewis base. The intermediate is in equilibrium with the dimeric species (iii), but only (ii) is the active species. Intermediate (ii) reacts with a second molecule of ZnR_2 giving the dinuclear zinc species (iv). The second molecule of ZnR_2 coordinates to the amino alcohol oxygen causing a change in the angle from 180º to 145º. Also, at this stage, the Zn-R bond becomes longer and the alkyl group acquires a more

nucleophilic character. These changes are responsible for the increase in reactivity of the dialkylzinc. Coordination of the aldehyde to the Lewis acid Zn atom originates (vi), which can alternatively result from coordination of the aldehyde to (ii) in the first place to give (v), followed by coordination of the second ZnR_2 molecule. As a result of coordination, the carbonyl carbon of the aldehyde becomes more electrophilic, thus enhancing its reactivity with respect to the transfer of the alkyl group, favoring the formation of (vii). This step is irreversible and it is the rate-determining step of the reaction. All other transformations are reversible. From (vii) the Zn alcoxide of the product alcohol is freed and (iv) or (v) are regenerated to participate in a new catalytic cycle.
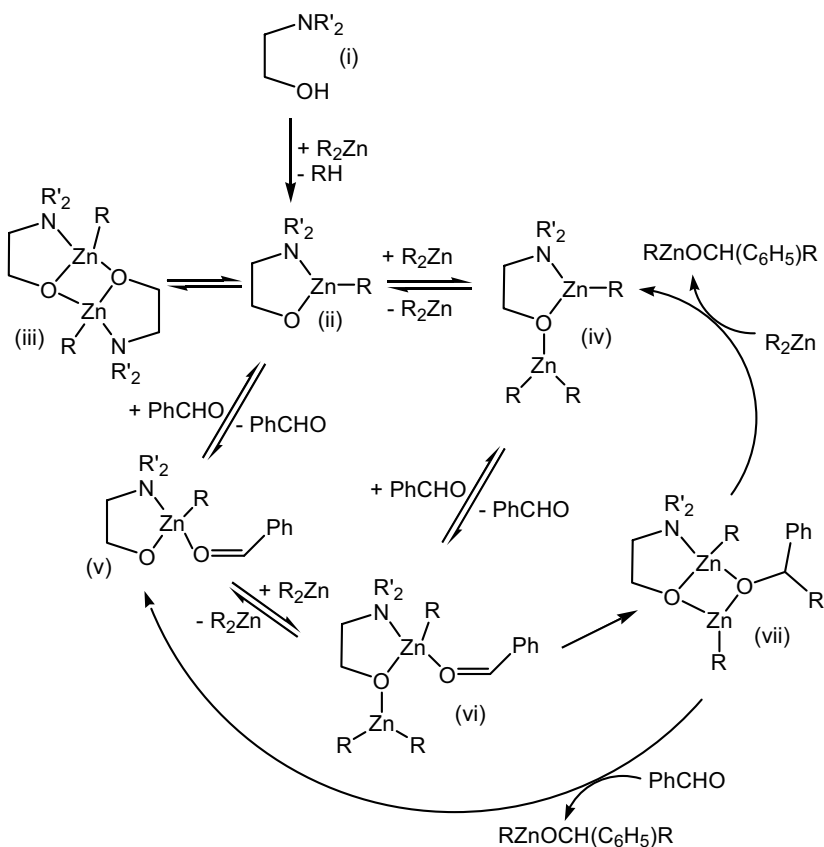
Figure 9 - Mechanism for the alkylation of aldehydes with organozinc reagents, in the presence of a chiral ligand.

408

The transition state leading to (vii) is the most important of the catalytic cycle because it is the one that determines the selectivity of the reaction. When β-amino alcohols are used, this transition state has a tricyclic structure with one 5-membered ring and two 4-membered rings. It is consequently identified as a 5-4-4 transition state, Figure 10.
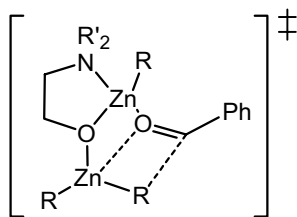
Figure 10 - Tricyclic 5-4-4 transition state.

There are four possible geometries for this transition state, Figure 11[13]. First of all, it may be classified as *syn* or *anti* depending on the relative position of the terminal rings. For each one of these, there are also two possibilities related to how the aldehyde coordinates, with the *Re* face or with the *Si* face. Consequently, the four possible geometries are *anti-Re, anti-Si, syn-Re* and *syn-Si*. Usually, the lower energy transition states are the *anti-Si* and *syn-Re*, where there are fewer repulsive interactions between groups. Which of the two enantiomers predominates in the reaction product depends on which of these two transition states presents fewer repulsive interactions. This is mainly determined by the specific structure of the chiral ligand used.
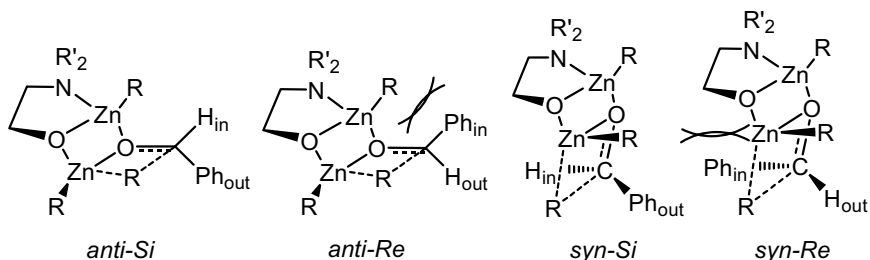
Figure 11 - Possible geometries for the 5-4-4 tricyclic transition state.

8.3.3. Factors influencing selectivity in enantioselective alkylations

Several factors are decisive in order for an enantioselective alkylation to be efficient. These are the structure of the chiral ligand, the type of substrate, the solvent and the reaction temperature.

8.3.3.1. Ligands

The type of chiral ligand used in enantioselective alkylations, as well as its specific structure is crucial in determining the selectivity of the process[14]. To date, aminoalcohols are the type of ligand that has given best results in enantioselective alkylations, in particular, the 1,2 difunctionalized ones, the β-amino alcohols. These ligands give rigid 5-4-4 transition states, which are more efficient in inducing chirality in the reaction product. For the same reason, ligands having cyclic structures, especially those in which the donor atoms are incorporated in the cycle or directly bonded to it, are excellent for giving products with high optical purity.

8.3.3.2. Substrates

The selectivity in enantioselective alkylations with diethylzinc is strongly dependant on the type of substrate used[15]. Although both aliphatic and aromatic aldehydes can be selectively alkylated, the latter usually lead to products with higher ee. Aliphatic aldehydes are more flexible, the transition state energy differences are smaller and so products with lower ee result. When substituents are present on the aromatic ring, if they are electron-attracting, products with higher ee are formed. However, if the substituents are electron-donationg, the ee are generally lower.

The position of the substituent on the aromatic ring also influences selectivity.

If it is in the *para* position, the ee are higher than when the same substituent is in the *ortho* or *meta* positions.

8.3.3.3. Solvents

Several solvents, both polar and apolar, have been used in the enantioselective alkylation of aldehydes, among which are cyclohexane, toluene, benzene, diethylether, tetrahydrofurane and dicholomethane[16]. The best solvents are the less polar ones, namely, cyclohexane and toluene, because the more polar solvents tend to coordinate with the dialkylzinc, destabilizing the transition states. Non polar solvents usually give quicker reactions and products with higher optical purity.

8.3.3.4. Temperature

Studies have established the best temperatures for enantioselective alkylations[17]. Reactions carried out at 0°C generally show higher selectivity, although they may be somewhat sluggish. Some alkylations are also very selective when carried out at room temperature. Temperatures below the 0°C-room temperature range usually give very sluggish reactions and those above this temperature range give reaction products with low optical purities.

8.3.4. Some examples of enantioselective alkylations with diethyl zinc

Some of the many chiral ligands that the literature presents as highly enantioselective in the alkylation of benzaldehyde with diethyl zinc are presented in Figure12[18]. Also referred are the ee observed for the reaction product in the presence of these ligands.
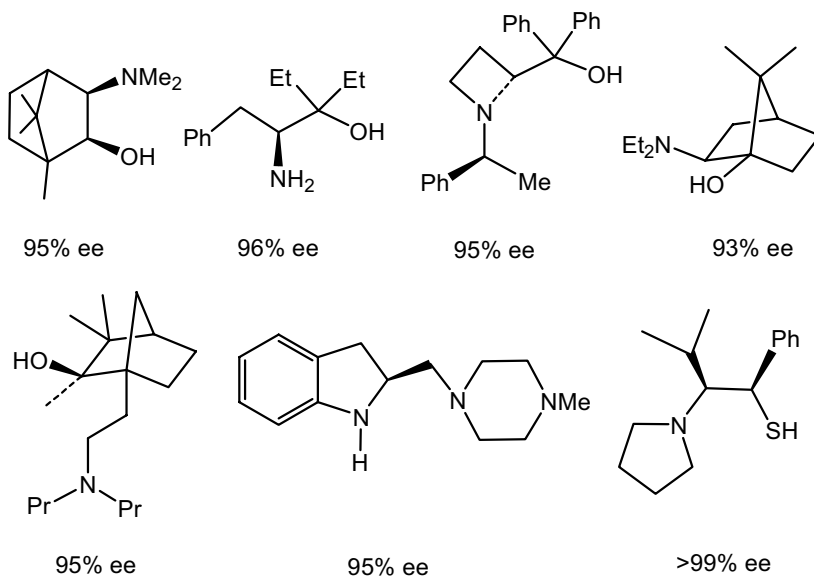
Figure 12 - Chiral ligands used in the enantioselective alkylation of benzaldehyde with diethyl zinc. Below each ligand is ee for the reaction product.

Figure 13 shows some examples of the ligands used in the enantioselective alkylation of an aliphatic aldehyde, cyclohexanecarboxaldehyde, as well as the ee of the products[19]. Although aliphatic aldehydes usually give lower selectivities, in these examples the ee are very high, greater than 97%.
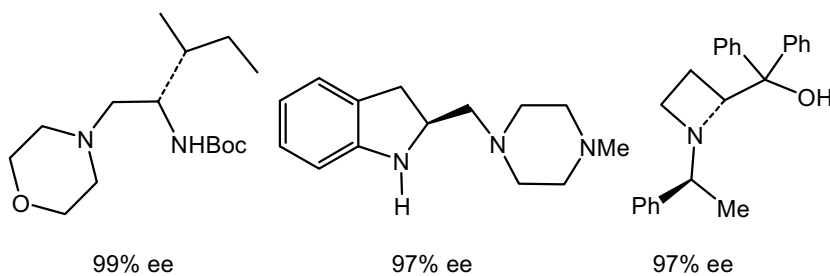
Figure 13 - Chiral ligands used in the enantioselective alkylation of cyclohexane-carboxaldehyde with diethyl zinc. Below each ligand is ee for the reaction product.

8.3.5. Enantioselective alkylations in the presence of titanium tetraisopropoxide

Not all chiral ligands used in enantioselective alkylations with organozinc reagents are strong Lewis bases. Some of them are weak Lewis bases or may even be slightly Lewis acidic. Examples of these ligands are diols, some diamines, disulfonamides and aminosulfonamides, among others. In these cases the alkylations with diethyl zinc alone do not go smoothly. When these types of ligands are used, the presence of an additional catalyst, a Lewis acid, is required. The most commonly used Lewis acid is Ti(O^{i}Pr)$_4$, whose function is to activate both the organozinc reagent and the aldehyde through coordination, thus favoring the reaction.

8.3.5.1. Mechanism of the enantioselective alkylation with organozinc reagents and titanium tetraisopropoxide

Although the mechanism of alkylations with organozinc reagents in the presence of Ti(O^{i}Pr)$_4$ is not completely understood, some proposals do exist [20]. One of these, presently the more generally accepted one, results from Walsh's mechanistic studies with binol. He suggests that the alkylation of the aldehyde involves two molecules of Ti(O^{i}Pr)$_4$. In the first part of the mechanism, Figure 14 a), the chiral ligand and the titanium complex react to give complex (i), followed by coordination of the aldehyde to give (ii). Through this coordination, the carbonyl carbon of the aldehyde becomes more electrophilic, thus activating the aldehyde for alkylation. A second molecule of Ti(O^{i}Pr)$_4$ reacts with a molecule of diethyl zinc, transferring an alkyl group to give complex (iii), Figure 14 b). It is this alkyl group that will subsequently be transferred to the aldehyde.
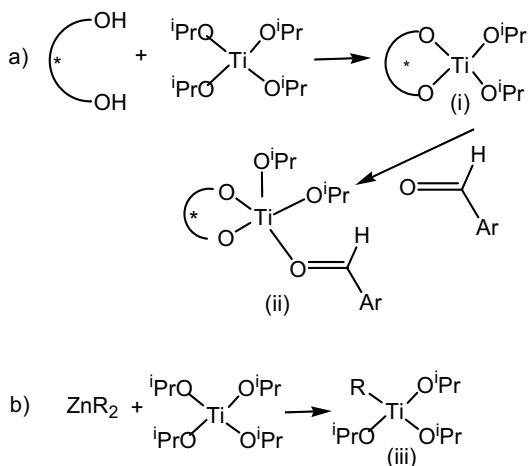
Figure 14 - Mehcanism for the alkylation of aldehydes with organozinc reagents in the presence of a chiral ligand and Ti(O^iPr)₄, first part.

For the second part of the mechanism, two proposals exist, Figure 15. In the first one, path **A**, two isolated complexes are involved and the R is transferred from (iii) to the aldehyde in the other titanium complex, (ii). In the second proposal, path **B**, a binuclear complex (iv) is formed from (ii) and (iii). Subsequently, transfer of R to the aldehyde occurs. Because it is an established fact that many titanium complexes tend to easily form binuclear species, the latter pathway, **B**, seems to be the most probable[21].
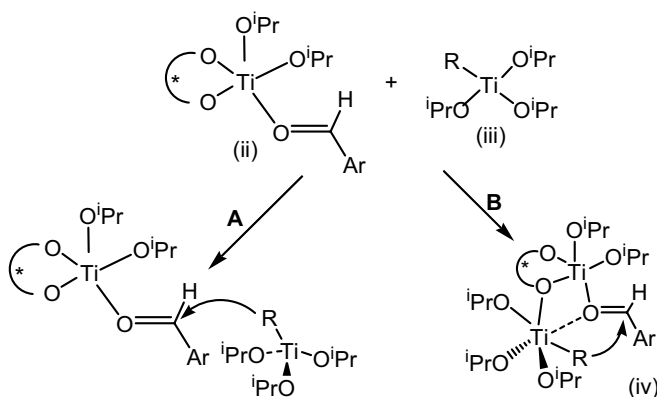

Figure 15 - Mechanism for the alkylation of aldehydes with organozinc reagents in the presence of a chiral ligand and Ti(O^iPr)₄, second part.

8.3.5.2. Factors influencing selectivity in enantioselective alkylations

The important factors for efficient enantioselective alkylations with organozinc reagents and $Ti(O^iPr)_4$, are basically the same as those previously mentioned for alkylations with organozinc reagents alone (see 8.2.3.). The titanium catalysed reactions, however, are usually carried out at lower temperatures for greater selectivity[22]. Temperatures in the range of -20ºC to -40ºC are the most commonly used for carrying out these reactions.

8.3.5.3. Some examples of enantioselective alkylations with diethyl zinc

Some examples of the enantioselective alkylation of benzaldehye with diethyl zinc using chiral ligands which require the presence of titanium complexes are indicated in Figure 16[23]. All of the products which are formed using these ligands have very high optical purity, greater than 90%.
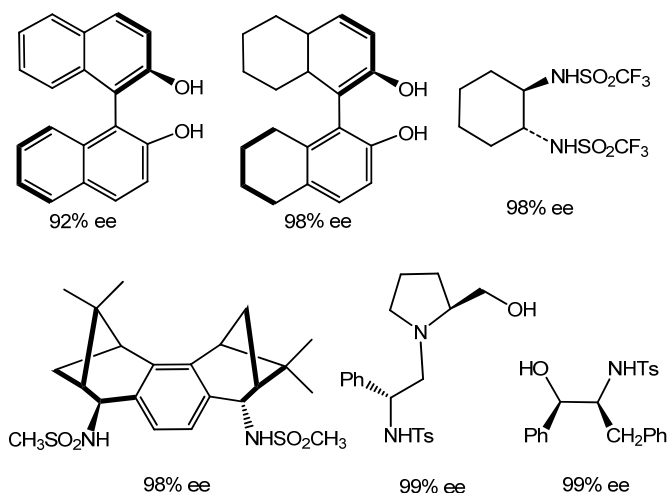
Figure 16 - Chiral ligands used in the enantioselective alkylation of benzaldehyde with diethyl zinc in the presence of $Ti(O^iPr)_4$. Below each ligand is the ee for the reaction product.

8.4. Conclusions

The enantioselective alkylation of aldehydes in the presence of organozinc reagents is an efficient and versatile method for the synthesis of optically active secondary alcohols. In these reactions, the presence of a chiral ligand serves two purposes. First of all, the chiral ligand is responsible for the induction of chirality in the reaction product. Secondly, the ligand is essential in order to activate the organozinc reagent by increasing the nucleophilicity of the alkyl group.

When the chiral ligands are strong Lewis bases, the alkylations of the aldehydes proceed smoothly, without the need of other additives. However, if the chiral ligands are weaker Lewis bases or if they are Lewis acids, the presence of $Ti(O^iPr)_4$ is essential for alkylation to occur. The function of the titanium complex is to increase the electrophilicity of the aldehyde and simultaneously the nucleophilicity of the organozinc reagent, in this way activating both reagents and favouring the alkylation reaction.

References

1. G.Q. Lin, Y.M. Li, A.S.C. Chan, *Principles and Applications of Asymmetric Synthesis*, John Wiley & Sons, Inc., New York, **2001**.

2. R. Whyman, *Applied Organometallic Chemistry and Catalysis*, Oxford University Press, Oxford, **1998**.

3. E.S.C. Temba, I.M.F. Oliveira, C.L. Donnici, *Quim. Nova,* **2003,** *26*, 112-122**.**

4. A.F. Pisarnitskii, *Applied Biochemistry and Microbiology*, **2001,** *37*, 552–560.

5. K. Tomioka, *Synthesis*, **1990**, 541-549.

6. a) S. Itsuno, K. Ito, A. Hirao, S. Nakahama, *J. Chem. Soc. Chem. Commun.,* **1983**, 469-470. b) S. Itsuno, K. Ito, Y. Sakurai, A. Hirao, S. Nakahama, *Bull. Chem. Soc. Jpn.,* **1987**, *60*, 395-396.

7. E.J. Corey, R.K. Bakshi, S. Shibata, *J. Am. Chem. Soc.,* **1987**, *109*, 5551-5553.

8. T. Mukaiyama, K. Soai, T. Sato, H. Shimizu, K. Suzuki, *J. Am. Chem. Soc.,* **1979**, *101*, 1455-1460.

9. K. Soai, N. Seiji, *Chem. Rev.,* **1992**, *92*, 833-856.

10. N. Oguni, T. Omi, *Tetrahedron Lett*., **1984**, 2823-2824.

11. M. Kitamura, S. Suga, K. Kawai, R. Noyori, *J. Am. Chem.* Soc., **1986**, *108*, 6071-6072.

12. a) M. Yamakawa, R. Noyori, *J. Am. Chem.* Soc., *1995, 117,* 6327-6335. b) M. Yamakawa, R. Noyori, *Organometallics*, **1999**, *18*, 128-133. c) B. Goldfuss, K.N. Houk, *J. Org. Chem.,* **1998**, *63,* 8998-9006

13. B. Goldfuss, see reference 12c).

14. a)K. Soai, T. Shibata in *Comprehensive Asymmetric Catalysis*, E.N. Jacobsen, A. Pfaltz, H. Yamamoto (Eds.), Springer-Verlag, Berlin, **1999**, vol. II, Chapter 26.1. b) L. Pu, H-B. Yu, *Chem. Rev.,* **2001**, *101*, 757-824. c) M. Casey, M.P. Smyth, *Synlett*, **2003**, 102-106.

15. a) S.L. Tseng, T.K. Yang, *Tetrahedron: Asymmetry*, **2004**, *15*, 3375-3380. b) A.L. Braga, R.M. Rubim, H.S. Schrekker, L.A. Wessjohann, M.W.G. Bolster, G. Zeni, J.A. Sehnem, *Tetrahedron: Asymmetry*, **2003**, *14*, 3291-3295. c) J. Mao, B. Wan, R. Wang, F. Wu, S. Lu, *J. Org. Chem.*, **2004**, *69*, 9123-9127.

16. a)Y. Hari, T. Aoyama, *Synthesis*, **2005**, *4*, 583-587. b)B. Fu, D.M. Du, J. Wang, *Tetrahedron: Asymmetry*, **2004**, *15*, 119-126. c)X.L. Bai, C.Q. Kang, X.D. Liu, L.X. Gao, *Tetrahedron: Asymmetry*, **2005**, *6*, 727-731. d) . Tanyeli, M. Stunbul, *Tetrahedron: Asymmetry*, **2005**, *16*, 2039-2043.

17. a)M.C. Wang, L.T. Liu, J.S. Zhang, Y.Y. Shi, D.K. Wang, *Tetrahedron: Asymmetry*, **2004**, *15*, 3853-3859. b) Y.W. Zhong, C.S. Jiang, M.H. Xu, G.Q. Lin, *Tetrahedron*, **2004**, *60*, 8861-8868. c) M. Yus, D.J. Ramón, O. Prieto, *Tetrahedron: Asymmetry*, **2003**, *14*, 1103-1114. d) M.P. Sibi, L.M. Stanley, *Tetrahedron: Asymmetry*, **2004**, *15*, 3353-3356. e) N. García-Delgado, M. Fontes, M.A. Pericàs, A. Riera, X. Verdaguer, *Tetrahedron: Asymmetry*, **2004**, *15*, 2085-2090.

18. a) M. Kitamura, *et. al.,* see ref. 11. b)C-S. Da, Z-J. Han, M. Ni, F. Yang, D-X Liu, Y.-F. Zhou, R. Wang, *Tetrahedron: Asymmetry,* **2003**, *14*, 659–665. c) P.J. Hermsen, J.G.O. Cremers, L. Thijs, B. Zwanenburg, *Tetrahedron Letters*, **2001**, *42*, 4243–4245. d) A.M. Garcıa, E.T. Vilar, A.G. Fraile, S.M. Cerero, P. Martınez-Ruiza, P.C. Villas, *Tetrahedron: Asymmetry,* **2002,** *13*, 1–4. e) A.L. Braga, *et. al.,* see ref. 15b). f) N. Hanyu, T. Aoki, T. Mino, M. Sakamoto, T. Fujitab, *Tetrahedron: Asymmetry,* **2000,** *11*, 4127–4136. g) M. Asami, H. Watanabe, K. Honda, S: Inoue, *Tetrahedron: Asymmetry,* **1998**, *9*, 4165-4173. h) S-L. Tseng, *et. al.,* see ref. 15a).

19. a) M.L. Richmond, C.T. Seto, *J. Org. Chem.,* **2003,** *68*, 7505-7508. b) M. Asami, *et. al.,* see ref. 18g). c) P.J. Hermsen, *et. al.,* see ref. 18c).

20. a) P.J. Walsh, *Acc. Chem. Res.,* **2003**, *36*, 739-749. b) J. Balsells, T.J. Davis, P. Carroll, P.J. Walsh, *J. Am. Chem. Soc.,* **2002**, *124*, 10336-10348. c) D.J. Ramón, M. Yus, *Chem. Rev.*, **2006**, *106*, 2126-2208.

21. a) P.J. Walsh, *see ref. 20a).* b) J. Balsells, et.al., see ref. 20b).

22. O. Prieto, D.J. Ramón, M. Yus, M., *Tetrahedron: Asymmetry*, **2000**, *11*, 1629-1644.

23. a) F-Y. Zhang C-W. Yip, R. Cao, A.S.C. Chan, *Tetrahedron: Asymmetry,* **1997**, *8*, 585-589. b)H. Takahashi, T. Kawakita, M. Ohno, M. Yoshioka, S. Kobayashi, S., *Tetrahedron,* **1992**, *48,* 5691-5700. c) L.A. Paquette, R. Zhou, *J. Org. Chem.,* **1999**, *64*, 7929-794. d) J. Mao, *et. al.,* see ref. 15c. e) J-S. You, M-Y. Shao, H-M. Gau, H-M., *Tetrahedron: Asymmetry,* **2001,** *12*, 2971–2975.

9. METHANOL CARBONYLATION: LIGANDS EVOLUTION

Zoraida Freixa

Institute of Chemical Research of Catalonia (ICIQ), Av. Països Catalans 16, 43007 – Tarragona, Spain

9.1. HISTORICAL DEVELOPMENT OF THE ACETIC ACID PRODUCTION

Acetic acid is a bulk chemical commodity industrially used for a wide range of applications, not only as a solvent, but also in the manufacture of cellulose acetate (for cigarette filters and photographic films) and vinyl acetate (paints, adhesives and textiles), as a bleach activator or in the manufacture of food, pharmaceuticals, pesticides, etc[1].

In fact, acetic acid is nearly as old as civilization itself. In all the cultures were beer or wine production was developed, they soon realized that vinegar was formed when exposed to air. The evolution of acetic acid production and the required technological development are strongly related to the historic availability of raw materials[2]. Although several synthetic (inorganic) routes were already known, until 1910 acetic acid was manufactured basically from wood or grain fermentation, which nowadays is still the preferred method for vinegar production.

Mercury catalyzed oxidation of acetylene (coming from coal) was the first industrial process for large-scale acetic acid production. The major disadvantages encountered (related to mercury toxicity) and the development of the petrochemical industry in the 1950s when the low-cost Middle East oil became available[3] prompted its replacement by the Wacker process; the Pd-Cu catalyzed synthesis of acetaldehyde coming for petroleum based ethylene. The sudden existence of an excess of light hydrocarbons (*n*-butane and naphtha) from the emerging petroleum refineries drove many companies to develop

oxidation processes to transform them into acetic acid (Mn or Co catalyzed). But these reactions usually lacked of selectivity, and many oxidation by-products were also formed[4,5].

With the continuous petroleum prices fluctuation (which ended with the crisis of 1973) many chemical industries soon realized of the importance of the development of new processes independent form petroleum prices[6]. In 1941 Reppe already demonstrated the potential of many metal carbonyls as catalysts for several reactions. In fact, in 1955 BASF commercialized the homogeneous methanol carbonylation route to acetic acid using nickel catalysts, which soon (in 1960) evolved to a iodide-promoted cobalt catalyzed process operating at elevated temperatures (200-250ºC) and pressures (500-700atm)[4], Figure 1.
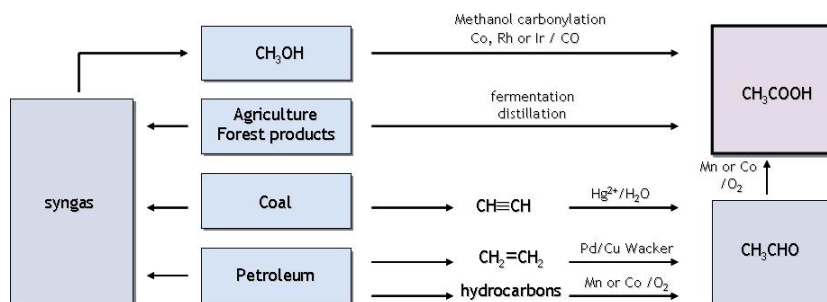
Figure 1 - Acetic acid production processes

In 1966, the rhodium-iodide process for methanol carbonylation was initiated at the Monsanto laboratories[7]. The rhodium catalyzed process operates at much milder conditions (180-220ºC, 30-40atm) compared to the cobalt based one, and with better performance, Table 1.

The first production plant based on this technology started operating in 1970 in Texas City with an initial capacity of 135,000 ton/y. In 1986 BP Chemicals (British Petroleum) acquired and further developed the technology while extending it all over the world. Nowadays the global production of acetic acid reaches eight million ton/y, and it is led by two companies, Celanese (using

"Monsanto" technology) and BP Chemicals with processes based on both rhodium and iridium[8].

TABLE 1 - Comparison of Rh and Co-based processes

	BASF	Monsanto-BP
metal	Co	Rh
temperature	230°C	150-200°C
pressure	600bar	30-60bar
[M]	10^{-1}M	10^{-3}M
selectivity (MeOH)	90 %	99%
selectivity (CO)	70%	90%

Methanol carbonylation, from an economical point of view, presents a clear advantage over all the former processes developed for the industrial production of acetic acid. Methanol and CO are relatively cheap feed-stocks, which can be obtained from different raw materials, which makes the whole process independent of petroleum prices. Methanol can be obtained from syngas (CO and H_2 mixture) coming from petroleum, natural gas or even from coal or biomass. These latest technologies are not yet on stream, but industries are considering them as powerful candidates for the future and pilot plants operate since the mid 1990s[9].

The process presents a 100% atom economy with all the atoms in the reactants going into the product (see Equation 1), and compared to previous methods benefits of a reduced waste and easier (and cheaper) product separation.

$$CH_3OH + CO \rightarrow CH_3COOH \quad \Delta G°=-17.8 \text{ kcal mol}^{-1}, \Delta H°= -135 \text{ kJ mol}^{-1} \quad (1)$$
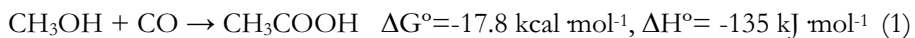
9.2. THE MONSANTO PROCESS

Mechanistically, the Monsanto process actually involves two interrelated catalytic cycles, one organometallic based on rhodium ionic species and an

organic one where iodide should be considered as the true catalyst, Figure 2. The two main components (rhodium and iodide) can be added in many forms. Under the reaction conditions RhI_3 is reduced by H_2O and CO to monovalent rhodium active species **1**, and methanol is converted to the iodo form, MeI.

The organometallic cycle comprises oxidative addition of MeI to $[RhI_2(CO)_2]^-$ **1** (generated *in situ*), which is considered to be the rate limiting step of the Monsanto process, ligand migration to generate the acyl complex **3**, CO coordination and reductive elimination of acyl iodide to regenerate the rhodium active species **1**. Acyl iodide enters the "organic" cycle where it is hydrolyzed to give acetic acid and HI which transforms MeOH into the more electrophilic MeI that comes into the organometallic cycle.
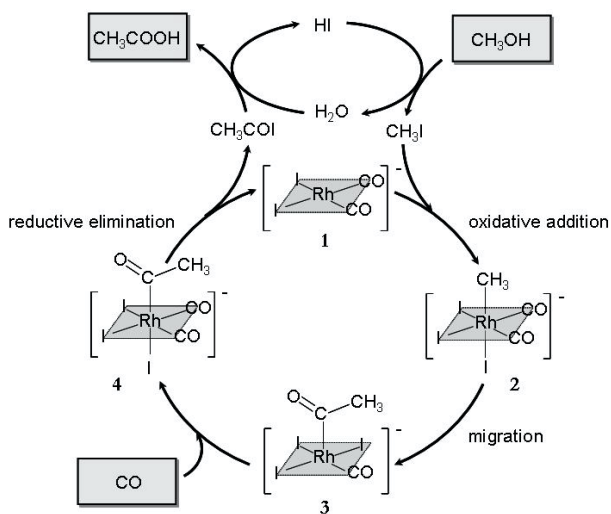
Figure 2 - Monsanto catalytic cycle.

It is important to notice that the two "organic" reactions ((2) and (3)) involving iodide show complete conversion. As a result, all of the iodide in the system occurs as a methyl iodide, and due to reaction (2), the rate of the catalytic cycle is independent of the methanol concentration[10]. This represents a very

important advantage from an economical point of view, because the whole process can operate in continuous at very high conversion diminishing the product separation costs.

$$CH_3OH + HI \rightarrow H_2O + CH_3I \tag{2}$$

$$CH_3COI + H_2O \rightarrow CH_3COOH + HI \tag{3}$$

One of the main drawbacks of the process is the loss of the expensive metal due to the formation of Rh(III) inactive species which, in areas of low CO pressure at the end of the reaction, precipitate as RhI_3. The inactive species $[RhI_4(CO)_2]^-$ can be produced by reaction of compounds **1** and **2** with HI according to reactions (4) and (5):

$$[RhI_2(CO)_2]^- + 2\ HI \rightarrow H_2 + [RhI_4(CO)_2]^- \tag{4}$$

$$[Rh(CH_3)I_3(CO)_2]^- + HI \rightarrow CH_4 + [RhI_4(CO)_2]^- \tag{5}$$

In the Monsanto process, Figure 3, this problem is solved by keeping the water content relatively high (around 14%), because it inhibits Rh precipitation by regenerating the Rh(I) active species from the labile $[RhI_4(CO)_2]^-$ through reaction (6):

$$[RhI_4(CO)_2]^- + H_2O + CO \rightarrow [RhI_2(CO)_2]^- + 2\ HI + CO_2 \tag{6}$$

In fact, the presence of water is controversial; it is needed to maintain the rhodium in the active Rh(I) form, but there are also several problems associated with keeping it at high concentrations:

a) The reaction of H_2O with CO (7) through the rhodium catalyzed water-gas shift reaction (WGSR) causes the loss of one of the feed-stocks and a selectivity in CO as low as 90%, Table 1.

$$CO + H_2O \rightarrow H_2 + CO_2 \tag{7}$$

b) For the synthesis of acetic anhydride, water needs to be removed from the product by distillation at the end of the reaction, increasing the production costs considerably.
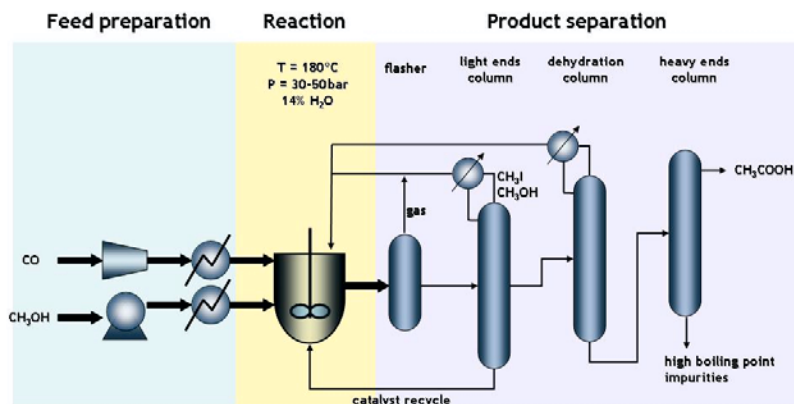
Figure 3 – Monsanto acetic acid process.

9.3. OXIDATIVE ADDITION OF MeI; THE RATE LIMITING STEP

Kinetic studies show that the whole process follows a second order rate-equation (8); first order dependence on both rhodium and MeI, and zero order in MeOH (as mentioned before) and CO.

$$\text{rate} = k \, [\{Rh(CO)_2I_2\}^-] \cdot [MeI] \tag{8}$$

These data point to the oxidative addition of MeI to **1** as being the rate-determining step of the rhodium-iodide catalyzed process. Kinetics on this elementary step can be performed by using *in situ* IR spectroscopy because the species involved (and in fact all the species in the Monsanto catalytic cycle) contain CO ligands. Due to their π acceptor capacity, the CO-stretching frequencies shift considerably when evolving from a Rh(I) to a Rh(III) complex

(the more electron rich centre, the lower the CO-stretching frequency), as exemplified in Figure 4 and Table 2.
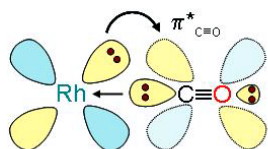
TABLE 2 – CO stretching frequencies of compounds 1-3.

species	$\nu_{CO\text{-stretching}}$ (cm^{-1})
$[Rh(CO)_2I_2]^-$ **1**	1980, 2050
$[Rh(CO)_2(CH_3)I_3]^-$ **2**	2104, 2065
$[Rh(CO)(COCH_3)I_3]^-$ **3**	2061, 1740(acyl)

Figure 4 - Schematic representation of CO coordination mode

The results obtained confirm a second order rate constant for the Monsanto system with k = 0.0293 $M^{-1} \cdot s^{-1}$, the species $[Rh(CO)_2I_2]^-$ **1** being the resting state of the catalyst, and oxidative addition as the rate limiting step.

It is generally accepted that the oxidative addition follows a two-step S_N2 mechanism; nucleophilic attack by the metal on the methyl carbon to displace iodide, presumably with inversion of configuration at the carbon atom, and a subsequent iodide coordination to the five-coordinate rhodium complex to give the alkyl-complex **2**, Figure 5[11,12]. The product of this reaction has been fully characterized spectroscopically[7a,13,14,15]. This mechanism is supported by the large negative activation entropy calculated that indicate a highly organized transition state (TS). Although there is general agreement on the mechanism, the theoretical calculations with respect to the geometry of the TS are still controversial, but the main interaction in the Rh-C bond formation seems to be between a full metal d_z^2-orbital and an empty C-I σ^*-orbital[16,17].
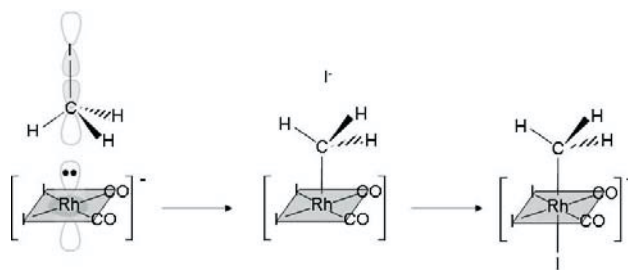
Figure 5 – Oxidative addition of MeI to species **1**.

A general approach to facilitate the oxidative addition of MeI to the active rhodium species, and therefore to enhance the rate of the overall process, is to increase the nucleophilicity of the metal center. This is accomplished by substituting CO and I for stronger donor ligands. In most of the cases either a chelating or two donating ligands are used, and a neutral [Rh(L)(CO)I] (L= chelating or two monodentate ligands) active species is generated.

In order to get an insight into the activity of the related ligand-modified systems, independent kinetic studies pertaining only to this elementary step can be performed by using IR spectroscopy (a CO ligand is still present!). Depending on the relative rates of oxidative addition/methyl migration, sometimes the directly corresponding acyl compound is observed, but occasionally (*vide infra*) the alkyl intermediate, the product of the oxidative addition, can be detected by IR spectroscopy or even isolated as the sole product of the reaction, Figure 6.
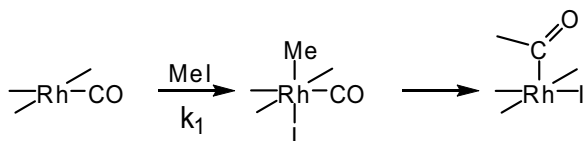
Figure 6 - MeI oxidative addition and subsequent migration steps

In Table 3 are presented the values of some second-order rate constants and activation parameters for MeI oxidative addition to rhodium complexes when

using several ligands (Scheme 1). They have been calculated by measuring pseudo first-order constants (k_{obs}) (using at least 10-fold excess of MeI in CH_2Cl_2) at different temperatures and MeI concentrations. In all the cases, a first-order dependence on both MeI and rhodium complex is observed for the reactions.

TABLE 3 - ν(CO)-IR of the complexes [RhX(CO)L] (X = Cl or I), and their reactivity toward MeI.

references	added ligand (L)	ν(CO) (cm^{-1}) [RhI(CO)L]	$10^3 k_1$ (M^{-1}s^{-1})	$\Delta H^{\neq}$ (kJmol^{-1})	$\Delta S^{\neq}$ (Jmol^{-1}K^{-1})
13,15	a)	2055, 1985	0.0293	50±1	-165±4
18	**2** PPh$_3$a)	1980	0.0276	43	-179
19	**2** PEt$_3$	1961	1.37	56±13	-112±44
21	**5**	1981	no reaction		
20	**6**	1970	no reaction		
22	**2** **7**b)	1943	0.0441	36±1	-189±3
	8	1987	1.19	47±1	-144±2
	9	1983	1.14	34±4	-188±13
	10	2011	1.41	40±1	-167±2

a) neat MeI; b) [MeI] = 1.6M, CH_2Cl_2, data concerning only the forward reaction.

| **5** | SPANphos **6** | **7** |

| dppms **8** | dppmo **9** | dppe **10** |

Scheme 1
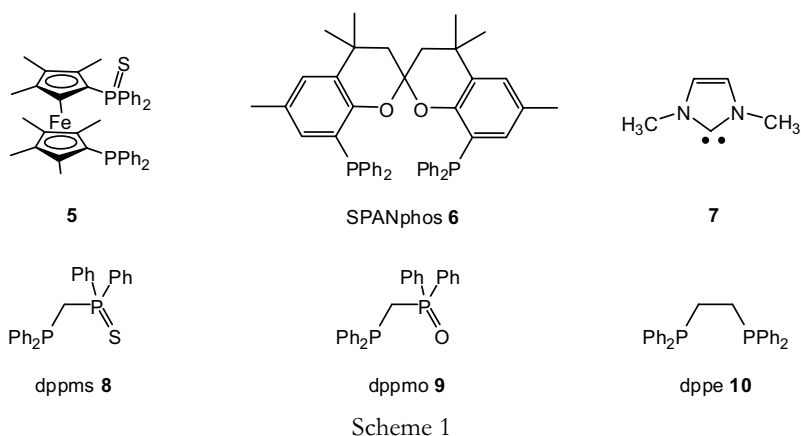
The frequency of the IR stretch vibration ν(CO) of the catalytically active complex [RhI(CO)L$_2$] is usually considered as a measure of the electron density

on the metal center, and consequently its nucleophilicity and reactivity toward MeI. It is generally accepted that the larger the electron density on the metal, the lower the ν(CO), due to electron back-donation on the π^*-orbital of the coordinated CO (*vide supra* Figure 4). If we compare the ν(CO) of the [Rh(CO)(PPh$_3$)$_2$Cl] and [Rh(CO)(PEt$_3$)$_2$Cl] we observe, as expected, a lower CO stretching frequency for the more basic PEt$_3$ derivative, and an enhanced reactivity of versus MeI (Table 3, Scheme 2). Nevertheless, some examples provide evidence that a direct correlation between the frequency of the IR stretch vibration of the coordinated CO and the reactivity of the rhodium complex versus MeI cannot be always established, but several other factors need to be taken into account.

$$\nu(CO)= 1961\,cm^{-1} \qquad \nu(CO)= 1980\,cm^{-1} \qquad \nu(CO)= 2010\,cm^{-1}$$
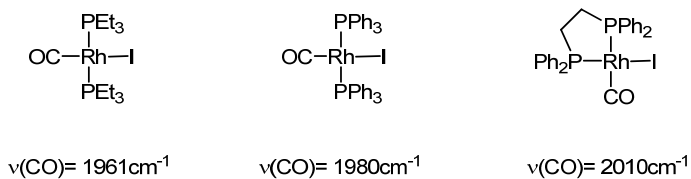
Scheme 2

First, the relative disposition of the ligands around the rhodium center plays a role. If we compare [RhI(CO)(dppe)] with [RhI(CO)(PEt$_3$)$_2$], Scheme 2, which each exhibit similar reactivity towards MeI, the frequencies of the corresponding ν(CO) differ by *ca.* 50 cm^{-1}. This can be attributed to the different relative disposition of the donor ligands in the corresponding active species (*cis* and *trans* respectively). A carbonyl trans to iodide experiences considerably more back-donation than one trans to a phosphine and it is reflected in a much lower ν(CO).

Secondly, not only electronic, but also steric effects play an important role in this elementary step. Ligands **5** and **6** (SPANphos) represent extreme cases[20,21]. If one compares ligands **5** and **8** (dppms), both with P and S donor atoms, and

identical disposition of the ligands in the "active" species [Rh(CO)Cl(L)] (with CO trans to the stronger sigma donor S), they show very similar CO stretching frequencies. Surprisingly complex [Rh(CO)Cl(**5**)] does not react with MeI via oxidative addition! This difference in reactivity is attributed to the fact that the backbone of the ligand eclipses one of the axial coordination sites of the rhodium center. In the case of SPANphos **6** this blockage is more evident; when using this trans-coordinating diphosphine, the backbone of the ligand completely occupies one of the axial sites of the metal centre, Figure 7. This strong steric hindrance is responsible of a complete inhibition of the oxidative addition (according to the S_N2 mechanism discussed before).
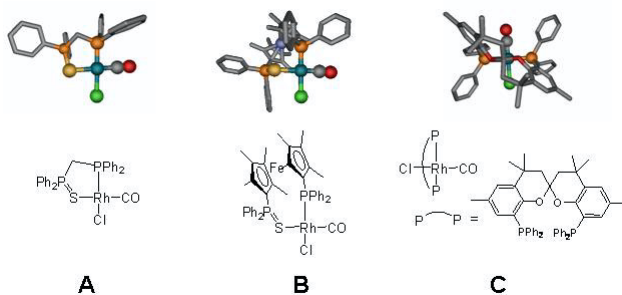
Figure 7 - Molecular structures (X-ray) of [Rh(CO)Cl(**5**)] **A**, [Rh(CO)Cl(**6**)] **B**, and [Rh(CO)Cl(**8**)] **C**.

In the case of ligand **7**[22], despite the higher nucleophilicity of the corresponding Rh-biscarbene complex that could be envisaged due to the low value of their corresponding ν(CO), they display a very low reactivity versus MeI, see Table 3. In this case it should be also attributed to the characteristic ligand disposition in which the NCN plane is perpendicular to the Rh(I) coordination plane, and therefore the R substituents partially block the rhodium axial sites inhibiting nucleophilic attack on MeI.

In order to accelerate the rate MeI oxidative addition (and consequently the rate of the overall process) electron donating ligands need to be used. The IR stretch vibration of the CO coordinated to the metal can be used to get an insight into the electron density on the rhodium center and its reactivity versus MeI, previously to further tests, but steric effects need to be also taken into account.

In general, the basic requirements for a ligand to generate an effective catalytic system for methanol carbonylation are: basicity in order to increase the nucleophilicity of the rhodium center and sterically not to block the axial positions of the square planar rhodium active species. As we will mention later stability is also a key feature!

9.4. LIGANDS DESIGN

In the last 20 years many effort has been directed to develop ligands able to increase the activity of the rhodium-iodide based Monsanto system. In some cases, even if they do not contribute with a significant reaction improvement, they are crucial for a better understanding of the reaction mechanism, and constitute basic pillars for further developments. An exhaustive recompilation of all the systems studies exceeds the scope of this book. In this chapter we will restrict to the most representative phosphine-based systems.

In 1997 Rankin *et al.* reported a PEt$_3$-rhodium modified system[23]. When employing this basic phosphine, pursuing an increase in the nucleophilicity of the rhodium active species, the rate of oxidative addition of MeI to [RhI(CO)(PEt$_3$)$_2$] becomes *ca.* 47 times higher than the one reported for **1** at 25°C. The basicity of the ligand produce a retard on migration, which becomes 38 times slower than in the original Monsanto system (but not enough to make it rate determining). Although in comparison to the Monsanto system there is a large increase in the rate of oxidative addition, it represents only an increase in

activity of 1.8 under catalytic conditions (150ºC). Unfortunately, at this temperature, loss of activity is observed after *ca.* 10 minutes, due to degradation of the catalytically active system to $[Rh(CO)_2I_2]^-$. Decomposition proceeds via reaction of $[RhI_2(CO)(CH_3)(PEt_3)_2]$ with HI to generate $[RhI_3(CO)(PEt_3)_2]$, which reductively eliminates $[PEt_3I]^+$ leading to $OPEt_3$.

Even though the use of basic phosphines, which increases the nucleophilicity of the rhodium center, was initially considered a very promising strategy[23], their instability under the harsh conditions of the process constituted a major drawback for their application. Attempts to circumvent the decomposition were undertaken by using bidentate diphosphines, which stabilize the active rhodium species by the chelate effect[24,25]. When using dppe **10** methyl iodide oxidative addition is approximately 48 times faster than the one observed with **1**, but no remarkable improvement is achieved under catalytic conditions[26]. Surprisingly, Carraz *et al.*[27] reported the use of the related asymmetrically substituted 1,2-ethanediyl diphosphines **11**, Scheme 3, that are very stable under the reaction conditions, although they do not represent an improvement on the catalytic activity when compared with the Monsanto process. At the end of the reaction a mixture of diphosphine Rh(III) carbonyl complexes can be isolated and characterized, and a second run can be performed without loss of activity.

Ph_2P PAr_2

11a Ar= C_6H_4OMe-4   **11d** Ar= $C_6H_3F_2$-3,5
11b Ar= C_6H_4F-3   **11e** Ar= $C_6H_2F_3$-3,4,5
11c Ar= $C_6H_4CF_3$-3   **11f** Ar= $C_6H_3(CF_3)_2$-3,5
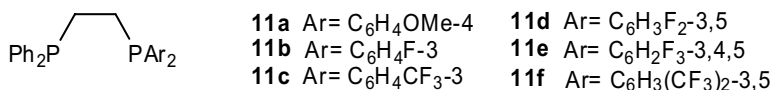
Scheme 3

An alternative strategy to increase the activity and attain stability of the systems is the use of hemilabile phosphine ligands (PX; X= O, S). They are supposed to accomplish both; stabilization of the complex via the "chelate" effect and

increase the nucleophilicity of the rhodium by coordination of a hetero-donor atom.

A comparative study of PS and PO ligands able to form 5-membered chelate rings (**8**[28] and **9**[29]) shows that the corresponding [RhI(CO)(PX)] complexes react between 35 and 50 times faster with MeI than **1**, an activity similar to the one observed with PEt$_3$[30,31]. This enhancement in activity is attributed to the good donor properties of the ligands.

Another example of this family of ligands using oxygen as a heteroatom is methyl 2-diphenylphosphinobenzoate **12**[32]. Depending on the stoichiometry of the reaction with [Rh(CO)$_2$Cl]$_2$, the corresponding rhodium species [RhCl(CO)(**12**)], and [RhCl(CO)(**12**)$_2$], are formed, Scheme 4. In the former complex, the ligand acts as a chelate through the P and O atoms, whereas in the latter two phosphines coordinate in a trans fashion, and secondary Rh-O interactions are suggested. Due to the increased nucleophilicity of the rhodium center, both systems show an activity that is *ca.* 1.5 times higher than Monsanto's system under the same catalytic conditions. This increase in nucleophilicity is in agreement with the low values of ν(CO) observed (1979 and 1949 cm^{-1} respectively). Nevertheless complex [RhCl(CO)(**12**)$_2$] shows slightly lower reaction rates, which is attributed to the increase in steric hindrance about the metal center on account of the presence of two ligands.
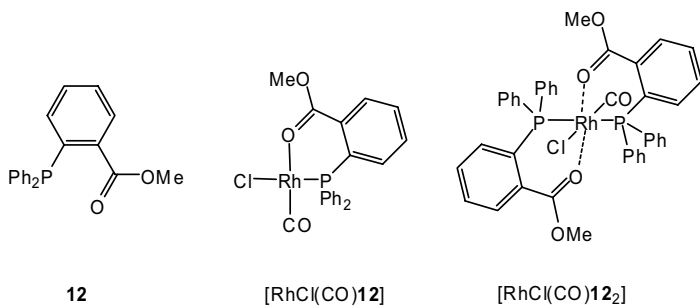
Scheme 4

Very recently, an extreme P-X system appeared in the literature[33], which can be considered as the fastest system for oxidative addition of MeI reported until now. It consists of a phosphine-cyclopentadienyl-linked anionic ligand. Several derivatives (with different substitution on the phosphorous atom and cyclopentadienyl moiety) and their corresponding rhodium (I) complexes have been prepared **13a-d** (Scheme 5).
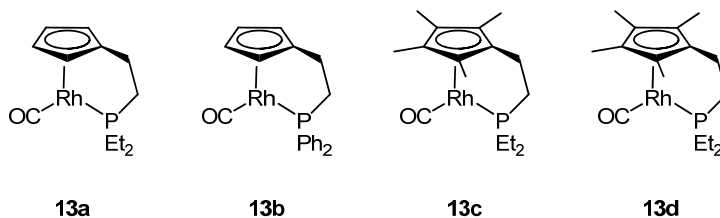
Scheme 5

TABLE 4 - ν(CO)-IR of the complexes 13 a-d, and their reactivity toward MeI.

	13a	13b	13c	13d
νCO (cm^{-1})	1938	1947	1924	1933
k (M^{-1}s^{-1})	n.d.	78 ·10^3	n.d.	2230 ·10^3

When studying the methyl iodide oxidative addition to these systems they showed a second order constants (see Table 4) 76000 times faster than the ones observed for the Monsanto's system! In the case of the more basic diethyl phosphine derivatives they could not even be measured. They also showed a good stability under catalytic conditions due to the chelate effect. Nevertheless the activity observed is only 1.2 times higher than the original rhodium without added ligands. It is postulated that the extraordinary increase of the electron density on the rhodium center produced by the cyclopentadienyl-phosphine ligands made the rate determining step of the reaction to be migration of the

methyl to for the acyl compound. This elementary step is known to be retarded with the use of extremely basic ligands.

In an effort to develop new systems able to combine both stability and the appropriate activity, Süss-Fink and co-workers reported a family of trans-spanning, but flexible diphosphines[34,35,36]. These ligands form stable complexes (due to the chelate effect) which resemble the ones obtained with PEt₃ (*trans*-[RhI(CO)(PEt₃)₂]) with the two phosphorus atoms in a trans disposition. These ligands are (as **12**) benzoic acid diphenylphosphine derivatives, and are supposed to increase the electron density on the rhodium center due to a weak Rh-O interaction, Scheme 6.
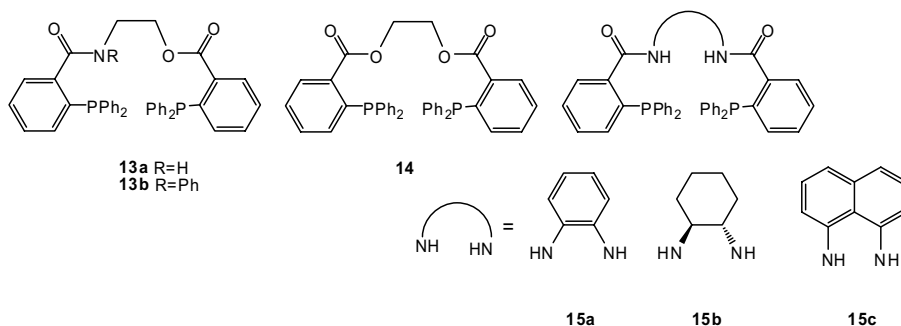
Scheme 6

When the corresponding rhodium complexes are tested in methanol carbonylation the activity obtained is *ca.* 2.5 times higher than the one obtained with the Monsanto system under the same conditions. The stability of the systems is evident by the ability to perform several runs without any noticeable loss in activity. From the residue of the reaction when ligand **13b** is employed, apart from the corresponding [RhI(CO)(**13b**)] complex, the dinuclear isomeric compounds **16a** and **16b** were isolated and characterized by X-ray diffraction. Presumably, these dinuclear compounds act as resting states for the acyl complex [RhI₂(COMe)(**13b**)] which arises from it by loss of diphosphine, Scheme 7.
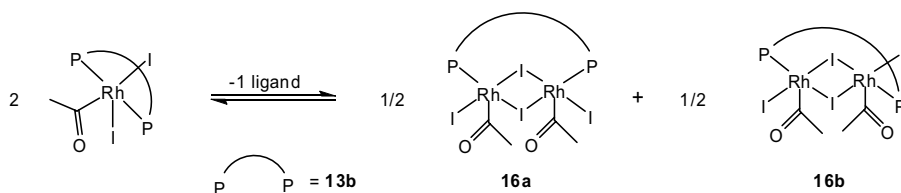
Scheme 7

Although the proposed catalytic cycle is analogous to Monsanto's one, recent studies on a related trans coordinating diphosphine, SPANphos **6**, suggest that a catalytic cycle involving only dinuclear species cannot be discarded[20]. Surprisingly, even if the corresponding trans-[RhI(CO)(**6**)] renders systems as active as the Süss-Fink analogues, when tested in an elementary step, they show no reaction in the oxidative addition of MeI (*vide supra*). The observed catalytic activity has been attributed to dinuclear species formed under catalytic conditions. The dinuclear compound [Rh$_2$(μ-Cl)$_2$(CO)$_2$(**6**)] reacts with MeI at 25 ºC with a k$_1$ value of *ca.* 0.025 s^{-1}M^{-1} and currently they represent the fastest phosphine based systems reported for methanol carbonylation. According to spectroscopic and GC-MS analysis, the products of the MeI oxidative addition are dinuclear monoacyl derivatives **17**, Scheme 8.
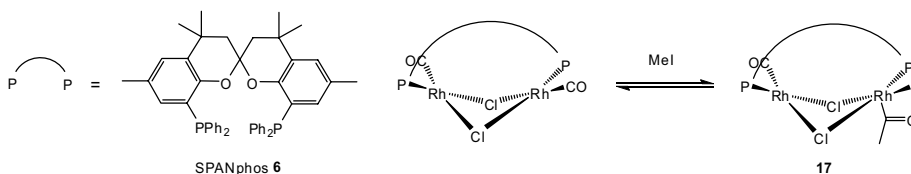
Scheme 8

The reactivity of dinuclear rhodium compounds toward MeI has been subject of study from the late 70's[37,38]. Unfortunately, no kinetic data is available, but the corresponding mono- and bis-acyl derivatives have been detected. Further

studies to corroborate the real mechanism of these promising systems are nowadays under development.

References

1. A. Haynes, *Educ. Chem.*, **2001**, *38*, 99-101.

2. R.P.A Sneeden. in *Comprehensive Organometallic Chemistry I*, G. Wilkinson, F.G.A. Sone, E.W. Abel (Eds.), Elsevier, **1982**, Vol.8, pp.73-79.

3. http://www.chemsystems.com/search/docs/prospectus/MC06_Polygeneration _Coal_%20Pros.pdf

4. N. Yoneda, S. Kusano, M. Yasui, P. Pujado, S. Wilcher, *Appl. Catal. A: Gen.*, **2001**, *221*, 253-265.

5. J.A. Moulijn, P.W.N.M. van Leeuwen, R.A. Santen in *Catalysis. An Integrated Approach toHomogeneous, Heterogeneous and Industrial Catalysis*, Elsevier, J.A. Moulijn, P.W.N.M. van Leeuwen, R.A. Santen (Eds) **1993**, pp.15.

6. J.R. Zoeller, V.H. Agreda, S.L. Cook, N.L. Lafferty, W. Polichnowski, D.M. Pond, *Catal. Today,* **1992**, *13*, 73-91.

7. a) D. Forster, *J. Am. Chem. Soc.,* **1976**, *98*, 846-848. b) D. Forster, *Adv. Organomet. Chem.*, **1979**, *17*, 255.

8. Q. Smejkal, D. Linke, M. Baerns, *Chem. Eng. Process.*, **2005**, *44,* 421-428.

9. http://www.greener-industry.org/

10. C. Claver, P.W.N.M. van Leeuwen in *Comprehensive Coordination Chemistry II*, Elsevier, J.A. McCleverty and T.J. Meyer (Eds.)*,* **2003**,Vol. 9, 141-206.

11. T.R. Griffin, D.B. Cook, A. Haynes, J.M. Pearson, D. Monti, G. Morris, *J. Am. Chem. Soc.*, **1996**, *118*, 3029-3030.

12. V. Chauby, J-C. Daran, C.S.B. Berre, F. Malbosc, P. Kalck, O.D. Gonzalez, C.E. Haslam, A. Haynes, *Inorg. Chem.*, **2002**, *41*, 3280-3290.

13. W. Adamson, J.J. Daly, D. Forster, *J. Organomet. Chem.*, **1974**, *1*, C17-C19.

14. A. Haynes, B.E. Mann, D.J. Gulliver, G.E. Morris, P.M. Maitlis, *J. Am. Chem. Soc.*, **1991**, *113*, 8567-8569.

15. A. Haynes, B.E. Mann, G.E. Morris, P.M. Maitlis, *J. Am. Chem. Soc.,* **1993**, *115*, 4093-4100.

16. M. Cheong, T. Ziegler, *Organometallics*, **2005**, *24* , 3053-3058.

17. M. Feliz, Z. Freixa, P.W.N.M. van Leeuwen, C. Bo, *Organometallics*, **2005**, *24*, 5718-5723.

18. I.C. Douek, G. Wilkinson, *J. Chem. Soc. (A)*, **1969**, 2604-2610.

19. a) J. Rankin, A.D. Poole, A.C. Benyei, D.J. Cole-Hamilton, *J. Chem. Commun.*, **1997**, 1835-1836. b) J. Rankin, A.C. Benyei, A.D. Poole, D.J. Cole-Hamilton, *J. Chem. Soc., Dalton Trans.*, **1999**, 3771-3782.

20. Z. Freixa, P.J.C. Kamer, M. Lutz, A.L. Spek, P.W.N.M. van Leeuwen, *Ang. Chem. Int. Ed.,* **2005**, *44*, 4385-4388.

21. R. Broussier, M. Laly, P. Perron, B. Gautheron, I.E. Nifant'ev, J.A.K. Howard, L.G. Kuz'mina, P. Kalck, *J. Organomet. Chem*., **1999**, *587*, 104-112.

22. H.C. Martin, N.H. James, J. Aitken, J.A. Gaunt, H. Adams, A. Haynes, *Organometallics,* **2003**, *22*, 4451-4458.

23. a) J. Rankin, A.D. Poole, A.C. Benyei, D. J. Cole-Hamilton, *J. Chem. Commun*., **1997**, 1835-1836. b) J. Rankin, A.C. Benyei, A.D. Poole, D.J. Cole-Hamilton, *J. Chem. Soc., Dalton Trans.*, **1999**, 3771-3782.

24. C.M. Bartish, (Air Products & Chemicals, Inc.) U.S. Patent 4,102,920, January 13, **1977**.

25. a) S. Gaemers, J.G. Sunley (BP Chemicals Limited) PCT Int. Appl. **2004**, WO 2004/101487. b) S. Gaemers, J.G. Sunley, (BP Chemicals Limited) PCT Int. Appl. **2004**, WO 2004/101488.

26. L. Gonsalvi, H. Adams, G.J. Sunley, E. Ditzel, A. Haynes, *J. Am. Chem. Soc.*, **1999**, *121*, 11233-11234.

27. a) C-A. Carraz, E.J. Ditzel, A.G. Orpen, D.D. Ellis, P.G. Pringle, G.J. Sunley, *Chem. Commun*., **2000**, 1277-1278.b) M. J. Baker, C-A. Carraz, E. J. Ditzel,; P. G. Pringle, G.J. Sunley, U.K. Pat. Appl. 2,336,154., March 31, **1999**.

28. M.J. Baker, M.F. Giles, A.G. Orpen, M.J. Taylor, R.J. Watt, *J. Chem. Soc., Chem. Commun.*, **1995**, 197-198.

29. R.W. Wegman, A.G. Abatjoglou, A.M. Harrison, *J. Chem. Soc. Chem. Commun.*, **1987**, 1891-1892.

30. L. Gonsalvi , H. Adams, G.J. Sunley, E. Ditzel, A. Haynes, *J. Am. Chem. Soc.*, **2002**, *124*, 13597-13612.

31. L. Gonsalvi, H. Adams, G.J. Sunley, E. Ditzel, A. Haynes, *J. Am. Chem. Soc.*, **1999**, *121*, 11233-11234.

32. D.K. Dutta, , J.D. Woollins, A.M.Z. Slawin, D. Konwar, P. Das, M. Sharma, P. Bhattacharyya, S.M. Autcott, *Dalton Trans.*, **2003**, 2674-2679.

33. A.C. McConnell, P.J. Pogorzelec, A.M.Z. Slawin, G.L. Williams, P.I.P. Elliott, A. Haynes, A.C. Marr, D.J. Cole-Hamilton, *Dalton Trans.*, **2006**, *1*, 91-107.

34. S. Burger, B. Therrien, G. Süss-Fink, *Helv. Chim. Acta*, **2005**, *88*, 478-486.

35. C.M. Thomas, G. Süss-Fink, *Coord. Chem. Rev.,* **2003**, *243*, 125-142.

36. C.M. Thomas, R. Mafia, B. Therrien, E. Rusanov, H. Stœckli-Evans, G. Süss-Fink, *Chem. Eur. J.*, **2002**, *8*, 3343-3352.

37. A. Mayanza, J-J. Bonnet, J. Galy, P. Kalck, R. Poilblanc, *J. Chem. Research (S)*, **1980**, 146.

38. M.J. Doyle, A. Mayanza, J-J. Bonnet, P. Kalck, R. Poilblanc, *J. Organomet. Chem.*, **1978**, *146*, 293-310.

10. Industrial Homogeneous Catalysis: from bulk to fine

Piet W.N.M. van Leeuwen and Zoraida Freixa

Institute of Chemical Research of Catalonia (ICIQ), Av. Països Catalans 16, 43007 – Tarragona, Spain (fax +34- 977 920 221, e-mail: pvanleeuwen@iciq.es).

10.1. Introduction

Chemists that are not familiar with catalysis, or more in particular homogeneous catalysis, usually have two misconceptions about homogeneous catalysis. Firstly, because of its presumed complexity and hence high costs it is not suited for bulk chemistry and applications can be expected for fine chemicals only; on the longer term perhaps one might find bulk chemical processes. Secondly, separation of the catalyst and the reaction product is an insurmountable problem that can only be solved at high cost. Neither one is true, but both complexity and separation are important issues in a somewhat different way. The complex nature of (homogeneous) catalysis makes that one can rarely take a catalyst from the shelf and use it for a new reaction as the results will often be mediocre. In transition metal complex catalysis usually one has to look into the metal salt precursor, the ligand, the solvents and activators to be used, the work-up method, recycling of reactants, catalyst stability and recovery, and thus several years of research may be needed before a catalyst can be used to our advantage. As a result, for fine chemicals, which have an annual turnover of only a few million or tens of millions of Euros, research costs for developing a new or modified catalyst may be too high. The history of homogeneous catalysis shows that the major developments took place as part of bulk chemical syntheses, such as oxidation of alkenes and methylaromatics, carbonylation of methanol and alkenes, oligomerization and polymerization of alkenes, and hydrocyanation of alkenes. Asymmetric hydrogenation forms an exception as this development started in the 70s and clearly concerned small

scale chemicals, but its broad potential was early recognized. It soon found commercial application in the synthesis of L-Dopa.

Here we will focus on metal catalysts in solution that have found widespread utilization in chemical industry for the manufacture of bulk chemicals, fine chemicals, and pharmaceuticals and in organic synthesis in the laboratory. The catalysts presented are important for a variety of reactions including hydrogenation, isomerization of alkenes, oligomerization, polymerization, carbonylation, hydroformylation, hydrocyanation, metathesis, polyester formation, etc. Many catalysts display high rates and selectivities for conversions that would have taken many steps in the absence of the catalyst or would not have been possible at all. Many of the catalytic reactions show a high atom economy, i.e. a high percentage of the atoms of the starting materials end up in the final product, as by-product formation is minimized.

Homogeneous catalysis concerns catalytic processes in which the catalyst and all reagents are in the same phase, and within this definition the oldest process, apart from enzymatic ones, is probably the lead chamber process for making sulfuric acid, all substances being in the gas phase. A modern example of gas phase catalysis includes ozone breakdown by chlorine atoms as catalyst! The many acid and base catalyzed reactions in organic chemistry that we know also belong to the realm of homogeneous catalysis. Most commonly today, we refer to transition metal catalyzed reactions when we talk about homogeneous catalysis. The oldest, industrially applied process is the addition of water to acetylene (from coal in electrically operated carbide ovens) catalyzed by mercury salts in sulfuric acid, a process operated in the twenties of the previous century. In spite of the catalyst, this is a very slow reaction and huge quantities of solvent and catalyst are required. The product made from this is acetic acid and it is interesting to follow its history in relation to circumstances and requirements.

The production of acetaldehyde after the beginning of the petrochemical era was based on ethylene and its oxidation via the Wacker process. Another route was already available using methanol (from syn gas), carbon monoxide, and cobalt carbonyl catalysts, but this required high pressures (600 bar), temperatures, gave low selectivities and was used by few companies only (BASF). Monsanto reported a first breakthrough, with highly selective and active rhodium catalysts. Nowadays the global production of acetic acid is led by two companies, Celanese (using "Monsanto" technology) and BP Chemicals with processes based on iridium as well.

Hydroformylation has been studied extensively and phosphorus ligand effects have led to highly active and selective catalysts. Nevertheless, only three ligands are of commercial importance, CO, PPh_3 and tppts. While alternative catalysts have become available both as ligand modified rhodium catalysts and catalysts based on other metals, for higher alkenes one still uses the classic cobalt catalysts.

Another important achievement of the last two decades has been the development of highly stereoselective catalysts for the synthesis of polyalkene polymers. By rational design, step by step improved catalysts have been found and both high rates and selectivities for e.g. polypropylene can be obtained. Industrial applications are still scarce and do not concern stereoselective polymers, but rather branched polyethylene!

When we neglect small differences, the number of processes (or better catalysts) used for making bulk chemicals is rather small and the life-time of a plant is rather long and thus it should not surprise us that the number of implementations is very low.

Application of homogeneous catalysts in the production of fine chemical intermediates is a somewhat more recent development. A large amount of knowledge on homogeneous catalysis has been collected while studying large-scale processes such as methanol carbonylation, hydroformylation, and

hydrocyanation. Reactions of importance now in fine chemicals are i.e. asymmetric hydrogenation, cross coupling, and epoxidation catalysis. In this chapter we will try to answer several of the implicit questions raised in the above.

10.2. ACETALDEHYDE

The production of acetaldehyde is a good example for showing the importance of feedstocks available in a certain period of history. In the acetylene era it was made via hydration of acetylene with the use of a mercury catalyst with low activity. We can calculate that large vessels of mercury sulfate and sulfuric acid were needed to carry out this reaction during the 1920s. Most likely this was the first metal catalyzed homogeneous reaction involving metal-to-carbon bonds (acetylene binds to mercury, and water attacks the activated acetylene); Friedel-Crafts reactions, using aluminum chloride are older than this reaction. The first reaction that attracts our interest in this context is the production of a bulk chemical.

Hydration of acetylene

$C_2H_2 + H_2O \rightarrow CH_3CHO$ ΔH = - 151 kJ/mol

60-80 °C, 1 bar, $HgSO_4$, 1-3 g/l in 25% H_2SO_4

Acetylene from coal, electricity, calcium carbide.

TOF 20-40 $m.m^{-1}.h^{-1}$

Today, a similar reaction is still used for the production of vinyl esters of higher acids for the paint industry, which uses the less toxic zinc metal to catalyze the addition of a carboxylic acid to acetylene. A schematic process scheme is shown below.

Scheme hydration acetylene (Lonza, Griesheim)

gas/liq separator
vent
condensor
H_2O
light ends

Reactor
$HgSO_4$ 10kg
H_2SO_4 25%
H_2O 3.5 m^3
80°C
1bar

scrubber

CH_3CHO

C_2H_2

gas recycle

10% product
in water

H_2O

distillation towers
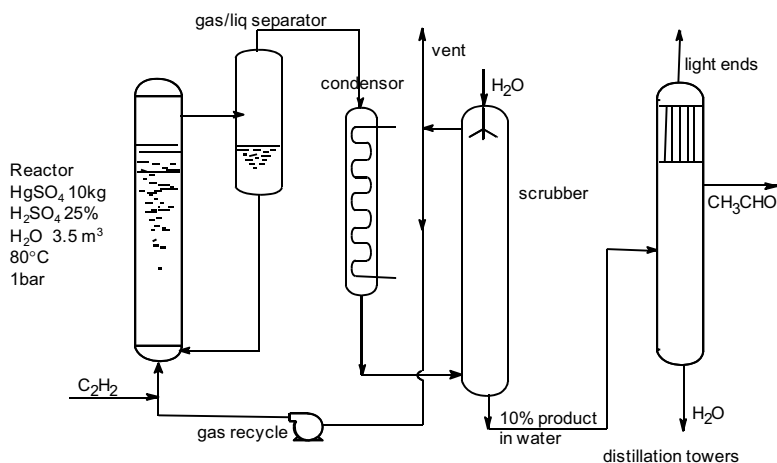
As the ancient literature did not reproduce pictures of the process scheme we used the same scheme as that used today for the Wacker process (see next process). Literature did give the size of the reactor, being only ~5 cubic meters. The space-time yield is roughly 10 kg per m^3 per hour, at least 10 times lower as that required today. The production with the reactor mentioned is only 400 tons a year, which today we would call a fine chemical! For Lonza in the south of Switzerland relatively cheap electricity was available for the manufacture of acetylene and this was the reason that the fabrication was located there. After new routes became available, this route was abandoned as the costs are several times higher.

$$C_2H_4 + 1/2\ O_2 \rightarrow CH_3CHO \qquad \Delta H = -244\ kJ/mol$$

$$C_2H_4 + Pd^{2+} + H_2O \rightarrow Pd(0) + 2\ H^+ + CH_3CHO$$
1894, Phillips

$$2\ Cu^{2+} + Pd(0) \rightarrow 2\ Cu^+ + Pd^{2+}$$

$$2\ Cu^+ + 1/2\ O_2 + 2H^+ \rightarrow 2\ Cu^{2+} + H_2O$$
1955, Smidt
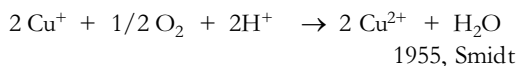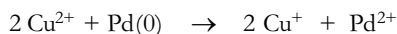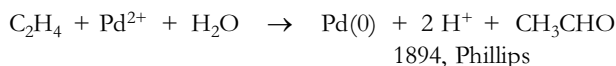
$$v = k[PdCl_4{}^{2-}][C_2H_4][H_3O^+]^{-1}[Cl^-]^{-2}$$

With the beginning of the "petroleum era" in the 1950s many processes changed and ethene became an important feedstock. Ethene (and propene and butadiene) were products of the cracking of higher alkanes. The Wacker process is the oxidation of ethene by divalent palladium to ethanal in the presence of water. The Wacker-Hoechst process has been studied in great detail and in all textbooks it occurs as the example of a homogeneous catalyst system illustrating nucleophilic addition to alkenes. Palladium chloride is the catalyst and palladium activates coordinating ethene toward a nucleophilic attack by water. The overall reaction is shown above. The reaction is highly exothermic as one might expect for an oxidation reaction. The figure below shows the reaction scheme. First coordination of ethene to palladium has to take place. One chloride ion is replaced by water and one by ethene. Ethene is activated towards nucleophilic attack by coordination to the electrophilic palladium ion. Then the key step occurs, the attack of water (hydroxide) to the activated ethene molecule. The nucleophilic attack of water or hydroxide takes place in an anti fashion; i.e. the oxygen attacks from outside the palladium complex and the reaction is not an insertion of ethene into the palladium oxygen bond.
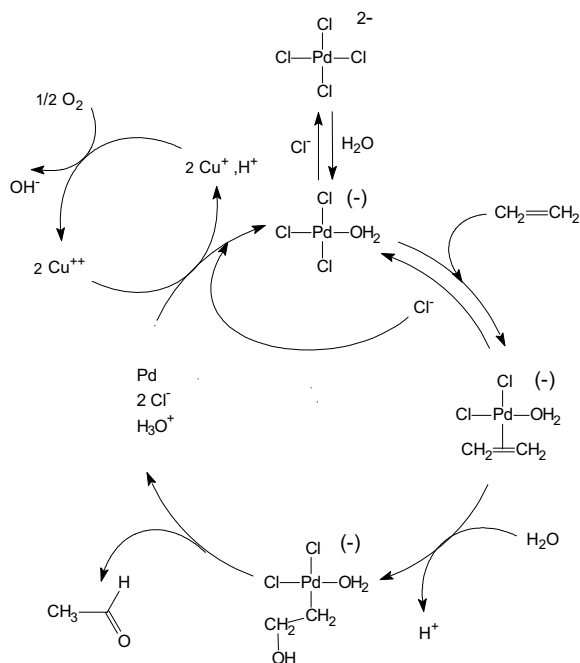
The attack of a nucleophile on an alkene coordinated to palladium is typical of "Wacker" type reactions. The rate equation is in agreement with the replacement reactions:

$v = k[PdCl_4^{2-}][C_2H_4][H_3O^+]^{-1}[Cl^-]^{-2}$

After rearrangement of the hydroxyethyl group, acetaldehyde (ethanal) forms and palladium zero is the reduced counter part. Including the palladium component, the reaction reads:

$C_2H_4 + Pd^{2+} + H_2O \rightarrow Pd(0) + 2 H^+ + CH_3CHO$

This reaction had been known since the beginning of the century. Re-oxidation of palladium directly by oxygen is extremely slow. The invention of Smidt (Wacker Chemie) involved copper as the intermediate in the recycling of divalent palladium:

$2 Cu^{2+} + Pd(0) \rightarrow 2 Cu^+ + Pd^{2+}$

$2 Cu^+ + 1/2 O_2 + 2H^+ \rightarrow 2 Cu^{2+} + H_2O$
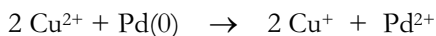
All kinetics are in support of the formation of a β-hydroxyethylpalladium complex as the intermediate. An important application of the Wacker chemistry is the reaction of ethene, acetic acid, and dioxygen over a heterogeneous catalyst containing palladium and a re-oxidation catalyst for the commercial production of vinyl acetate. The process scheme is the same as that for acetylene, replacing acetylene by ethene and oxygen, raising the temperature to 100 °C and the total pressure to 100 bar. The catalyst is a mixture of palladium and copper chloride. By-products include chlorinated ethanes, which present an environmental disadvantage.

10.3. ACETIC ACID

Carbonylation of methanol, thermodynamics

$$CH_3OH + CO \rightarrow CH_3COOH$$
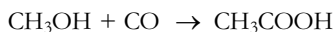
ΔG, standard conditions, – 75 kJ.mol^{-1}

Catalysts: cobalt, rhodium, palladium, iridium
always with the use of methyl iodide

The synthesis of acetic acid is another example that shows how the feedstocks determine the chemistry of our processes of major products. Acetic acid in ancient times was made from ethanol oxidation by bacteria of the genus acetobacter and it was used as such in a diluted form in water. Later acetic acid was made from acetaldehyde, obtained either from acetylene or ethylene. Today the most attractive route is to make it from methanol and carbon monoxide both stemming from synthesis gas, which can be made from any carbon source, carbon, methane, or natural products. Thermodynamically, the carbonylation of methanol is highly favorable, although the formation of methane and carbon

dioxide (not shown) is even better. Thus the formation of acetic acid is kinetically controlled.

Carbonylation of Methanol: Catalytic cycle
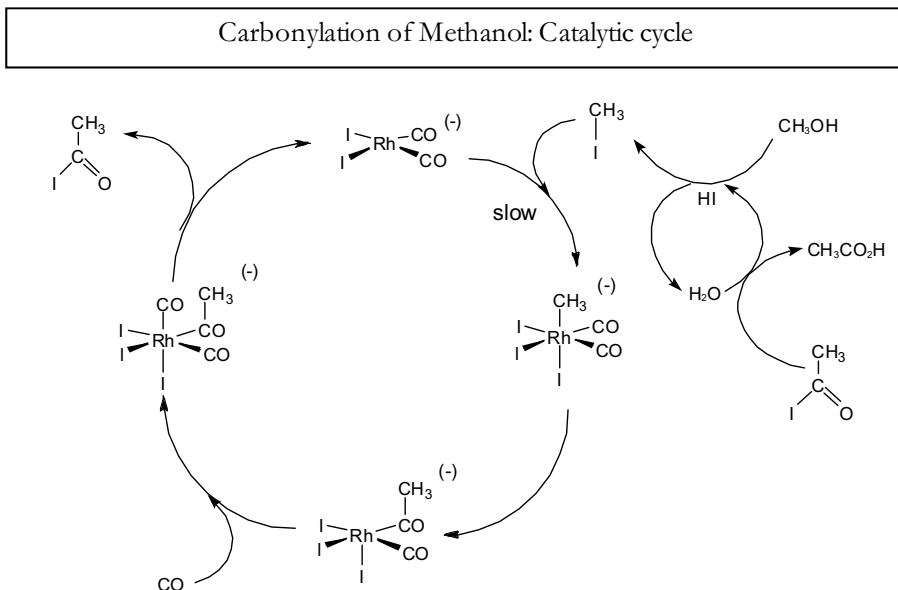
The first process used cobalt as the catalyst and employed high pressures (700 bar) and temperatures (BASF process). Apart from the drastic conditions, the selectivity was also a drawback, by-products being methane and propionic acid. The carbonylation of methanol under mild conditions was developed by Monsanto in the late sixties. It is a large-scale operation employing a rhodium/iodide catalyst converting methanol and carbon monoxide into acetic acid. Since the nineties, an iridium/iodide based catalyst has been used by BP.

The rhodium and iridium catalysts have several distinct advantages over the cobalt catalyst; they are much faster and far more selective. The higher rate is, in process terms, translated into much lower pressures (60 bar).

The rate-determining step in this process is the oxidative addition of methyl iodide. Within the operation window of the process the reaction rate is independent of the carbon monoxide pressure. Furthermore, the methyl iodide formation from methanol is almost complete which makes the reaction rate

also practically independent of the methanol concentration. As a result of the kinetics and the equilibria involved, all iodide in the system occurs as methyl iodide. Hence, up to high conversions the rate does not depend on the concentrations of the two reactants! The process scheme is presented below.

Carbonylation of methanol, process scheme
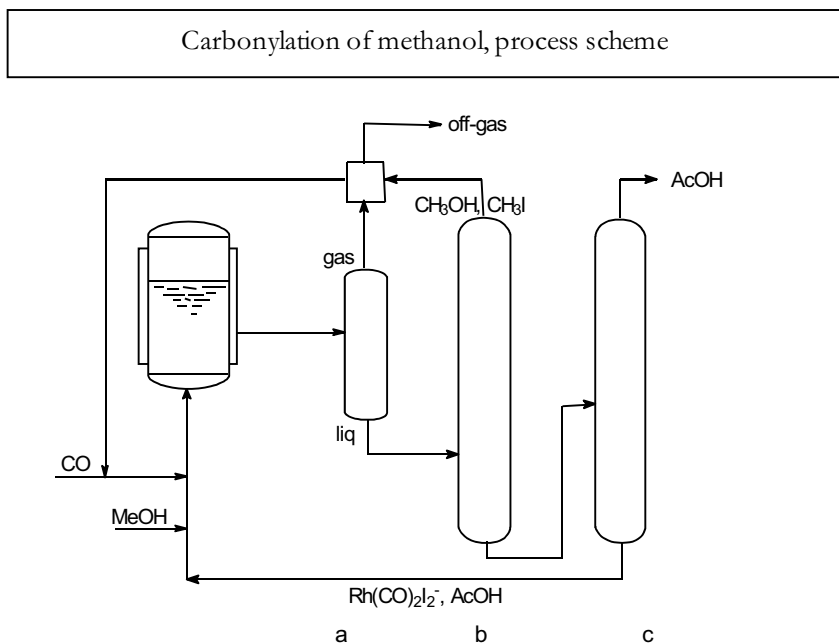
The product is taken out of the reactor in a liquid stream also containing the catalyst. After flashing (a) and distilling off the volatiles (b), the acetic is distilled off and the bottom containing rhodium and iodide is returned to the reactor.

10.4. ADIPONITRILE

Hydrocyanation 1960s,
DuPont, adiponitrile, phosphites, Tolman parameters
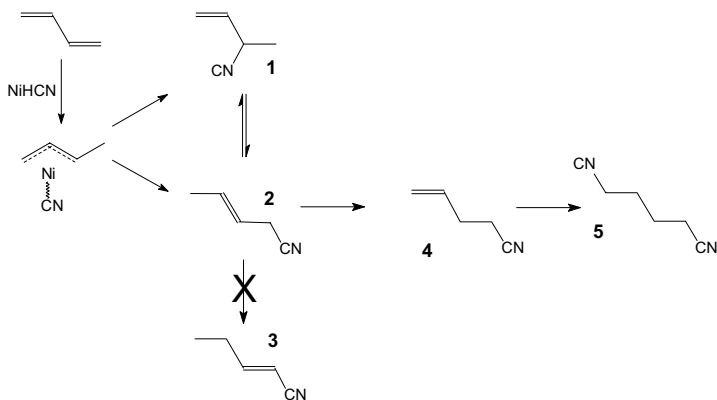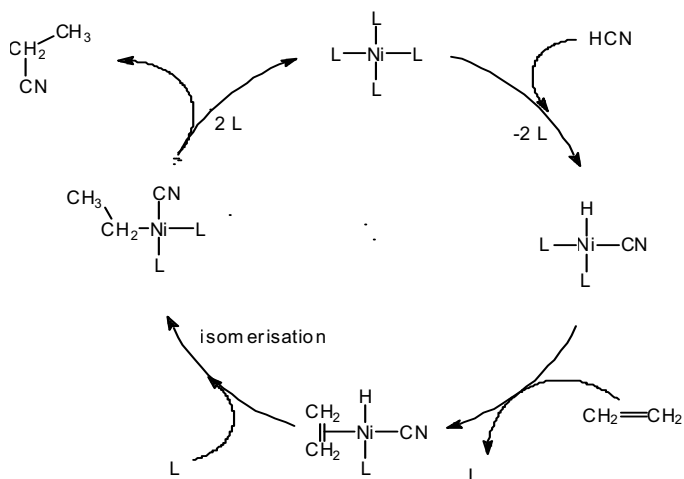
The reductive elimination of the nitrile is the rate determining step, and therefore phosphites –stabilizing nickel zero complexes- are the only ligands that give satisfactory results. Phosphines do not lead to active catalysts, until it was discovered that wide bite angle phosphines also stimulate the formation of nickel(0) complexes from divalent ones via reductive elimination:

Hydrocyanation
bite angle effect of bidentate phosphines on the rate

Yield %

PPh₂   PPh₂

90   110   130   angle
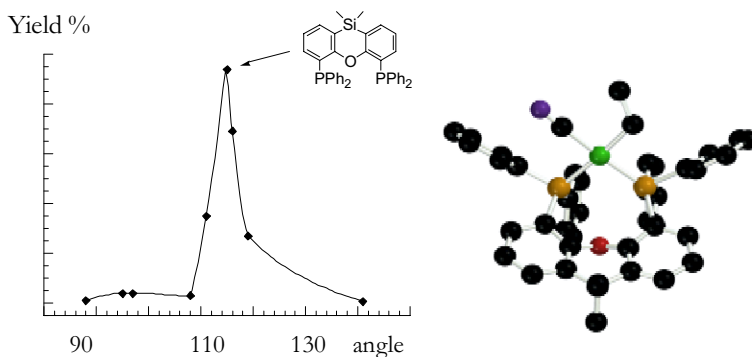
Kranenburg, Goertz, Vogt, van Leeuwen *Chemistry, Eur. J.* **2001**, *7*, 1614.
Dalton Trans. **1998**, 2981. *Chem. Commun.* **1997**, 1521.

In the figure it is seen that classic bite angles around 90 degrees do not give active catalysts and only around 109 degrees we see good activity. These reactions were carried out with styrene as this is easier to handle and give less side products than butadiene. Subsequently, companies such as DuPont have looked at wide bite angle diphosphites and these turned out to be even better than both monophosphites and the diphosphines shown above, as might be expected.

10.5. HIGHER OLEFINS

Alkene Oligomerization
Shell Higher Olefins Process, Kinetics

$$\gamma = \frac{[C_{n+2}]}{[C_n]} = \frac{k_g}{k_g + k_t} \qquad \text{or} \qquad \frac{\overset{\sim}{\underset{n+2}{\Sigma}}[C_n]}{[C_n]} = \frac{k_g}{k_t}$$

Geometric oligomer distribution
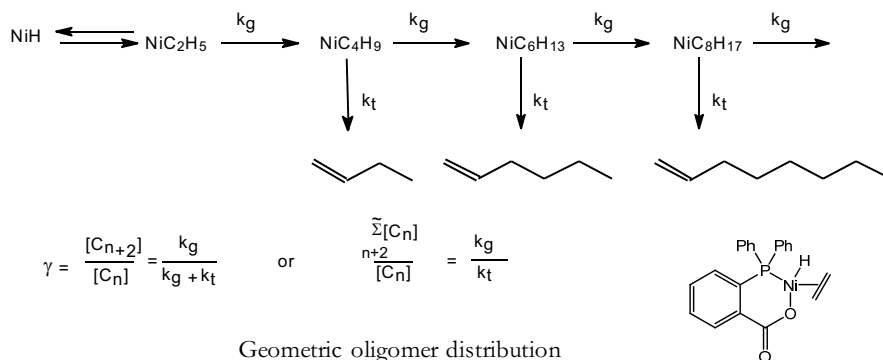
Kinetics determine Mw and distribution!

1-Alkenes, or linear α-olefins as they are called in industry, are desirable starting materials for a variety of products. Polymers and detergents are the largest end-uses. We mention a few applications:

C4	polybutylene
C6-8	comonomers in HDPE, LLDPE, synthetic esters
C6-10	alcohols (hydroformylation) as phthalates for PVC plasticizers
C8-10	as trimers in synthetic lub-oils
C10-14	after hydroformylation, detergents
C14-16	sulfates and sulfonates in detergents

Industrially, alkenes are obtained from several reactions, one being ethene oligomerization. Two processes are based on aluminum alkyl compounds and one on nickel catalysts.

Shell-Higher-Olefins-Process

Many transition metal hydrides will polymerize ethene to polymeric material or, alternatively, dimerize it to butene. Fine-tuning of these catalysts to one that will give a mixture of say predominantly C10 to C20 oligomers is not at all trivial. Nickel complexes have been extensively studied by Wilke and his co-workers for their activity as alkene oligomerization catalysts. In the late sixties Keim and co-workers at Shell discovered a homogeneous nickel catalyst which selectively oligomerizes ethene to higher homologues (see pervious page).

-oligomerization

The catalyst is prepared in a pre-reactor from nickel salts with boron hydrides as the reductor under a pressure of ethene and then ligand is added. Polar solvents such as alcohols are used for the dissolution of the catalyst. The catalyst solution and ethene are led to the reactor, a stirred autoclave, which is maintained at 80-120 ºC and 100 bar of ethene.

Alkene Oligomerization
Schulz-Flory, 0.78

Ethene oligomerisation, Schulz-Flory

$0.78 = \gamma$

61 wt % C_{6-20}
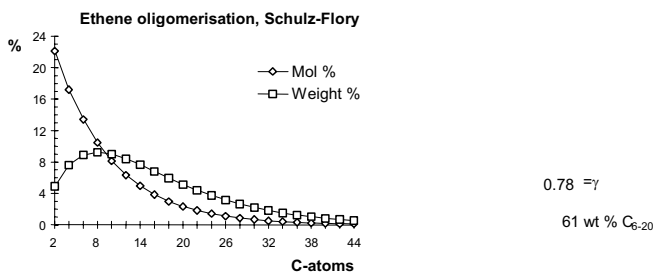
-separation

The product alkenes are insoluble in the alcohol and phase separation takes place. After settling, the alcohol layer goes to a regeneration unit. The alkene layer is washed and ethene is recycled to the reactor. The products are distilled and the desired fractions are collected.

Simple flow scheme of Shell Higher Olefins Process, oligomerisation
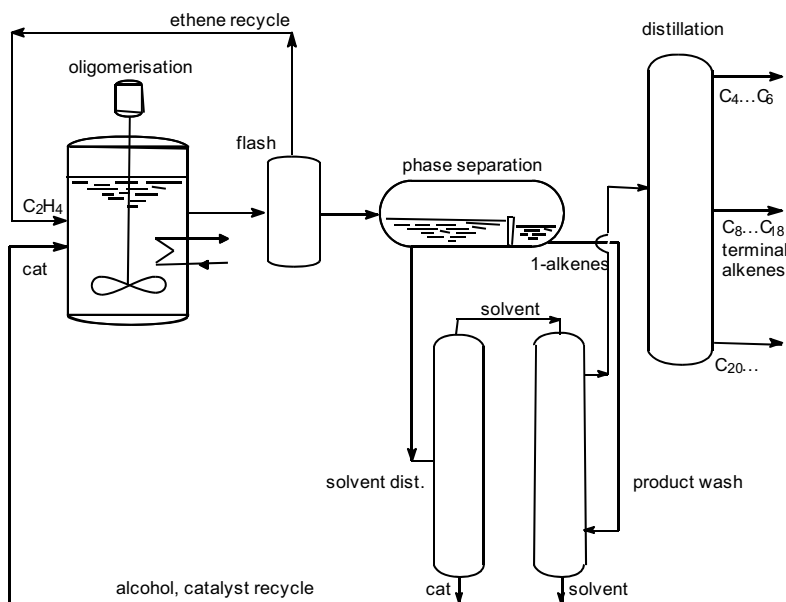
-purification and metathesis

The lower alkenes and the heavy alkenes must be "disproportionated" to give the full range of alkenes. To this end the light and heavy alkenes are sent to an isomerization reactor after having passed a purification bed, a simple absorbent to remove alcohol and ligand impurities. The isomerized mixture is then passed over a commercial molybdenum metathesis catalyst (CoMox), also a fixed bed reactor, to give a broad mixture of internal alkenes. After distillation the C11-14 fraction ($\pm$15%) is used as a feedstock for alcohol production via cobalt catalysts. The light and heavy products are recycled. A bleed stream of the heavy ends must limit the build-up of branched products and polymers.

The total production of higher olefins via this and similar routes is estimated to be 2 million tons annually. A large part of the alkenes are produced for captive use.

Metathesis section of the Shell Higher Olefins Process

purification   isomerisation   metathesis   distillation

$C_4...C_8$

$C_{11}...C_{14}$ internal alkenes

$C_{15}...$ recycle, internal alkenes

bleed stream heavy ends branched alkenes

$C_4...C_8$ and $C_{20}...$ recycle, terminal alkenes
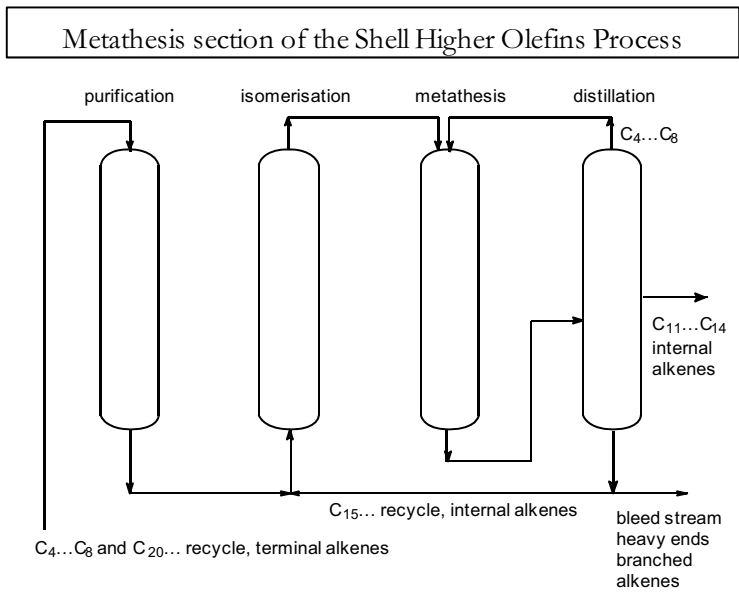
10.6. HYDROFORMYLATION

Introduction

Functionalization of hydrocarbons from petroleum sources is mainly concerned with the introduction of oxygen into the molecule. Roughly speaking, two ways are open: oxidation and carbonylation. Oxidation is the preferred route inter alia for aromatic acids, acrolein, maleic anhydride, ethene oxide, propene oxide, and acetaldehyde. Hydroformylation (older literature and technical literature say "oxo" reaction) is employed for the large-scale preparation of butanal and butanol, 2-ethyl hexanol, and detergent alcohols. Butanal and butanol are used in many applications as a solvent, in esters, in polymers etc. The main use of 2-ethylhexanol is in phthalate esters, which are softeners (plasticizers) in PVC. The catalysts applied are based, again, on cobalt and rhodium.

"normal"
linear product

"iso"
branched product
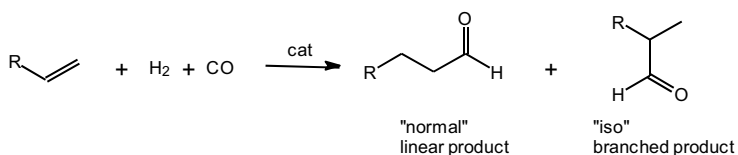
The hydroformylation reaction

Cobalt-based oxo-process

Roelen accidentally discovered the hydroformylation of alkenes in the late thirties while he was studying the conversion of synthesis gas to liquid fuels (Fischer-Tropsch reaction) using a heterogeneous cobalt catalyst. It took more than a decade before the reaction was taken further, but now it was the conversion of petrochemical hydrocarbons into oxygenates that was the driving force. It was discovered that the reaction was not catalyzed by the supported cobalt but in fact by $HCo(CO)_4$ formed in the liquid phase.

A key issue in the hydroformylation reaction is the ratio of "normal" (linear) and "iso" (branched) product being produced. The linear ("normal") product is the desired product; the value of butanal is higher because this is the product which can be converted to 2-ethyl hexanol via a base catalyzed aldol condensation and a hydrogenation. The detergent alcohols should be preferably linear because their biodegradability was reported to be better than that of the branched product. The linearity obtained in the cobalt catalyzed process is 60-80 %. The reaction mechanism for cobalt is similar to that of rhodium, which will be discussed in the next section.

H(O)CC₂H₄R

$H(O)CC_2H_4R$

$\begin{array}{c} H \\ CO-Co-CO \\ CO \quad CO \end{array}$

$CH_2=CHR$

CO

H_2

$\begin{array}{c} CH_2-R \\ CH_2 \\ O= \\ CO-Co-CO \\ CO \quad CO \end{array}$

$\begin{array}{c} CH_2=CHR \\ H-Co-CO \\ CO \quad CO \end{array}$

CO

$\begin{array}{c} R \\ CH_2 \\ CH_2 \\ CO-Co-CO \\ CO \quad CO \end{array}$

CO
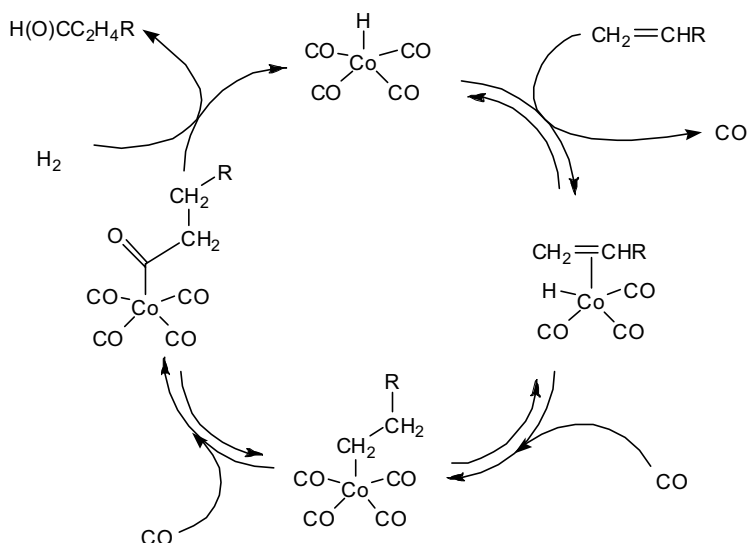
Thermodynamics of hydroformylation and hydrogenation at standard conditions are as follows:

$$H_2 + CH_3CH=CH_2 + CO \rightarrow CH_3CH_2CH_2C(O)H$$

	H_2	$CH_3CH=CH_2$	CO	$CH_3CH_2CH_2C(O)H$	
ΔG	15		-33	-28 (l)	= -10 kcal/mol
ΔH	5		-26	-57	= -36 kcal/mol

$$H_2 + CH_3CH=CH_2 \rightarrow CH_3CH_2CH_3$$

	H_2	$CH_3CH=CH_2$	$CH_3CH_2CH_3$	
ΔG	15		-6	= -21 kcal/mol
ΔH	5		-25	= -30 kcal/mol

Thus the reaction is highly exothermic and favored by thermodynamics at temperatures roughly below 200 °C. Hydrogenation of the alkene to alkane is thermodynamically even more attractive. Often this reaction is observed as a side-reaction.

CO/H$_2$ alkene

reactors

depress.

crude
aldehyde/
alcohol

dist. dist.

alkene

CO/H$_2$
hydrogen poor

CO/H$_2$
hydrogen rich

HCoL(CO)$_3$, alcohol, heavy ends

heavy ends
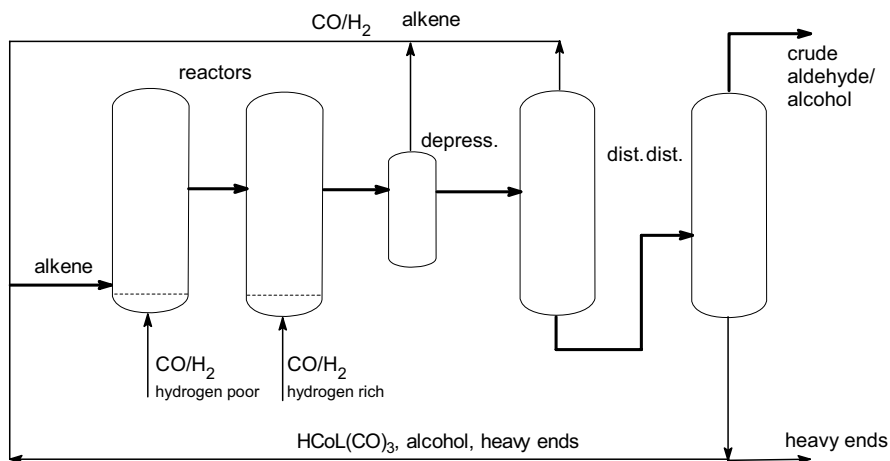
In industrial practice the older cobalt catalyst is still used today for the conversion of higher alkenes to detergent aldehydes or alcohols (> C12). The cobalt process requires high pressures (70-100 bar) and temperatures (140-170 °C). Aldol condensation and hydrogenation of the alkene to alkane (~ 10%) are undesirable side reactions for the detergent alcohols. Interestingly, the cheaper internal alkenes can be used for this process and yet the outcome is mainly a terminally hydroformylated, linear aldehyde/alcohol. Often the separation of catalyst, product, by-product and starting material is tedious. For propene the most economic processes are based rhodium catalysts commercialized in the seventies.

Rhodium-based hydroformylation

Fundamental work by Nobel-laureate Wilkinson demonstrated that rhodium triphenylphosphine catalysts allowed the operation of the hydroformylation reaction at much lower pressure (1 bar was reported by Wilkinson) and temperature than the cobalt process. The selectivity was also reported to be

considerably higher, virtually no hydrogenation was observed and the linearity was in some cases as high as 95%. The rhodium catalysts were reported to be three orders of magnitude faster in rate. The resulting milder reaction conditions would give much less condensation products. In 1971 Union Carbide Corporation, Johnson and Matthey, and Davy Powergas (now Kvearner) joined forces to develop a process based on this new finding. As yet it is only applied for propene. Hydroformylation of propene is of prime importance and world-wide probably more than 7 million tons of butanal are produced this way annually.

A convenient catalyst precursor is $RhH(CO)(PPh_3)_3$. Under ambient conditions it will slowly convert 1-alkenes into the expected aldehydes. Internal alkenes exhibit hardly any reaction. At higher temperatures (100-120 °C) pressures of 10-30 bar are required. Unless a large excess of ligand is present the catalyst will also show some isomerization activity, but the internal alkenes thus formed will not be hydroformylated. The 2-alkene concentration will increase and the 1-alkene concentration will decrease; this will slow down the rate of the hydroformylation reaction. This makes the rhodium catalyst less suited for the conversion of alkenes other than propene for which isomerization is irrelevant. To date, hydroformylation of higher alkenes is industrially still carried out with cobalt catalysts.

Propene hydroformylation can be done yielding a linearity ranging from 60 to 95% depending on the phosphine concentration. At very high phosphine concentration the rate is low, but the linearity achieves its maximum value. The commercial process operates presumably around 30 bar of syn-gas, at 120 °C, at high phosphine concentrations, and linearities around 92%. The estimated turnover frequency of moles of product per mole of rhodium complex per hour is in the order of 300. Low ligand concentrations, with concomitant low linearities, will give turnover frequencies in the order of 10,000 at 10 bar and 90 °C. In the presence of carbon monoxide this rhodium catalyst has no activity

for hydrogenation and the selectivity based on starting material is virtually 100%. The n-butanal produced contains no alcohol and can be converted both to butanol, to 2-ethyl-hexanol-1 and to other products as desired.

The most likely mechanism for the reaction is given below. Note the trigonal bipyramidal structure (tbp) of the rhodium catalysts. The σ-bonded hydrido group or the alkyl group are bound in an apical position of the tbp structure. This leaves three equatorial and one apical position for the remaining four ligands, carbon monoxide, phosphorus ligands and the alkene substrate. As usual, the ligand replacement equilibria have been simplified. After an insertion step, a 16-electron species is formed which restores its 18-electron count with a new CO molecule. There is consensus in the literature that the catalytic species with two phosphine ligands plays a major role, certainly when L=PPh$_3$. The high preference for linear aldehyde formation is ascribed to steric factors: congestion at the rhodium center favors the formation of linear alkyl and acyl species. Especially when two phosphine ligands coordinate bis-equatorially, there is a strong preference for the formation of *n*-alkyl groups. Later we will see how one can make use of this concept to obtain highly selective catalysts.

For rhodium-phosphine catalysts, the kinetics show that one of the first steps, complexation of alkene or migratory insertion of the alkene, is the rate-determining step. A first order in alkene is observed, while there is a negative dependence on the CO and/or phosphine concentration, which also stems from the replacement reaction. The rate of reaction is independent of the hydrogen concentration.

Ligand effects in hydroformylation
Ligand effects on the selectivity of the rhodium catalyzed hydroformylation have been extensively studied. The rate may vary several orders of magnitude and also the selectivity to either the branched or the linear product may vary

dramatically with minor changes in the electronic and steric properties of the ligand.

H(O)CC$_2$H$_4$R

CH$_2$=CHR

CO

CO

CO

L

H$_2$
- CO

CO

CO

CO

CO
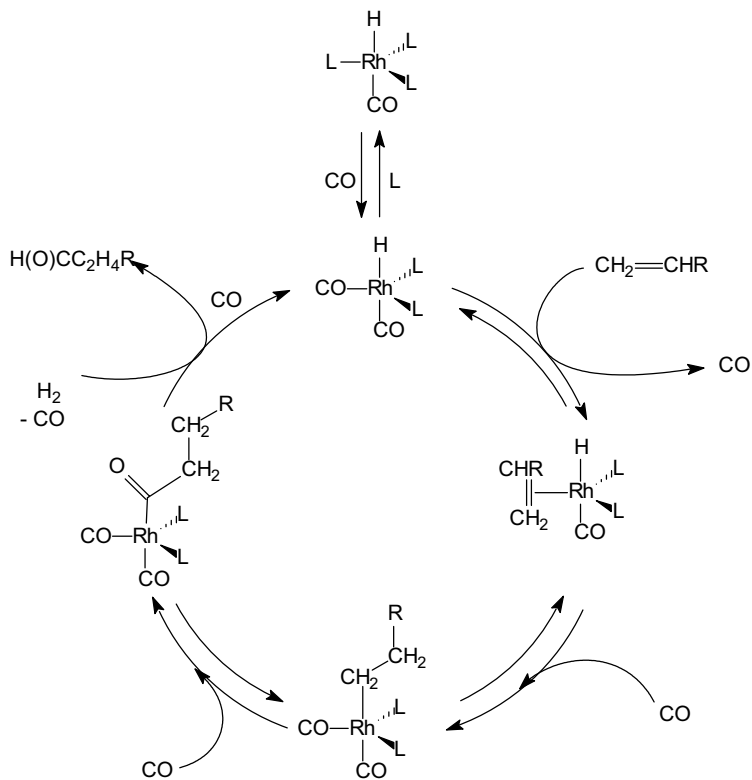
Bidentates with constrained bite angles

A few classes of new ligands have been introduced that give very high selectivity for linear products. All use the concept that a bis-equatorial coordination of the phosphorus ligands is needed to raise the selectivity to linear product. As mentioned above for triphenylphosphine, it was thought that also in this instance this coordination mode gave rise to the desired selectivity. The two structures are shown:
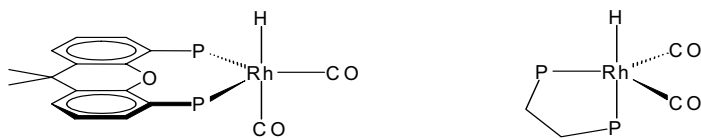
Bidentate ligands have been made and used extensively in many studies on coordination compounds and organometallic compounds. The majority of bidentate ligands, however, lead to "bite" angle of the bidentate on the metal between 75 and 95°. If a bidentate is to coordinate in a bis-equatorial fashion, it should have a bite angle of ~ 120°. Only very few ligands are available. Three of them are shown below. Molecular modeling and crystallographic studies by Casey and Van Leeuwen have learned that indeed the "natural" bite angle of these ligands is 110-120°. They give linear to branched product ratios up to 100!

Ligands leading to high l/b ratios in rhodium catalyzed hydroformylation

"BISBI"   general formula of bisphosphite   Xantphos
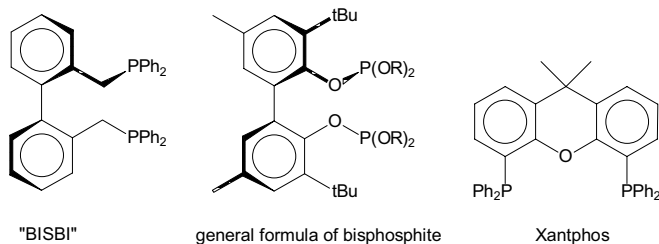
Two-phase hydroformylation: water-soluble catalysts

In the eighties a new process has come on stream, employing a two-phase system with rhodium in a water phase and the substrate and the product in an organic phase. The catalyst used is a rhodium complex trisulphonated triphenylphosphine (tppts) which is highly water-soluble (in the order of 1 kg of the ligand "dissolves" in 1 kg of water). The ligand forms complexes with

rhodium that are very similar to the ordinary triphenylphosphine complexes (i.e. RhH(CO)(PPh$_3$)$_3$). The rhodium complex resides in the aqueous phase.
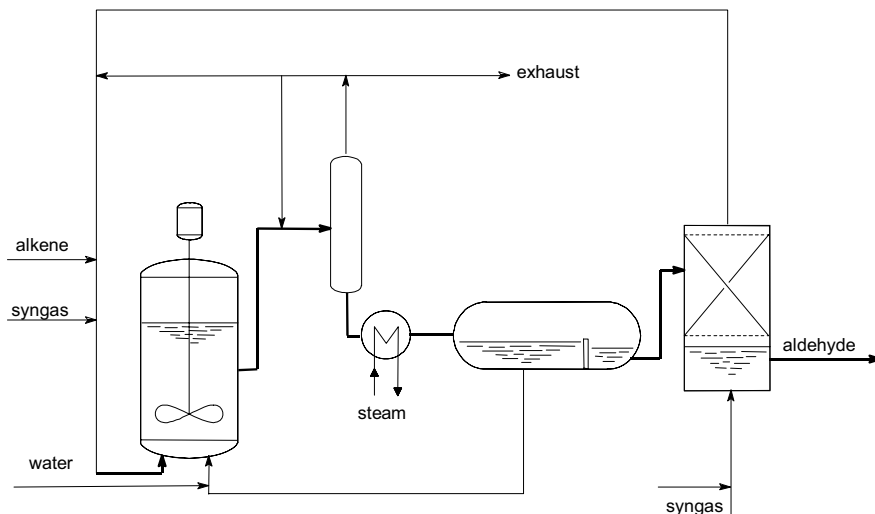
The substrates, propene/CO/H$_2$, are only slightly soluble in water. Upon reaction a second phase forms, the organic phase, consisting of the product butanal and dissolved propene and syn gas. The two phases are intensely stirred to ensure a fast transport of the gases from the gas phase to the organic and water phase.

The two phases are removed from the reactor and separated in a settler tank after the heat and the gases have been removed. Often in organic synthesis the separation of two layers is not such an easy process step, but in this particular instance a very clean separation of the two layers occurs. Most importantly, the rhodium/ligand components remain completely in the aqueous phase. This type of separation is very attractive on a large scale, continuous process. Ruhrchemie has commercialized the process, after the initial work had been done by workers at Rhone-Poulenc, for the production of butanal from propene. The linearity of the product amounts to 92%. The process is not applicable to the hydroformylation of higher alkenes because:

- the isomerization cannot be completely suppressed with aryl phosphines, thus leading to the formation of 2-alkenes which cannot be separated from the 1-alkenes in the recycle.

- the solubility of higher alkenes in water is very low.

10.7. TITANIUM AND ZIRCONIUM CATALYZED POLYMERIZATION OF ALKENES

The titanium catalyst for the stereoselective polymerization of propene to isotactic polymers was discovered by Ziegler and Natta in the mid-fifties. Soon after its discovery it was turned into commercial exploitation and until today isotactic polypropylene is one of the most important commodity polymers. Polymers with side-arms, polypropylene (PP) being the simplest one containing methyl groups, may possess stereoregularity in the arrangement of these side-arms. For example, if all methyl groups in PP are oriented toward the same direction in the stretched polymer chain, we say this polypropene is isotactic. If the methyl groups are alternatingly facing to the front and the back, we say the polymer has a syndiotactic microstructure. Random organization of the methyl groups is found in atactic polymers. The stereoregularity of a polymer has an enormous influence on the properties of the polymer. Isotactic PP is the well-known semi-crystalline material that we all know, while atactic PP is a rubber-like material. The degree of isotacticity determines the "melting point" of the polymer.

isotactic polypropene

syndiotactic polypropene
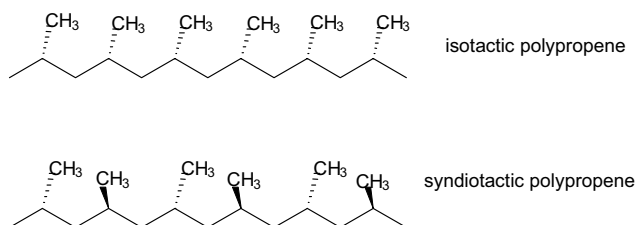
The catalyst and the concomitant technology have undergone drastic changes over the years. The titanium catalysts can be prepared by the interaction of $TiCl_4$ and alkylaluminum compounds in a hydrocarbon solvent. This reaction can be carried out with numerous variations to give a broad range of catalysts. It is a heterogeneous high-surface $TiCl_3$ material of which the active site is titanium in an unknown valence state. It is quite likely that alkyltitanium groups at the surface are responsible for the coordination polymerization. Since the eighties titanium catalysts supported on magnesium salts are used.

The Cossee-Arlman mechanism

The mechanism proposed for the solid titanium chloride catalysts is essentially the same for all catalysts and it is usually referred to as the Cossee-Arlman mechanism. Titanium is hexa-coordinated in the $TiCl_3$ catalysts or supported analogues by three bridging chlorides, one terminal chloride, and one terminal chloride that is replaced by an alkyl group by the alkylating agent (Et_2AlCl or Et_3Al), and a vacancy that is available for propene coordination. This simple picture yields an asymmetric titanium site, but by considering the lattice surface four bridging chlorides may also lead to an asymmetric site.
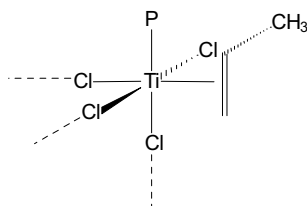
In Cossee's view, one way or another, the site has to control the way a propene molecule inserts, by doing this in a very controlled manner one can imagine that a stereoregular polymer will form.

Site control versus chain-end control.

Over the years two mechanisms have been put forward as being responsible for the stereo-control of the growing polymer chain, firstly the site-control mechanism and secondly the chain-end control mechanism. In the site control mechanism the structure of the catalytic site determines the way the molecule of 1-alkene will insert (enantiomorphic-site control). As we have seen previously, propene is prochiral and a catalyst may attack either the re-face or the si-face. If the catalyst itself is chiral as the one drawn above, a diastereomeric complex forms and there may be a preference for the formation of particular diastereomer. If the catalysts adds to the same face of each subsequent propene molecule, we say isotactic PP is formed (a definition proposed by Natta). Thus, we see that stereoregular polymerization is concerned with asymmetric catalysis.

When we look more closely at the intermediate polymer chain we see that an alternative explanation emerges. After the first insertion has taken place a stereogenic center has been obtained at carbon 2. Coordination with the next propene may take place preferentially either with the re-face or the si-face, or as displayed below, with the methyl group pointing up or down.
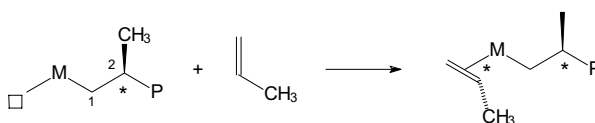
Summarizing, in the chain-end control mechanism the last monomer inserted determines how the next molecule of 1-alkene will insert. Proof for this stems from catalysts not containing a stereogenic center that do give stereoregular polymer. Secondly, whatever site-control we try to induce, the chain that we are making will always contain, by definition, an asymmetric center. These two points would strongly support the chain-end control mechanism. As we have mentioned above, the nature of the solid catalysts had an enormous influence

on the product, and this underpins the Cossee site-control mechanism. Thus both are operative and both are important. Occasionally, chain-end control only suffices to ensure enantiospecifity.

The analysis of the products using high resolution ^{13}C NMR has greatly contributed to the mechanistic insight and distinction between the various catalysts. NMR analysis gives a detailed picture of the relative orientation of the methyl groups in the chain, i.e. the regular ones, but more in particular the mistakes that were made.

Homogeneous catalysts

In the seventies the first reports appeared concerning the homogeneous stereospecific polymerization, but they received relatively little attention as during the same years the first highly active heterogeneous titanium catalysts, immobilized on magnesium salts, were reported and the industrial interest in homogeneous catalysts diminished.

The development of the new family of homogeneous catalysts based on biscyclopentadienyl Group 4 metal complexes for the stereoselective polymerization of alkenes is mainly due to Kaminsky, Ewen and Brintzinger. In 1980 Kaminsky and Sinn reported on an extremely fast homogeneous catalyst for the polymerization of ethene formed from the interaction of $Cp_2Zr(CH_3)_2$ and $(CH_3AlO)_n$ (=MAO). At 8 bar of ethene and 70 °C an average rate of insertion of ethene was reported amounting 3.107 mole of ethene per mole of Zr per hour! For propene this catalyst led to completely atactic polymer. Ewen was the first to report the synthesis of stereoregular polymers with soluble Group 4 metal complexes and MAO as the co-catalyst. He found that Cp_2TiPh_2 with MAO and propene gives isotactic polypropene. This catalyst does not contain an asymmetric site that would be able to control the stereoregularity. A stereoblock polymer is obtained, see below. Formation of

this sequence of regular blocks is hold for a proof of the chain-end control mechanism.

catalyst
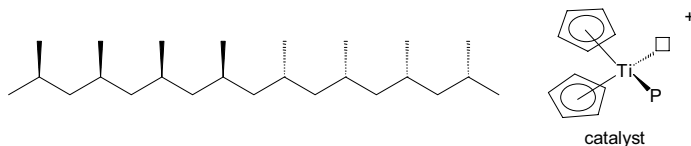
Using an intrinsically chiral titanium compound (rac ethylene-bis-indenyl *titanium* dichloride), first described by Brintzinger, Ewen obtained polypropene that was in part isotactic. Kaminsky and Brintzinger have shown that highly isotactic polypropene can be obtained using the racemic *zirconium* analogue of the ethylene-bis(indenyl) compound. Modification of the cyclopentadienyl ligands has led to a very rich chemistry and a great variety of microstructures and combination thereof has been obtained including isotactic polymer with melting points above 160 °C, syndiotactic polypropene, block polymers, hemi-isotactic polymers etc.
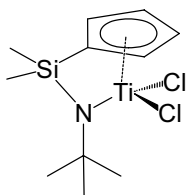
Only one commercialization of the new metallocene catalysts will be mentioned here as an example, the so-called "Single Site Catalyst" developed by Dow, see above. It is not a stereospecific catalyst as it simply polymerizes ethene and added higher alkenes. It gives a narrow MW and a high rate of (re-)insertion of higher alkenes. The control of branching and the extent of long-chain branching leads to a product that can be easily processed.

10.8. ASYMMETRIC HYDROGENATION

When a metal complex is chiral, either because it contains a chiral ligand or a chiral metal center, and then forms a complex to a "prochiral alkene", the resulting complex is a diastereomer. Thus, a mixture of diastereomers can form when the chiral complex coordinates to each face of the alkene. These diastereomers have different properties and, more interestingly for catalysis, the diastomeric energies also have different free energies and thus enantioselective hydrogenation may occur. The asymmetric hydrogenation of cinnamic acid derivatives has been developed by Knowles at Monsanto. The synthesis of L-dopa, a drug for the treatment of Parkinson's disease, has been developed and applied on an industrial scale. The reaction is carried out with a cationic rhodium complex and an asymmetric diphosphine as the ligand that induces the enantioselectivity. Surprisingly, the reaction is not very sensitive to the type of diphosphine used, although it must be added that most ligands tested are bis(diphenylphosphino) derivatives. On the other hand the reaction is very sensitive to the type of substrate and the polar substituents, prerequisites for a successful asymmetric hydrogenation.
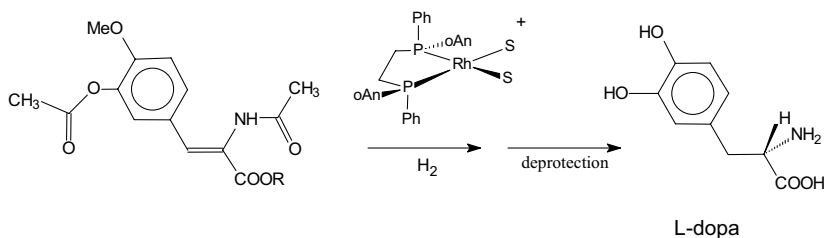
The hydrogenation reaction is carried out with a substituted cinnamic acid. The acetamido group is of particular importance because it functions as a secondary complexation function in addition to the alkene functionality. In the first step the alkene coordinates to the cationic rhodium species for which there are two possibilities, binding to the re-face and the si-face. This new chiral center, combined with the ligand chirality, leads to the formation of two diastereomers,

which have different free energies. Thus, a preference for just one enantiospecific pathway may result. For a few systems in situ characterizations have been carried out and both complexes have been identified. The final product is not necessarily derived from the most abundant isomer; all that matters is through which pathway the fastest reaction takes place that produces most of the product.

A large series of asymmetric ligands have been developed most of which having the asymmetric "center" in the bridge rather than at the phosphorus atoms as is the case in DIPAMP, the ligand shown above for the L-dopa synthesis.

10.9. ASYMMETRIC ISOMERIZATION, MENTHOL

An important application of an isomerization is found in the Takasago process for the commercial production of (-)menthol from myrcene. The catalyst used is a rhodium complex of BINAP. BINAP is an asymmetric ligand based on the atropisomerism of substituted dinaphthyl, introduced by Noyori. Atropisomers of diphenyl and the like are formed when ortho-substituents do not allow rotation around the central carbon-carbon bond. As a result two enantiomers are formed.
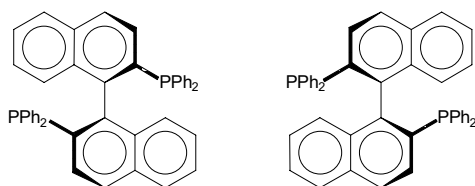
BINAP has been extensively used for the asymmetric hydrogenation, transfer hydrogenation and isomerization of double bonds using both ruthenium and rhodium complexes. The synthesis of menthol is given in the reaction scheme. The key reaction is the enantioselective isomerization of the allylamine to the

asymmetric enamine. It has been proposed that this reaction proceeds via an allylic intermediate.
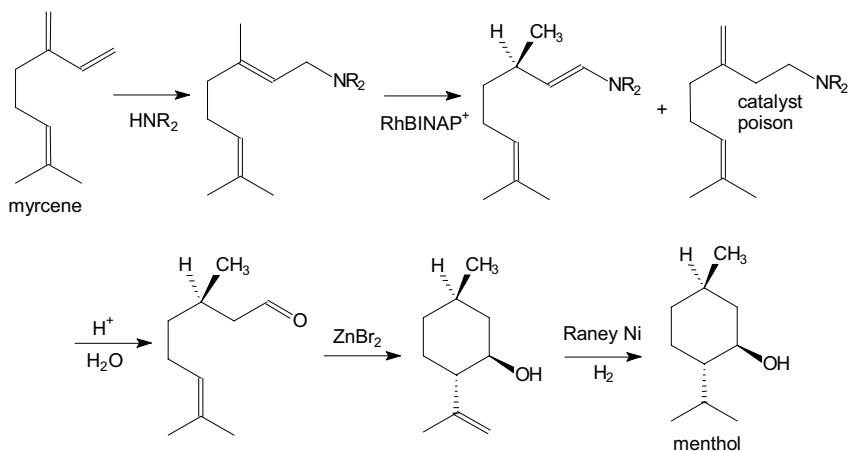
This is the only step that needs to be steered to the correct enantiomer, since the other two are produced in the desired stereochemistry with the route depicted. Of the eight possible isomers only this one (1R,3R,4S) is important. After the enantioselective isomerization the enamine is hydrolyzed. A Lewis acid catalyzed ring closure gives the menthol skeleton. In a subsequent step the isopropenyl group is hydrogenated over a heterogeneous Raney nickel catalyst.

10.10. PALLADIUM CATALYSED CROSS-COUPLING REACTIONS

Heck reaction

The Heck reaction involves the coupling of an aryl halide (or pseudo halide) with an alkene in the presence of a base. Owing to the latter, as in the cross coupling reaction an equivalent of base is formed. In the base case, the Heck reaction will produce substituted styrenes. These products can also be made in the cross coupling reaction discussed above. It is attractive that the Heck reaction does not involve Grignard type reagents and thus it allows the

presence of groups reactive towards Grignard reagents such as esters, acids, ketones, etc.
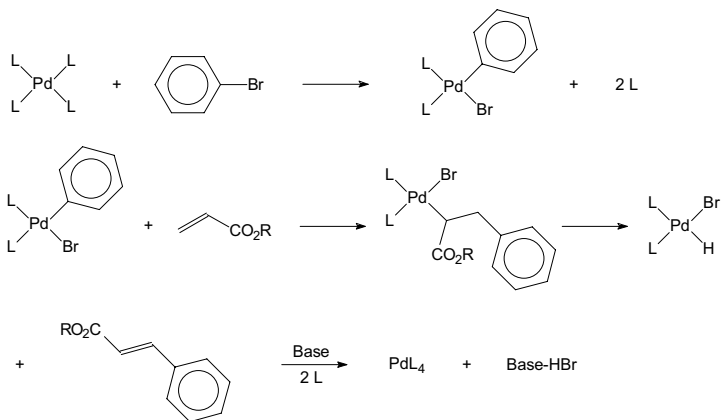
The reaction starts with the oxidative addition of an aryl halide (Br or I) to palladium zero. The next step is the insertion of an alkene into the palladium carbon bond just formed. The third step is β-elimination giving the organic product and a palladium hydrido halide. The latter reductively eliminates HX that reacts with base to give a salt. In modern Heck chemistry the halide is replaced by non-coordinating anions such as O_3SCF_3. The advantage is that the palladium center is now much less saturated and more positively charged (and hence more reactive) during the alkene coordination and insertion steps. The example below shows the synthesis of Naproxen as carried out by Albemarle using a Heck reaction.
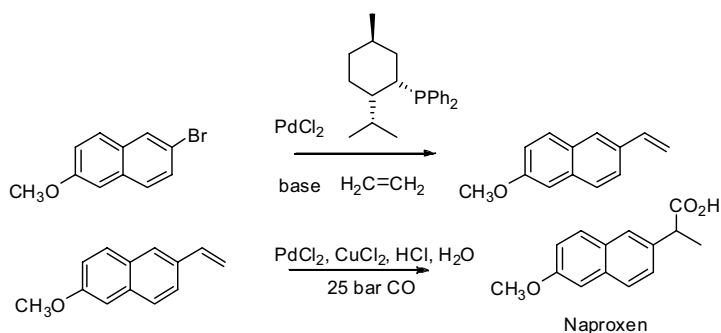
The synthesis of Merck's L 699,392 involves two Heck reactions and an asymmetric H-transfer reaction:

Merck L 699,392
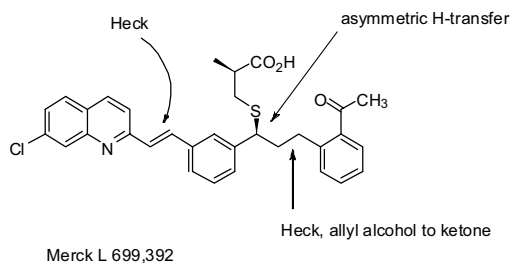
Cross coupling

The making of carbon-to-carbon bonds from carbo-cations and carbo-anions is a straightforward and simple reaction. Easily accessible carbo-anions are Grignard reagents RMgBr and lithium reagents RLi. They can be conveniently obtained from the halides RBr or RCl and the metals Mg and Li. They are both highly reactive materials, for instance with respect to water.

The reactions of these carbon centered anions with polar compounds such as esters, ketones, and metal chlorides are indeed very specific and give high yields. The reaction of Grignard reagents and the like with alkyl or aryl halogenides, however, is extremely slow giving many side-products, if anything happens at all.

472

The "cross coupling" reaction has found wide application both in organic synthesis in the lab and in industrial environment. The transition metal catalysts are usually nickel and palladium. In addition to organomagnesium and organolithium a great variety of organometallic precursors can be used. Also, many precursors can serve as starting materials for the carbocation. Last but not least, the ligand on the transition metal plays an important role in determining the rate and selectivity of the reaction. Here we will present only the main scheme and take palladium as the catalyst example. The general scheme of the palladium catalyzed cross coupling reaction reads as follows:
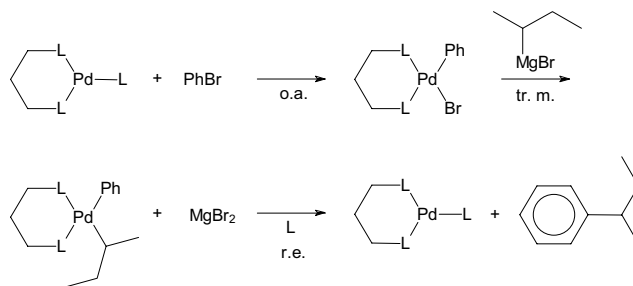
We can start with palladium(II) or palladium(0), but for the present explanation the latter is more convenient. Oxidative addition of an aryl halide to palladium zero takes place and a square planar Pd(II) complex is formed. Subsequently the inorganic bromide reacts with the Grignard or lithium alkyl reagent (here 2-BuMgBr) giving a diorganopalladium complex and magnesium dibromide. The third reaction that occurs is the reductive elimination giving the organic "cross-coupling" product and the palladium(0) catalyst in its initial state. This particular example shows a large bite angle effect and especially DPEphos gives high rates, yields, and selectivity.

Less reactive organometallics derived from tin and boron can also be used. These reagents do not react with water, but they are still able to alkylate the palladium bromide intermediate. As mentioned above, their formation does involve one more step because they are also made via Grignard type reagents. A

reagent based on boron was introduced by Suzuki. The boronic ester derivative is made from trimethyl borate and an aryl anion reagent followed by hydrolysis of the two remaining methyl ester groups. This phenylboronic acid is soluble in water and the coupling reaction can even be carried out in water:
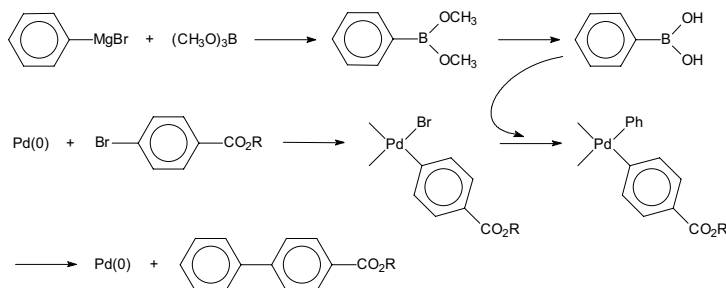
The cross coupling reaction is applied industrially in the synthesis of alkyl-aryl compounds that are used in liquid crystals, aryl-aryl compounds in agrochemicals, pharmaceuticals, etc. An example from Clariant and Zeneca is shown below:
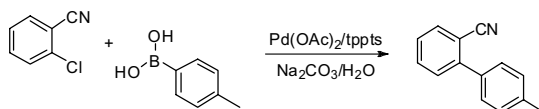
Bibliography

P.W.N.M. Van Leeuwen, *Homogeneous Catalysis; Understanding the Art,* Springer, London (formerly Kluwer Academic Publishers, Dordrecht), **2004**.

G.W. Parshall, S.D. Ittel, *Homogeneous Catalysis*, Wiley, New York, **1992**.

R. Fink, G. Mülhaupt, H.H. Brintzinger (eds.), *Ziegler Catalysts.* Springer, Berlin, **1995**.

R. Noyori, *Asymmetric Catalysis in Organic Chemistry.* Wiley, New York, **1995**.

B.Cornils, W.A. Herrmann (eds.), *Applied Homogeneous Catalysis with Organometallic Compounds.* VCH, Weinheim, **1996**.

M. Beller, C. Bolm (eds.), *Transition Metals for Organic Synthesis; Building Blocks and Fine Chemicals*, Wiley-VCH, Weinheim, **1998**.

F. Diederich, P.J Stang. (eds.), *Metal-catalyzed Cross-coupling Reactions*, Wiley-VCH, Weinheim, **1998**.

B. Cornils, W.A. Herrmann (eds.), *Aqueous Phase Organometallic Catalysis-Concepts and Applications*, Wiley-VCH, Weinheim, **1998**.

R.A. van Santen, P.W.N.M. van Leeuwen, J.A. Moulijn, B.A. Averill, (eds.) *Catalysis, an Integrated Approach*, 3rd edition. Elsevier, Amsterdam, **1999**.

P.W.N.M. van Leeuwen, C.Claver, (eds.) *Rhodium Catalyzed Hydroformylation. Catalysis by Metal Complexes*, Kluwer Academic Publishers, Dordrecht, **2000**.

(Página deixada propositadamente em branco)

SECTION C

PHOTOCATALYSIS

(Página deixada propositadamente em branco)

1. THE HETEROGENEOUS PHOTOCATALYTIC PROCESS

Joaquim Luís Faria

Laboratório de Catálise e Materiais, Departamento de Engenharia Química, Faculdade de Engenharia, Universidade do Porto - Rua Dr. Roberto Frias, 4200-465 Porto, Portugal.

1.1. INTRODUCTION

The heterogeneous photocatalytic process, like other heterogeneous catalytic processes, is of outmost interest for industrial applications, with respect to minimization of energy consumption, reducing pollution and increasing efficiency. It's probably one of the fields where very substantial developments and achievements have been made in the last 30 years, mainly due to the recent developments in materials science (especially in the semiconductor field) and light technologies (particularly in the development of different radiant sources). In most cases, these incredible scientific and technological developments are still awaiting to be put into operation because of the high capital costs and, to a lesser extent, due to the traditional scepticism of industrial chemists and engineers when confronted with a new, not completely clear technology. In spite of the enormous effort made by the scientists in this field and the fact that the photocatalytic process is very simple in its essence, there is a great difficulty in understanding the role of light as reactant and the emerging relationships between the structure and reactivity of all participants in the process. Understanding what photocatalysis stands for and knowing the photo-mechanisms involved is crucial to understand the photocatalyst operation, and therefore to optimize the whole photocatalytic system and its application.

Application of heterogeneous photocatalysis spawns over a wide range of reactions, most of them oxidations. Other examples to be found in the current literature are dehydrogenation, hydrogen and electron transfer, metal

deposition, water decontamination, removal of air pollutants, energy production and storage.

As far as degradation of organic pollutants in water and air is concerned, there is an important class of technologies, normally designated as Advanced Oxidation Processes (AOP), where light is used to in-situ generate highly efficient chemical oxidants, such as the hydroxyl radical (HO•), which is able to react rapidly and non-selectively with a wide range of organic compounds. Some of the AOP have been developed to a point close to full-scale commercialization. However treatment costs are normally considered using as reference a somewhat loose concept of unit volume of a particular effluent, which does not take in account the concentration of the contaminant or the level of degradation, rendering any decision on the adoption of such method somehow arbitrary.

The first landmark for the understanding of the heterogeneous photocatalytic process was set in 1972 with the description of the water splitting on titanium dioxide (TiO$_2$) electrodes[1]. This work was on the base of a new promising and alternative method, for the photocatalytic degradation of biphenyl and chlorobiphenyl derivatives in water in the presence of TiO$_2$ published some 4 years later[2]. Since those days the number of ISI referred articles inspired on the application of TiO$_2$-based photocatalysts for complete conversion of organics in air effluents or waste waters has surpassed 5000. In these works many researchers have demonstrated the efficiency of irradiating TiO$_2$ in the UV-Visible spectrum (even using sunlight) as a mean of detoxification.

1.2. THE PHOTOCATALYTIC REACTION

An heterogeneous photocatalytic system for oxidative degradation of organic or inorganic oxidizable compounds includes the following components: (1) a reactant; (2) a photon of the appropriate wavelength; (3) a catalyst surface (normally a semiconductor like TiO$_2$); (4) a strong oxidizing agent. At first,

catalysis by light is a common misconception. Light always acts as a reactant never as catalyst. This is even more evident when dealing with heterogeneous photocatalysis. By definition photocatalysis has been described as a change in the rate of a chemical reaction, or its initiation under the action of ultraviolet, visible, or infrared radiation in the presence of a substance – the photocatalyst – that absorbs light and is involved in the chemical transformation of the reaction partners[3]. However, there is no universal agreement on this definition and photocatalysis is probably better described as a catalytic reaction involving light absorption by a catalyst or by a substrate[4].

In conventional heterogeneous catalysis, the overall process consists of a sequence events, which can be decomposed in five elementary steps:

I. Diffusion of the reactants through the bulk to the surface.

II. Adsorption of at least one reactant.

III. Reaction in the adsorbed phase.

IV. Desorption of the products.

V. Removal of products away from the interface.

In heterogeneous photocatalysis, the only difference lies in step III whereas the usual thermal activation is now replaced by photonic activation[5]. Although the irradiation of the solid may change its surface properties and therefore some photo-adsorption may occur (step II), as well some photo-desorption (step IV), this is not to be concerned with activation. The photoinduced molecular transformations and reactions, involving electron transfer or energy transfer, will take place at the surface of the catalyst solely in step III. In heterogeneous photocatalysis, either the catalyst substrate (normally a semiconductor), or the adsorbed molecule, or both, are in the excited state during the catalytic step III. It is the subsequent deexcitation process that leads to chemical reactions.

One of the most important events that may take place involves electron transfer. An electron transfer process is a reaction in which a single electron is transferred from an occupied orbital of the donor to an empty orbital of the acceptor. The initial excitation may occur at either acceptor adsorbed molecule (A → A*), donor adsorbed molecule (D → D*) or catalyst substrate. The following electron transfer will result in an ion pair (Equation 1) of the donor cation (D$^+$) and acceptor anion (A$^-$).

$$A(ads) + D(ads) \xrightarrow{\ h\nu\ } A^-(ads) + D^+(ads) \tag{1}$$

When the initial photon absorption occurs in an adsorbate molecule, which then interacts with the ground state catalyst substrate, the process is a catalyzed photoreaction. If the absorption of the photons occurs in the catalyst substrate and the photoexcited catalyst then transfers its excitation (by means of energy or electron) to a ground state adsorbed molecule, the process is referred to as sensitized photoreaction.

1.3. THE SENSITIZED PHOTOREACTION

The initial process of the sensitized photo reaction is the photo-generation of a bound electron/hole pair (e$^-$/h$^+$) at the bulk of the semiconductor particle, Figure 1. In a semiconductor, there is a void energy region extending from the top of the occupied valence band (VB, HOMO) to the bottom of the unoccupied conduction band (CB, LUMO) designated by bandgap (E$_g$), which determines the necessary energy for activation. Taking TiO_2 as an example, following excitation with light of the appropriate wavelength, i.e. with photon energy in excess of the semiconductor bandgap (in this case E$_g$ > 3.23 eV) a electron/hole pair (e$^-$/h$^+$) is generated at the bulk of the metal oxide particle, Figure 1[6,7].
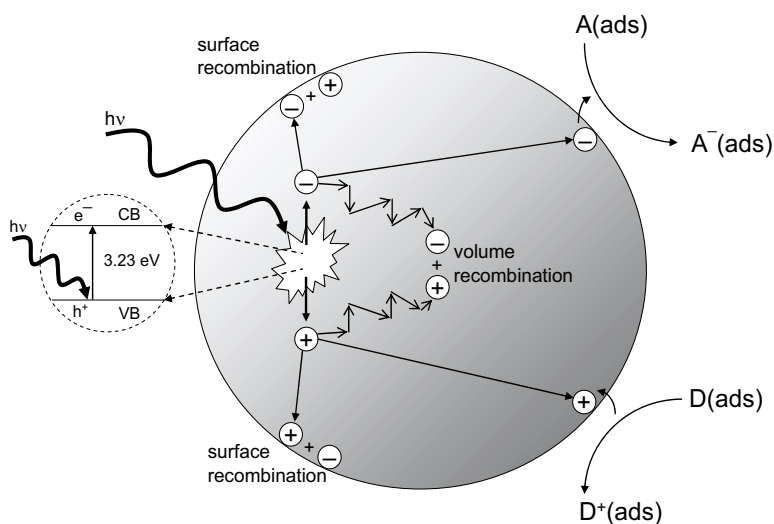
Figure 1 - Schematic photoexcitation taking place in a semiconductor spherical particle (taking TiO_2 as example) followed by deexcitation in the presence of an acceptor (A) and donor (D) molecules (adapted from ref. [7]).

The lifetime of the bound (e^-/h^+) pair lies on the nanosecond time scale and once generated electrons and holes can either recombine (no photocatalysis will take place) or diffuse to the interfacial region. Once at the surface, on the absence of any suitable acceptors (for e^-) or donors (for h^+), recombination will occur with other counterparts - again no photocatalysis will take place. Attention should be drawn to the fact that bimolecular recombination is not the only pathway of deactivation. The charge carriers could be single trapped in lattice defects, and recombination could occur through these defects. All these processes account for catalyst deactivation. On the other hand, while scanning the different interfacial sites the charge carriers are able to reduce the suitable adsorbed electron acceptors, A(ads), or to oxidize the adsorbed electron donors, D(ads), in competition with the described deactivation by surface recombination.

$$A*(ads) + e^- \rightarrow A^-(ads) \tag{2}$$
$$D*(ads) + h^+ \rightarrow D^+(ads) \tag{3}$$

The efficiency of the photocatalytic process can be measured in terms of the quantum yield of the process (number of events per photon absorbed), or in terms of turnover number (number of product chemical species per number of photoactive sites). In either case, it is difficult to have an accurate measure: the number of absorbed photons is difficult to evaluate in heterogeneous systems due to light diffraction, correspondingly the number of active sites in irradiation is equally difficult to measure. A somewhat loose concept of apparent quantum yield is normally preferred, but has the disadvantage of depending on the operational conditions of each experiment.

In TiO_2 aerated aqueous suspensions molecular oxygen is adsorbed on the surface and acts as electron acceptor, whereas adsorbed water molecules and hydroxyl anions will be available as electron donors to generate the very oxidizing $HO^{\bullet}$ radical. In the presence of an organic molecule the generated $HO^{\bullet}$ radical is the primary oxidizing entity, reacting by adduct formation followed by structural breakdown into several intermediates till, eventually, total mineralization.

If the organic reactant is able to compete with oxygen and water molecules for the active sites of the semiconductor, then direct electron transfer to an active hole is also conceivable, as the first step of an oxidative degradation. The overall process can be described by a set of sequential and concurrent multielectron transfers (Equations 4-9).

$$TiO_2 \xrightarrow{\ h\nu\ } TiO_2(h_{VB}^+ + e_{CB}^-) \tag{4}$$

$$TiO_2(e_{CB}^-) + O_2 \rightarrow TiO_2 + O_2^{\bullet-} \tag{5}$$

$$TiO_2(h_{VB}^+) + H_2O(ads) \rightarrow TiO_2 + OH^{\bullet}(ads) + H^+(ads) \tag{6}$$

$$TiO_2(h_{VB}^+) + OH^-(ads) \rightarrow TiO_2 + OH^{\bullet}(ads) \tag{7}$$

$$TiO_2(h_{VB}^+) + R(ads) \rightarrow TiO_2 + R^{\bullet+}(ads) \tag{8}$$

$$OH^{\bullet}(ads) + R(ads) \rightarrow Intermediate \rightarrow Mineralization \tag{9}$$
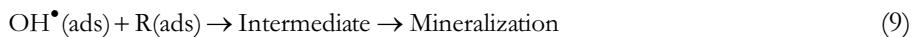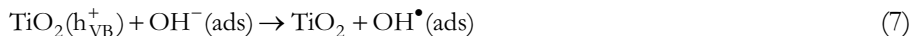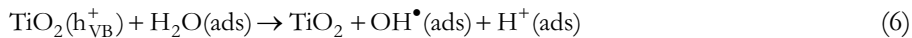
It should be noticed that because of Equation 7 there is a pH dependency, given the water dissociation into ions. On the other hand the role of oxygen can be more complex than suggested by Equation 5. There are many different oxidizing chemical species which can be generated from the reduction of molecular oxygen and will take part in the oxidation of the organic reactant (Equations 10-11).

$$O_2^{\bullet-} + H^+ \rightarrow HO_2^{\bullet} \tag{10}$$

$$H^+ + O_2^{\bullet-} + HO_2^{\bullet} \rightarrow H_2O_2 + O_2 \tag{11}$$

The generated H_2O_2 will undergo thermal desorption from the TiO_2 surface and it is known that in solution upon direct photolysis with UV radiation can lead to the formation of $HO^{\bullet}$ radicals (Equation 12) which may contribute to the oxidation of the organic molecule.

$$H_2O_2 \xrightarrow{h\nu} 2OH^{\bullet} \tag{12}$$

However, the contribution of this type of reaction is expected to be marginal in normal conditions of operation, where formation of $HO^{\bullet}$ radicals by Equations 6 and 7 is expected to dominate. In the presence of the oxidizing radicals, oxidative degradation should occur through formation of oxygenated radical intermediates, which will break down to lower molecular weight species as referred earlier.

1.4. PHOTOCATALYTIC REACTORS

The choice of the reactor will depend on the type of reaction to be considered, especially in the medium to be considered: gas phase, pure organic liquid phase, or aqueous solution. When liquid phase is to be considered the trivial solution uses the knowledge from chemical engineering reactors for thermal reactions, which means that the best way of irradiating a solution is to sink the light

source inside of the reaction mixture. This type of reactor is best known as immersion photochemical reactor and one of the simplest configurations is shown in Figure 2.
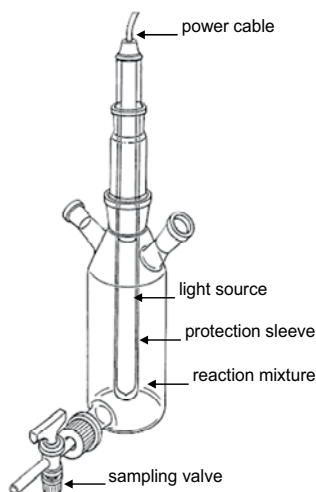
Figure 2 - Scheme of a typical immersion photochemical reactor. The light source is connected to an external power unit. Depending on the type of lamp refrigeration of the lamp may be needed (adapted from a Heraeus commercial leaflet).

In spite of its very simple design, this type of reactor poses a certain number of issues. The most relevant is the fact that in comparison with the perfectly stirred reactor where the thermal reaction is statistically distributed all over the volume, in the photoreactor the photochemical reaction can only occur at the points where light can reach. The transmission of irradiation in a highly scattering and absorbing medium made of an aqueous suspension of TiO_2 is a fundamental issue in the design and application of photocatalytic reactors. Therefore the design of a reactor for special purpose applications must take in consideration the type of source used and how this will reflect in the reactor geometry and accessories.

Radiation sources include arc lamps, incandescent filaments, fluorescent lamps, and lasers. Their operation mode and power demand is very variable, as well as

their need to be cooled – this is an important issue if the thermal activation is to be avoided. In Figure 2 some modifications can be introduced to include a cooling jacket between the protection sleeve and the light source. In addition sunlight, natural or artificial, concentrated or not, is also a possibility for illumination.

In the immersion photoreactor, the source (lamp) is placed inside of the reaction mixture. Other arrangements can use an external light source where the lamps are outside the reactor pot, therefore not in contact with the reaction mixture. Another possibility is to use distributed light sources where the light is conveyed to the reaction medium by means of reflectors and mirrors.

For heterogeneous photocatalysis there are basically two types of reactors:

> I. The slurry photocatalytic reactors, where the catalyst is basically suspended or dispersed in the fluid phase;
>
> II. The fixed bed photocatalytic reactors, where the catalyst is immobilized into a fixed support or dispersed over a stationary phase.

Due to the development of new materials, a new prototype of photocatalytic reactors has been appearing recently, in which the semiconductor is incorporated in a glass matrix used to build the reactor. This type of approach is based on self-cleaning non-fogging property of TiO_2 composites, for example as used at commercial scale in the composition of the rear-mirrors of some automobiles.

When comparing the two types of reactors several advantages and disadvantages can be listed in either case.

Photocatalytic slurry reactors are easy to handle. Depending on the efficiency of stirring, the distribution of the catalyst is uniform. No mass transfer limitations are normally associated to its operation and the ratio surface area to treated volume is normally very favourable, especially if nanostructured particles are used. The main disadvantage is the fact that scattering of light lowers the

efficiency of the process and in the case of very deeply coloured fluids there may be a deficient illumination of all catalyst particles. In addition a post-separation process is needed to isolate the catalyst particles, but being a simple physical process this is not of great concern in many of the current applications. Photocatalytic fixed bed reactors do not pose the problem of additional catalyst post-separation, they can operate in a continuous fashion and in the case where a support is used to disperse the catalyst they can benefit of some synergetic effects to improve photo-efficiency. On the other hand, mass transfer limitations are an issue to take into consideration. The ratio surface area to volume is not so favourable as in the slurry due to the loss of surface area imposed by immobilization. Finally, while the glass containing semiconductor materials are not fully developed, the immobilization is normally constrained to rapid degradation, leaching and wash out, because of mechanical stress.

The semiconductors used as photocatalysts include various metal oxides, besides TiO_2, such as ZnO, ZrO_2, WO_3, CeO_2, etc... or even sulfides like CdS and ZnS. TiO_2 is the most popular material in photocatalytic applications, mainly due to its strong oxidizing power, high chemical stability and relative inexpensiveness. It exists in different crystalline forms such as anatase, rutile and brookite. Anatase and brookite are thermodynamically metastable and can be irreversibly transformed to the most thermodynamically stable rutile at temperatures above 600 ºC. In many applications described, the catalyst used is titania from Degussa P-25, Table 1. Titania can be commercially obtained from other sources, or even synthesized. Sometimes can be modified by metal deposition or inserted in a matrix of other materials, such as different carbon phases.

TiO_2 can be prepared by both liquid and gas phase processes. The sol-gel method is one of the most used liquid phase techniques to synthesize thin films, powders and membranes. Among the many advantages of this technique are ease of processing, control over composition, purity and homogeneity of

the obtained materials. Titanium alkoxides are generally used as starting material for sol-gel formation, or precipitation, by hydrolysis followed by condensation. Acid catalysis is known to optmize hydrolysis rates leading to the formation of crystalline powders. The synthesis is followed by a thermal treatment to remove the organic part and to induce crystallization.

TABLE 1 - Physical chemistry properties of commercial titania P-25 (adapted from Degussa)

Crystal structure	$\approx$80% anatase : $\approx$20% rutile
Density (g cm-3)	3.8
BET Surface Area (m2g-1)	$\approx$55
Average particle size (nm)	30
Aqueous solution pH	3 – 4
Porosity	non-porous
CHEMICAL COMPOSITION	
SiO_2	<0.2 %
Al_2O_3	<0.3 %
Fe_2O_3	<0.01 %
TiO_2	>97 %
HCl	>0.3 %

The physical-chemical properties are found to be directly related to the preparation parameters, such as type of Ti(IV)-alkoxide precursor, solvent, aging time and calcination temperature. On the other hand, the photocatalytic efficiency is influenced by the crystal structure, surface area, size distribution, porosity, band gap and surface hydroxyl density.

1.5. HETEROGENEOUS PHOTOCATALYTIC REACTION RATES

The rate of photoconversion in a heterogeneous process can be expressed in terms of a limited number of variables and parameters that should include not only the concentrations of the present species, but also the reactor volume, and the amount of catalyst irradiated in this volume. Either in the case of the slurry

or fixed bed photoreactor a number of reasonable assumptions can be made, leading to an expression to the rate (r) of photoconversion[8]:

$$r = \frac{V}{W_{irr}} \frac{dC}{dt} = \sum_k \upsilon_k R_k \qquad (13)$$

with V being the reaction volume (L), W_{irr} the unit weight of irradiated catalyst (g), C the instantaneous concentration (mol/L), t time (s), υ_k a dimensionless stochiometric coefficient of the organic reactant under consideration involved in the reaction step k with a particular rate of photoconversion R_k (mol/g_{cat}s). This equation involves some assumptions better adapted to slurry than to fixed-bed reactors. At first, it assumes that the W_{irr} is know. However care should be taken since the same weight of catalyst does not mean the same number of illuminated active sites, especially in case of the fixed-bed photoreactor, as mentioned earlier. A similar approach can be adopted using the more meaningful external area of irradiated catalyst (A_{irr}). Another issue refers to the fact that the expression was derived considering a one pot reaction or batch mode operation which is not normally the case for fixed-bed photoreactors. Finally it is assumed that the illuminated section of the reactor is uniform and a quasi constant reaction rate can be assumed; this will require absence of mass transfer limitations, uniform light scattering, therefore a good fluid circulation and effective mixing. Also it should be noted that the irradiated volume (V_{irr}) is not necessarily identical to the reaction volume. Hence, the observed conversion for a given organic reactant in a specific reactor geometry depends on the weight of catalyst irradiated and volume of mixture illuminated. The kinetic parameters are then subjected to corrections, if they are meant to be used in predictive models. In terms of true rate constants (k), for a first order usual photoconversion, the rate constant derived from Equation 13 can be expressed in terms of apparent rate constants (k_{app}) defined according to the referred parameters[8]:

$$k_{app} = k'_{app} \frac{V_{irr}}{V} = k''_{app} \frac{A_{irr}}{V} = k \frac{W_{irr}}{V} \qquad (14)$$

The rate is normally identified with the true rate constant of the Langmuir-Hinshelwood kinetic model described by the following expression:

$$r = k\theta = \frac{kKC}{1+KC} \qquad (15)$$

where θ is the fractional surface coverage defined by the Langmuir isotherm expression and K is the adsorption equilibrium constant defined by the ratio between the adsorption and desorption rate constants ($K=k_{ads}/k_{des}$). The model assumes that a fast adsorption equilibrium is established (Equation 16) and the rate controlling step is the desorption of the adsorbed products (Equation 17)

$$C(bulk) \underset{k_{des}}{\overset{k_{ads}}{\rightleftarrows}} C(ads) \qquad (16)$$

$$C(ads) \xrightarrow{k} Products \qquad (17)$$

However if desorption of the reactants is fast, Equation 16 does not hold, thus reactant adsorption/desorption equilibrium is not established during reaction. Because of continuous illumination active centre reactivity (i.e. formation of e^-/h^+) is continuous, no equilibrium being established. On the other hand it was observed[9] that the Langmuir-Hinshelwood apparent kinetic terms (rate and equilibrium constants) were found to depend in the intensity of irradiation (Φ) with the same observed dependency, either to Φ or $\Phi^{1/2}$. Also a dependency of k in the oxygen coverage was found[9]. These findings resulting in the derivation of the pseudo-steady state kinetic model with a rate expression slightly different[9] from Equation 15. This was a warning that the traditional approach to kinetic analysis based solely on the evidence provided by kinetics can be misleading. Analysis of the heterogeneous photocatalytic process requires the determination of all kinetic parameters of a more fundamental rate equation

that that used currently. That includes all the physical parameters governing the kinetics: mass of catalyst, wavelength and radiant flux of irradiating source, quantum yields or turnover numbers for of the photocatalytic process, initial concentration of reactants, influence of oxygen pressure and temperature.

1.6. THE PHOTOCATALYTIC DEGRADATION OF TEXTILE DYES

In spite of the growing concern from industry towards minimization of environmental impacts, certain specific technologies still involve hazardous compounds that need careful treatment prior to release into the environment. This is the case of industrial dyestuffs including textile dyes, of which more than half are azo compounds, recognized as one of the most important threatens to the environment. Here we will give the example of degradation of 3 azo dyes, Figure 3, currently used in textile industry, respectively Solophenyl Green BLE 155 (SG, a trisazo dye), Erionyl Red B (ER, a disazo dye) and Chromotrop 2R (C2R a monoazo dye).
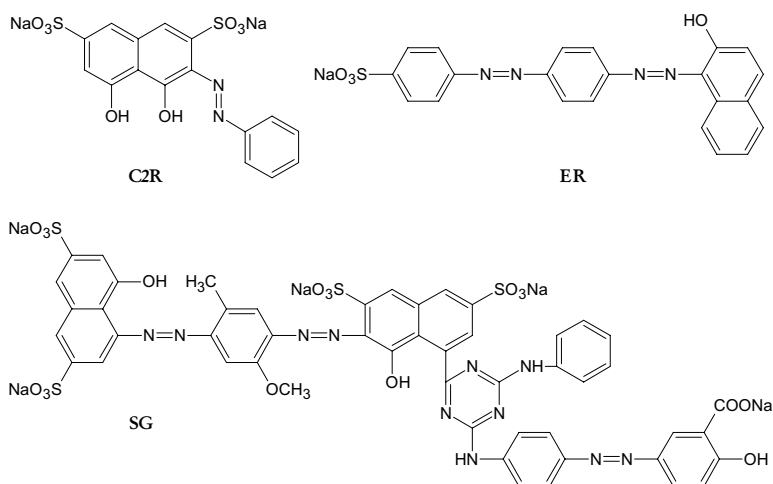
Figure 3 - Molecular forms of the used azo dyes: Chromotrop 2R (C2R, $C_{16}H_{10}N_2O_8S_2Na_2$, m.w.= 468.37 g/mol, molecular composition: 40% C; 25% H; 5% N; 20% O; 5% S; 5% Na); Erionyl Red B (ER, $C_{22}H_{15}N_4O_4SNa$, m.w.= 454.43 g/mol, molecular composition: 46.81% C; 31.91% H; 8.51% N; 8.51% O; 2.13 S; 2.13% Na); Solophenyl Green BLE 155 (SG, $C_{49}H_{32}N_{11}O_{18}S_4N_5$, m.w.= 1306.05 g/mol, molecular composition: 41.18% C; 26.89% H; 9.24% N; 15.13% O; 3.36% S; 4.20% Na).

The dyes were independently introduced in aqueous suspensions of TiO_2 and the photocatalytic process used UV-Visible irradiation (λ_{exc} = 253.7 nm). The used set-up was an immersion photocatalytic reactor of the same type of the one represented in Figure 2. It was observed that the solutions bleached, becoming completely colourless at the end of the treatment. First-order kinetics were recovered when measuring the change in absorption of the dye solution at the λ_{max} of each dye. The apparent rate constant was found to increase with catalyst load, in line with the heterogeneous photocatalytic nature of the process.

In this case the kinetics were well described by a modified Langmuir-Hinshelwood model, thus leading to the kinetic rate constants (k) and adsorption equilibrium constants (K) given in Table 2.

TABLE 2 - Kinetic and equilibrium parameters for dye degradation

Dye	k / (mg L^{-1}min^{-1})	K / (mg^{-1} L)
SG	1.58	0.0923
ER	2.43	0.1428
C2R	1.26	0.1284

Catalyst deactivation due to the adsorption is one of the drawbacks to the application of TiO_2 to photocatalytic degradation of organic pollutants. The observed colour change of the used catalyst may indicate the presence of chemisorbed species. By means of spectroscopic analysis (UV-Vis diffuse reflectance spectroscopy) of initial and used TiO_2 catalyst, surface modification was confirmed. The used catalysts were treated thermally and re-used. The recovered photo-catalysts do show a slight decline on the rate of degradation, which could be attributed to the presence of adsorbed species on the active sites of the catalyst surface, or to change of the particle dimension, which may occur during the recovery process.

The study, here briefly described, is an example of how organic complex molecules, normally refractory to classical methods can be degraded by means of the heterogeneous photocatalytic process.

Acknowledgments

References

1. A. Fujishima, K. Honda, *Nature,* **1972**, *238*, 37.

2. J.H. Carey, J. Lawrence, H.M. Tosine, *Bulletin of Environmental Contamination and Toxicology*, **1976**, *16*, 697.

3. S.E. Braslavsky, *Pure Appl. Chem.*, **2007**, *79*, 293.

4. *IUPAC Compendium of Chemical Terminology*, Electronic version (Copyright © 2005, 2006 International Union of Pure and Applied Chemistry), http://goldbook.iupac.org/P04580.html.

5. J.M. Herrmann, *Top. Catal.,* **2005**, *34*, 49.

6. A.L. Linsebigler, L. Guangquan, J.T. Yates Jr, *Chem. Rev.*, **1995**, *95*, 735.

7. A. Mills, S. Le Hunte, *J. Photochem. Photobiol. A: Chem.,* **1997**, *108*, 1.

8. H. Lasa, B. Serrano, M. Salaices, *Photocatalytic Reaction Engineering*, Springer, New York, **2005**.

9. D.F. Ollis, *Top. Catal.,* **2005**, *35*, 217.

2. HOMOGENEOUS PHOTOCATALYSIS

Hugh D. Burrows, M. Emília Azenha and Carlos J. P. Monteiro

Departamento de Química da Universidade de Coimbra, Rua Larga, 3004-535 Coimbra, Portugal.

Photochemistry is the study of the chemical effects of light absorption. It can therefore be considered an extension of spectroscopy. In this chapter we will concentrate on the catalytic photodegradation of substrates induced by the presence of light. Various interpretations and definitions of the concept photocatalysis have been given, and are discussed in the preceding Chapter. However, for our consideration of homogeneous photocatalysis we will take this to mean cyclic processes in a single homogeneous phase (usually the liquid phase) in which substrates react under the influence of light, leading to spontaneous regeneration of the catalyst such that this will allow the sequence to continue indefinitely until all the substrate has reacted. A more detailed discussion is given elsewhere[1,2].

In this Chapter, we will discuss both the fundamental basis of photochemistry and photocatalysis, together with some relevant applications. These include areas such as Advanced Oxidation Processes (AOPs) for treatment of pollutants[3], solar energy conversion[4], and photochemical synthesis of value added materials[5]. We will start with a brief review of basic photochemical processes.

Visible and ultraviolet light, like other forms of electromagnetic radiation, have energy (E), which is given by the Planck relationship

$$E = h\upsilon = hc/\lambda$$

where υ is the frequency, c the velocity of light in vacuum, λ the wavelength and h Planck's constant (6.626×10^{-34} J s). This is similar to the energy of many

chemical bonds, e.g. 400 nm (violet) light has an energy 3.1 eV (300 kJ mol^{-1}), which is almost identical to the dissociation energy of the hydrogen-iodine bond in HI (299 kJ mol^{-1}). Upon light absorption, this can dissociate to produce hydrogen and iodine atoms.

$$HI + h\nu \rightarrow H^\bullet + I^\bullet$$

Light of shorter wavelengths has even higher energy and may, therefore, induce homolytic cleavage of many other chemical bonds. Of particular importance for the photochemistry of organic systems are weak bonds, such as peroxy (ROOR) or azo (RN=NR) linkages. Under certain conditions even stronger bonds, such as C-C or C-H ones, may photodissociate upon UV excitation. However, as we will see, many photochemical reactions do not involve this photodissociation pathway, but instead chemical change occurs through reactions of electronically excited states.

There are certain spectroscopic and photophysical requirements for photochemical processes to occur. The first of these was presented nearly two centuries ago by Grötthus and Draper, and can be stated: "only light that is absorbed can induce a chemical change". This is sometimes referred to as the First Law of Photochemistry, and indicates that at least part of the absorption spectrum of molecules must fall within the spectral range of the exciting light source. In Table 1 we show the various regions of the electromagnetic spectrum of interest in photochemistry, together with the corresponding energies of the radiation, while Table 2 gives the most important lines of the commonly used low and medium pressure mercury lamp[6]. Further details of the emission wavelengths of common lasers and other light sources, together with a discussion of the solar spectrum are given elsewhere[6].

TABLE 1 - Approximate regions of the electromagnetic spectrum of interest in photochemistry.

Region	Wavelength / nm	Energy cm^{-1}	Energy eV
Near infrared	750-2500	13300-4000	1.65-0.50
visible	400-750	25 000-13 300	3.10-1.65
UV-A	320-400	31 250-25 000	3.87-3.10
UV-B	290-320	34 500-31 250	4.28-3.87
UV-C	220-290	50 000-34 500	6.20-4.28
Far UV	190-220	52 630-50 000	6.53-6.20
vacuum UV	40-190	250 000-50 000	31.00-6.53

$$1 \text{ eV} = 96.5 \text{ kJ mol}^{-1}$$

TABLE 2 - Most important emission lines (in nm) with relative intensities in the spectra of low and medium pressure mercury lamps.

Low pressure		Medium pressure	
wavelength /nm	relative intensity	wavelength /nm	relative intensity
253.7	100	253.7	9.1
296.7	0.74	302.3	16
312.9	2.2	312.9	33
365.4	3.0	365.4	100
404.7	2.2	404.7	24
435.8	8.0	435.8	37
546.1	4.8	546.1	33
		577.0	20
		579.1	29

The UV-A and UV-B regions in Table 1 correspond to the regions of transmission of light by glass and the ozone layer of the atmosphere respectively. For photochemical processes using light of shorter wavelength it is necessary to use quartz reaction vessels and optics. General photochemical techniques have been described in detail elsewhere[7]. In addition to the above light sources, a number of cheap light emitting diodes and diode lasers are now available which are likely to be excellent excitation sources for photocatalysis.

The Second Law of Photochemistry, due to Stark and Einstein, resulted from the development of quantum theory, and can be stated: "in the primary photochemical step each molecule will only absorb one quantum of light (photon)". Although, particularly with the development of high power lasers, a number of multiphoton processes are known, and two-photon photochemistry is a rapidly developing area for chemical and biomedical applications[8], the Stark-Einstein generalisation still holds true in the vast majority of cases.

We can thus represent the primary process in photochemistry as light absorption to produce an electronically excited state (**A***), which may reemit the light, lose the excess energy as heat, or undergo unimolecular or bimolecular reactions to form new products, in the processes:

A + hν → A*   **light absorption**

A* → A + hν′   **light emission** Φ_e

A* → A + heat   **nonradiative processes** Φ_{nr}

A* → products   **unimolecular photochemical reactions** Φ_{upr}

A* + B → products   **bimolecular photochemical reactions** Φ_{bpr}
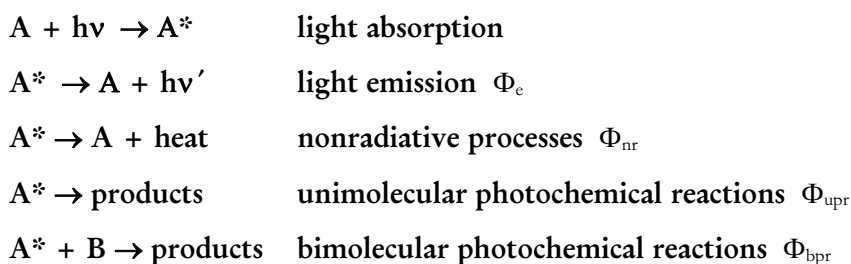
From the Stark-Einstein relation we can introduce an important parameter to measure the relative importance of these processes, the quantum yield (Φ). This can be defined as the number of molecules of reactant following a particular

pathway per photon absorbed. For a purely photochemical process the maximum quantum yield is 1. Some researchers prefer to use quantum efficiencies as percentages, such that the maximum yield is 100%. More details on this and general definitions can be found in the Glossary of Terms in Photochemistry, which has been prepared by IUPAC[9].

From the, Second Law of Photochemistry, the sum of quantum yields for purely photochemical reactions is 1, such that in the above scheme

$$\Phi_e + \Phi_{nr} + \Phi_{upr} + \Phi_{bpr} = 1$$

If we know the quantum yields of some of these processes from independent measurements, then we can calculate those of the other ones. We should note though that in a number of cases there may be secondary reactions following the initial photochemical step, such that quantum yields much greater than unity are observed. For example, the photolysis of chlorine in the presence of hydrogen involves the chain reaction

$$Cl_2 + h\nu \rightarrow Cl^{\bullet} + Cl^{\bullet}$$

$$Cl^{\bullet} + H_2 \rightarrow HCl + H^{\bullet}$$

$$H^{\bullet} + Cl_2 \rightarrow HCl + Cl^{\bullet}$$
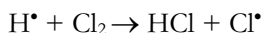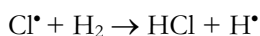
where the primary process is the homolytic photodissociation of a Cl-Cl bond. This produces chlorine atoms, which in subsequent secondary reactions form hydrogen and chlorine atoms as chain carriers, leading to very high quantum yields ($> 10^3$) of chlorine degradation or hydrogen chloride formation, in some cases with explosive results. Photochemically induced chain reactions may also be relevant in photocatalysis, particularly where reactive oxygen species such as hydrogen peroxide and hydroxyl radicals are involved.

We will now consider in more detail the physical processes of deactivation of excited states. A fundamental concept in quantum theory is the Born-Oppenheimer approximation, which states that we can break down the total energy of a molecule into a number of modes which can be treated

independently in terms of electronic, vibrational, rotational, translational and other contributions.

$$E_{total} = E_{electronic} + E_{vibrational} + E_{rotational} + E_{translational} + \ldots$$

This results from the fact that the magnitudes of the various contributions to the total energy of a molecule are very different, and provides us with the advantage that we can treat each of these energies separately. In photochemistry, the most important of these terms are the electronic and vibrational modes. We consider that each molecule has a well defined set of electronic states, and that associated with each of these there is a set of vibrational levels. Absorption of light of a particular wavelength will lead to an excited vibrational level of a particular electronic excited state. Boltzmann's distribution law relates the relative populations of two states (n_2/n_1) to their energy difference (ΔE)

$$n_2/n_1 = \exp(-\Delta E/RT)$$

and as a consequence, at equilibrium there must be many more molecules in the ground state than in excited states. Following light absorption, the excited states must therefore lose their excess energy to return to the ground state of the same or a different chemical species. The initial process is loss of excess vibrational energy, predominantly through collision with other molecules and subsequent conversion to thermal energy, i.e. heat. The process is termed vibrational relaxation, and this heat loss can be measured directly using photothermal techniques, such as photoacoustic calorimetry[10,11], which provide valuable information on both the energetics and yields of these pathways.

It is now necessary to consider a further dimension of electronic states, their spin multiplicities. Most organic and many inorganic molecules have a ground state in which all electron spins are paired – the singlet state (termed S_0). Light absorption will normally produce an excited singlet state (S_1), which typically has a lifetime of a few ns. However, there is a small but finite possibility that one of the electrons can invert its spin in a forbidden process to produce the

triplet state (T_1) in which two electrons have the same spin. From Pauli's exclusion principle, these must be in different orbitals. The ground (S_0), and excited singlet (S_1) and triplet (T_1) states are represented schematically below, Figure 1.

ground singlet state   **excited singlet state**   **excited tripet state**
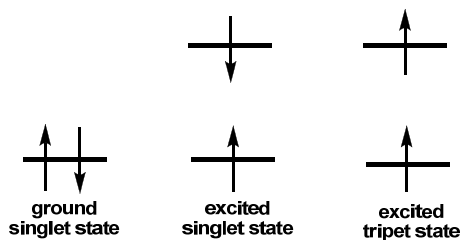
Figure 1- Schematic representation of singlet and triplet states.

From quantum mechanics (Hund's rule), the energy of the triplet state T_1 will be lower than that of the corresponding singlet (S_1). Triplet states also normally have much longer lifetimes than excited singlet states, with values typically of the order of μs or ms in solution and even longer in the solid state. In solution, these are normally quenched in the presence of molecular oxygen to give submicrosecond lifetimes. As we will see later, these bimolecular quenching reactions of excited triplet states with molecular oxygen are of particular importance for photocatalysis since they frequently produce singlet oxygen or other reactive oxygen species.

 Following vibrational relaxation to the lowest vibrational level of a particular excited electronic state, the molecule will now be transformed into a lower electronic state through radiative or nonradiative (radiationless) photophysical processes. The possible radiative processes, which will lead to light emission, are fluorescence, involving states of the same spin multiplicity (typically $S_1 \rightarrow S_0$) and phosphorescence involving states of different spin multiplicities (normally $T_1 \rightarrow S_0$). The nonradiative processes, which lead to the interconversion between isoenergetic levels of two electronic states, are internal conversion (IC) involving states of the same spin multiplicities and intersystem

crossing (ISC), where the processes occurs between states of different spin multiplicities.

All these processes are commonly represented in terms of the Jablonski-Perrin diagram[9,12], Figure 2, where the corresponding efficiencies are given as quantum yields (Φ). A detailed understanding of the photophysics of these system also requires determination of the rate constants (k) and lifetimes ($\tau = 1/k$) of all the radiative and nonradiative pathways. These can be obtained from fast reaction techniques such as flash photolysis, pulse radiolysis and time-correlated single photon counting[13].
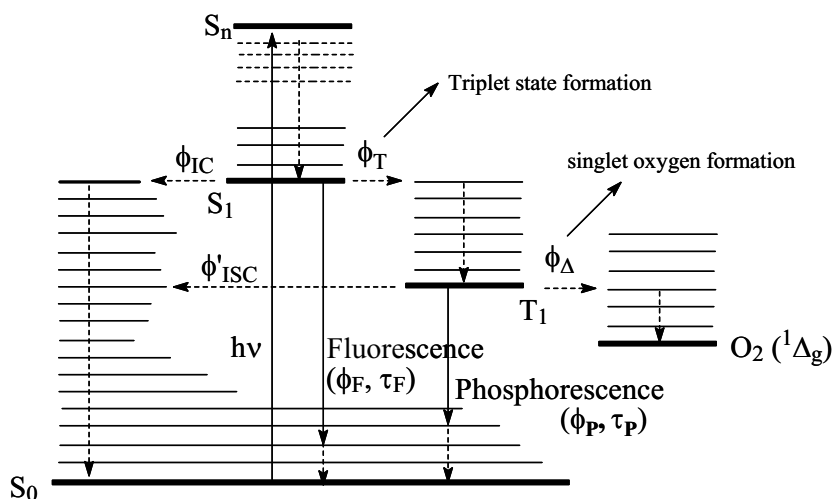
Figure 2 - Jablonski-Perrin diagram.

One important approximation arises as a consequence of the relative rates of the various processes involved, the Kasha-Vavilov rule[12]. This can be expressed as: "photophysical and photochemical processes in general only occur from the lowest excited state of a given spin multiplicity". This is a generalisation, and a number of important exceptions are known, particularly azulene, which fluoresces from emits S_2 state[9]. Nevertheless, the Kasha-Vavilov rule greatly simplifies our treatment of photochemistry, since we normally only need to

consider the lowest singlet (S_1) and triplet (T_1) excited states of a particular molecule.

Detailed description of the factors which affect the importance of the different radiative and radiationless processes are beyond the scope of this Chapter, and are given in any standard textbook of photochemistry[12,14]. However, we will indicate three factors which are particularly relevant for photocatalysis:

(a) Radiative processes are generally favoured with structurally rigid compounds, such as aromatic systems. Further, within any group of aromatic compounds, systems having a more rigid structure will generally show higher fluorescence quantum yields than conformationally flexible ones. For example, the fluorescence quantum yield (Φ_F) of biphenyl (**1**) in nonpolar solvents is 0.18, whereas with the rigid fluorene (**2**), this increases to $\Phi_F = 0.68$[6];

(b) Triplet state formation is favoured by the presence of lowest lying excited states involving nonbonding electrons, such as the so-called n,π^* states present in carbonyl containing compounds[14]. For example, the formation of the triplet state of benzophenone (**3**) occurs with 100% efficiency (lowest excited state (n,π^*), $\Phi_T = 1$)[6], whereas with benzene (lowest excited state (π,π^*)) the quantum yield is much lower ($\Phi_T = 0.25$ in nonpolar solvents)[6]. This has been discussed in more quantitative detail elsewhere in terms of El Sayed's rules[15];

(c) The presence of heavy atoms (halogens, metal centres, etc.) in molecules greatly increases the quantum yields of intersystem crossing ($S_1 \leadsto T_1$ and $T_1 \leadsto S_0$) through increased spin-orbit coupling, the so-called heavy atom effect.[16] This is illustrated nicely with the quantum yields for triplet state formation of benzene ($\Phi_T = 0.25$), chlorobenzene ($\Phi_T = 0.76$) and 1,4-dichlorobenzene ($\Phi_T = 0.95$)[6].

| 1 | 2 | 3 |
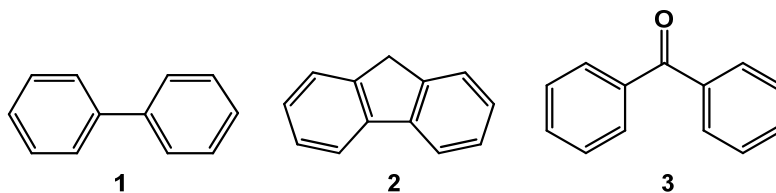
In addition to the above intramolecular photophysical processes, another photophysical pathway which is of great importance in many systems, including photocatalysis, involves the intermolecular transfer of electronic energy from an excited donor molecule (D*) to an energy acceptor (A):

$$D^* + A \rightarrow D + A^*$$
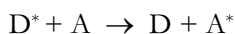
For this to occur, the excited state energy of A must be equal to or less than that of D. In addition, there are other requirements which depend on the energy transfer mechanism. The most important of these are the exchange mechanism associated with Dexter[17], and the Förster mechanism involving dipole-dipole interactions[18]. Both of these require good overlap between the emission spectrum of the donor and the absorption spectrum of the acceptor. In addition, the Dexter mechanism normally proceeds *via* collision between excited donor and acceptor in its ground state, and requires a correlation between the overall spins of the initial and final donor-acceptor pair. More detailed discussion on kinetic and energetic aspects of energy transfer can be found elsewhere[19]. Probably the most important cases of Dexter transfer for photocatalysis involve the sensitisation of a triplet state by an appropriate donor, and the interaction between triplet donor and ground state (triplet) molecular oxygen to form singlet oxygen:

$$^3D^* + A \rightarrow D + {}^3A^*$$

$$^3D^* + O_2\,(^3\Sigma_g^-) \rightarrow D + {}^1O_2^*\,(^1\Delta_g)$$
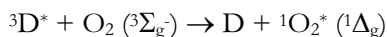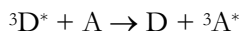
Förster energy transfer does not require collision and can take place over distances much larger than molecular diameters (up to *ca* 100 Å). The most relevant cases for photocatalysis involve relatively rigid media.

Before discussing homogeneous photocatalysis, we will comment briefly on the effects of excitation on the chemical properties of molecules. From the Kasha-Vavilov rule[13], we will normally only consider the lowest excited state of a molecule with a particular spin multiplicity. Excitation of an electron from the highest occupied molecular orbital (HOMO) to the lowest unoccupied molecular orbital (LUMO) will change the electron distribution, and hence the chemical properties. Excited states are thus distinct chemical entities with different behaviour from the corresponding ground state. This includes properties such as oxidation potentials[20] and acidities[21], examples are in Table 3.

TABLE 3- Example of oxidation potentials and acidities in ground and excited states.

Couple	E^o / $V(a_{H^+} = 1\ M)$	Compound	pK_a
UO_2^{2+} / UO_2^+	+ 0.163	PhOH	10.0
$*UO_2^{2+}$ / UO_2^+	+ 2.60	$^1PhOH^*$	3.60

These will change the reactivity of excited states in relation to both redox and acid-base reactions. In addition, changes of electron density within the LUMO may favour other processes, such as atom transfer. Our discussion of photocatalysis will include examples of reactions in which these factors are driving forces. Naturally, with such a wide area it is necessary to be selective, and we make no apologies for focussing much of the discussion on our own work in this area.

As a starting point, photosynthesis in green plants is often taken as a classic case of photocatalysis

$$6H_2O + 6CO_2 \rightarrow C_6H_{12}O_6 + 6O_2$$

This occurs in the chloroplast, and involves metalloporphyrins, in particular magnesium porphyrins, in a somewhat complex pathway. Although the general features are understood[22], there are still outstanding questions, and this is probably not the best model for homogeneous photocatalysis. However, it does

show one important facet of many photocatalytic processes in that it involves a redox reaction, with oxidation of water to produce oxygen and accompanying reduction of carbon dioxide. The majority of homogeneous photocatalytical processes which have been studied involve related redox reactions.

A further relevant result from the example of photosynthesis is the involvement of metalloporphyrins both as catalysts and light harvesting species. Porphyrins, phthalocyanines and related cyclic tetrapyrroles have very strong absorptions in the visible region and represent an extremely important class of homogeneous photocatalysts[5,23-27]. In many photocatalytical processes, the substrate (X) does not absorb light in the region of interest, but is activated or reacts through a photosensitised process *via* a sensitiser (Sens):

$$Sens \ + \ h\nu \rightarrow \ Sens^*$$

$$Sens^* \ + \ X \rightarrow Sens + X^*$$

$$X^* \rightarrow Products$$

$$\Phi(products) \leq 1$$
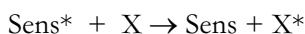
Porphyrins and related compounds have an intense absorption band (the Soret band) around 400-420 nm, and a series of weaker bands (Q bands) in the 500-650 nm region[28]. They can therefore be used as good sensitisers with visible light. Two photosensitised pathways are typically presented[13,29] for this class of compounds, Type I, involving atom or electron transfer, and Type II, which occurs in the presence of molecular oxygen and produces singlet oxygen.

Type I mechanism involving electron transfer

$$Sens \ + \ h\nu \rightarrow \ {}^1Sens^*$$

$$Sens^* + X \rightarrow {}^1(Sens^{\bullet\bullet}X)^*$$

$${}^1(Sens^{\bullet\bullet}X)^* \rightarrow Sens^{\bullet+} + X^{\bullet-} \ (or \ Sens^{\bullet-} + X^{\bullet+}) \rightarrow Products$$

Type II mechanism

$$Sens \ + \ h\nu \rightarrow \ {}^1Sens^* \rightarrow {}^3Sens^*$$

$${}^3Sens^* + O_2 \rightarrow Sens + {}^1O_2^*$$

$${}^1O_2^* + X \rightarrow Products$$
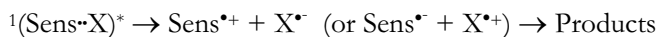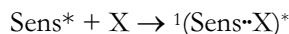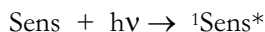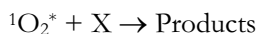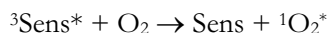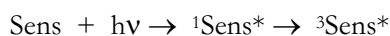
In the presence of water and/or oxygen both these pathways can produce a variety of reactive oxygen species, the properties of which are summarised below[30].

TABLE 4 – Oxidation potential and pKa of some reactive oxygen species.

Species	E^o / V (relative to NHE, [H^+] = 1 M)	pKa
$^\bullet OH$	1.90 ($^\bullet OH/OH^-$)	11.9 ($^\bullet OH/O^{\bullet-}$)
$O_2^{\bullet-}$	-0.16 ($O_2/O_2^{\bullet-}$)	4.8 ($HO_2^\bullet/ O_2^{\bullet-}$)
$HO_2^\bullet$	0.75 ($HO_2^\bullet/HO_2^-$)	
$^1O_2^*$	0.83 ($^1O_2^*/O_2^{\bullet-}$)	
O_3	1.01 ($O_3/O_3^{\bullet-}$)	
H_2O_2	1.44 (H^+, $HO_2^\bullet/H_2O_2$)	

We will start by considering some porphyrin sensitised reactions occurring through the Type II pathway. Singlet oxygen is a highly reactive species, which can react with double bonds either via cycloaddition to give endoperoxides or in the *ene* reaction to give hydroperoxides[31]. These have the weak peroxide and hydroperoxide bonds which can undergo further thermal or photochemical degradation, leading to formation of final products containing carbonyl and/or hydroxyl groups. Photocatalysed oxidation of 1,5-dihydroxynaphthalene (4) in air saturated solutions in the presence of different porphyrins leads to formation of the important compound 5-hydroxynaphthoquinone (5) (juglone) in high yields through formation of singlet oxygen and its subsequent reaction with the substrate[5], Scheme 1. The porphyrin *meso*-tetrakis(2,6-dichlorophenyl)porhyrin is found to be a particularly good sensitiser both in terms of product yields and photostability. The high yield of singlet oxygen formation with such chlorinated tetraphenylporphyrins probably results from

high $S_1 \leadsto T_1$ intersystem crossing yields due to the heavy atom effect. A detailed study of the heavy atom effect in porphyrins has been presented[32].
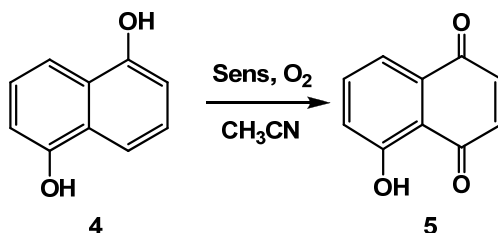
Scheme 1

We should note that the lifetime of singlet oxygen is very strongly dependent upon solvent[33,34], varying from 2 μs in water, 32 μs, 25 μs in toluene, 40 μs in acetonitrile and 700 μs in carbon tetrachloride[33]. Choice of appropriate solvent conditions is therefore an important consideration in photocatalysed reactions involving singlet oxygen. In addition for designing such Type II photocatalysed processes, it can be valuable using available kinetic data for the reaction of singlet oxygen substrates in solution[33,35].

Similar Type II processes involving free base and metalloporphyrins as sensitisers have been used in the catalysed photodegradation of pollutants such as chlorophenols[24,25] and triazine pesticides[26]. General aspects of the photodegradation of chlorophenols[36] and pesticides[37] have been given elsewhere. The compound *meso*-tetrakis(2,6-dichloro-3-sulfophenyl)porphyrin (6) and its metal containing derivatives (7) have been developed as particularly efficient photocatalysts.

6   **7**
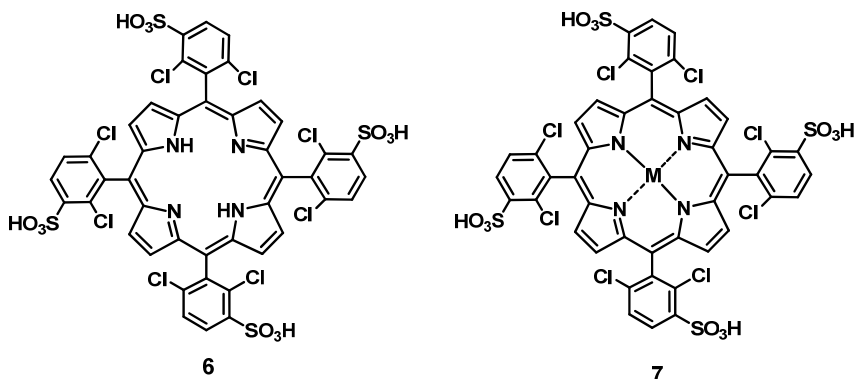
As we have remarked earlier, incorporation of a heavy atom, such as chlorine, will significantly enhance the yield of triplet state formation, and hence of singlet oxygen production, whilst the sulfonate group makes the compound water soluble. As a model reaction, we can consider the photosensitized degradation of 4-chlorophenol (4-CP) (**8**) by iron *meso*-tetrakis(2,6-dichloro-3-sulfophenyl)porphyrin (FeTDCPPS) (**7**, M=Fe) in aerated aqueous solution, which is shown to lead to formation of *p*-benzoquinone (**9**) and *p*-hydroquinone (**10**) as main photoproducts, Scheme 2[24].
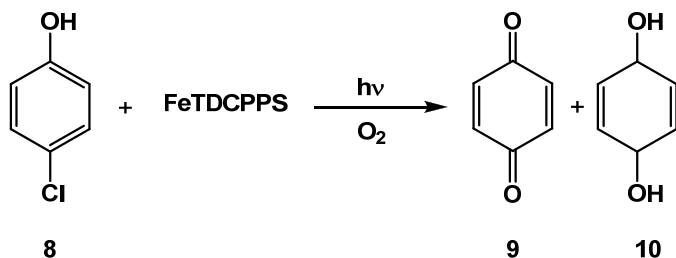
Scheme 2

In deaerated solution no *p*-benzoquinone was formed, while laser flash photolysis, time resolved singlet oxygen phosphorescence measurements and the slower rate of photolysis in aerated solution and in the presence of the singlet oxygen quencher sodium azide (NaN$_3$) all supporting the idea that under these conditions, Type II sensitisation is one of the dominant mechanisms of 4-CP degradation. However, there are also indications of direct reaction between

the excited porphyrin and 4-CP, indicating that there are two mechanisms involved in the chlorophenol photodegradation. The balance between the reactions seems to be strongly dependent on both the nature and metal ion involved[25].

Application of photocatalytic pathways to the degradation of pollutant molecules has as principal objective their photomineralisation, or conversion of organic species into relatively inert inorganic products such as carbon dioxide, water, halide ions and ammonia. Although porphyrins have excellent spectral and photophysical properties which make them good sensitisers using visible light, and their properties can be modulated by appropriate structural modification, considerable research is still necessary to produce photocatalytic systems with them which will lead to complete substrate mineralisation. In addition, there are problems with their long term photostability, which at present limits the number of catalytic cycles possible.

Metal complexes avoid some of these limitations, and show strong potential as homogeneous photocatalysts. The uranyl ion (UO_2^{2+}) is a strong oxidant in excited state but only weakly oxidising in ground state, and its photoreactivity has been described in detail elsewhere[20,38]. In addition, its luminescence and excited state absorption provide excellent tools to study mechanistic details of its photoreactivity, making it an excellent model compound for understanding details of homogeneous photocatalysis. Two main pathways have been identified, examples of which are given below.

Hydrogen atom abstraction

$$*UO_2^{2+} + R_2CHOH \rightarrow UO_2H^{2+} + R_2{}^\bullet COH$$

$$UO_2H^{2+} \rightarrow UO_2^+ + H^+$$

Electron transfer

$$*UO_2^{2+} + PhOH \rightarrow UO_2^+ + PhOH^{\bullet+}$$
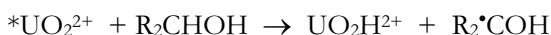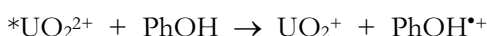
The reduced uranium(V) species itself undergoes disproportionation in aqueous solutions

$$2UO_2^+ + 4H^+ \rightarrow U(IV) + UO_2^{2+} + 2H_2O$$

In addition, U(IV) and UO_2^+ are oxidised to UO_2^{2+} by molecular oxygen in aqueous solutions. With substrates such as alkanes, alkenes, alcohols and aldehydes, uranyl catalysed photoxidation with molecular oxygen has been demonstrated[39]. In addition, detailed mechanistic studies have been reported on the photocatalytic oxidation of alcohols through hydrogen abstraction[40], and of chlorophenols through electron transfer[41]. The reaction with aliphatic alcohols is particularly valuable as it is stereospecific towards the α-carbon atom.

$$*UO_2^{2+} + R_1R_2CHOH \rightarrow UO_2H^{2+} + R_1R_2{}^\bullet COH$$

$$R_1R_2{}^\bullet COH + UO_2{}^{2+} \rightarrow R_1R_2CO + UO_2^+ + H^+$$
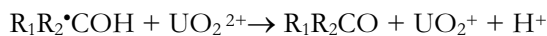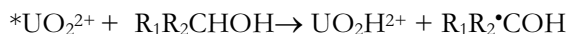
However, one limitation is the relatively slow rate of reoxidation of U(V) or U(IV) to UO_2^{2+} by molecular oxygen, which depends on pH, oxygen pressure and the particular counter-ions used[39,42]. A more serious drawback is the concern over possible hazards associated with the use of the radioactive uranium. As a consequence, a considerable amount of research has been devoted to the development of other oxometallic species a potential photocatalysts.

The most successful of these involve polyoxometallates (POM)[43,44], which have the general formula $M_xO_y{}^{q-}$. A good example is $XW_{12}O_{40}{}^{z-}$ (X=P, Si; Z=3, 4), whose structure is given below, in Figure 3.
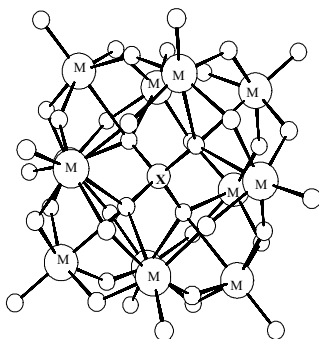
Figure 3 - Structure of $XW_{12}O_{40}{}^{z-}$.

Polyoxometallate photocatalyst presents similarities both with that of the uranyl ion, and of inorganic semiconducting particles such as TiO_2[43,44], and thus bridges the gap between homogeneous and heterogeneous photocatalysis. In many cases, reactions involve generation of the reactive hydroxyl radical ($HO^\bullet$). Both mechanistic[36,37,45] and kinetic[46] details are available on reactions of the hydroxyl radical with both organic and inorganic substrates. The most important reactions of the $OH^\bullet$ radical are:

Electron transfer

$$HO^\bullet + P \rightarrow OH^- + P^{\bullet+}$$

Hydrogen atom abstraction

$$HO^\bullet + PH \rightarrow H_2O + P^\bullet$$
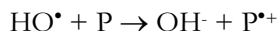
Addition to aromatic rings

$$HO^\bullet + P \rightarrow P\text{-}OH^\bullet$$

The radicals formed will then undergo further reactions to form the final stable products, leading in many cases to mineralization. We will consider other routes to solution generation of hydroxyl radicals, which have particular applications in AOPs, like below.

Hydrogen Peroxide Homolysis

$$H_2O_2 + h\nu \rightarrow 2HO^\bullet$$

Ozone photolysis

$$O_3 + h\nu \rightarrow O_2 + O^\bullet$$

$$O^\bullet + H_2O \rightarrow 2HO^\bullet$$

Photo-Fenton reaction

$$H_2O_2 + Fe^{2+} \rightarrow Fe^{3+} + {}^-OH + HO^\bullet$$

$$Fe^{3+} + H_2O + h\nu \rightarrow Fe^{2+} + HO^\bullet + H^+$$
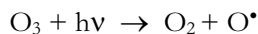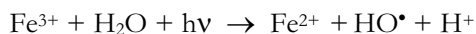
Of these, only the photo-Fenton reaction is strictly photocatalytic. However, the other two routes means of photogeneration of hydroxyl radicals which involve relatively cheap substrates are also important in areas such as waste water treatment. The photo-Fenton reaction is strongly dependent upon pH[47], and the most reactive species appears to be the complex $Fe(OH)^{2+}$. Systems involving this species have been developed and shown to be capable of inducing the complete mineralisation of various organic pollutants[48].

In addition to the strongly oxidizing hydroxyl radical, a number of other inorganic radicals, including hydrogen atoms, hydroperoxyl radicals, $HO_2^{\bullet}$, sulfate radical anion, $SO_4^{\bullet-}$, dihalide radical anions, $X_2^{\bullet-}$, and the azide. radical, $N_3^{\bullet}$, can be produced and used in photocatalytic systems. Details on many of these can be found on the very valuable website of the Notre Dame Radiation Chemical Data Center[49]. We will consider the reaction of one of these, the $SO_4^{\bullet-}$ radical anion, produced in the sacrificial reaction between the excited tris(2,2'-bipyridyl)ruthenium(II) cation ($[Ru(bpy)_3]^{2+}$) and persulfate anion ($S_2O_8^{2-}$)[50,51].

$$[Ru(bpy)_3]^{2+} + S_2O_8^{2-} + h\nu \rightarrow [Ru(bpy)_3]^{3+} + SO_4^{\bullet-} + SO_4^{2-}$$
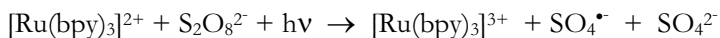
The ruthenium complex has a strong absorption in much of the visible spectrum, making it suitable for photocatalysis using solar radiation, and possesses lowest excited state which can be both strongly reducing and oxidizing and whose properties have been extensively reviewed[52]. In this particular case, the excited ruthenium complex transfers an electron to the persulfate ion leading to formation of two strongly oxidizing species, the trivalent $[Ru(bpy)_3]^{3+}$ and the sulfate radical anion. In photoreactions in the presence of oxygen with substrates such as chlorophenols[50,51], both the oxidizing species may react with substrate, in the former case leading to reduction of the ruthenium(III) complex back to ruthenium(II), making the overall process photocatalytic, and leading to less harmful compounds and in many cases to photomineralisation. We should note, however, that recent

results have questioned whether the $SO_4{}^{\bullet-}$ radical anion is the true oxidizing species when reactions are carried out in the presence of oxygen[53], and more research is needed to clarify this. However, this does not detract from the overall efficiency of the process.

Homogeneous catalysts in general suffer the limitation in comparison with heterogeneous ones that some separation process is needed for practical applications. The principal strategy to avoid this involves the immobilisation of photocatalysts on an inorganic or polymeric solid support. Aspects of immobilization of homogeneous catalysts in general have been reviewed elsewhere[54,55]. For photocatalysis, in which reactive radical species may be produced, inorganic supports, such as aluminas, zeolites and clays would appear to be particularly valuable, and this is currently an area of active research.

Acknowledgements

References

1. N. Serpone, E. Pelizzetti, *Photocatalysis- Fundamentals and Applications*, Wiley, New York, **1989**.

2. M. Chanon (Ed.), *Homogeneous Catalysis*, Wiley, Chichester, **1997**.

3. O. Legrini, E. Oliveros A.M. Braun, *Chem. Rev.*, **1993**, *93*, 671.

4. See, for example, B. O'Regan, M. Grätzel, *Nature*, **1991**, *353*, 737.

5. D. Murtinho, M. Pinheiro, M.M. Pereira, A.M.d'A. Rocha Gonsalves, L.G. Arnaut, M. da G. Miguel, H.D. Burrows, *J. Chem. Soc. Perkin Trans. 2*, **2000**, 2441.

6. M. Montali, A. Credi, L. Prodi, M.T. Gandolfi, *Handbook of Photochemistry*, CRC Taylor and Francis, Boca Raton, 3rd edn., **2005**.

7. J. Calvert, J.N. Pitts, *Photochemistry*, John Wiley & Sons, Inc., **1966**.

8. W. Denk, J. Strickler, W.W. Webb, *Science*, **1990**, *248*, 73.

9. S.E. Braslavsky, *Pure Appl. Chem.*, **2007**, *79*, 293.

10. S.E. Braslavsky, G.E. Heibel, *Chem. Rev.*, **1992**, *92*, 1381.

11. L.G. Arnaut, R.A. Caldwell, J.E. Elbert, L.A. Melton, *Rev. Sci. Instruments,* **1992**, *63*, 5381.

12. R.P. Wayne, *Principles and Applications of Photochemistry*, Oxford Science Publications, Oxford, **1988**.

13. R.V. Bensasson, E.J. Land, T.G. Truscott, *Excited States and Free Radicals in Biology and Medicine*, Oxford University Press, Oxford, **1993**.

14. See, for example, N. Turro, *Modern Molecular Photochemistry*, University Science Books, Sausalito Ca., **1991**.

15. M.A. El-Sayed, *Acc. Chem. Res.,* **1968**, *1*, 8.

16. J.C. Koziar, D.O. Cowan, *Acc. Chem. Res.,* **1978**, *11*, 334.

17. D.L. Dexter, *J. Chem. Phys.,* **1953**, *21*, 836.

18. T. Förster, *Disc. Faraday Soc.*, **1959**, *27*, 7.

19. V. Balzani, F. Bolletta, F. Scandola, *J. Am. Chem. Soc.,* **1980**, *102*, 2152.

20. S.J. Formosinho, H.D. Burrows, M. da G. Miguel, M.E. Azenha, I.M. Saraiva, A.C.D.N. Ribeiro, I.V. Khudyakov, R.G. Gasanov, M. Bolte, M. Sarakha, *Photochem. Photobiol. Sci.,* **2003**, *2*, 569.

21. J.F. Ireland, P.A.H. Wyatt, *Adv. Phys. Org. Chem.,* **1976**, *12*, 131.

22. See, for example, *Photosynthesis: Mechanisms and Effects*, G. Garab (Ed.), Kluwer. New York, **1999**.

23. H. Hennig, S. Knoblauch, D. Scholz, *New J. Chem.,* **1997**, *21*, 701.

24. E. Silva, M.M. Pereira, H.D. Burrows, M.E. Azenha, M. Sarakha, M. Bolte, *Photochem. Photobiol. Sci.*, **2004**, *3*, 200.

25. C.J.P. Monteiro, M.M. Pereira, M.E. Azenha, H.D. Burrows, C. Serpa, L.G. Arnaut, M.J. Tapia, M. Sarakha, P. Wong-Wah-Chung, S. Navaratnam, *Photochem. Photobiol. Sci.*, **2005**, *4*, 617.

26. S.L.H. Rebelo, A. Melo, R. Coimbra, M.E. Azenha, M.M. Pereira, H.D. Burrows, M. Sarakha, *Environ. Chem. Lett.*, **2007**, *5*, 29.

27. D. Gryglik, J.S. Miller, S. Ledakowicz, *Solar Energy*, **2004**, *77*, 615.

28. M. Gouterman, *J. Mol. Spectroscopy*, **1961**, *6*, 138.

29. C.S. Foote, *Photochem. Photobiol.,* **1991**, *54*, 659.

30. Data from D.M. Stanbury, *Adv. Inorg. Chem.,* **1989**, *33*, 70.

31. A.A. Gorman, M.A.J. Rodgers, *Chem. Soc. Rev.,* **1981**, *10*, 205.

32. E.G. Azenha, A.C. Serra, M. Pineiro, M.M. Pereira, J. Seixas de Melo, L.G. Arnaut, S.J. Formosinho, A.M.d'A. Rocha Gonsalves, *Chem. Phys.,* **2002,** *280*, 177.

33. F. Wilkinson, J. Brumer, *J. Phys. Chem. Ref. Data,* **1981**, *10*, 809.

34. F. Wilkinson, W.P. Helman, A.B. Ross, *J. Phys. Chem. Ref. Data,* **1993**, *22*, 113.

35. F. Wilkinson, W.P. Helman, A.B. Ross, *J. Phys. Chem. Ref. Data,* **1995**, *24*, 663.

36. H.D. Burrows, L.S. Ernestova, T.J. Kemp, Y.I. Skurlatov, A.P. Purmal, A.N. Yermakov, *Prog. Reaction Kinetics,* **1998**, *23*, 145.

37. H.D. Burrows, M.L. Canle, J.A. Santaballa, S. Steenken, *J. Photochem. Photobiol. B: Biol.*, **2002**, *67*, 71.

38. H.D. Burrows, T.J. Kemp, *Chem. Soc. Rev.*, **1974**, *3*, 139.

39. W.D. Wang, A. Bakac, J.H. Espenson, *Inorg. Chem.,* **1995**, *34*, 6034.

40. M.E. Azenha, H.D. Burrows, S.J. Formosinho, M.G.M. Miguel, *J. Chem. Soc., Faraday Trans.1,* **1989**, *85*, 2625.

41. M. Sarakha, M. Bolte, H.D. Burrows, *J. Phys .Chem. A*, **2000**, *104*, 3142.

42. K.R. Howes, A. Bakac, J.H. Espenson, *Inorg. Chem.*, **1988**, *27*, 791.

43. A. Hiskia, A. Mylonas, E. Papaconstantinou, *Chem. Soc. Rev.,* **2001**, *30*, 62.

44. P. Kormali, A. Troupis, T. Triantis, A. Hiskia, E. Papaconstantinou, *Catal. Today,* **2007**, *124*, 149.

45.   S. Steenken, *Topics Curr. Chem.,* **1996**, *177*, 125.

46. G.V. Buxton, C.L. Greenstock, W.P. Helman, A.B. Ross, *J. Phys. Chem. Ref. Data,* **1988**, *17*, 513.

47. H.J. Benkelberg, P.Warneck, *J. Phys .Chem.,* **1995**, *99*, 5214.

48. G. Mailhot, M. Sarakha, B. Lavédrime, J.Cáceres, S. Malato, *Chemosphere,* **2002**, *49*, 525.

49. http://allen.rad.nd.edu/, accessed 13th January 2008.

50. M.I. Silva, H.D. Burrows, M.G. Miguel, S.J. Formosinho, *Ber. Bunsenges Phys. Chem.*, **1996**, *100*, 138.

51. M.I. Silva, H.D. Burrows, S.J. Formosinho, L. Alves, A. Godinho, M.J. Antunes, D. Ferreira, *Environ. Chem. Le*tt., **2007**, *5*, 143.

52. See, for example, A. Juris, V. Balzani, S. Campagna, P. Belser, A. von Zelewsky, *Coord. Chem. Rev.,* **1988**, *84*, 85.

53. K. Clarke, R. Edge, E. Land, S. Navaratnam, T.G. Truscott, *Radiat. Phys .Chem.,* **2008**, *77*, 49.

54. P.M. Price, J.H. Clark, D.J. Macquarrie, *J. Chem. Soc. Dalton Trans.,* **2000**, 101.

55. N.E. Leadbetter, M. Marco, *Chem. Rev.,* **2002**, *102*, 3217.

(Página deixada propositadamente em branco)

SECTION D

ELECTROCATALYSIS

(Página deixada propositadamente em branco)

1. ELECTROCATALYSIS: ELECTRODES AS HETEROGENEOUS CATALYSTS AND APPLICATION IN SENSORS AND FUEL CELLS

Christopher M.A. Brett

Departamento de Química da Universidade de Coimbra, Rua Larga, 3004-535 Coimbra, Portugal.

1.1. INTRODUCTION

Electrode reactions occur through charge transfer, normally of electrons, between an electrode and an electroactive species immersed in a contacting electrolyte solution. The rate of these processes depends on the energy of the electrons which are transferred, as well as on the quantity present close to the electrode surface. The energy of these electrons can be altered by external control through the applied potential, thus directly determining the possibility and extent of the reaction and thence the ability to carry out oxidation and reduction reactions. The electrode itself can therefore be viewed as a controllable heterogeneous catalyst. Different electrode materials can influence the electrode kinetics by decreasing or increasing the activation energy barrier to electron transfer, manifested by a change in the potential necessary to carry out an oxidation or a reduction, the basis of electrocatalysis.

In this chapter, the fundamentals aspects of electrode processes necessary for an understanding of electrocatalysis will be indicated and applications in sensors and in fuel cells will be described.

1.2. ELECTRODE PROCESSES AND ELECTROCATALYSIS

Electrochemistry is concerned with the study of phenomena associated with charge transfer and charge separation[1]. The charge transfer can occur homogeneously in solution or at the surface of electrodes immersed in electrolyte solution, at one of which occurs oxidation (anode) and at the other

reduction (cathode) in order to ensure electroneutrality. An electrical circuit is formed, via the electrolyte solution between the two electrodes and externally through conducting wires and possibly through a load. With a load, the energy change of the chemical reactions is converted into electrical energy which is used to power and send current through the external load (galvanic cell). By contrast, externally furnished electrical energy can be used to force non-spontaneous chemical conversions to occur, which is the case in electrolysis (electrolytic cell). In both of these situations the conversion between chemical and electrical energy should be as efficient as possible. This means that the chemical species that reacts at the electrodes should be supplied at least as fast as it is consumed and that the kinetics of the electrode reactions is fast, corresponding to a low activation energy barrier.

We now consider briefly the processes occurring at a single metallic electrode, illustrating with the simple case where the electrode acts only as a source or sink of electrons, the reaction being

$$O + ne^- \rightarrow R$$
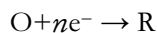
Here, O and R are the oxidised and reduced forms of the redox species in solution, respectively. There must be a correspondence between the energy of the electrons transferred between the electrode and the redox species in solution, i.e. the Fermi energy, E_F, in the electrode, and the donor/acceptor orbital energy in the redox species. Reference to Figure.1 shows that in the case of reduction, there is a minimum energy that the transferable electrons from the electrode must have for transfer to be able to occur, which corresponds to a sufficiently negative potential (in volts). In the case of oxidation, E_F must be lower than the energy E_{redox} in order to be able to receive electrons from the redox species in solution, corresponding to a sufficiently positive potential (in volts).
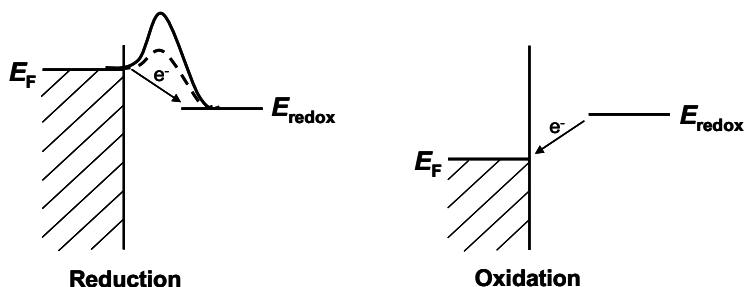
Figure 1 - Scheme of electron transfer between a redox species in solution and an inert metal electrode. The externally controlled potential alters the Fermi energy, E_F, the energy of the highest occupied electronic energy level in the electrode, facilitating reduction (more negative potential) or oxidation (more positive potential). The reduction process also shows an activation energy barrier (solid line) which can be reduced in height by electrocatalysis (dashed line).

If the electron transfer were able to take place directly without any barriers to electron movement, then a modified form of the general Nernst equation

$$E_{eq} = E^{\ominus\prime} + \frac{RT}{nF}\ln\frac{\prod[O_i]^{\nu_i}}{\prod[R_i]^{\nu_i}}$$

can be directly applied at the surface of the electrode, where E_{eq} is the equilibrium potential for the concentrations of oxidised and reduced species with ν_i their stoichiometric coefficients, $E^{\ominus\prime}$ is the formal potential, F the Faraday constant (the charge corresponding to one mole of electrons) and R and T have their usual meanings. The formal potential is related directly to the standard electrode potential (the potential relative to the standard hydrogen electrode reference, taken as 0 V) and includes all activity effects with respect to species intervening in the electrode reaction in the electrolyte solution where it takes place. Experimentally, it is always the formal potential that is determined since it is the number of electrons transferred, i.e. the current, that is measured, which is proportional to the amount of chemical species, hence to their concentration.

In practice, the electrode process may not occur as predicted by the Nernst equation, owing to kinetic barriers, as shown in Figure 1. The rate of the electrode reaction is then governed by the kinetics. The formulation of electrode kinetics leads to expressions for the rate constants as

$$k_a = k_0 \exp[a_a nF(E - E^{\ominus}{}') / RT]$$

for an anodic process, and

$$k_c = k_0 \exp[-a_c nF(E - E^{\ominus}{}') / RT]$$

for a cathodic process. In these equations, k_a and k_c are the rate constants for anodic and cathodic processes, respectively, and k_0 is the standard rate constant at the formal potential $E^{\ominus}{}'$. The charge transfer coefficients $_a$ and $_c$ depend on the position of the activation energy barrier between reagents and products. Their values are usually around 0.5 for simple electrode reactions - large deviations suggest either a more complex electrode process when soluble species are involved, or occur in processes such as metal dissolution. Further details on electrode kinetics may be found in Reference 1.

The extra energy (potential) which is needed to overcome the activation energy barrier is called the *activation overpotential*, or often just the *overpotential*, since kinetic limitations represent the most important source of overpotential in electrode reactions in most aqueous liquid electrolyte solutions.

In this context, the essential role of an electrocatalyst can be readily understood, which is to reduce the height of the activation energy barrier, as can also be seen in Figure 1. In experimental terms, this means that the value of the standard rate constant is increased and that the reaction begins to occur at a less positive potential (oxidation) or at a less negative potential (reduction).

A second type of overpotential can be identified, which is not due to the kinetic barrier. This is the *concentration overpotential,* arising in situations when species are unable to reach the electrode surface fast enough i.e. diffusion is too

slow. Since diffusion occurs along a concentration gradient, this means that an extra potential must be applied to induce a higher concentration gradient.

In designing an industrial electrode process or a sensor it is normally required to reduce the overpotential to as small a value as possible, in order to improve the response and, in the case of electrolysis, save electrical energy. It means that electrocatalysts and good engineering of electrochemical cells are both needed. This can be aided by the judicious choice of electrode materials and much effort has gone and is continuing to go into this area. The structure of the interfacial region and the way that the redox species interacts with the surface - perhaps by being adsorbed as part of the reaction mechanism - can be highly important and which depends on both the electrode material and the electrolyte in which the reaction takes place.

One further aspect which must be borne in mind is the potential range in which an electrode material can be used. This is usually limited by solvent decomposition - in aqueous solutions by the formation of oxygen (oxidation) or hydrogen (reduction), which is pH dependent. Potential ranges can vary significantly as well as the associated overpotential. For example, at pH 7 hydrogen evolution occurs at platinum electrodes at $\sim$–0.42 V vs SHE whereas in the most extreme case of mercury it occurs at around –1.8 V vs SHE, so that - in principle - more possibilities of carrying out reduction reactions in aqueous electrolytes without hydrogen evolution become possible. (In practice this is little exploited due to mercury's toxicity and, unfortunately, no substitute for mercury with such a large potential range in the negative direction and which is non-toxic, has yet been found.).

Additionally, now that it is possible to examine and design materials at the nanoscale, nanostructured materials are being investigated for electrocatalytic effects and which, besides reducing the overpotential, can also lead to significantly increased conversion efficiencies due to their high surface area.

Electrochemistry has had an impact in many fields, ranging from sensors and fuel cells (see below) to industrial electrolysis and batteries[2]. Industrially, one of the most important electrolysis processes which demonstrates the importance of electrode materials is the chlor-alkali process, the electrolysis of brine. The anode reaction is oxidation of chloride ion to chlorine and was formerly carried out at carbon electrodes, having an overpotential of ~0.5 V with extensive consumption of the anode material. With the invention of dimensionally stable anodes (DSA) which are precious metal oxides such as RuO_2 on a titanium substrate, the overpotential was reduced to 40 mV and electrode longevity was significantly increased. Since then, DSA's have found application in a number of other areas such as in the degradation of environmental pollutants by anodic oxidation. Modern chlor-alkali cells also use a perfluorosulphonated cation exchange membrane to separate the anodic and cathodic reaction compartments; this type of membrane has also found application in proton exchange membrane fuel cells (see below).

A second industrial example which had an important impact in the manufacture of Nylon 66 is the hydrodimerization of acrylonitrile to adiponitrile using bipolar electrodes in a stack in a mainly aqueous, complex electrolyte mixture which, besides increasing the selectivity of the conversion in relation to the alternative chemical route, also brought environmental benefits through the use of mainly aqueous solvents. Many other examples of industrial processes in which electrolysis has been successful in increasing selectivity, the electrode acting as a heterogeneous catalyst, often with the added benefit of electrocatalysis, could be given. The same electrochemical technology can often be applied to environmental treatment and clean energy conversion[3]. Often the electrochemical processes can be carried out at, or close to, room temperature, they can be continuously monitored and turned on and off when desired, and electrons are essentially clean reagents. The engineering of the cells is very

important in order to exploit the cell reactions and catalytic effects to the maximum.

1.3. ELECTROCHEMICAL SENSORS AND BIOSENSORS AND ELECTROCATALYSIS

An electrochemical sensor[4,5] is a type of chemical sensor in which the transducer and sensorial element are combined: the electrochemical recognition reaction produces an electrical current which can then be analysed. This can have advantages in instrumental terms and in simplicity of operation. The selectivity and specificity of these sensors usually arises from the applied potential at which oxidation or reduction of the chemical species occurs and possibly also from the electrode materials. Electrocatalytic effects are inherent and the correct electrode material can permit the distinction between two analytes which would otherwise be oxidised or reduced at very similar potentials with overlapping response. Nevertheless, interferences caused by the reaction or adsorption of other substances present in complex matrices can occur, depending on the concentration level of potential interferents in the medium where the sensor is inserted, so that extra measures for increasing specificity and protection of the electrode surface may need to be taken to avoid them.

In an electrochemical biosensor, the recognition element is biological and is therefore separate form the transducer. A further chemical reaction is then needed to transform the product of the biological reaction into an electrical current. Examples of biological recognition elements are enzymes, antibodies and bacteria, the aim of all of which is to add a very high degree of specificity to the sensor.

In this section, examples of both types of sensor will be given based on recent developments using small, carbon film electrodes and using nanoparticle-modified electrodes.

The carbon film electrodes are made from cylindrical carbon film electrical resistors, the carbon film being produced by pyrolysis in a rotating oven on a cylindrical ceramic substrate, length 6 mm and diameter 1.5 mm, which are then capped at each end with metal contacts and an external connecting wire. To make them into electrodes, one of the resistor's metal caps plus external connecting wire is removed, the other being sheathed and protected by epoxy resin to leave a cylindrical surface with end disc exposed. These electrodes are easy to make, are small and have interesting properties which them amenable to a variety of sensing applications, including in flow systems.

Modification of electrode surfaces can lead to changes in the rates of electrode reactions. Recent investigations suggested that the modification of electrode surface by metal hexacyanoferrates would lead to interesting electrocatalytic effects, the motivation being mainly their use for measurement of the hydrogen peroxide produced in oxidase enzyme reactions, to be described in more detail below. Figure 2 shows current-voltage profiles obtained on cycling the applied potential following three different ways of forming films of copper hexacyanoferrate on carbon film electrode substrates[6]. Of particular note is the fact that the chemical deposition gives a profile which is most consistent with a simple oxidation/reduction between Fe(II) and Fe(III) in the film formed, and the Cu(I)/Cu(II) couple at lower potential s suppressed. Small kinetic effects are demonstrated by the close proximity of oxidation and reduction peaks which are of much higher intensity for Fe(II)/Fe(III) than for the other two preparation methods.

The different profiles therefore reflect different film morphologies and structures, which have important effects on their electrocatalytic behaviour, confirmed by electrochemical impedance spectroscopy.
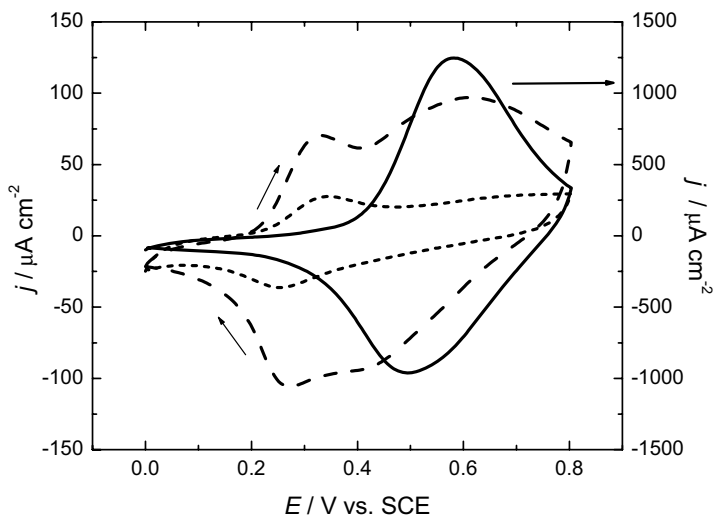
Figure 2 - Current voltage profiles by potential cycling (scan rate 50 mV s^{-1} in 0.05 M KCl solution of copper hexacyanoferrate films on carbon film substrates prepared from a solution containing 10 mM Cu^{2+}, 10 mM K$_3$Fe(CN)$_6$, and 100 mM KCl: (——) chemically by immersing the electrodes for 50 min in the solution of the precursor salts, (----) galvanostatically by applying a current of -100 mA cm^{-2} for 300 s, or (········) by cycling the potential 25 times between +0.25 and +0.90 V vs SCE at 50 mV s^{-1}.

It was also discovered that ascorbate is particularly easily oxidised at copper hexacyanoferrate, at lower potentials than at other substrates[7]. This strategy was used to design a sensor that operates at 0.05 V vs saturated calomel electrode (SCE) reference compared to higher potentials for all others described in the literature, representing an enhanced electrocatalytic effect.

Electrochemical enzyme biosensors very often employ oxidase enzymes, which usually consume oxygen and produce hydrogen peroxide. The latter can either be oxidised directly on an electrode, which occurs at a very high potential (around 0.7 V vs SCE at carbon), or can be made to react homogeneously with a redox mediator. The redox mediator is then regenerated at the electrode and the current necessary to make this happen is proportional to the concentration of the enzyme substrate (the analyte). This is the principle used in the disposable strip sensor for blood glucose for diabetics.

Metal hexacyanoferrates have been explored as redox mediators, but more recently electropolymerised neutral red dye has been investigated, the electropolymerisation being done directly on the electrode surface to form a thin film. The enzyme is then immobilised in a porous layer above this film by reticulation or encapsulation such that the enzyme substrate can diffuse in from the outside solution. An interesting response of this biosensor assembly was found. At the potentials used for this biosensor assembly, around -0.25 - 0.30 V vs SCE, it would be predicted that the hydrogen peroxide produced during reaction of the enzyme substrate would be reduced, oxidising the polymer which then has to be regenerated by a reduction (cathodic current), Figure 3a - this was observed, for example, with pyruvate and pyruvate oxidase enzyme[8]. However, for glucose with glucose oxidase an anodic response was obtained[9]. The explanation for this is that the poly(neutral red) reacts directly with glucose oxidases's inherent co-factor flavine adenine dinucloeotide (FAD), as shown in Figure 3b. In fact, the two processes can compete - which is dominant depends on the concentrations of enzyme substrate and oxygen, indicative of a complex catalytic mechanism.
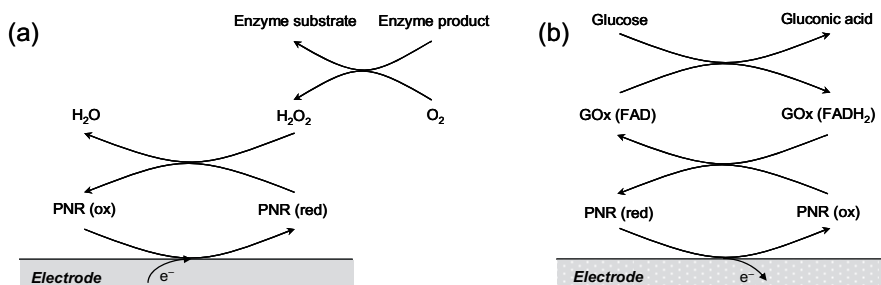
Figure 3 - Scheme of operation of poly(neutral red) (PNR) redox-mediated enzyme biosensors operating at -0.25V vs SCE. (a) General scheme for reaction of hydrogen peroxide leading to a cathodic response (b) Specific case of reaction of glucose with FAD in glucose oxidase (GOx) leading to an anodic response.

A final example concerns the direct oxidation of monosaccharides[10] which is known to be enhanced in the presence of copper, possibly due to Cu(III) surface species initiating the electrocatalysis. This was studied at several different electrode materials: glassy carbon modified by copper nanoparticles at open circuit or by electrodeposition, copper nanoparticle-modified gold and bulk copper. Each of them leads to a different response, the Cu-modified Au being found to be the most stable and with the largest linear range, being highly selective for monosaccharides, (fructose, glucose, galactose, xylose), as opposed to disaccharides.

1.4. Fuel Cells

A fuel cell is, in effect, a type of battery in which the reactants are fed externally: there is a constant flow of fuel and oxidant to anode and cathode, respectively, in order to generate electrical energy[11] and possibly some heat and chemicals[12]. It parallels classic combustion reactions with oxygen but with the major part of the energy being produced directly in electrical form. Today, most fuel cells are based on hydrogen fuel and the oxidant is oxygen - this has a benefit in that it does not increase the amount of carbon dioxide in the atmosphere. It is not practical to feed naturally-occurring hydrocarbons but they can be used to form hydrogen by steam reforming, for example methane with water leads to carbon dioxide and hydrogen.

Figure 4 shows the basic construction of a fuel cell - it should be particularly noted that both the anode and cathode require electrocatalysts.
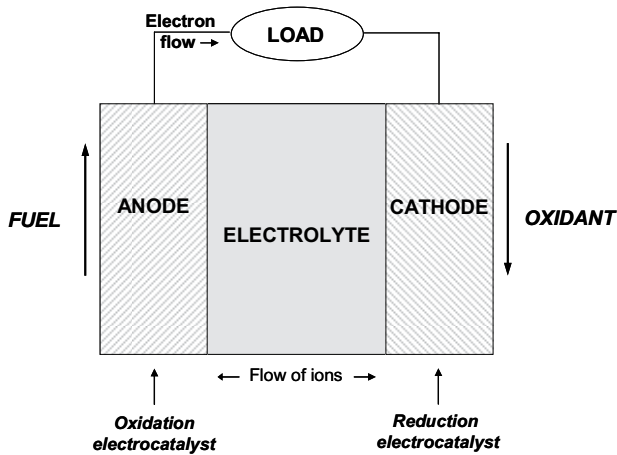
Figure 4 - Basic scheme of operation of a fuel cell

The different types of fuel cells are:

PEMFC   Proton exchange membrane fuel cell

DMFC   Direct methanol fuel cell

AFC   Alkaline fuel cell

PAFC   Phosphoric acid fuel cell

MCFC   Molten carbonate fuel cell

SOFC   Solid oxide fuel cell

and the reactions that occur are:

	Cathode	*Anode*
PEMFC	$O_2 + 2H^+ + 4e^- \rightarrow 2H_2O$	$H_2 \rightarrow 2H^+ + 2e^-$
DMFC	$O_2 + 2H^+ + 4e^- \rightarrow 2H_2O$	$CH_3OH + H_2O \rightarrow CO_2 + 6H^+ + 6e^-$
AFC	$O_2 + 2H_2O + 4e^- \rightarrow 4OH^-$	$H_2 + 2OH^- \rightarrow 2H_2O + 2e^-$
PAFC	$O_2 + 2H^+ + 4e^- \rightarrow 2H_2O$	$H_2 \rightarrow 2H^+ + 2e^-$
MCFC	$O_2 + 2CO_2 + 4e^- \rightarrow 2CO_3^{2-}$	$H_2 + CO_3^{2-} \rightarrow H_2O + CO_2 + 2e^-$
SOFC	$O_2 + 4e^- \rightarrow 2O^{2-}$	$H_2 + O^{2-} \rightarrow H_2O + 2e^-$

Important characteristics of fuel cells are shown in Table 1. The operating temperature varies from just above room temperature to 1000ºC and, in general, the efficiency increases as the temperature is raised, as does the maximum power generation.

TABLE 1 - Types of fuel cell and their principal characteristics

Fuel cell type	Typical electrolyte	Operating temperature	Catalyst	Max. power output	Efficiency	Applications
PEMFC*	Solid organic polymer perfluoro-sulphonic acid	50-100ºC	Pt on carbon support	250 kW	Electric 50 - 60%	Back-up power, transportation
AFC	KOH (aq,) soaked in a matrix	90-100ºC	Variety	100 kW	Electric 60 - 70%	Military, space
PAFC	Liquid H_3PO_4 soaked in a Teflon-bonded SiC matrix	150-200ºC	Pt	1 MW	Electric 40% Total 85%	Power generation
MCFC	Liquid solution of Li, K or Na carbonates soaked in a $LiAlO_2$ matrix	600-700ºC	Variety	1 MW	Electric 60% Total 85%	Power generation
SOFC	Solid zirconium oxide + yttria	650-1000ºC	Variety	3 MW	Electric 60% Total 85%	Power generation

* DMFC are a subset of PEMFC, small and portable with power up to 100 W and operating at 60-90ºC.

Each cell has a number of advantages and disadvantages. One of the important criteria is the choice of catalyst, which can be an expensive part of the total cost, particularly if the catalyst is subject to poisoning. The PEMFC's solid electrolyte reduces corrosion problems and the low temperature means that start-up is fast, but it suffers from the disadvantage that the platinum catalyst is highly sensitive to any impurities in the fuel, particularly CO (so that CO_2 must be removed), and hydrogen purification can represent a significant extra cost. The alkaline medium in the AFC increases the efficiency of the cathodic reaction, but any CO_2 has to be removed from the fuel and air streams to avoid precipitation of carbonates. The PAFC has a high efficiency but the ratio of power to size/weight is not very good. Both the two high temperature fuel cells are highly efficient for power generation and are more flexible for use with other fuels, but suffer from a high corrosion rate owing to the elevated temperature, and start-up is slow.

The ideal situation for any fuel cell is that no matter what current is drawn from it the cell voltage remains the same, at the reversible, thermodynamic value.

Theoretically this is possible, since the reactants can be supplied at a constant rate. However, in practice it is not the case for several reasons, which are due to the kinetics of the electrode reactions, the electrical resistance of both electrolyte and electrode, and difficulties with respect to the reactants being able to reach the electrode surfaces as higher currents are drawn.

The practical performance of fuel cells will be illustrated for the PEMFC, for which the current-voltage characteristics are depicted schematically in Figure 5. In this type of cell[13], the electrolyte is typically a thin (75-300 μm) perfluorosulphonic acid polymer membrane with an anode of Pt black and a cathode of platinized carbon. On the outside of each is carbon fibre paper (the gas diffusion layer) which allows the gases to permeate through into the porous electrodes, electrocatalyst being deposited on the surfaces of the pores to maximise contact. The electrolyte membrane serves to transport protons produced in the anode reaction to the cathode where they are needed for the reduction of oxygen.
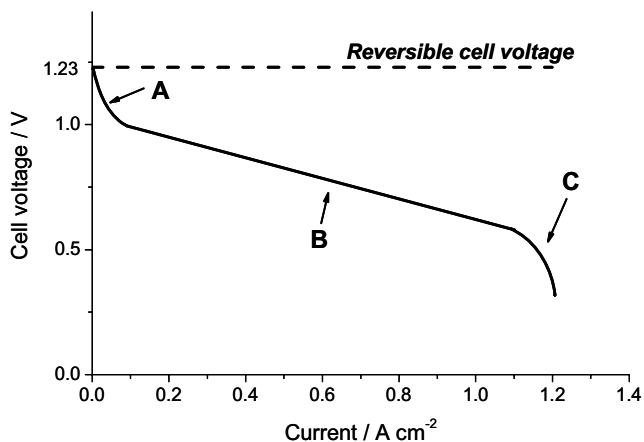

Figure 5 - Basic performance characteristics of a PEM fuel cell. The three polarisation regions are due to: A activation polarisation (reaction rate losses), B ohmic polarisation (resistance losses), C concentration polarisation (gas transport losses).

Reference to Figure 5 shows that there are three regions in the current-voltage curve. In region A, kinetic effects reduce the cell voltage, which is then followed by a straight line region, B, where ohmic losses predominate. Finally, at much higher currents insufficient supply of reactants causes the cell voltage to fall further. The main challenges for this, and all fuel cells are therefore seen to be first to reduce the activation overpotential in region A by employing improved electrocatalysts, secondly to reduce the resistance of the cell assembly, possibly by improved or thinner electrolyte membranes, in region B and last, to improve the characteristics of the gas diffusion layer and the electrocatalyst, where nanostructure plays an important role. As an example of this, metal nanoparticles grown and held within dendrimers in layer-by-layer structures can be particularly effective as electrocatalysts for oxygen reduction, as was recently shown[14].

Much effort is devoted to all these questions as well as to the engineering associated with making robust cells and cell stacks and with adequate storage of the hydrogen fuel. This is particularly important for some for the applications which are now being, such as transportation by fuel cell hybrid vehicles and portable power sources for instruments and portable computers.

A final interesting application of fuel cells but with power output in the μW range is biofuel cells[15]. These fuel cells use biocatalysts, i.e. enzymes or microbes, and once again, operation consists in separating the oxidation and reduction reactions that occur naturally and harnessing this energy as electrical energy. One of the advantages is that they operate under mild conditions, i.e. near neutral pH and 20~40ºC.

One of the first successful examples of a microbially catalysed system is direct electrochemical communication of *Shewanella putrefaciens* with an anode via cellular membrane cytochromes[16]

$$\text{Lactate} \xrightarrow{\text{microbes}} \text{wastes} + \text{(membrane\_cytochrome)}^-$$

Anode: $\text{(membrane\_cytochrome)}^- \longrightarrow \text{(membrane\_cytochrome)} + e^-$

Cathode: O_2 reduction

which eventually leads to carbon dioxide and water, being used for feedstock destruction.

Enzyme based systems have usually been geared towards special applications where small amounts of power are needed for implantable devices, sensors, drug delivery etc.[17]. The anode can incorporate an oxidising enzyme and the cathode a reducing enzyme. An important example is a specially-functionalised glucose oxidase (GOx) attached to a gold electrode which follows the sequence of reactions shown below[18].

Au-elec.-PQQ-FAD-GOx + Glucose → Au-elec.-PQQ-FADH$_2$-GOx + Gluconic acid
Au-elec.-PQQ-FADH$_2$-GOx → Au-elec.-PQQH$_2$-FAD-GOx
Au-elec.-PQQH$_2$-FAD-GOx → Au-elec.-PQQ-FAD-GOx + 2H$^+$ + 2e$^-$

Cathode: H_2O_2 reduction with microperoxidase

with oxidation of glucose to gluconic acid, the hydrogen peroxide produced by this reaction being reduced at the cathode. The cell voltage was 0.3 V and the power output 160 μW. Since this cell was conceived, many improvements have been suggested to increase the robustness of the system with the eventual aim of making biofuel cells the power source for a continuously operating glucose monitor for diabetics.

1.5. FINAL REMARKS

It is hoped that this chapter has shown the catalytic nature of electrode processes as well as the importance of electrocatalysts in the conversion of chemical substances and in the generation of electrical energy. The examples shown of sensors and fuel cells indicate an increasing importance in the future

owing to the present concerns of increasing energy efficiency and of clean sources of power, together with the high selectivity and specificity that can be obtained in electrochemical processes, electrochemical sensors and electrochemical power sources.

References

1. C.M.A. Brett, A.M. Oliveira Brett, *Electrochemistry. Principles, Methods and Applications*, Oxford University Press, Oxford, **1993**.

2. Ref.1 Chapter 15.

3. F.C. Walsh, *Pure Appl. Chem.*, **2001**, *73*, 1819.

4. R.W. Cattrall, *Chemical sensors*, Oxford University Press, Oxford, **1997**.

5. C.M.A. Brett, A.M. Oliveira Brett, *Electroanalysis*, Oxford University Press, Oxford, **1998**.

6. R. Pauliukaite, M. Florescu, C.M.A. Brett, *J. Solid State Electrochem.*, **2005**, *9*, 354.

7. R. Pauliukaite, M.E. Ghica, C.M.A. Brett, *Anal. Bioanal. Chem.*, **2005**, *381*, 972.

8. M.E. Ghica, C.M.A. Brett, *Electroanalysis*, **2006**, *18*, 748.

9. R. Pauliukaite, M.E. Ghica, M. Barsn, C.M.A. Brett, *J. Solid State Elctrochem.*, **2007**, *11*, 899.

10. H. Mohammadi, A. Amine, M. El Rhazi, C.M.A. Brett, *Talanta*, **2004**, *62*, 951.

11. V.S. Bagotzky, N.V. Osetrova, A.M. Skundin, *Russ. J. Elctrochem.*, **2003**, *39*, 919.

12. F. Alcaide, P.-L. Cabot, E. Brillas, *J. Power Sources*, **2006**, *153*, 47.

13. S. Litster, G. McLean, *J. Power Sources*, **2004**, *130*, 61.

14. F.N. Crespilho, F.C. Nart, O.N. Oliveira Jr., C.M.A. Brett, *Electrochim. Acta*, **2007**, *52*, 4649.

15. F. Davis, S.P.J. Higson, *Biosens. Bioelectron.*, **2007**, *22*, 1224.

16. H.J. Kim, H.S. Park, M.S. Hyun, I.S. Chang, M. Kim, B.H. Kim, *Enzyme Microb. Technol.*, **2002**, *30*, 145.

17. J. Kim, H. Jia, P. Wang, *Biotechnol. Adv.*, **2006**, *24*, 296.

18. I. Willner, E. Katz, F. Patolsky, A.F. Buckmann, *J. Chem. Soc., Perkin Trans.*, **1998**, *2*, 1817.

(Página deixada propositadamente em branco)

2. Electrocatalysis: Applications In Coordination, Bioinorganic And Organometallic Chemistries

Armando J. L. Pombeiro

Centro de Química Estrutural, Complexo I, Instituto Superior Técnico, Av. Rovisco Pais, 1049-001 Lisboa, Portugal.

Summary

Electron-transfer (ET) is known to induce a wide variety of reactions and processes which, in some cases, can be of a catalytic nature, namely within the following general types: redox or mediated ET catalysis (in particular coordination electrocatalysis) and electron transfer-chain (ETC) catalysis. The bases of these forms of catalysis and of their applications in synthesis are presented, with focus on the apparent contradiction with Thermodynamics and, for the latter type, on the role of the electron as a catalyst, what confers a "magic" behaviour with a number of advantages over conventional processes, namely in terms of energy saving.

Examples of significance in Coordination, Bioinorganic and Organometallic Catalyses are discussed, namely involving the Michaelis-Menten electrocatalytic oxidation of biological thiols by Amavadine as an ET mediator, reduction of dinitrogen to ammonia (nitrogen fixation), isomerization of a carbonyl complex and alkyne polymerization.

2.1. Introduction

The word "Electrocatalysis" immediately reminds us of the relevance of the involvement of an "Electron" and of "Catalysis", somehow associated. The participation of the former ("electron") can be considered in a simple electron-transfer (ET) step in which, for instance, an oxidized form of a molecule (S^{ox}) is

reduced to the corresponding reduced form (S^{red}). From this simple ET often results a chemical reaction (C) which thus is induced by ET, in an overall process denoted by EC (E: electron transfer step; C: chemical step – reaction 1).

$$S^{ox} \; \underset{\longleftarrow}{\overset{e}{\longrightarrow}} \; S^{red} \longrightarrow P \qquad (EC)$$

(1)

Let us now consider at which stage we can introduce a catalytic behaviour: either to the chemical reaction (C) or to the electron-transfer (or the electron itself).

The former usually corresponds to a process of Chemical Catalysis in which the formation of an active species is promoted by an ET and does not fit the aim of this work, while the latter situation, in contrast, falls within the scope of Electrocatalysis.

Two relevant types of Electrocatalysis can now be introduced. In one of them the catalysis is associated to ETs in reverse directions, via a mediator between the electrode (or, more generally, a suitable redox agent) and the substrate , Scheme 1. Hence, e.g., reduction of the mediator (M^{ox}) at the electrode leads to an active form (M^{red}) which reduces the substrate ($S^{ox} \to S^{red}$), being reoxidized to the inactive M^{ox} form which, however, upon reduction at the electrode (there is charge consumption), regenerates the reducing active form (M^{red}). The mediator thus acts as the catalyst in this type of Electrocatalysis that is named[1] "Mediated ET Catalysis" or "Redox Catalysis".

In the other type of Electrocatalysis, the electron itself is the catalyst, being consumed and regenerated along the catalytic cycle which involves no overall charge consumption, apart from a limited initial one just to trigger the process, Scheme 2. This type of Electrocatalysis is known[1] as "ET Chain Catalysis" (ETC Catalysis)

$$S^{ox} \; \underset{\longleftarrow}{\overset{e}{\longrightarrow}} \; S^{red} \longrightarrow P \qquad (EC)$$
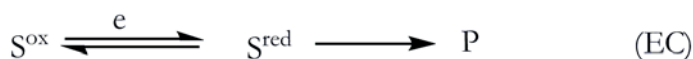
(other designations have been given, such as "Electrocatalysis", in a more simplified but less clear way).

Catalyst: Mediator

Scheme 1

Catalyst: Electron

Scheme 2
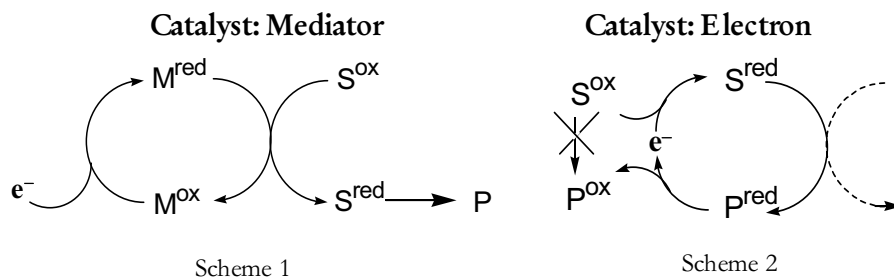
In the following sections, the above forms of Electrocatalysis[1-3] will be treated in greater detail and illustrated with examples that, in some cases, have been investigated in the author's laboratory. They often involve coordination compounds i.e. those with a central metal coordinated by various ligands, with significance in Coordination, Bioinorganic and/or Organometallic Chemistries. However, applications in other fields, namely in Organic Chemistry[4], are also well documented.

2.2. MEDIATED ET CATALYSIS OR REDOX CATALYSIS

2.2.1. Relevance in Biology and in Chemistry

This type of catalysis concerns an oxidation or reduction, either chemical or electrochemical, by a catalyst that acts as a mediator for the ET between the redox agent (either a chemical reagent or the electrode) and the substrate, Scheme 1.

It has relevance in Biology (see, e.g. the regeneration of the reduced Fe^{II} form of cytochrome P-450 via a chain of ET-mediators, Scheme 3), in Chemistry (see, e.g. the regeneration of active Pd^{II} in the Wacker oxidation of ethylene to acetaldehyde, Scheme 4) and in Electrochemistry in which the reducing or oxidizing agent is an electrode, as discussed below in more detail.

NADPH (red) · reductase (FMN, FAD)$_{ox}$ · P-450 (Fe^{II}) · O$_2$, RH
NADP$^+$ (ox) · reductase (FMN, FAD)$_{red}$ · P-450 (Fe^{III}) · ROH, H$_2$O

<center>Scheme 3</center>

CH$_3$CHO · Pd^{II} · 2Cu^{II} · 1/2O$_2$
H$_2$O
C$_2$H$_4$ · Pd^0 · 2Cu^I · H$_2$O
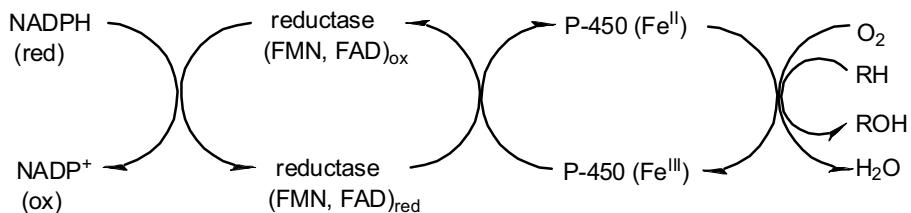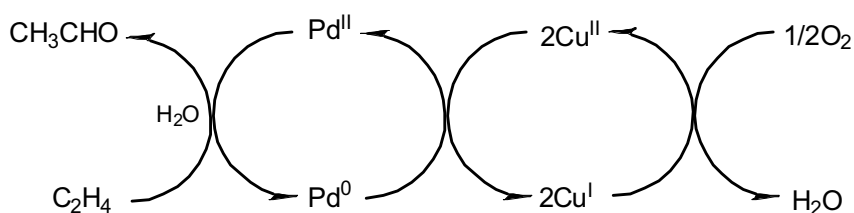
<center>Scheme 4</center>

2.2.2. Mediated ET Electrocatalysis or Redox Electrocatalysis

2.2.2.1. Indirect and direct ET. Driving a thermodynamically unfavourable ET

In order to better understand the process and the role of the mediator, let us compare the situations with and without the use of the mediating agent, which correspond to an indirect and a direct ET between the electrode and the substrate, respectively.

In the former case (indirect or mediated ET), Scheme 1 assumes the form of Scheme 5a), while the direct ET can be represented by Scheme 5b), both assuming a reductive process (similar treatments could be applied, *mutatis mutandis*, to an oxidative process).
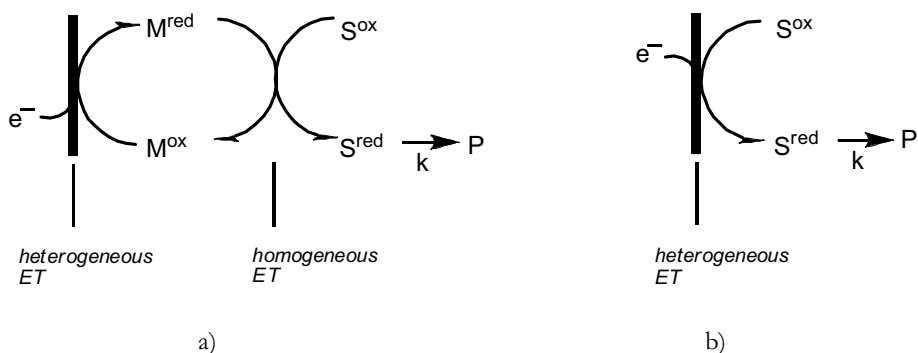
Scheme 5

A relevant difference concerns the required applied potential at the electrode: while for the direct ET the potential has to be that required for the reduction of the substrate, in the case of the indirect ET, everything proceeds at the potential required for the reduction of the mediator, what can be much more accessible (less cathodic for a reduction process or less anodic for an oxidation one), thus resulting in an *energy saving*. This effect can be quite dramatic, corresponding (see below) to the use of a more favourable potential up to ca. 1.0 V!

In other words, for the case of the reduction, we are using a mediator, with a $M^{ox/red}$ redox potential that can be much higher (less cathodic) than that of the substrate ($S^{ox/red}$), to act as a *reducing* agent of the latter, in apparent conflict with the thermodynamics, since the thermodynamically favourable reaction would be the reversed one, i.e., the mediator acting as an oxidizing (rather than a reducing) agent of the substrate (see also below)!

This intriguing behaviour, which corresponds to *driving an unfavourable ET* (against the normal redox potential gradient), can be accounted for by considering the following effects on shifting the equilibrium $M^{red} + S^{ox} \rightleftarrows M^{ox} + S^{red}$ towards the thermodynamically unfavourable products (M^{ox} and S^{red}): the consumption of S^{red} to give the final product P via an

543

irreversible reaction, Scheme 5a), and the consumption of M^{ox} by its reduction (to M^{red}) at the electrode.

Hence, the remarkable reduction of the substrate by a mediator that would be expected to act as an oxidant rather than a reducer, is a consequence of the catalytic nature of the mediator (regeneration of the reduced form by reduction of M^{ox}) and of the conversion of S^{red} into the final product P, in a thermodynamically acceptable (although not immediately perceptible) way.

Let us now quantify these effects. The equations involved, Scheme 5a), can be indicated in the more common forms (2) (heterogeneous ET), (3) (homogeneous ET) and (4) (irreversible chemical steps), where k_1, k_2 and k are the rate constants of the corresponding reactions and K_{eq} is the equilibrium constant of the homogeneous ET (it has a value $<< 1$ on account of the thermodynamically unfavourable character of this reaction).

$$M^{ox} + e^- \rightleftharpoons M^{red} \tag{2}$$

$$M^{red} + S^{ox} \underset{k_2}{\overset{k_1}{\rightleftharpoons}} M^{ox} + S^{red} \tag{3}$$

$$S^{red} \xrightarrow{k} P \tag{4}$$
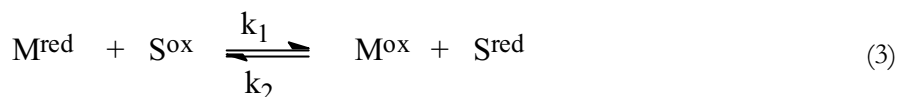
The kinetics, referred to the substrate, are given by equation (5) which, under the steady-state hypothesis expressed by equations (6), assumes the form (7) or (8), the latter by considering the definition of K_{eq}

$$-d[S^{ox}]/dt = k_1[M^{red}][S^{ox}] - k_2[M^{ox}][S^{red}] \tag{5}$$

$$d[S^{red}]/dt = 0 = \underbrace{k_1[M^{red}][S^{ox}] - k_2[M^{ox}][S^{red}]}_{-d[S^{ox}]/dt} - k[S^{red}] \tag{6}$$

$$d[S^{ox}]/dt = -k[S^{red}] \tag{7}$$

$$d[S^{ox}]/dt = -k\,K_{eq}\,\frac{[M^{red}][S^{ox}]}{[M^{ox}]} \tag{8}$$

Hence, the kinetics of the electrocatalytic process are determined not only by the unfavourable equilibrium constant K_{eq} but also by the rate of the final chemical reaction (k) and by the ratio of the concentrations of the active (reduced) and inactive (oxidized) forms of the mediator, $[M^{red}]/[M^{ox}]$, which is promoted by a high rate constant for the heterogeneous ET (reaction 2).

Therefore, a low value of K_{eq} (even much lower than 1 as expected from the known expression (9) in which ΔE^o, given by equation 10, is < 0) can be compensated by a high value of the rate constant k, making possible the reduction of the substrate at the more accessible reduction potential of the mediator which interestingly (opposing the thermodynamic gradient) is acting as a reducing agent of the substrate.

$$\ln K_{eq} = \frac{nF}{RT} \Delta E^o \qquad (9)$$

$$\Delta E^o = E^o(S^{ox/red}) - E^o(M^{ox/red}) \qquad (10)$$

Obviously, related considerations would apply to oxidations.

2.2.2.2. Properties and types of mediators

A number of requirements has to be followed in order that a species can act as a mediator such as:

- Its redox potential has to be more accessible (i.e., less cathodic for a reduction, or less anodic for an oxidation) than that of the substrate; otherwise, the direct reduction or oxidation of the substrate, rather than the mediator, would occur.
- The ET of the mediator should be reversible (equation 2) and both redox forms, M^{ox} and M^{red}, should be stable. To account for these features which can allow the use of a catalytic amount of the mediator, both redox forms should present nearly identical structures.

- The ETs of the mediator with the electrode and with the substrate should be fast, thus overcoming the usual overpotential (difference between the electrode potential and the normal potential of the substrate) required for the direct (heterogeneous) reduction (or oxidation) of the substrate particularly if involving bond breaking or formation. In fact, the heterogeneous ET is confined to the restricted two-dimensional space of the electrode surface, whereas the homogeneous ET (between the mediator and the substrate) occurs in the three-dimensional space of the bulk solution, allowing to optimise their mutual orientation for the minimum activation energy for ET.
- Electrode passivation by the mediator should be negligible.
- Both mediator redox forms should be soluble in the electrolytic medium (except in biphasic systems).

Two main *types* of mediators have been considered, named by Shono[3] as homomediators and heteromediators (or chemiomediators). More complex designations were given by Savéant: redox catalysts and mediators of chemical catalysis with electrochemical regeneration, respectively. We'll follow the former names, for simplicity reasons.

A homomediator acts as a simple ET agent to (from) the substrate, being involved in an outer-sphere type mechanism. Examples include metallocenes (e.g. ferrocene/ferricinium) or aromatic amines $NAr_3^{o/+}$ redox pairs for oxidations, and polyaromatics (o/-) for reductions. In biological systems, flavodoxins, Fe/S proteins (e.g. ferredoxins) or cytochromes can also behave in such a way.

A homomediator can allow the use of a more favourable potential up to ca. 0.6 V relatively to that of the direct reduction (or oxidation) of the substrate.

In the case of an hetero- or chemio-mediator, the ET occurs by a chemical reaction (bond formation) between the mediator and the substrate, following an inner-sphere mechanism, the redox reaction being coupled to a chemical one.

Such a type of behaviour is typically displayed by transition metal ions and their complexes, positively charged halogenated species, hypohalous ions or halogens obtained by anodic oxidation of halide ions.

The use of a heteromediator can lead to a saving of up to ca. 1.0 V in comparison with the potential required for the direct reduction (or oxidation) of the substrate.

2.2.2.3. Coordination electrocatalysis

Relevant situations in electrocatalysis are provided by using metal complexes (coordination compounds) as mediators, namely as heteromediators (the field then being named Coordination Electrocatalysis).

An intermediate complex (MS) is formed between the mediator and the substrate (S), Scheme 6, and the process occurs at the redox potential of this intermediate, rather than at those of the free mediator M or the free substrate (S). Moreover, upon coordination to M, the substrate can be further activated towards ET, and remarkably large over potentials (up to ca. 1.0 V) can be overcome. More complex variations of such a type of electrocatalytic processes are known, e.g. when the active form of the mediator (M) is generated by ET to (from) an inactive one but are not considered further.
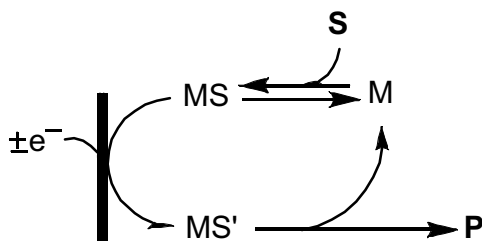
Scheme 6

2.2.2.4. Indirect *versus* direct electrosynthesis

The redox catalysis (or mediated ET catalysis) is based on an indirect ET process, as we have discussed above, and can be used for preparative purposes, thus being applied to indirect electrosynthesis.

In this type of electrosynthesis, the product is formed at the redox potential of the mediator rather than at that of the substrate, in contrast with the direct electrosynthetic methods, and the main advantages of the former are as follows:

- Use of a more favourable potential, what can also result from the following features;
- Decrease of the electrode passivation (the only species that undergoes ET with the electrode is the mediator) which is common during the direct electrolysis and could lead to a drastic current density decrease;
- Overcome of the overpotential required by the direct electrolysis for an acceptable current density (such a requirement in the case of the direct electrolysis results from the above reason and from the restriction of the substrate, in this type of electrolysis, to the two-dimensional space of the electrode surface);
- Possible control, in some cases, of the number of transferred electrons upon selection of the type of mediator (a single- or a two-electron transfer);
- By using an activating metal centre, a reaction that is impossible for the free substrate may become viable in coordination electrocatalysis, e.g. N_2, CO_2 or organohalide reduction upon binding to a suitable activating metal centre (the coordination of the substrate to the metal site is usually a selective process and thus the coordination electrocatalysis improves the selectivity in comparison with the direct electrosynthesis);
- From the above, the following two relevant advantages can be stressed: energy saving and selectivity gain.

2.2.3. The first Michaelis-Menten type mechanism in electrocatalysis. Amavadine as an ET mediator for the oxidation of thiols.

Amavadine is an intriguing natural bare vanadium complex present in some beautiful *amanita* toadstools, formulated as an octacoordinated V^{4+} complex with two tribasic forms of $2,2'$-(hydroxyimino)dipropionic acid, $[VL_2]^{2-}$ [L = $^-ON\{CH(CH_3)(COO^-)\}_2$ = $HIDPA^{3-}$]. Its molecular structure, as well as that of its model $[VL_2]^{2-}$ [L = $^-ON(CH_2COO^-)_2$ = $HIDA^{3-}$] are depicted in Scheme 7.
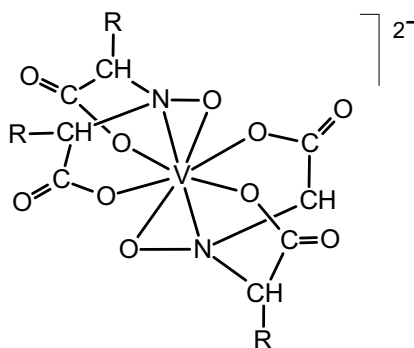
Scheme 7

Both *amavadine* and its model undergo, in aqueous medium and at a Pt electrode, a fully electrochemical and chemical reversible $V^{IV/V}$ oxidation and act as ET mediators for the electrocatalytic oxidation of some thiols (HSR), such as mercaptoacetic or mercaptopropionic acid $HS(CH_2)_nCOOH$ (n = 1 or 2, respectively) and cysteine $HSCH_2CH(NH_2)COOH$, to the corresponding disulfides RS-SR which were isolated upon bulk preparative indirect electrolyses,[5] Scheme 8.
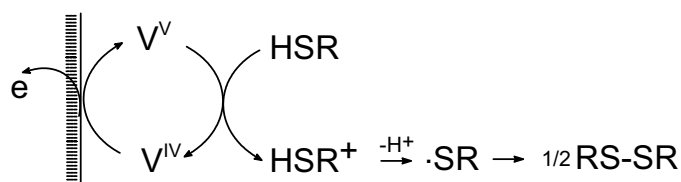
Scheme 8

The mechanism was studied in detail by digital simulation of cyclic voltammetry[5] and shown to exhibit a saturation effect with the concentration of the thiol, involving Michaelis-Menten type kinetics with formation of an intermediate species {V.HSR} (with half-life time of ca. 0.3 s) derived from the interaction of the substrate with the oxidized vanadium (V) complex (the active form of the mediator which acts as an inner-sphere oxidant of the thiol).

$$V^{IV} - e^- \rightleftharpoons V^V \qquad \textbf{\textit{ET at the electrode}}$$

$$V^V + HSR \underset{k_{-1}}{\overset{k_1}{\rightleftharpoons}} \{V \cdot HSR\} \qquad \textbf{\textit{inner-sphere}}$$

$$\{V \cdot HSR\} \xrightarrow{k_2} V^{IV} + 1/2\ RS\text{-}SR + H^+$$
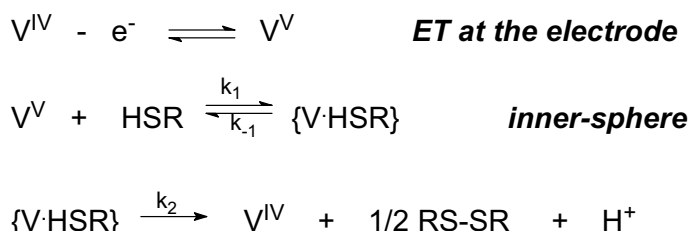
Scheme 9

The implications of this study were quite interesting. It suggested a possible biological role of *Amavadine* in the defensive system of the mushroom by S-S cross-coupling of protein fibers in damaged tissues. Even more importantly, it showed that *Amavadine*, in spite of its simplicity, could have a behaviour typical of an enzyme, following Michaelis-Menten kinetics. As a further step, since vanadium-haloperoxidases are well known, could *Amavadine* behave as an haloperoxidase or even a peroxidase towards some types of substrates? This oriented our subsequent research that lead to the discovery that *Amavadine*

and other V-complexes are quite remarkably efficient catalysts for the single-pot partial oxidation of alkanes under mild conditions,[6-11] i.e. (i) their peroxidative oxidation to alcohols and ketones, (ii) their peroxidative halogenation to organohalides, and (iii) their carboxylation to carboxylic acids. These catalytic studies were inspired on the above electrocatalytic behaviour.

2.2.4. Electrocatalytic reduction of dinitrogen to ammonia mediated by a metal centre

Dinitrogen (N_2) is a very stable species, with a strong N-N triple bond, a very negative electron affinity (very difficult to reduce) and a very high ionisation potential (very difficult to oxidize). It corresponds to a main abiotic source of nitrogen, an essential element to life, but cannot be assimilated by living organisms. For this purpose, it has to be firstly reduced to ammonia (NH_3), which can be incorporated in the living matter. This conversion is very energy demanding but can be achieved in Nature, under ambient conditions, by metalloenzymes called nitrogenases, and the process is named Nitrogen Fixation. Concomitant proton reduction also occurs in the biological systems and the overall reaction normally follows a $8H^+/8e^-$ process (reaction 11).

$$N_2 \ + \ 8H^+ + 8e^- \ \longrightarrow \ 2NH_3 \ + \ H_2 \qquad\qquad (11)$$
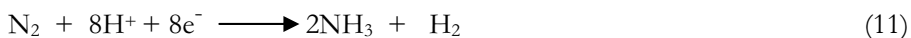
In contrast, the industrial Haber process for the synthesis of ammonia from N_2 and H_2, developed in the early XXth century, requires quite drastic conditions, at high temperatures and pressures, in the presence of a solid metal catalyst. However, the field of Chemical Nitrogen Fixation[12] underwent an effective impetus since the 60s due to remarkable achievements from the pioneering works of Vol'pin, Allen and Senoff, Chatt, Richards, Leigh, Hidai, Berclaw, Shilov, Tamaru, van Tamelen, etc.

A common feature of all these systems is that N_2 is activated by coordination to a suitable transition metal centre, what results in a weakening of the NN bond, in an asymmetric electronic distribution and eventually in a promotion of its chemical reactivity. A particularly interesting case was provided by van Tamelen,[13] involving the electrochemical reduction of N_2 to NH_3 by a system composed of titanium(IV)iso-propyloxide $[Ti(OPr^i)_4]/Al(OPr^i)_3$/naphthalene (Np) in 1,2-dimethoxyethane, according to Scheme 10.
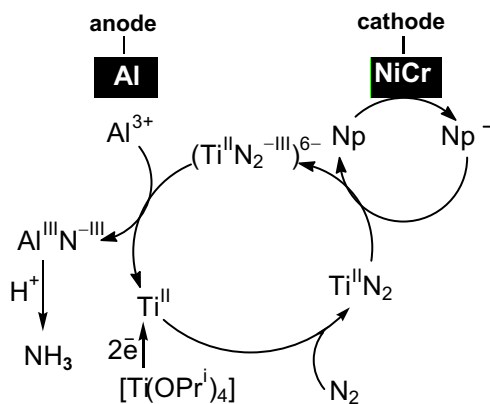
Scheme 10

Naphthalene behaves as an outer-sphere ET mediator between the Ni/Cr cathode and a dinitrogen Ti^{II} species formed by coordination of N_2 to a Ti^{II} centre (derived from cathodic reduction of the starting Ti^{IV} complex). The active Ti^{II} centre acts an inner-sphere ET mediator to N_2 which, upon stepwise reductive steps, is converted to nitride (N^{3-}).

The nitrile ligand is abstracted by Al^{3+} (Lewis acid) formed at the Al anode, to form aluminum nitride, AlN, with regeneration of the active Ti^{II} which further binds N_2 and the reductive cycle is repeated. Final nitride hydrolysis, after the electrolysis, liberates the ammonia (yield of ca. 6 mol NH_3/mol Ti).

This interesting process combines a form of coordination electrocatalysis (the Ti^{II}-N_2 species corresponds to the complex MS of Scheme 6 with the use of a homomediator [naphthalene in this case, or M in Scheme 5a)] that promotes the ET between the electrode and the complex MS. It thus occurs at the very favourable reduction potential of naphthalene, instead of the extremely cathodic potential required by the direct reduction of N_2.

Based on a systematic chemical and electrochemical investigation of Mo- or W-dinitrogen complexes with phosphine ligands, Chatt and Richards have proposed a stepwise pathway, Scheme 11, for the biological reduction of N_2 to NH_3.[12]

N_2 is activated by coordination to a metal centre (M) of the active site of the enzyme (although not yet established, the metal can be Mo or V, in the Mo- or V-nitrogenases, respectively, or Fe in such cases or in the alternative nitrogenase without Mo and V). The metal centre M not only activates N_2 to protonation, but also acts as an inner-sphere ET mediator (heteromediator) to N_2 and the derived protonated/reduced forms.

The N_2 reduction is thus occurring at the reduction potentials of the M-N_2 and derived species, which are much more accessible than that required by free N_2.

The model can be viewed as a complex example of coordination electrocatalysis in which the reducing agents are natural reducers instead of a cathode. It can also account for the liberation of H_2 upon concomitant proton reduction, via formation of a di-hydride intermediate, MH_2, from which H_2 is evolved upon replacement by N_2.
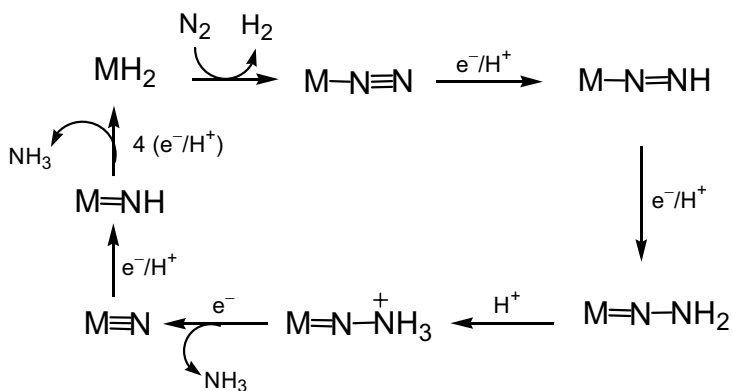
Scheme 11

2.3. ET Chain (ETC) Catalysis

This type of Electrocatalysis was initially found in Inorganic Chemistry by Taube. The reaction is triggered by ET, but the electron (or electron hole) is the catalyst and commonly there is no overall net redox change between the reagent (A) and the product (B) (overall reactions 12 or 13). The first applications in Electrochemistry were reported by Savéant, Amatore and Feldberg.

As the ET agent, one can use an electrode, an initiator or even light. As examples of one-electron oxidative initiators one can cite $[Ru^{III}(bpy)_3]^{3+}$, $ArN_3^{.+}$, Ag^+ or $[Fe^{III}(Cp)_2]^{.+}$ (Cp = η^5-C_5H_5), while one-electron reductive initiators include Na, $Na^+(C_{10}H_8)^{.-}$, $Na[Mn^I(Cp^*)_2]$ (Cp* = η^5-C_5Me_5), $[Fe^I(Cp^*)(C_6Me_6)]^.$, $[Fe^0(C_6Me_6)_2]$, $[Co^{II}(Cp^*)_2]^.$, $[Fe^I(Cp)(C_6H_6)]^.$.

$$A \xrightarrow{\ \pm e\ } B \tag{12}$$

$$A + C \xrightarrow{\ \pm e\ } B + D \tag{13}$$

Most of the general types of reactions have been electrocatalysed according to the above pattern, namely ligand exchange (the most usual case), insertion or dissociation, isomerization and chelation, but not oxidative addition.

2.3.1. ETC catalytic isomerization

The relative isomeric stability of coordination compounds is often dependent on the metal oxidation state and on the electron count of the molecule and a geometrical isomerization can be induced by simple ET. The subject has been reviewed[14,15] and the conversion in a few cases can proceed via ETC catalysis, as observed[16] in the *cis*-to-*trans* isomerization of the carbonyl complex *cis*-[ReCl(CO)(dppe)$_2$] (dppe = Ph$_2$PCH$_2$CH$_2$PPh$_2$) that is triggered by an oxidative initiation and which we have investigated in detail.

Let us first understand the basis of the catalytic process [the overall reaction is given by equation (14), in which *A* is the *cis*-carbonyl complex and *B* is the *trans* isomer, in the same redox state]. The reaction starts with an oxidative initiation step, denoted by $\vec{\mathbf{E}}$ (1, Scheme 12), by a catalytic amount of an oxidizing reagent (initiator I$^+$), an anode or light (for a reductive initiation, a related Scheme could be easily proposed).

This oxidation leads to an acceleration of the overall reaction (*cis*-to-*trans* isomerization, i.e. A$^+$ → B$^+$, first propagation step 2) due to a high kinetic gain at the radical 17-electron A$^+$ and B$^+$ species which are less stable than the parent 18-electron complex A.

$$ A \xrightarrow{\text{- e}} B \tag{14} $$

Since B$^+$ is an oxidizing agent relative to A (it has to be in order the ETC catalysis can occur), B$^+$ once formed oxidizes A by the cross-redox reaction 3 (2nd propagation step, homogeneous) that closes the cycle and drives the

isomerization reaction 2 if it is reversible (even if thermodynamically unfavourable!).

B^+ is also an oxidant of the initiator I (see the qualitative scale of the relative potentials of the redox couples), thus regenerating I^+ and forming further B (back ET step 4, denoted by $\overleftarrow{E}$). Moreover, if the process was initiated anodically, i.e., at the $E^o(A+/A)$ potential (or close to it), B^+ can be reduced at the electrode regenerating B (step 4). Therefore the process is clearly catalytic in electrons, following an $\overrightarrow{E}C\overleftarrow{E}$ mechanism (notation proposed by Feldberg) and requiring only a catalytic amount of charge to be triggered.

The *Coulombic efficiency* is defined as the number of molecules of B formed per electron transferred (or the number of moles of B formed per mole of electrons transferred, i.e., per Faraday) by the initiator (redox reagent or electrode).

$\overrightarrow{E}C\overleftarrow{E}$ mechanism

$\overrightarrow{E}$ – initiation b ET (**1**)

C – chemical propagation step (**2**)

$\overleftarrow{E}$ – back ET (or cross-ET) step f the propagation (**3** or **4**)
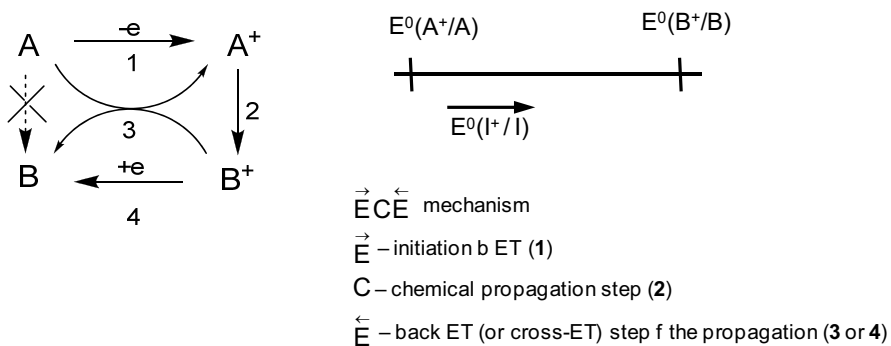
Scheme 12

In our case,[16] Scheme 13, exhaustive CPE at the oxidation potential of the *cis* isomer (A), E^o (*cis*$^{o/+}$), consumes only 0.018 F/mol, for its full conversion into

the *trans* isomer (B), what corresponds to a Coulombic efficiency of $1/0.018 =$ 56 mol/F.

The mechanism was investigated in detail by digital simulation of cyclic voltammetry, Figure 1a) as an example, that has allowed to estimate the various rate constants involved. The low value of $\Delta S^{\ddagger}$ (although with a high uncertainty) is suggestive that the isomerization could occur via an intramolecular twist rather than a dissociative (bond rupture) mechanism.[16]

Multiple cyclic voltammetric scans clearly show the oxidative *cis*-to-*trans* isomerisation, Figure 1b).

The relative stability of the two geometrical isomers and its variation upon oxidation have also been studied by quantum chemical calculations[17] that corroborate the observed electrochemical behaviour.


Scheme 13

557
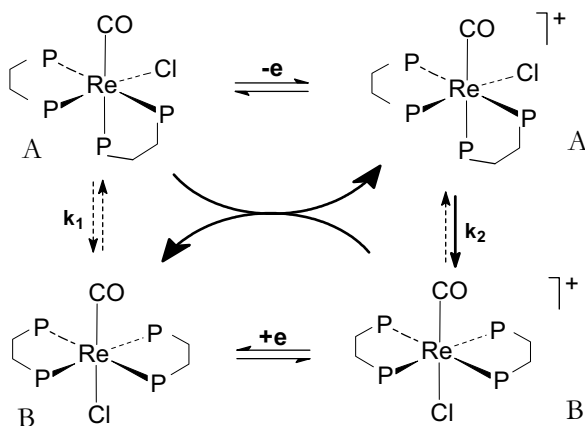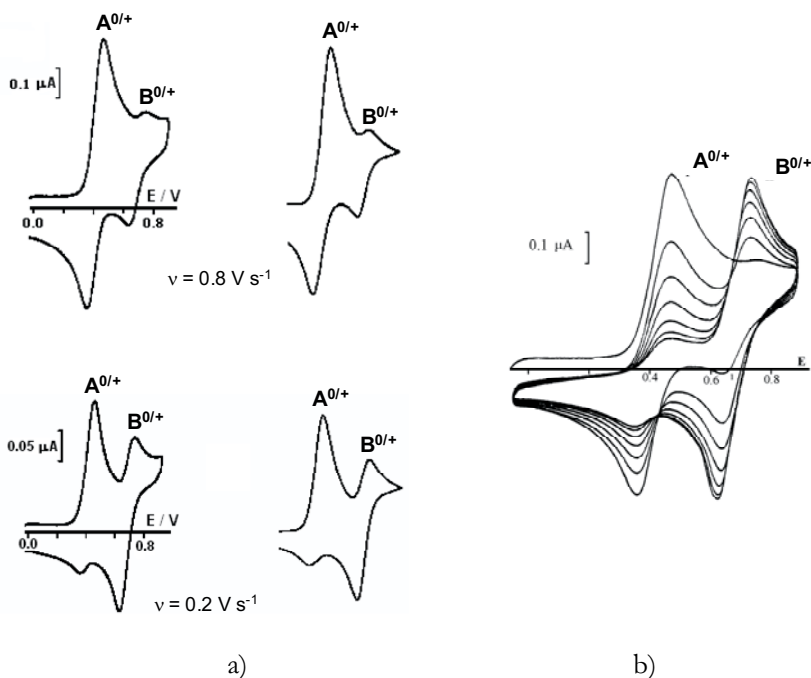
Figure 1 - a) Experimental (left) and simulated cyclic voltammograms of *cis*-[ReCl(CO)(dppe)$_2$]$^+$ at 0.8 and 0.2 Vs^{-1}. b) Multiple scans cyclic voltammetry. In CH$_2$Cl$_2$/0.2 M [NBu$_4$][BF$_4$]/Pt disc electrode, at -40 ºC. Potentials in V *vs*. SCE. Waves I and II due to the oxidation of the *cis* and the *trans* complex, respectively.

2.3.2. ETC catalytic ligand replacement. Coupling with organometallic catalysis

Reactions involving more than one reagent – e.g. A and C to afford B and D equation (15) – can also be triggered by an ET according to an ETC catalytic process, as shown by the general Scheme 14. They concern the case of oxidative initiation, but the reductive initiation could be treated similarly.

$$A + C \xrightarrow{\ -e\ } B + D \tag{15}$$

$\overrightarrow{E}C\overleftarrow{E}$ mechanism
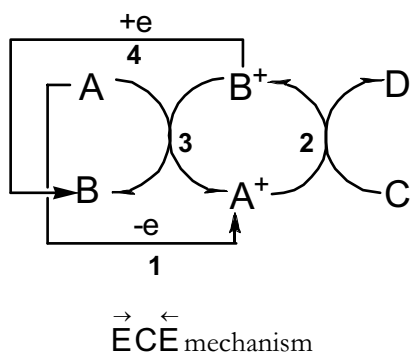
Scheme 14
(for the meaning of the steps and the order of the redox potentials, see Scheme 12)

Scheme 14, apart from requiring a second reagent (C) and leading to a second product (D), has good analogies with the simpler and previous one, 12, and will not be discussed now in detail. It is possibly sufficient to indicate that 1 is the oxidative initiation step (in the same way as previously), 2 is the first propagation step (homogeneous) giving one of the products, 3 and 4 are further propagation steps, the former (homogeneous) by cross-redox reaction (B^+ has to be a better oxidant than A^+) that drives 2 if it is reversible (it can be thermodynamically unfavourable) and the latter 4 by ET with the initiator (B^+ oxidizes homogeneously the reduced form I) or by ET with the electrode (heterogeneous).

The general Scheme 14 can be adapted to a ligand replacement reaction by considering that C is the incoming ligand and D is the displaced one. Let us apply it to an interesting case involving also organometallic catalysis in which the chemical catalyst is quickly generated *in situ* by ETC ligand exchange catalysis. This occurs in the fast polymerization of 1-alkynes by $[W(CO)_3(NCMe)_3]$ in the presence of a small amount (one-tenth molar ratio) of the ferricinium salt $[FeCp_2]^+[PF_6]^-$ (the reaction is practically instantaneous with the initiator, while it takes one week in its absence).[18]

By following the above described ETC catalytic mechanism, triggered by the oxidative initiation step 1 by ferricinium, for the sequential replacement of two acetonitriles by two alkynes (weaker electron-donors), Scheme 15, there occurs a fast generation of the active species $[W(CO)_3(HC\equiv CR)_2(NCMe)]$ denoted, in a simplified way, by $M(HC\equiv CR)_2$, which acts as the catalyst for the alkyne polymerization according to a Katz "metathesis-like" mechanism, represented in Scheme 16, involving insertions of the alkynes into the metal-carbene double bonds.
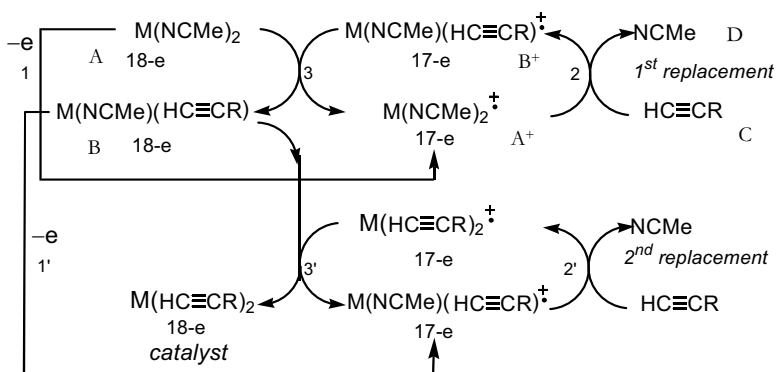
Scheme 15

Scheme 16

560
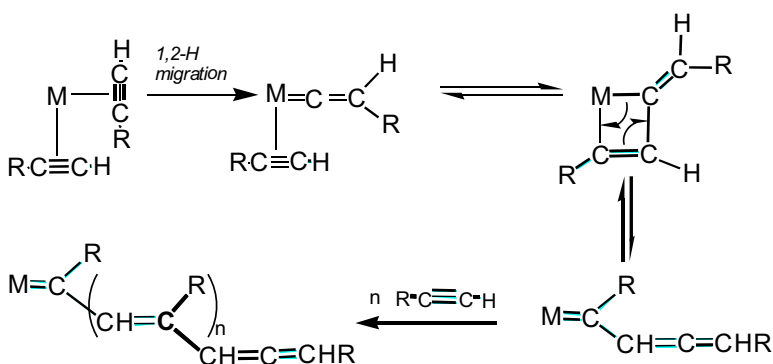
The authors[18] have thus achieved, in an ingenious and advantageous way, [18] to couple ETC catalysis and organometallic catalysis. Other possibilities and combinations are worthwhile to be further investigated.

2.4. FINAL REMARKS

We have shown illustrative cases on the basis and understanding of Electrocatalysis, as well as on its synthetic applications namely in Coordination and Organometallic Chemistries.

By using a mediator, it is possible, in a catalytic way, to inject (or abstract) an electron to (or from) a system which is thus activated towards further reactions with synthetic significance.

The electron itself can act as a catalyst in the catalytic cycle that it initiates.

Any of the main types of Electrocatalysis, i.e. either the mediated ET catalysis or the ETC catalysis, can promote reactions against the thermodynamic potential gradient and opposing the thermodynamic equilibrium constant, thus showing a kind of "magic" behaviour.

The mediator and the electron appear as magic agents ("magic wands") that induce unfavourable behaviours, apparently (but not in reality) in contradiction with Thermodynamics, and the Electrocatalysis evolves as an "Electronic Magic" to add to other much more popular magic forms such as Natural, White or Black Magics…

"E-Magic" Catalysis thus feeds our childhood dreams of making impossible things to happen! Isn't this a marvellous mystery that deserves to be further explored?

Acknowledgements

Thanks are due to the other authors of joint publications, in particular, Dr. M.F. Guedes da Silva who performed the electrocatalytic studies in the author's laboratory and kindly prepared the Schemes and Figures.

References

1. D. Astruc, *Electron-Transfer and Radical Processes in Transition-Metal Chemistry*, VCH, New York, **1995**, Chp. 6 and 7, pp. 413-566.

2. A.J.L. Pombeiro, C. Amatore (Eds.), *Trends in Molecular Electrochemistry*, Marcel Dekker/Fontis Media, New York/Lausanne, **2004**.

3   T. Shono, *Electroorganic Chemistry as a Tool in Organic Synthesis*, Springer-Verlag, Berlin, **1984**, Chp. 2.9, pp. 114-124.

4. J. Simonet, J.-F. Pilard, in H. Lund, O. Hammerich (Eds.), *Organic Electrochemistry*, Marcel Dekker, New York, **2001**, Chp. 29, pp. 1163-1225.

5. M.F.C. Guedes da Silva, J.A.L. da Silva, J.J.R. Fraústo da Silva, A.J.L. Pombeiro, C. Amatore, J.-N. Verpeaux, *J. Am. Chem. Soc.*, **1996**, *118*, 7568.

6. P.M. Reis, J.A.L. Silva, J.J.R. Fraústo da Silva, A.J.L. Pombeiro, *J. Chem. Soc., Chem. Commun.*, **2000**, 1845.

7. P.M. Reis, J.A.L. Silva, A.F. Palavra, J.J.R. Fraústo da Silva, T. Kitamura, Y. Fujiwara, A.J.L. Pombeiro, *Angew. Chem.*, *Int. Ed.*, **2003**, *42*, 821.

8. A.J.L. Pombeiro, J.J.R. Fraústo da Silva, Y. Fujiwara, J.A.L. Silva, P.M. Reis, A.F. Palavra, Patent WO 2004/037416 A3.

9. P.M. Reis, J.A.L. Silva, A.F. Palavra, J.J.R. Fraústo da Silva, A.J.L. Pombeiro, *J. Cat.*, **2005**, *235*, 333.

10. G.S. Mishra, J.J.R. Fraústo da Silva, A.J.L. Pombeiro, *J. Mol. Cat. A: Chem.*, **2006**, *265*, 59.

11. G.S. Mishra, A.J.L. Pombeiro, *Appl. Cat. A: Gen.*, **2006**, *304*, 185.

12. J. Chatt, L.M. Câmara Pina, R.L. Richards (Eds.), *New Trends in the Chemistry of Nitrogen Fixation*, Academic Press, **1980**.

13. E.E. van Tamelen, *Acc. Chem. Res.*, **1970**, *3*, 361.

14. A.J.L. Pombeiro, M.F.C. Guedes da Silva, M.A.N.D.A. Lemos, *Coord. Chem. Rev.*, **2001**, *219-221*, 53.

15. A.J.L. Pombeiro, M.F.C. Guedes da Silva, in A.J.L. Pombeiro, C. Amatore (Eds.), *Trends in Molecular Electrochemistry*, Marcel Dekker / Fontis Media, New York/Lausanne, **2004**, Chp. 5, pp. 153-186.

16. M.F.C. Guedes da Silva, C.M.P. Ferreira, J.J.R. Fraústo da Silva, A.J.L. Pombeiro, *J. Chem. Soc., Dalton Trans.*, **1998**, 4139.

17. M.L. Kuznetsov, A.J.L. Pombeiro, *Dalton Trans.*, **2003**, 738.

18. M.-H. Desbois, D. Astruc, *New J. Chem.*, **1989**, *13*, 595.

(Página deixada propositadamente em branco)

SECTION E

EXPERIMENTAL DESIGN

(Página deixada propositadamente em branco)

1. EXPERIMENTAL DESIGN

Alberto Canelas Pais

Departamento de Química da Universidade de Coimbra, Rua Larga, 3004-535 Coimbra, Portugal

In Chemistry, many tasks possess well defined objectives and the variables upon which control may be exerted are easy to identify. At the same time, many processes are too complex to tackle using first principles. One of the areas in which these statements apply is chemical synthesis. A black-box approach, see Figure 1, may provide significant insight into the process, a rationale for the observations and is often the only way to circumvent less controlled effects.
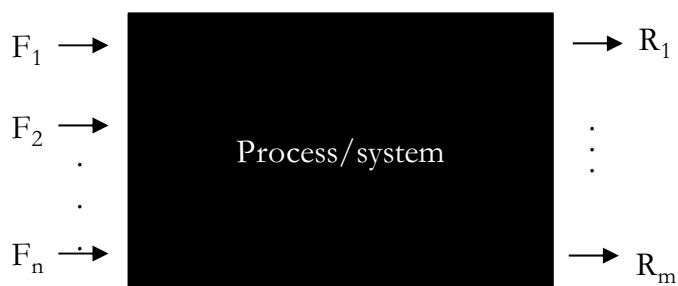
Figure 1 - The blackbox view of a process or a system. Factors, F, control the output or system responses, R. Usually, n >> m.

Experimental design consists of planning having in view the optimisation of the process. It is thus directly connected with carrying out experiments so as to identify the most relevant factors, the interaction effects and, finally, choose the best values for the operation variables (the degrees of freedom of the process). It embodies classical chemometrics[1], and has a variety of applications from analytical chemistry[2] to industrial catalysis[3] or pharmaceutical development[4], not to mention other, totally disparate, sciences.

Methods can be divided using a number of different criteria, but for the experimentalist one of the key issues is the number of experiments that are

necessary. In some approaches it is not possible to make an estimate of the number of trials that will ultimately lead to the outcome, which consists either of a deeper understanding of the process, many times in the form of a model, or simply establishes the best conditions for operation. Many methods are essentially directed at finding extrema for the response variable(s), using the degrees of freedom as factors or independent variables. They do not provide an overall description of the system, and the number of experiments is governed by a convergence criterion. This makes it difficult to estimate the workload involved in the optimisation, and each experiment is the result of previous experiments. However, the degree of proximity to the optimal solution is, in principle, arbitrarily large. Other methods rely on a set of well defined experiments that often are capable of making a screen of factors and providing the optimal solution, being sometimes called *simultaneous* methods. These approaches usually rely on simple models that, in some cases, are not adequate to the process. This may result both in poor description and in poor optimisation. To circumvent such shortcomings approaches are also devised. They rely on a simple rule: the larger the number of experiments, the more complex may the model be and the best is the system described. This rule possesses a counterpart: for a limited number of experiments the description of the process is of a lesser quality, but the cost of the design is also lower.

In what follows, we will present a brief overview of some methods used in the optimisation of chemical processes, with a definite emphasis on factorial design.

1.1. GENERAL ASPECTS

An optimisation procedure relies on the description of the system on the basis of a response or responses determined by a set of factors (see Figure 1). These factors must be carefully selected according to some criterion. The experimentalist's previous experience is clearly a major asset for this choice.

1.2. SIMPLEX OPTIMISATION

The simplex methods are based on an initial design of k+1 trials, where k is the number of variables. A k+1 geometric figure in a k-dimensional space is called a simplex. The corners of this figure are called vertices (see Figure 2).
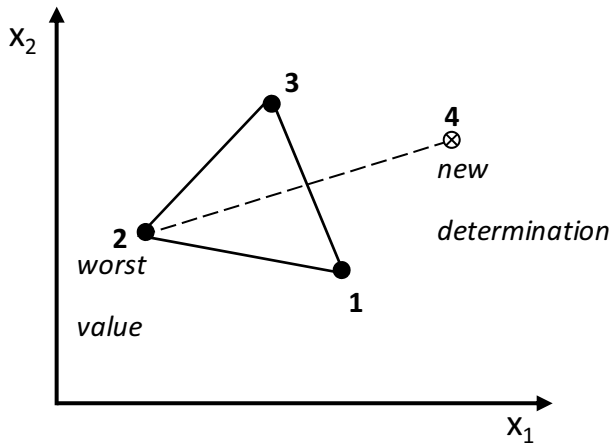
Figure 2 - A schematic description of the initial simplex in two-dimensions, and the direction of search for the next step.

With two variables, the first simplex design is based on three trials, for three variables it is four trials, etc. This number of trials is also the minimum for defining a direction of improvement. Therefore, it is a timesaving and economical way to start an optimization project.

After the initial trials the simplex process is sequential, with the addition and assessment of one new point at a time. The simplex searches systematically for the best (higher or lower depending on what is being searched) values of the response. The optimization process ends when it is sufficiently close to the optimum. The simplex algorithm advances such that the test point with the least favourable response value in the current simplex is discarded, and a new set of control variable levels (the word level denotes a specific value of a

controlled variable) is calculated, by reflection into the control variable space opposite this undesirable result. The new trial replaces the least favourable one in the simplex. This leads to a new least favourable response in the new simplex that, in turn, leads to another new trial, and so on. At each step one moves away from the more undesirable conditions. Naturally, one can never return to control variable levels that have just been rejected. Without this second rule, the simplex would just oscillate between the two control variable levels if the calculated reflection in the control variables produces a least favourable result. The problem is eliminated by choosing the second best condition and moving away from it.

Basic simplex optimisation relies on a fixed length for the side of the (hyper-)triangle, which is reduced when new points produce some rotation about a central point. The process is halted when this rotation occurs for a very short radius, which indicates proximity with the optimal conditions.

A number of more efficient procedures have been offered in which the size of the simplex is modified in the course of the search. It should be mentioned, however, that in most of these methods an increased efficiency is usually obtained at the expense of robustness.

The method and its variants have the significant advantage of being *direct search* methods, i.e., they do not require a model or parameter estimation. However, the usually high number of experiments to achieve convergence, and the fact that the number of experiments is not known *a priori*, may discourage their use.

1.3. FACTORIAL DESIGN

Factorial design is based on systematic changes in the factors (variables, degrees of freedom) that allow an assessment of the respective influence upon the response. Designs based on two levels for each factor, sometimes called

screening designs, are very common. They correspond to the full factorial design at two levels and rely on performing 2^k experiments, where k is the number of factors. Unlike other areas, in factorial design the number of parameters in a function that relates factors and response may be very close or equal to the number of experiments.

Factorial design has several important features. First, it has great flexibility for exploring or enhancing the signal or response in experimental studies. Whenever we are interested in examining variations in the degrees of freedom, factorial designs should be strong candidates as the designs of choice. Second, factorial designs are efficient. Instead of conducting a series of independent studies we are effectively able to combine these studies into one. Finally, factorial designs are the only effective way to examine interaction effects. Also, they allow for a set of experiments conducted within operational conditions that are chosen in advance, and do not result from previous experiments. This is especially convenient when one is faced with experimental restrictions.

1.3.1. The main effect

A main effect is an outcome that is a consistent difference between levels of a factor. It is calculated from the effect of a single factor, i.e., the difference in the response at the two levels of this factor, for each level of the others.

1.3.2. The interaction

Factorial designs would be useful, even if only the main effects would be assessed. However, because of the way we combine levels in factorial designs, they also enable us to examine the interaction effects that exist between factors. An interaction effect exists when differences on one factor depend on the level you are on another factor. It is important to recognize that an interaction is between factors, not levels.

1.3.3. How to proceed

Let us assume that we have two variables in the process (e.g. pressure and temperature). A full factorial design of two levels would require 2^2 experiments (see Figure 3), and would allow to establish a function with up to 4 parameters. In a black-box study, the obvious choice is

$$R = a_0 + a_1 x_1 + a_2 x_2 + a_{12} x_1 x_2 \tag{1}$$

where R is the value of the system response, and x_1 and x_2 denote the two factors. The first problem is to set the values of the two levels for each of the variables, whose combination defines the four experiments. This is often based on the definition of a meaningful range, within the usual operational conditions. In the above example, the two temperatures and the two pressures would be chosen within equipment restrictions and based on previous experience in similar systems.
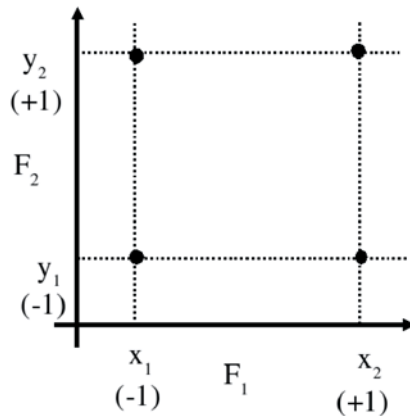

Figure 3 - Scheme for a two-factor, two-level design. Also indicated is the most common coding scheme.

The next step is to carry out the experiments, with two or three repetitions in all or most combinations of levels, so as to obtain a set of responses. See Table 1 for a numerical example.

The parameters in Equation (1) can be determined directly on the basis of this Table. The procedure corresponds essentially to a simple least squares fit to the data. The actual values of the variables are input and all the 8 responses (or 4 if we use the average for each combination of the levels) used in the fitting. This is a useful way to predict optimal values for the temperature and pressure so as to obtain the maximum yield. Equation (1) now naturally takes the form

$$R = a_0 + a_1 T + a_2 P + a_{12} TP \tag{2}$$

and the optimum (it can also be a minimum!) comes from the system

$$\begin{cases} \dfrac{\partial R}{\partial T} = 0 \\ \dfrac{\partial R}{\partial P} = 0 \end{cases} \tag{3}$$

which gives $T=-a_2/a_{12}$ and $P=-a_1/a_{12}$. Unfortunately, this approach does not provide a significant insight in the importance of the factors or the interaction. An alternative is to use coded levels, i.e., the actual values of the independent variables are replaced by another representation of the lower and upper level. A frequent coding scheme is to use -1 for the lower level and +1 for the higher. There are significant advantages in this scheme. Firstly, a_0 corresponds to the central point in a centred design, thus being given by the average value of the experiments in each level. Secondly, the inspection of the relative values of the remaining coefficients is sufficient to present a first notion of the relative importance of the factors and of the interaction for the chosen intervals. Thirdly, it is very easy to transform back to the original variables. If these, on the other hand, are used for the least-squares procedure, the coefficients are

strongly dependent on their actual values and do not directly reflect the importance of the factors. The constant is also meaningless. A fourth aspect that should not be neglected is related with the use of qualitative factors. It is hard to include a catalyst, an action (e.g. agitate, pulverize or not), etc. in a numerical treatment. However, it can be easily done if the absence of a catalyst is denoted as -1, and its presence as +1, or if catalyst A is given as -1 and catalyst B as +1. Naturally, when qualitative factors are introduced something is lost: the ability to estimate optimum conditions involving all the variables. Optimization is now restricted to situations in which these qualitative factors are frozen.

TABLE 1 - Results for a chemical reaction in which two factors have been controlled, pressure and temperature. Two repetitions are indicated for each combination of the levels.

Experiment	Temperature/°C	Pressure/bar	Yield/%
1	40	5	90.5, 91.2
2	40	10	94.5, 93.9
3	80	5	89.5, 88.3
4	80	10	90.2, 90.8

1.3.4. The algorithm

In a more mathematical sense, parameters a_i and $a_{i,j,...}$ correspond to the main effects of factor i and the interaction between factors i, j, etc. Following our two-level two-factor scheme, the main effect of the temperature would correspond simply to the average of the effects (i.e. the result of changing) this variable at the two levels of the pressure. In a obvious notation

$$a_1 = \frac{1}{2}\left\{\left(\overline{R}_3 - \overline{R}_1\right) + \left(\overline{R}_4 - \overline{R}_2\right)\right\} \tag{4}$$

with a similar expression for the main effect of pressure. The interaction can be expressed as

$$a_{12} = \frac{1}{2}\left\{\left(\overline{R}_1 + \overline{R}_4\right) - \left(\overline{R}_2 + \overline{R}_3\right)\right\} \tag{5}$$

and is given by the difference between the value of the effect of T for the lower level of P to this effect for the higher level. The above equations show that both the main effects and the interaction resort to *all* the system responses.

There is a more systematic approach (see for example Reference 1) to the calculation of parameters in Equation (1). It can also be extended to any model of the same type. We note that such models rarely go beyond squared dependences on one factor or interactions between sets of three factors.

Firstly we build a matrix that describes the sets of experiments, D, and the column vector of the corresponding responses, R, for example

$$D = \begin{bmatrix} -1 & -1 \\ -1 & -1 \\ -1 & +1 \\ -1 & +1 \\ +1 & -1 \\ +1 & -1 \\ +1 & +1 \\ +1 & +1 \end{bmatrix} \quad R = \begin{bmatrix} 90.5 \\ 91.2 \\ 94.5 \\ 93.9 \\ 89.5 \\ 88.3 \\ 90.2 \\ 90.8 \end{bmatrix}$$

The matrix D is then enlarged to matrix X, closely following the order of parameters in the model function. For expression (1) the expanded matrix would have in the first row unitary values, in the second the values of the levels in factor 1, the third would be given by the values of levels for factor 2 and the fourth would be products of the values of factor 1 and 2.

$$X = \begin{bmatrix} +1 & -1 & -1 & +1 \\ +1 & -1 & -1 & +1 \\ +1 & -1 & +1 & -1 \\ +1 & -1 & +1 & -1 \\ +1 & +1 & -1 & -1 \\ +1 & +1 & -1 & -1 \\ +1 & +1 & +1 & +1 \\ +1 & +1 & +1 & +1 \end{bmatrix}$$

In case the function comprises squares of the factors there would be rows with squares of the values of the levels, etc. Recall that both coded levels or the actual values of the variables can be used. A simple succession of matrix operations

$$(X'X) = \begin{bmatrix} 8 & 0 & 0 & 0 \\ 0 & 8 & 0 & 0 \\ 0 & 0 & 8 & 0 \\ 0 & 0 & 0 & 8 \end{bmatrix} \qquad (X'R) = \begin{bmatrix} 728.9 \\ -11.3 \\ 9.9 \\ -3.5 \end{bmatrix}$$

$$a = (X'X)^{-1}(X'R) = \begin{bmatrix} 91.11 \\ -1.41 \\ 1.24 \\ -0.44 \end{bmatrix}$$

would lead to the final model

$$R = 91.11 - 1.41x_1 + 1.24x_2 - 0.44x_1 x_2$$

This succession is implemented more easily using a package such as Matlab or similar (Octave, Scilab, etc.) but it can also be easily developed by means of a

spreadsheet. For example, the functions Transpose, Matmult, Invert would make most of the work resorting to Excel.

1.3.5. The analysis

The analysis is not as trivial as the development of the method, but usually the amount of information that is obtained is worth the effort. The idea is to answer questions such as:

- what factors are relevant?
- how do they affect the response?
- do they interact and how?
- can the model explain the results?
- is the model really adequate?

Once again, it should be stressed that such questions are better answered on the basis of coded levels.

The relevance of the factors can be assessed, on a first attempt, using the relative values of the respective coefficients. This is sufficient in most problems (see below). It also allows to have an idea if the interaction is significant or not. The way they affect the system response is not as obvious: a negative value of the main effect would suggest a decrease in the response when we move to the upper level, but the interaction effect may alter this view. For the simple two-level/two-factor scheme it is possible to combine the main effect of one factor with the interaction and have

$$R = a_0 + (a_1 + a_{12} x_2) x_1 + a_2 x_2 \tag{6}$$

This clearly highlights what has previously been mentioned: the interaction is the alteration in the main effect caused by a change in level of the other factor.

It also gives a way to directly vary the main effect, but such a procedure becomes cumbersome for complex models.

A more accurate way to look into the significance of the factors is to use, for example, t-statistics.

The procedure is again, straightforward[5]:

1.   Calculate the matrix $\mathbf{b} = \left(X'X \right)^{-1}$

2.   Calculate the error sum of squares between the values predicted by the model and the actual experimental values

$$S_{residual} = \sum_{i=1}^{n° \text{ of experiments}} \left(R_i - R_{model} \right)^2 ;$$

3.   Calculate the mean, dividing $S_{residual}$ by the number of degrees of freedom available for testing the fitting, i.e., the total number of experimental points minus the number of parameters

$$s = S_{residual} / \left(n° \text{ of experiment s - } n° \text{ of parameters} \right) ;$$

4.   For each of the parameters in the model, take the appropriate diagonal element, b_{ii} from the matrix of step 1; this corresponds to the variance, υ, associated to each parameter a;

5.   For each coefficient calculate $t = a / \sqrt{s \, \upsilon}$; naturally, higher values of this ratio correspond to more significant coefficients;

6.   Obtain the statistical significance from a two-tailed t distribution.

Note that the concept of a more significant coefficient does not overlap with that of a coefficient that strongly influences the process, as derived from the simple assessment of magnitude. A significant coefficient is one for which the uncertainty is small, but it may at the same time be irrelevant to the process.

This means that the two observations have to be coupled for a correct interpretation.

A standard ANOVA procedure would convey more information, mostly in what concerns the adequacy of the model and the relevance of the regression (see e.g., Reference 4). It is often the case that the regression is significant, i.e., the procedure explains most of the variations in the process and, even for simple models, experimental responses are approached. A common conclusion is also that the model is not (at least not fully) adequate. This poses a problem: should we look for a better objective function? In what follows we approach the question of how to either simplify or improve the quality of the model. However, in most cases if the predictive capabilities or the information conveyed for rationalization are deemed sufficient, the inadequacy of the model as extracted from the ANOVA procedure may not be an issue.

1.3.6. Simpler or more complete models?

Sometimes, the performance of our models is really low and we have no alternative but to improve the corresponding capabilities for the description of the process. In the type of models described above, the improvement may be carried out in a more or less systematic way. Essentially, the sequence would be to consider first main effects, then two-way interactions, squares of main effects, three-way interactions, etc. All the procedure of extension must follow in a very careful way. It is well known in general least squares doctrine that increasing the number of parameters increases the quality of the fitting, but it also makes the model more unstable towards both interpolation and extrapolation. Also, parsimony criteria should be included to establish how much is gained with a new parameter. Naturally, the number of experiments must concomitantly increase. In factorial design it is relevant that the information conveyed by the new experiments be used in conjunction with that previously determined. The so-called central composite design is a natural

extension of the full 2^k factorial approach. Figure 4 depicts that approach for the two-factor case, but extrapolation for higher-dimensional problems is straightforward. A central experiment is placed in the center of the design, which is extremely useful to control the curvature of the response surface. The description is also improved because intermediate points, slightly displaced to introduce clear new levels, are placed midway between the two levels in each factor.
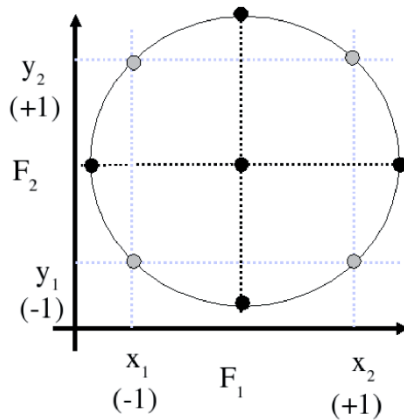

Figure 4 - Central composite design for a two-factor process. The new experiments (in black) are indicated on top of the previous 2^2 (grey) indicated in Figure 3. All these 9 levels belong to the improving scheme.

Note that 9 types of experiments allow for the use of a 9 parameter expression, but a more conservative choice is probably sufficient,

$$R = a_0 + a_1 x_1 + a_2 x_2 + a_{12} x_1 x_2 + a_{11} x_1^2 + a_{22} x_2^2 \qquad (7)$$

Sometimes the number of factors is high, and a full factorial 2^k design requires an excessive number of experiments. There are several schemes to reduce this number. A popular one is the Plackett-Burman (PB) plan, which relies on statistics and combinatorial analysis. Only the main effects are determined in

this plan. For this type of analysis, the term 'screening design' is much more adequate than for factorial plans in general. It refers, in this case, to an experimental plan that is intended to find the few significant factors from a list of many potential ones, or identify significant main effects, rather than interaction effects.

The scheme was described in 1946, when R.L. Plackett and J.P. Burman published their famous paper "The Design of Optimal Multifactorial Experiments" in Biometrika (vol. 33). This paper describes the construction of very economical designs with the run number a multiple of four (rather than a power of 2). PB designs are very efficient screening designs if the main effects are considered dominant or interactions negligible. However, main effects are in general heavily confounded with two-factor interactions. The PB design in N runs, for example, may be used for an experiment containing up to N-1 factors. A test plan of this type, with seven factors is shown in Table 2.

TABLE 2 - Plackett-Burman plan for seven factors.

Entry	A	B	C	D	E	F	G
1	+	+	+	-	+	-	-
2	+	+	-	+	-	-	+
3	+	-	+	-	-	+	+
4	-	+	-	-	+	+	+
5	+	-	-	+	+	+	-
6	-	-	+	+	+	-	+
7	-	+	+	+	-	+	-
8	-	-	-	-	-	-	-

The calculation of the main effects is conducted by adding the measurements, with the signs listed in the columns, and the sum is divided by four.

1.3.7 Incorporating restrictions

Restrictions in factorial design are usually introduced without difficulty. These are of different types, and may affect the controlled variables or the response. An example of the former is the use of mass or molar fractions in mixtures. Let us take the simple example of Equation (1) and assume that the variables x_1 and x_2 are the molar fraction in some binary mixture. Then

$$x_1 + x_2 = 1$$

which means that the independent term, a_0, can be written as $a_0(x_1 + x_2)$ which translated in the model yields

$$R = (a_0 + a_1)x_1 + (a_0 + a_2)x_2 + a_{12}x_1x_2$$

being equivalent to write

$$R = a_1'x_1 + a_2'x_2 + a_{12}x_1x_2$$

i.e., the model no longer possesses the independent parameter. For restrictions upon the response, especially for restrictions upon the respective domain other approaches must be used. A common situation is having the response expressed in percentage, limited to the 0-100% range. In this case, one possibility is to rewrite the model in terms a 100% response[6,7]

$$100 = a_0 + a_1x_1 + a_2x_2 + a_{12}x_1x_2$$

especially if an optimization is being conducted. As such, there will be a range of x_1 and x_2 (now depending functionally on each other) values that may be used in predicting the maximum output. Practical considerations, e.g. in terms of the experimental limitations, will provide a guide for selecting appropriate values of the variables that can be used to test the validity of the prediction.

1.3.8 A case study

In what follows we describe a practical application of factorial design in hydroformylation reactions (this example is described in detail in reference 7). The controlled variables are the ligands used (2 different molecules), temperature and pressure. The response is the fraction of branched aldheyd obtained. A full 2^3 factorial design on these variables has produced the results depicted in Table 3.

TABLE 3 - Coded values of controlled variables, *D*, in the order temperature, pressure and ligand, and responses, *R*, for the hydroformylation example.

$$
D = \begin{bmatrix}
-1 & -1 & -1 \\
-1 & -1 & +1 \\
-1 & +1 & -1 \\
-1 & +1 & +1 \\
+1 & -1 & -1 \\
+1 & -1 & -1 \\
+1 & -1 & +1 \\
+1 & +1 & -1 \\
+1 & +1 & -1 \\
+1 & +1 & +1 \\
+1 & +1 & +1
\end{bmatrix}
\qquad
R = \begin{bmatrix}
72.4 \\
83.0 \\
67.7 \\
59.3 \\
90.0 \\
90.2 \\
91.2 \\
87.0 \\
86.0 \\
81.4 \\
82.0
\end{bmatrix}
$$

The actual determination of the parameters, and the respective characterisation was made using the Octave (essentially also compatible with Matlab) program shown in the Appendix, in which some efficiency is lost for the sake of clarity. From Table 4 it is seen that both pressure and temperature are important variables in the process, but the direct effect of the ligand is negligible: the respective coefficient cannot be distinguished from zero. However, the effect of the ligand is clearly dependent on temperature as can be extracted from the

interaction coefficient a_{LT}, while the interaction with pressure, from a_{LP} is less significant. A visible interaction between ligand structure and temperature can be related to the differential flexibility of the chelate rings.

TABLE 4 - Values of coefficients, *t* and probability for a Student's *t-test*. Only main and two-variable interaction effects are considered.

Coefficient	Value	t	Probability/%
a_0	79.1	95.7	>99.9
a_P	8.5	10.3	>99.9
a_T	-5.3	6.4	99.7
a_L	-0.1	0.1	5.6
a_{PT}	1.8	2.2	90.3
a_{TL}	-2.7	3.4	97.2
a_{LP}	-0.6	0.7	49.9

A standard analysis using ANOVA was also carried out on this design (Table 5). It indicates that, although the model is not fully adequate, it is still highly significant and explains the major part of the deviations from the corresponding mean values.

TABLE 5 - Analysis of variance in the case study.

	Degrees of freedom	Sum of squares	Mean square	F	Significance/%
Total	10	1057.5			<0.1
Regression	6	1030.4	171.7	190.8	
Residual	4	27.1	6.8		
Lack of fit	1	24.4	24.4	27.2	<5
Pure error	3	2.7	0.9		

Appendix

Program used for the analysis of data in Table 3, producing the results in Tables 4 and 5. Please note comments along the lines. The notation used in the calculations is standard.

```
%number of parameters for model
% R=ao+a1x1+a2x2+a3x3+a12x1x2+a23x2x3+a13x1x3
nparam=7
% number of different experiments, including
% repetitions
nexp=11
% calculation of degrees of freedom
dgf=nexp-nparam
ndif=8 % number of different experiments
dgfregr=nparam-1
dgfresid=dgf
dgferr=nexp-ndif
dgflof=dgfresid-dgferr
x = [ 1,-1,-1,-1,+1,+1,+1;
1,-1,-1,+1,+1,-1,-1;
1,-1,+1,-1,-1,-1,+1;
1,-1,+1,+1,-1,+1,-1;
1,+1,-1,-1,-1,+1,-1;
1,+1,-1,-1,-1,+1,-1;
1,+1,-1,+1,-1,-1,+1;
1,+1,+1,-1,+1,-1,-1;
1,+1,+1,-1,+1,-1,-1;
1,+1,+1,+1,+1,+1,+1;
1,+1,+1,+1,+1,+1,+1 ]
y = [ 72.4;
83.0;
67.7;
59.3;
90.0;
90.2;
91.2;
87.0;
86.0;
81.4;
82 ]
% calculation of model
% parameters
b = inv (x'*x)
a = b*x'*y
% determination of the significance
```

```
f = x*a
s = sum(x*a,2)
df1=(s-y)
df2=df1'
ss=df2*df1
s=ss/dgf
v=diag(b)
sv=sqrt(s*v)
t=a./sv
conf=100*(t_cdf(abs(t),dgf));
conf=2*conf-100 % degree of confidence
teste=x*a % check on the model
% ANOVA analysis for lack-of-fit (lof) and regression
% (regr).
averagey=sum(y)/nexp;
dif1=(y-averagey);
sstotal=dif1'*dif1
dif2=(teste-y);
dgfresid
ssresid=dif2'*dif2
msresid=ssresid/dgfresid
dgfregr
ssregr=sstotal-ssresid
msregr=ssregr/dgfregr
yrep=[ 72.4;
83.0;
67.7;
59.3;
90.1;
90.1;
91.2;
87.5;
87.5;
81.7;
81.7
];
diferr=y-yrep;
dgferr
sserr=diferr'*diferr
mserr=sserr/dgferr
F1=msregr/mserr
dgflof
F1teor=f_cdf(F1,dgfregr,dgferr)
sslof=ssresid-sserr
mslof=sslof/dgflof
F2=mslof/mserr
F2teor=f_cdf(F2,dgflof,dgferr)
```

References

1. D.L. Massart, B.M.G. Vandeginste, S.N. Deming, Y.Michotte, and L.Kaufman. *Chemometrics: a Textbook*. Elsevier, Amsterdam, **1988.**

2. R. Kellner, J.-M. Mermet, M. Otto, M. Valcárcel, and H.M. Widmer (Eds.). *Analytical Chemistry,* 2nd ed. Wiley, Weinheim, **2004**.

3. J. Hagen. *Industrial Catalysis: a Pratical Approach,* 2nd ed. Wiley, Weinheim, **2006**.

4. R. Phan-Tan-Luu, G.A. Lewis and D. Mathieu *Pharmaceutical Experimental Design*. Marcel Dekker, New York, **1999**.

5. R. G. Brereton (Ed.). *Chemometrics: Data Analysis for the Laboratory and Chemical Plant*. Wiley, Chichester, **2003**.

6. P.J.S. Gomes, C.M. Nunes, A.A.C.C. Pais, T.M.V.D. Pinho e Melo, and L.G. Arnaut., *Tetrahedron Lett.*, **2006**, *47,* 5475–5479.

7. A. F. Peixoto, M. M. Pereira, and A.A.C.C. Pais, *J. Mol. Cat. A: Chem.*, **2007**, *267,* 234–240.

Série

Investigação

•

· U · C ·